BioMed Research International

Accelerating Precision Medicine through Integrated Analysis of Multiscale Biological Data

Lead Guest Editor: Jian-Xin Shi
Guest Editors: Chang Gu, Jun Yang, Yue Wang, and Xufeng Pan

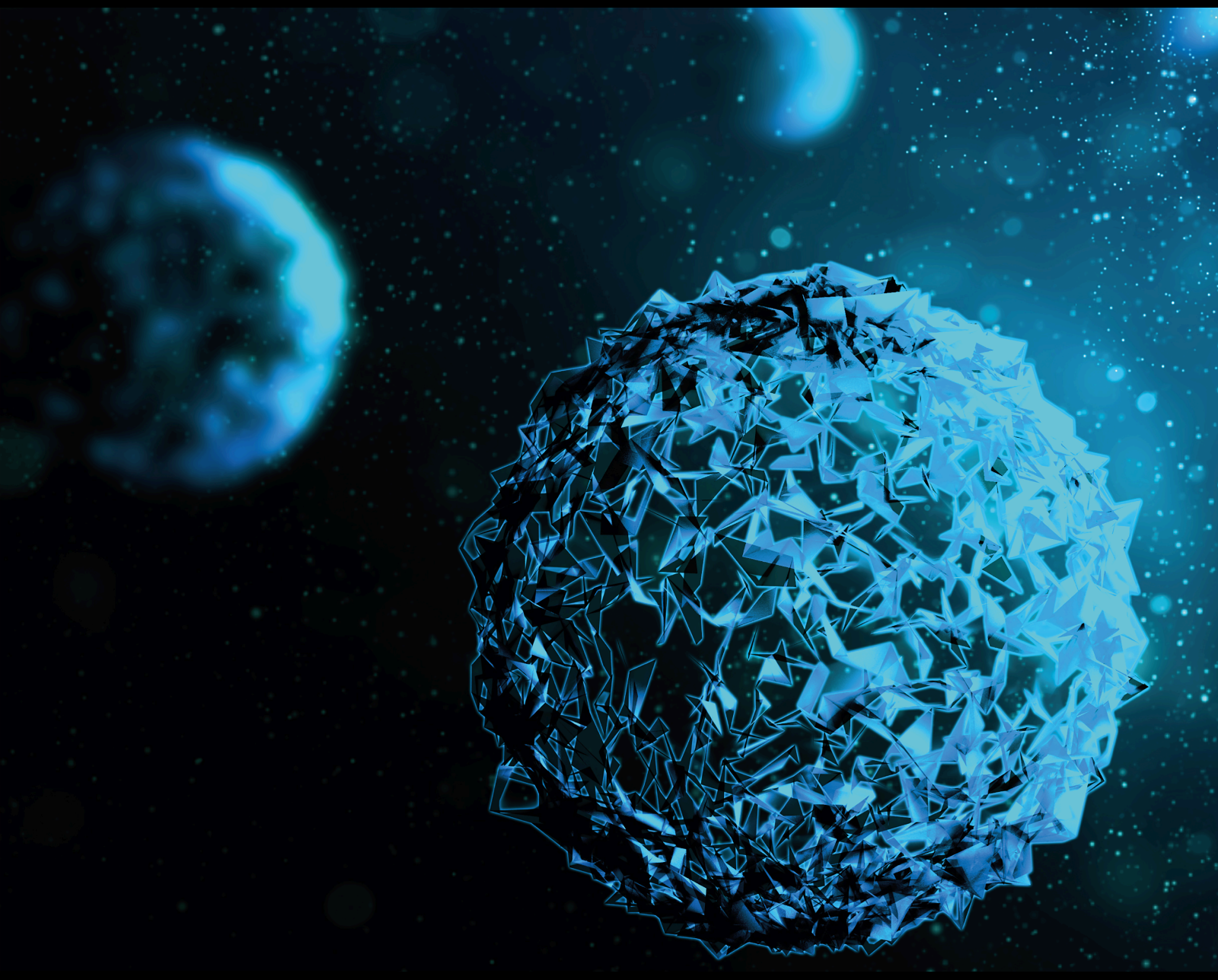

Accelerating Precision Medicine through Integrated Analysis of Multiscale Biological Data

BioMed Research International

Accelerating Precision Medicine through Integrated Analysis of Multiscale Biological Data

Lead Guest Editor: Jian-Xin Shi
Guest Editors: Chang Gu, Jun Yang, Yue Wang, and Xufeng Pan

Section Editors

Penny A. Asbell, USA
David Bernardo, Spain
Gerald Brandacher, USA
Kim Bridle, Australia
Laura Chronopoulou, Italy
Gerald A. Colvin, USA
Aaron S. Dumont, USA
Pierfrancesco Franco, Italy
Raj P. Kandpal, USA
Fabrizio Montecucco, Italy
Mangesh S. Pednekar, India
Letterio S. Politi, USA
Jinsong Ren, China
William B. Rodgers, USA
Harry W. Schroeder, USA
Andrea Scribante, Italy
Germán Vicente-Rodriguez, Spain
Momiao Xiong, USA
Hui Zhang, China

Academic Editors

Bioinformatics

Contents

Retracted: Expression of miR-210, miR-137, and miR-153 in Patients with Acute Cerebral Infarction
BioMed Research International
Retraction (1 page), Article ID 9894720, Volume 2024 (2024)

Retracted: Study on the Efficacy and Safety of Ambroxol Combined with Methylprednisolone in Patients with Acute Lung Injury
BioMed Research International
Retraction (1 page), Article ID 9894363, Volume 2024 (2024)

Retracted: Investigation on Risk Stratification and the Prognostic Value of hs-TnT Combined with MMP-2 in Patients with Acute Coronary Syndrome
BioMed Research International
Retraction (1 page), Article ID 9893040, Volume 2024 (2024)

Retracted: LncRNA PVT1 Promotes Hypoxia-Induced Cardiomyocyte Injury by Inhibiting miR-214-3p
BioMed Research International
Retraction (1 page), Article ID 9873517, Volume 2024 (2024)

Retracted: Effects of High-Flux Dialysis Combined with Hemoperfusion on Serum GRP78 and miR-495-3p in Renal Failure Patients
BioMed Research International
Retraction (1 page), Article ID 9867817, Volume 2024 (2024)

Retracted: The Protective Effects of miR-21-Mediated Fibroblast Growth Factor 1 in Rats with Coronary Heart Disease
BioMed Research International
Retraction (1 page), Article ID 9867070, Volume 2024 (2024)

Retracted: Expression of lncRNA-ANRIL before and after Treatment and Its Predictive Value for Short-Term Survival in Patients with Coronary Heart Disease
BioMed Research International
Retraction (1 page), Article ID 9864190, Volume 2024 (2024)

Retracted: Analysis on the Clinical Effect of High-Dose Glucocorticoids Combined with Immunosuppressants on Patients with Myasthenia Gravis Undergoing Video-Assisted Thoracoscopic Surgery
BioMed Research International
Retraction (1 page), Article ID 9863429, Volume 2024 (2024)

Retracted: Disorder Genes Regulate the Progression of Ischemic Stroke through the NF-κB Signaling Pathway
BioMed Research International
Retraction (1 page), Article ID 9859240, Volume 2024 (2024)

Retracted: The Functionalities and Clinical Significance of Tumor-Infiltrating Immune Cells in Esophageal Squamous Cell Carcinoma
BioMed Research International
Retraction (1 page), Article ID 9858395, Volume 2024 (2024)

Retracted: Changes of Serum Ferritin, Hemoglobin, and Serum Iron (SI) and Treatment Effect of Iron Proteinsuccinylate Oral Solution Combined with Vitamin A and D Drops on Children with Nutritional Iron Deficiency Anemia
BioMed Research International
Retraction (1 page), Article ID 9856043, Volume 2024 (2024)

Retracted: Effects of Sevoflurane on Apoptosis of Myocardial Cells in IRI Rats
BioMed Research International
Retraction (1 page), Article ID 9853194, Volume 2024 (2024)

Retracted: Protein Arginine Methyltransferase 5 Promotes the Migration of AML Cells by Regulating the Expression of Leukocyte Immunoglobulin-Like Receptor B4
BioMed Research International
Retraction (1 page), Article ID 9852462, Volume 2024 (2024)

Retracted: Treatment of Severe Ptosis by Conjoint Fascial Sheath Suspension
BioMed Research International
Retraction (1 page), Article ID 9850985, Volume 2024 (2024)

Retracted: The Function of circRNA-0047604 in Regulating the Tumor Suppressor Gene DACH1 in Breast Cancer
BioMed Research International
Retraction (1 page), Article ID 9845035, Volume 2024 (2024)

Retracted: miR-10b-5p Suppresses the Proliferation and Invasion of Primary Hepatic Carcinoma Cells by Downregulating EphA2
BioMed Research International
Retraction (1 page), Article ID 9834789, Volume 2024 (2024)

Retracted: Correlation Analysis of Acute Coronary Syndrome with Serum IL-18, MMP-9, hs-CRP, and Plasma FIB
BioMed Research International
Retraction (1 page), Article ID 9824926, Volume 2024 (2024)

Retracted: Clinical Efficacy of Methotrexate Combined with Iguratimod on Patients with Rheumatoid Arthritis and Its Influence on the Expression Levels of HOTAIR in Serum
BioMed Research International
Retraction (1 page), Article ID 9823071, Volume 2024 (2024)

Contents

Retracted: Long-Term Carbohydrate-Containing Late-Evening Snack Significantly Improves the Ratio of Branched Chain Amino Acids to Aromatic Amino Acids in Adults with Liver Cirrhosis due to Hepatitis B
BioMed Research International
Retraction (1 page), Article ID 9821414, Volume 2024 (2024)

Retracted: PFNA-II Internal Fixation Helps Hip Joint Recovery and Improves Quality of Life of Patients with Lateral-Wall Dangerous Type of Intertrochanteric Fracture
BioMed Research International
Retraction (1 page), Article ID 9808357, Volume 2024 (2024)

Retracted: Protective Effect of Luteolin on D-Galactosamine (D-Gal)/Lipopolysaccharide (LPS) Induced Hepatic Injury by in Mice
BioMed Research International
Retraction (1 page), Article ID 9807363, Volume 2024 (2024)

Retracted: The Expression of miR-23a And miR-146a in the Saliva of Patients with Periodontitis and Its Clinical Significance
BioMed Research International
Retraction (1 page), Article ID 9793809, Volume 2024 (2024)

Retracted: The Influence of ICAM1 3#UTR Gene Polymorphism on the Occurrence and Metastasis of Primary Liver Cancer
BioMed Research International
Retraction (1 page), Article ID 9793607, Volume 2024 (2024)

Retracted: Radiosensitizing Effect of Celastrol by Inhibiting G2/M Phase Arrest Induced by the c-myc Gene of Human SW1353 Chondrosarcoma Cells: Network and Experimental Analyses
BioMed Research International
Retraction (1 page), Article ID 9784090, Volume 2024 (2024)

Retracted: Clinical Effect of Clarithromycin Combined with Tinidazole on Helicobacter pylori-Related Gastritis and Its Influence on COX-2 Expression
BioMed Research International
Retraction (1 page), Article ID 9783981, Volume 2024 (2024)

Retracted: lncRNA FGD5-AS1 and miR-130a Can Be Used for Prognosis Analysis of Patients with Chronic Periodontitis
BioMed Research International
Retraction (1 page), Article ID 9781459, Volume 2024 (2024)

Retracted: Curcumin Improves Pulmonary Hypertension Rats by Regulating Mitochondrial Function
BioMed Research International
Retraction (1 page), Article ID 9769323, Volume 2024 (2024)

Retracted: Effect of Dexmedetomidine Combined with Ropivacaine on Cognitive Dysfunction and Inflammatory Response in Patients Undergoing Craniocerebral Surgery
BioMed Research International
Retraction (1 page), Article ID 9760679, Volume 2024 (2024)

Retracted: miR-1226-3p Promotes eNOS Expression of Pulmonary Arterial Endothelial Cells to Mitigate Hypertension in Rats via Targeting Profilin-1
BioMed Research International
Retraction (1 page), Article ID 9758259, Volume 2024 (2024)

[Retracted] Radiosensitizing Effect of Celastrol by Inhibiting G2/M Phase Arrest Induced by the c-myc Gene of Human SW1353 Chondrosarcoma Cells: Network and Experimental Analyses
Jin Qian, Zhen Zhang, Xiao Han, Liulong Zhu, Zhenyu Bian, and Tao Xie
Research Article (20 pages), Article ID 1948657, Volume 2022 (2022)

[Retracted] The Function of circRNA-0047604 in Regulating the Tumor Suppressor Gene DACH1 in Breast Cancer
Bingkun Zhao, Rong Zhou, Changle Ji, Diya Liu, Tianqi Wu, Hui Xu, Dongmei Lan, Chao Yao, Yuanzhi Xu, and Lin Fang
Research Article (10 pages), Article ID 6589651, Volume 2022 (2022)

[Retracted] Changes of Serum Ferritin, Hemoglobin, and Serum Iron (SI) and Treatment Effect of Iron Proteinsuccinylate Oral Solution Combined with Vitamin A and D Drops on Children with Nutritional Iron Deficiency Anemia
Yan Ma, Yanbo Ma, Xiuqing Zhang, Xuejing Wang, and Zhigang Sun
Research Article (6 pages), Article ID 2972617, Volume 2022 (2022)

[Retracted] Correlation Analysis of Acute Coronary Syndrome with Serum IL-18, MMP-9, hs-CRP, and Plasma FIB
Yuexia Yang, Guoming Li, and Ruiqin Zhang
Research Article (9 pages), Article ID 5984184, Volume 2022 (2022)

[Retracted] Effects of Sevoflurane on Apoptosis of Myocardial Cells in IRI Rats
Shikun Zhang, Xiaoyan Du, Kun Zhang, and Haiyan Wang
Research Article (6 pages), Article ID 3347949, Volume 2021 (2021)

[Retracted] miR-10b-5p Suppresses the Proliferation and Invasion of Primary Hepatic Carcinoma Cells by Downregulating EphA2
Xu Niu, Haitao Sun, Feng Qiu, Jing Liu, Tianchi Yang, and Wei Han
Research Article (12 pages), Article ID 1382061, Volume 2021 (2021)

[Retracted] lncRNA FGD5-AS1 and miR-130a Can Be Used for Prognosis Analysis of Patients with Chronic Periodontitis
Miao Yu and Chunyuan Chi
Research Article (7 pages), Article ID 8544914, Volume 2021 (2021)

Contents

[Retracted] Analysis on the Clinical Effect of High-Dose Glucocorticoids Combined with Immunosuppressants on Patients with Myasthenia Gravis Undergoing Video-Assisted Thoracoscopic Surgery
Pei Liu, Haoyue Wang, Jiejie Hu, Xiaobin Zhai, and Zhaoming Ge
Research Article (6 pages), Article ID 5854056, Volume 2021 (2021)

[Retracted] Expression of lncRNA-ANRIL before and after Treatment and Its Predictive Value for Short-Term Survival in Patients with Coronary Heart Disease
Jinhui Sun and Shi Qiu
Research Article (8 pages), Article ID 5431985, Volume 2021 (2021)

Cystic Fibrosis: Systems Biology Analysis from Homozygous p.Phe508del Variant Patients' Samples Reveals Perturbations in Tissue-Specific Pathways
Joice de Faria Poloni, Thaiane Rispoli, Maria Lucia Rossetti, Cristiano Trindade, and José Eduardo Vargas
Research Article (16 pages), Article ID 5262000, Volume 2021 (2021)

[Retracted] Expression of miR-210, miR-137, and miR-153 in Patients with Acute Cerebral Infarction
Hongtao Tian, Yan Zhao, Chao Du, Xiao Zong, Xiuping Zhang, and Xia Qiao
Research Article (9 pages), Article ID 4464945, Volume 2021 (2021)

[Retracted] The Protective Effects of miR-21-Mediated Fibroblast Growth Factor 1 in Rats with Coronary Heart Disease
Bin Zhang, Hongguang Liu, Guoping Yang, Yongmei Wang, and Yan Wang
Research Article (9 pages), Article ID 3621259, Volume 2021 (2021)

[Retracted] Effect of Dexmedetomidine Combined with Ropivacaine on Cognitive Dysfunction and Inflammatory Response in Patients Undergoing Craniocerebral Surgery
Yang Liu, Hongwei Zhang, and Wenhua Zhang
Research Article (8 pages), Article ID 4968300, Volume 2021 (2021)

[Retracted] Clinical Effect of Clarithromycin Combined with Tinidazole on Helicobacter pylori-Related Gastritis and Its Influence on COX-2 Expression
Chenxi He, Fanting Kong, Xinying Zhu, Fanlei Kong, Wei Zhao, Yanling Liu, and Kuixiang Wang
Research Article (9 pages), Article ID 4171019, Volume 2021 (2021)

[Retracted] The Expression of miR-23a and miR-146a in the Saliva of Patients with Periodontitis and Its Clinical Significance
Lanhua Kang, Ning Li, and Lexiu Wang
Research Article (8 pages), Article ID 5135278, Volume 2021 (2021)

[Retracted] Study on the Efficacy and Safety of Ambroxol Combined with Methylprednisolone in Patients with Acute Lung Injury
Weiwei Su, Qinglian Dong, and Fangfang Jiao
Research Article (8 pages), Article ID 5771101, Volume 2021 (2021)

[Retracted] The Influence of ICAM1 3#UTR Gene Polymorphism on the Occurrence and Metastasis of Primary Liver Cancer
Li He, Suwen Wang, and Xusheng Ma
Research Article (11 pages), Article ID 7377299, Volume 2021 (2021)

[Retracted] PFNA-II Internal Fixation Helps Hip Joint Recovery and Improves Quality of Life of Patients with Lateral-Wall Dangerous Type of Intertrochanteric Fracture
Weilu Mu and Junlin Zhou
Research Article (6 pages), Article ID 5911868, Volume 2021 (2021)

[Retracted] Investigation on Risk Stratification and the Prognostic Value of hs-TnT Combined with MMP-2 in Patients with Acute Coronary Syndrome
Ying Li, Li Li, Kun Wang, Pengtao Wu, and Yijie Cui
Research Article (5 pages), Article ID 1040171, Volume 2021 (2021)

Analysis of the Expression and Prognostic Value of MSH2 in Pan-Cancer Based on Bioinformatics
Wenli Qiu, Ke Ding, Lusheng Liao, Yongchang Ling, Xiaoqiong Luo, and Junli Wang
Research Article (12 pages), Article ID 9485273, Volume 2021 (2021)

[Retracted] Long-Term Carbohydrate-Containing Late-Evening Snack Significantly Improves the Ratio of Branched Chain Amino Acids to Aromatic Amino Acids in Adults with Liver Cirrhosis due to Hepatitis B
Wei Hou, Zheng Lv, Jing Yang, Jing Wu, Zhong-ying Wang, and Qing-hua Meng
Research Article (11 pages), Article ID 1074565, Volume 2021 (2021)

[Retracted] Treatment of Severe Ptosis by Conjoint Fascial Sheath Suspension
Pengfei Sang, Mingsong Fang, Xuan Li, Chang Liu, and Qingchun Xi
Research Article (6 pages), Article ID 1837458, Volume 2021 (2021)

[Retracted] LncRNA PVT1 Promotes Hypoxia-Induced Cardiomyocyte Injury by Inhibiting miR-214-3p
Chuanliang Liu, Jieqiong Zhang, Xuejie Lun, and Lei Li
Research Article (9 pages), Article ID 4604883, Volume 2021 (2021)

Screening of Parkinson's Differential MicroRNA Based on GEO Database and Its Clinical Verification
Xuping Jiang, Lili Xiao, Xumei Jiang, Guangsheng Li, and Zhijuan Lu
Research Article (9 pages), Article ID 8171236, Volume 2021 (2021)

[Retracted] Clinical Efficacy of Methotrexate Combined with Iguratimod on Patients with Rheumatoid Arthritis and Its Influence on the Expression Levels of HOTAIR in Serum
Jingya Tan, Jiaqiang Dan, and Yi Liu
Research Article (7 pages), Article ID 2486617, Volume 2021 (2021)

Contents

[Retracted] miR-1226-3p Promotes eNOS Expression of Pulmonary Arterial Endothelial Cells to Mitigate Hypertension in Rats via Targeting Profilin-1
Jie Jian and Liang Xia
Research Article (7 pages), Article ID 1724722, Volume 2021 (2021)

[Retracted] Disorder Genes Regulate the Progression of Ischemic Stroke through the NF-κB Signaling Pathway
Wei Wei, Wenqiang Xin, Yufeng Tang, Zhonglun Chen, Yue Heng, Mingjun Pu, Bufan Yang, Jiacai Zuo, and Jingfeng Duan
Research Article (11 pages), Article ID 2464269, Volume 2021 (2021)

[Retracted] Protein Arginine Methyltransferase 5 Promotes the Migration of AML Cells by Regulating the Expression of Leukocyte Immunoglobulin-Like Receptor B4
Lu Zhao, Bingqing Cheng, Jie Xiong, Dan Ma, Xin Liu, Li Wang, Xi Zhang, and Jishi Wang
Research Article (18 pages), Article ID 7329072, Volume 2021 (2021)

A Wavelet-Based Learning Model Enhances Molecular Prognosis in Pancreatic Adenocarcinoma
Binhua Tang, Yu Chen, Yuqi Wang, and Jiafei Nie
Research Article (17 pages), Article ID 7865856, Volume 2021 (2021)

[Retracted] Effects of High-Flux Dialysis Combined with Hemoperfusion on Serum GRP78 and miR-495-3p in Renal Failure Patients
Wei Fan, Xudong Li, Xiangjun Xu, and Hong Chu
Research Article (6 pages), Article ID 9591177, Volume 2021 (2021)

Bioinformatics Analysis of ZBTB16 as a Prognostic Marker for Ewing's Sarcoma
Ke Ding, Wenli Qiu, Dianbo Yu, Huade Ma, Kangqi Xie, Fuqiang Luo, Shanlang Li, Zaiyong Li, and Jihua Wei
Research Article (8 pages), Article ID 1989917, Volume 2021 (2021)

Gene Expression Characteristics of Liver Tissue Reveal the Underlying Pathogenesis of Hepatocellular Carcinoma
Congfang Guo, Xiang Guo, Yudong Rong, Yirui Guo, and Li Zhang
Research Article (11 pages), Article ID 9458328, Volume 2021 (2021)

[Retracted] The Functionalities and Clinical Significance of Tumor-Infiltrating Immune Cells in Esophageal Squamous Cell Carcinoma
Jishuai Zhang, Haifeng Wang, Haitao Wu, and Guangliang Qiang
Research Article (9 pages), Article ID 8635381, Volume 2021 (2021)

[Retracted] Curcumin Improves Pulmonary Hypertension Rats by Regulating Mitochondrial Function
Jing Chen, Wen Jiang, Fei Zhu, Qiong Wang, Haiyan Yang, and Jinhua Wu
Research Article (10 pages), Article ID 1078019, Volume 2021 (2021)

[Retracted] Protective Effect of Luteolin on D-Galactosamine (D-Gal)/Lipopolysaccharide (LPS) Induced Hepatic Injury by in Mice

Yiwei Pu, Zhaocong Yang, and Xuming Mo

Research Article (8 pages), Article ID 2252705, Volume 2021 (2021)

Hindawi
BioMed Research International
Volume 2024, Article ID 9894720, 1 page
https://doi.org/10.1155/2024/9894720

Retraction

Retracted: Expression of miR-210, miR-137, and miR-153 in Patients with Acute Cerebral Infarction

BioMed Research International

Received 12 March 2024; Accepted 12 March 2024; Published 20 March 2024

This article has been retracted by Hindawi following an investigation undertaken by the publisher [1]. This investigation has uncovered evidence of one or more of the following indicators of systematic manipulation of the publication process:

(1) Discrepancies in scope

(2) Discrepancies in the description of the research reported

(3) Discrepancies between the availability of data and the research described

(4) Inappropriate citations

(5) Incoherent, meaningless and/or irrelevant content included in the article

(6) Manipulated or compromised peer review

The presence of these indicators undermines our confidence in the integrity of the article's content and we cannot, therefore, vouch for its reliability. Please note that this notice is intended solely to alert readers that the content of this article is unreliable. We have not investigated whether authors were aware of or involved in the systematic manipulation of the publication process.

Wiley and Hindawi regrets that the usual quality checks did not identify these issues before publication and have since put additional measures in place to safeguard research integrity.

We wish to credit our own Research Integrity and Research Publishing teams and anonymous and named external researchers and research integrity experts for contributing to this investigation.

The corresponding author, as the representative of all authors, has been given the opportunity to register their agreement or disagreement to this retraction. We have kept a record of any response received.

References

[1] H. Tian, Y. Zhao, C. Du, X. Zong, X. Zhang, and X. Qiao, "Expression of miR-210, miR-137, and miR-153 in Patients with Acute Cerebral Infarction," *BioMed Research International*, vol. 2021, Article ID 4464945, 9 pages, 2021.

Hindawi
BioMed Research International
Volume 2024, Article ID 9894363, 1 page
https://doi.org/10.1155/2024/9894363

Retraction

Retracted: Study on the Efficacy and Safety of Ambroxol Combined with Methylprednisolone in Patients with Acute Lung Injury

BioMed Research International

Received 12 March 2024; Accepted 12 March 2024; Published 20 March 2024

This article has been retracted by Hindawi following an investigation undertaken by the publisher [1]. This investigation has uncovered evidence of one or more of the following indicators of systematic manipulation of the publication process:

(1) Discrepancies in scope

(2) Discrepancies in the description of the research reported

(3) Discrepancies between the availability of data and the research described

(4) Inappropriate citations

(5) Incoherent, meaningless and/or irrelevant content included in the article

(6) Manipulated or compromised peer review

The presence of these indicators undermines our confidence in the integrity of the article's content and we cannot, therefore, vouch for its reliability. Please note that this notice is intended solely to alert readers that the content of this article is unreliable. We have not investigated whether authors were aware of or involved in the systematic manipulation of the publication process.

Wiley and Hindawi regrets that the usual quality checks did not identify these issues before publication and have since put additional measures in place to safeguard research integrity.

We wish to credit our own Research Integrity and Research Publishing teams and anonymous and named external researchers and research integrity experts for contributing to this investigation.

The corresponding author, as the representative of all authors, has been given the opportunity to register their agreement or disagreement to this retraction. We have kept a record of any response received.

References

[1] W. Su, Q. Dong, and F. Jiao, "Study on the Efficacy and Safety of Ambroxol Combined with Methylprednisolone in Patients with Acute Lung Injury," *BioMed Research International*, vol. 2021, Article ID 5771101, 8 pages, 2021.

Hindawi
BioMed Research International
Volume 2024, Article ID 9893040, 1 page
https://doi.org/10.1155/2024/9893040

Retraction

Retracted: Investigation on Risk Stratification and the Prognostic Value of hs-TnT Combined with MMP-2 in Patients with Acute Coronary Syndrome

BioMed Research International

Received 12 March 2024; Accepted 12 March 2024; Published 20 March 2024

This article has been retracted by Hindawi following an investigation undertaken by the publisher [1]. This investigation has uncovered evidence of one or more of the following indicators of systematic manipulation of the publication process:

(1) Discrepancies in scope

(2) Discrepancies in the description of the research reported

(3) Discrepancies between the availability of data and the research described

(4) Inappropriate citations

(5) Incoherent, meaningless and/or irrelevant content included in the article

(6) Manipulated or compromised peer review

The presence of these indicators undermines our confidence in the integrity of the article's content and we cannot, therefore, vouch for its reliability. Please note that this notice is intended solely to alert readers that the content of this article is unreliable. We have not investigated whether authors were aware of or involved in the systematic manipulation of the publication process.

Wiley and Hindawi regrets that the usual quality checks did not identify these issues before publication and have since put additional measures in place to safeguard research integrity.

We wish to credit our own Research Integrity and Research Publishing teams and anonymous and named external researchers and research integrity experts for contributing to this investigation.

The corresponding author, as the representative of all authors, has been given the opportunity to register their agreement or disagreement to this retraction. We have kept a record of any response received.

References

[1] Y. Li, L. Li, K. Wang, P. Wu, and Y. Cui, "Investigation on Risk Stratification and the Prognostic Value of hs-TnT Combined with MMP-2 in Patients with Acute Coronary Syndrome," *BioMed Research International*, vol. 2021, Article ID 1040171, 5 pages, 2021.

Hindawi
BioMed Research International
Volume 2024, Article ID 9873517, 1 page
https://doi.org/10.1155/2024/9873517

Retraction

Retracted: LncRNA PVT1 Promotes Hypoxia-Induced Cardiomyocyte Injury by Inhibiting miR-214-3p

BioMed Research International

Received 12 March 2024; Accepted 12 March 2024; Published 20 March 2024

This article has been retracted by Hindawi following an investigation undertaken by the publisher [1]. This investigation has uncovered evidence of one or more of the following indicators of systematic manipulation of the publication process:

(1) Discrepancies in scope

(2) Discrepancies in the description of the research reported

(3) Discrepancies between the availability of data and the research described

(4) Inappropriate citations

(5) Incoherent, meaningless and/or irrelevant content included in the article

(6) Manipulated or compromised peer review

The presence of these indicators undermines our confidence in the integrity of the article's content and we cannot, therefore, vouch for its reliability. Please note that this notice is intended solely to alert readers that the content of this article is unreliable. We have not investigated whether authors were aware of or involved in the systematic manipulation of the publication process.

Wiley and Hindawi regrets that the usual quality checks did not identify these issues before publication and have since put additional measures in place to safeguard research integrity.

We wish to credit our own Research Integrity and Research Publishing teams and anonymous and named external researchers and research integrity experts for contributing to this investigation.

The corresponding author, as the representative of all authors, has been given the opportunity to register their agreement or disagreement to this retraction. We have kept a record of any response received.

References

[1] C. Liu, J. Zhang, X. Lun, and L. Li, "LncRNA PVT1 Promotes Hypoxia-Induced Cardiomyocyte Injury by Inhibiting miR-214-3p," *BioMed Research International*, vol. 2021, Article ID 4604883, 9 pages, 2021.

Hindawi
BioMed Research International
Volume 2024, Article ID 9867817, 1 page
https://doi.org/10.1155/2024/9867817

Retraction

Retracted: Effects of High-Flux Dialysis Combined with Hemoperfusion on Serum GRP78 and miR-495-3p in Renal Failure Patients

BioMed Research International

Received 12 March 2024; Accepted 12 March 2024; Published 20 March 2024

This article has been retracted by Hindawi following an investigation undertaken by the publisher [1]. This investigation has uncovered evidence of one or more of the following indicators of systematic manipulation of the publication process:

(1) Discrepancies in scope

(2) Discrepancies in the description of the research reported

(3) Discrepancies between the availability of data and the research described

(4) Inappropriate citations

(5) Incoherent, meaningless and/or irrelevant content included in the article

(6) Manipulated or compromised peer review

The presence of these indicators undermines our confidence in the integrity of the article's content and we cannot, therefore, vouch for its reliability. Please note that this notice is intended solely to alert readers that the content of this article is unreliable. We have not investigated whether authors were aware of or involved in the systematic manipulation of the publication process.

Wiley and Hindawi regrets that the usual quality checks did not identify these issues before publication and have since put additional measures in place to safeguard research integrity.

We wish to credit our own Research Integrity and Research Publishing teams and anonymous and named external researchers and research integrity experts for contributing to this investigation.

The corresponding author, as the representative of all authors, has been given the opportunity to register their agreement or disagreement to this retraction. We have kept a record of any response received.

References

[1] W. Fan, X. Li, X. Xu, and H. Chu, "Effects of High-Flux Dialysis Combined with Hemoperfusion on Serum GRP78 and miR-495-3p in Renal Failure Patients," *BioMed Research International*, vol. 2021, Article ID 9591177, 6 pages, 2021.

Hindawi
BioMed Research International
Volume 2024, Article ID 9867070, 1 page
https://doi.org/10.1155/2024/9867070

Retraction

Retracted: The Protective Effects of miR-21-Mediated Fibroblast Growth Factor 1 in Rats with Coronary Heart Disease

BioMed Research International

Received 12 March 2024; Accepted 12 March 2024; Published 20 March 2024

This article has been retracted by Hindawi following an investigation undertaken by the publisher [1]. This investigation has uncovered evidence of one or more of the following indicators of systematic manipulation of the publication process:

(1) Discrepancies in scope

(2) Discrepancies in the description of the research reported

(3) Discrepancies between the availability of data and the research described

(4) Inappropriate citations

(5) Incoherent, meaningless and/or irrelevant content included in the article

(6) Manipulated or compromised peer review

The presence of these indicators undermines our confidence in the integrity of the article's content and we cannot, therefore, vouch for its reliability. Please note that this notice is intended solely to alert readers that the content of this article is unreliable. We have not investigated whether authors were aware of or involved in the systematic manipulation of the publication process.

Wiley and Hindawi regrets that the usual quality checks did not identify these issues before publication and have since put additional measures in place to safeguard research integrity.

We wish to credit our own Research Integrity and Research Publishing teams and anonymous and named external researchers and research integrity experts for contributing to this investigation.

The corresponding author, as the representative of all authors, has been given the opportunity to register their agreement or disagreement to this retraction. We have kept a record of any response received.

References

[1] B. Zhang, H. Liu, G. Yang, Y. Wang, and Y. Wang, "The Protective Effects of miR-21-Mediated Fibroblast Growth Factor 1 in Rats with Coronary Heart Disease," *BioMed Research International*, vol. 2021, Article ID 3621259, 9 pages, 2021.

Hindawi
BioMed Research International
Volume 2024, Article ID 9864190, 1 page
https://doi.org/10.1155/2024/9864190

Retraction

Retracted: Expression of lncRNA-ANRIL before and after Treatment and Its Predictive Value for Short-Term Survival in Patients with Coronary Heart Disease

BioMed Research International

Received 12 March 2024; Accepted 12 March 2024; Published 20 March 2024

This article has been retracted by Hindawi following an investigation undertaken by the publisher [1]. This investigation has uncovered evidence of one or more of the following indicators of systematic manipulation of the publication process:

(1) Discrepancies in scope

(2) Discrepancies in the description of the research reported

(3) Discrepancies between the availability of data and the research described

(4) Inappropriate citations

(5) Incoherent, meaningless and/or irrelevant content included in the article

(6) Manipulated or compromised peer review

The presence of these indicators undermines our confidence in the integrity of the article's content and we cannot, therefore, vouch for its reliability. Please note that this notice is intended solely to alert readers that the content of this article is unreliable. We have not investigated whether authors were aware of or involved in the systematic manipulation of the publication process.

Wiley and Hindawi regrets that the usual quality checks did not identify these issues before publication and have since put additional measures in place to safeguard research integrity.

We wish to credit our own Research Integrity and Research Publishing teams and anonymous and named external researchers and research integrity experts for contributing to this investigation.

The corresponding author, as the representative of all authors, has been given the opportunity to register their agreement or disagreement to this retraction. We have kept a record of any response received.

References

[1] J. Sun and S. Qiu, "Expression of lncRNA-ANRIL before and after Treatment and Its Predictive Value for Short-Term Survival in Patients with Coronary Heart Disease," *BioMed Research International*, vol. 2021, Article ID 5431985, 8 pages, 2021.

Hindawi
BioMed Research International
Volume 2024, Article ID 9863429, 1 page
https://doi.org/10.1155/2024/9863429

Retraction

Retracted: Analysis on the Clinical Effect of High-Dose Glucocorticoids Combined with Immunosuppressants on Patients with Myasthenia Gravis Undergoing Video-Assisted Thoracoscopic Surgery

BioMed Research International

Received 12 March 2024; Accepted 12 March 2024; Published 20 March 2024

This article has been retracted by Hindawi following an investigation undertaken by the publisher [1]. This investigation has uncovered evidence of one or more of the following indicators of systematic manipulation of the publication process:

(1) Discrepancies in scope

(2) Discrepancies in the description of the research reported

(3) Discrepancies between the availability of data and the research described

(4) Inappropriate citations

(5) Incoherent, meaningless and/or irrelevant content included in the article

(6) Manipulated or compromised peer review

The presence of these indicators undermines our confidence in the integrity of the article's content and we cannot, therefore, vouch for its reliability. Please note that this notice is intended solely to alert readers that the content of this article is unreliable. We have not investigated whether authors were aware of or involved in the systematic manipulation of the publication process.

Wiley and Hindawi regrets that the usual quality checks did not identify these issues before publication and have since put additional measures in place to safeguard research integrity.

We wish to credit our own Research Integrity and Research Publishing teams and anonymous and named external researchers and research integrity experts for contributing to this investigation.

The corresponding author, as the representative of all authors, has been given the opportunity to register their agreement or disagreement to this retraction. We have kept a record of any response received.

References

[1] P. Liu, H. Wang, J. Hu, X. Zhai, and Z. Ge, "Analysis on the Clinical Effect of High-Dose Glucocorticoids Combined with Immunosuppressants on Patients with Myasthenia Gravis Undergoing Video-Assisted Thoracoscopic Surgery," *BioMed Research International*, vol. 2021, Article ID 5854056, 6 pages, 2021.

Hindawi
BioMed Research International
Volume 2024, Article ID 9859240, 1 page
https://doi.org/10.1155/2024/9859240

Retraction

Retracted: Disorder Genes Regulate the Progression of Ischemic Stroke through the NF-κB Signaling Pathway

BioMed Research International

Received 12 March 2024; Accepted 12 March 2024; Published 20 March 2024

This article has been retracted by Hindawi following an investigation undertaken by the publisher [1]. This investigation has uncovered evidence of one or more of the following indicators of systematic manipulation of the publication process:

(1) Discrepancies in scope

(2) Discrepancies in the description of the research reported

(3) Discrepancies between the availability of data and the research described

(4) Inappropriate citations

(5) Incoherent, meaningless and/or irrelevant content included in the article

(6) Manipulated or compromised peer review

The presence of these indicators undermines our confidence in the integrity of the article's content and we cannot, therefore, vouch for its reliability. Please note that this notice is intended solely to alert readers that the content of this article is unreliable. We have not investigated whether authors were aware of or involved in the systematic manipulation of the publication process.

Wiley and Hindawi regrets that the usual quality checks did not identify these issues before publication and have since put additional measures in place to safeguard research integrity.

We wish to credit our own Research Integrity and Research Publishing teams and anonymous and named external researchers and research integrity experts for contributing to this investigation.

The corresponding author, as the representative of all authors, has been given the opportunity to register their agreement or disagreement to this retraction. We have kept a record of any response received.

References

[1] W. Wei, W. Xin, Y. Tang et al., "Disorder Genes Regulate the Progression of Ischemic Stroke through the NF-κB Signaling Pathway," *BioMed Research International*, vol. 2021, Article ID 2464269, 11 pages, 2021.

Hindawi
BioMed Research International
Volume 2024, Article ID 9858395, 1 page
https://doi.org/10.1155/2024/9858395

Retraction

Retracted: The Functionalities and Clinical Significance of Tumor-Infiltrating Immune Cells in Esophageal Squamous Cell Carcinoma

BioMed Research International

Received 12 March 2024; Accepted 12 March 2024; Published 20 March 2024

This article has been retracted by Hindawi following an investigation undertaken by the publisher [1]. This investigation has uncovered evidence of one or more of the following indicators of systematic manipulation of the publication process:

(1) Discrepancies in scope

(2) Discrepancies in the description of the research reported

(3) Discrepancies between the availability of data and the research described

(4) Inappropriate citations

(5) Incoherent, meaningless and/or irrelevant content included in the article

(6) Manipulated or compromised peer review

The presence of these indicators undermines our confidence in the integrity of the article's content and we cannot, therefore, vouch for its reliability. Please note that this notice is intended solely to alert readers that the content of this article is unreliable. We have not investigated whether authors were aware of or involved in the systematic manipulation of the publication process.

Wiley and Hindawi regrets that the usual quality checks did not identify these issues before publication and have since put additional measures in place to safeguard research integrity.

We wish to credit our own Research Integrity and Research Publishing teams and anonymous and named external researchers and research integrity experts for contributing to this investigation.

The corresponding author, as the representative of all authors, has been given the opportunity to register their agreement or disagreement to this retraction. We have kept a record of any response received.

References

[1] J. Zhang, H. Wang, H. Wu, and G. Qiang, "The Functionalities and Clinical Significance of Tumor-Infiltrating Immune Cells in Esophageal Squamous Cell Carcinoma," *BioMed Research International*, vol. 2021, Article ID 8635381, 9 pages, 2021.

Hindawi
BioMed Research International
Volume 2024, Article ID 9856043, 1 page
https://doi.org/10.1155/2024/9856043

Retraction

Retracted: Changes of Serum Ferritin, Hemoglobin, and Serum Iron (SI) and Treatment Effect of Iron Proteinsuccinylate Oral Solution Combined with Vitamin A and D Drops on Children with Nutritional Iron Deficiency Anemia

BioMed Research International

Received 12 March 2024; Accepted 12 March 2024; Published 20 March 2024

This article has been retracted by Hindawi following an investigation undertaken by the publisher [1]. This investigation has uncovered evidence of one or more of the following indicators of systematic manipulation of the publication process:

(1) Discrepancies in scope

(2) Discrepancies in the description of the research reported

(3) Discrepancies between the availability of data and the research described

(4) Inappropriate citations

(5) Incoherent, meaningless and/or irrelevant content included in the article

(6) Manipulated or compromised peer review

The presence of these indicators undermines our confidence in the integrity of the article's content and we cannot, therefore, vouch for its reliability. Please note that this notice is intended solely to alert readers that the content of this article is unreliable. We have not investigated whether authors were aware of or involved in the systematic manipulation of the publication process.

Wiley and Hindawi regrets that the usual quality checks did not identify these issues before publication and have since put additional measures in place to safeguard research integrity.

We wish to credit our own Research Integrity and Research Publishing teams and anonymous and named external researchers and research integrity experts for contributing to this investigation.

The corresponding author, as the representative of all authors, has been given the opportunity to register their agreement or disagreement to this retraction. We have kept a record of any response received.

References

[1] Y. Ma, Y. Ma, X. Zhang, X. Wang, and Z. Sun, "Changes of Serum Ferritin, Hemoglobin, and Serum Iron (SI) and Treatment Effect of Iron Proteinsuccinylate Oral Solution Combined with Vitamin A and D Drops on Children with Nutritional Iron Deficiency Anemia," *BioMed Research International*, vol. 2022, Article ID 2972617, 6 pages, 2022.

Hindawi
BioMed Research International
Volume 2024, Article ID 9853194, 1 page
https://doi.org/10.1155/2024/9853194

Retraction

Retracted: Effects of Sevoflurane on Apoptosis of Myocardial Cells in IRI Rats

BioMed Research International

Received 12 March 2024; Accepted 12 March 2024; Published 20 March 2024

This article has been retracted by Hindawi following an investigation undertaken by the publisher [1]. This investigation has uncovered evidence of one or more of the following indicators of systematic manipulation of the publication process:

(1) Discrepancies in scope

(2) Discrepancies in the description of the research reported

(3) Discrepancies between the availability of data and the research described

(4) Inappropriate citations

(5) Incoherent, meaningless and/or irrelevant content included in the article

(6) Manipulated or compromised peer review

The presence of these indicators undermines our confidence in the integrity of the article's content and we cannot, therefore, vouch for its reliability. Please note that this notice is intended solely to alert readers that the content of this article is unreliable. We have not investigated whether authors were aware of or involved in the systematic manipulation of the publication process.

Wiley and Hindawi regrets that the usual quality checks did not identify these issues before publication and have since put additional measures in place to safeguard research integrity.

We wish to credit our own Research Integrity and Research Publishing teams and anonymous and named external researchers and research integrity experts for contributing to this investigation.

The corresponding author, as the representative of all authors, has been given the opportunity to register their agreement or disagreement to this retraction. We have kept a record of any response received.

References

[1] S. Zhang, X. Du, K. Zhang, and H. Wang, "Effects of Sevoflurane on Apoptosis of Myocardial Cells in IRI Rats," *BioMed Research International*, vol. 2021, Article ID 3347949, 6 pages, 2021.

Hindawi
BioMed Research International
Volume 2024, Article ID 9852462, 1 page
https://doi.org/10.1155/2024/9852462

Retraction

Retracted: Protein Arginine Methyltransferase 5 Promotes the Migration of AML Cells by Regulating the Expression of Leukocyte Immunoglobulin-Like Receptor B4

BioMed Research International

Received 12 March 2024; Accepted 12 March 2024; Published 20 March 2024

This article has been retracted by Hindawi following an investigation undertaken by the publisher [1]. This investigation has uncovered evidence of one or more of the following indicators of systematic manipulation of the publication process:

(1) Discrepancies in scope

(2) Discrepancies in the description of the research reported

(3) Discrepancies between the availability of data and the research described

(4) Inappropriate citations

(5) Incoherent, meaningless and/or irrelevant content included in the article

(6) Manipulated or compromised peer review

The presence of these indicators undermines our confidence in the integrity of the article's content and we cannot, therefore, vouch for its reliability. Please note that this notice is intended solely to alert readers that the content of this article is unreliable. We have not investigated whether authors were aware of or involved in the systematic manipulation of the publication process.

Wiley and Hindawi regrets that the usual quality checks did not identify these issues before publication and have since put additional measures in place to safeguard research integrity.

We wish to credit our own Research Integrity and Research Publishing teams and anonymous and named external researchers and research integrity experts for contributing to this investigation.

The corresponding author, as the representative of all authors, has been given the opportunity to register their agreement or disagreement to this retraction. We have kept a record of any response received.

References

[1] L. Zhao, B. Cheng, J. Xiong et al., "Protein Arginine Methyltransferase 5 Promotes the Migration of AML Cells by Regulating the Expression of Leukocyte Immunoglobulin-Like Receptor B4," *BioMed Research International*, vol. 2021, Article ID 7329072, 18 pages, 2021.

Hindawi
BioMed Research International
Volume 2024, Article ID 9850985, 1 page
https://doi.org/10.1155/2024/9850985

Retraction

Retracted: Treatment of Severe Ptosis by Conjoint Fascial Sheath Suspension

BioMed Research International

Received 12 March 2024; Accepted 12 March 2024; Published 20 March 2024

This article has been retracted by Hindawi following an investigation undertaken by the publisher [1]. This investigation has uncovered evidence of one or more of the following indicators of systematic manipulation of the publication process:

(1) Discrepancies in scope

(2) Discrepancies in the description of the research reported

(3) Discrepancies between the availability of data and the research described

(4) Inappropriate citations

(5) Incoherent, meaningless and/or irrelevant content included in the article

(6) Manipulated or compromised peer review

The presence of these indicators undermines our confidence in the integrity of the article's content and we cannot, therefore, vouch for its reliability. Please note that this notice is intended solely to alert readers that the content of this article is unreliable. We have not investigated whether authors were aware of or involved in the systematic manipulation of the publication process.

Wiley and Hindawi regrets that the usual quality checks did not identify these issues before publication and have since put additional measures in place to safeguard research integrity.

We wish to credit our own Research Integrity and Research Publishing teams and anonymous and named external researchers and research integrity experts for contributing to this investigation.

The corresponding author, as the representative of all authors, has been given the opportunity to register their agreement or disagreement to this retraction. We have kept a record of any response received.

References

[1] P. Sang, M. Fang, X. Li, C. Liu, and Q. Xi, "Treatment of Severe Ptosis by Conjoint Fascial Sheath Suspension," *BioMed Research International*, vol. 2021, Article ID 1837458, 6 pages, 2021.

Hindawi
BioMed Research International
Volume 2024, Article ID 9845035, 1 page
https://doi.org/10.1155/2024/9845035

Retraction

Retracted: The Function of circRNA-0047604 in Regulating the Tumor Suppressor Gene DACH1 in Breast Cancer

BioMed Research International

Received 12 March 2024; Accepted 12 March 2024; Published 20 March 2024

This article has been retracted by Hindawi following an investigation undertaken by the publisher [1]. This investigation has uncovered evidence of one or more of the following indicators of systematic manipulation of the publication process:

(1) Discrepancies in scope

(2) Discrepancies in the description of the research reported

(3) Discrepancies between the availability of data and the research described

(4) Inappropriate citations

(5) Incoherent, meaningless and/or irrelevant content included in the article

(6) Manipulated or compromised peer review

The presence of these indicators undermines our confidence in the integrity of the article's content and we cannot, therefore, vouch for its reliability. Please note that this notice is intended solely to alert readers that the content of this article is unreliable. We have not investigated whether authors were aware of or involved in the systematic manipulation of the publication process.

Wiley and Hindawi regrets that the usual quality checks did not identify these issues before publication and have since put additional measures in place to safeguard research integrity.

We wish to credit our own Research Integrity and Research Publishing teams and anonymous and named external researchers and research integrity experts for contributing to this investigation.

The corresponding author, as the representative of all authors, has been given the opportunity to register their agreement or disagreement to this retraction. We have kept a record of any response received.

References

[1] B. Zhao, R. Zhou, C. Ji et al., "The Function of circRNA-0047604 in Regulating the Tumor Suppressor Gene DACH1 in Breast Cancer," *BioMed Research International*, vol. 2022, Article ID 6589651, 10 pages, 2022.

Hindawi
BioMed Research International
Volume 2024, Article ID 9834789, 1 page
https://doi.org/10.1155/2024/9834789

Retraction

Retracted: miR-10b-5p Suppresses the Proliferation and Invasion of Primary Hepatic Carcinoma Cells by Downregulating EphA2

BioMed Research International

Received 12 March 2024; Accepted 12 March 2024; Published 20 March 2024

This article has been retracted by Hindawi following an investigation undertaken by the publisher [1]. This investigation has uncovered evidence of one or more of the following indicators of systematic manipulation of the publication process:

(1) Discrepancies in scope

(2) Discrepancies in the description of the research reported

(3) Discrepancies between the availability of data and the research described

(4) Inappropriate citations

(5) Incoherent, meaningless and/or irrelevant content included in the article

(6) Manipulated or compromised peer review

The presence of these indicators undermines our confidence in the integrity of the article's content and we cannot, therefore, vouch for its reliability. Please note that this notice is intended solely to alert readers that the content of this article is unreliable. We have not investigated whether authors were aware of or involved in the systematic manipulation of the publication process.

Wiley and Hindawi regrets that the usual quality checks did not identify these issues before publication and have since put additional measures in place to safeguard research integrity.

We wish to credit our own Research Integrity and Research Publishing teams and anonymous and named external researchers and research integrity experts for contributing to this investigation.

The corresponding author, as the representative of all authors, has been given the opportunity to register their agreement or disagreement to this retraction. We have kept a record of any response received.

References

[1] X. Niu, H. Sun, F. Qiu, J. Liu, T. Yang, and W. Han, "miR-10b-5p Suppresses the Proliferation and Invasion of Primary Hepatic Carcinoma Cells by Downregulating EphA2," *BioMed Research International*, vol. 2021, Article ID 1382061, 12 pages, 2021.

Hindawi
BioMed Research International
Volume 2024, Article ID 9824926, 1 page
https://doi.org/10.1155/2024/9824926

Retraction

Retracted: Correlation Analysis of Acute Coronary Syndrome with Serum IL-18, MMP-9, hs-CRP, and Plasma FIB

BioMed Research International

Received 12 March 2024; Accepted 12 March 2024; Published 20 March 2024

This article has been retracted by Hindawi following an investigation undertaken by the publisher [1]. This investigation has uncovered evidence of one or more of the following indicators of systematic manipulation of the publication process:

(1) Discrepancies in scope

(2) Discrepancies in the description of the research reported

(3) Discrepancies between the availability of data and the research described

(4) Inappropriate citations

(5) Incoherent, meaningless and/or irrelevant content included in the article

(6) Manipulated or compromised peer review

The presence of these indicators undermines our confidence in the integrity of the article's content and we cannot, therefore, vouch for its reliability. Please note that this notice is intended solely to alert readers that the content of this article is unreliable. We have not investigated whether authors were aware of or involved in the systematic manipulation of the publication process.

Wiley and Hindawi regrets that the usual quality checks did not identify these issues before publication and have since put additional measures in place to safeguard research integrity.

We wish to credit our own Research Integrity and Research Publishing teams and anonymous and named external researchers and research integrity experts for contributing to this investigation.

The corresponding author, as the representative of all authors, has been given the opportunity to register their agreement or disagreement to this retraction. We have kept a record of any response received.

References

[1] Y. Yang, G. Li, and R. Zhang, "Correlation Analysis of Acute Coronary Syndrome with Serum IL-18, MMP-9, hs-CRP, and Plasma FIB," *BioMed Research International*, vol. 2022, Article ID 5984184, 9 pages, 2022.

Hindawi
BioMed Research International
Volume 2024, Article ID 9823071, 1 page
https://doi.org/10.1155/2024/9823071

Retraction

Retracted: Clinical Efficacy of Methotrexate Combined with Iguratimod on Patients with Rheumatoid Arthritis and Its Influence on the Expression Levels of HOTAIR in Serum

BioMed Research International

Received 12 March 2024; Accepted 12 March 2024; Published 20 March 2024

This article has been retracted by Hindawi following an investigation undertaken by the publisher [1]. This investigation has uncovered evidence of one or more of the following indicators of systematic manipulation of the publication process:

(1) Discrepancies in scope

(2) Discrepancies in the description of the research reported

(3) Discrepancies between the availability of data and the research described

(4) Inappropriate citations

(5) Incoherent, meaningless and/or irrelevant content included in the article

(6) Manipulated or compromised peer review

The presence of these indicators undermines our confidence in the integrity of the article's content and we cannot, therefore, vouch for its reliability. Please note that this notice is intended solely to alert readers that the content of this article is unreliable. We have not investigated whether authors were aware of or involved in the systematic manipulation of the publication process.

Wiley and Hindawi regrets that the usual quality checks did not identify these issues before publication and have since put additional measures in place to safeguard research integrity.

We wish to credit our own Research Integrity and Research Publishing teams and anonymous and named external researchers and research integrity experts for contributing to this investigation.

The corresponding author, as the representative of all authors, has been given the opportunity to register their agreement or disagreement to this retraction. We have kept a record of any response received.

References

[1] J. Tan, J. Dan, and Y. Liu, "Clinical Efficacy of Methotrexate Combined with Iguratimod on Patients with Rheumatoid Arthritis and Its Influence on the Expression Levels of HOTAIR in Serum," *BioMed Research International*, vol. 2021, Article ID 2486617, 7 pages, 2021.

Hindawi
BioMed Research International
Volume 2024, Article ID 9821414, 1 page
https://doi.org/10.1155/2024/9821414

Retraction

Retracted: Long-Term Carbohydrate-Containing Late-Evening Snack Significantly Improves the Ratio of Branched Chain Amino Acids to Aromatic Amino Acids in Adults with Liver Cirrhosis due to Hepatitis B

BioMed Research International

Received 12 March 2024; Accepted 12 March 2024; Published 20 March 2024

This article has been retracted by Hindawi following an investigation undertaken by the publisher [1]. This investigation has uncovered evidence of one or more of the following indicators of systematic manipulation of the publication process:

(1) Discrepancies in scope

(2) Discrepancies in the description of the research reported

(3) Discrepancies between the availability of data and the research described

(4) Inappropriate citations

(5) Incoherent, meaningless and/or irrelevant content included in the article

(6) Manipulated or compromised peer review

The presence of these indicators undermines our confidence in the integrity of the article's content and we cannot, therefore, vouch for its reliability. Please note that this notice is intended solely to alert readers that the content of this article is unreliable. We have not investigated whether authors were aware of or involved in the systematic manipulation of the publication process.

Wiley and Hindawi regrets that the usual quality checks did not identify these issues before publication and have since put additional measures in place to safeguard research integrity.

We wish to credit our own Research Integrity and Research Publishing teams and anonymous and named external researchers and research integrity experts for contributing to this investigation.

The corresponding author, as the representative of all authors, has been given the opportunity to register their agreement or disagreement to this retraction. We have kept a record of any response received.

References

[1] W. Hou, Z. Lv, J. Yang, J. Wu, Z.-y. Wang, and Q.-h. Meng, "Long-Term Carbohydrate-Containing Late-Evening Snack Significantly Improves the Ratio of Branched Chain Amino Acids to Aromatic Amino Acids in Adults with Liver Cirrhosis due to Hepatitis B," *BioMed Research International*, vol. 2021, Article ID 1074565, 11 pages, 2021.

Hindawi
BioMed Research International
Volume 2024, Article ID 9808357, 1 page
https://doi.org/10.1155/2024/9808357

Retraction

Retracted: PFNA-II Internal Fixation Helps Hip Joint Recovery and Improves Quality of Life of Patients with Lateral-Wall Dangerous Type of Intertrochanteric Fracture

BioMed Research International

Received 12 March 2024; Accepted 12 March 2024; Published 20 March 2024

This article has been retracted by Hindawi following an investigation undertaken by the publisher [1]. This investigation has uncovered evidence of one or more of the following indicators of systematic manipulation of the publication process:

(1) Discrepancies in scope

(2) Discrepancies in the description of the research reported

(3) Discrepancies between the availability of data and the research described

(4) Inappropriate citations

(5) Incoherent, meaningless and/or irrelevant content included in the article

(6) Manipulated or compromised peer review

The presence of these indicators undermines our confidence in the integrity of the article's content and we cannot, therefore, vouch for its reliability. Please note that this notice is intended solely to alert readers that the content of this article is unreliable. We have not investigated whether authors were aware of or involved in the systematic manipulation of the publication process.

Wiley and Hindawi regrets that the usual quality checks did not identify these issues before publication and have since put additional measures in place to safeguard research integrity.

We wish to credit our own Research Integrity and Research Publishing teams and anonymous and named external researchers and research integrity experts for contributing to this investigation.

The corresponding author, as the representative of all authors, has been given the opportunity to register their agreement or disagreement to this retraction. We have kept a record of any response received.

References

[1] W. Mu and J. Zhou, "PFNA-II Internal Fixation Helps Hip Joint Recovery and Improves Quality of Life of Patients with Lateral-Wall Dangerous Type of Intertrochanteric Fracture," *BioMed Research International*, vol. 2021, Article ID 5911868, 6 pages, 2021.

Hindawi
BioMed Research International
Volume 2024, Article ID 9807363, 1 page
https://doi.org/10.1155/2024/9807363

Retraction

Retracted: Protective Effect of Luteolin on D-Galactosamine (D-Gal)/Lipopolysaccharide (LPS) Induced Hepatic Injury by in Mice

BioMed Research International

Received 12 March 2024; Accepted 12 March 2024; Published 20 March 2024

This article has been retracted by Hindawi following an investigation undertaken by the publisher [1]. This investigation has uncovered evidence of one or more of the following indicators of systematic manipulation of the publication process:

(1) Discrepancies in scope

(2) Discrepancies in the description of the research reported

(3) Discrepancies between the availability of data and the research described

(4) Inappropriate citations

(5) Incoherent, meaningless and/or irrelevant content included in the article

(6) Manipulated or compromised peer review

The presence of these indicators undermines our confidence in the integrity of the article's content and we cannot, therefore, vouch for its reliability. Please note that this notice is intended solely to alert readers that the content of this article is unreliable. We have not investigated whether authors were aware of or involved in the systematic manipulation of the publication process.

Wiley and Hindawi regrets that the usual quality checks did not identify these issues before publication and have since put additional measures in place to safeguard research integrity.

We wish to credit our own Research Integrity and Research Publishing teams and anonymous and named external researchers and research integrity experts for contributing to this investigation.

The corresponding author, as the representative of all authors, has been given the opportunity to register their agreement or disagreement to this retraction. We have kept a record of any response received.

References

[1] Y. Pu, Z. Yang, and X. Mo, "Protective Effect of Luteolin on D-Galactosamine (D-Gal)/Lipopolysaccharide (LPS) Induced Hepatic Injury by in Mice," *BioMed Research International*, vol. 2021, Article ID 2252705, 8 pages, 2021.

Hindawi
BioMed Research International
Volume 2024, Article ID 9793809, 1 page
https://doi.org/10.1155/2024/9793809

Retraction

Retracted: The Expression of miR-23a And miR-146a in the Saliva of Patients with Periodontitis and Its Clinical Significance

BioMed Research International

Received 12 March 2024; Accepted 12 March 2024; Published 20 March 2024

This article has been retracted by Hindawi following an investigation undertaken by the publisher [1]. This investigation has uncovered evidence of one or more of the following indicators of systematic manipulation of the publication process:

(1) Discrepancies in scope

(2) Discrepancies in the description of the research reported

(3) Discrepancies between the availability of data and the research described

(4) Inappropriate citations

(5) Incoherent, meaningless and/or irrelevant content included in the article

(6) Manipulated or compromised peer review

The presence of these indicators undermines our confidence in the integrity of the article's content and we cannot, therefore, vouch for its reliability. Please note that this notice is intended solely to alert readers that the content of this article is unreliable. We have not investigated whether authors were aware of or involved in the systematic manipulation of the publication process.

Wiley and Hindawi regrets that the usual quality checks did not identify these issues before publication and have since put additional measures in place to safeguard research integrity.

We wish to credit our own Research Integrity and Research Publishing teams and anonymous and named external researchers and research integrity experts for contributing to this investigation.

The corresponding author, as the representative of all authors, has been given the opportunity to register their agreement or disagreement to this retraction. We have kept a record of any response received.

References

[1] L. Kang, N. Li, and L. Wang, "The Expression of miR-23a and miR-146a in the Saliva of Patients with Periodontitis and Its Clinical Significance," *BioMed Research International*, vol. 2021, Article ID 5135278, 8 pages, 2021.

Hindawi
BioMed Research International
Volume 2024, Article ID 9793607, 1 page
https://doi.org/10.1155/2024/9793607

Retraction

Retracted: The Influence of ICAM1 3′UTR Gene Polymorphism on the Occurrence and Metastasis of Primary Liver Cancer

BioMed Research International

Received 12 March 2024; Accepted 12 March 2024; Published 20 March 2024

This article has been retracted by Hindawi following an investigation undertaken by the publisher [1]. This investigation has uncovered evidence of one or more of the following indicators of systematic manipulation of the publication process:

(1) Discrepancies in scope

(2) Discrepancies in the description of the research reported

(3) Discrepancies between the availability of data and the research described

(4) Inappropriate citations

(5) Incoherent, meaningless and/or irrelevant content included in the article

(6) Manipulated or compromised peer review

The presence of these indicators undermines our confidence in the integrity of the article's content and we cannot, therefore, vouch for its reliability. Please note that this notice is intended solely to alert readers that the content of this article is unreliable. We have not investigated whether authors were aware of or involved in the systematic manipulation of the publication process.

Wiley and Hindawi regrets that the usual quality checks did not identify these issues before publication and have since put additional measures in place to safeguard research integrity.

We wish to credit our own Research Integrity and Research Publishing teams and anonymous and named external researchers and research integrity experts for contributing to this investigation.

The corresponding author, as the representative of all authors, has been given the opportunity to register their agreement or disagreement to this retraction. We have kept a record of any response received.

References

[1] L. He, S. Wang, and X. Ma, "The Influence of ICAM1 3′UTR Gene Polymorphism on the Occurrence and Metastasis of Primary Liver Cancer," *BioMed Research International*, vol. 2021, Article ID 7377299, 11 pages, 2021.

Hindawi
BioMed Research International
Volume 2024, Article ID 9784090, 1 page
https://doi.org/10.1155/2024/9784090

Retraction

Retracted: Radiosensitizing Effect of Celastrol by Inhibiting G2/M Phase Arrest Induced by the c-myc Gene of Human SW1353 Chondrosarcoma Cells: Network and Experimental Analyses

BioMed Research International

Received 12 March 2024; Accepted 12 March 2024; Published 20 March 2024

This article has been retracted by Hindawi following an investigation undertaken by the publisher [1]. This investigation has uncovered evidence of one or more of the following indicators of systematic manipulation of the publication process:

(1) Discrepancies in scope

(2) Discrepancies in the description of the research reported

(3) Discrepancies between the availability of data and the research described

(4) Inappropriate citations

(5) Incoherent, meaningless and/or irrelevant content included in the article

(6) Manipulated or compromised peer review

The presence of these indicators undermines our confidence in the integrity of the article's content and we cannot, therefore, vouch for its reliability. Please note that this notice is intended solely to alert readers that the content of this article is unreliable. We have not investigated whether authors were aware of or involved in the systematic manipulation of the publication process.

Wiley and Hindawi regrets that the usual quality checks did not identify these issues before publication and have since put additional measures in place to safeguard research integrity.

We wish to credit our own Research Integrity and Research Publishing teams and anonymous and named external researchers and research integrity experts for contributing to this investigation.

The corresponding author, as the representative of all authors, has been given the opportunity to register their agreement or disagreement to this retraction. We have kept a record of any response received.

References

[1] J. Qian, Z. Zhang, X. Han, L. Zhu, Z. Bian, and T. Xie, "Radiosensitizing Effect of Celastrol by Inhibiting G2/M Phase Arrest Induced by the c-myc Gene of Human SW1353 Chondrosarcoma Cells: Network and Experimental Analyses," *BioMed Research International*, vol. 2022, Article ID 1948657, 20 pages, 2022.

Hindawi
BioMed Research International
Volume 2024, Article ID 9783981, 1 page
https://doi.org/10.1155/2024/9783981

Retraction

Retracted: Clinical Effect of Clarithromycin Combined with Tinidazole on Helicobacter pylori-Related Gastritis and Its Influence on COX-2 Expression

BioMed Research International

Received 12 March 2024; Accepted 12 March 2024; Published 20 March 2024

This article has been retracted by Hindawi following an investigation undertaken by the publisher [1]. This investigation has uncovered evidence of one or more of the following indicators of systematic manipulation of the publication process:

(1) Discrepancies in scope

(2) Discrepancies in the description of the research reported

(3) Discrepancies between the availability of data and the research described

(4) Inappropriate citations

(5) Incoherent, meaningless and/or irrelevant content included in the article

(6) Manipulated or compromised peer review

The presence of these indicators undermines our confidence in the integrity of the article's content and we cannot, therefore, vouch for its reliability. Please note that this notice is intended solely to alert readers that the content of this article is unreliable. We have not investigated whether authors were aware of or involved in the systematic manipulation of the publication process.

Wiley and Hindawi regrets that the usual quality checks did not identify these issues before publication and have since put additional measures in place to safeguard research integrity.

We wish to credit our own Research Integrity and Research Publishing teams and anonymous and named external researchers and research integrity experts for contributing to this investigation.

The corresponding author, as the representative of all authors, has been given the opportunity to register their agreement or disagreement to this retraction. We have kept a record of any response received.

References

[1] C. He, F. Kong, X. Zhu et al., "Clinical Effect of Clarithromycin Combined with Tinidazole on Helicobacter pylori-Related Gastritis and Its Influence on COX-2 Expression," *BioMed Research International*, vol. 2021, Article ID 4171019, 9 pages, 2021.

Hindawi
BioMed Research International
Volume 2024, Article ID 9781459, 1 page
https://doi.org/10.1155/2024/9781459

Retraction

Retracted: lncRNA FGD5-AS1 and miR-130a Can Be Used for Prognosis Analysis of Patients with Chronic Periodontitis

BioMed Research International

Received 12 March 2024; Accepted 12 March 2024; Published 20 March 2024

This article has been retracted by Hindawi following an investigation undertaken by the publisher [1]. This investigation has uncovered evidence of one or more of the following indicators of systematic manipulation of the publication process:

(1) Discrepancies in scope

(2) Discrepancies in the description of the research reported

(3) Discrepancies between the availability of data and the research described

(4) Inappropriate citations

(5) Incoherent, meaningless and/or irrelevant content included in the article

(6) Manipulated or compromised peer review

The presence of these indicators undermines our confidence in the integrity of the article's content and we cannot, therefore, vouch for its reliability. Please note that this notice is intended solely to alert readers that the content of this article is unreliable. We have not investigated whether authors were aware of or involved in the systematic manipulation of the publication process.

Wiley and Hindawi regrets that the usual quality checks did not identify these issues before publication and have since put additional measures in place to safeguard research integrity.

We wish to credit our own Research Integrity and Research Publishing teams and anonymous and named external researchers and research integrity experts for contributing to this investigation.

The corresponding author, as the representative of all authors, has been given the opportunity to register their agreement or disagreement to this retraction. We have kept a record of any response received.

References

[1] M. Yu and C. Chi, "lncRNA FGD5-AS1 and miR-130a Can Be Used for Prognosis Analysis of Patients with Chronic Periodontitis," *BioMed Research International*, vol. 2021, Article ID 8544914, 7 pages, 2021.

Hindawi
BioMed Research International
Volume 2024, Article ID 9769323, 1 page
https://doi.org/10.1155/2024/9769323

Retraction

Retracted: Curcumin Improves Pulmonary Hypertension Rats by Regulating Mitochondrial Function

BioMed Research International

Received 12 March 2024; Accepted 12 March 2024; Published 20 March 2024

This article has been retracted by Hindawi following an investigation undertaken by the publisher [1]. This investigation has uncovered evidence of one or more of the following indicators of systematic manipulation of the publication process:

(1) Discrepancies in scope

(2) Discrepancies in the description of the research reported

(3) Discrepancies between the availability of data and the research described

(4) Inappropriate citations

(5) Incoherent, meaningless and/or irrelevant content included in the article

(6) Manipulated or compromised peer review

The presence of these indicators undermines our confidence in the integrity of the article's content and we cannot, therefore, vouch for its reliability. Please note that this notice is intended solely to alert readers that the content of this article is unreliable. We have not investigated whether authors were aware of or involved in the systematic manipulation of the publication process.

Wiley and Hindawi regrets that the usual quality checks did not identify these issues before publication and have since put additional measures in place to safeguard research integrity.

We wish to credit our own Research Integrity and Research Publishing teams and anonymous and named external researchers and research integrity experts for contributing to this investigation.

The corresponding author, as the representative of all authors, has been given the opportunity to register their agreement or disagreement to this retraction. We have kept a record of any response received.

References

[1] J. Chen, W. Jiang, F. Zhu, Q. Wang, H. Yang, and J. Wu, "Curcumin Improves Pulmonary Hypertension Rats by Regulating Mitochondrial Function," *BioMed Research International*, vol. 2021, Article ID 1078019, 10 pages, 2021.

Hindawi
BioMed Research International
Volume 2024, Article ID 9760679, 1 page
https://doi.org/10.1155/2024/9760679

Retraction

Retracted: Effect of Dexmedetomidine Combined with Ropivacaine on Cognitive Dysfunction and Inflammatory Response in Patients Undergoing Craniocerebral Surgery

BioMed Research International

Received 12 March 2024; Accepted 12 March 2024; Published 20 March 2024

This article has been retracted by Hindawi following an investigation undertaken by the publisher [1]. This investigation has uncovered evidence of one or more of the following indicators of systematic manipulation of the publication process:

(1) Discrepancies in scope

(2) Discrepancies in the description of the research reported

(3) Discrepancies between the availability of data and the research described

(4) Inappropriate citations

(5) Incoherent, meaningless and/or irrelevant content included in the article

(6) Manipulated or compromised peer review

The presence of these indicators undermines our confidence in the integrity of the article's content and we cannot, therefore, vouch for its reliability. Please note that this notice is intended solely to alert readers that the content of this article is unreliable. We have not investigated whether authors were aware of or involved in the systematic manipulation of the publication process.

Wiley and Hindawi regrets that the usual quality checks did not identify these issues before publication and have since put additional measures in place to safeguard research integrity.

We wish to credit our own Research Integrity and Research Publishing teams and anonymous and named external researchers and research integrity experts for contributing to this investigation.

The corresponding author, as the representative of all authors, has been given the opportunity to register their agreement or disagreement to this retraction. We have kept a record of any response received.

References

[1] Y. Liu, H. Zhang, and W. Zhang, "Effect of Dexmedetomidine Combined with Ropivacaine on Cognitive Dysfunction and Inflammatory Response in Patients Undergoing Craniocerebral Surgery," *BioMed Research International*, vol. 2021, Article ID 4968300, 8 pages, 2021.

Hindawi
BioMed Research International
Volume 2024, Article ID 9758259, 1 page
https://doi.org/10.1155/2024/9758259

Retraction

Retracted: miR-1226-3p Promotes eNOS Expression of Pulmonary Arterial Endothelial Cells to Mitigate Hypertension in Rats via Targeting Profilin-1

BioMed Research International

Received 12 March 2024; Accepted 12 March 2024; Published 20 March 2024

This article has been retracted by Hindawi following an investigation undertaken by the publisher [1]. This investigation has uncovered evidence of one or more of the following indicators of systematic manipulation of the publication process:

(1) Discrepancies in scope

(2) Discrepancies in the description of the research reported

(3) Discrepancies between the availability of data and the research described

(4) Inappropriate citations

(5) Incoherent, meaningless and/or irrelevant content included in the article

(6) Manipulated or compromised peer review

The presence of these indicators undermines our confidence in the integrity of the article's content and we cannot, therefore, vouch for its reliability. Please note that this notice is intended solely to alert readers that the content of this article is unreliable. We have not investigated whether authors were aware of or involved in the systematic manipulation of the publication process.

Wiley and Hindawi regrets that the usual quality checks did not identify these issues before publication and have since put additional measures in place to safeguard research integrity.

We wish to credit our own Research Integrity and Research Publishing teams and anonymous and named external researchers and research integrity experts for contributing to this investigation.

The corresponding author, as the representative of all authors, has been given the opportunity to register their agreement or disagreement to this retraction. We have kept a record of any response received.

References

[1] J. Jian and L. Xia, "miR-1226-3p Promotes eNOS Expression of Pulmonary Arterial Endothelial Cells to Mitigate Hypertension in Rats via Targeting Profilin-1," *BioMed Research International*, vol. 2021, Article ID 1724722, 7 pages, 2021.

Hindawi
BioMed Research International
Volume 2024, Article ID 9784090, 1 page
https://doi.org/10.1155/2024/9784090

Retraction

Retracted: Radiosensitizing Effect of Celastrol by Inhibiting G2/M Phase Arrest Induced by the c-myc Gene of Human SW1353 Chondrosarcoma Cells: Network and Experimental Analyses

BioMed Research International

Received 12 March 2024; Accepted 12 March 2024; Published 20 March 2024

This article has been retracted by Hindawi following an investigation undertaken by the publisher [1]. This investigation has uncovered evidence of one or more of the following indicators of systematic manipulation of the publication process:

(1) Discrepancies in scope

(2) Discrepancies in the description of the research reported

(3) Discrepancies between the availability of data and the research described

(4) Inappropriate citations

(5) Incoherent, meaningless and/or irrelevant content included in the article

(6) Manipulated or compromised peer review

The presence of these indicators undermines our confidence in the integrity of the article's content and we cannot, therefore, vouch for its reliability. Please note that this notice is intended solely to alert readers that the content of this article is unreliable. We have not investigated whether authors were aware of or involved in the systematic manipulation of the publication process.

Wiley and Hindawi regrets that the usual quality checks did not identify these issues before publication and have since put additional measures in place to safeguard research integrity.

We wish to credit our own Research Integrity and Research Publishing teams and anonymous and named external researchers and research integrity experts for contributing to this investigation.

The corresponding author, as the representative of all authors, has been given the opportunity to register their agreement or disagreement to this retraction. We have kept a record of any response received.

References

[1] J. Qian, Z. Zhang, X. Han, L. Zhu, Z. Bian, and T. Xie, "Radiosensitizing Effect of Celastrol by Inhibiting G2/M Phase Arrest Induced by the c-myc Gene of Human SW1353 Chondrosarcoma Cells: Network and Experimental Analyses," *BioMed Research International*, vol. 2022, Article ID 1948657, 20 pages, 2022.

Hindawi
BioMed Research International
Volume 2022, Article ID 1948657, 20 pages
https://doi.org/10.1155/2022/1948657

Research Article

Radiosensitizing Effect of Celastrol by Inhibiting G2/M Phase Arrest Induced by the c-myc Gene of Human SW1353 Chondrosarcoma Cells: Network and Experimental Analyses

Jin Qian, Zhen Zhang, Xiao Han, Liulong Zhu, Zhenyu Bian, and Tao Xie

Department of Orthopedic Surgery, Affiliated Hangzhou First People's Hospital, Zhejiang University School of Medicine, Hangzhou 310006, China

Correspondence should be addressed to Zhenyu Bian; abe-august@163.com and Tao Xie; todxietao2021@163.com

Received 14 August 2021; Accepted 30 October 2021; Published 31 January 2022

Academic Editor: Chang Gu

Objective. Studies have unveiled that the components of *Tripterygium wilfordii* Hook F (TWHF) such as celastrol could attenuate apoptosis and proliferation of various tumor cells. This study is focused on the radiosensitization effect and apoptotic pathways of celastrol via the inhibition of the *c-myc* gene and the influence of which combined with radiotherapy on the proliferation, apoptosis, invasion, and metastasis of chondrosarcoma cells. *Methods*. A variety of bioinformatic tools were applied to explore the expression level and prognosis of the *c-myc* gene in different tumor cells and chondrosarcoma cells. We used pharmacology network to analyze the components, pathways, targets, molecular functions of TWHF and explore the relevant effective components over the MYC gene. Clone formation assay, CCK-8 assay, flow cytometry, and transwell migration assay were applied to detect the effects of celastrol on the expression of *c-myc* gene, cell apoptosis, and cell cycle. Radiation therapy was used to observe the radiosensitization effect of celastrol on chondrosarcoma. *Results*. This study shows that the c-myc gene is overexpressed in various tumor cells and bone tumor cells to varying degrees. Celastrol can significantly inhibit the expression of the *c-myc* gene, induce G2/M phase arrest through regulation of G2/M phase-related proteins, and promote SW1353 cell apoptosis through the mitochondrial signaling pathway. In addition, we also found that the use of triptorubin to inhibit *c-myc* gene expression in combination with radiotherapy can increase the osteosarcoma cells' apoptosis rate through the mitochondrial signaling pathway significantly. *Conclusions*. Our study validated the radiosensitization effect of celastrol through knocking down the expression of the c-myc gene to induce G2/M phase arrest and provides a new idea for the treatment of refractory or recurrent chondrosarcoma that is not sensitive to radiotherapy.

1. Introduction

Chondrosarcoma is a highly malignant tumor characterized by the production of the cartilage matrix by tumor cells, which is the second most commonly malignant bone tumor, with an incidence of 1 in 1,000,000 people [1, 2]. Chondrosarcoma itself has poor blood supply and lymphatic circulation and is insensitive to radiotherapy and chemotherapy; local or extensive surgical resection is the main method of treatment of chondrosarcoma to prevent local recurrence and distant metastasis [3–5]. However, for certain parts of the body, such as the pelvis or skull, it is difficult to achieve broad-side resection and the incidence of recurrence and metastasis is still high [6]. Radiotherapy is still a better palliative treatment [7, 8].

The proto-oncogene *c-myc* encodes a transcription factor c-Myc, which is of great importance in controlling cell growth and vitality. c-Myc belongs to a small family of transcription factors that contain basic, helix-loop-helix, and leucine zipper domains. c-Myc displays sequence-specific DNA-binding properties only when bound to Max, its heterodimeric partner. The interaction with Max has been shown to be necessary for most of the physiological effects of c-Myc, including the promotion of cell growth and

apoptosis [9–11]. *c-myc* expression is absent in quiescent cells but is rapidly induced upon the addition of growth factors. A large body of physiological evidence shows that either upregulation or downregulation of intracellular c-Myc activity has profound consequences on cell cycle progression. There were some studies suggesting that c-Myc may stimulate the activity of cyclin E/cyclin-dependent kinase 2 (Cdk2) complexes and antagonize the action of the Cdk inhibitor $p27^{KIP1}$. Cyclin D/Cdk4/6 complexes have also been implicated as targets of c-Myc activity. Its abnormal expression leads to 30–50% of malignant tumors, overexpression in more than 70% of human malignancies, and high expression in sarcomas [12, 13]. Overexpression of the *c-myc* gene leads to increased replication origin activity, followed by DNA damage and checkpoint activation [14, 15]. On the contrary, reducing *c-myc* expression by antisense methods or deletion of the gene by homologous recombination lead to a lengthening of the cell cycle. *c-myc* null cells display a lengthening of both the G1 and G2 phases of the cell cycle, while S phase duration remains unchanged. The expression of MYC can also induce CCNB1 to encode the mitotic driver cyclin B1, which reduces the G2/M arrest induced by DNA damage and enters inappropriate mitosis [10, 15]. Evidence showed that tumors arrest at the G2/M stage and more sensitive to radiotherapy [16]. Consequently, the combination of radiotherapy and downregulation of the c-myc gene may be a new strategy for the treatment of chondrosarcoma to deal with refractory or relapsed chondrosarcoma.

Tripterygium wilfordii Hook F (TWHF), a plant of the Euonymus family, has been used to treat rheumatoid arthritis as early as centuries ago and has now been used for a broad-spectrum treatment of autoimmune and inflammatory diseases [17, 18]. It contains diterpenoids such as triptolide, triterpenes such as celastrol, and other components, which have anti-inflammatory, antitumor, immunosuppressive, antioxidant, and antiobesity pharmacological effects [19, 20]. Among them, TWHF has been confirmed to be a natural proteasome inhibitor with antitumor activity [21]. With the deepening of research, it has a clear killing effect on leukemia, multiple myeloma, liver cancer, glioma, melanoma, and breast cancer [21, 22]. Related literature reports on its antitumor mechanisms are also divergent, including nuclear factor-κB (nuclear factor-kappaB, (NF-κB)), proteasome, mitogen-activated protein kinase (mitogen-activated protein kinase (MAPK)), and serine/threonine protein kinase B (PI3K/AKT), but it is still unclear which is its direct or main target [22–25]. At present, there is no literature report that *Tripterygium wilfordii* or some of its components can inhibit c-myc gene expression, thereby exerting antitumor effects and radiosensitization effects.

Hopkins [26] proposed the concept of network pharmacology in 2007, using bioinformatics methods to comprehensively carry out high-throughput screening and network analysis to reveal the relationship between drug components, targets, and diseases. This provides us with effective experimental assistance and theoretical basis for screening and developing drugs with high activity and low toxicity from *Tripterygium wilfordii* to treat chondrosarcoma.

In our literature, we aimed to determine the role of core components of TWHF such as celastrol in the treatment of chondrosarcoma and its potential related targets in the chondrosarcoma cell line SW1353. Meanwhile, we also attempted to observe the inhibitory effect of celastrol on the proliferation of chondrosarcoma cells and explore the mechanism of its antitumor effect. Our results demonstrated that celastrol can exert the effect of radiotherapy sensitization by inhibiting the *c-myc* gene, which provided a new method for the treatment of refractory or relapsed chondrosarcoma.

2. Method

2.1. Analysis of Pan-Cancer MYC Gene and Sarcoma Gene Expression. Gene expression matrices of different tumor and sarcoma cell lines were obtained from the Cancer Cell Line Encyclopedia (CCLE) dataset (https://portals.broadinstitute.org/ccle/about) [27], built, and visualized with R v4.0.3 package ggplot2 (v3.3.3). The limma software package (version: 3.40.2) of R software was used to study the differentially expressed mRNAs in sarcoma. The adjusted *P* value was analyzed in the Cancer Genome Atlas (TCGA) or the Genotype-Tissue Expression (GTEx) to correct false-positive results. "Adjusted $P < 0.05$ and log2 (fold change) > 1 or log2 (fold change) < −1" are defined as a threshold level for the differential expression.

2.2. The Prognostic Analysis of the MYC Gene for Sarcoma. The raw count of RNA sequencing data (level 3) of sarcoma and the corresponding clinical information were obtained from The Cancer Genome Atlas (TCGA) dataset (https://portal.gdc.com). The logrank was used to test the Kaplan–Meier (KM) survival analysis to compare the survival difference between the above two or more groups, and the time-dependent ROC curve (timeROC) analysis was performed to compare the prediction accuracy and risk score of the MYC gene. timeROC and the area under timeROC curve (AUC) were generated with R package "timeROC." The *P* value and the hazard ratio (HR) with 95% confidence interval (CI) were obtained via logrank test and Cox proportional hazard regression for the Kaplan-Meier curve. All the above analysis methods and R software packages were executed using R (v4.0.3). $P < 0.05$ was considered statistically significant.

2.2.1. Network Pharmacology Analysis

(1) Search for Active Components of Tripterygium wilfordii and Related Targets. We searched "*Tripterygium wilfordii*" in the traditional Chinese medicine systems pharmacology database and analysis platform (TCMSP) database to obtain the known pharmaceutical ingredients and all possible targets. The obtained targets were annotated through the UniProt database, and the human-derived target gene name and its ID of the corresponding target were obtained. We then searched "chondrosarcoma" in the GeneCards, OMIM, PharmGKB, TTD, DrugBank databases for related targets and aggregated and merged all potential targets for chondrosarcoma.

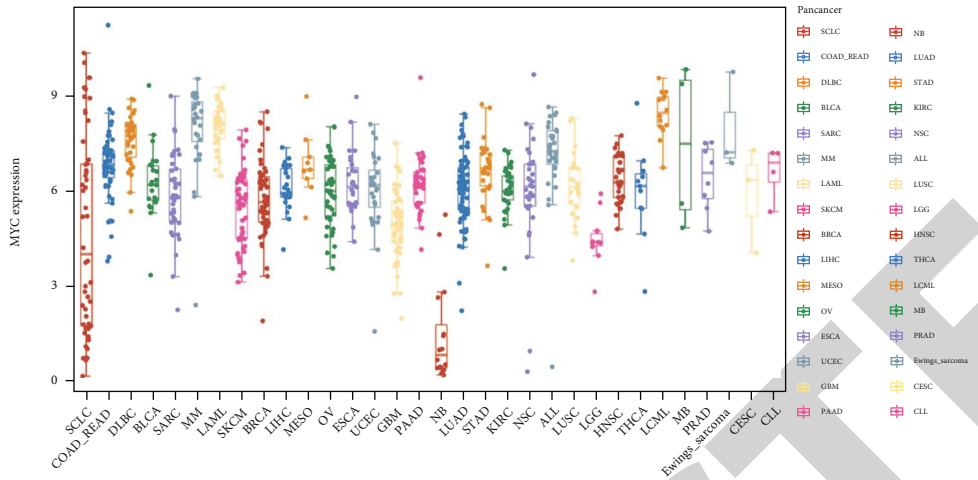

(a)

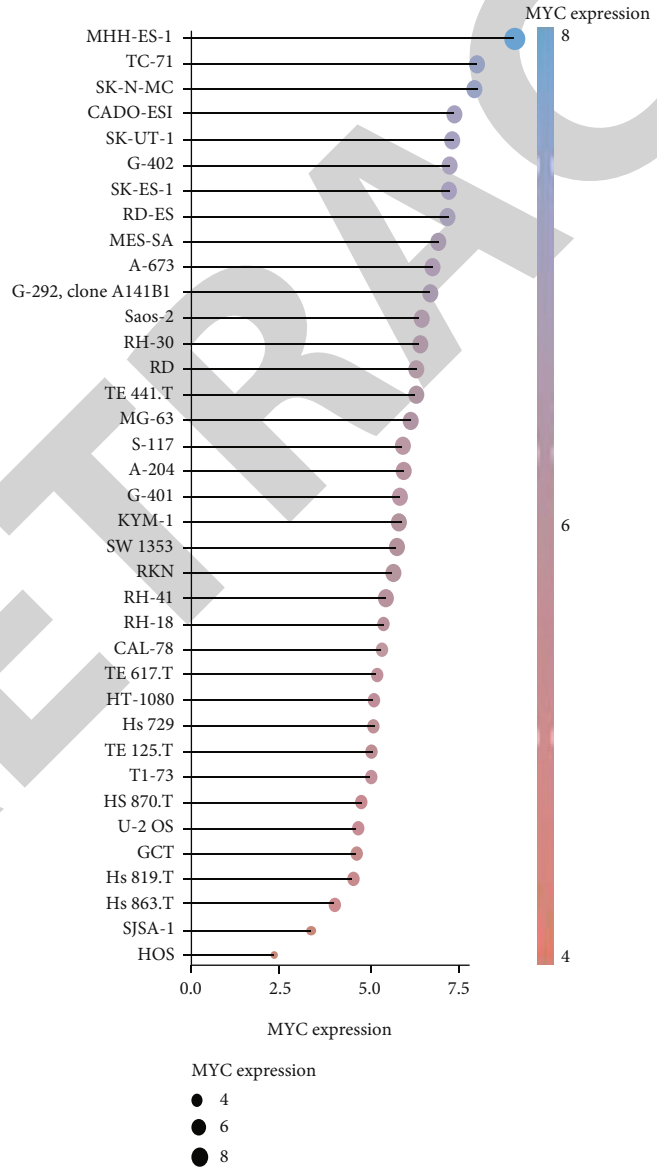

(b)

Figure 1: Continued.

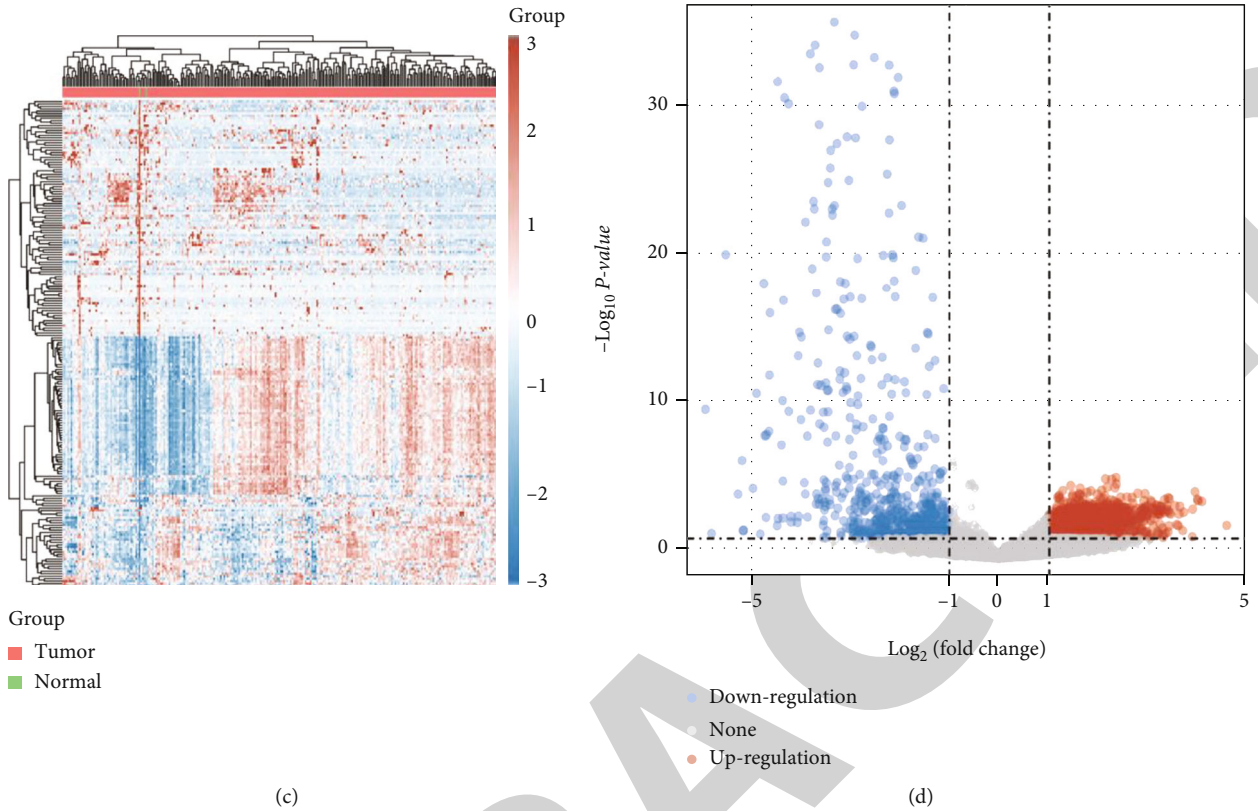

Figure 1: The differential expression of the myc gene and the differential analysis of sarcoma cell lines. (a) The expression distribution of the MYC gene in different tumor tissues. (b) The expression distribution of the MYC gene in sarcoma cell lines. (c) Volcano plots. (d) Hierarchical clustering analysis of mRNAs.

(2) Construction of Protein–Protein Interactions (PPIs). We obtained the intersection of the drug target and disease target through R software drew the Venn diagram of the *Tripterygium*-chondrosarcoma action target to visualize the intersection of the drug-disease target. The STRING database (http://www.string-db.org) is a computerized and powerful global resource for studying the interactions between the predicted and experimental interactions of proteins. We then entered the obtained disease-drug common target set into the STRING11.0 database and set the biological category to "*Homo sapiens*," and the interaction confidence score > 0.4, to build the PPI network. We next imported the obtained PPI network file into Cytoscape 3.8.0 software for editing and then analyzed the topological properties of the network and calculated the node's betweenness centrality (BC), closeness centrality (CC), and other related information. Genes greater than the median value were selected and saved. We finally screened twice to obtain the core target in the PPI network.

(3) Construction of the Component-Target Network of Tripterygium wilfordii Hook F (TWHF). The active ingredients of TWHF and their possible targets integrated in steps 1 and 2 were regarded as two types of "nodes." If the interaction between the drug ingredients and the target was related, "Edge" was used to connect, and Cytoscape 3.8.0 software was imported to build a "drug component-target" network. We then imported the core target obtained in step 4 into the component-target network graph, used the network analyzer to analyze the characteristic parameters of the network node, and determined the core component according to the degree.

(4) GO and KEGG Enrichment Analyses. Genes in modules of interest were extracted for further functional enrichment analysis. A Gene Ontology (GO) analysis was used to identify characteristic biological attributes. A Kyoto Encyclopedia of Genes and Genomes (KEGG) pathway enrichment analysis was performed to identify functional attributes. GO annotation analysis and KEGG pathway enrichment analysis of DEGs in this study were performed using the Database for Annotation, Visualization and Integrated Discovery (DAVID) tools (https://david.ncifcrf.gov/). GO was widely used to annotate functional genes, including the molecular function (MF), biological pathway (BP), and cell composition (CC). Threshold correction was set as $P < 0.05$; targets were sorted from small to large and ranked in top 10 biological processes or pathways. The top 20 pathways in the KEGG pathway were analyzed by Cytoscape to construct a "pathway-target" network. The significance of the signal pathway is indicated by the size and color of the bubble. The larger the bubble is, the more genes in the signal pathway are and the more important the pathways are.

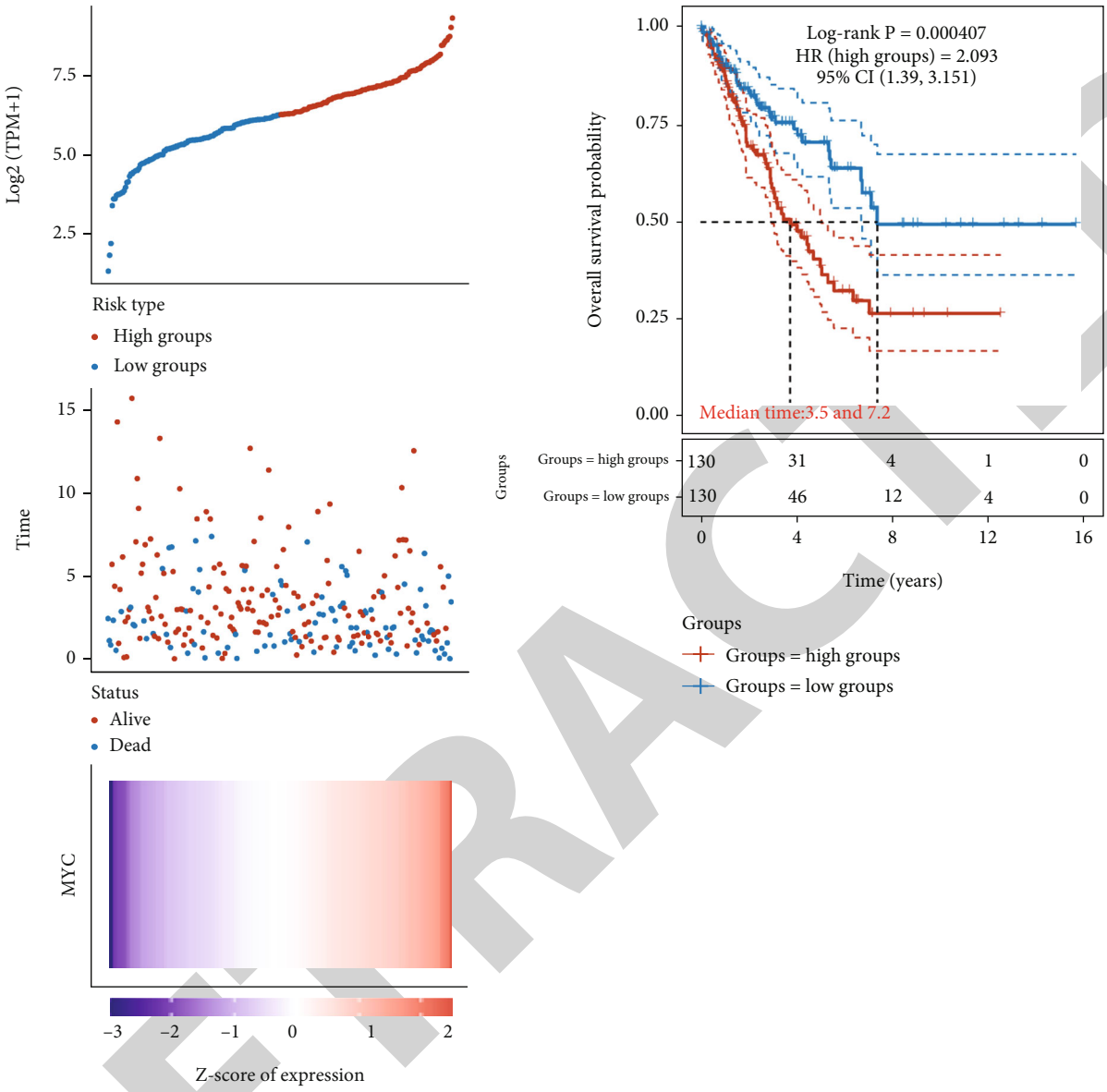

Figure 2: Continued.

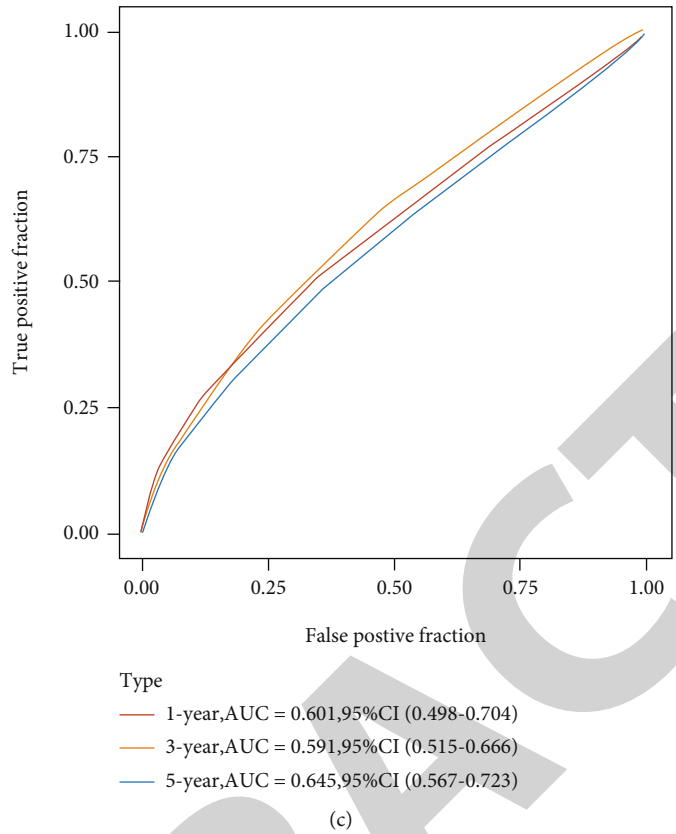

Figure 2: Prognostic analysis of the gene signature in the TCGA set. (a) TCGA dataset. (b) KM survival curve distribution of the MYC gene in the TCGA dataset. (c) ROC curve and AUC of the gene at different times.

(5) Review and Find Target Genes and Corresponding Drug Ingredients. We found and reviewed the active ingredients of the drug corresponding to the MYC gene and summarized the drug ingredients.

2.2.2. Experimental Verification

(1) Cell Culture and Treatment. Cultured in DMEM containing 10% fetal bovine serum and 1% double antibody (100 U/ml penicillin and 100 μg/ml streptomycin), human chondrosarcoma cells SW1353 were placed at 37°C with a 5% CO_2 constant-temperature cell incubator. The cells in the logarithmic growth phase were digested with trypsin containing EDTA, and the chondrosarcoma cells were seeded in the cell plate and cultured for 24 hours to make them adherent. Different concentrations of TWHF were added to the treatment, and the control group was treated with 0.1% DMSO in volume fraction for 24 h and 48 h.

(2) Cytotoxicity and Proliferation Assays. Seeded on a 96-well plate at a density of 5×10^3 cells/well, cells were incubated for 48 h in an incubator, washed twice with medium, added with 100 ml CCK-8 solution (MedChemExpress) and DMEM medium (1 : 10) mixture to each well, and incubated for 60 minutes in the dark. Minutes later, the absorbance value of each well was measured on the MR7000 microplate reader (Dynatech) at 450 nm absorbance. For cell proliferation assay, cells were cultured on 5×10^3 cells/well in a 96-well plate. After drug treatment, we added CCK8 in the culture as above and measured the absorbance. According to the cell inhibition rate (%) = 1-cell survival rate, we took drug concentration as the abscissa and the cell inhibition rate as ordinate to draw the CCK-8 line chart.

(3) Colony Formation Assay. After the cells are treated with drugs or radiotherapy, they are seeded in a 6-well plate at 1000 cells/well and cultured at 37°C for 2 weeks. When there are macroscopic clones in the culture dish, the culture is immediately terminated. After washing 3 times with PBS, a mixture of 4% polymethanol and 0.1% crystal violet was added, fixed, and stained at 37°C for 30 minutes. Rinse the dye slowly with tap water. The count > 50 cell clones under a light microscope (magnification, ×200). Cell clone formation rate (PE) = (number of clones/number of inoculated cells) × 100%, and cell survival rate = cell clone formation rate of each experimental group/control group cell clone formation rate × 100%.

(4) Cell Cycle Analysis. After 0, 24, 48, 72, and 96 hours, the siRNA-transfected cells were digested and washed with PBS twice and fixed with 75% ethanol overnight in a 20°C environment. Cells were added with propidium iodide (BD Biosciences) and incubated for 15 minutes in the dark. We used the FACSCalibur flow cytometer (BD Biosciences) to analyze the cell cycle and used ModFit software to analyze the data.

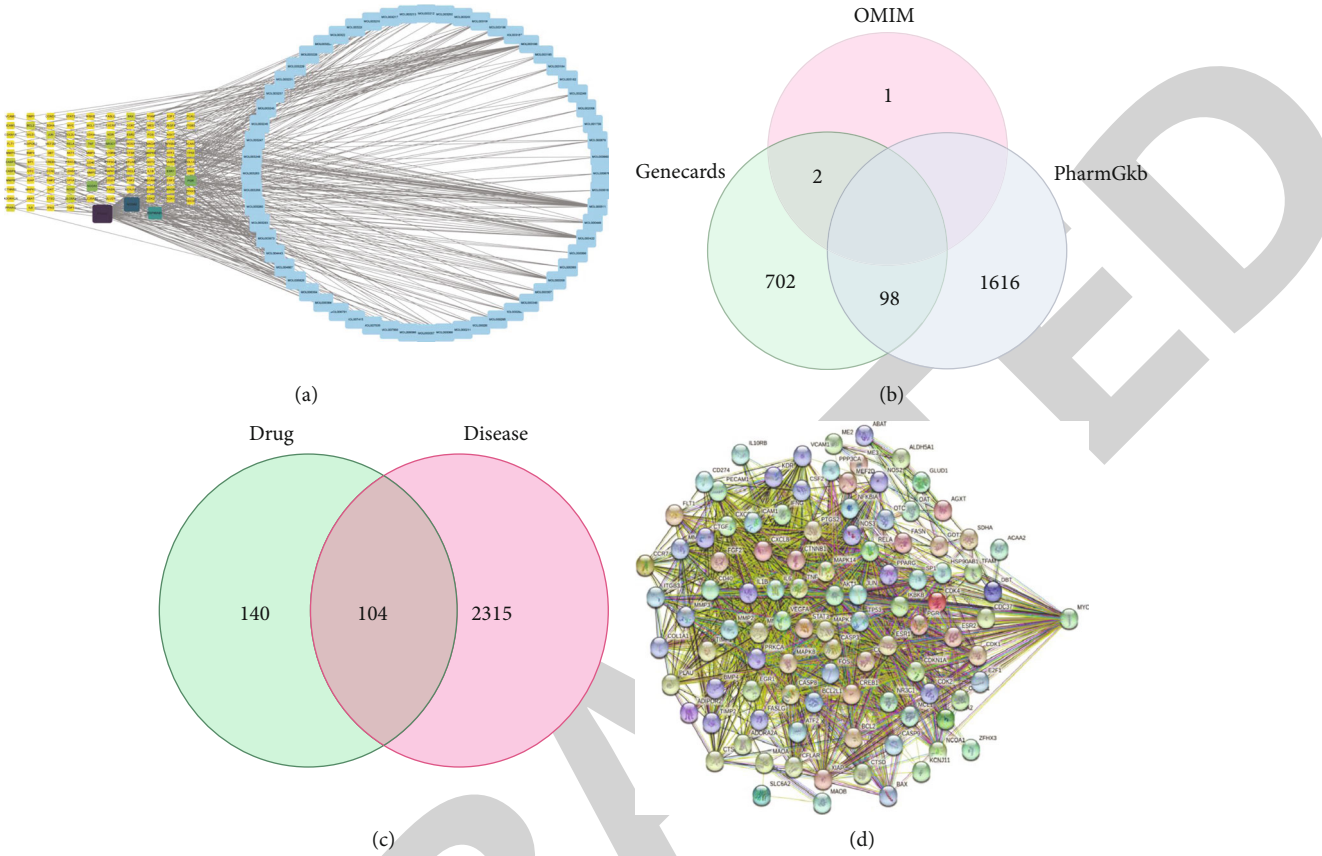

Figure 3: Construction of the C-T network of TWHF for chondrosarcoma treatment. (a) Constructing the relationship between all the therapeutic targets of TWHF and all the drug components. (b) The intersection of chondrosarcoma target genes in different databases. (c) The intersection of TWHF treatment targets and chondrosarcoma disease targets. (d) Constructing a PPI network of TWHF for the treatment of chondrosarcoma based on STRING.

(5) Cell Apoptosis Analysis. Annexin V FITC (Thermo Fisher) was used to analyze cell apoptosis. We digested the cells and washed them with PBS and then resuspended it in 1x binding buffer. Subsequently, we transferred the cells to 100 μl of the resuspension mixture solution (1×10^5 cells) into a culture tube (5 ml). V FITC (5 μl) and PI (5 μl) were added to the test tube and incubated at room temperature for 15 minutes. Finally, we added 400 μl of 1x binding buffer to each test tube. Flow cytometry (BD Biosciences) was used for cell apoptosis analysis, and FlowJo software was used for data analysis.

(6) Radiotherapy. The drug-treated SW1353 cells were seeded (200 cells per well) in 6-well plates and cultured at 37°C with 5% CO_2 for 24 hours. We used an X-ray equipment (Precision X-Ray) to irradiate cells at dose rates of 2, 4, 6, and 8 Gy. Subsequently, SW1353 cells were cultured for 10 days until colonies were visible to the naked eye.

(7) Western Blotting. The treated SW1353 cells were digested and lysed in RIPA lysis buffer (Sigma Aldrich). After 30 minutes, the protein concentration was measured at 570 nm wavelength by using the BCA protein analysis kit (Thermo Fisher). The same amount of protein (40 μg) by SDS-PAGE (12% polyacrylamide gel) was separated.

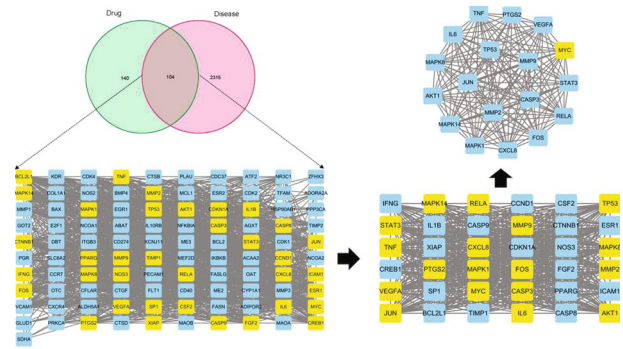

Figure 4: Obtaining the core target of TWHF for the treatment of chondrosarcoma.

Electrophoresis was manipulated at 100 V for 1.5 h, and the separated protein was transferred to PVDF membrane, blocked with 5% skim milk in TBS-T for 1 hour at 37°C, and incubated with primary antibody (Cell Signaling Technology) overnight at 4°C. After washing the protein three times with TBS-T, we diluted it with HRP anti-rabbit (cat. no. FD0128) or anti-mouse IgG (cat. no. FD0142) antibody (Fdbio Science) in 5% skim milk (1 : 5000) at room temperature for 1 hour. The protein bands were visualized by using WESTAR SUPERNOVA-1 Kit (Cyanagen) and Molecular

Table 1: Summary of GO function enrichment of *Tripterygium wilfordii* Hook F (TWHF) chondrosarcoma targets.

Ontology	ID	Description	*P*.adjust
BP	GO:0032496	Response to lipopolysaccharide	$2.00E-22$
	GO:0002237	Response to molecule of bacterial origin	$5.25E-22$
	GO:0042493	Response to drug	$9.74E-22$
	GO:0070482	Response to oxygen levels	$4.77E-16$
	GO:0048545	Response to steroid hormone	$5.18E-14$
	GO:0009411	Response to UV	$5.26E-14$
	GO:0097191	Extrinsic apoptotic signaling pathway	$7.06E-14$
	GO:0051090	Regulation of DNA-binding transcription factor activity	$8.31E-14$
	GO:0009314	Response to radiation	$8.55E-14$
	GO:2001237	Negative regulation of extrinsic apoptotic signaling pathway	$1.35E-13$
CC	GO:0005759	Mitochondrial matrix	$1.07E-07$
	GO:0045121	Membrane raft	$1.15E-06$
	GO:0098857	Membrane microdomain	$1.15E-06$
	GO:0005667	Transcription regulator complex	$1.03E-05$
	GO:0031968	Organelle outer membrane	$1.03E-05$
	GO:0019867	Outer membrane	$1.03E-05$
	GO:0005741	Mitochondrial outer membrane	$2.93E-05$
	GO:0000307	Cyclin-dependent protein kinase holoenzyme complex	$8.19E-05$
	GO:0090575	RNA polymerase II transcription regulator complex	$8.19E-05$
	GO:1904813	Ficolin-1-rich granule lumen	$9.39E-05$
MF	GO:0140297	DNA-binding transcription factor binding	$1.17E-09$
	GO:0061629	RNA polymerase II-specific DNA-binding transcription factor binding	$6.55E-08$
	GO:0033613	Activating transcription factor binding	$6.55E-08$
	GO:0001216	DNA-binding transcription activator activity	$2.30E-06$
	GO:0031072	Heat shock protein binding	$2.30E-06$
	GO:0005126	Cytokine receptor binding	$2.41E-06$
	GO:0002020	Protease binding	$2.85E-06$
	GO:0005125	Cytokine activity	$4.09E-06$
	GO:0005178	Integrin binding	$4.45E-06$
	GO:0001228	DNA-binding transcription activator activity, RNA polymerase II specific	$6.10E-06$

Imager (Bio-Rad). We used ImageJ 1.8.0 software for density analysis.

2.2.3. Data Analysis. Data were expressed as mean ± standard deviation (SD) and analyzed with SPSS17.0 (SPSS Inc.) software. We used the *t*-test to calculate the difference between the two groups and used one-way analysis of variance to compare the differences between three or more groups and then performed the Tukey post test. Two-tailed test was used for the test, and $P < 0.05$ was considered statistically significant.

3. Result

3.1. Bioinformatic Analysis of the MYC Gene and Chondrosarcoma Cells. We collected the *MYC* gene expression matrix of 946 different tumors and 37 sarcoma cell lines from the CCLE database, analyzed, and obtained the violin pilot of the pan-cancer analysis of the *MYC* gene (Figure 1(a)) and the difference map of the *MYC* gene expression in sarcoma cell lines, respectively (Figure 1(b)). We also made the gene expression volcano map expression (Figure 1(c)) and heat map of the differential gene expression (Figure 1(d)) of the sarcoma by acquiring the RNA sequencing data (level 3) and related information of 260 sarcomas from the TCGA database.

We then drew *MYC* gene expression and survival time and status of sarcoma patients (Figure 2(a)), as well as the distribution of the KM survival curve (Figure 2(b)), ROC curve, and AUC of the MYC gene at different times (Figure 2(c)) according to the raw count of RNA sequencing data of 260 sarcomas and corresponding clinical

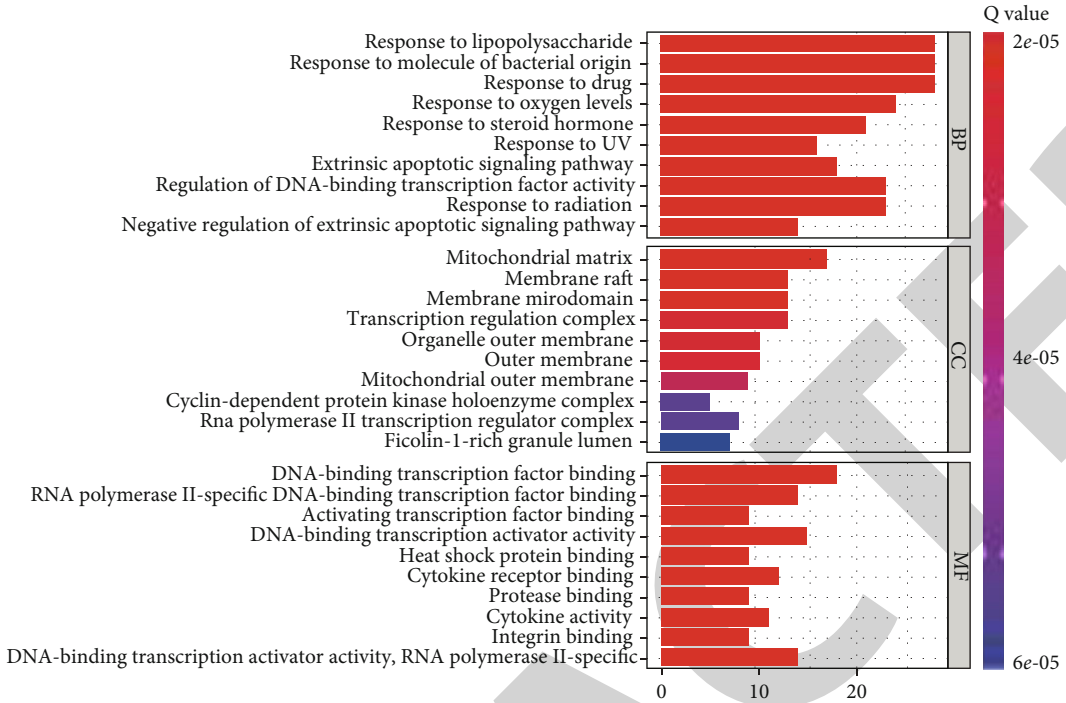

(a)

Figure 5: Continued.

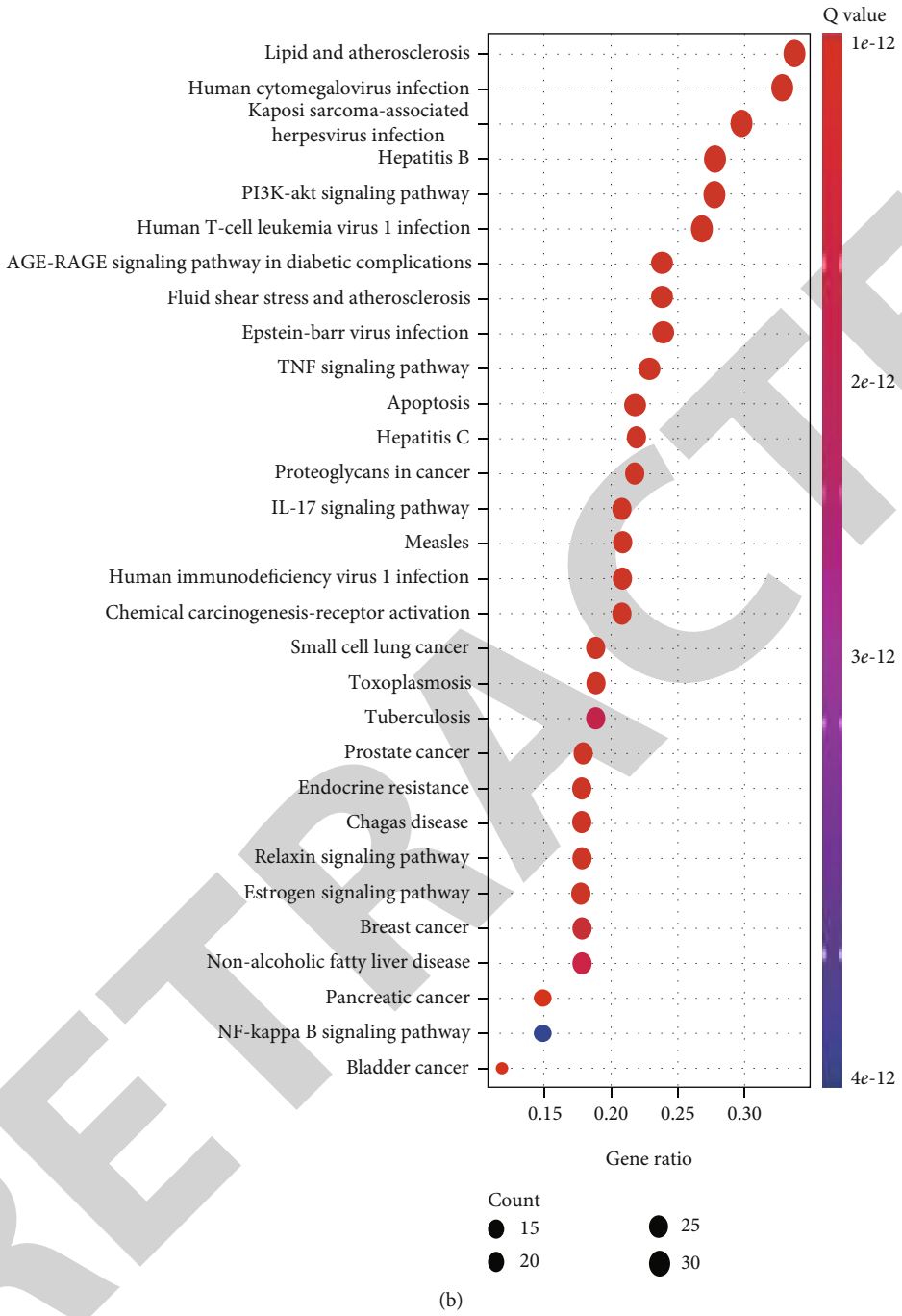

(b)

Figure 5: Continued.

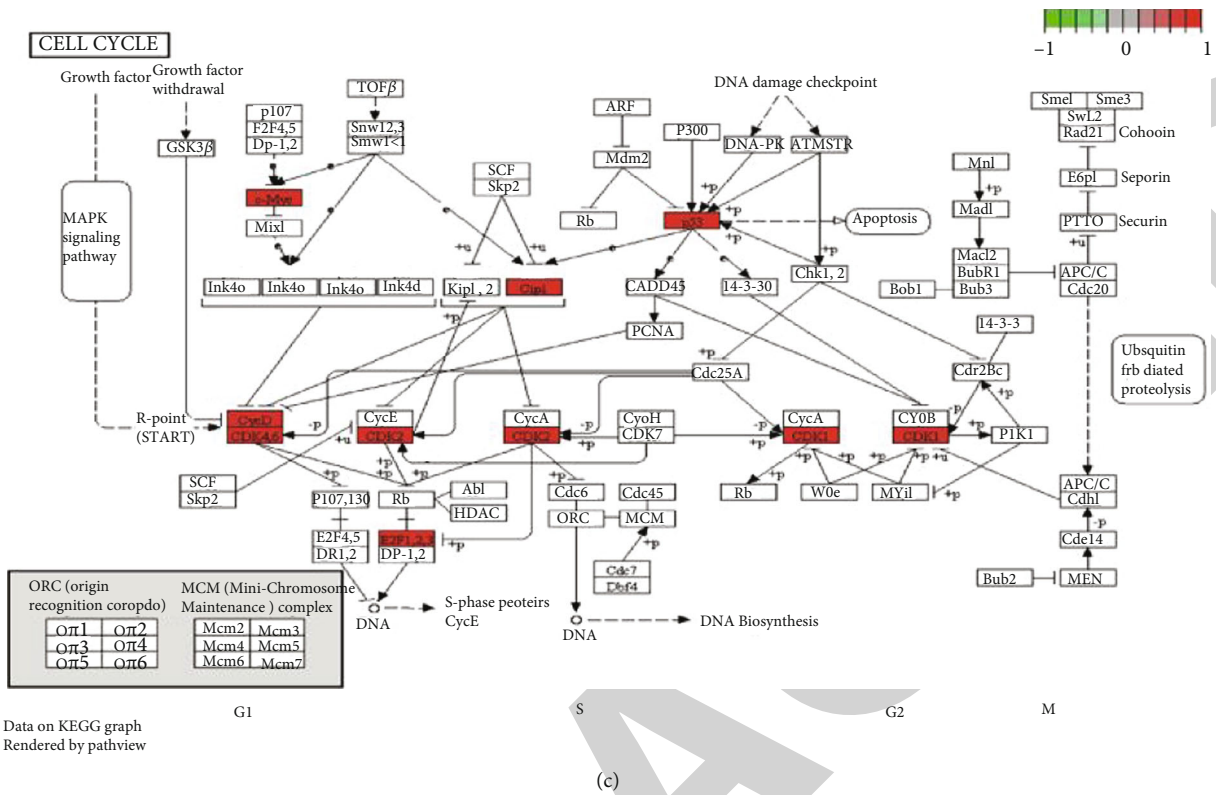

(c)

Figure 5: Gene enrichment analysis based on GO and KEGG. (a) Histogram of GO function enrichment at the intersection target of TWHF and chondrosarcoma. (b) Histogram of KEGG enrichment at the intersection target of TWHF and chondrosarcoma. (c) Schematic diagram of core genes involved in the cell cycle pathway enrichment based on KEGG analysis.

information from TCGA. The gene is proved to be a risk factor according to the risk score and gene expression trend after sorting gene expression from low to high (Figure 2(a)). The median overall survival (OS) of the high-expression group was 3.5 years and that of the low-expression group was 7.2 years. However, the AUC value shows that the predictive ability of the gene is general. We found that compared with normal samples, the MYC gene is overexpressed in tumor patients and sarcoma patients and MYC gene expression is in correlation negatively with the OS of patients.

3.2. Construction of the Compound-Target Network of Tripterygium wilfordii Hook F (TWHF). We searched TCMSP (https://old.tcmsp-e.com/tcmsp.php), got 143 chemical constituents of *Tripterygium wilfordii* Hook F (TWHF) and 134 potential drug targets, and drew a CT network diagram of TWHF (Figure 3(a)), where the circles represent the active components of TWHF and the squares represent the drug targets. It shows that multiple active ingredients act on multiple targets, reflecting the multicomponent and multitarget synergistic treatment characteristics of TWHF. We collected 802, 4, 1714, 0, and 0 potential chondrosarcoma targets from GeneCards, OMIM, PharmGKB, TTD, and DrugBank, respectively. We summarized and merged all data and obtained a total of 2419 chondrosarcoma-related targets (Figure 3(b)).

3.3. Construction of Protein–Protein Interactions (PPIs). After summarizing the previously-obtained drug and disease targets, we obtained 104 active ingredient-disease common targets by using the R language to take the intersection and draw the Venn diagram (Figure 3(c)). STRING 11.0 was applied to analyze common targets and collect protein interactions. In STRING, the confidence score was set more than 0.4 and the isolated edges was deleted. The PPI network has 104 nodes and 1631 edges and the average degree of this network is 31.4 (Figure 4). We then used Cytoscape 3.8.0 software to revisualize and analyze the active ingredient-disease common target network. The larger the node and the darker the color is, the higher the degree parameter value is, indicating that it may be the key target to find. After filtering the nodes twice according to each parameter, 18 nodes and 153 edges are finally obtained (Figure 4). It is confirmed that the core targets obtained in the final screening are MAPK8, VEGFA, CASP3, CXCL8, TP53, FOS, MMP9, IL6, AKT1, TNF, JUN, STAT3, MAPK14, PTGS2, MYC, MMP2, MAPK1, and RELA.

3.4. GO and KEGG Enrichment Analyses. GO enrichment analysis was used, and we obtained 1908 items related to biological processes, 35 items related to cell components, and 145 items related to molecular functions, which were sorted and summarized according to the corrected *P* value (Table 1) and plotted as a histogram (Figure 5(a)). We got

Table 2: Summary table of KEGG function enrichment of TWHF-chondrosarcoma targets.

ID	Description	*P*.adjust
hsa05417	Lipid and atherosclerosis	$8.28E-27$
hsa05163	Human cytomegalovirus infection	$4.15E-25$
hsa05167	Kaposi sarcoma-associated herpesvirus infection	$1.62E-23$
hsa04933	AGE-RAGE signaling pathway in diabetic complications	$2.37E-23$
hsa05161	Hepatitis B	$2.37E-23$
hsa04668	TNF signaling pathway	$8.76E-21$
hsa05418	Fluid shear stress and atherosclerosis	$6.58E-20$
hsa04657	IL-17 signaling pathway	$8.02E-20$
hsa05166	Human T-cell leukemia virus 1 infection	$1.12E-18$
hsa04210	Apoptosis	$1.16E-17$
hsa05222	Small cell lung cancer	$2.72E-17$
hsa05160	Hepatitis C	$2.41E-16$
hsa05162	Measles	$2.71E-16$
hsa05169	Epstein-Barr virus infection	$2.86E-16$
hsa05145	Toxoplasmosis	$1.01E-15$
hsa05215	Prostate cancer	$1.26E-15$
hsa01522	Endocrine resistance	$1.43E-15$
hsa05142	Chagas disease	$2.87E-15$
hsa04151	PI3K-Akt signaling pathway	$1.42E-14$
hsa05205	Proteoglycans in cancer	$4.71E-14$
hsa05212	Pancreatic cancer	$1.64E-13$
hsa04926	Relaxin signaling pathway	$1.75E-13$
hsa05219	Bladder cancer	$4.46E-13$
hsa04915	Estrogen signaling pathway	$5.38E-13$
hsa05170	Human immunodeficiency virus 1 infection	$8.36E-13$
hsa05207	Chemical carcinogenesis-receptor activation	$8.36E-13$
hsa05224	Breast cancer	$1.47E-12$
hsa04932	Nonalcoholic fatty liver disease	$3.60E-12$
hsa05152	Tuberculosis	$4.16E-12$
hsa04064	NF-kappa B signaling pathway	$1.41E-11$
hsa04620	Toll-like receptor signaling pathway	$1.41E-11$

144 items through KEGG pathway analysis, and the top 30 items were screened out based on the corrected *P* value, and a bubble chart (Figure 5(b) and Table 2) and a cell cycle pathway diagram were drawn (Figure 5(c)).

3.5. Analysis of MYC Gene-Targeted Drugs. Having reviewed the information collected in network pharmacology, we found that celastrol (NSC 70931) is the only drug component of TWHF that targets the *MYC* gene. We then analyzed and summarized the corresponding targets of celastrol (Table 3).

3.6. Celastrol Inhibits SW1353 Proliferation and Induces Caspase-Dependent Cell Apoptosis. We first investigated the influence of celastrol (0, 1.0, 2.0, 3.0, 4.0, and 5.0 μM) on human chondrosarcoma cells SW1353. The cell proliferation assay (Figure 6(a)) and the clone formation assay (Figure 6(b)) showed that celastrol not only inhibits the cell viability of the SW1353 cell lines in a dose-dependent manner but also in a time-dependent manner. The maximum inhibition rate of celastrol appeared at 48 hours at 5.0 μM (Figure 6(a)).

The apoptosis assay (Figure 6(c)) showed that the proportion of early and late apoptotic cells in SW1353 increased after celastrol treatment. The involved pathways were determined by Western blotting (Figure 6(d)). Celastrol inhibits the expression of the *c-myc* gene, increases the expression of cleaved PARP and cleaved caspase-3 protein, and reduces caspase-9, caspase-3, Bid, Bcl-2, Bax, and PARP protein expression. The ratio of Bcl-2/Bax was reduced by gray

Table 3: Summary of celastrol information.

Drug name	Target	Symbol
Tripterine	NR3C1	Glucocorticoid receptor
	VEGFA	Vascular endothelial growth factor A
MOL003186	CCND1	G1/S-specific cyclin-D1
	BCL2	Apoptosis regulator Bcl-2
	BCL2L1	Bcl-2-like protein 1
	BAX	Apoptosis regulator BAX
	FLT1	Vascular endothelial growth factor receptor 1
	KDR	Vascular endothelial growth factor receptor 2
	MMP9	Matrix metalloproteinase-9
	JUN	Transcription factor AP-1
	PTGS2	Prostaglandin G/H synthase 2
	BIRC5	Baculoviral IAP repeat-containing protein 5
	BIRC2	Baculoviral IAP repeat-containing protein 2
	CFLAR	CASP8 and FADD-like apoptosis regulator
	AKR1B1	Aldose reductase
	CDC37	Hsp90 cochaperone Cdc37
	MMP2	72 kDa type IV collagenase
	TIMP1	Metalloproteinase inhibitor 1
	TIMP2	Metalloproteinase inhibitor 2
	MMP1	Interstitial collagenase
	MYC	Myc proto-oncogene protein
	FNDC3B	Fibronectin
	COL7A1	Collagen alpha-1 (VII) chain
	COL4A4	Transforming growth factor beta-1
	RELA	Collagen alpha-4 (IV) chain

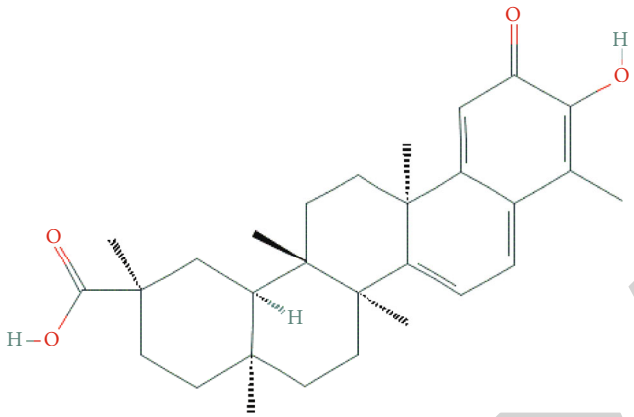

analysis. Above that, the apoptosis caused by *Tripterygium wilfordii* may be related to the mitochondrial signaling pathway.

The results of cell cycle detection by flow cytometry (Figure 7(a)) showed that the proportion of cells in the G2 phase in the control group and the 0.5, 1.0, and 1.5 μM triptoergrin intervention groups were 14.07%, 25.79%, 24.07%, and 22.45%, respectively, which indicate that the drug can block the cell cycle of chondrosarcoma at the G2/M stage and is concentration dependent. When the concentration of TWHF reaches 1 μM (about half of the IC50), the maximum arrest in the G2/M stage occurs accompanied by an increase in the proportion of the S phase. Western blotting assay showed that the expression of cell cycle regulatory proteins p21, cyclin D1, cyclin B1, and Cdc2 was downregulated (Figure 7(b)), which may be the direct cause of G2/M phase arrest.

3.7. Measure the Radiosensitivity of SW1353 Cells. SW1353 cells were irradiated with 2, 4, 6, and 8 Gy to determine their radiosensitivity. As shown in Figure 7(c), the colony survival rates calculated based on the number of communities in the radiotherapy group/the number of communities in the NC group were 71.3%, 29.3%, 58%, and 0.0%, respectively. The cell survival rate was significantly reduced in a dose-dependent manner. In order to rule out that the intensity of radiotherapy directly leads to cell death, the radiation dose of 2 Gy is used in subsequent radio sensitization experiments.

3.8. Celastrol Achieves the Effect of Radiotherapy Sensitization by Inducing G2/M Phase Arrest. According to the clone formation experiment (Figure 8(a)), the average number of colonies in the NC, celastrol, 2 Gy, and celastrol + 2 Gy groups with a seeding density of 200/well were 81, 54, 51, and 9, respectively, and the colony formation rate in the celastrol + 2 Gy group is significantly reduced. Western blot analysis showed (Figure 8(b)) that the expression of cell cycle regulatory proteins cyclinB1 and p21, Cdc2, and cyclinD1 in the celastrol and celastrol + 2 Gy groups was downregulated. Apoptosis-related proteins c-myc, caspase-9, caspase-3, Bid, Bcl-2, Bax, and PARP protein expression decreased, while cleaved PARP and cleaved caspase-3 protein expression increased. The result confirms that the combination therapy promotes the apoptosis of chondrosarcoma, which is attributed to the radiosensitization effect of celastrol by downregulating the expression of c-myc and inducing the G2/M phase arrest and the induction of chondrosarcoma apoptosis through the mitochondrial signaling pathway.

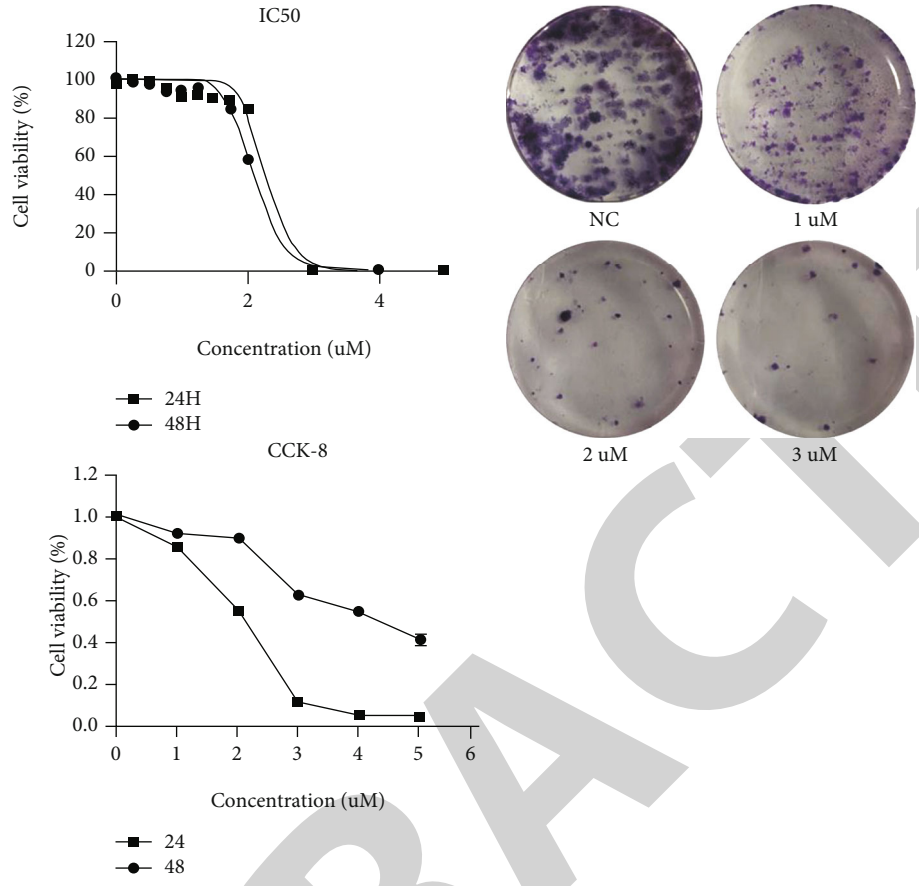

Figure 6: Continued.

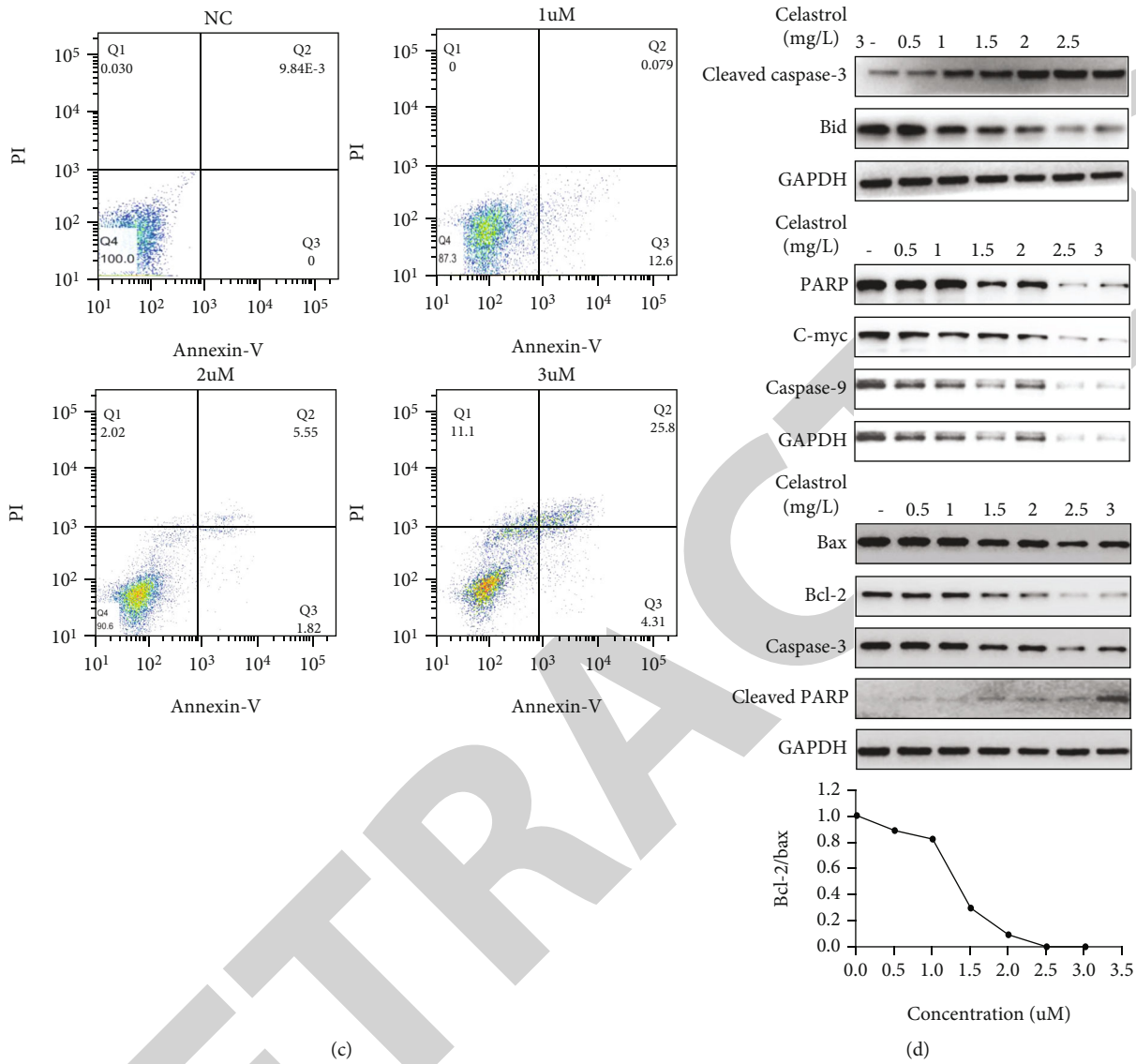

Figure 6: TWHF inhibits the proliferation of osteosarcoma cells by inhibiting the expression of the C-myc gene and induces caspase-dependent cell apoptosis. (a) Cell survival rate and drug IC50. (b) Colony formation assay. (c) Flow cytometry assay. (d) Western blotting detects the caspase-dependent apoptosis pathway.

4. Discussion

Chondrosarcoma was strongly resistant to X-rays, which has caused great limitations in the treatment of chondrosarcoma [7]. Accumulating evidence indicates that cell cycle G2/M phase arrest is one of the key factors to enhance the sensitivity of radiotherapy [15, 28, 29]. Inhibition of *c-myc* expression can effectively inhibit tumor cell proliferation and induce G2/M phase arrest and apoptosis of sarcoma cells [15, 30–33]. This study shows that celastrol can effectively inhibit the expression of the *c-myc* gene and significantly inhibit the growth of tumors. At the same time, celastrol can promote the radiosensitization caused by G2/M phase arrest by inhibiting the expression of the c-myc gene and enhance the apoptosis caused by the mitochondrial signaling pathway.

Through bioinformatics analysis, we found that the *MYC* gene is highly expressed in a variety of tumor and sarcoma cell lines to varying degrees and is negatively correlated with the OS of patients. Many components of TWHF have been confirmed to have antitumor activity, but no reports have been found on drug components directly related to the MYC gene [34, 35]. Through the network pharmacology summary, we revealed that *Tripterygium wilfordii* has the characteristics of multicomponent, multipathway, multitarget, multibiological function, etc., playing a therapeutic effect on chondrosarcoma, and found its biological process in GO enrichment analysis (BP is related to response to radiation, CC is related to cyclin-dependent protein kinase, and MF is related to transcription factor binding). This laid the foundation for us to find a good radiosensitizer and *MYC* gene inhibitor in

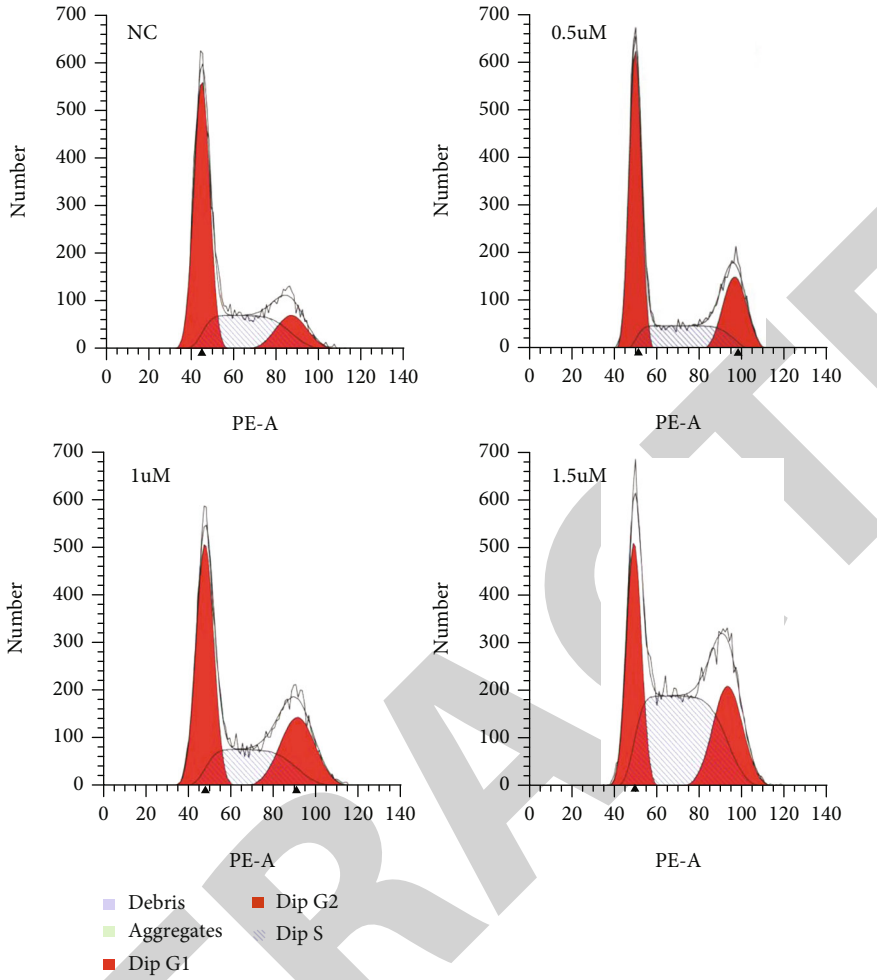

(a)

Radiation dose	0GY	2GY	4GY	6GY	8GY
Number of colonies	83	57	22	4	0
	80	54	25	6	0
	78	60	23	4	0
Mean	80	57	23	5	0
Survival rate		71.3%	29.3%	5.8%	0%

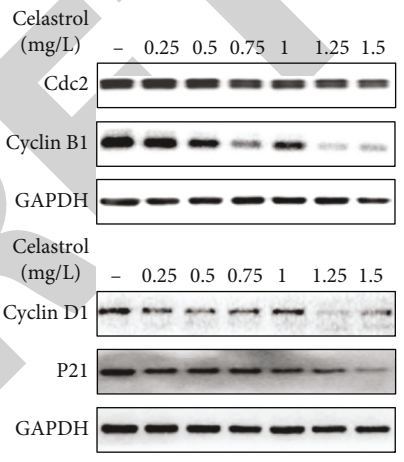

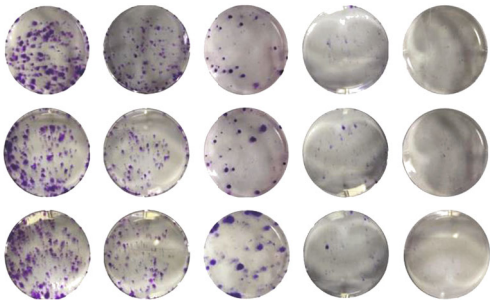

(b)

Figure 7: Continued.

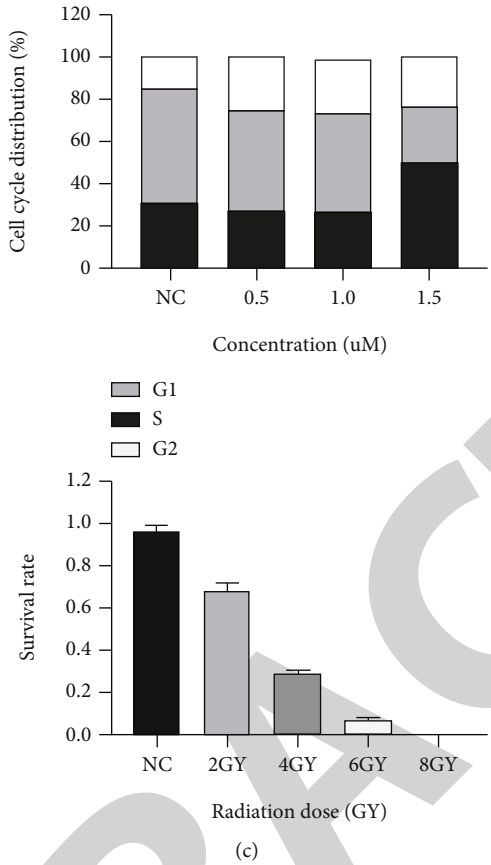

Figure 7: Celastrol influences the cell cycle of SW1353 by regulating cell cycle regulator proteins and assesses its radiosensitivity. (a) Flow cytometry analysis. (b) Western blotting. (c) SW1353 cells were irradiated with 0, 2, 4, 6, and 8 Gy, colony formation experiments were performed, and the radiosensitivity of the cells was evaluated.

the active ingredients of TWHF. The proto-oncogene *c-myc* encodes a transcription factor c-Myc, which is greatly important in controlling cell growth and vitality. The quantity of c-Myc is carefully controlled by many mechanisms, and its actions to induce and repress genes are modulated by interactions with other regulatory proteins. Previous studies showed that celastrol inhibits chondrosarcoma proliferation, migration, and invasion through suppression of the CIP2A/c-MYC signaling pathway. We discovered that celastrol was the only active component of the drug related to the *MYC* gene, and its drug targets are mostly related to radiation, which is consistent with the literature report [36].

Radiotherapy has become an important part of cancer treatment [37]. Radiation therapy induces apoptosis by destroying DNA and inhibiting checkpoint activation of the cell cycle [38, 39]. As a response to DNA damage, cells mainly stagnate at the junction of cell checkpoints G1/S and G2/M, which is the core mechanism that controls DNA replication and repair and cell division in eukaryotic cells [15]. G1/S arrest prevents damaged DNA from entering the S phase, and G2/M arrest prevents damaged DNA from entering mitosis. Therefore, in order to deal with DNA damage, normal cells prevent the activation of Cdc2/cyclin B through various mechanisms, such as the cytoplasmic isolation of the key components of Cdc2 activation (cyclin B and Cdc25C) [10, 15]. Therefore, how to reduce the cyclin B1/Cdc2 complex and induce cell G2/M arrest is the key to sensitizing tumor cells to the effect of radiotherapy.

Tumor cells have a strong ability to proliferate and are accompanied by cell cycle disorders. The *c-myc* gene can directly induce the high expression of the cell cycle-regulating genes CDC2-L1 and Cyclin B1 and can maintain the abnormally high expression of cyclin B1 under the induction of ionizing radiation (IR), causing the cells with DNA damage to enter inappropriately the S phase, thereby enhancing the resistance to ionizing radiation [15, 30, 40].

In *in vitro* experiments, we found that celastrol can effectively inhibit the expression of the *c-myc* gene and reduce the expression of cyclin B1 and Cdc2 (CDK1) proteins, resulting in chondrosarcoma cell G2/M phase arrest and effective inhibition proliferation of chondrosarcoma cells [29, 41]. Although c-Myc gene is related to caspase-3 related pathways to promote cell apoptosis, inhibiting the cyclin B1/Cdc2 complex and inducing G2/M phase arrest are still the main driving forces for inhibiting the

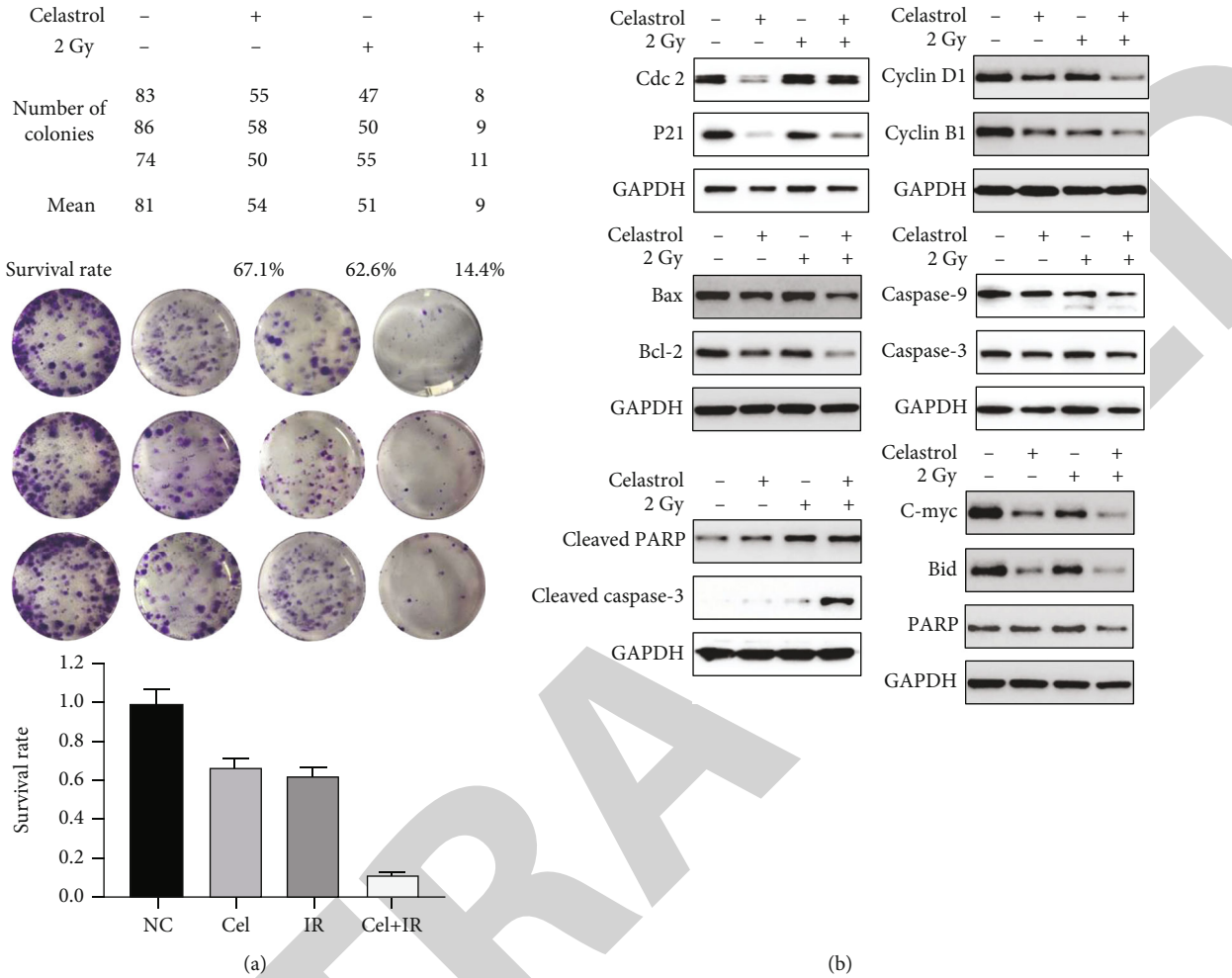

Figure 8: Celastrol downregulates the c-myc gene and induces G2/M phase block to cause radiosensitization of SW1353 cells. (a) The radiosensitization caused by celastrol was detected by the colony formation experiment. (b) Western blotting proved that the radiosensitization effect caused by t celastrol is to induce SW1353 cell apoptosis through the regulation of cycle regulator proteins and through the mitochondrial signaling pathway.

c-myc gene to control tumorigenesis [11, 16, 28]. We also found that the expression of P21 protein in chondrosarcoma cells decreased with the increase of drug concentration, which may be related to the multitarget effect of celastrol and the time of action of drugs or radiation. Further research is needed [5, 7, 42]. In vitro experiments confirmed that celastrol can interfere with cyclin-dependent protein kinases by inhibiting the *MYC* gene-encoding transcription factors and lead to radiosensitization, which verified the accuracy of the conclusions of network pharmacology.

In summary, this study proved that celastrol can inhibit the proliferation of chondrosarcoma cells by downregulating the *c-myc* gene and induce cell cycle arrest in the G2/M phase. At the same time, the combined application of radiotherapy and celastrol makes the apoptosis rate of chondrosarcoma cells significantly higher than that of any single treatment method. This method can not only reduce the liver and kidney toxicity caused by the single use of large doses of drugs but also reduce the impact of the single use of large doses of radiotherapy on the cells of the whole body. Therefore, we believe that celastrol is a radiosensitizer that inhibits the expression of the *c-myc* gene and is an effective strategy to improve the sensitivity of clinical tumor radiotherapy, providing a new way of treatment for chondrosarcoma.

Data Availability

The authors confirm that the data supporting the findings of this study are available within the article.

Disclosure

This article contained no human participants or animals performed by any of the authors.

Conflicts of Interest

The authors declare no competing interests.

Authors' Contributions

J.Q. conceived and designed the study, participated in experimental research, and wrote this manuscript. Z.Z. searched the database and performed data analysis and participated in experimental research. X.H. and LL.Z. prepared the initial draft of the manuscript. T.X. and ZY.B. participated in the interpretation of data, helped in drafting the manuscript, and critically reviewed the manuscript. All authors read and approved the final manuscript. Jin Qian and Zhen Zhang contributed equally to this study as co-first authors.

Acknowledgments

We thank the staff of the Department of Orthopaedic Surgery for their assistance during this study. This research was supported by the Zhejiang Provincial Natural Science Foundation of China (Grant no. Q17H160012), Medical Scientific Research Foundation of Zhejiang Province, China (Grant no. 2021KY864), Scientific and Technological Developing Scheme of Hangzhou Province (Grant no. 20170533B38), and Medical Health Science and Technology Project of Zhejiang Provincial Health Commission (Grant no. 2019324649).

References

[1] E. Nazeri, M. Gouran Savadkoohi, K. Majidzadeh-A, and R. Esmaeili, "Chondrosarcoma: an overview of clinical behavior, molecular mechanisms mediated drug resistance and potential therapeutic targets," *Critical Reviews in Oncology/Hematology*, vol. 131, pp. 102–109, 2018.

[2] Z. Ouyang, S. Wang, M. Zeng et al., "Therapeutic effect of palbociclib in chondrosarcoma: implication of cyclin-dependent kinase 4 as a potential target," *Cell Communication and Signaling*, vol. 17, no. 1, p. 17, 2019.

[3] A. Italiano, O. Mir, A. Cioffi et al., "Advanced chondrosarcomas: role of chemotherapy and survival," *Annals of Oncology*, vol. 24, no. 11, pp. 2916–2922, 2013.

[4] M. Koizumi, N. G. Tanjung, A. Chen et al., "Administration of salubrinal enhances radiation-induced cell death of SW1353 chondrosarcoma cells," *Anticancer Research*, vol. 32, no. 9, pp. 3667–3673, 2012.

[5] N. Girard, E. Lhuissier, J. Aury-Landas et al., "Heterogeneity of chondrosarcomas response to irradiations with X-rays and carbon ions: a comparative study on five cell lines," *Journal of Bone Oncology*, vol. 22, 2020.

[6] A. M. van Maldegem, H. Gelderblom, E. Palmerini et al., "Outcome of advanced, unresectable conventional central chondrosarcoma," *Cancer*, vol. 120, no. 20, pp. 3159–3164, 2014.

[7] F. Chevalier, D. H. Hamdi, C. Lepleux et al., "High LET radiation OvercomesIn VitroResistance to X-rays of chondrosarcoma cell lines," *Technology in Cancer Research & Treatment*, vol. 18, 2019.

[8] O. Bloch and A. T. Parsa, "Skull base chondrosarcoma: evidence-based treatment paradigms," *Neurosurgery Clinics of North America*, vol. 24, no. 1, pp. 89–96, 2013.

[9] E. M. Meškytė, S. Keskas, and Y. Ciribilli, "MYC as a multifaceted regulator of tumor microenvironment leading to metastasis," *International Journal of Molecular Sciences*, vol. 21, no. 20, 2020.

[10] S. Littler, O. Sloss, B. Geary, A. Pierce, A. D. Whetton, and S. S. Taylor, "Oncogenic MYC amplifies mitotic perturbations," *Open Biology*, vol. 9, no. 8, 2019.

[11] L. M. Boxer and C. V. Dang, "Translocations involving c-_myc_ and c- _myc_ function," *Oncogene*, vol. 20, no. 40, pp. 5595–5610, 2001.

[12] M. Li, Y. Liu, Y. Wei et al., "Zinc-finger protein YY1 suppresses tumor growth of human nasopharyngeal carcinoma by inactivating c-Myc-mediated _microRNA-141_ transcription," *The Journal of Biological Chemistry*, vol. 294, no. 15, pp. 6172–6187, 2019.

[13] J. K. Mito, X. Qian, V. Y. Jo, and L. A. Doyle, "MYC expression has limited utility in the distinction of undifferentiated radiation-associated sarcomas from sporadic sarcomas and sarcomatoid carcinoma," *Histopathology*, vol. 77, no. 4, pp. 667–672, 2020.

[14] D. Dominguez-Sola, C. Y. Ying, C. Grandori et al., "Non-transcriptional control of DNA replication by c-Myc," *Nature*, vol. 448, no. 7152, pp. 445–451, 2007.

[15] J. H. Sheen, J. K. Woo, and R. B. Dickson, "c-Myc alters the DNA damage-induced G2/M arrest in human mammary epithelial cells," *British Journal of Cancer*, vol. 89, no. 8, pp. 1479–1485, 2003.

[16] H. J. Cho, Y. J. Oh, S. H. Han et al., "Cdk1 Protein-mediated Phosphorylation of Receptor-associated Protein 80 (RAP80) Serine 677 Modulates DNA Damage-induced G_2/M Checkpoint and Cell Survival," *The Journal of Biological Chemistry*, vol. 288, no. 6, pp. 3768–3776, 2013.

[17] Y. Liu, S. Tu, W. Gao et al., "Extracts of *Tripterygium wilfordii* Hook F in the treatment of rheumatoid arthritis: a systemic review and meta-analysis of randomised controlled trials," *Evidence-Based Complementary and Alternative Medicine*, vol. 2013, Article ID 410793, 11 pages, 2013.

[18] T. W. Corson and C. M. Crews, "Molecular understanding and modern application of traditional medicines: triumphs and trials," *Cell*, vol. 130, no. 5, pp. 769–774, 2007.

[19] L. Tu, P. Su, Z. Zhang et al., "Genome of *Tripterygium wilfordii* and identification of cytochrome P450 involved in triptolide biosynthesis," *Nature Communications*, vol. 11, no. 1, p. 971, 2020.

[20] D. Qiu and P. N. Kao, "Immunosuppressive and anti-inflammatory mechanisms of triptolide, the principal active diterpenoid from the Chinese medicinal herb *Tripterygium wilfordii* Hook. f," *Drugs in R & D*, vol. 4, no. 1, pp. 1–18, 2003.

[21] H. Yang, D. Chen, Q. C. Cui, X. Yuan, and Q. P. Dou, "Celastrol, a triterpene extracted from the Chinese "Thunder of God Vine, " is a potent proteasome inhibitor and suppresses human prostate cancer growth in nude mice," *Cancer Research*, vol. 66, no. 9, pp. 4758–4765, 2006.

[22] X. Liu, P. Zhao, X. Wang et al., "Celastrol mediates autophagy and apoptosis via the ROS/JNK and Akt/mTOR signaling pathways in glioma cells," *Journal of Experimental & Clinical Cancer Research*, vol. 38, no. 1, 2019.

[23] Y. Dai, J. T. DeSano, Y. Meng et al., "Celastrol potentiates radiotherapy by impairment of DNA damage processing in human prostate cancer," *International Journal of Radiation Oncology • Biology • Physics*, vol. 74, no. 4, pp. 1217–1225, 2009.

[24] G. Sethi, K. S. Ahn, M. K. Pandey, and B. B. Aggarwal, "Celastrol, a novel triterpene, potentiates TNF-induced apoptosis and suppresses invasion of tumor cells by inhibiting NF-κB–

Hindawi
BioMed Research International
Volume 2024, Article ID 9845035, 1 page
https://doi.org/10.1155/2024/9845035

Retraction

Retracted: The Function of circRNA-0047604 in Regulating the Tumor Suppressor Gene DACH1 in Breast Cancer

BioMed Research International

Received 12 March 2024; Accepted 12 March 2024; Published 20 March 2024

This article has been retracted by Hindawi following an investigation undertaken by the publisher [1]. This investigation has uncovered evidence of one or more of the following indicators of systematic manipulation of the publication process:

(1) Discrepancies in scope

(2) Discrepancies in the description of the research reported

(3) Discrepancies between the availability of data and the research described

(4) Inappropriate citations

(5) Incoherent, meaningless and/or irrelevant content included in the article

(6) Manipulated or compromised peer review

The presence of these indicators undermines our confidence in the integrity of the article's content and we cannot, therefore, vouch for its reliability. Please note that this notice is intended solely to alert readers that the content of this article is unreliable. We have not investigated whether authors were aware of or involved in the systematic manipulation of the publication process.

Wiley and Hindawi regrets that the usual quality checks did not identify these issues before publication and have since put additional measures in place to safeguard research integrity.

We wish to credit our own Research Integrity and Research Publishing teams and anonymous and named external researchers and research integrity experts for contributing to this investigation.

The corresponding author, as the representative of all authors, has been given the opportunity to register their agreement or disagreement to this retraction. We have kept a record of any response received.

References

[1] B. Zhao, R. Zhou, C. Ji et al., "The Function of circRNA-0047604 in Regulating the Tumor Suppressor Gene DACH1 in Breast Cancer," *BioMed Research International*, vol. 2022, Article ID 6589651, 10 pages, 2022.

Hindawi
BioMed Research International
Volume 2022, Article ID 6589651, 10 pages
https://doi.org/10.1155/2022/6589651

Research Article

The Function of circRNA-0047604 in Regulating the Tumor Suppressor Gene DACH1 in Breast Cancer

Bingkun Zhao,[1,2,3] Rong Zhou,[1] Changle Ji,[2] Diya Liu,[2] Tianqi Wu,[2] Hui Xu,[2] Dongmei Lan,[4] Chao Yao,[4] Yuanzhi Xu ,[1] and Lin Fang [1,2]

[1]*Department of Stomatology, Shanghai Tenth People's Hospital, Tongji University School of Medicine, Shanghai 200072, China*
[2]*Department of Breast and Thyroid Surgery, Shanghai Tenth People's Hospital, Shanghai 200072, China*
[3]*Department of Plastic Surgery, Affiliated Hospital of Xuzhou Medical University, Xuzhou, Jiangsu 221000, China*
[4]*Medical College of Anhui University of Science and Technology, Huainan, Anhui 232000, China*

Correspondence should be addressed to Yuanzhi Xu; amyxyz01@hotmail.com and Lin Fang; fanglin2017@126.com

Received 29 September 2021; Revised 14 December 2021; Accepted 17 December 2021; Published 20 January 2022

Academic Editor: Jun Yang

Breast cancer is the most common cancer among females. Dachshund Homolog 1 (DACH1) gene is regarded as an important tumor suppressor gene in breast cancer which plays an important regulatory role in the development disease progression, particularly in carcinomas. Circular RNAs (circRNAs) and microRNA (miRNA), regarded as a novel group of noncoding RNAs, are always involved in regulating gene expression. In this work, hsa_circ_0047604 expressed lower in breast cancer tissue and played the role of sponge of miR-548o. By this way, hsa_circ_0047604 could upregulate DACH1 to inhibit breast cancer. In conclusion, this study revealed that hsa_circ_0047604 acted as a tumor suppressor and regulated breast cancer progression via hsa_circ_0047604–miR-548o–DACH1 axis, which might provide a therapeutic method for breast cancer.

1. Introduction

Breast cancer is one of the most common cancers, accounting for 23% of female malignant tumors. It is the second leading cause of cancer-related death in women worldwide [1]. Although great progress has been made in recent years to improve the development of an earlier diagnosis, tumor recurrence and distant metastasis remain the most pressing problem to be solved.

Dachshund Homolog 1 (DACH1) is a member of the DACH family and plays an essential role in promoting the differentiation of the *Drosophila* eye and limb subfamily of nuclear protein [2]. Results from a recent study of more than 2,000 human breast cancer cases indicate that reduction of DACH1 is correlated with a poor breast cancer prognosis [3]. Accordingly, it is found that it can inhibit breast tumor growth and suppress oncogene-induced breast cancer cell migration and invasion [3, 4]. Moreover, DACH1 is involved in a broad variety of signal transduction pathways and may act as a significant target gene for ER (estrogen receptor) negative breast cancer patients [5]. Therefore, it is important to identify the mechanism of DACH1 downregulation in breast cancer.

More and more evidence confirmed that noncoding RNA (ncRNA) plays an important role in mediating breast cancer genesis and progression [6]. MicroRNAs (miRNA) are small noncoding RNAs with nucleotides of 19-25 in length that can regulate posttranscription gene expression. They can combine to the 3′-untranslated regions (UTR) of target mRNAs to block translation [7]. Circular RNAs (circRNAs) belong to the endogenous noncoding RNAs (ncRNAs) which is formed from exons or introns through special selective shearing [8]. It is a single-stranded covalently closed circular transcripts which make it more stable and harder to degrade in cells [9]. Recently, circRNAs have been confirmed as diagnostic biomarkers of many diseases like cardiovascular diseases, rheumatoid arthritis, kidney disease, and cancer [10–13]. Nowadays, the underlying mechanism of circRNA function significantly lies in the miRNA or protein sponges, enhancer of protein function,

protein scaffolding, protein recruitment, and templates for peptides translation [9]. So it cannot be overlooked that circRNA plays an important role in regulating tumor-associated genes.

Given that they play a significant role in regulating genes, miRNA is often involved in various biological and pathological processes, such as proliferation, morphogenesis, apoptosis, and carcinogenesis [14]. It is reported that half of human miRNAs are located in cancer-related regions, indicating that miRNA could function as a critical part of tumor development [15]. Accordingly, miRNA is a significant feature in cancer-associated gene dysfunction, and thus, can not only improve cancer diagnosis success rates but also provide a range of clinical applications with targeted research [16]. miR-548o has a highly putative function because it can directly combine to and suppress the expression of DACH1 according to bioinformatics analysis. However, the function of miR-548o in tumor development remains to be researched at length.

Circ_0047604 originated from mothers against decapentaplegic homolog 2 (SMAD2). SMAD family has distinct effects on mammary development and homeostasis [17]. From previous research, upregulate and stabilize SMAD2 protein would contribute to breast cancer progression [18, 19], but the function of circ_0047604 is still unknown.

In this work, we have confirmed that circ_0047604 exerted its antioncogenic role in breast cancer *via* acting as a sponge of miR-548o to regulate DACH1 expression. This study was the first to provide an insight into the mechanism by circRNA regulating DACH1.

2. Materials and Methods

2.1. Tumor Sample. Tumor and their adjacent normal tissues from breast cancer patients without any treatment before surgery were collected from the Department of Breast and Thyroid Surgery of Shanghai Tenth People's Hospital of Tongji University (Shanghai, China) with patients informed and consent. Our study was approved by Institutional Ethics Committees of Shanghai Tenth People's Hospital (approval number: SHSY-IEC-KY-4.0/17-83/01) and adhered to the standards outlined in the Declaration of Helsinki.

2.2. Cell Culture. The breast cancer cell line MDA-MB-231, MCF-7, and the nonmalignant breast epithelial cell line MCF-10A were acquired from The Chinese Academy of Sciences in Shanghai, China. First, these cells were cultured in a Dulbecco Modified Eagle Medium (DMEM) (Gibco, USA) and supplemented with 10% Fetal Bovine Serum (FBS) (Gibco), penicillin (100 units/ml), and streptomycin (100 μg/ml) (Enpromise, China). Second, these cells were incubated in an incubator at 37°C in a humidified chamber supplemented with a 5% CO_2 environment. Finally, these cells were split at a ratio of 1 : 3 for every 2-3 days when cell confluence reached approximately 80-90%.

2.3. Transfection Assay. The miR-548o mimic, inhibitor, and negative control (NC) were synthesized by Shanghai Genepharma Co., Ltd. (Shanghai, China). Si-RNA specifically targeting hsa_circ_0047606 (si-circ_0047604), negative control (NC) was purchased from IBSBio (Shanghai, China), and a lentivirus plasmid containing circ_0053063 was assembled by ZORIN (Shanghai, China). Plasmid extraction was finished by DNA Midiprep Kits (Qiagen, Hilden, Germany). First, six-well plates were used to culture transfected cells with 1.2×10^6 cells per well. No serum DMEM was added. Second, the MiR-548o mimics, miR-548o inhibitor, circ_0047604 circ_0047604, and (negative control) NC were transfected by using Lipofectamine 3000 (Invitrogen, Carlsbad, CA, USA) according to the manufacturer instructions when the cells reached 30-50%. Third, after 12 hours of incubation, the DMEM medium was substituted for DMEM with 10% FBS. Finally, all cells were incubated at 37°C in a CO_2 incubator for 36 hours prior to further testing.

2.4. Western Blot Analysis. After transfection, cells were washed twice with precooling PBS and resuspended in a RIPA lysis buffer (100 μL/well, Beyotime). After the cell lysate was collected, it was centrifuged for 20 minutes at 4°C (Eppendorf 5804R, Eppendorf Biotech, Germany). The supernatants were collected, and the protein concentrations were quantified using the BCA protein assay kit (Beyotime). 6 × SDS loading buffers (Beyotime) were added to the extracted protein samples, and these samples were degenerated at 100°C for 10 minutes. The total protein was separated by using 10% sodium dodecyl sulfate polyacrylamide gel electrophoresis (SDS-PAGE, Beyotime) and transferred to a 0.45 μm nitrocellulose membrane (Beyotime). This membrane was incubated overnight at 4°C with primary antibodies against DACH1 (1 : 2,000; Bioworld Technology, China) and β-actin (1 : 3,000; Bioworld Technology, China). After incubation, the membranes were washed with PBST, and secondary antibodies were used to incubate the washed membranes for 60 minutes at room temperature. Finally, immune reactive protein bands were detected using The Odyssey Scanning System.

2.5. Quantitative Reverse-Transcription PCR (qRT-PCR). In accordance with manufacturer protocol, the total RNA was extracted from the cells or tissues using TRIzol (Invitrogen, Carlsbad, CA, USA). The PCR parameters for relative quantification were as follows: 2 minutes at 95°C, followed by 40 cycles of 45 seconds at 57°C and 45 seconds at 72°C. The relative expression was evaluated following the relative quantification equation: $2^{-\Delta\Delta CT}$. Each sample was tested in triplicate. Primers used in this article are presented in Supplementary Table 1.

2.6. Dual-Luciferase Reporter Assay. 293T cells were seeded in 48 well plates (BD, USA) and cultured until they reached 80% confluence. The mRNA sequence of the hsa_circ_0047604 and DACH1 3′UTR segments, along with the predicted miR-548o binding sites, and the corresponding mutant constructs of the miR-548o binding site was designed and synthesized by IBSBio (Shanghai, China). Cells were cotransected with the constructed reporter plasmids, together with miR-548o or NC using Lipofectamine® 2000 (Invitrogen; Thermo Fisher Scientific, USA). Finally, after

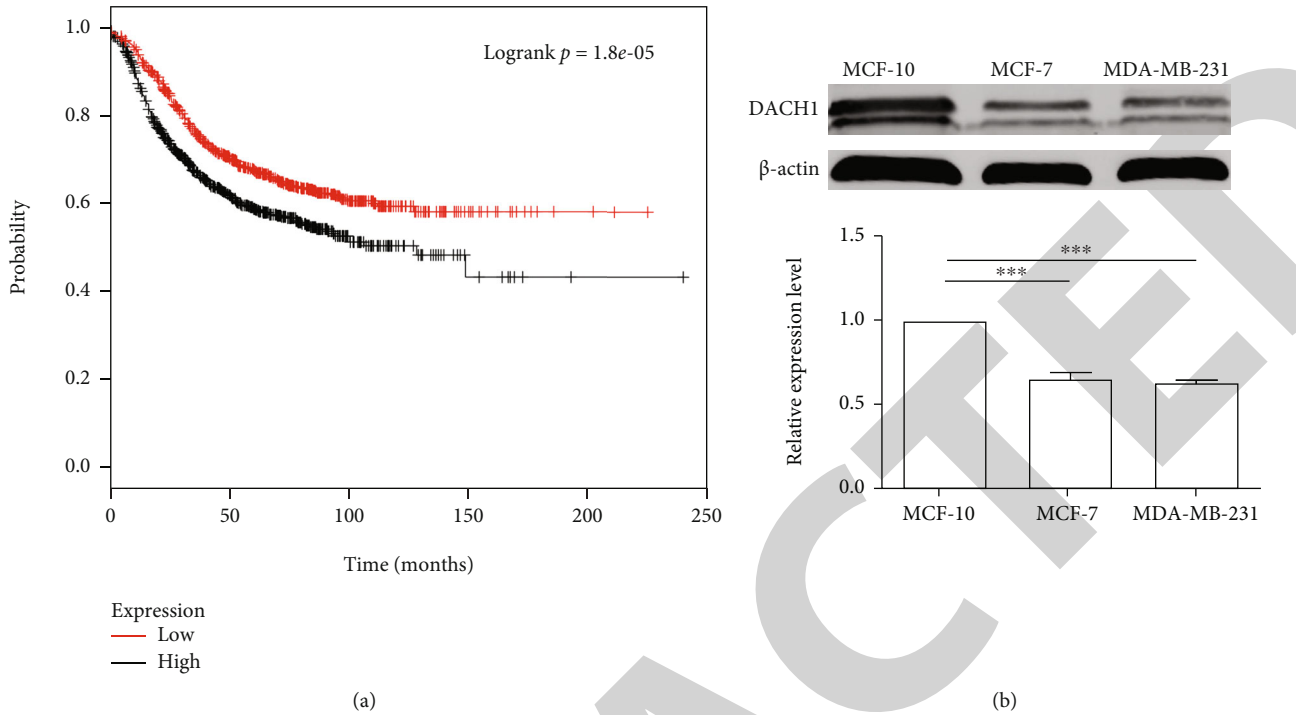

Figure 1: Survival related to expression level of DACH1 and its expression level in cell lines. (a) The expression level of DACH1 relationship with survival rate. (b) The expression level of DACH1 is also lower in MCF-7 and MDA-MB-231 compared with MCF-10. The graph represents the compared values ± SD; $^{***}P < 0.001$.

48 hours, firefly and renilla luciferase activities were measured using a Dual Luciferase Assay (Promega, Madison, WI, USA). The firefly luciferase activity was normalized to renilla, and the ratio of firefly to renilla was presented.

2.7. Cell Proliferation Assay. The CCK8 assay kit (Sigma, Santa Clara, CA, USA) was applied in accordance with manufacturer instructions to detect for cell proliferation. The transfected cells (2×10^3 cells/well) were seeded into 96-well plates and incubated overnight at 37°C with a 5% CO_2 environment. Cell proliferation was assessed after replacing medium by 10 μL CCK-8 assays plus 200 μL culture medium per well at 24, 48, 72, and 96-hour intervals. Two hours after incubation, an optical density of 450 nm wavelength was determined at room temperature using a microplate spectrophotometer. Each sample was tested with five replicates.

2.8. Wound Healing Assays. Cells were seeded in 12-well plates with 1 mL cell culture medium. After seeding density reach 90%, we produced a scratch by using 1000 μL pipette tip. The scratch area was accessed after 0 h, 24 h by microscope.

2.9. Colony Formation Assay. 800 cells were separately seeded in 12-well plates after transfection. After 7 days, when the colonies were visible, the culture was terminated and the plates were washed twice with phosphate-buffered saline (PBS) to remove this medium. These colonies were fixed using 95% ethanol for 10 minutes and dried and stained with 0.1% crystal violet solution for another 10 minutes. Each plate was washed three times with water.

2.10. Bioinformation Analysis. A survival analysis of the DACH1 and miR-548o relationship was carried out using patient data by reference to the following website (http://kmplot.com) including all cancer stage and pathological type [20].

The predicted miRNA for targeting DACH1 and miRNA potential target of circRNA was selected by starbase (http://starbase.sysu.edu.cn/) [21]. Expression data including miR-548o and DACH1 relationship was also identified by starbase (http://starbase.sysu.edu.cn/).

2.11. Statistical Analysis. This data was calculated using the mean ± the standard deviation (SD) of at least three independent experiments. Student t-tests and one-way ANOVA were used to evaluate the differences between each group using SPSS 20.0 software. These differences were considered significant for P values < 0.05.

3. Results

3.1. Breast Cancer with Low Expression of DACH1 Has a Poor Outcome in Breast Cancer Patients, and DACH1 Is Underexpressed in Breast Cancer Cell Line. A lower level of expression was found for DACH1, and this has been related to tumor development and progression [22–24]. The DACH1 expression level in 1809 patients was analyzed using Kaplan-Meier Plots. It was shown that this lower level of expression in breast cancer was significantly correlated with a lower survival rate as showed in Figure 1(a). The expression level of DACH1 in the MDA-MB-231, MCF-7, and MCF-10A breast cancer cell lines was further identified.

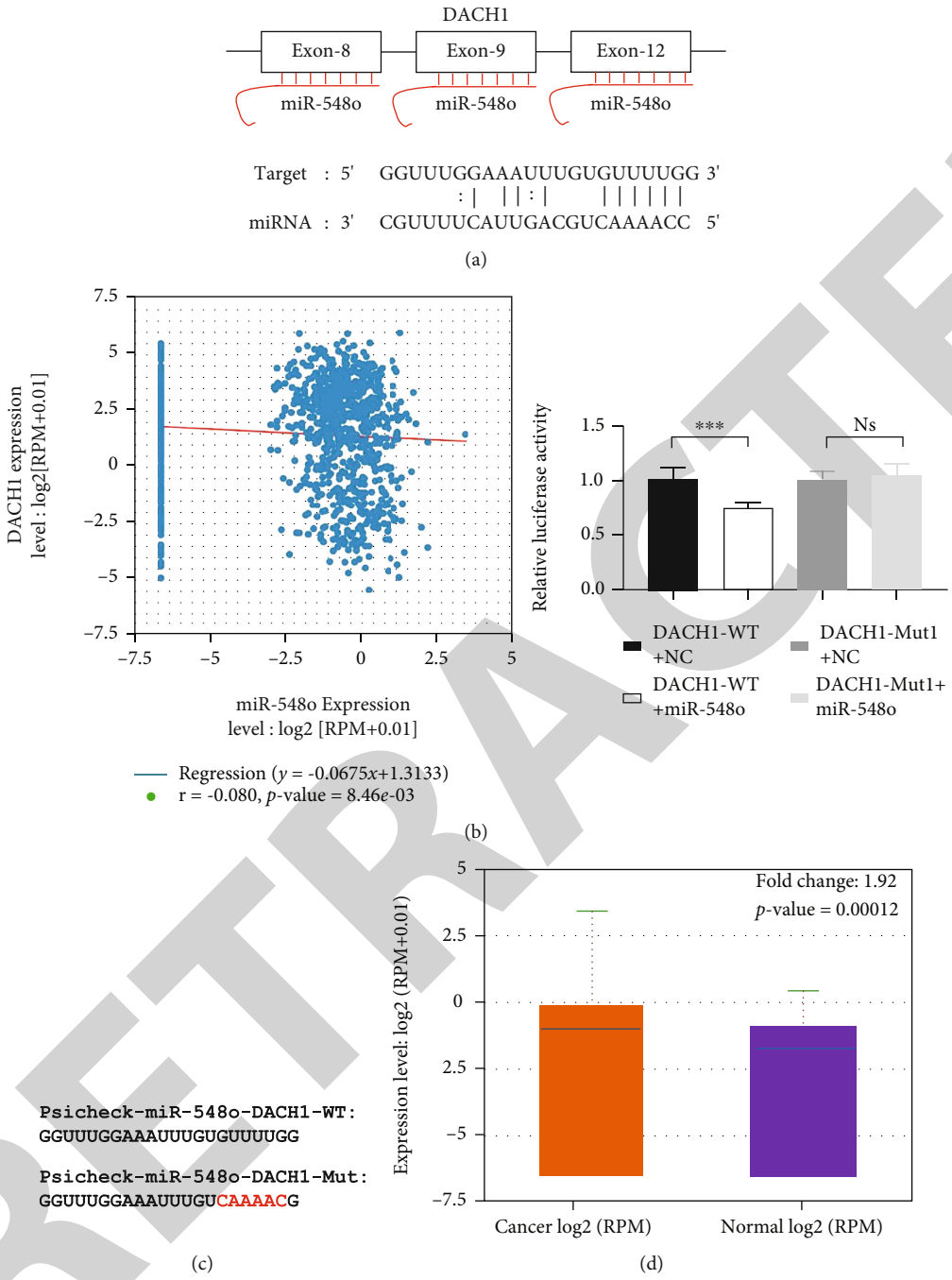

Figure 2: Continued.

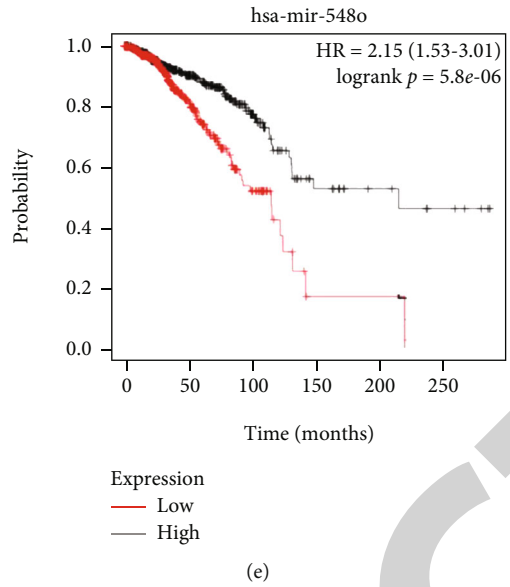

(e)

Figure 2: DACH1 is a direct target of miR-548o. (a) The binding site for miR-548o in 3′-UTR of DACH1 mRNA. (b) The coexpression level between DACH1 and miR-548o. (c) The wild and the mutation sequence of the binding site. The relative luciferase activity was measured in 293T cells after cotransfecting the DACH1 luciferase construct with either miR-548o or NC. (d) The expression level of miR-548o. (e) The expression level of miR-548o relationship with survival rate. $^{*}P < 0.05$, $^{**}P < 0.01$, $^{***}P < 0.001$.

These results show that the DACH1 expression level is also downregulated and is consistent with reported clinical results (Figure 1(b)).

3.2. miR-548o Directly Targets DACH1 in Breast Cancer Cells. The database of starbase indicated a strong possibility that miR-548o could be a candidate regulator in binding microRNAs to DACH1 mRNA (Figure 2(a)). To investigate whether miR-548o can bind to DACH1 3′-UTR, a luciferase reporter assay was carried out in 293T cells. The DACH1 original 3′-UTR predicted region was replaced by a mutation sequence as shown in Figure 2(b). As shown in Figure 2(b), the luciferase activity decreased after cotransfection with psi-CHECK-2/DACH1 3′-UTR and miR-mimics in comparison with control groups. This supports that miR-548o specifically binds to the 3′-UTR of DACH1 mRNA. From correlation between miRNA-548o and DACH1 expression level, it is shown that miRNA-548o and DACH1 showed negative correlation in 1085 breast cancer samples (Figure 2(c)). miR-548o showed a higher expression level, and higher expression of miR-548o showed a poorer survival rate (Figures 2(d) and 2(e)).

3.3. Increase miR-548o Expression Level Will Promote the Proliferation of Breast Cancer Cells. Given that miR-548o has an absent function in tumors, the miR-548o mimics and the miR-548o inhibitor were transfected into MDA-MB-231 and MCF-7 cells to investigate the impacts of miR-548o functions in breast cancer cells. CCK8 assays were used to assess cell proliferation at 24, 48, 72, and 96-hour intervals after the miR-548o mimics and inhibitor were transfected and proliferation abilities was calculated. As shown in Figure 3(a), miR-548o mimics can promote cell proliferation in a time-dependent manner, while the miR-548o inhibitor produced opposite results. The colony formation assays (Figure 3(b)) also showed the same trend because miR-548o formed colony areas were more and larger than those formed under negative controls, while the miR-548o inhibitor produced opposite results. Ultimately, these results revealed that an overexpression of miR-548o can promote a cellular proliferation ability.

Further research into the migration role of miR-548o in mediating breast cancer was identified using wound healing assay. Cells transfected with miR-548o mimics and miR-548o inhibitor groups were compared to miR-NC and miR-NC inhibitor transfection groups. As is shown in Figure 3(c), the miR-548o mimics group showed an apparently smaller scratched area, while the miR-548o inhibitor group showed a contrary trend.

3.4. Circ_0047604 Is an Important Factor to Regulate miR-548o. Recent research revealed important treatment with wild-type circ_0047604 showed decreased luciferase activity, but not the mutation-type (Figure 4(b)). From western blot assays, it shows that increased circ_0047604 would upregulate DACH1 level and decreased circ_0047604 would inhibit DACH1 expression (Figure 4(c)). We further tested the DACH1 and circ_0047604 expression level. As Figures 4(d) and 4(e) show, both DACH1 and circ_0047604 expressed significant lower in tumor tissues than that in normal tissues. Pearson correlation analysis of DACH1 expression and circ_0047604 expression in 11 samples showed a markedly positive correlationship (Figure 4(f)).

3.5. Circ_0047604 Can Inhibit Cancer Cell Proliferation and Migration. At last, we further test the function of circ_0047604. Circ_0047604 can inhibit breast cancer cell proliferation (Figure 5(a)). The colony formation assays

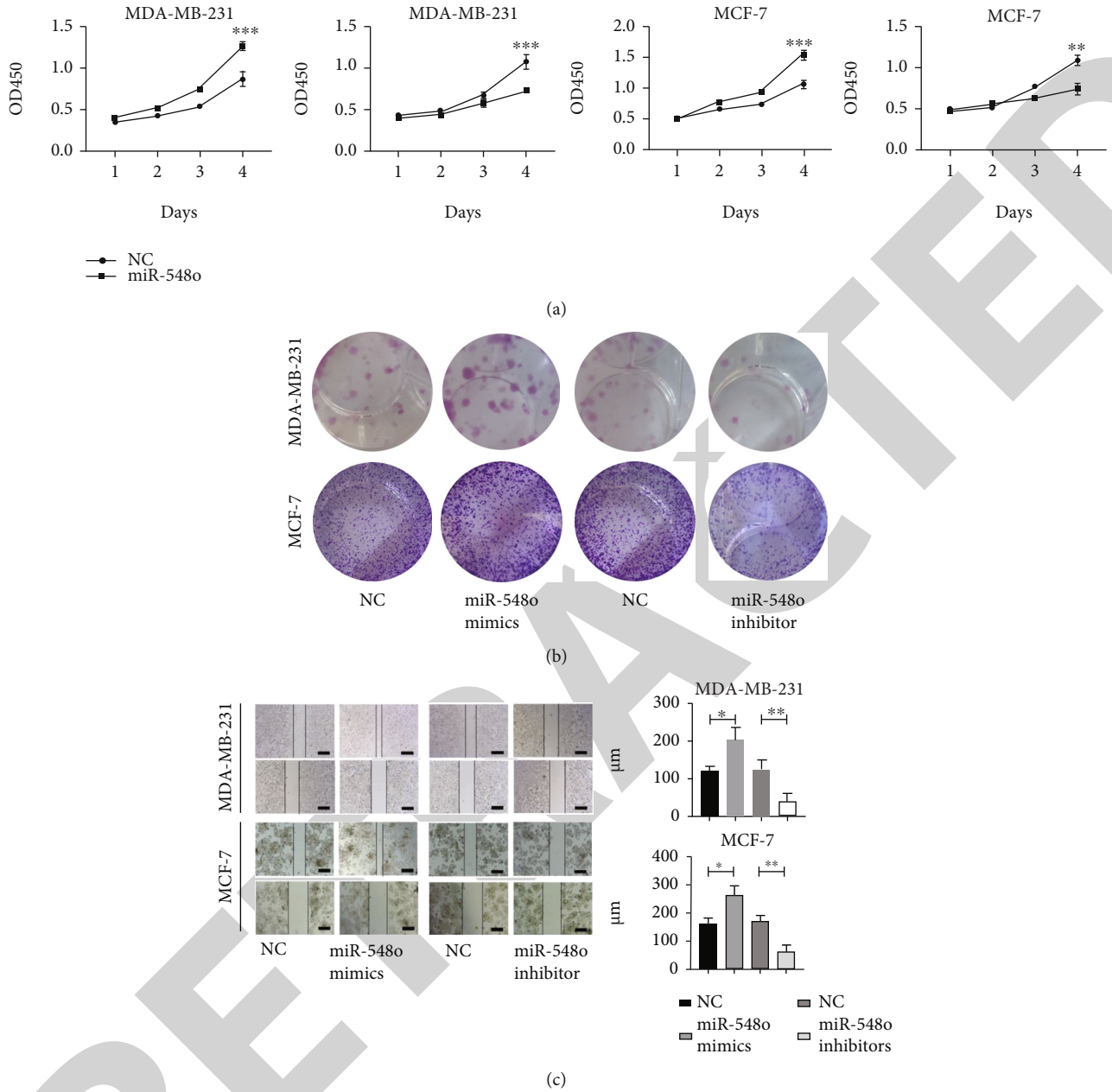

Figure 3: miR-548o can promote tumor cell growth and immigration. (a) The CCK-8 assay was carried out to monitor the proliferation level of MDA-MB-231 and MCF-7 cells at 1, 2, 3, and 4 days. (b) Images of crystal violet stained colonies of MDA-MB-231 and MCF-7 cells transfected with NC, miR-548o, and miR-548o inhibitor. (c) Wound healing assays to test cell migration after transfection of NC, miR-548o, and miR-548o inhibitor. $^{*}P < 0.05$, $^{**}P < 0.01$, $^{***}P < 0.001$.

(Figure 5(b)) also showed the same trend. From wound healing assays, it is shown that overexpressed circ_0047604 can inhibit cell migration and inhibition of circ_0047604 could act as a carcinogenic factor.

4. Discussion

According to recent studies, DACH1 is identified as an important marker related to breast cancer prognosis [25]. These studies indicate that the presence of DACH1 in different tumors indicates that it can suppress the growth and invasion of tumor cells through a signal pathway in a variety of researches [26–29]. Previous reports have implicated that DACH1 could suppress tumor cell proliferation, migration, and invasion by mediating other important biomarkers, such as Estrogen Receptor-α, Peroxiredoxin 3, Wnt/β-catenin signaling Smad4, and TGF-β [5, 30–33].

MicroRNA is often involved in many aspects of biology, including embryogenesis, aging, metabolism, and immunity. However, the microRNAs related to the pathogenesis and progression of various human diseases are considerably more important [34]. A novel class of drugs called antimirs and miRNA-mimics capable of regulating miRNA level is currently in various stages of preclinical and clinical

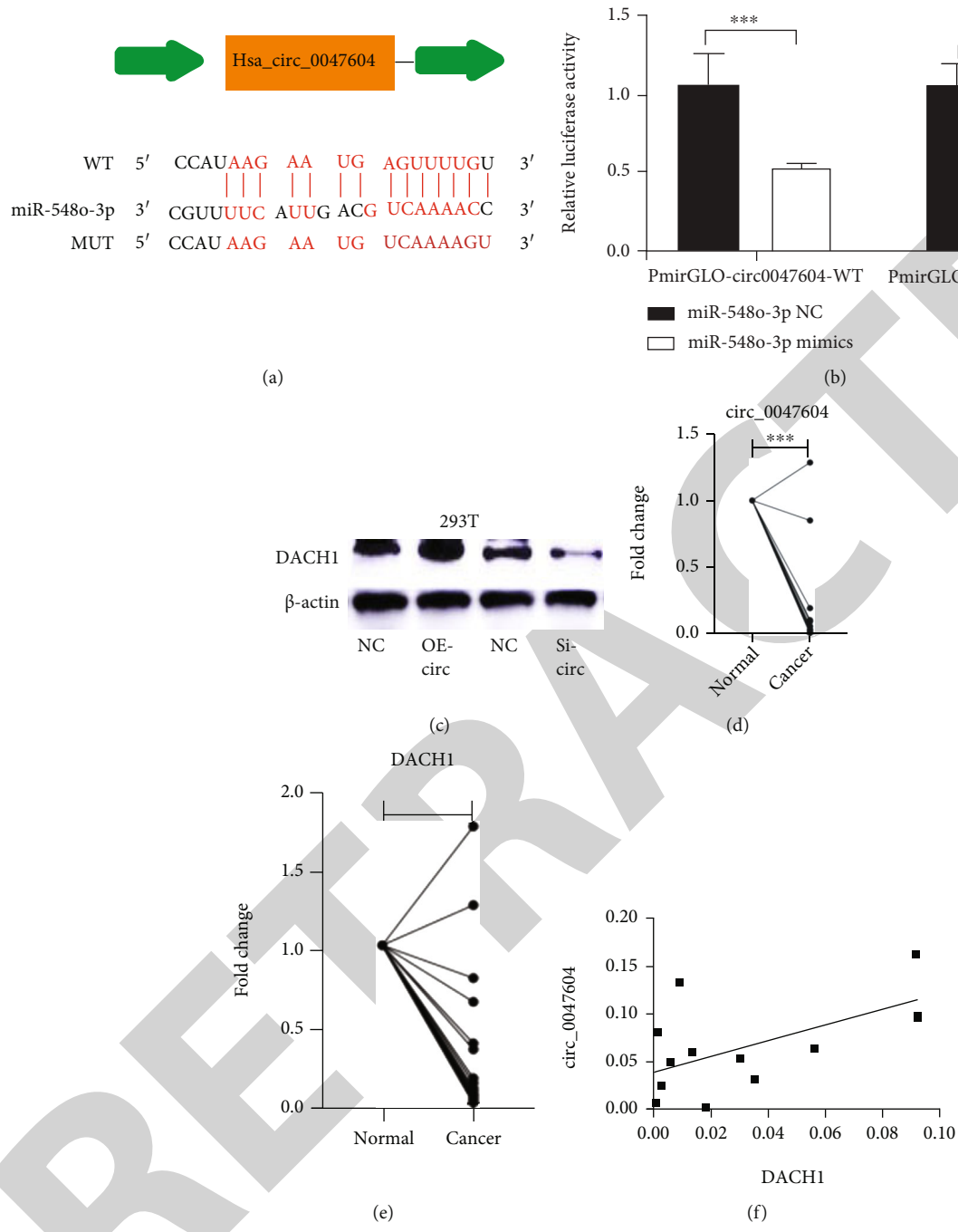

Figure 4: Circ_0047604 can be a sponge of miR-548o. (a) The binding site for miR-548o in circ_0047604. (b) The wild and the mutation sequence of the binding site. The relative luciferase activity was measured in 293T cells after cotransfecting the circ-0047604 luciferase construct with either miR-548o or NC. (c) DACH1 expression level after up/downregulating circ_0047604. (d) and (e) The expression levels of DACH1 and circ_0047604 in tumor tissues. (f) The coexpression level between DACH1 and circ_0047604. $^{*}P < 0.05$, $^{**}P < 0.01$, $^{***}P < 0.001$.

testing. This brings about the hope that someday a miRNA-based therapeutic approach can be used to treat common human diseases [35]. The function of miR-548o on tumors has not yet been reported, and almost no research has been conducted on miR-548o. In this study, it has been shown that miR-548o can regulate DACH1 expression directly and can enhance both the proliferation and migration of breast cancer cells *in vitro*. Normally, microRNAs could be grouped in relation to their function into two types: onco-miRs (an oncogene-like microRNA) or tumor suppressor-miRs (a tumor suppressor-like microRNA) [36]. Preliminary results showed that miR-548o could be regarded as an oncogene-like microRNA by regulating DACH1 expression, and miR-548o could be regarded as a tumor oncogene-like miRNA involved in mediating breast cancer.

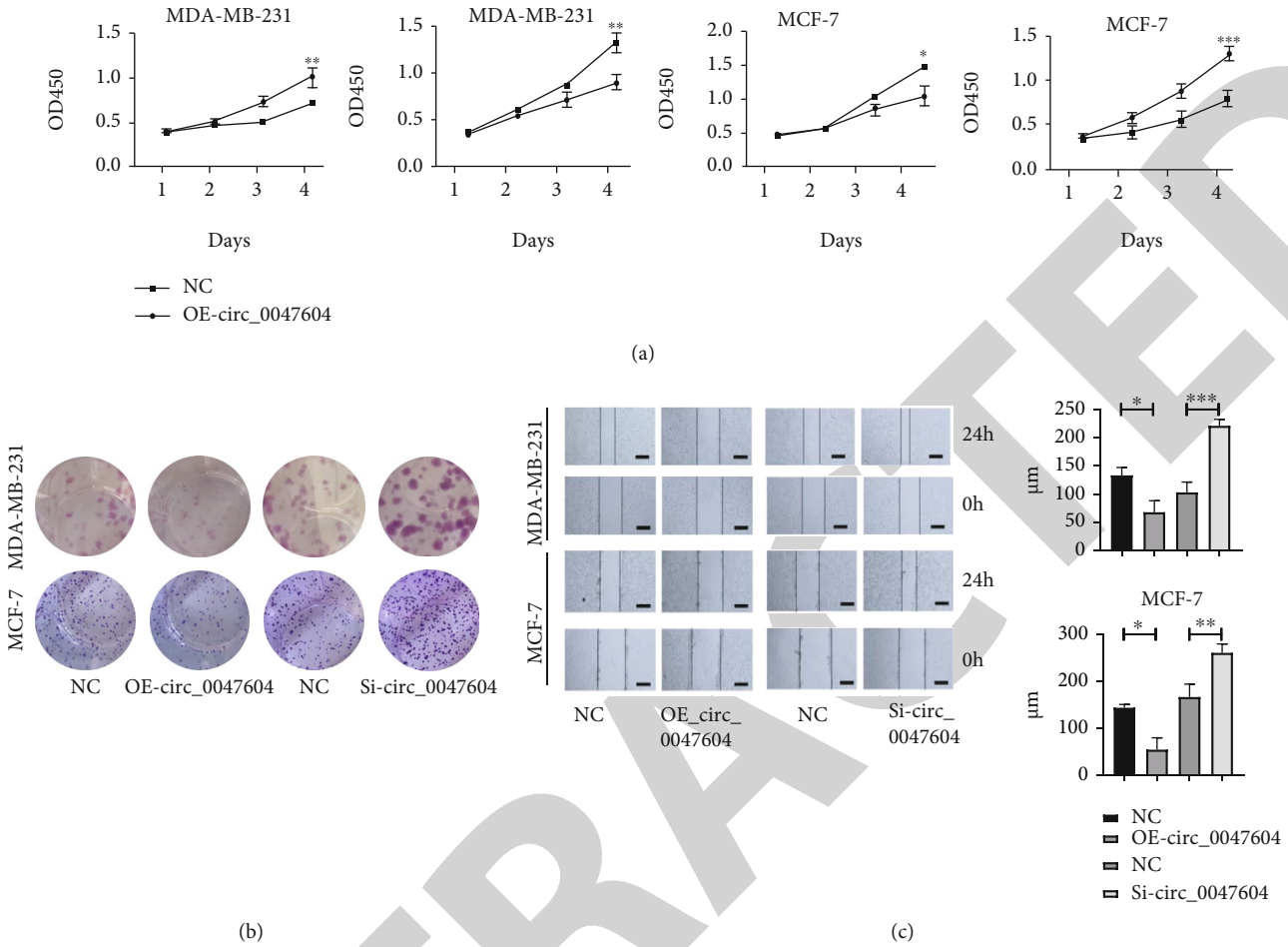

Figure 5: Circ_0047604 can inhibit tumor cell growth and immigration. (a) The CCK-8 assay was carried out to monitor the proliferation level of MDA-MB-231 and MCF-7 cells at 1, 2, 3, and 4 days. (b) Images of crystal violet stained colonies of MDA-MB-231 and MCF-7 cells after up or downregulation of circ_0047604. (c) Wound healing assays of cell migration after up or downregulation of circ_0047604. $^{*}P < 0.05$, $^{**}P < 0.01$, and $^{***}P < 0.001$.

Recent reports indicate that circRNA can act as miRNA sponge and interacting with proteins to affect gene expression level to influence transcription and translation [37–39]. After further analyzing circRNA on breast cancer sample, we found that circ_0047604 expression level is lower in tumors. It could bind to miR-548o and, to a large degree, also affect DACH1 expression. Considering that circ_0047604 is originated from SMAD2 gene and SMAD2 always acts as an oncogenic gene in breast cancer [40], it means circ_0047604 exerts contrary to original SMAD2 protein. Therefore, the relationship between SMAD2 mRNA transcription and circRNA production is not clear and still needs further investigation. More clinical cases, different tumor progressions, and other physiological processes are needed.

Data Availability

All data included in this study are available upon request by contact with the corresponding author. Pro. Lin Fang, Department of Breast and Thyroid Surgery, Shanghai Tenth People's Hospital, Tongji University, 301 Yanchang Road, Jing'an Area, Shanghai 200072, China. E-mail: fanglin2017@126.com; Pro. Yuanzhi Xu, Department of Stomatology, Shanghai Tenth People's Hospital, Tongji University School of Medicine, 301 Yanchang Road, Shanghai 200072, China. E-mail: amyxyz01@hotmail.com. Dr. Bingkun Zhao, Department of Breast and Thyroid Surgery, Shanghai Tenth People's Hospital, Tongji University, 301 Yanchang Road, Jing'an Area, Shanghai 200072, China. E-mail: zhaobingkun0506@163.com.

Conflicts of Interest

The authors declare that they have no conflicts of interest.

Authors' Contributions

Bingkun Zhao, Rong Zhou, and Changle Ji contributed equally to this work.

Acknowledgments

This work was supported by grants from the National Natural Science Foundation of China (no. 82073204) and the Shanghai Municipal Health Commission (no. 202040157). We thank the Department of Thyroid and Breast Surgery, Shanghai Tenth People's Hospital, Shanghai, China, for providing the BC tissue samples and related anonymous clinical data.

Supplementary Materials

Supplementary Table 1: nucleotide sequences of primers used for qRT-PCR. *(Supplementary Materials)*

References

[1] A. Jemal, F. Bray, M. M. Center, J. Ferlay, E. Ward, and D. Forman, "Global cancer statistics," *CA: a Cancer Journal for Clinicians*, vol. 61, no. 2, pp. 69–90, 2011.

[2] G. Mardon, N. M. Solomon, and G. M. Rubin, "Dachshund encodes a nuclear protein required for normal eye and leg development in drosophila," *Development*, vol. 120, no. 12, pp. 3473–3486, 1994.

[3] R. Neshige and H. Lüders, "Recording of event-related potentials (P300) from human cortex," *Journal of Clinical Neurophysiology*, vol. 9, no. 2, pp. 294–298, 1992.

[4] K. Wu, S. Katiyar, A. Li et al., "Dachshund inhibits oncogene-induced breast cancer cellular migration and invasion through suppression of interleukin-8," *Proceedings of the National Academy of Sciences of the United States of America*, vol. 105, no. 19, pp. 6924–6929, 2008.

[5] V. M. Popov, J. Zhou, L. A. Shirley et al., "The cell fate determination factor DACH1 is expressed in estrogen receptor-alpha-positive breast cancer and represses estrogen receptor-alpha signaling," *Cancer Research*, vol. 69, no. 14, pp. 5752–5760, 2009.

[6] Y. Zhang, Q. Mao, Q. Xia et al., "Noncoding RNAs link metabolic reprogramming to immune microenvironment in cancers," *Journal of Hematology & Oncology*, vol. 14, no. 1, p. 169, 2021.

[7] R. I. Gregory, T. P. Chendrimada, N. Cooch, and R. Shiekhattar, "Human RISC couples microRNA biogenesis and posttranscriptional gene silencing," *Cell*, vol. 123, no. 4, pp. 631–640, 2005.

[8] Y. Li, Q. Zheng, C. Bao et al., "Circular RNA is enriched and stable in exosomes: a promising biomarker for cancer diagnosis," *Cancer Research*, vol. 25, no. 8, pp. 981–984, 2015.

[9] L. S. Kristensen, M. S. Andersen, L. V. W. Stagsted, K. K. Ebbesen, T. B. Hansen, and J. Kjems, "The biogenesis, biology and characterization of circular RNAs," *Nature Reviews Genetics*, vol. 20, no. 11, pp. 675–691, 2019.

[10] H. Song, Y. Yang, Y. Sun et al., "Circular RNA Cdyl promotes abdominal aortic aneurysm formation by inducing M1 macrophage polarization and M1-type inflammation," *Molecular Therapy*, 2021.

[11] Y. Cai, R. Liang, S. Xiao et al., "Circ_0088194 promotes the invasion and migration of rheumatoid arthritis fibroblast-like synoviocytes via the miR-766-3p/MMP2 axis," *Front Immunol*, vol. 12, p. 628654, 2021.

[12] A. J. van Zonneveld, M. Kölling, R. Bijkerk, and J. M. Lorenzen, "Circular RNAs in kidney disease and cancer," *Nature Reviews Nephrology*, vol. 17, no. 12, pp. 814–826, 2021.

[13] X. Wang, R. Ma, X. Zhang et al., "Crosstalk between N6-methyladenosine modification and circular RNAs: current understanding and future directions," *Molecular Cancer*, vol. 20, no. 1, p. 121, 2021.

[14] A. Esquela-Kerscher and F. J. Slack, "Oncomirs – microRNAs with a role in cancer," *Nature Reviews Cancer*, vol. 6, no. 4, pp. 259–269, 2006.

[15] L. He and G. J. Hannon, "MicroRNAs: small RNAs with a big role in gene regulation," *Nature Reviews Genetics*, vol. 5, no. 7, pp. 522–531, 2004.

[16] C. Jay, J. Nemunaitis, P. Chen, P. Fulgham, and A. W. Tong, "miRNA profiling for diagnosis and prognosis of human cancer," *DNA and Cell Biology*, vol. 26, no. 5, pp. 293–300, 2007.

[17] M. Zabala, N. A. Lobo, J. Antony et al., "LEFTY1 is a dual-SMAD inhibitor that promotes mammary progenitor growth and tumorigenesis," *Cell Stem Cell*, vol. 27, no. 2, pp. 284–299.e8, 2020.

[18] Y. Zhuang, X. Li, P. Zhan, G. Pi, and G. Wen, "MMP11 promotes the proliferation and progression of breast cancer through stabilizing Smad2 protein," *Oncology Reports*, vol. 45, no. 4, 2021.

[19] L. Zhang, Z. Zhu, H. Yan et al., "Creatine promotes cancer metastasis through activation of Smad2/3," *Cell Metabolism*, vol. 33, no. 6, pp. 1111–1123.e4, 2021.

[20] B. Győrffy, A. Lanczky, A. C. Eklund et al., "An online survival analysis tool to rapidly assess the effect of 22,277 genes on breast cancer prognosis using microarray data of 1,809 patients," *Breast Cancer Research and Treatment*, vol. 123, no. 3, pp. 725–731, 2010.

[21] J. H. Li, S. Liu, H. Zhou, L. H. Qu, and J. H. Yang, "starBase v2.0: decoding miRNA-ceRNA, miRNA-ncRNA and protein-RNA interaction networks from large-scale CLIP-Seq data," *Nucleic Acids Research*, vol. 42, no. D1, pp. D92–D97, 2014.

[22] F. Nan, Q. Lü, J. Zhou et al., "Altered expression of DACH1 and cyclin D1 in endometrial cancer," *Cancer Biology & Therapy*, vol. 8, no. 16, pp. 1534–1539, 2009.

[23] H. Xu, S. Yu, X. Yuan et al., "DACH1 suppresses breast cancer as a negative regulator of CD44," *Scientific Reports*, vol. 7, no. 1, p. 4361, 2017.

[24] X. Jiao, Z. Li, M. Wang et al., "*Dachshund* Depletion Disrupts Mammary Gland Development and Diverts the Composition of the Mammary Gland Progenitor Pool," *Stem Cell Reports*, vol. 12, no. 1, pp. 135–151, 2019.

[25] K. Wu, A. Li, M. Rao et al., "DACH1 is a cell fate determination factor that inhibits cyclin D1 and breast tumor growth," *Molecular Cell Biology*, vol. 26, no. 19, pp. 7116–7129, 2006.

[26] K. Chen, K. Wu, S. Cai et al., "Dachshund binds p53 to block the growth of lung adenocarcinoma cells," *Cancer Research*, vol. 73, no. 11, pp. 3262–3274, 2013.

[27] K. Wu, S. Katiyar, A. Witkiewicz et al., "The cell fate determination factor dachshund inhibits androgen receptor signaling and prostate cancer cellular growth," *Cancer Research*, vol. 69, no. 8, pp. 3347–3355, 2009.

[28] K. Wu, X. Jiao, Z. Li et al., "Cell Fate Determination Factor Dachshund Reprograms Breast Cancer Stem Cell Function," *The Journal of Biological Chemistry*, vol. 286, no. 3, pp. 2132–2142, 2011.

Hindawi
BioMed Research International
Volume 2024, Article ID 9856043, 1 page
https://doi.org/10.1155/2024/9856043

Retraction

Retracted: Changes of Serum Ferritin, Hemoglobin, and Serum Iron (SI) and Treatment Effect of Iron Proteinsuccinylate Oral Solution Combined with Vitamin A and D Drops on Children with Nutritional Iron Deficiency Anemia

BioMed Research International

Received 12 March 2024; Accepted 12 March 2024; Published 20 March 2024

This article has been retracted by Hindawi following an investigation undertaken by the publisher [1]. This investigation has uncovered evidence of one or more of the following indicators of systematic manipulation of the publication process:

(1) Discrepancies in scope

(2) Discrepancies in the description of the research reported

(3) Discrepancies between the availability of data and the research described

(4) Inappropriate citations

(5) Incoherent, meaningless and/or irrelevant content included in the article

(6) Manipulated or compromised peer review

The presence of these indicators undermines our confidence in the integrity of the article's content and we cannot, therefore, vouch for its reliability. Please note that this notice is intended solely to alert readers that the content of this article is unreliable. We have not investigated whether authors were aware of or involved in the systematic manipulation of the publication process.

Wiley and Hindawi regrets that the usual quality checks did not identify these issues before publication and have since put additional measures in place to safeguard research integrity.

We wish to credit our own Research Integrity and Research Publishing teams and anonymous and named external researchers and research integrity experts for contributing to this investigation.

The corresponding author, as the representative of all authors, has been given the opportunity to register their agreement or disagreement to this retraction. We have kept a record of any response received.

References

[1] Y. Ma, Y. Ma, X. Zhang, X. Wang, and Z. Sun, "Changes of Serum Ferritin, Hemoglobin, and Serum Iron (SI) and Treatment Effect of Iron Proteinsuccinylate Oral Solution Combined with Vitamin A and D Drops on Children with Nutritional Iron Deficiency Anemia," *BioMed Research International*, vol. 2022, Article ID 2972617, 6 pages, 2022.

Hindawi
BioMed Research International
Volume 2022, Article ID 2972617, 6 pages
https://doi.org/10.1155/2022/2972617

Research Article

Changes of Serum Ferritin, Hemoglobin, and Serum Iron (SI) and Treatment Effect of Iron Proteinsuccinylate Oral Solution Combined with Vitamin A and D Drops on Children with Nutritional Iron Deficiency Anemia

Yan Ma,[1] Yanbo Ma,[2] Xiuqing Zhang,[1] Xuejing Wang,[1] and Zhigang Sun[2]

[1]*Pediatric Internal Medicine, The Second People's Hospital of Liaocheng, The Second Hospital of Liaocheng Affiliated to Shandong First Medical University, 252600 Liaocheng, Shandong Province, China*
[2]*Child Healthcare Department, The Second People's Hospital of Liaocheng, The Second Hospital of Liaocheng Affiliated to Shandong First Medical University, 252600 Liaocheng, Shandong Province, China*

Correspondence should be addressed to Zhigang Sun; sibi9378@163.com

Received 8 August 2021; Revised 8 November 2021; Accepted 11 November 2021; Published 13 January 2022

Academic Editor: Jianxin Shi

Objective. The purpose was to evaluate the treatment effect of iron proteinsuccinylate oral solution combined with vitamin A and D drops on children with nutritional iron deficiency anemia. *Methods*. 124 children treated in the outpatient department of our hospital from January 2017 to January 2020 were selected as the study subjects. They were randomly divided into control and observation two groups. The control group was treated with iron proteinsuccinylate oral solution (1.5 mL/kg) in the morning and evening, respectively. The observation group received adjuvant treatment with oral vitamin A and D drops based on the treatment of the control group. The treatment effect of proteinsuccinylate oral solution combined with vitamin A and D drops was evaluated by the serum iron (SI), serum ferritin (SF), and transferrin (TRF) levels, the values of $CD3^+$, $CD4^+$, and $CD4^+/CD8^+$, and other evaluation indicators. *Results*. After treatment, the SI and SF levels of children in both groups significantly increased ($P < 0.01$) while the TRF level significantly decreased ($P < 0.01$), and the SI and SF levels in the observation group increased more significantly, and the TRF level decreased more significantly compared with those in the control group ($P < 0.01$). After treatment, the values of $CD3^+$, $CD4^+$, and $CD4^+/CD8^+$ of children in both groups significantly increased compared with those before treatment ($P < 0.01$), and the values of $CD3^+$, $CD4^+$, and $CD4^+/CD8^+$ increased more significantly in the observation group compared with those in the control group ($P < 0.01$). In addition, the evaluation results of treatment effect showed that the markedly effective rate in the observation group was significantly higher than that in the control group ($P < 0.01$). *Conclusion*. Iron proteinsuccinylate oral solution combined with vitamin A and D drops can better improve the anemia symptoms in children, with high application value.

1. Introduction

Iron, an essential trace element in human body, plays an important role in maintaining the activities of hemoglobin, myoglobin, and metabolic-related enzymes in human body and can participate in various physiological activities of human body. Patients with iron deficiency are often accompanied by oxygen transport disorders, resulting in metabolic disorders and eventually anemia [1–3]. Iron deficiency anemia is more common in children, whose pathogenesis has a variety of reasons including unreasonable dietary structure, massive iron loss caused by chronic bleeding, and iron malabsorption in the body, which has a serious impact on the development and growth of children [4–6]. At present, to treat this chronic disease, dietary therapy, iron preparations, and other methods are often used in the intervention, including increasing the intake of liver, lean meat, and soy products to improve the internal environment of children or directly supplementing iron preparations to raise the iron level in the body, promoting the synthesis of

Table 1: General information of patients.

Items	Control group	Observation group	t	P
Sex ratio	15 : 16	1 : 1	0.03	0.83
Average age (years old)	6.73 ± 0.53	6.69 ± 0.59	0.40	0.44
Body mass index (kg/m^2)	13.98 ± 0.53	13.97 ± 0.56	0.10	0.75
SI level (μmol/L)	11.98 ± 2.09	12.01 ± 2.13	0.08	0.77
SF level (μg/L)	85.29 ± 8.03	85.29 ± 8.03	0.06	0.81
Serum TRF level (μg/L)	7.23 ± 1.19	7.27 ± 1.11	0.19	0.63
$CD3^+$ level (%)	40.29 ± 3.29	40.31 ± 3.27	0.03	0.83
$CD4^+$level (%)	37.09 ± 2.09	37.03 ± 2.07	0.16	0.71

hemoglobin in vivo and thereby improve the symptoms of anemia [7–9]. In clinic, iron preparations for the treatment of iron deficiency anemia in children mainly include ferrous gluconate and iron proteinsuccinylate [10–12]. However, some studies have shown that iron deficiency anemia is associated with some vitamin deficiencies in children [13, 14]. Based on this, 124 children treated in the outpatient department of our hospital from January 2017 to January 2020 were selected as the study subjects in this study. Vitamin A and D drops were used based on iron proteinsuccinylate to evaluate the symptom improvement before and after treatment through SI, SF, TRF, and immune levels, which is aimed at providing a reference for the treatment of iron deficiency anemia in children.

2. Materials and Methods

2.1. General Information. This study was approved by the hospital ethics committee. 124 children treated in the outpatient department of our hospital from January 2017 to January 2020 were selected as the study subjects. The general data of the patients are shown in Table 1.

2.2. Screening Criteria. Inclusion criteria are as follows: (1) the patients were clinically diagnosed with iron deficiency anemia; (2) the guardians of the children had a detailed understanding of the content of the study; (3) the patient had symptoms such as pale skin, decreased appetite, and depression; (4) the guardians of the children voluntarily signed the informed consent; (5) the children were aged 3-9 years old; (6) the children had never received intervention with iron preparations.

Exclusion criteria are as follows: (1) children with hemolytic anemia, (2) children with aplastic anemia, (3) children with iron utilization disorder and other symptoms, (4) children with hematopoietic disorder, and (5) children could not cooperate with clinical follow-up.

2.3. Treatment Methods. 124 children were randomly divided into two groups for control and observation. The children in the control group were treated with iron proteinsuccinylate oral solution, once in the morning and once in the evening, with a total dose of 1.5 mL/kg. The children in the observation group received adjuvant treatment with vitamin A and D drops based on the treatment of the control group, with oral administration of one vitamin A (12,000 IU/pill) and one vitamin D_3 (700 IU/pill) daily.

Drug information is as follows: iron proteinsuccinylate oral solution (Italfarmaco S.p.A; SFDA No.: H20160143) and vitamin A and D drops (Shandong Dyne Marine Biopharmaceutical Co., Ltd.; SFDA No.: H37022974).

2.4. Observation Indexes. Determination of SI, SF, and TRF levels: 2 mL of venous blood was taken before and after treatment in fasting state to detect SI, SF, and TRF levels. Bipyridine colorimetry was used to detect the SI, and chemiluminescence immunoassay was used to detect the SF and TRF levels.

Determination of immune level: the levels of $CD3^+$, $CD4^+$, and $CD8^+$ of T lymphocyte subsets in children were measured by a flow cytometry, and the ratio of $CD4^+$/$CD8^+$ was calculated.

Clinical efficacy: the treatment effect was divided into markedly effective, effective, and ineffective according to the appetite, spirit, skin, and mucosal color of children, SI, SF, and TRF levels, and the improvement of $CD3^+$, $CD4^+$, and $CD4^+/CD8^+$ of children.

2.5. Data Analysis. The data obtained in this study were processed by SPSS 20.0. The measurement data and count data were tested by t-test and χ^2, respectively. The difference was statistically significant when $P < 0.05$.

3. Results

3.1. Comparison of SI Levels between the Two Groups of Children before and after Treatment. The SI levels of children in the two groups before and after treatment are shown in Figure 1. After treatment, the SI levels of children in both groups significantly increased compared with those before treatment ($P < 0.01$), and the SI level in the observation group increased more significantly compared with that in the control group ($P < 0.01$).

3.2. Comparison of SF Levels between the Two Groups of Children before and after Treatment. The SF levels of children in the two groups before and after treatment are shown in Figure 2. After treatment, the SF levels of children in both

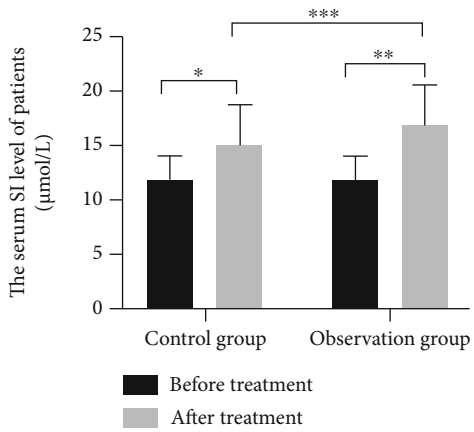

Figure 1: Comparison of SI levels between the two groups of children before and after treatment. Note: The abscissa represents the groups, and the ordinate represents the SI level of patients. * indicated that there was a significant difference in the SI levels of children in the control group before treatment (11.97 ± 2.13 μmol/L) and after treatment (15.09 ± 3.69 μmol/L; $t = 4.99$ and $P = 1.6e-5$). ** indicated that there was a significant difference in the SI levels of children in the observation group before treatment (11.99 ± 2.09 μmol/L) and after treatment (16.91 ± 3.71 μmol/L; $t = 4.50$ and $P = 8.2e-5$). *** indicated that there was a significant difference in the SI levels of children in both groups after treatment ($t = 2.74$ and $P = 4.5e-3$).

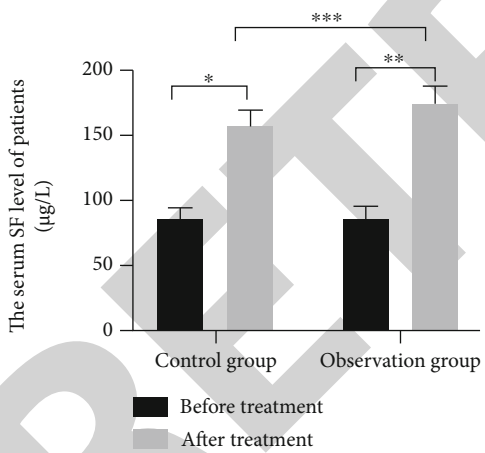

Figure 2: Comparison of SF levels between the two groups of children before and after treatment. Note: The abscissa represents the groups, and the ordinate represents the SF level of patients. * indicated that there was a significant difference in the SF levels of children in the control group before treatment (85.31 ± 8.96 μg/L) and after treatment (156.19 ± 12.97 μg/L; $t = 3.84$ and $P < 0.01$). * * indicated that there was a significant difference in the SF levels of children in the observation group before treatment (85.69 ± 8.99 μg/L) and after treatment (173.32 ± 13.32 μg/L; $t = 3.47$ and $P < 0.01$). *** indicated that there was a significant difference in the SF levels of children in both groups after treatment ($t = 7.26$ and $P < 0.01$).

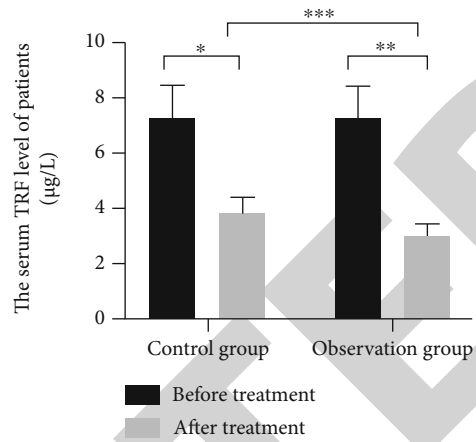

Figure 3: Comparison of TRF levels between the two groups of children before and after treatment. Note: The abscissa represents the groups, and the ordinate represents the serum TRF level of patients. * indicated that there was a significant difference in the serum TRF levels of children in the control group before treatment (7.23 ± 1.21 μg/L) and after treatment (3.77 ± 0.61 μg/L; $t = 12.41$ and $P < 0.01$). ** indicated that there was a significant difference in the serum TRF levels of children in the observation group before treatment (7.29 ± 1.09 μg/L) and after treatment (2.95 ± 0.43 μg/L; $t = 16.38$ and $P < 0.01$). *** indicated that there was a significant difference in the serum TRF levels of children in both groups after treatment ($t = 8.65$ and $P < 0.01$).

groups significantly increased compared with those before treatment ($P < 0.01$), and the SF level in the observation group increased more significantly compared with that in the control group ($P < 0.01$).

3.3. Comparison of TRF Levels between the Two Groups of Children before and after Treatment. The serum TRF levels of children in the two groups before and after treatment are shown in Figure 3. After treatment, the serum TRF levels of children in both groups significantly decreased compared with those before treatment ($P < 0.01$), and the TRF level in the observation group decreased more significantly compared with that in the control group ($P < 0.01$).

3.4. Comparison of the Immune Level between the Two Groups of Children before and after Treatment. The changes of immune level of children in the two groups before and after treatment are shown in Table 2. After treatment, the values of $CD3^+$, $CD4^+$, and $CD4^+/CD8^+$ of children in both groups significantly increased compared with those before treatment ($P < 0.01$), and the values of $CD3^+$, $CD4^+$, and $CD4^+/CD8^+$ increased more significantly in the observation group compared with that in the control group ($P < 0.01$).

3.5. Comparison of Treatment Effect between the Two Methods. The treatment effect of the two methods is shown in Table 3. The proportion of children with obviously improved symptoms in the observation group was significantly higher than that in the control group ($P < 0.05$).

Table 2: Immune level of children in two groups.

Indicators	Groups	Cases	Before treatment	After treatment	t	P
$CD3^+$ (%)	Control group	62	40.32 ± 3.57	49.13 ± 3.35	5.88	6.5*e*-6
	Observation group	62	40.27 ± 3.16	55.09 ± 4.19	5.29	3.1*e*-6
	t		0.08	8.75		
	P		0.77	5.6*e*-8		
$CD4^+$ (%)	Control group	62	37.13 ± 2.21	41.97 ± 3.03	6.53	9.6*e*-7
	Observation group	62	37.29 ± 2.13	45.29 ± 3.31	6.10	3.6*e*-7
	t		0.41	5.83		
	P		0.42	5.3*e*-6		
$CD4^+/CD8^+$	Control group	62	1.17 ± 0.19	1.39 ± 0.23	5.48	5.9*e*-6
	Observation group	62	1.15 ± 0.17	1.63 ± 0.27	4.67	5.7*e*-5
	t		0.62	5.33		
	P		0.31	4.9*e*-6		

Table 3: Treatment effect between the two methods.

Groups	Cases	Marked effective	Effective	Ineffective	Effective rate (%)
Control group	62	25	26	11	82.56
Observation group	62	36	23	3	95.16
χ^2		6.74			
P		0.007			

4. Discussion

Iron deficiency anemia is a common chronic disease in children, which not only leads to poor body development and slow growth of children but also seriously affects their intellectual development [15, 16]. Iron proteinsuccinylate is a widely used iron supplement in clinical practice, which can effectively improve the iron deficiency in children. However, iron deficiency anemia in children is a comprehensive metabolic disease, and the treatment of simply supplementing iron has certain limitations [17, 18]. Therefore, it is of positive significance to select a reasonable treatment for children with iron deficiency anemia.

SI, SF, and TRF levels are often used to reflect the severity of iron deficiency anemia in patients [19]. In this study, the changes of SI, SF, and TRF levels of children were used to reflect their iron level in vivo. Compared with those before treatment, the SI and SF levels of children in both groups increased significantly after treatment while the TRF level decreased significantly, indicating that long-term administration of iron proteinsuccinylate could significantly improve the body iron level of children and thereby improve the symptoms of anemia. Iron proteinsuccinylate is a commonly used iron supplement in clinical practice, which is often used to treat anemia caused by iron malabsorption in pregnant and lactating women and children. In addition, compared with the control group, the SI and SF levels of children in the observation group increased more significantly after treatment while the TRF level decreased more significantly, indicating that the adjuvant treatment of vitamin A and D drops can better improve the iron deficiency in children, so as to further alleviate the anemia symptoms. The vitamin A level is significantly correlated with iron deficiency anemia in children. Larson et al. [20] found that vitamin A could directly reflect the degree of anemia in preschool and school-age children as an independent factor through investigation. In addition, Altemose et al. [21] showed that vitamin D deficiency also increased the risk of iron deficiency anemia in children. These studies indicate that increased vitamins A and D can help improve the symptoms of anemia in children.

The immune level of children is significantly correlated with the content of iron ions in their blood and can directly reflect their health [22]. In this study, the levels of $CD3^+$ and $CD4^+$ and the ratio of CD4/CD8 were used to observe the changes in immunity of children before and after treatment. Compared with those before treatment, the levels of $CD3^+$ and $CD4^+$ and the ratio of CD4/CD8 in both groups increased significantly after treatment, indicating that long-term administration of iron proteinsuccinylate can significantly improve the immunity of children, thereby effectively reducing the incidence of complications caused by iron deficiency anemia in children. In addition, compared with the control group, the levels of $CD3^+$ and $CD4^+$ and the ratio of CD4/CD8 increased more significantly in the observation group after the adjuvant treatment of vitamin A and D drops, indicating that vitamin A and D drops as an adjuvant treatment could better improve the immunity of children

and effectively improve their health level. Studies have shown that the deficiency of vitamins A and D is significantly related to the incidence of various diseases in children, and the supplementation of vitamins A and D can effectively improve the immune level of children and enhance their resistance to viruses [23, 24]. These studies suggest that vitamin A and D supplementation can help to improve the immune level of children. In addition, Houghton et al. [25] found that the majority of children with iron deficiency anemia included in their study had severe deficiencies in vitamins A and D. This finding also supports the conclusion of this study, indicating that vitamin A and D supplementation has a positive effect on improving the symptoms of anemia in children.

In conclusion, our study demonstrated that iron protein-succinylate oral solution combined with vitamin A and D drops can better improve the anemia symptoms in children, indicating this approach can transform nutritional status assessment and monitoring globally.

Data Availability

The authors confirm that the data supporting the findings of this study are available within the article.

Conflicts of Interest

The authors declare that they have no conflicts of interest.

Authors' Contributions

Yan Ma, Xiuqing Zhang, and Xuejing Wang performed the experiments, analyzed data, and wrote the manuscript. Yanbo Ma and Zhigang Sun designed the study. All the authors agreed to be accountable for the accuracy and integrity of all aspects of the research.

References

[1] R. Eltayeb, D. A. Rayis, M. E. Sharif, A. B. A. Ahmed, O. Elhardello, and I. Adam, "The prevalence of serum magnesium and iron deficiency anaemia among Sudanese women in early pregnancy: a cross-sectional study," *Transactions of the Royal Society of Tropical Medicine and Hygiene*, vol. 113, no. 1, pp. 31–35, 2019.

[2] M. S. Field, P. Mithra, D. Estevez, and J. P. Peña-Rosas, "Wheat flour fortification with iron for reducing anaemia and improving iron status in populations," *Cochrane Database of Systematic Reviews*, vol. 7, article CD011302, 2020.

[3] B. D. Keeler, E. A. Dickson, J. A. Simpson et al., "The impact of pre-operative intravenous iron on quality of life after colorectal cancer surgery: outcomes from the intravenous iron in colorectal cancer-associated anaemia (IVICA) trial," *Anaesthesia*, vol. 74, no. 6, pp. 714–725, 2019.

[4] T. P. Gwetu, M. K. Chhagan, M. Taylor, S. Kauchali, and M. Craib, "Anaemia control and the interpretation of biochemical tests for iron status in children," *BMC Research Notes*, vol. 10, no. 1, p. 163, 2017.

[5] A. Geletu, A. Lelisa, and K. Baye, "Provision of low-iron micronutrient powders on alternate days is associated with lower prevalence of anaemia, stunting, and improved motor milestone acquisition in the first year of life: a retrospective cohort study in rural Ethiopia," *Maternal & Child Nutrition*, vol. 15, no. 3, article e12785, 2019.

[6] R. Rodrigo, A. Allen, A. Manampreri et al., "Haemoglobin variants, iron status and anaemia in Sri Lankan adolescents with low red cell indices: a cross sectional survey," *Blood Cells, Molecules & Diseases*, vol. 71, pp. 11–15, 2018.

[7] B. Rogers, J. Kramer, S. Smith, V. Bird, and E. I. Rosenberg, "Sodium chloride pica causing recurrent nephrolithiasis in a patient with iron deficiency anemia: a case report," *Journal of Medical Case Reports*, vol. 11, no. 1, p. 325, 2017.

[8] C. K. Kubuga, H. G. Hong, and W. O. Song, "Hibiscus sabdariffa meal improves iron status of childbearing age women and prevents stunting in their toddlers in northern Ghana," *Nutrients*, vol. 11, no. 1, p. 198, 2019.

[9] L. M. de-Regil, M. E. D. Jefferds, and J. P. Peña-Rosas, "Point-of-use fortification of foods with micronutrient powders containing iron in children of preschool and school-age," *Cochrane Database of Systematic Reviews*, vol. 2017, no. 11, p. CD009666, 2017.

[10] G. Russo, V. Guardabasso, F. Romano et al., "Monitoring oral iron therapy in children with iron deficiency anemia: an observational, prospective, multicenter study of AIEOP patients (Associazione Italiana Emato-Oncologia Pediatrica)," *Annals of Hematology*, vol. 99, no. 3, pp. 413–420, 2020.

[11] A. Martínez Francés and J. Leal Martínez-Bujanda, "Efficacy and tolerability of oral iron protein succinylate: a systematic review of three decades of research," *Current Medical Research and Opinion*, vol. 36, no. 4, pp. 613–623, 2020.

[12] A. Córdova, J. Mielgo-Ayuso, C. I. Fernandez-Lazaro, A. Caballero-García, E. Roche, and D. Fernández-Lázaro, "Effect of iron supplementation on the modulation of iron metabolism, muscle damage biomarkers and cortisol in professional cyclists," *Nutrients*, vol. 11, no. 3, p. 500, 2019.

[13] S. Soofi, G. N. Khan, K. Sadiq et al., "Prevalence and possible factors associated with anaemia, and vitamin B 12 and folate deficiencies in women of reproductive age in Pakistan: analysis of national-level secondary survey data," *BMJ Open*, vol. 7, no. 12, article e018007, 2017.

[14] N. Kucuk, Z. Orbak, C. Karakelloglu, and F. Akcay, "The effect of therapy on plasma ghrelin and leptin levels, and appetite in children with iron deficiency anemia," *Journal of Pediatric Endocrinology & Metabolism*, vol. 32, no. 3, pp. 275–280, 2019.

[15] Y. Gelaw, B. Woldu, and M. Melku, "The role of reticulocyte hemoglobin content for diagnosis of iron deficiency and iron deficiency anemia, and monitoring of iron therapy: a literature review," *Clinical Laboratory*, vol. 65, no. 12/2019, 2019.

[16] A. Gafter-Gvili, A. Schechter, and B. Rozen-Zvi, "Iron deficiency anemia in chronic kidney disease," *Acta Haematologica*, vol. 142, no. 1, pp. 44–50, 2019.

[17] S. Mahadev, M. Laszkowska, J. Sundström et al., "Prevalence of celiac disease in patients with iron deficiency anemia-a systematic review with meta-analysis," *Gastroenterology*, vol. 155, no. 2, pp. 374–382.e1, 2018.

[18] J. Wesström, "Safety of intravenous iron isomaltoside for iron deficiency and iron deficiency anemia in pregnancy," *Archives of Gynecology and Obstetrics*, vol. 301, no. 5, pp. 1127–1131, 2020.

[19] J. C. Barton, J. C. Barton, and L. F. Bertoli, "Pagophagia in men with iron-deficiency anemia," *Blood Cells, Molecules & Diseases*, vol. 77, pp. 72–75, 2019.

Hindawi
BioMed Research International
Volume 2024, Article ID 9824926, 1 page
https://doi.org/10.1155/2024/9824926

Retraction

Retracted: Correlation Analysis of Acute Coronary Syndrome with Serum IL-18, MMP-9, hs-CRP, and Plasma FIB

BioMed Research International

Received 12 March 2024; Accepted 12 March 2024; Published 20 March 2024

This article has been retracted by Hindawi following an investigation undertaken by the publisher [1]. This investigation has uncovered evidence of one or more of the following indicators of systematic manipulation of the publication process:

(1) Discrepancies in scope

(2) Discrepancies in the description of the research reported

(3) Discrepancies between the availability of data and the research described

(4) Inappropriate citations

(5) Incoherent, meaningless and/or irrelevant content included in the article

(6) Manipulated or compromised peer review

The presence of these indicators undermines our confidence in the integrity of the article's content and we cannot, therefore, vouch for its reliability. Please note that this notice is intended solely to alert readers that the content of this article is unreliable. We have not investigated whether authors were aware of or involved in the systematic manipulation of the publication process.

Wiley and Hindawi regrets that the usual quality checks did not identify these issues before publication and have since put additional measures in place to safeguard research integrity.

We wish to credit our own Research Integrity and Research Publishing teams and anonymous and named external researchers and research integrity experts for contributing to this investigation.

The corresponding author, as the representative of all authors, has been given the opportunity to register their agreement or disagreement to this retraction. We have kept a record of any response received.

References

[1] Y. Yang, G. Li, and R. Zhang, "Correlation Analysis of Acute Coronary Syndrome with Serum IL-18, MMP-9, hs-CRP, and Plasma FIB," *BioMed Research International*, vol. 2022, Article ID 5984184, 9 pages, 2022.

Hindawi
BioMed Research International
Volume 2022, Article ID 5984184, 9 pages
https://doi.org/10.1155/2022/5984184

Research Article

Correlation Analysis of Acute Coronary Syndrome with Serum IL-18, MMP-9, hs-CRP, and Plasma FIB

Yuexia Yang,[1] Guoming Li,[1] and Ruiqin Zhang[2]

[1]*Department of Cardiology, Yidu Central Hospital, Weifang 262500, Shandong Province, China*
[2]*Blood Purification Centre, Weifang People's Hospital, Weifang 261041, Shandong Province, China*

Correspondence should be addressed to Ruiqin Zhang; rongbirang92008870@163.com

Received 20 September 2021; Accepted 3 November 2021; Published 4 January 2022

Academic Editor: Jun Yang

Aim. This study attempted to investigate the diagnostic value of interleukin-18 (IL-18), matrix metalloproteinase-9 (MMP-9), high-sensitivity C-reactive protein (hs-CRP), and fibrinogen (FIB) in acute coronary syndrome (ACS) and their correlation with the degree of vascular lesions. *Materials and Methods*. Altogether 206 patients with coronary heart disease admitted to our hospital were selected as research objects, including 136 patients with ACS (group A), 70 patients with stable angina pectoris (SAP) (group B), and 60 patients with noncoronary heart disease who had normal coronary angiography during the same period were selected as group C. The levels of IL-18, MMP-9, and hs-CRP in the serum were detected by enzyme-linked immunosorbent assay (ELISA), and the level of FIB in plasma was detected by automatic coagulation analyzer. *Results*. Serum IL-18, MMP-9, hs-CRP, and plasma FIB levels in group A were significantly higher than those in group B and group C ($p < 0.05$). ROC curve and multivariate logistic regression showed that the sensitivity and specificity of combined diagnosis of ACS with serum IL-18, MMP-9, hs-CRP, and plasma FIB were 86.03% and 95.71%, respectively. Serum IL-18, MMP-9, hs-CRP, and plasma FIB were positively correlated with Gensini grading ($p < 0.001$). Serum IL-18, MMP-9, hs-CRP, and plasma FIB levels were positively correlated ($p < 0.001$). *Conclusion*. The combined detection of serum IL-18, MMP-9, hs-CRP, and plasma FIB has good diagnostic value for ACS, and these index levels are positively correlated with the degree of vascular lesions.

1. Introduction

Coronary heart disease is a kind of stable or unstable disease, which can rapidly develop into acute coronary syndrome (ACS) within a few years, cause myocardial infarction, and then lead to sudden death of patients [1]. ACS is defined as ST-segment elevation myocardial infarction (STEMI), non-ST-segment elevation myocardial infarction (NSTEMI), and unstable angina pectoris (UAP). ACS is a serious manifestation of cardiovascular diseases and is one of the major diseases with high mortality in the world including China [2]. At present, the diagnosis of ACS mainly depends on electrocardiogram, clinical symptoms, and biochemical markers. A single biochemical marker lacks certain specificity. However, patients with ACS often have poor prognosis if they are not treated in time [3]. Therefore, the timely diagnosis and evaluation of ACS is of great significance for subsequent treatment.

Inflammatory reaction plays a key role in the occurrence and promotion of atherosclerosis, which can trigger ACS by inducing plaque instability [4]. The occurrence of ACS is closely related to unstable plaque and secondary thrombosis. Inflammatory cells in plaque and its inflammatory products may be the inducement of plaque instability and rupture [5]. Proinflammatory cytokine interleukin-18 (IL-18) is a proatherosclerotic cytokine. Elevated IL-18 levels and the genetic variation of the IL-18 have been previously linked with acute coronary events and cardiovascular mortality among patients with coronary artery disease (CAD). Previously, it has been shown that IL-18 receptor subunits as well as IL-18 are expressed in atherosclerotic lesions [6]. IL-18 has been associated with the development of subclinical atherosclerosis [3–6]. The production of IL-18 seems to affect not only the overall amount of atherosclerosis but also the stability of atherosclerotic lesions. IL-18 stimulates the production of interferon c (IFN-c), and the proatherogenic

Table 1: Baseline data of three groups (n (%))/($\bar{x} \pm$ SD).

Category	Group A ($n = 136$)	Group B ($n = 70$)	Group C ($n = 60$)	$t/F/\chi^2$	P
Sex				0.630	0.730
Male	71 (52.21)	38 (54.29)	35 (58.33)		
Female	65 (47.79)	32 (45.71)	25 (41.67)		
Age (years)	64.4 ± 9.6	63.6 ± 7.5	63.4 ± 9.7	0.326	0.722
BMI (kg/m^2)	21.24 ± 1.73	20.97 ± 1.29	21.62 ± 1.45	2.804	0.062
Hypertension				5.868	0.053
Yes	73 (53.68)	29 (41.43)	22 (36.67)		
No	63 (46.32)	41 (58.57)	38 (63.33)		
Diabetes				0.419	0.811
Yes	28 (20.59)	14 (20.00)	10 (16.67)		
No	108 (79.41)	56 (80.00)	50 (83.33)		
Hyperlipidemia				3.397	0.183
Yes	46 (30.88)	18 (25.71)	11 (18.33)		
No	94 (69.12)	52 (74.29)	49 (81.67)		
Drinking history				0.310	0.856
Yes	42 (30.88)	23 (32.86)	17 (28.33)		
No	94 (69.12)	47 (67.14)	43 (71.67)		
Smoking history				1.828	0.401
Yes	64 (47.06)	31 (44.29)	22 (36.67)		
No	72 (52.94)	39 (55.71)	38 (63.33)		
Glu (mmol/L)	5.16 ± 0.72	5.02 ± 0.67	5.29 ± 0.51	2.681	0.070
Urea (mmol/L)	5.41 ± 1.52	5.18 ± 1.39	5.09 ± 0.97	1.356	0.260
Scr (μmol/L)	70.85 ± 15.73	69.52 ± 15.74	66.15 ± 10.87	2.106	0.124
BUN (mmol/L)	4.34 ± 1.57	4.27 ± 1.32	4.16 ± 1.28	0.326	0.723
AST (U/L)	26.26 ± 11.07	25.28 ± 10.46	23.85 ± 9.28	1.104	0.333
ALT (U/L)	30.47 ± 10.25	28.58 ± 8.14	27.53 ± 7.45	2.450	0.088
Course of disease (year)	1.6 ± 0.9	1.5 ± 0.8	—	0.784	0.434

Table 2: Comparison of serum IL-18, MMP-9, hs-CRP, and plasma FIB levels in three groups ($\bar{x} \pm$ SD).

Indicator	Group A ($n = 136$)	Group B ($n = 70$)	Group C ($n = 60$)	F	P
IL-18 (ng/mL)	51.25 ± 13.45$^{*,\#}$	37.68 ± 9.56*	20.68 ± 11.48	136.000	<0.001
MMP-9 (ng/mL)	103.48 ± 28.59$^{*,\#}$	83.69 ± 23.68*	77.15 ± 21.32	44.060	<0.001
hs-CRP (mg/L)	6.73 ± 1.46$^{*,\#}$	5.08 ± 1.07*	3.32 ± 0.63	169.500	<0.001
FIB (g/L)	4.91 ± 1.33$^{*,\#}$	3.67 ± 1.04*	2.81 ± 0.96	77.220	<0.001

Note: *compared with group C, $p < 0.05$; $^{\#}$compared with group B, $P < 0.05$.

Table 3: Diagnostic value of serum IL-18, MMP-9, hs-CRP, and plasma FIB for ACS.

Indicator	AUC	95% CI	S. E	Cut-off	Sensitivity (%)	Specificity (%)
IL-18 (ng/mL)	0.804	0.746-0.863	0.030	45.62	70.59	75.71
MMP-9 (ng/mL)	0.814	0.754-0.874	0.030	84.70	78.68	70.00
hs-CRP (mg/L)	0.842	0.789-0.894	0.027	6.12	65.44	90.00
FIB (g/L)	0.795	0.734-0.856	0.031	4.72	59.56	92.86
IL-18+MMP-9+hs-CRP+FIB	0.958	0.932-0.983	0.013	0.71	86.03	95.71

Table 4: Logistic regression analysis of predicting ACS by serum IL-18, MMP-9, hs-CRP, and plasma FIB.

Variable	*B*	S. E	Wals	*P*	OR	95% CI
IL-18 (ng/mL)	0.106	0.025	17.342	<0.001	1.112	1.058-1.168
MMP-9 (ng/mL)	0.062	0.014	19.583	<0.001	1.064	1.035-1.094
hs-CRP (mg/L)	0.830	0.219	14.301	<0.001	2.293	1.492-3.526
FIB (g/L)	0.883	0.218	16.423	<0.001	2.417	1.577-3.704
Constant	-18.201	2.745	43.971	<0.001	—	—

and atherosclerotic plaque destabilizing influence of IL-18 is likely due to this IL-18-dependent production of interferon-γ (IFN-γ) [6]. Matrix metalloproteinase-9 (MMP-9), also known as gelatinase B, which has numerous substrates, is involved in a wide range of physiological functions, including regulation of protease and cytokine activity. In addition, MMP-9 plays a role in elastin degradation, which promotes breakdown of the thin, fibrous caps of plaques [7]. MMP-9, an important member of the matrix metalloproteinase family, is involved in the invasion and metastasis of cancer cells, inflammation, and angiogenesis, as well as the initiation and development of atherosclerosis. One study has demonstrated that MMP-9 levels were significantly higher in patients with vulnerable atherosclerotic plaques than in patients without vulnerable atherosclerotic plaques, indicating that MMP-9 levels were closely associated with vulnerable atherosclerotic plaques [7]. Hypersensitive C-reactive protein (hs-CRP) is a kind of systemic inflammatory reactant in acute phase and is an established marker of cardiovascular risk. The level of hs-CRP is closely related to the degree of atherosclerosis and is a clinical marker of potential modifiable risk for patients with coronary artery disease [8]. hs-CRP is produced by hepatocytes and is involved in inflammation. Clinical studies have demonstrated that hs-CRP levels can be used as predictors of cardiovascular disease. Levels of hs-CRP change with coronary artery plaque characteristics, and hs-CRP is also a predictor of coronary artery disease-associated mortality. Fibrinogen (FIB) is a complex protein, which can reflect hypercoagulable state of blood and is a marker of atherosclerosis activity [9]. Although there have been many studies on IL-18, MMP-9, hs-CRP, and FIB in ACS [10–13] in the past, there are few studies on the diagnostic value of combined detection of these indicators in ACS and the correlation with the degree of vascular lesions.

In this study, the levels of IL-18, MMP-9, hs-CRP, and FIB in the peripheral blood of ACS patients were detected to explore the diagnostic value of IL-18, MMP-9, hs-CRP, and FIB in ACS and the correlation with the severity of coronary artery lesions.

2. Materials and Methods

2.1. General Information. Altogether 206 patients with coronary heart disease admitted to our hospital were selected as research objects, including 136 patients with ACS (group A), 70 patients with stable angina pectoris (SAP) (group B), and 60 patients with noncoronary heart disease who had normal coronary angiography during the same period were selected as group C. In group A, there were 71 males and 65 females, aged 52-77 years with an average age of 64.4 ± 9.6 years. In group B, there were 38 males and 32 females, aged 52-76 years with an average age of 63.6 ± 7.5 years. In group C, there were 35 males and 25 females, aged 50-76 years, with an average age of 63.4 ± 9.7 years. This study was approved by the Ethics Committee of our hospital. The subjects and their families were informed and signed a fully informed consent form.

2.2. Inclusion and Exclusion Criteria. The inclusion criteria were as follows: Group A met ACS diagnostic criteria of American College of Cardiology and American Heart Association (ACC/AHA) [14], accompanied by chest pain, abnormal electrocardiogram, and elevated serum troponin I level, etc.; group B met the SAP diagnostic criteria in ACC/AHA [15]; patients with complete clinical data. The exclusion criteria were as follows: nonsteroidal anti-inflammatory drugs and immunosuppressants were used one week before admission; patients combined with severe liver and kidney dysfunction, coronary artery malformation, valvular heart disease, malignant tumor, hypertrophic obstructive cardiomyopathy, severe organic diseases, mental diseases, dilated cardiomyopathy, heart failure, cognitive dysfunction, thyroid dysfunction, infectious diseases, stroke, renal artery stenosis, an dautoimmune diseases.

2.3. Detection Method. A total of 4 mL of fasting venous blood was sampled from the subjects and placed in blood collection tube without anticoagulant and containing sodium citrate anticoagulant. Then, the blood was centrifuged at $1450 \times g$ for 10 min with a centrifuge radius of 10 cm. The upper serum was separated for later use. The levels of IL-18, MMP-9, and hs-CRP in serum were detected by enzyme-linked immunosorbent assay (ELISA) [16], and the detection was carried out with reference to the instruction manual of human IL-18, MMP-9, and hs-CRP ELISA kit (Shanghai Guang Rui Biological Technology Co., Ltd., China, batch number: 1057, 716, 1497). A blank well, a sample well to be tested, and a standard well were set up, and no samples and enzyme-labeled reagents were added to the blank well; 50 μL of standard substance and 50 μL of streptomycin HRP were added to the standard well, and 40 μL of sample, 10 μL of antibody ,and 50 μL of streptomycin HRP were added to the sample well to be tested; then, the wells were covered with film and incubated at 37°C for 60 min; the liquid were discarded and dried, and the rinse were repeated for 5 times; 50 μL of developer A and then 50 μL of developer B were added to each well. The mixture was shaken and mixed evenly. The color reaction was developed

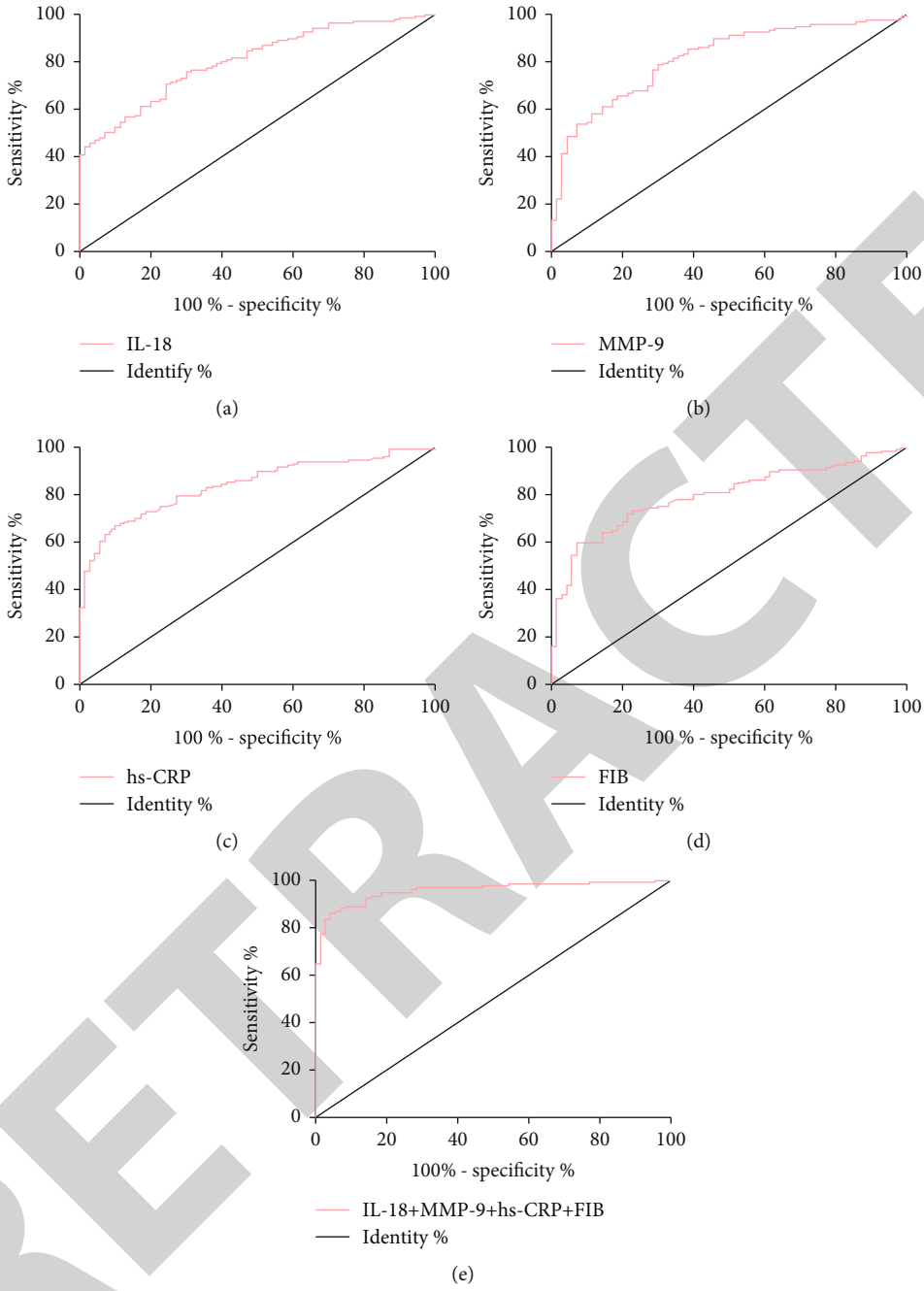

Figure 1: ROC curve of serum IL-18, MMP-9, hs-CRP, and plasma FIB diagnosing ACS. (a) The sensitivity and specificity of serum IL-18 in diagnosing ACS were 70.59% and 75.71%, respectively. (b) The sensitivity and specificity of serum MMP-9 in diagnosing ACS were 78.68% and 70.00%, respectively. (c) The sensitivity and specificity of serum hs-CRP in diagnosing ACS were 65.44% and 90.00%, respectively. (d) The sensitivity and specificity of plasma FIB in diagnosing ACS were 59.56% and 92.86%, respectively. (e) The sensitivity and specificity of combined diagnosis of ACS by serum IL-18, MMP-9, hs-CRP, and plasma FIB were 86.03% and 95.71%, respectively. IL-8: interleukin-8; MMP-9: matrix metalloproteinase-9; hs-CRP: high-sensitivity C-reactive protein; FIB: fibrinogen.

at 37°C in the dark for 10 min. A 50 μL of stop solution was added to each well to stop the reaction. The absorbance (OD value) of each well was measured sequentially at 450 nm wavelength using RAD550 microplate reader (Bio-Rad, Hercules, CA, USA), and IL-18, MMP-9, and hs-CRP levels were calculated. Sta-R Evolution fully automatic hemagglutination analyzer (Sichuan Asia-Core Medical Instruments Co., Ltd., China) was used to detect the level of FIB in plasma. The detection process was strictly carried out in accordance with the operation instructions of the instrument and kit.

2.4. Coronary Gensini Score. Coronary angiography was performed using NSX-6000SONATA digital vascular X-ray machine (General Electric Company, Schenectady, NY, USA). Left and right coronary angiographies were performed sequentially. The left coronary artery was observed

Table 5: Comparison of serum IL-18, MMP-9, hs-CRP, and plasma FIB levels ($\bar{x} \pm SD$).

Indicator	n	IL-18 (ng/mL)	MMP-9 (ng/mL)	hs-CRP (mg/L)	FIB (g/L)
Mild lesion	31	39.15 ± 10.65	86.48 ± 22.18	5.25 ± 1.43	3.94 ± 1.02
Moderate lesion	40	47.53 ± 12.69*	93.37 ± 24.63*	6.59 ± 1.44*	4.62 ± 1.25*
Severe lesion	65	57.37 ± 13.56*,#	116.28 ± 29.53*,#	7.16 ± 1.53*,#	5.64 ± 1.38*,#
F	—	18.970	16.670	17.450	20.790
P	—	<0.001	<0.001	<0.001	<0.001

Note: *compared with mild lesions, $p < 0.05$; #compared with moderate lesions, $P < 0.05$.

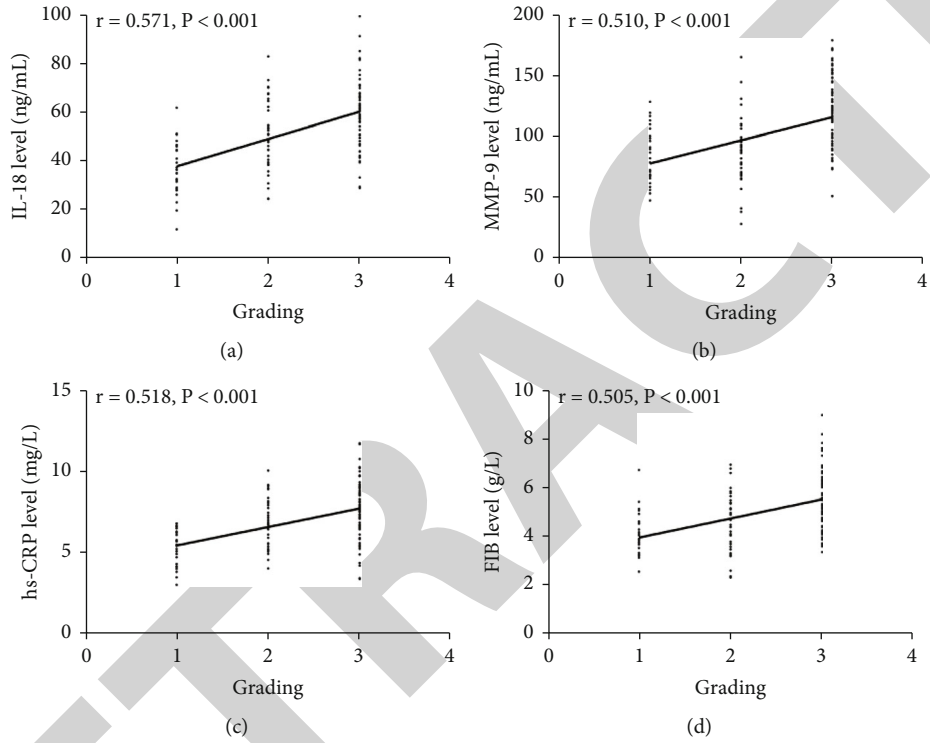

Figure 2: Correlation between serum IL-18, MMP-9, hs-CRP, and plasma FIB levels and Gensini score grading in group A. (a) Serum IL-18 level was positively correlated with Gensini score classification ($r = 0.571$, $p < 0.001$). (b) Serum MMP-9 level was positively correlated with Gensini score classification ($r = 0.510$, $p < 0.001$). (c) hs-CRP level was positively correlated with Gensini grading ($r = 0.518$, $p < 0.001$). (d) Plasma FIB level was positively correlated with Gensini score classification ($r = 0.505$,$p < 0.001$). IL-8: interleukin-8; MMP-9: matrix metalloproteinase-9; hs-CRP: high-sensitivity C-reactive protein; FIB: fibrinogen.

at more than or equal to 5 positions, the right coronary artery was observed at more than or equal to 2 positions, and the stenosis degree of vascular lesions was measured. The Gensini score was evaluated combining the stenosis degree results of coronary angiography [17]. A degree of 100% stenosis indicates 32 points, 91%-99% indicates 16 points, 76%-90% indicates 8 points, 51%-75% indicates 4 points, 26%-50% indicates 2 points, and 1%-25% indicates 1 point. The lesions in the middle and distal segments of the left circumflex branch and distal segment of descending branches represent 1 point, lesions in the right coronary artery represent 1 point, lesions in the middle segment of the left anterior descending branch represent 1.5 points, lesions in the proximal segment of the left anterior circumflex branch and descending branch represent 2.5 points, and lesions in the left main artery represent 5 points. The coronary artery Gensini score was obtained by multiplying the lesion site and stenosis degree score and then adding the products together. Gensini grade: mild lesion: less than 50 points; moderate lesions: 50-99 points; severe lesions: more than or equal to 100 points. In group A, there were 31 cases of mild lesions, 40 cases of moderate lesions, and 65 cases of severe lesions.

2.5. Statistical Method. SPSS 22.0 (IBM Corp, Armonk, NY, USA) was used for statistical analysis. The measurement data were expressed by mean ± standard deviation ($\bar{x} \pm SD$). Independent sample t-test was used for the comparison of measurement data between groups, and paired t-test was used for the comparison before and after treatment within the group. Counting data was expressed by the number of cases/percentage (n (%)), and chi-square test was used for

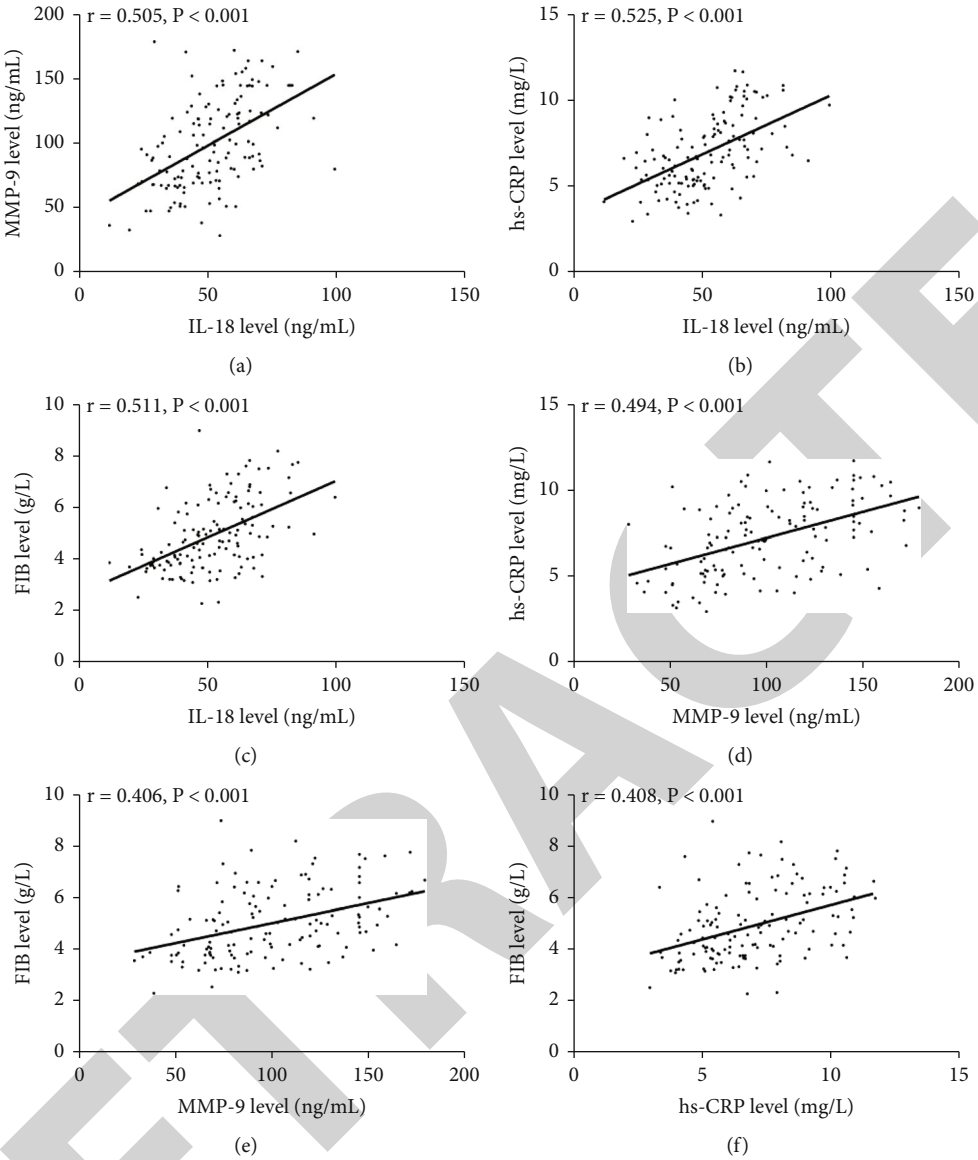

Figure 3: Correlation between serum IL-18, MMP-9, hs-CRP, and plasma FIB levels in group A. (a) Serum IL-18 level is positively correlated with MMP-9 ($r = 0.505$, $p < 0.001$). (b) Serum IL-18 level was positively correlated with hs-CRP ($r = 0.525$, $p < 0.001$). (c) Serum IL-18 level was positively correlated with plasma FIB ($r = 0.511$, $p < 0.001$). (d) Serum MMP-9 level was positively correlated with hs-CRP ($r = 0.494$, $p < 0.001$). (e) Serum MMP-9 level was positively correlated with plasma FIB ($r = 0.406$, $p < 0.001$). (f) Serum hs-CRP level was positively correlated with plasma FIB ($r = 0.408$, $p < 0.001$). IL-8: interleukin-8; MMP-9: matrix metalloproteinase-9; hs-CRP: high-sensitivity C-reactive protein; FIB: fibrinogen.

comparison of counting data between groups. One-way ANOVA was used for the comparison of multiple groups' mean values, and LSD-t test was used for pairwise comparison in multiple groups. ROC curve and multivariate logistic regression were used to analyze the diagnostic value of IL-18, MMP-9, hs-CRP, and FIB in ACS. Spearman's correlation coefficient was used to analyze the correlation of serum IL-18, MMP-9, hs-CRP, and plasma FIB levels with Gensini grading. Pearson's correlation coefficient was used to analyze the correlation between serum IL-18, MMP-9, hs-CRP, and plasma FIB. The p value less than 0.05 was regarded as the statistical significance.

3. Results

3.1. Baseline Data of Three Groups. There was no significant difference in clinical baseline data such as gender, age, body mass index (BMI), hypertension, diabetes, hyperlipidemia, drinking history, smoking history, blood glucose (Glu), blood urea (urea), serum creatinine (Scr), blood urea nitrogen (BUN), aspartate aminotransferase (AST), alanine aminotransferase (ALT) among groups A, B, and C ($p < 0.05$). There was no significant difference in the disease course between group A and group B ($p < 0.05$), see Table 1.

3.2. Results of Serum IL-18, MMP-9, hs-CRP, and Plasma FIB Levels in Three Groups. The levels of serum IL-18, MMP-9, hs-CRP, and plasma FIB in group A were significantly higher than those in group B and group C ($p < 0.05$). The levels of serum IL-18, MMP-9, hs-CRP, and plasma FIB in group B were significantly higher than those in group C ($p < 0.05$), see Table 2.

3.3. Diagnostic Value of Serum IL-18, MMP-9, hs-CRP, and Plasma FIB Levels in ACS. The ROC curves of serum IL-18, MMP-9, hs-CRP, and plasma FIB for diagnosing ACS were drawn. The optimal critical value of serum IL-18 for diagnosing ACS was 45.62 ng/mL, the diagnostic sensitivity was 70.59%, and the specificity was 75.71%. The optimal critical value of serum MMP-9 in diagnosing ACS was 84.70 ng/mL, the diagnostic sensitivity was 78.68%, and the specificity was 70.00%. The optimal critical value of serum hs-CRP for diagnosing ACS was 6.12 mg/L, the diagnostic sensitivity was 65.44%, and the specificity was 90.00%. The optimal critical value of plasma FIB for diagnosing ACS was 4.72 g/L, the diagnostic sensitivity was 59.56%, and the specificity was 92.86%. We further drew ROC curves of combined diagnosis of ACS by serum IL-18, MMP-9, hs-CRP, and plasma FIB levels and established a combined detection model of IL-18, MMP-9, hs-CRP, and FIB according to logistic regression analysis. The combined model was $\text{Logit}(p) = -18.201 + 0.106 \times \text{IL} - 18 + 0.062 \times \text{MMP} - 9 + 0.830 \times \text{hs} - \text{CRP} + 0.883 \times \text{FIB}$. The area under curve of combined detection was fitted by the probability value in the model. The sensitivity and specificity of combined diagnosis of ACS by serum IL-18, MMP-9, hs-CRP, and plasma FIB were 86.03% and 95.71%, see Tables 3 and 4 and Figure 1.

3.4. Correlation of Serum IL-18, MMP-9, hs-CRP, and Plasma FIB with Gensini Score Grading in Group A. The levels of serum IL-18, MMP-9, hs-CRP, and plasma FIB in patients with severe lesions were significantly higher than those in patients with mild and moderate lesions ($p < 0.05$). The levels of serum IL-18, MMP-9, hs-CRP, and plasma FIB in patients with moderate lesions were significantly higher than those in patients with mild lesions ($p < 0.001$). According to Gensini grading, patients with mild lesions were set as 1, patients with moderate lesions as 2, and patients with severe lesions as 3. Spearman's correlation coefficient showed that serum IL-18, MMP-9, hs-CRP, and plasma FIB were positively correlated with Gensini score classification ($r = 0.571$, $p < 0.001$; $r = 0.510$, $p < 0.001$; $r = 0.518$, $p < 0.001$; $r = 0.505$, $p < 0.001$), see Table 5 and Figure 2.

3.5. Correlation between Serum IL-18, MMP-9, hs-CRP, and Plasma FIB Levels in Group A. The level of serum IL-18 in group A was positively correlated with MMP-9, hs-CRP, and plasma FIB ($r = 0.505$, $p < 0.001$; $r = 0.525$, $p < 0.001$; $r = 0.511$, $p < 0.001$); serum MMP-9 level was positively correlated with hs-CRP and plasma FIB ($r = 0.494$, $p < 0.001$; $r = 0.406$, $p < 0.001$); serum hs-CRP level was positively correlated with plasma FIB ($r = 0.408$, $p < 0.001$), see Figure 3.

4. Discussion

ACS is a kind of coronary heart disease emergency, which is caused by unstable rupture of arterial plaque and can cause sudden cardiac death [18]. ACS is characterized by inflammatory reaction, platelet activation, and myocardial ischemia, with the key link of thrombosis [19]. ACS has the characteristics of rapid onset, rapid disease change, and high mortality rate [20]. Therefore, the early diagnosis of ACS and the prediction of the severity of coronary artery disease are of great significance to the prevention, treatment, and prognosis of ACS.

A large number of studies have confirmed the close relationship between inflammation and ACS [21]. During the development of ACS, the interaction between leukocytes and endothelial cells can promote the release of various cytokines, which can stimulate liver synthesis of acute phase reaction proteins (including CRP and FIB) [22]. IL-18 is an important pro-inflammatory factor, and its expression is elevated in atherosclerotic plaques [23]. MMP-9 is an enzyme analog that damages the elastic membrane of blood vessels and is closely related to atherosclerotic plaque and vascular reconstruction [24]. hs-CRP is an indicator of inflammatory state, and the level of hs-CRP can change with the characteristics of coronary plaque, which is a predictor of coronary disease-related mortality [25]. FIB can promote the proliferation of vascular smooth muscle cells and the formation of atherosclerotic plaques, which is an indicator of thrombosis [26]. There have been many studies on IL-18, MMP-9, hs-CRP, and FIB in ACS in the past. For example, in the study of Li et al. [27], the plasma levels of IL-18 and IL-10 in SAP patients are closely related to the occurrence of ACS. The increased IL-18/IL-10 ratio has positive predictive value for the occurrence of ACS in SAP patients. In the study of Inokubo et al. [28], elevated plasma MMP-9 and TIMP-1 levels can be detected in coronary circulation of ACS patients, which are involved in the process of active plaque rupture in ACS. However, studies by Shi et al. [29] have confirmed that the plasma FIB level of ACS patients is significantly higher than that of stable coronary heart disease patients and healthy people. High CRP and FIB levels are predictive factors for long-term poor prognosis of ACS patients. In this study, the levels of serum IL-18, MMP-9, hs-CRP, and plasma FIB in group A are significantly higher than those in groups B and C, which indicates that IL-18, MMP-9, hs-CRP, and FIB may participate in the occurrence and development of ACS, and is similar to the above research. Although IL-18, MMP-9, hs-CRP, and FIB play an important role in the occurrence and development of ACS, there is little research on the diagnostic value of combined detection of these indicators for ACS. The study further showed that the sensitivity and specificity of the combined detection of serum IL-18, MMP-9, hs-CRP, and plasma FIB in the diagnosis of ACS were 86.03% and 95.71%, respectively. The combined detection of the four has good predictive value for ACS. The Gensini score is a scoring system for stenosis degree of coronary artery disease, which is of great significance for prognosis prediction of patients with coronary heart

disease [30]. In this study, serum IL-18, MMP-9, hs-CRP, and plasma FIB are positively correlated with Gensini score grading, indicating that IL-18, MMP-9, hs-CRP, and FIB were positively correlated with vascular lesion degree. Guo et al. [31] believe that the levels of hs-CRP and MMP-9 are significantly correlated with the severity of coronary artery lesions, and the levels of serum estrogen, hs-CRP, and MMP-9 are also significantly correlated, which can be used as biomarkers for the severity of coronary artery lesions and the stability of coronary artery plaques. In the study by Wang et al. [32], the levels of serum hs-CRP and IL-6 in the serum of ACS patients are significantly increased, which can be used to determine the stability of plaque and has some correlation in the development of ACS, and is of great significance to the prognosis judgment of ACS patients. In this study, serum IL-18, MMP-9, hs-CRP, and plasma FIB levels in ACS patients are positively correlated. FIB can increase the viscosity of blood, regulate the synthesis of inflammatory cells and endothelial cells, and mediate inflammatory reactions by changing hemorheology and damaging endothelium, thus participating in the progress of atherosclerosis [33]. Therefore, the occurrence and development of ACS may be the result of the synergistic effect of inflammatory reaction and thrombosis, but the mechanism remains to be further observed.

This study confirmed the diagnostic value and effect of combined detection of serum IL-18, MMP-9, hs-CRP, and plasma FIB on ACS, but there are still some deficiencies in the experiment. First, the risk factors of ACS are not observed. Second, the role of IL-18, MMP-9, hs-CRP, and FIB in the prognosis of ACS patients has not been studied. These deficiencies need to be further supplemented in future research.

The combined detection of serum IL-18, MMP-9, hs-CRP, and plasma FIB has a good diagnostic value for ACS, and these index levels are positively correlated with the degree of vascular lesions.

Data Availability

The authors confirm that the data supporting the findings of this study are available within the article.

Conflicts of Interest

The authors declare that they have no conflict of interest.

Authors' Contributions

Yuexia Yang and Guoming Li performed the experiments, analyzed data, and wrote the manuscript. Ruiqin Zhang designed the study. All the authors agreed to be accountable for the accuracy and integrity of all aspects of the research. Yuexia Yang and Guoming Li contributed equally to this study as co-first author.

References

[1] H. Chung, H. M. Kwon, J. Y. Kim et al., "Lipoprotein-associated phospholipase A2Is related to plaque stability and is a potential biomarker for acute coronary syndrome," *Yonsei Medical Journal*, vol. 55, no. 6, pp. 1507–1515, 2014.

[2] C. Zhang, P. Liu, K. Xia et al., "Association of serum prealbumin with angiographic severity in patients with acute coronary syndrome," *Medical Science Monitor*, vol. 23, pp. 4041–4049, 2017.

[3] E. Danese and M. Montagnana, "An historical approach to the diagnostic biomarkers of acute coronary syndrome," *Annals of Translational Medicine*, vol. 4, no. 10, p. 194, 2016.

[4] M. Krintus, M. Kozinski, A. Stefanska et al., "Value of C-reactive protein as a risk factor for acute coronary syndrome: a comparison with apolipoprotein concentrations and lipid profile," *Mediators of Inflammation*, vol. 2012, Article ID 419804, 10 pages, 2012.

[5] C. Y. Ma, Z. Y. Xu, S. P. Wang et al., "Change of inflammatory factors in patients with acute coronary syndrome," *Chinese Medical Journal*, vol. 131, no. 12, pp. 1444–1449, 2018.

[6] H. O. El-Mesallamy, N. M. Hamdy, A. K. El-Etriby, and E. F. Wasfey, "Plasma granzyme B in ST elevation myocardial infarction versus non-ST elevation acute coronary syndrome: comparisons with IL-18 and fractalkine," *Mediators of Inflammation*, vol. 2013, Article ID 343268, 8 pages, 2013.

[7] M. H. Tayebjee, G. Y. Lip, and R. J. MacFadyen, "Matrix metalloproteinases in coronary artery disease: clinical and therapeutic implications and pathological significance," *Current Medicinal Chemistry*, vol. 12, no. 8, pp. 917–925, 2005.

[8] M. Qintar, P. P. Sharma, Y. Pokharel et al., "Prevalence and predictors of elevated high-sensitivity C-reactive protein in post–myocardial infarction patients: insights from the VIRGO and TRIUMPH registries," *Clinical Cardiology*, vol. 40, no. 12, pp. 1205–1211, 2017.

[9] A. C. van Dijk, S. J. Donkel, T. Zadi et al., "Association between fibrinogen and fibrinogen γ' and atherosclerotic plaque morphology and composition in symptomatic carotid artery stenosis: Plaque-At- RISK study," *Thrombosis Research*, vol. 177, pp. 130–135, 2019.

[10] J. Zhou, G. Deng, T. Yang, Q. Ma, and X. Luo, "Association between interleukin-18 and Global Registry of Acute Coronary Events score in patients with acute coronary syndrome," *Zhong Nan Da Xue Xue Bao. Yi Xue Ban*, vol. 39, no. 6, pp. 570–576, 2014.

[11] I. V. Santana and J. E. Tanus-Santos, "Serum or plasma matrix metalloproteinase (MMP)-9 levels and cardiovascular diseases," *Journal of Cardiovascular Translational Research*, vol. 11, no. 6, pp. 524-525, 2018.

[12] N. Fernandez Machulsky, J. Gagliardi, B. Fabre et al., "Matrix metalloproteinases and psychosocial factors in acute coronary syndrome patients," *Psychoneuroendocrinology*, vol. 63, pp. 102–108, 2016.

[13] S. P. Whelton, V. Narla, M. J. Blaha et al., "Association between resting heart rate and inflammatory biomarkers (high- sensitivity C-reactive protein, interleukin-6, and fibrinogen) (from the multi-ethnic study of atherosclerosis)," *The American Journal of Cardiology*, vol. 113, no. 4, pp. 644–649, 2014.

[14] F. Rodriguez and K. W. Mahaffey, "Management of patients with NSTE-ACS: a comparison of the recent AHA/ACC and

Hindawi
BioMed Research International
Volume 2024, Article ID 9853194, 1 page
https://doi.org/10.1155/2024/9853194

Retraction

Retracted: Effects of Sevoflurane on Apoptosis of Myocardial Cells in IRI Rats

BioMed Research International

Received 12 March 2024; Accepted 12 March 2024; Published 20 March 2024

This article has been retracted by Hindawi following an investigation undertaken by the publisher [1]. This investigation has uncovered evidence of one or more of the following indicators of systematic manipulation of the publication process:

(1) Discrepancies in scope

(2) Discrepancies in the description of the research reported

(3) Discrepancies between the availability of data and the research described

(4) Inappropriate citations

(5) Incoherent, meaningless and/or irrelevant content included in the article

(6) Manipulated or compromised peer review

The presence of these indicators undermines our confidence in the integrity of the article's content and we cannot, therefore, vouch for its reliability. Please note that this notice is intended solely to alert readers that the content of this article is unreliable. We have not investigated whether authors were aware of or involved in the systematic manipulation of the publication process.

Wiley and Hindawi regrets that the usual quality checks did not identify these issues before publication and have since put additional measures in place to safeguard research integrity.

We wish to credit our own Research Integrity and Research Publishing teams and anonymous and named external researchers and research integrity experts for contributing to this investigation.

The corresponding author, as the representative of all authors, has been given the opportunity to register their agreement or disagreement to this retraction. We have kept a record of any response received.

References

[1] S. Zhang, X. Du, K. Zhang, and H. Wang, "Effects of Sevoflurane on Apoptosis of Myocardial Cells in IRI Rats," *BioMed Research International*, vol. 2021, Article ID 3347949, 6 pages, 2021.

Hindawi
BioMed Research International
Volume 2021, Article ID 3347949, 6 pages
https://doi.org/10.1155/2021/3347949

Research Article

Effects of Sevoflurane on Apoptosis of Myocardial Cells in IRI Rats

Shikun Zhang,[1] Xiaoyan Du,[2] Kun Zhang,[3] and Haiyan Wang[1]

[1]*Department of Cardiovascular Disease, Gaomi People's Hospital, 77 Gaomi Zhenfu Street, Weifang, 261500 Shandong, China*
[2]*Department of Ophthalmology, Gaomi People's Hospital, 77 Gaomi Zhenfu Street, Weifang, 261500 Shandong, China*
[3]*Department of Geriatrics, Gaomi People's Hospital, 77 Gaomi Zhenfu Street, Weifang, 261500 Shandong, China*

Correspondence should be addressed to Haiyan Wang; wanghaiyan751227@163.com

Received 21 September 2021; Revised 29 October 2021; Accepted 30 October 2021; Published 31 December 2021

Academic Editor: Jianxin Shi

Background. Cardiomyocyte apoptosis functions essentially in ischemia/reperfusion- (I/R-) induced myocardial injury. It is suggested that autophagy is widely implicated in the regulation of cell survival and death. Sevoflurane, as a largely used inhalational general anesthetic, has been shown to have a protective effect on cardiomyocytes. However, it was yet elusive on the underlying mechanisms. *Aim*. The objective of this study is to investigate the association of sevoflurane-mediated cardioprotective effects with autophagy regulation. *Methods*. An in vitro hypoxia model was established in primary cardiomyocytes from fresh myocardial tissue of the rats. The apoptosis rate of myocardial cells treated with hypoxia and treated with sevoflurane was measured. Western blot and immunocytochemical assay were used to measure the protein expression. The cell proliferation rate and cell apoptosis were measured using the MTT assay and flow cytometry, respectively. *Results*. The expression of apoptotic proteins including B cell lymphoma-2 (Bcl-2), CCAAT/enhancer-binding protein homologous protein (CHOP), glucose-regulated protein 78 (GRP78), and Bcl-2-associated X protein (BAX) in myocardium treated with sevoflurane was significantly lower than that in myocardium treated with hypoxia. The expression of adhesion proteins such as intercellular adhesion molecule-1 (ICAM-1), vascular cell adhesion molecule-1 (VCAM-1), and E-selectin in myocardium treated with sevoflurane was higher than that in myocardium treated with hypoxia, suggesting better connectivity of the myocardium. *Conclusion*. Sevoflurane treatment reduced the apoptosis of myocardial cells after hypoxia treatment.

1. Introduction

General anesthesia is a reversible state induced by drugs [1]. Under the condition of maintaining physiological stability, patients will have a reversible state such as coma, forgetfulness, antisyncope, and immobility [2]. Since the first public display of diethyl ether as a general anesthetic at Massachusetts General Hospital (MGH) in 1846, the practice of anesthesiology has revolutionized surgery and spurred the advance of modern medicine [3]. Today, more than 170 years later, the administration of diethyl ether derivatives remains the basis of anesthesiology [4]. Fluoromethyl hexafluoroisopropyl ether, also known as sevoflurane, is a derivative of diethyl ether, which is widely used in current clinical practice [5].

The change of diet and the improvement of living standard make the incidence of cardiovascular disease in China rise rapidly [6]. At present, the main treatment method is to restore normal blood supply to the heart by recanalization of blocked coronary arteries by surgical operation or intervention. Cardiac surgery is more susceptible to external factors than surgery on other solid organs, so anesthesia is more carefully used [7]. Improper use or concentration of anesthetic drugs can cause patients with arrhythmia, tachycardia, bradycardia and other symptoms, or even death [8].

Sevoflurane, as a new sort of inhalation anesthetic, produces excellent anesthesia quality and is commonly employed in cardiac surgeries since it exerts more fast and smooth recovery than other inhaled anesthesia. It was demonstrated that the application of sevoflurane at the onset of

reperfusion (sevoflurane postconditioning) was a protective stimulus to decrease ischemia/reperfusion (I/R) injury in patients undergoing coronary bypass surgery [9]. Studies have found that sevoflurane can not only improve the myocardial contractility but also reduce the myocardial infarction area, which has a protective effect on the myocardium [9, 10]. Sevoflurane pretreatment of isolated rat right ventricular muscle can effectively promote the recovery of myocardial contractility after reperfusion. Studies have shown that sevoflurane pretreatment and posttreatment can both reduce the area of heart infarction, but posttreatment is more widely used than sevoflurane preconditioning in clinical therapy [9]. Additionally, *in vivo* studies and clinical observations have shown that sevoflurane can increase left ventricular pressure (LVDP) and reduce left ventricular end-diastolic pressure (LV-EDP) [11].

Therefore, in this study, we aimed to investigate the effects of sevoflurane treatment in rat-derived primary cardiomyocytes. We demonstrated the protective effect of sevoflurane on hypoxic cardiomyocytes. And this protective effect was demonstrated by reducing the expression of apoptotic proteins in myocardial cells.

2. Methods

2.1. Primary Cell Culture. The fresh myocardial tissue of the rats was cut into 1–2 mm^3 heart fragments in phosphate-buffered saline (PBS) containing 0.1% trypsin and 0.1% collagenase. After the digestion of tissues 3-4 times, 5 minutes each time, the digested cells from the tissues were collected and centrifuged in DMEM containing 10% FBS. Finally, the cells were cultured in DMEM containing 10% FBS. The cell suspensions were mixed and plated at a cell culture flask in 37°C in a 5% CO_2 incubator for 30 min cultivation. The cells were then cultured in 6-well and 96-well plates and kept at 37°C and 5% CO_2. On the first 2 days, 100 mM 5-bromo-29-deoxyuridine (BrdU; BioVision, USA) inhibits nonmyocyte proliferation. The cells were cultured for 3 days.

2.2. Hypoxia Treatment and Experimental Grouping. For hypoxia treatment, oxygen-control incubator (Thermo Fisher Scientific Inc., Waltham, MA) was used. Cardiomyocytes were randomly divided into three groups. To study the protective effect of sevoflurane against hypoxia in cardiomyocytes, cells cultured under normal oxygen conditions (normal control) were set up. Cells were cultured in an anaerobic chamber with 2% CO_2 and 95% N_2 for 24 h (hypoxia group). For anesthetic agent treatment, cells pretreated with 1.8 mg/mL sevoflurane were incubated in an anesthesia induction chamber immediately after hypoxia treatment at 37°C, 2% O_2 for 12 h (hypoxia+sevoflurane group).

2.3. Cell Viability. The effect of sevoflurane on cell proliferation was determined using the MTT method.

Briefly, the cells were treated as described above and were placed in a 96-well plate and cultured overnight in DMEM and 10% FBS containing 0.5 mg/mL of MTT (Biotech, Shanghai, China). An automated microplate reader was used to measure the absorbance at 490 nm (Molecular Devices, Sunnyvale, CA).

2.4. Flow Cytometry Assay. After different treatments, the cells were plated in six-well plates. The medium was replaced with cold 75% ethanol to fix the cells at 4°C overnight. Then, 10 μL of Annexin V-fluorescein isothiocyanate (FITC) binding buffer (Sigma-Aldrich, USA) and 5 μL of propidium iodide (PI) (Sigma-Aldrich, USA) were added to each well to incubate cells for 20 min in the dark. The apoptosis rate of each well was detected by using a FACScan flow cytometer (Beckman-Coulter, California, USA).

2.5. Western Blot. Western blot was performed to detect then expression levels of B cell lymphoma-2 (Bcl-2), CCAAT/enhancer-binding protein homologous protein (CHOP), glucose-regulated protein 78 (GRP78), Bcl-2-associated X protein (BAX), intercellular adhesion molecule-1 (ICAM-1), vascular cell adhesion molecule-1 (VCAM-1), and E-selectin in the heart cells from control, hypoxia, and sevoflurane groups. Cells were homogenized and protein isolated using the RIPA lysis buffer system (Thermo Fisher, Massachusetts, USA). Protein concentrations were quantified using the BCA protein assay (Beyotime, Shanghai, China), and all samples were loaded with equal protein onto 10% polyacrylamide gel with 0.1% sodium dodecyl sulfate (SDS). Proteins were then separated by electrophoresis and transferred onto nitrocellulose membranes. Nonspecific binding sites were blocked with Tris-buffered saline solution (TBS) containing 5% dry milk. The membranes were incubated with primary antibodies against ICAM (ab171123, Abcam; 1 : 500), E-selectin (ab18981, Abcam; 1 : 1000), VCAM (ab134047, Abcam; 1: 500), Bcl-2 (ab32124, Abcam; 1 : 500), BAX (ab32503, Abcam; 1 : 500), GRP78 (ab21685, Abcam; 1 : 500), and β-actin (ab8226, Abcam; 1 : 1000). After the membranes were cleaned, protein blots were detected by enhanced chemiluminescence (ECL) (Beyotime). The intensity of the identified bands was detected by densitometry software (Quantity One software; Bio-Rad, Hercules, CA, USA).

2.6. Statistical Analysis. The representative data were expressed as the mean ± standard deviation (SD) from three independent experiments. SPSS version 19.0 software (IBM Corp., Armonk, NY, USA) was employed for statistical analysis. Data among multiple groups were compared with one-way analysis of variance (ANOVA), and data between two groups were compared by Student's *t*-test. A P value < 0.05 was considered to be statistically significant.

3. Results

Flow cytometry was used to analyze the cell death of myocardial cells in three groups (control group, hypoxia group, and hypoxia+sevoflurane group). Compared with the control group, 12-hour hypoxia treatment resulted in a large number of myocardial cell apoptosis (Figure 1(a)), but in the sevoflurane group, the apoptosis caused by hypoxia was alleviated (Figure 1(b)). This confirmed that sevoflurane inhibited apoptosis.

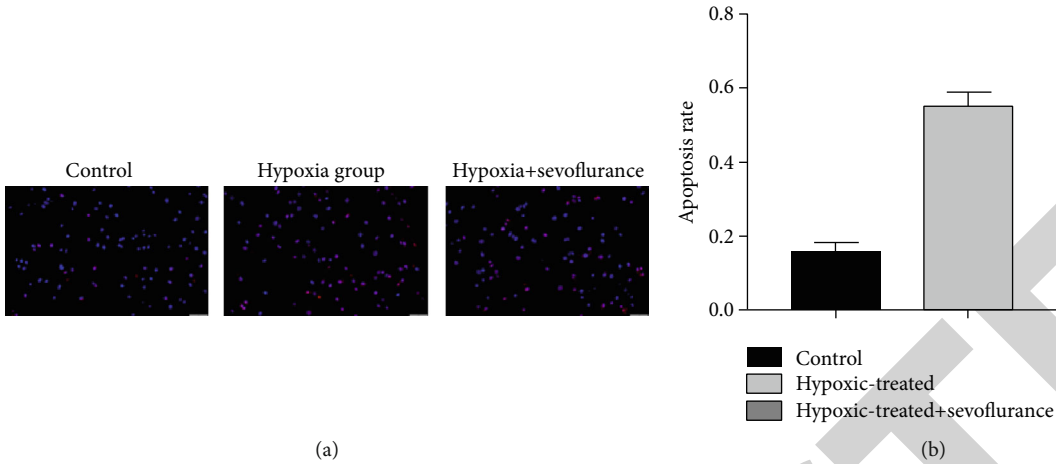

Figure 1: The sevoflurane treatment group showed less apoptosis. (a, b) TUNEL staining demonstrated an increased apoptosis rate of myocardial cells in the hypoxia group. However, the apoptosis rate of myocardial cells in the hypoxia group was decreased after sevoflurane treatment. $^{*}P < 0.05$ and $^{**}P < 0.01$.

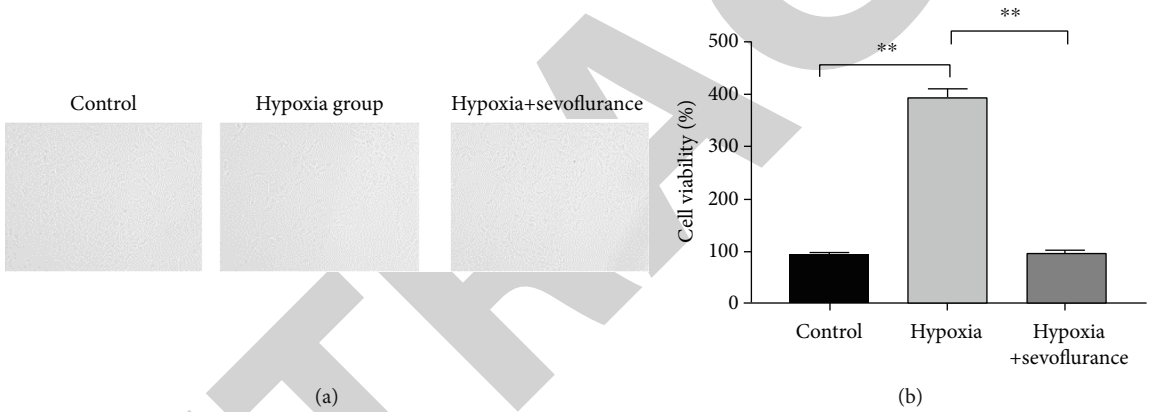

Figure 2: The survival ability of myocardial cells treated with sevoflurane increased compared with that treated with hypoxia. (a) The morphology of the cells did not change after hypoxia or sevoflurane treatment. (b) The cell viability test showed that the myocardial viability of the sevoflurane treatment group was significantly better than that of the hypoxia treatment group. $^{*}P < 0.05$ and $^{**}P < 0.01$.

The morphology of the cells did not change after hypoxia or sevoflurane treatment (Figure 2(a)).

In the same culture condition, the cell proliferation ability and cell density decreased after hypoxia treatment. The addition of sevoflurane alleviates the cell loss. In the cell survival assay, the cell survival index of hypoxia treatment was significantly lower than that of the control group (Figure 2(b)). Similar to the results of apoptosis test, the proliferation ability of cells treated with sevoflurane was enhanced.

To investigate the molecular biological causes of sevoflurane's inhibition of hypoxic cell apoptosis, western blot was used to detect protein expression. Apoptosis-promoting proteins such as CHOP, CRP78, and BAX were significantly increased in the hypoxia group, while apoptosis-inhibiting protein Bcl-2 was significantly higher in the sevoflurane group than in the hypoxia group (Figures 3(a) and 3(b)). This explains why the apoptosis of sevoflurane-treated cells was significantly lower than that of the hypoxia group.

In addition, we examined intercellular adhesion molecule-1 (ICAM-1), vascular cell adhesion molecule-1 (VCAM-1), and E-selectin proteins, which are thought to be expressed in the presence of myocardial injury. Western blot detection revealed that these proteins were highly expressed in 12-hour hypoxic cardiomyocytes and significantly decreased in cells treated with sevoflurane (Figures 4(a) and 4(b)). This revealed the protective effect of sevoflurane on myocardial cells during anesthesia.

4. Discussions

Commonly used inhalation drugs for volatile general anesthesia include halothane, isoflurane, sevoflurane, and other internal halogenated alkanes [12]. Pain, high price, and non-explosive characteristics are widely favored by patients and doctors. With the increase in frequency and dosage, halothane anesthesia is gradually exposed to poisons in various systems of the body, in addition to degenerative damage to

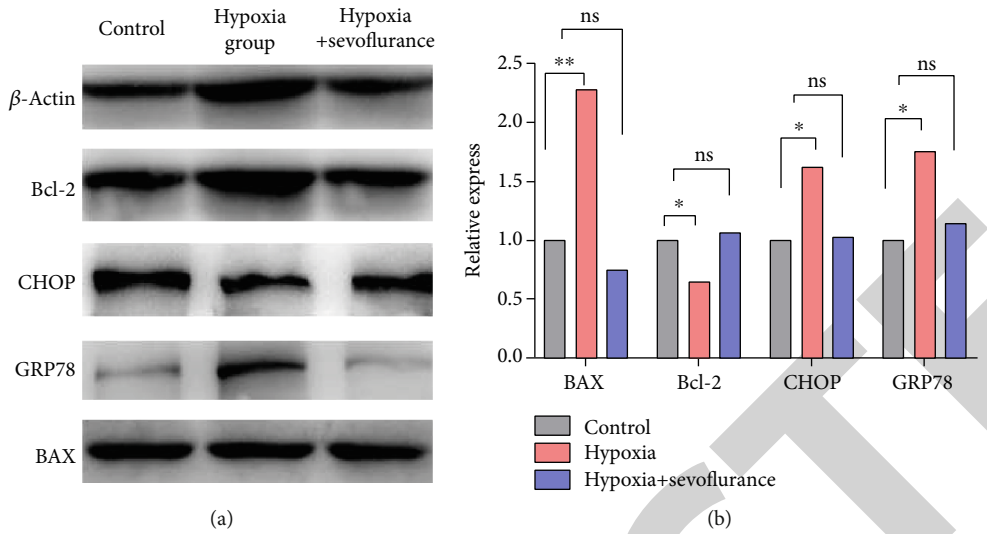

Figure 3: Expression of apoptotic proteins in the hypoxia- and sevoflurane-treated groups. (a, b) Western blot was used to detect the expression of apoptotic proteins such as Bcl-2, CHOP, GRP78, and BAX. $^{*}P < 0.05$ and $^{**}P < 0.01$. ICAM-1: intercellular adhesion molecule-1; VCAM-1: vascular cell adhesion molecule-1.

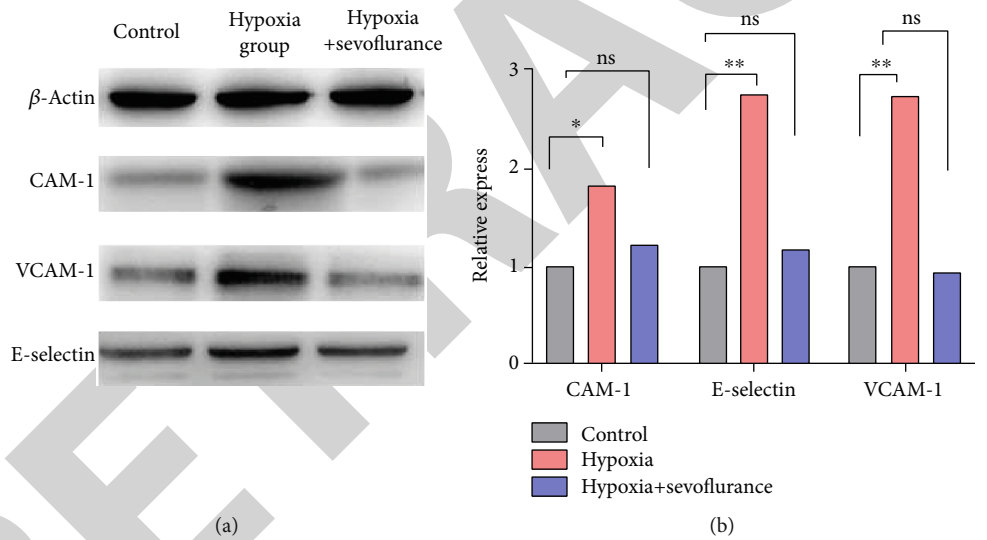

Figure 4: Expression of cell adhesion protein in the hypoxia- and sevoflurane-treated groups. (a, b) Western blot was used to detect the expression of adhesion proteins such as ICAM-1, VCAM-I, and E-selectin. $^{*}P < 0.05$ and $^{**}P < 0.01$. ICAM-1: intercellular adhesion molecule-1; VCAM-1: vascular cell adhesion molecule-1.

the nervous system, liver cancer damage, and cardiovascular suppression [13]. The anesthetic drug sevoflurane has the characteristics of rapid induction and depth of anesthesia, and many studies have shown that sevoflurane has a lighter cardiovascular inhibitory response and has a certain myocardial protective effect [14, 15].

Early structural and functional damage to vascular endothelial cells is the basis of the pathophysiology of I/R injury, and vascular endothelial cells are oxygen free radicals, adhesion molecules, and other biologically active substances during I/R injury source [16]. Autophagy plays an important role in the pathogenesis and progression of cardiovascular diseases such as myocardial ischemia-reperfusion, myocardial infarction, and heart failure. Excessive autophagosome accumulation and autophagy activation were observed in mouse undergoing myocardial I/R injury, thereby contributing to cardiomyocyte death [16]. Furthermore, autophagy is also thought to participate in ischemic postconditioning-mediated cardioprotection [16]. Nonetheless, the function of autophagy in this process is complicated considering it plays a promoting or suppressing role in cardioprotection.

Apoptosis is the programmed death of type I cells performed by activated caspase (Caspase), which is a highly evolved gene-regulated cell process, which eliminates cells without producing harmful substances [17, 18]. Apoptosis is involved in acute and chronic loss of cardiomyocytes in

various cardiovascular diseases, such as myocardial infarction, ischemic heart disease, various cardiomyopathy, and heart failure, and inhibiting apoptosis is a potential way to treat cardiovascular disease.

Sevoflurane postconditioning (SpostC) has previously been shown to enhance cardiac resistance to I/R injury in experimental and clinical studies [10, 11]. SpostC was used to treat Sprague-Dawley rats with I/R injury, and the data showed that SpostC dramatically reduced the infarct size and improved cardiac function by activation of the ERK pathway [19]. SpostC promoted autophagosome clearance in vitro, reduced cell damage, and enhanced cell viability to reduce hypoxia-reoxygenation (H/R) injury in H9C2 cells. Another study showed that the SpostC-induced cardioprotection in I/R injury in Sprague-Dawley rats was modulated by the activation of the PI3K/Akt/mTOR pathway, and SpostC protected mitochondrial functions and had an antiapoptotic role in I/R-injured rats [20]. SpostC protects the heart from I/R injury through multiple mechanisms that involve the nuclear factor-erythroid-2-related factor-2 (NRF2) pathway, the reduction of reactive oxygen species (ROS) levels, and extracellular signal-regulated kinase (ERK) phosphorylation [21–24].

Oxidative stress and inflammation-induced endothelial dysfunction play a critical role in the pathogenesis of cardiovascular diseases. The anesthetic confers cytoprotective effects by virtue of its anti-inflammatory properties in various pathologies such as systemic inflammatory response syndrome and I/R injury. Sevoflurane, one of the most commonly used anesthetics, was proven to be effective in combating oxidative stress and inflammation and protecting organs against stress-induced injury in various conditions. Sevoflurane preconditioning could greatly attenuate tumor necrosis factor α- (TNF-α-) induced permeability and activation of p38 MAPK in rat pulmonary microvascular endothelial cells by reducing ICAM-1 expression. In our study, the expression of adhesion proteins in sevoflurane-treated myocardium was higher than that in myocardium treated with hypoxia, suggesting better connectivity of the myocardium.

Sevoflurane, as a commonly used anesthetic, has the characteristics of fast onset and easy regulation. Many studies have shown that sevoflurane inhibits cardiovascular responses less. Moreover, some evidence suggests that sevoflurane has a protective effect on the heart. It also affects the expression of various cytokines such as tumor necrosis factor (TNF-α), ICAM-1 in endothelial cells, and the level of cellular inflammation.

We used rats as model organisms and used in vitro cultured primary cells for hypoxia modeling. Our results revealed that sevoflurane treatment could reduce apoptosis of cardiomyocytes, similar to previous conclusion that sevoflurane ameliorated H/R-induced cardiomyocyte apoptosis by autophagy inhibition via reducing Beclin-1/PI3KC3 formation and PI3KC3 activity [25]. Also, our conclusion was consistent with Yu et al., who described that the cardiomyocyte apoptosis inhibited by sevoflurane postconditioning may influence the modulation of the expression of pro- and antiapoptotic proteins, specifically Bcl-2, BAX, and phosphor-Bad [26]. Besides, the study has indicated that sevoflurane could significantly improve the hypoxia-reoxygenation injury of the rats via decreasing the apoptosis of cardiomyocytes [27].

Collectively, our study provides evidence for the effect of sevoflurane on myocardial capacity and provides reference for clinical medicine. These preliminary findings require validation with further *in vitro* and *in vivo* studies. More studies should pay attention to investigating the roles of sevoflurane and the molecular basis for cardiac protection by sevoflurane *in vivo* (especially in human cardiac tissues) or in hypoxia injury in cardiomyocytes *in vitro*.

Data Availability

The authors confirm that the data supporting the findings of this study are available within the article.

Conflicts of Interest

There is no conflict of interest.

Authors' Contributions

Yingchun Zhang and Xiaojuan Chu performed the experiments, analyzed data, and wrote the manuscript. Qingjie Wei designed the study. All the authors agreed to be accountable for the accuracy and integrity of all aspects of the research.

References

[1] M. T. Alkire, A. G. Hudetz, and G. Tononi, "Consciousness and anesthesia," *Science*, vol. 322, no. 5903, pp. 876–880, 2008.

[2] E. N. Brown, R. Lydic, and N. D. Schiff, "General anesthesia, sleep, and coma," *New England Journal of Medicine*, vol. 363, no. 27, pp. 2638–2650, 2010.

[3] G. D. Shorten, E. De Robertis, Z. Goldik, S. Kietaibl, L. Niemi-Murola, and O. Sabelnikovs, "European section/board of anaesthesiology/european society of anaesthesiology consensus statement on competency-based education and training in anaesthesiology," *European Journal of Anaesthesiology*, vol. 37, no. 6, pp. 421–434, 2020.

[4] D. A. Hashimoto, E. Witkowski, L. Gao, O. Meireles, and G. Rosman, "Artificial intelligence in anesthesiology: current techniques, clinical applications, and limitations," *Anesthesiology*, vol. 132, pp. 379–394, 2020.

[5] J. S. Gaynor, J. Wimsatt, C. Mallinckrodt, and D. Biggins, "A comparison of sevoflurane and isoflurane for short-term anesthesia in polecats (Mustela eversmanni)," *Journal of Zoo and Wildlife Medicine*, vol. 28, no. 3, pp. 274–279, 1997.

[6] D. S. Celermajer, C. K. Chow, E. Marijon, N. M. Anstey, and K. S. Woo, "Cardiovascular disease in the developing world: prevalences, patterns, and the potential of early disease detection," *Journal of the American College of Cardiology*, vol. 60, no. 14, pp. 1207–1216, 2012.

[7] R. L. Mueller and T. A. Sanborn, "The history of interventional cardiology: cardiac catheterization, angioplasty, and related interventions," *American Heart Journal*, vol. 129, no. 1, pp. 146–172, 1995.

[8] D. J. Hausenloy, P. K. Mwamure, V. Venugopal et al., "Effect of remote ischaemic preconditioning on myocardial injury in

Hindawi
BioMed Research International
Volume 2024, Article ID 9834789, 1 page
https://doi.org/10.1155/2024/9834789

Retraction

Retracted: miR-10b-5p Suppresses the Proliferation and Invasion of Primary Hepatic Carcinoma Cells by Downregulating EphA2

BioMed Research International

Received 12 March 2024; Accepted 12 March 2024; Published 20 March 2024

This article has been retracted by Hindawi following an investigation undertaken by the publisher [1]. This investigation has uncovered evidence of one or more of the following indicators of systematic manipulation of the publication process:

(1) Discrepancies in scope

(2) Discrepancies in the description of the research reported

(3) Discrepancies between the availability of data and the research described

(4) Inappropriate citations

(5) Incoherent, meaningless and/or irrelevant content included in the article

(6) Manipulated or compromised peer review

The presence of these indicators undermines our confidence in the integrity of the article's content and we cannot, therefore, vouch for its reliability. Please note that this notice is intended solely to alert readers that the content of this article is unreliable. We have not investigated whether authors were aware of or involved in the systematic manipulation of the publication process.

Wiley and Hindawi regrets that the usual quality checks did not identify these issues before publication and have since put additional measures in place to safeguard research integrity.

We wish to credit our own Research Integrity and Research Publishing teams and anonymous and named external researchers and research integrity experts for contributing to this investigation.

The corresponding author, as the representative of all authors, has been given the opportunity to register their agreement or disagreement to this retraction. We have kept a record of any response received.

References

[1] X. Niu, H. Sun, F. Qiu, J. Liu, T. Yang, and W. Han, "miR-10b-5p Suppresses the Proliferation and Invasion of Primary Hepatic Carcinoma Cells by Downregulating EphA2," *BioMed Research International*, vol. 2021, Article ID 1382061, 12 pages, 2021.

Hindawi
BioMed Research International
Volume 2021, Article ID 1382061, 12 pages
https://doi.org/10.1155/2021/1382061

Research Article

miR-10b-5p Suppresses the Proliferation and Invasion of Primary Hepatic Carcinoma Cells by Downregulating EphA2

Xu Niu,[1] Haitao Sun,[1] Feng Qiu,[1] Jing Liu,[2] Tianchi Yang,[1] and Wei Han[1]

[1]*General Surgery, Luhe Hospital, Capital Medical University, Beijing 101100, China*
[2]*General Surgery, Tongren Hospital, Capital Medical University, Beijing 101100, China*

Correspondence should be addressed to Wei Han; weizi8662@163.com

Received 7 July 2021; Revised 25 October 2021; Accepted 27 October 2021; Published 29 December 2021

Academic Editor: Jun Yang

Objective. To analyze the function of miR-10b-5p in suppressing the invasion and proliferation of primary hepatic carcinoma cells by downregulating erythropoietin-producing hepatocellular receptor A2 (EphA2). *Material and Methods*. Eighty-six hepatic carcinoma (HCC) tissue specimens and 86 corresponding adjacent tissue specimens were collected, and the mRNA expression of miR-10b-5p and Ephrin type-A receptor 2 (EphA2) in the specimens was determined using a reverse transcription-polymerase chain reaction (RT-PCR) assay. Western blot was employed to quantify EphA2, B-cell chronic lymphocytic leukemia/lymphoma-2 (Bcl-2), Bcl-2-associated X protein (Bax), and Caspase-3 in the cells, and CCK8, Transwell assay, and flow cytometry were applied to evaluate the proliferation, invasion, and apoptosis of cells, respectively. Moreover, the dual luciferase reporter assay was utilized for correlation analysis between miR-10b-5p and EphA2. *Results*. miR-10b-5p was lowly expressed in HCC, while EphA2 was highly expressed. Cell experiments revealed that miR-10b-5p overexpression or EphA2 knockdown could reduce cell proliferation, accelerate apoptosis, strongly upregulate Bax and Caspase-3, and downregulate Bcl-2. In contrast, miR-10b-5p knockdown or EphA2 overexpression gave rise to reverse biological phenotypes. Furthermore, dual luciferase reporter assay verified that miR-10b-5p was a target of EphA2, and the rescue experiment implied that transfection of pCMV-EphA2 or Si-EphA2 could reverse EphA2 expression and cell biological functions caused by miR-10b-5p overexpression or knockdown. *Conclusions*. miR-10b-5p reduced HCC cell proliferation but accelerate apoptosis by regulating EphA2, suggesting it has the potential to be a clinical target for HCC.

1. Introduction

Hepatic carcinoma (HCC) is a familiar clinical malignant tumor in the digestive system and is also one of the major reasons for cancer-related death [1]. In recent years, with the changes of social environment and living habits, HCC shows an increasingly higher incidence and mortality [2]. With the progression of medical technology, a considerable progress has been made in the treatment of HCC recently. However, due to the strong invasiveness of HCC cells, the prognosis of most HCC patients after hepatic carcinectomy and intervention embolization is still unsatisfactory [3, 4]. Therefore, it is of great clinical significance to understand the pathogenesis of HCC and uncover new therapeutic targets for HCC patients for the treatment of HCC.

miRNA is a noncoding microRNA, and its role and mechanism in tumors have captured a growing attention over the years [5]. Many studies have been carried out on the role of miRNAs in tumors including HCC. For instance, one study has stated that miR-197-3p can be taken as a prognostic marker and potential treatment target for HCC [6], and one other study has revealed that miR-532-3p can promote the development of HCC by targeting protein tyrosine phosphatase receptor T (PTPRT) [7]. Those studies all imply the strong correlation between miRNA and development and progression of HCC. miR-10b-5p, belonging to the miR-10 family, is located on 2q31.1 chromosome. Some previous studies have reported abnormal expression of miR-10b-5p in tumors such as glioma and renal cell carcinoma [8, 9], and some studies have also found through sequencing

abnormal expressed miRNA that miR-10b-5p is a highly dysregulated miRNA in HCC [10]. However, no further research has been conducted on its role and mechanism in the cancer.

We found a targeting relationship between miR-10b-5p and EphA2 through biological information prediction, and Ephrin type-A receptor 2 (EphA2) was reported to be related to the development, metastasis, and prognosis of HCC cells [11]. Therefore, we attempted to investigate the role of miR-10b-5p on the biological functions of HCC cells.

2. Materials and Methods

2.1. Clinical Data. Eighty-seven patients with primary HCC admitted to our hospital from March 2014 to June 2016 were enrolled, and 87 HCC tissue specimens and 87 corresponding tumor-adjacent tissue specimens were extracted from. The inclusion criteria of the patients were as follows: HCC patients were confirmed according to pathological diagnosis and those with expected survival longer than 3 months. The exclusion criteria of them were as follows: patients with severe infection disease, patients with other comorbid malignant tumors, patients who had received any treated before the experiment, and patients with immune system disorder. All participants and their relatives gave their consent to participate in the experiment and also provided their signed informed consent forms. The experiment was approved by the permission of the Ethics Committee of our hospital.

2.2. Experiment Reagents and Materials. Human HCC cell strains (HepG2, BEL-7402, Huh-7, and SMMC-7721) and human normal hepatic cell (HL-7702) from the American Type Culture Collection (ATCC), quantitative reverse transcription-polymerase chain reaction (qRT-PCR), and reverse transcription kit (TransGen Biotech Co., Ltd., Beijing, China), Trizol reagent (Thermo Fisher Scientific-CN), phosphate-buffered saline (PBS) (Gibco Company, United States), dual luciferase reporter gene assay kit (Beijing Biolab Technology Co., Ltd.), CCK-8 kit (Promega Company, the United States), Transwell kit (Costar Company, United States), Annexin V-FITC/PI apoptosis assay kit (Biolab Technology Co., Ltd., Beijing, China), RIPA and BCA kits (Thermo Fisher Scientific, United States), EphA2, Caspase-3, Bax, Bcl-2, and GAPDH antibodies (Cell Signaling Technology), goat anti-rabbit immunoglobulin G (IgG) secondary antibody (BOSTER Biological Technology Co., Ltd., Wuhan, China), electrochemiluminescence (ECL) developer (Thermo Company), and PCR instrument (ABI company, United States). All primers were synthesized by Shanghai Sangon Biotech Co., Ltd., and EphA2 plasmid (pCMV-EphA2) and empty plasmid (pCMV) were synthesized by OriGene (Rockville, Maryland, United States).

2.3. qRT-PCR Assay. Total RNA was extracted from collected tissues and cells with a TRIzol kit, and its purity and concentration were determined using an ultraviolet spectrophotometer. Subsequently, 1 μL cDNA was taken from cDNA synthesized by reverse transcription of 5 μg total RNA from tissues and cells, separately, under kit instructions for amplification. Three repeated wells were set for each sample, and the experiment was repeated three times with U6 as an internal reference for miR-10-5p and glyceraldehyde-3-phosphate dehydrogenase (GAPDH) as an internal reference for EphA2. Data in this experiment were analyzed using the $2^{-\Delta\Delta CT}$. See Table 1 for primer sequences.

2.4. Cell Culture and Transfection. HCC cell lines were cultured in Dulbecco's modified Eagle medium (DMEM) with 10% PBS under 5% CO_2 at 37°C. Upon reaching 85% confluency in adherent growing, the cells were digested with 25% trypsin and then cultured in the medium for passage. miR-10b-5p-mimics (overexpression sequence), miR-10b-5p-inhibitor (inhibition sequence), miR negative control (miR-NC), targetedly inhibited EphA2 (si-EphA2), negative control RNA (Si-NC), EphA2 plasmid (pCMV-EphA2), and empty plasmid (pCMV) were transfected into cells using a Lipofectamine 2000 kit, separately, in strict accordance with the kit instructions.

2.5. Western Blot Assay. The RIPA lysis method was applied to lyse cells to extract the total protein, and the concentration of the extracted protein was determined using the BCA method. With concentration adjusted to 4 μg/μL, the protein was subject to sodium dodecyl sulfate-polyacrylamide gel electrophoresis (SDS-PAGE) and then transferred to a PVDF membrane. Afterwards, the membrane was cultured with EphA2 (1 : 500), Caspase-3 (1 : 500), Bax (1 : 500), Bcl-2 (1 : 500), and GAPDH (1 : 1000) at 4°C for one night after being sealed with 5% skim milk for 2 h. The membrane was washed to remove the primary antibody, added with horseradish peroxidase-labeled goat anti-rabbit secondary antibody (1 : 1000), cultured at 37°C for 1 h, and rinsed with PBS three times, 5 min each time. Then, the membrane was made to be luminescent with ECL and developed.

2.6. Cell Proliferation Assay. The proliferation ability of HepG2 and Huh-7 cells was evaluated by a CCK-8 kit. After being transfected for 48 hours, the cells were collected and diluted to 3×10^4 cell/mL and transferred to a 96-well plate at 100 μL per well. The plate was cultured under 5% CO_2 at 37°C, and then, 10 μL CCK8 solution was added into each well at 0 h, 24 h, 48 h, and 72 h after adherent growth of the cells. After addition of the solution, the plate was continuously cultured at 37°C for 2 h each time, and the optical density of each well at 450 nm was analyzed using an enzyme mark instrument to analyze proliferation of the cells and draw growth curves of the cells. The experiment was tripled.

2.7. Transwell Assay. After being transfected for 24 hours, the cells were transferred to a 24-well plate at $3 * 10^3$ cells/well, digested with trypsin, and then transferred to the upper compartment, followed by addition of 200 μL RPMI 1640. RPMI1640 with 10% FBS was put into the lower compartment. Afterwards, the chamber was cultured at 37°C for 48 h, and the substrates and cells not penetrating the microporous membrane were wiped off. The membrane was washed with PBS three times, immobilized with

Table 1: Primer sequences.

Factor	Upstream sequence	Downstream sequence
miR-10b-5p	5′-GGGTACCCTGTAGAACCG-3′	5′-AACTGGTGTCGTGGAGTCGGC-3′
U6	5′-CTCGCTTCGGCAGCACA-3′	5′-AACGCTTCACGAATTTGCGT-3′
EphA2	5′-GGGACCTGATGCAGAACATC-3′	5′-AGGCATTTCACTCACAGGGG-3′
GAPDH	5′-GGAGTCAACGGATTTGGT-3′	5′-GTGATGGGATTTCCATTGAT-3′

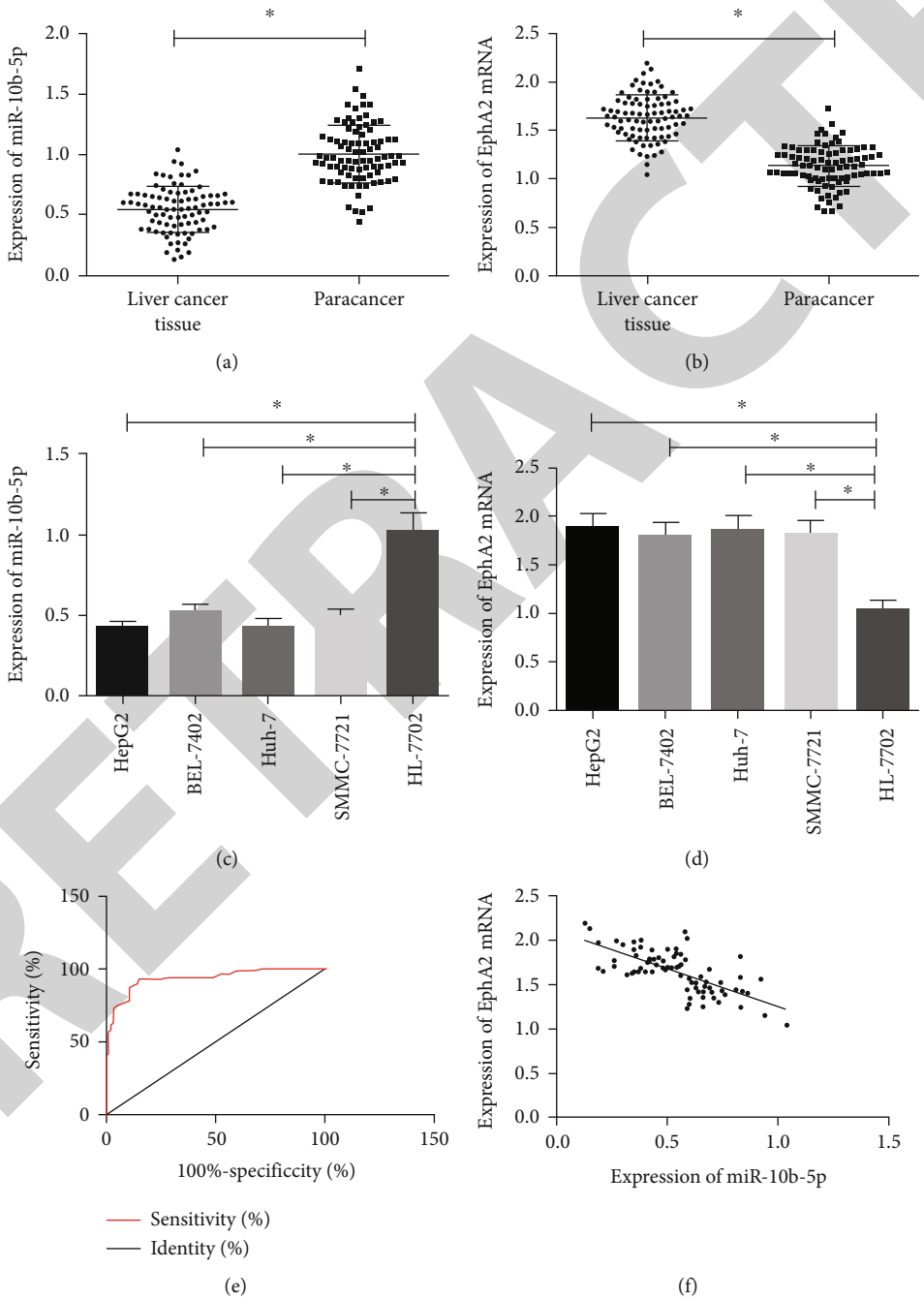

Figure 1: Expression of miR-10b-5p in HCC tissues and cells. (a) Expression of miR-10b-5p in HCC tissues. (b) Expression of EphA2 mRNA in HCC cells. (c) Expression of miR-10b-5p in HCC cells. (d) Expression of EphA2 mRNA in HCC cells. (e) ROC curves of miR-10b-5p for HCC. (f) Correlation between miR-10b-5p and EphA2. ∗ indicates $p < 0.05$.

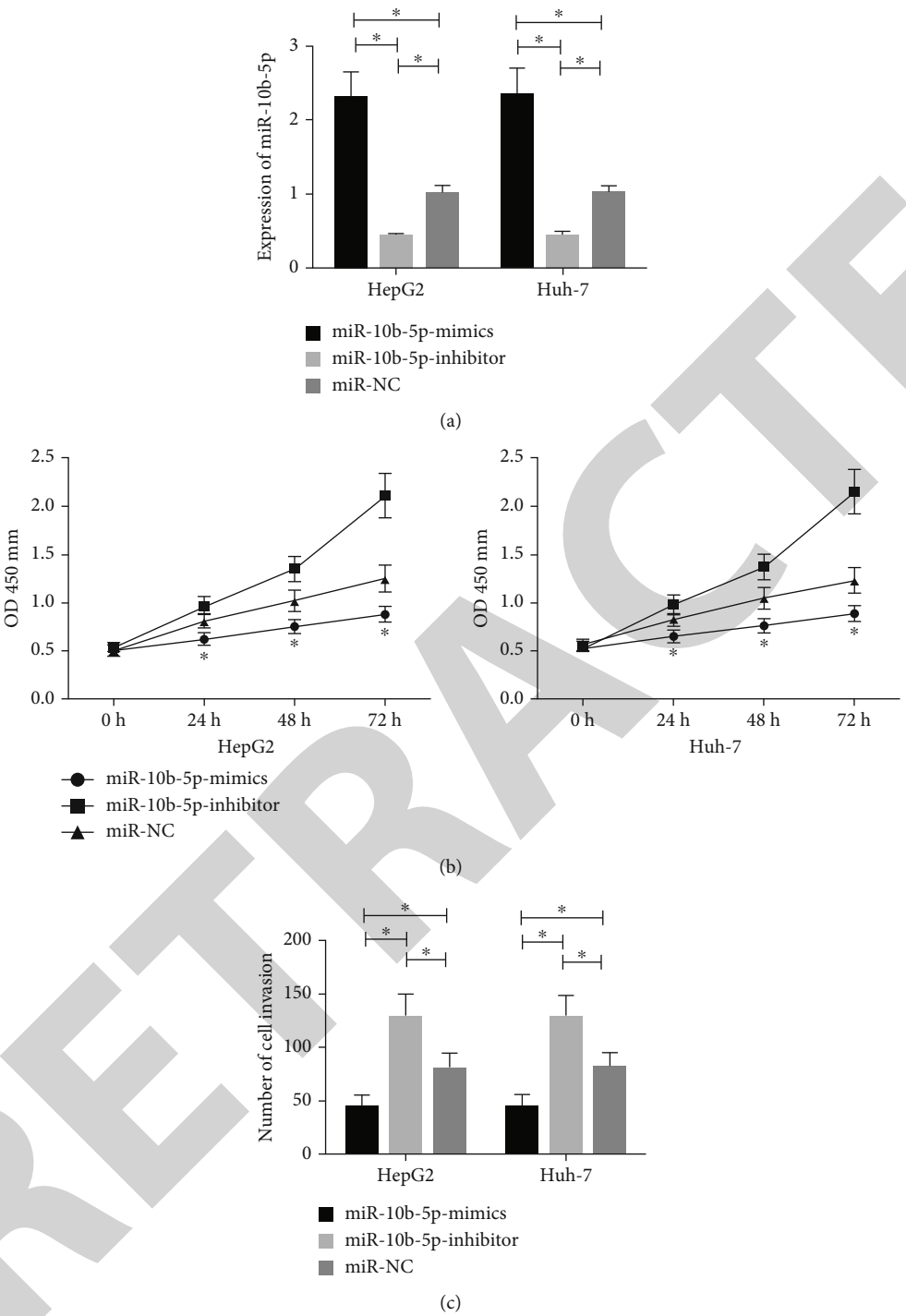

Figure 2: Continued.

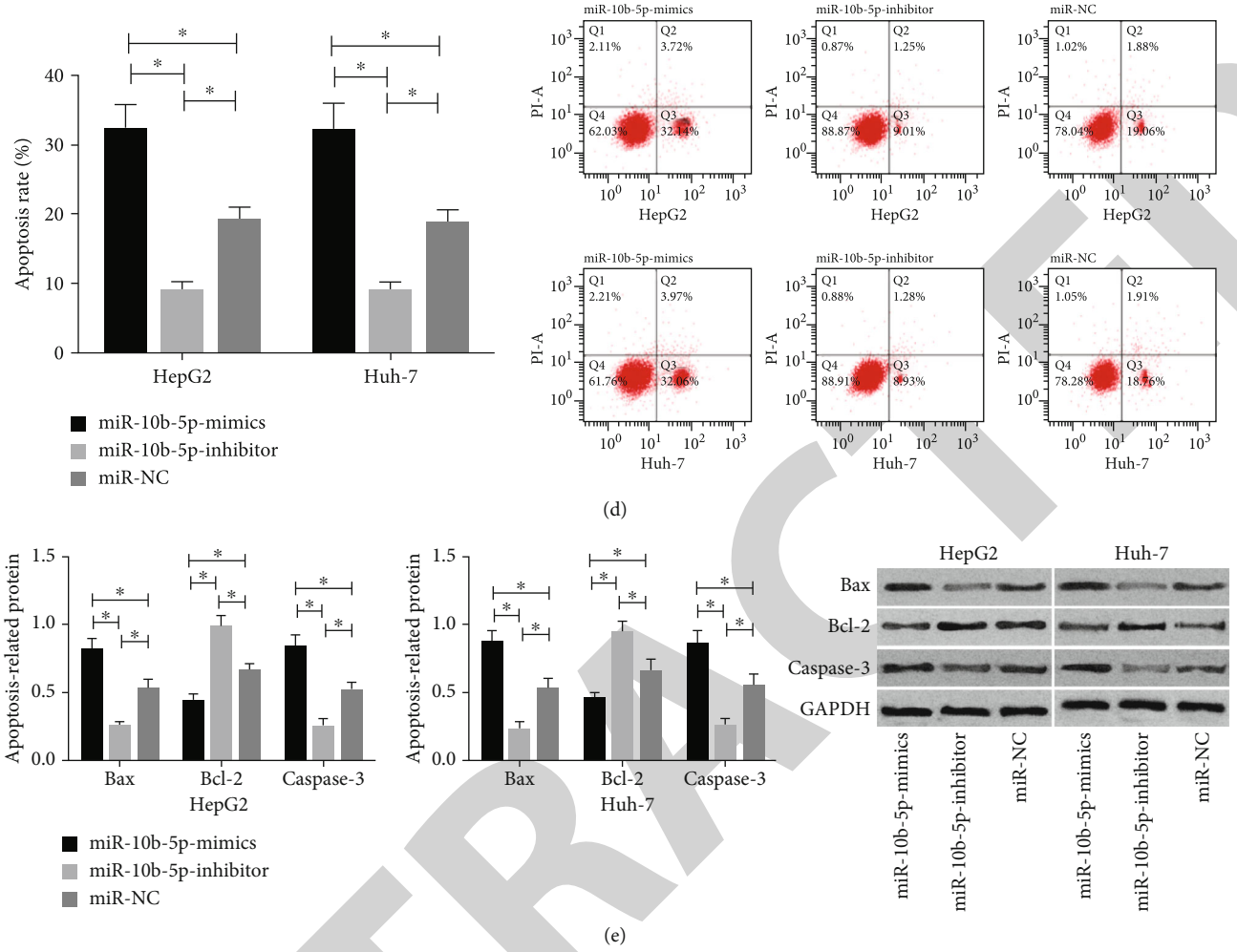

Figure 2: Influences of miR-10b-5p on the biological functions of HCC cells. (a) Expression of miR-10b-5p in transfected cells. (b) Influences of miR-10b-5p on the proliferation ability of HCC cells. (c) Influences of miR-10b-5p on the invasion ability of HCC cells. (d) Influences of miR-10b-5p on the apoptosis rate of HCC cells. (e) Influences of miR-10b-5p on apoptosis-related proteins in HCC cells. * indicates $p < 0.05$.

paraformaldehyde for 10 min, and washed with double distilled water three times again, and it was then stained with 0.5% crystal violet after being dried out. Finally, cell migration was analyzed using a microscope.

2.8. Apoptosis Assay. The transfected cells were trypsinized with 0.25% trypsin. After it, the cells were washed with PBS twice and then added with 100 μL binding buffer to prepare $1 * 10^6$ cells/mL suspension. Annexin V-FITC and PI were put into the suspension in order, and the suspension was cultured in the dark at indoor temperature for 5 min and then detected using the FACS Verse flow cytometer system. The experiment was tripled, and the data were averaged as results.

2.9. Dual Luciferase Assay. The EphA2-3′UTR wild-type (Wt) and EphA2-3′UTR mutant type (Mut) as well as miR-10b-5p-mimics, miR-10b-5p-inhibitor, and miR-NC were transferred into HepG2 and Huh-7 cells by a Lipofectamine 2000 kit. After transfection for 48 hours, the luciferase activity of the cells was measured with a dual luciferase reporter gene assay kit (Promega).

2.10. Statistical Analysis. In this study, the collected data were analyzed statistically using SPSS20.0 and visualized into required figures using GraphPad 7. Comparison between groups was conducted using the independent t-test, and multigroup comparison was carried out using the one-way ANOVA. Post hoc pairwise comparison was carried out using the LSD t-test. Pearson's correlation was conducted for correlation analysis between miR-10b-5p and EphA2. $p < 0.05$ implies a significant difference.

3. Results

3.1. Reduction of miR-10b-5p in HCC Tissues and Cells. The RT-PCR assay revealed that compared with tumor-adjacent tissues and normal hepatic cells, HCC tissues and cells showed a great decrease in the expression of miR-10b-5p ($p < 0.05$) and an increase in the expression of EphA2

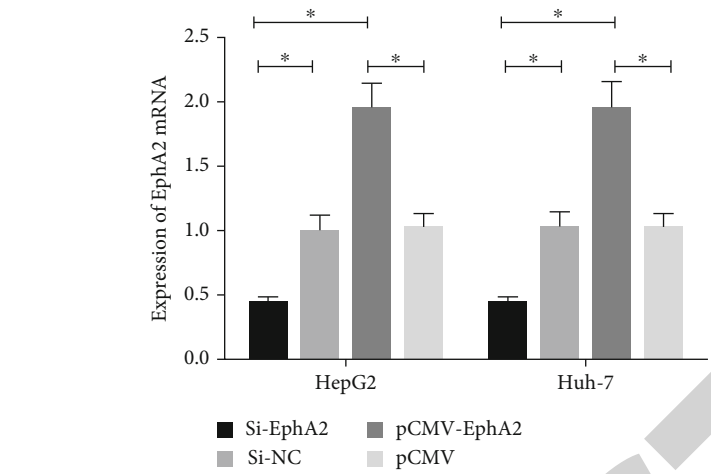

(a)

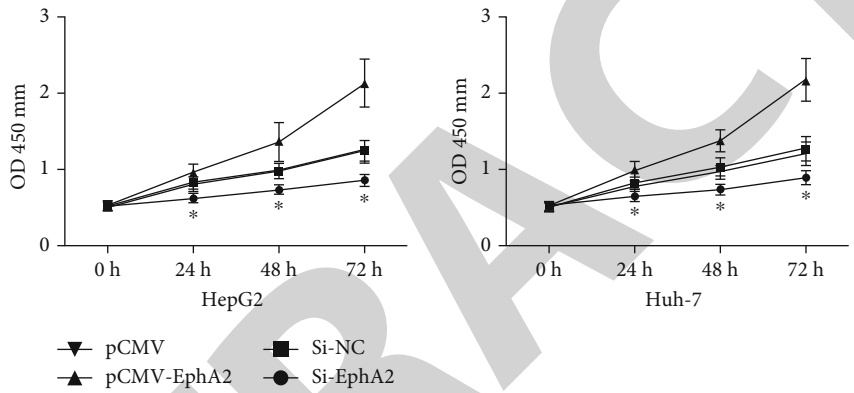

(b)

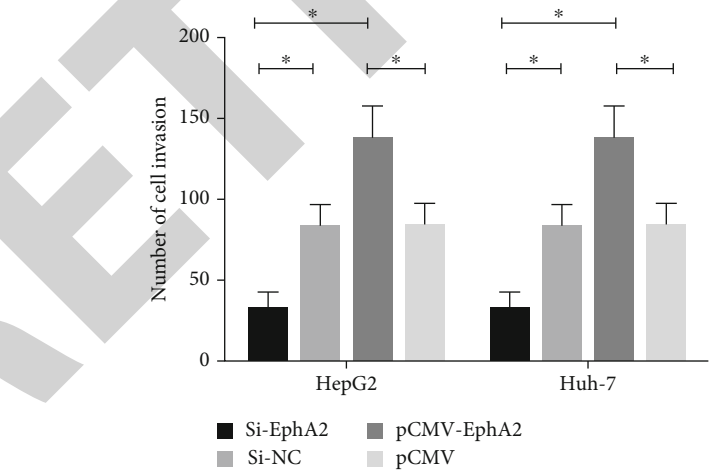

(c)

Figure 3: Continued.

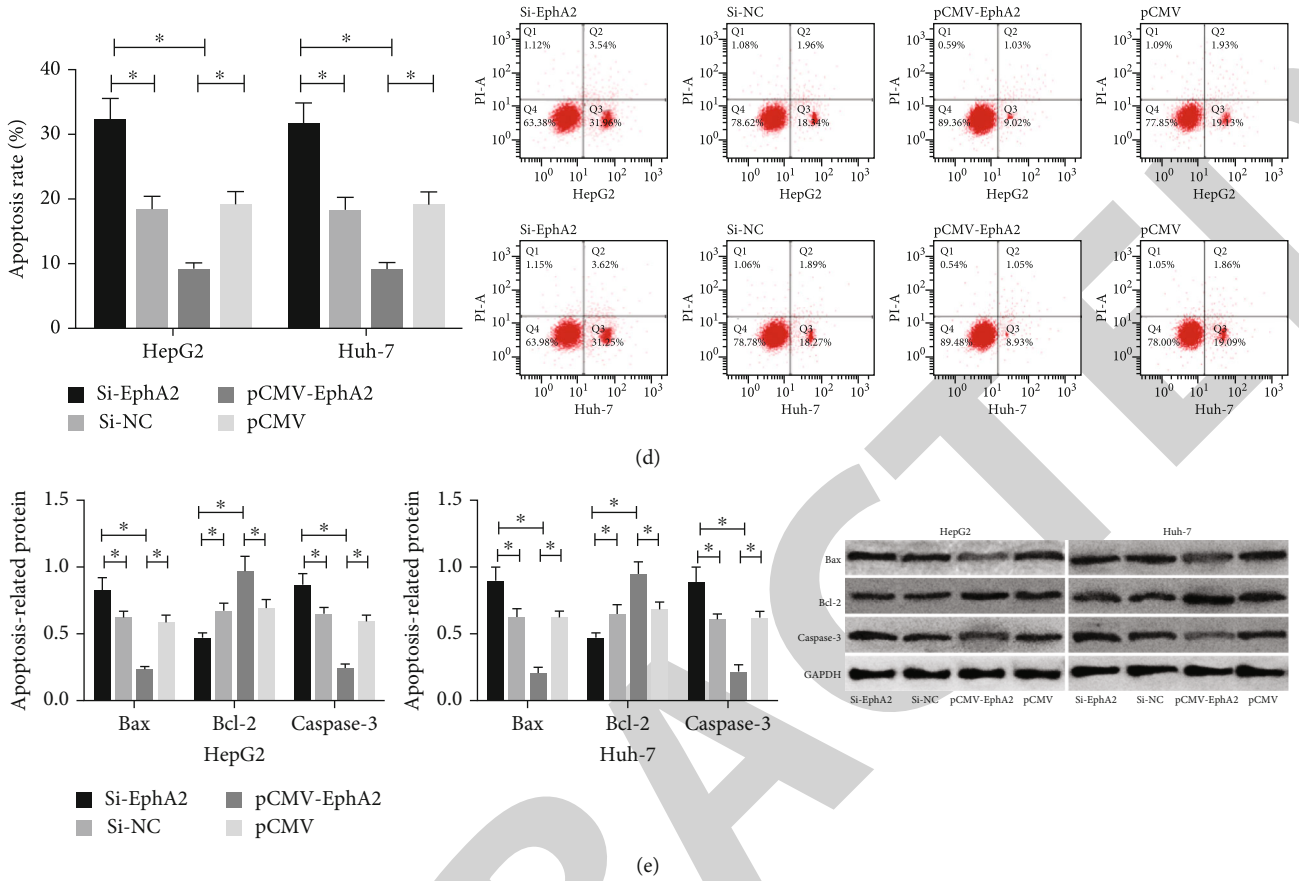

Figure 3: Influences of EphA2 on the biological functions of HCC cells. (a) Expression of EphA2 mRNA in transfected cells. (b) Influences of EphA2 on the proliferation ability of HCC cells. (c) Influences of EphA2 on the invasive ability of HCC cells. (d) Influences of EphA2 on the apoptosis of HCC cells. (e) Influences of EphA2 on apoptosis-related proteins in HCC cells. ∗ indicates $p < 0.05$.

($p < 0.05$), and the expression of miR-10b-5p was negatively related to that of EphA2 ($r = -0.698$, $p < 0.05$). ROC curves indicated that the area-under-the-curve of miR-10b-5p in diagnosing HCC was 0.937 ($p < 0.05$) (Figure 1).

3.2. Influences of miR-10b-5p on Biological Functions of HCC Cells. Compared with HepG2 and Huh-7 cells transfected with miR-10b-5p-mimics, those transfected with miR-NC showed a great increase in the expression of miR-10b-5p, while those transfected with miR-10b-5p-inhibitor showed a great decrease in it. The detection of the biological functions of cells in the two groups revealed that compared with the miR-NC group, the cells transfected with miR-10b-5p-mimics showed significantly weakened proliferation and invasion abilities and significantly increased apoptosis rate, while those transfected with miR-10b-5p-inhibitor showed significantly strengthened proliferation ability and significantly decreased apoptosis rate. In addition, compared with the miR-NC group, cells transfected with miR-10b-5p-mimics showed significantly downregulated Bcl-2 and significantly upregulated Caspase-3 and Bax, while those transfected with miR-10b-5p-inhibitor showed significantly upregulated Bcl-2 and significantly down-regulated Caspase-3 and Bax (Figure 2).

3.3. Influences of EphA2 on the Biological Functions of HCC Cells. Compared with HepG2 and Huh-7 cells transfected with Si-EphA2, those transfected with Si-NC presented a great decrease in the expression of EphA2, while those transfected with pCMV-EphA2 showed a great increase in the expression of EphA2. Detection of the biological functions of cells in the two groups revealed that compared with the Si-NC group, cells transfected with Si-EphA2 showed significantly weakened proliferation and invasion abilities and significantly increased apoptosis rate, significantly downregulated Bcl-2, and significantly upregulated Caspase-3and Bax. In addition, compared with the pCMV group, cells transfected with pCMV-EphA2 showed significantly strengthened proliferation and invasion abilities, significantly weakened apoptosis, significantly upregulated Bcl-2, and significantly downregulated Caspase-3 and Bax (Figure 3).

3.4. Dual Luciferase Reporter Assay. In order to further understand the correlation of miR-10b-5p with EphA2, Targetscan 7.2 was utilized to predict downstream target genes of miR-10b-5p, and it was found that there was a targeted binding locus between EphA2 and miR-10b-5p. To confirm it, we carried out a dual luciferase reporter assay, finding that

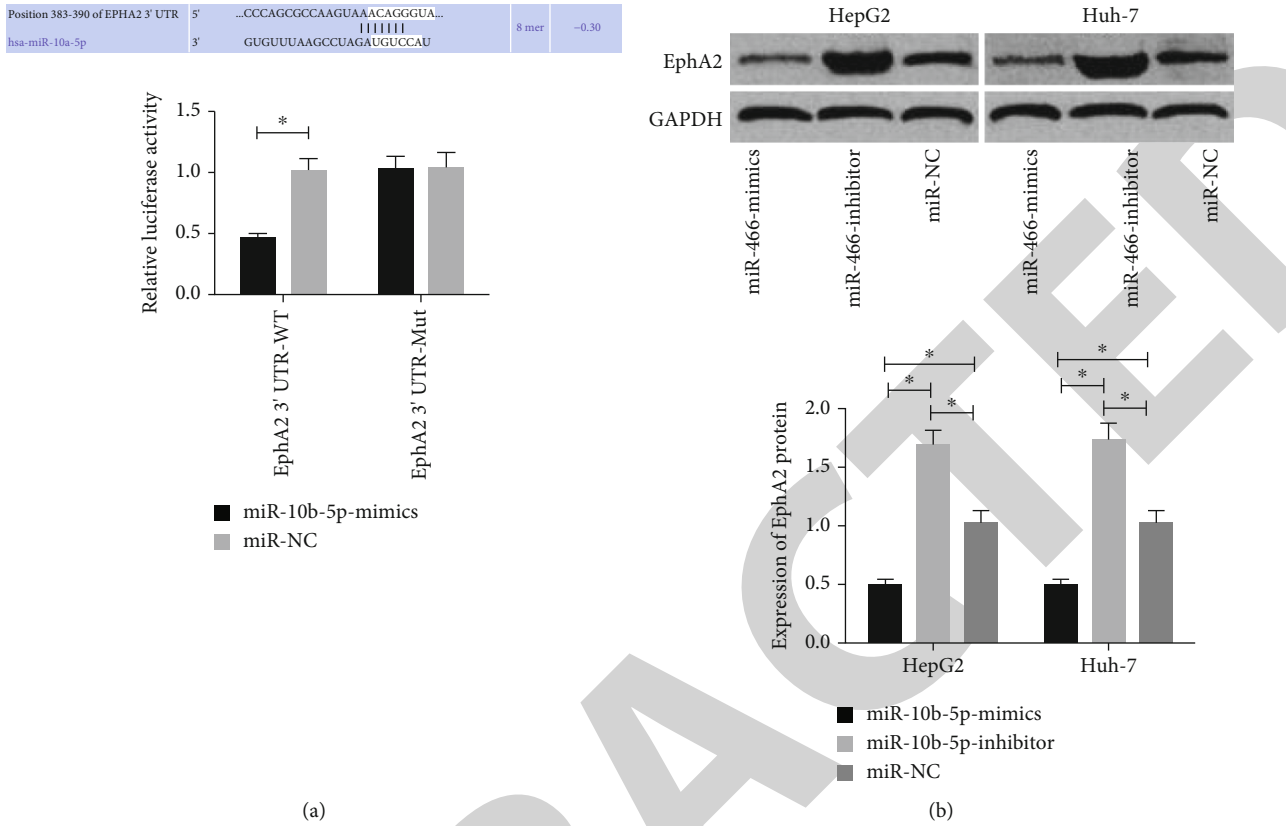

Figure 4: Dual luciferase reporter assay. (a) Influences of miR-10b-5p on dual luciferase activity of EphA2. (b) Influences of miR-10b-5p on EphA2. ∗ indicates $p < 0.05$.

overexpression of miR-10b-5p strongly lowered the luciferase activity of EphA2-3′UTR Wt ($p < 0.05$) but exerted no effect on that of EphA2-3′UTR Mut ($p > 0.05$). The western blot (WB) assay revealed that transfection of miR-10b-5p-mimics greatly decreased the expression of Rap1b in HepG2 and Huh-7 cells and transfection of miR-10b-5p-inhibitor greatly lowered it in the cells (both $p < 0.05$) (Figure 4).

3.5. Rescue Experiment. miR-10b-5p-mimics+pCMV-EphA2 or miR-10b-5p-inhibitor+Si-EphA2 was cotransfected into HepG2 and Huh-7 cells, and it came out that cotransfection with pCMV-EphA2 reversed the downregulation of EphA2 caused by overexpression of miR-10b-5p and cotransfection of Si-EphA2 also reversed the upregulation of it caused by ablating miR-10b-5p. Moreover, detection of biological functions revealed that EphA2 could reverse the influence of miR-10b-5p on the proliferation, invasion, and apoptosis of HCC cells (Figure 5).

4. Discussion

HCC is a malignant tumor with high incidence. Its symptoms are usually insidious, so most patients have already missed the optimal treatment opportunity at the time of diagnosis, causing unfavorable prognosis [11]. Many studies have reported the dysregulation of miRNA in HCC, and they believe that dysregulation of miRNA and its functions as an oncogene or tumor suppressor gene are one of the main driving forces for HCC [12, 13]. Therefore, it is of great significance to identify the function and functional mechanism of miRNA in HCC for diagnosis and treatment of the cancer.

miR-10b-5p has been proved to play different roles in different tumors. For instance, the expression of it decreased in breast cancer and increased in colorectal cancer [14, 15]. However, the expression of miR-10b-5p in HCC and relevant mechanisms are still under investigation. In our study, it was found that the expression of miR-10b-5p in HCC tissues and cells decreased, and ROC curves revealed the high diagnostic value of miR-10b-5p in the disease. One study has stated that miR-10b-5p is able to inhibit the proliferation of glioma and terminate the cell cycle [16]. In our study, we uncovered that overexpression of miR-10b-5p could strongly hinder the invasion and proliferation of HCC cells and accelerate apoptosis of them, while reducing miR-10b-5p would give rise to opposite results, which suggested that miR-10b-5p acted as a tumor suppressor gene in HCC. One previous study has also found reduced miR-10b-5p in colorectal cancer patients under liver metastasis [17]. However, there are no more demonstrations on the functional mechanism of miR-10b-5p in HCC, so for the purpose of further exploring the mechanism, we have predicted targeting relationship between EphA2 and miR-10b-5p based on the biological information website Targetscan.

EphA2 is one of the members of receptor tyrosine kinase, and it has been reported to be crucial in the

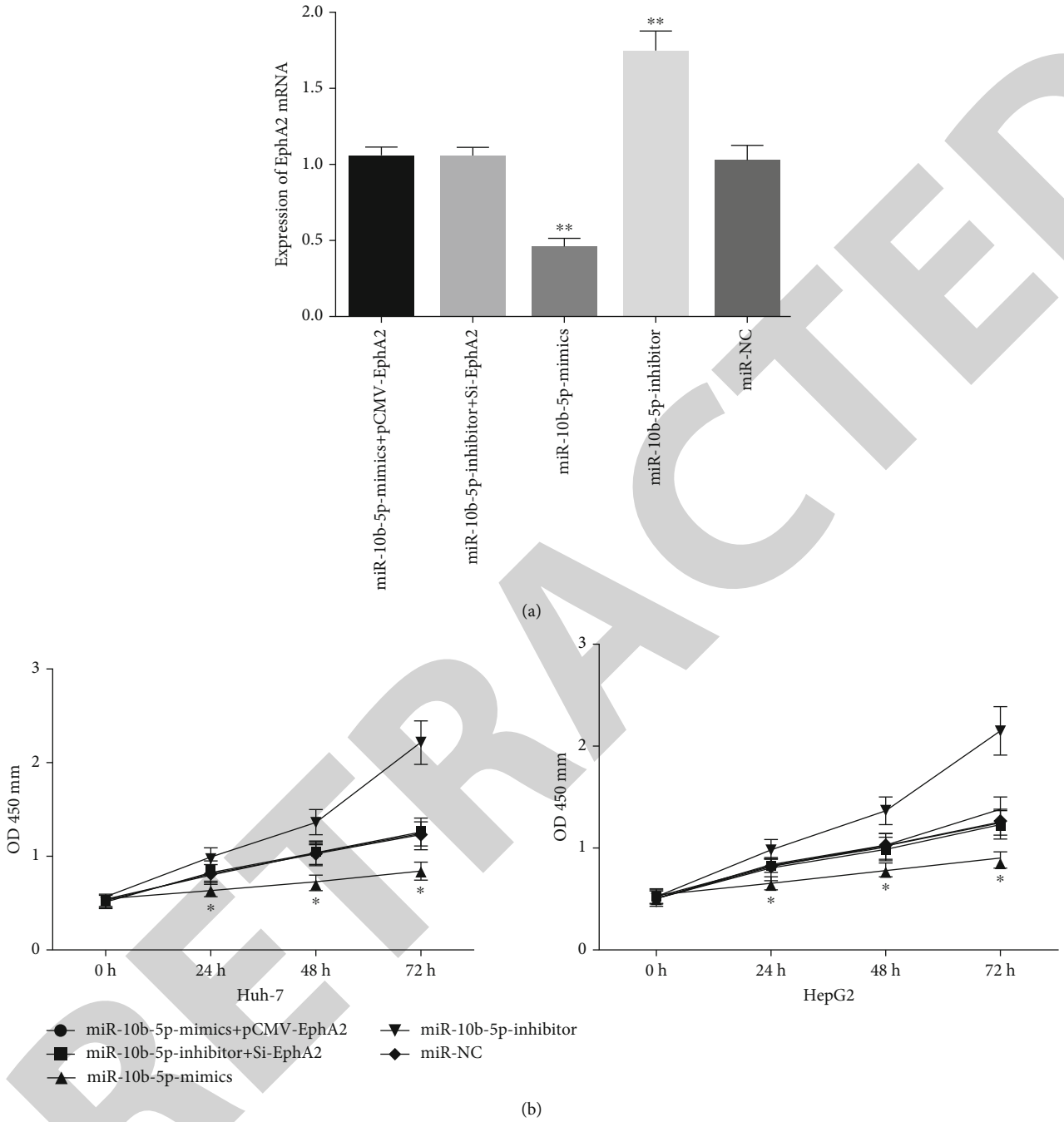

Figure 5: Continued.

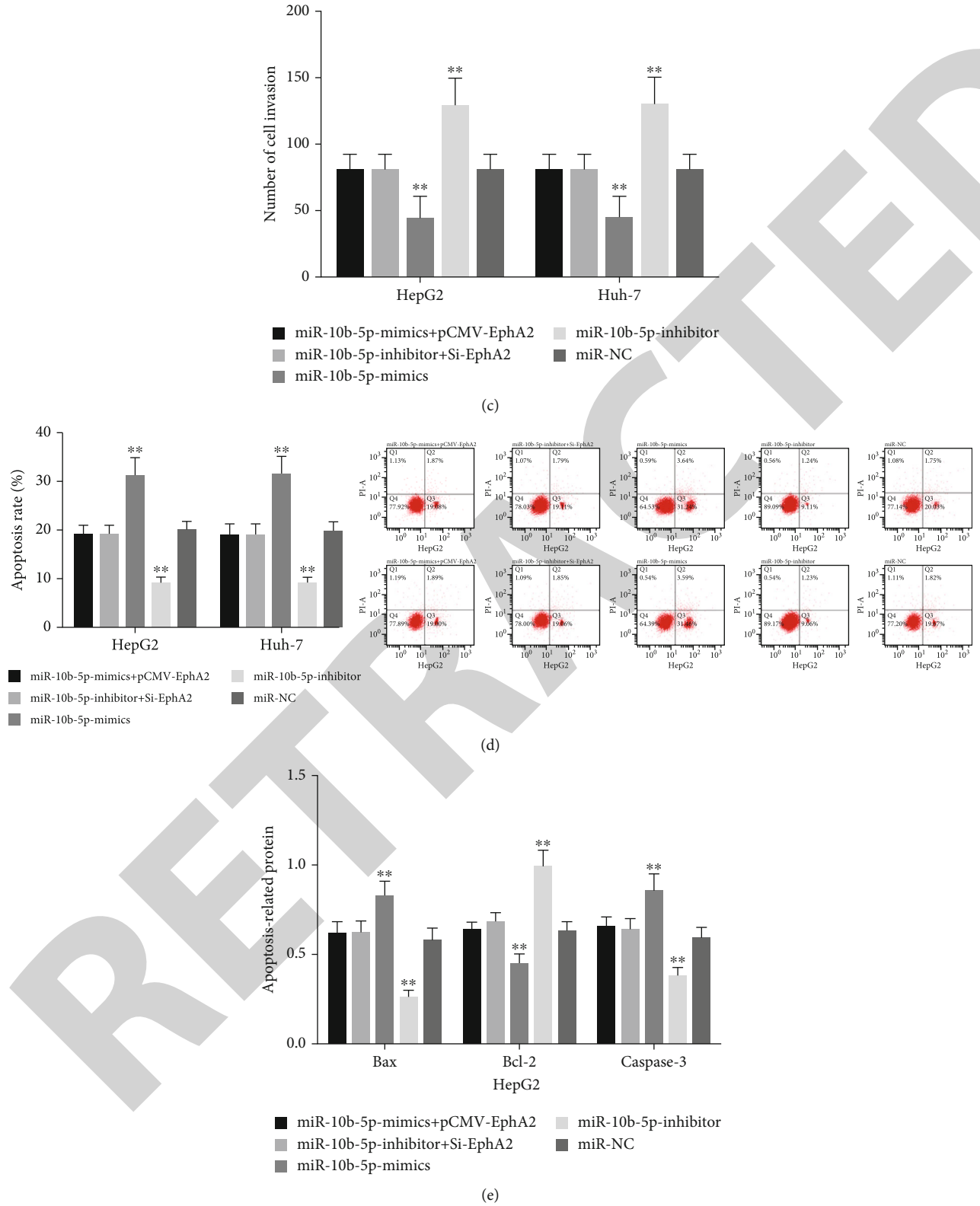

Figure 5: Rescue experiment. (a) Expression of EphA2 mRNA in co-transfected cells. (b) Influences of cotransfection on the proliferation ability of HCC cells. (c) Influences of cotransfection on the invasion ability of HCC cells. (d) Influences of cotransfection on the apoptosis of HCC cells. (e) Influences of cotransfection on apoptosis-related proteins of HCC cells. ∗∗ indicates that in comparison of other groups, $p < 0.05$; ∗ indicates $p < 0.05$.

proliferation, metastasis, and growth of tumors [18]. EphA2 showed overexpression in HCC tissues and cells in our study, and it was regulated in various cancers including gastric cancer and lung cancer according to some studies [19, 20]. In order to further verify the influences of EphA2 on HCC cells, we regulated EphA2 expression in HCC cells, and it came out that downregulation of EphA2 expression strongly inhibited the invasion and proliferation of HCC cells. We also transfected plasmids of EphA2 into HCC cells, finding that after transfection, the invasion and proliferation of HCC cells were strengthened and the apoptosis of it was weakened. These results suggested that EphA2 played a role of oncogene in HCC. One previous study has concluded that downregulation of EphA2 in HCC cells can inhibit cell invasion [21], which is consistent with our results. Moreover, one study has reported the relation between EphA2 and the metastasis and prognosis of HCC [22], and one other study has pointed out that miR-26a can suppress the migration and invasion of HCC cells by downregulating EphA2 [23]. These studies further illustrate the role of EphA2 in HCC. In our study, correlation analysis revealed the negative correlation between miR-10b-5p and EphA2, and the dual luciferase reporter assay further verified the targeting correlation between them. In order to further verify that miR-10b-5p affects HCC cells by regulating EphA2, we carried out a rescue experiment, finding that pCMV-EphA2 could reverse the downregulation of EphA2 and influences on biological functions caused by overexpression of miR-10b-5p, and Si-EphA2 could reverse the upregulation of EphA2 and influences on cells caused by inhibition of miR-10b-5p, which further proved that miR-10b-5p exerted its effect on HCC cells by regulating EphA2. As far as I know, this is the first time that we have proved that miR-10b-5p can inhibit the expression of EphA2 to affect the invasion, proliferation, and apoptosis of HCC cells.

5. Conclusion

miR-10b-5p can suppress the invasion and proliferation of primary HCC cells and accelerate apoptosis of them by downregulating EphA2, so it has the potential to be a target for diagnosis and treatment of HCC. However, there are still some deficiencies in this study. For example, we have not conducted any animal experiments to further verify the role of miR-10b-5p in vivo. Secondly, we have not conducted any experiments on the downstream mechanism of EphA2. In the future, we will further improve our experiments to provide support for our conclusions with more data.

Data Availability

The data used during the present study are available from the corresponding author upon reasonable request.

Conflicts of Interest

The authors declare no conflict of interest.

References

[1] H. Nakagawa, M. Fujita, and A. Fujimoto, "Genome sequencing analysis of liver cancer for precision medicine," *Seminars in Cancer Biology*, vol. 55, pp. 120–127, 2019.

[2] S. C. Melkonian, M. A. Jim, B. Reilley et al., "Incidence of primary liver cancer in American Indians and Alaska Natives, US, 1999-2009," *Cancer Causes & Control*, vol. 29, no. 9, pp. 833–844, 2018.

[3] J. Colombo, B. V. Jardim-Perassi, J. P. S. Ferreira et al., "Melatonin differentially modulates NF-κB expression in breast and liver cancer cells," *Anti-Cancer Agents in Medicinal Chemistry*, vol. 18, no. 12, pp. 1688–1694, 2018.

[4] A. Cast, L. Valanejad, M. Wright et al., "C/EBPα-dependent preneoplastic tumor foci are the origin of hepatocellular carcinoma and aggressive pediatric liver cancer," *Hepatology*, vol. 67, no. 5, pp. 1857–1871, 2018.

[5] E. Callegari, M. Domenicali, R. C. Shankaraiah et al., "MicroRNA-based prophylaxis in a mouse model of cirrhosis and liver cancer," *Molecular Therapy-Nucleic Acids*, vol. 14, pp. 239–250, 2019.

[6] J. S. Ni, H. Zheng, Z. P. Huang et al., "MicroRNA-197-3p acts as a prognostic marker and inhibits cell invasion in hepatocellular carcinoma," *Oncology Letters*, vol. 17, no. 2, pp. 2317–2327, 2019.

[7] Y. Wang, Z. Yang, L. Wang et al., "miR-532-3p promotes hepatocellular carcinoma progression by targeting _PTPRT_ ," *Biomedicine & Pharmacotherapy*, vol. 109, pp. 991–999, 2019.

[8] W. Li, C. Li, Q. Xiong, X. Tian, and Q. Ru, "MicroRNA-10b-5p downregulation inhibits the invasion of glioma cells via modulating homeobox B3 expression," *Experimental and Therapeutic Medicine*, vol. 17, no. 6, pp. 4577–4585, 2019.

[9] Y. Li, D. Chen, Y. Li et al., "Oncogenic cAMP responsive element binding protein 1 is overexpressed upon loss of tumor suppressive miR-10b-5p and miR-363-3p in renal cancer," *Oncology Reports*, vol. 35, no. 4, pp. 1967–1978, 2016.

[10] A. Wojcicka, M. Swierniak, O. Kornasiewicz et al., "Next generation sequencing reveals microRNA isoforms in liver cirrhosis and hepatocellular carcinoma," *The International Journal of Biochemistry & Cell Biology*, vol. 53, pp. 208–217, 2014.

[11] A. Hiraoka, T. Kumada, K. Michitaka, and M. Kudo, "Newly proposed ALBI grade and ALBI-T score as tools for assessment of hepatic function and prognosis in hepatocellular carcinoma patients," *Liver Cancer*, vol. 8, no. 5, pp. 312–325, 2019.

[12] H. Dong, J. Wang, Y. Yang et al., "Overexpression of miR-451a inhibits cell proliferation by targeted macrophage migration inhibitory factor in HepG2 cells," *Xi Bao Yu Fen Zi Mian Yi Xue Za Zhi*, vol. 34, no. 12, pp. 1091–1098, 2018.

[13] B. Liu, X. F. Yang, X. P. Liang et al., "Expressions of MiR-132 in patients with chronic hepatitis B, posthepatitic cirrhosis and hepatitis B virus-related hepatocellular carcinoma," *European Review for Medical and Pharmacological Sciences*, vol. 22, no. 23, pp. 8431–8437, 2018.

[14] J. Wang, Y. Yan, Z. Zhang, and Y. Li, "Role of miR-10b-5p in the prognosis of breast cancer," *PeerJ*, vol. 7, article e7728, 2019.

[15] K. Schee, S. Lorenz, M. M. Worren et al., "Deep sequencing the microRNA transcriptome in colorectal cancer," *PLoS One*, vol. 8, no. 6, article e66165, 2013.

Hindawi
BioMed Research International
Volume 2024, Article ID 9781459, 1 page
https://doi.org/10.1155/2024/9781459

Retraction

Retracted: lncRNA FGD5-AS1 and miR-130a Can Be Used for Prognosis Analysis of Patients with Chronic Periodontitis

BioMed Research International

Received 12 March 2024; Accepted 12 March 2024; Published 20 March 2024

This article has been retracted by Hindawi following an investigation undertaken by the publisher [1]. This investigation has uncovered evidence of one or more of the following indicators of systematic manipulation of the publication process:

(1) Discrepancies in scope

(2) Discrepancies in the description of the research reported

(3) Discrepancies between the availability of data and the research described

(4) Inappropriate citations

(5) Incoherent, meaningless and/or irrelevant content included in the article

(6) Manipulated or compromised peer review

The presence of these indicators undermines our confidence in the integrity of the article's content and we cannot, therefore, vouch for its reliability. Please note that this notice is intended solely to alert readers that the content of this article is unreliable. We have not investigated whether authors were aware of or involved in the systematic manipulation of the publication process.

Wiley and Hindawi regrets that the usual quality checks did not identify these issues before publication and have since put additional measures in place to safeguard research integrity.

We wish to credit our own Research Integrity and Research Publishing teams and anonymous and named external researchers and research integrity experts for contributing to this investigation.

The corresponding author, as the representative of all authors, has been given the opportunity to register their agreement or disagreement to this retraction. We have kept a record of any response received.

References

[1] M. Yu and C. Chi, "lncRNA FGD5-AS1 and miR-130a Can Be Used for Prognosis Analysis of Patients with Chronic Periodontitis," *BioMed Research International*, vol. 2021, Article ID 8544914, 7 pages, 2021.

Hindawi
BioMed Research International
Volume 2021, Article ID 8544914, 7 pages
https://doi.org/10.1155/2021/8544914

Research Article

lncRNA FGD5-AS1 and miR-130a Can Be Used for Prognosis Analysis of Patients with Chronic Periodontitis

Miao Yu and Chunyuan Chi

Department of Stomatology, Weifang People's Hospital, Weifang, 261000 Shandong Province, China

Correspondence should be addressed to Chunyuan Chi; kanganchun0570@163.com

Received 12 June 2021; Revised 18 October 2021; Accepted 19 October 2021; Published 10 December 2021

Academic Editor: Jianxin Shi

Background. lncRNA and microRNA affect the occurrence and development of many diseases, so they are expected to become diagnostic or predictive indicators. But the relationship between lncRNA FGD5-AS1 and miR-130a and the prognosis of chronic periodontitis is still unclear. The purpose of this study is to explore the prognostic value of the two in chronic periodontitis. *Objective*. This study set out to investigate the prognostic value of lncRNA FGD5-AS1 and miR-130a in chronic periodontitis. *Methods*. Eighty-seven patients with chronic periodontitis who visited our hospital from March 2016 to August 2017 were collected as an observation group (OG), and 72 subjects with periodontal health who underwent physical examination at the same time were collected as a control group (CG). The FGD5-AS1 and miR-130a expression levels of subjects in the two groups were compared, and prognosis of 87 patients who were reviewed one year later was counted. The expression levels of patients with different prognoses were compared when they were admitted to our hospital. We drew the ROC curve and explored the prognostic value of FGD5-AS1 and miR-130a. The risk factors for adverse prognosis were analyzed through logistic regression. *Results*. FGD5-AS1 was lowly expressed in patients, while miR-130a was highly expressed. FGD5-AS1 and miR-130a had certain diagnostic and predictive value in chronic periodontitis and patient prognosis. The higher the periodontal pocket, the higher the attachment loss. Lower FGD5-AS1 and higher miR-130a levels were independent prognostic risk factors. *Conclusion*. lncRNA FGD5-AS1 is lowly expressed in patients with chronic periodontitis, while miR-130a is highly expressed. Both of them have certain diagnostic and prognostic value in chronic periodontitis and may be potential diagnostic and prognostic indicators.

1. Introduction

Periodontitis is the most common inflammatory disease in the world, which affects about 50% of adults and 60% of people over 65 years old. It is also an oral disease with extremely high morbidity in China [1, 2]. It is often caused by poor oral hygiene and bacterial infection. The release of inflammatory factors after its onset will destroy the balance of alveolar bone absorption and attachment, resulting in bone loss and gradual destruction of oral tissues [3]. Inflammation of chronic periodontitis has long duration. Soft tissue and hard tissue around teeth will be affected, which will often lead to tooth loss or dentition dysfunction in patients at the later stage of development [4]. Moreover, there are also some references showing that the risk of chronic periodontitis patients complicated with cardiovascular diseases, chronic respiratory diseases, cancer, and other diseases is dramatically higher than that of people without chronic periodontitis, so the treatment and control of chronic periodontitis become critical [5]. Prognosis of patients in the treatment of chronic periodontitis is a key point that we must consider, so that we can better adjust the treatment plan and support effective treatment decisions [6].

Long noncoding RNA (lncRNA) is a noncoding single-stranded RNA with a length of more than 200 nucleotides [7]. There are some lncRNA that affect the development of periodontitis, and their expression levels are dramatically different between patients and normal people [8]. lncRNA FGD5-AS1 is an lncRNA [9] discovered recently that can interfere with the development of periodontitis through the

Table 1: Primer sequence.

	Upstream primers	Downstream primers
FGD5-AS1	5′-GAAGGGCCGAAGAG CTCAAT-3′	5′-GGCTCGCAAAGTGTCTGTTG-3′
miR-130a	5′-GGCAGTCAATGCAATGTTAAAAG-3′	5′-CAGTGCGTGTCGTGGAGT-3′
GAPDH	5′-TATGATGATATCAAGAGGGT AGT-3′	5′-TGTATCCAAACTCATTGTCATAC-3′
U6	5′-CTCGCTTCGGCAGCACATATACTA-3′	5′-ACGAATTTGCGTGTCATCCTTGCG-3′

Table 2: Clinical data table.

	Observation group (OG) ($n = 87$)	Control group (CG) ($n = 72$)	X^2/t	P
Gender				
Male	39 (44.83)	41 (56.94)	2.314	0.128
Female	48 (55.17)	31 (43.06)		
Age (years)	48.1 ± 9.5	47.6 ± 8.5	0.346	0.730
BMI (kg/m^2)	22.26 ± 2.46	21.75 ± 2.69	1.247	0.214
History of smoking				
Yes	39 (44.83)	23 (31.94)	2.749	0.097
No	48 (55.17)	49 (68.06)		
History of alcoholism				
Yes	18 (20.69)	11 (15.28)	0.774	0.379
No	69 (79.31)	61 (84.72)		
Number of teeth (teeth)	25.22 ± 4.05	26.57 ± 2.67	2.425	0.016
Gingival index	1.94 ± 0.58	0.21 ± 0.09	25.048	<0.001
Plaque index	1.43 ± 0.60	0.17 ± 0.06	17.736	<0.001
Sulcus bleeding index	2.63 ± 0.89	0.24 ± 0.11	22.632	<0.001
Pocket depth (mm)	3.93 ± 0.88	2.06 ± 0.47	16.213	<0.001
Attachment loss (mm)	4.22 ± 0.75	1.23 ± 0.27	32.134	<0.001

SOCS6/NF-KB pathway. However, it is still unclear whether FGD5-AS1 can be used for prognostic analysis of patients with chronic periodontitis.

The regulation process of lncRNA is often to bind mRNA by acting as a competitive endogenous RNA (ceRNA) so as to target and regulate the microRNA and target protein expression levels to affect the occurrence and development of diseases [10]. ceRNAs are transcripts as microRNA spongesthat regulate each other at the post-transcriptional level through competitivebinding with other microRNAs. ceRNAs has been found to include protein-codingmRNAs and non-coding RNA, in which non-coding RNA includes pseudogene transcripts,lncRNA, and circular RNA etc. The presence of ceRNAs affect the functional activity ofmicroRNAs. ceRNAsactivity can form a large-scale transcriptional regulatory network, which canexpand the functional genetic information in the human genome and play a rolein pathological conditions. MicroRNA is an endogenous noncoding RNA, which also participates in the development and regulation of some diseases [11, 12]. Venugopal et al. [13] found that the miR-125b, miR-100, and miR-21 expression levels in periodontitis patients were abnormal with normal people and affected periodontitis through the interaction of some signal pathways and cytokines. miR-130a is an inflammation-related microRNA; it has abnormal expression in patients with osteoarthritis and leukemia inflammation, so does periodontitis [14–16]. However, there is little research on the prognostic value of lncRNA FGD5-AS1 and miR-130a in chronic periodontitis.

Therefore, in this study, we hope to observe the FGD5-AS1 and miR-130a expression levels in different prognoses of chronic periodontitis to analyse their prognostic value and provide the basis and direction for clinical practice.

2. Methods

2.1. Patient Data. Eighty-seven patients with chronic periodontitis who visited our hospital from March 2016 to August 2017 were collected as an observation group (OG), including 39 males and 48 females with an average age of 48.1 ± 9.5 years and an age range of 31-64 years. Seventy-two subjects with periodontal health who underwent physical examination during the same period were also collected as a control group (CG), including 41 males and 31 females with an average age of 47.6 ± 8.5 years and an age range of 26-60 years. This study was conducted with the approval

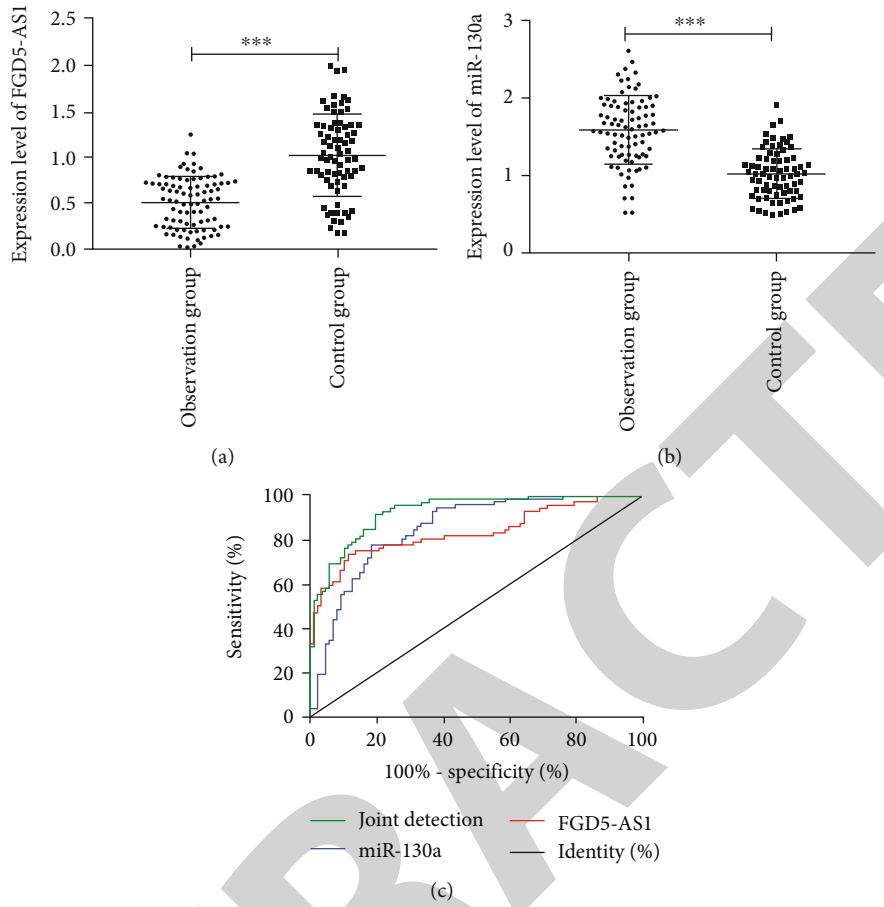

Figure 1: Expression differences and diagnosis ROC curve of lncRNA FGD5-AS1 and miR-130a in the OG and CG. (a) FGD5-AS1 expression levels in the OG were dramatically lower than those in the CG ($t = 8.899$, $P < 0.001$). (b) miR-130a expression levels in the OG were dramatically higher than those in the CG ($t = 9.166$, $P < 0.001$). (c) ROC curve of lncRNA FGD5-AS1 and miR-130a in diagnosing chronic periodontitis. $***$ indicates $P < 0.001$.

of the Medical Ethics Committee, and all patients were informed and signed an informed consent form.

2.2. Inclusion and Exclusion Criteria. Inclusion criteria were as follows: patients were diagnosed with chronic periodontitis by imaging [17], no anti-inflammatory drugs were used for nearly 3 months, their clinical data were complete, and the treatment and follow-up were coordinated.

Exclusion criteria were as follows: patients had implant or orthodontic appliance, patients took bactericide orally in the past 3 months, patients had less than 18 natural teeth in the full mouth, and patients were complicated with diabetes.

2.3. Detection Methods. Specimens of gingival crevicular fluid from all subjects were collected and stored into EP tubes at -80°C for later use. The collected samples were extracted with the EasyPure miRNA kit, and the purity, concentration, and integrity were tested by using ultraviolet spectrophotometer and agarose gel electrophoresis. Total RNA was reversely transcribed through the TransScript® miRNA RT Enzyme Mix and 2×TS miRNA Reaction Mix (Transgen Biotech Co., Ltd., Beijing, ER601-01, AT351-01), and the operation steps were strictly in accordance with the manufacturer's kit. Then, PCR amplification experiment was carried out under a PCR instrument (ABI, USA, 7500). A PCR reaction system was as follows: cDNA 1 μL, upstream and downstream primers 0.4 μL each, 2×TransTaq® Tip Green qPCR SuperMix 10 μL, passive reference dye (50×) 0.4 μL, and ddH_2O supplemented to 20 μL. PCR reaction conditions were as follows: predenaturation at 94°C for 30 s, denaturation at 94°C for 5 s, and annealing at 60°C for 30 s. The above three steps had 40 cycles in total. Each sample was provided with 3 repeated wells, and the experiment was carried out 3 times. In this study, FGD5-AS1 used GAPDH as an internal reference, miR-130a used U6 as an internal reference, and $2^{-\triangle\triangle ct}$ was employed to analyze the data. The left and right primers were provided by Sangon Biotech (Shanghai) Co., Ltd., and the primer sequence is shown in Table 1.

2.4. Outcome Measures

2.4.1. Main Outcome Measures. The differences of lncRNA FGD5-AS1 and miR-130a expression levels in the OG and the CG were compared, and the prognosis of the patients

Table 3: ROC curve data.

Indicators	AUC	95% CI	Specificity	Sensitivity	Youden index	Cut-off
FGD5-AS1	0.835	0.769-0.901	88.51%	72.22%	42.21%	>0.805
miR-130a	0.851	0.792-0.910	80.46%	77.78%	58.24%	<1.227
Joint detection	0.929	0.891-0.933	80.46%	90.28%	70.74%	>0.321

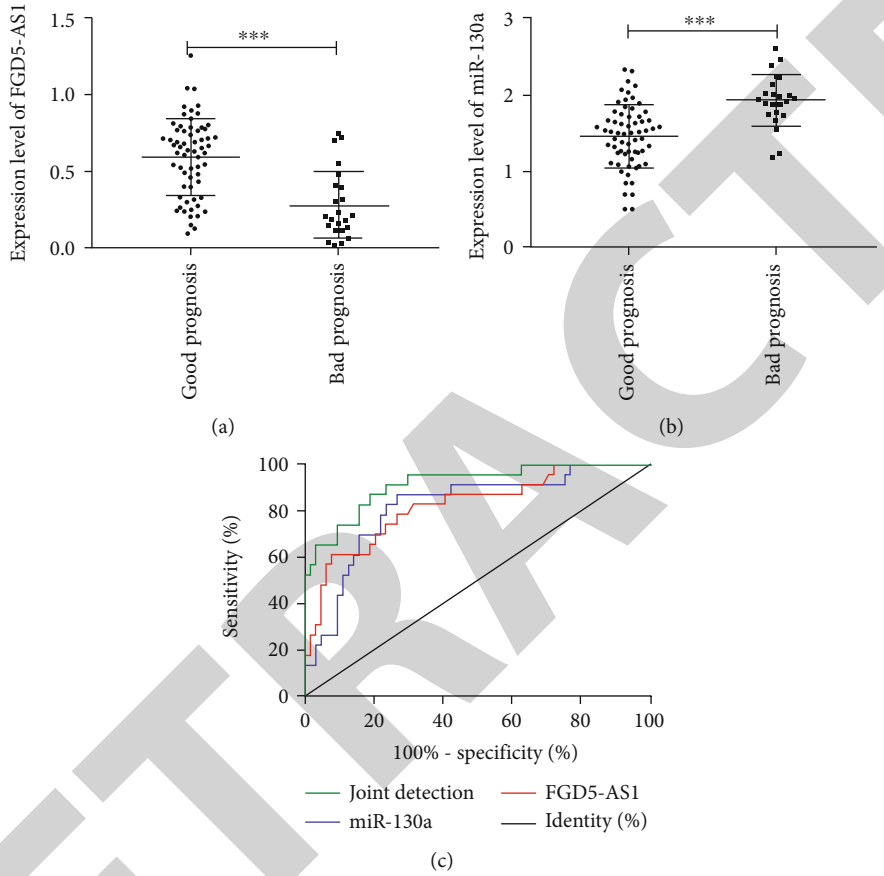

Figure 2: Expression differences and prognosis ROC curve of FGD5-AS1 and miR-130a in different prognosis groups. (a) FGD5-AS1 expression levels in the GPG were markedly higher than those in the PPG ($t = 5.205$, $P < 0.001$). (b) miR-130a expression levels in the GPG were markedly lower than those in the PPG ($t = 5.023$, $P < 0.001$). (c) ROC curve; *** indicates $P < 0.001$.

one year after discharge was counted. The prognosis was good if PD < 4 mm reexamined after one year and poor if PD ≥ 4 mm. According to their prognosis, they were divided into the good prognosis group (GPG) and poor prognosis group (PPG), and their independent prognostic risk factors were analyzed by multivariate logistic regression.

2.4.2. Secondary Outcome Measures. The diagnostic value and prognostic value of FGD5-AS1 and miR-130a in patients with chronic periodontitis were analyzed by the receiver operating characteristic (ROC) curve.

2.5. Statistical Analysis. The collected data were statistically analyzed via SPSS 20.0 (SPSS Co., Ltd., Chicago, USA). Their pictures were drawn by using GraphPad Prism 7 (GraphPad Software Co., Ltd., San Diego, USA). The counting data usage was expressed as n (%) and checked by X^2. The measurement data were expressed as mean ± standard deviation (mean ± SD), and all those conformed to normal distribution. Comparison between the two groups was under the independent samples t-test. Multivariate analysis of prognosis was under the multivariate logistic regression test. $P < 0.05$ indicates statistically significant differences.

3. Results

3.1. Clinical Data. By comparing the clinical data of the OG and the CG, we found that there was no remarkable difference in gender, age, BMI, and history of smoking or alcoholism of subjects between the two groups, while there were remarkable differences in the number of teeth, gingival index, plaque index, sulcus bleeding index, pocket depth, and attachment loss ($P < 0.05$) (Table 2).

Table 4: Univariate analysis table (n (%)).

	Good prognosis group (GPG) ($n = 64$)	Poor prognosis group (PPG) ($n = 23$)		
Gender				
Male	31 (48.44)	8 (34.78)	1.276	0.259
Female	33 (51.56)	15 (65.22)		
Age (years)	47.8 ± 9.9	49.0 ± 8.5	0.517	0.607
BMI (kg/m^2)	22.45 ± 2.37	21.75 ± 2.69	1.172	0.245
History of smoking				
Yes	25 (39.06)	14 (60.87)	3.253	0.071
No	39 (60.94)	9 (39.13)		
History of alcoholism				
Yes	13 (20.31)	5 (21.74)	0.021	0.885
No	51 (79.69)	18 (78.26)		
Number of teeth (teeth)	25.33 ± 4.15	24.92 ± 3.80	0.415	0.674
Gingival index	1.84 ± 0.54	2.22 ± 0.60	2.811	0.006
Plaque index	1.31 ± 0.50	1.74 ± 0.75	3.075	0.003
Sulcus bleeding index	2.45 ± 0.87	3.13 ± 0.76	3.318	0.001
Pocket depth (mm)	3.73 ± 0.78	4.50 ± 0.88	3.924	<0.001
Attachment loss (mm)	4.25 ± 0.95	1.23 ± 0.43	5.547	<0.001
FGD5-AS1	0.59 ± 0.25	0.28 ± 0.23	5.205	<0.001
miR-130a	1.45 ± 0.41	1.93 ± 0.34	5.023	<0.001

3.2. Expression Differences and Diagnosis ROC of lncRNA FGD5-AS1 and miR-130a in the Two Groups. By comparing the lncRNA FGD5-AS1 and miR-130a expression levels in both groups, we found that FGD5-AS1 (0.51 ± 0.28) in the OG was obviously lower than that in the CG (1.03 ± 0.45) ($t = 8.899$, $P < 0.001$) ($P < 0.05$), and miR-130a (1.58 ± 0.44) in the OG was obviously higher than that in the CG (1.01 ± 0.32) ($t = 9.166$, $P < 0.001$) ($P < 0.05$). The ROC curve for diagnosis of chronic periodontitis revealed that the area under the lncRNA FGD5-AS1 curve was 0.835 and the best specificity and sensitivity were 88.51% and 72.22%, respectively, when the cut-off point was 0.805; the area under the miR-130a curve was 0.851 and the best specificity and sensitivity were 80.46% and 77.78%, respectively, when the cut-off point was 1.227; and the area under the joint detection curve was 0.929 and the best specificity and sensitivity were 80.46% and 90.28%, respectively, when the cut-off point was 0.321 (Figure 1, Table 3).

3.3. Expression of lncRNA FGD5-AS1 and miR-130a in Different Prognosis Groups and Diagnosis of ROC. Prognosis of the patients in the OG reviewed after one year was collected. Sixty-four patients had good prognosis and 23 patients had poor prognosis. According to their prognosis, they were divided into GPG ($n = 64$) and PPG ($n = 23$). The FGD5-AS1 expression levels (0.59 ± 0.25) in the GPG were markedly higher than those in the PPG (0.28 ± 0.23) ($t = 5.205$, $P < 0.001$) ($P < 0.05$). The miR-130a expression levels (1.45 ± 0.41) in the GPG were dramatically lower than those in the PPG (1.93 ± 0.34) ($t = 5.023$, $P < 0.001$) ($P < 0.05$). The predicted prognosis ROC curve revealed that the area under the lncRNA FGD5-AS1 curve was 0.822 and the best specificity and sensitivity were 90.63% and 60.87%, respectively, when the cut-off point was 0.237; the area under the miR-130a curve was 0.819 and the best specificity and sensitivity were 73.44% and 82.61%, respectively, when the cut-off point was 1.686; and the area under the joint detection curve was 0.916 and the best specificity and sensitivity were 81.25% and 82.61%, respectively, when the cut-off point was 0.295 (Figure 2, Table 3).

3.4. Univariate Analysis. Through univariate analysis of the clinical data of the GPG and the PPG, it was found that there were statistical differences in the gingival index, plaque index, sulcus bleeding index, pocket depth, attachment loss, FGD5-AS1, and miR-130a between the two groups ($P < 0.05$), while there were no statistical differences in gender, age, BMI, history of smoking, history of alcoholism, and number of teeth ($P > 0.05$) (Table 4).

3.5. Multivariate Analysis of Prognosis. We included the indicators with differences in univariate analysis into the evaluation (the evaluation table is shown in Table 5). Then, we chose to proceed with LR to perform multivariate logistic regression analysis. The results revealed that the gingival index, plaque index, and sulcus bleeding index were not independent risk factors for patients' prognosis, while periodontal pocket, attachment loss, FGD5-AS1, miR-130a, miR-17-5p, and miR-130a were independent risk factors for poor prognosis of patients (Table 6).

Table 5: Assignment table.

Factor	Assignment
Gingival index	Data are a continuous variable and are analyzed using original data
Plaque index	Data are a continuous variable and are analyzed using original data
Sulcus bleeding index	Data are a continuous variable and are analyzed using original data
Pocket depth	Data are a continuous variable and are analyzed using original data
Attachment loss	Data are a continuous variable and are analyzed using original data
FGD5-AS1	Data are a continuous variable and are analyzed using original data
miR-130a	Data are a continuous variable and are analyzed using original data
Prognosis	Poor prognosis = 1, good prognosis = 0

Table 6: Multivariate analysis table.

Factor	B	S.E.	Wals	Sig.	Exp(B)	95% CI of Exp(B)	
						Lower limit	Upper limit
Periodontal pocket	1.398	0.694	4.054	0.044	4.047	1.038	15.782
Attachment loss	1.570	0.744	4.457	0.035	4.805	1.119	20.635
FGD5-AS1	-6.441	2.239	8.273	0.004	0.002	0.001	0.129
miR-130a	2.875	1.363	4.451	0.035	11.726	1.227	56.187

4. Discussion

Many evidences display that microRNA and lncRNA play a role in the occurrence and development of diseases, and the same regulatory mechanism exists in periodontosis [18–20]. Lian et al. [21] found that miR-335-5p could promote osteoblast activity and reduce periodontal bone destruction and inflammation in periodontitis, so as to prevent periodontitis and bone loss. Han et al. [22] discovered that lncRNA TUG1 could reduce inflammation caused by lipopolysaccharide and regulate cell proliferation and apoptosis of periodontal ligament cells.

In this research, we found that the FGD5-AS1 expression in periodontitis patients was remarkably lower than that in healthy people, while the miR-130a expression was remarkably higher than that in healthy people, suggesting that FGD5-AS1 and miR-130a expression levels were probably altered in patients. The ROC curve analysis found that the area under the FGD5-AS1 and miR-130a curve presented with considerable specificity and sensitivity, respectively, and the sensitivity of combined detection was better than that of single detection of two indexes. Additionally, we found that the FGD5-AS1 expression levels in patients with good prognosis were remarkably higher than those in patients with poor prognosis, while the miR-130a expression levels were remarkably lower than those in patients with poor prognosis; this indicated that the FGD5-AS1 and miR-130a expression levels were tied to the prognosis of periodontitis patients.

We then explored the independent risk factors for poor prognosis of patients with chronic periodontitis and found that the higher the periodontal pockets, the higher the loss of attachment; lower FGD5-AS1 and higher miR-130a levels were independent risk factors for their prognosis. In previous studies, age, bone height, and periodontal pocket were mentioned as prognostic factors of patients [23, 24], while our study first found that FGD5-AS1 and miR-130a were also independent prognostic factors of chronic periodontitis. Hence, in the future, we can predict the prognosis of patients through the levels of two indicators, so as to implement the corresponding treatment plans.

Nevertheless, there are still some limitations in this study. In the first place, the study did not consider the treatment plan of patients, so it was not clear whether different treatment plans would have different effects on the FGD5-AS1 and miR-130a expression levels, and whether there would be differences in their expression levels in patients with different efficacies had not been explored. In the second place, we did not study the specific mechanism of FGD5-AS1 and miR-130a regulating chronic periodontitis, and we did not predict the target gene and target protein mediated by the two. Finally, we were still not clear whether there was a certain relationship between FGD5-AS1 and miR-130a. Hence, we hope to increase the corresponding basic experiments in the later stage to explore the specific impact mechanism of FGD5-AS1 and miR-130a and their interrelation.

To summarize, lncRNA FGD5-AS1 is lowly expressed in patients with chronic periodontitis while miR-130a is highly expressed. Both of them have certain diagnostic and prognostic value in chronic periodontitis and may be potential diagnostic and prognostic indicators.

Data Availability

The data used during the present study are available from the corresponding author upon reasonable request.

Hindawi
BioMed Research International
Volume 2024, Article ID 9863429, 1 page
https://doi.org/10.1155/2024/9863429

Retraction

Retracted: Analysis on the Clinical Effect of High-Dose Glucocorticoids Combined with Immunosuppressants on Patients with Myasthenia Gravis Undergoing Video-Assisted Thoracoscopic Surgery

BioMed Research International

Received 12 March 2024; Accepted 12 March 2024; Published 20 March 2024

This article has been retracted by Hindawi following an investigation undertaken by the publisher [1]. This investigation has uncovered evidence of one or more of the following indicators of systematic manipulation of the publication process:

(1) Discrepancies in scope

(2) Discrepancies in the description of the research reported

(3) Discrepancies between the availability of data and the research described

(4) Inappropriate citations

(5) Incoherent, meaningless and/or irrelevant content included in the article

(6) Manipulated or compromised peer review

The presence of these indicators undermines our confidence in the integrity of the article's content and we cannot, therefore, vouch for its reliability. Please note that this notice is intended solely to alert readers that the content of this article is unreliable. We have not investigated whether authors were aware of or involved in the systematic manipulation of the publication process.

Wiley and Hindawi regrets that the usual quality checks did not identify these issues before publication and have since put additional measures in place to safeguard research integrity.

We wish to credit our own Research Integrity and Research Publishing teams and anonymous and named external researchers and research integrity experts for contributing to this investigation.

The corresponding author, as the representative of all authors, has been given the opportunity to register their agreement or disagreement to this retraction. We have kept a record of any response received.

References

[1] P. Liu, H. Wang, J. Hu, X. Zhai, and Z. Ge, "Analysis on the Clinical Effect of High-Dose Glucocorticoids Combined with Immunosuppressants on Patients with Myasthenia Gravis Undergoing Video-Assisted Thoracoscopic Surgery," *BioMed Research International*, vol. 2021, Article ID 5854056, 6 pages, 2021.

Hindawi
BioMed Research International
Volume 2021, Article ID 5854056, 6 pages
https://doi.org/10.1155/2021/5854056

Research Article

Analysis on the Clinical Effect of High-Dose Glucocorticoids Combined with Immunosuppressants on Patients with Myasthenia Gravis Undergoing Video-Assisted Thoracoscopic Surgery

Pei Liu, Haoyue Wang, Jiejie Hu, Xiaobin Zhai, and Zhaoming Ge

Department of Neurology, Lanzhou University Second Hospital, Lanzhou, 730030 Gansu Province, China

Correspondence should be addressed to Zhaoming Ge; bei0217438@163.com

Received 8 August 2021; Accepted 30 October 2021; Published 6 December 2021

Academic Editor: Jianxin Shi

Objective. The purpose of the study was to investigate the clinical effect of high-dose glucocorticoids (GCS) combined with immunosuppressants on the treatment of myasthenia gravis (MG) with video-assisted thoracoscopic surgery (VATS). *Methods*. A total of 106 MG patients admitted to the neurology department of our hospital from February 2016 to February 2020 were selected as the study subjects and divided into experimental group ($n = 53$) and control group ($n = 53$). The patients in the control group underwent VATS, while the patients in the experimental group were treated with high-dose GCS combined with immunosuppressants on the basis of VATS treatment. The clinical efficacy of different MG treatment methods was analyzed. *Results*. No significant differences were observed in visual analogue score (VAS) at T1 between the two groups ($P > 0.05$), while VAS scores at T2, T3, and T4 in the experimental group were significantly lower than those in the control group ($P < 0.001$). In the experimental group, the overall response rate was significantly higher than the control group ($P < 0.05$). Cytotoxic T-lymphocyte-associated protein 4 (CTLA4) level in regulatory T (Treg) cells in experimental groups after treatment was significantly higher, compared to that in before treatment and the control group ($P < 0.05$). Similar results of each quantitative MG score were displayed in both groups after treatment, compared to before treatment and the control group ($P < 0.05$). Clinical performance of patients with lower incidence of adverse reactions in the experimental groups after treatment was significantly higher than those in the control group ($P < 0.001$). *Conclusion*. GCS combined with immunosuppressants can effectively relieve patients' clinical symptoms and improve their quality of life, with significant clinical efficacy and high safety, which is worthy of application and promotion.

1. Introduction

Myasthenia gravis (MG), as an immune disease in neurology, refers to weak contraction in skeletal muscles caused by impairment of neuromuscular transmission. The clinical hallmark of MG consists of fluctuating fatigability and weakness affecting ocular, bulbar, and (proximal) limb skeletal muscle groups. A pragmatic clinical classification distinguishes pure ocular myasthenia from generalized myasthenia with mild, moderate, and severe manifestation. Ocular myasthenia exclusively affects the outer ocular muscles including the M. levator palpebrae and presents with ptosis and double vision. Ptosis and double vision may be transient, fluctuating, or progressive during the day. Only 10–20% of patients show muscle fatigability and weakness persistently restricted to the outer ocular muscles. The majority of patients proceed to generalized muscle fatigability and weakness within 24 months after the disease onset [1, 2]. Investigations have found that MG, which has affected 730000 patients across the whole world, can occur at any age and be specifically divided into generalized and ocular types, with higher prevalence rate in women than in men [3]. At present, the top priority for MG treatment is drug therapy, in which glucocorticoids (GCS) and immunosuppressants have been widely used, as GCS can effectively improve thymus immune function, inhibit germinal center

formation, and promote the secretion of acetylcholine at the neuromuscular junction, thus greatly relieving clinical symptoms [4, 5]. However, clinical practice confirms that long-term implementation of drug therapy can contribute to multiple complications, hence increasing the difficulty of treatment. Some scholars have pointed out that immunosuppressants combined with GCS can greatly shorten treatment time and effectively avoid the side effect caused by the long-term use of hormones, thus exerting the synergistic effect of drugs and improving therapeutic effect [6]. As a minimally invasive treatment method, video-assisted thoracoscopic surgery (VATS), which is performed with the assistance of high-definition video-assisted photographic technology and high-tech equipment, with the advantages of less trauma and obvious clinical efficacy, has been widely applied in thoracic surgery [7]. This study provides more evidence for MG treatment by further investigating the clinical effect of high-dose GCS combined with immunosuppressants on MG treatment with VATS, and the study is reported as follows.

2. Materials and Methods

2.1. General Information. A total of 106 MG patients admitted to the neurology department of our hospital from February 2016 to February 2020 were selected as the study subjects and divided into experimental group ($n = 53$) and control group ($n = 53$), according to the number table method. In the experimental group, there were 28 males and 25 females, with the average age of 46.52 ± 5.83 years old, average course of disease of 5.63 ± 1.24 months, and average body mass index (BMI) of $21.43 \pm 1.22\,kg/m^2$, including 24 patients in the acute phase and 29 in the remission phase, while in the control group, there were 27 males and 26 females, with the average age of 46.54 ± 5.81 years old, average course of disease of 5.66 ± 1.26 months, and average BMI of $21.46 \pm 1.23\,kg/m^2$, including 26 patients in the acute phase and 27 in the remission phase, with comparability.

This study was approved by the Hospital Ethics Committee, and patients and their family members were informed of the purpose and processes of this study and signed the informed consent.

2.2. Inclusion Criteria. Patients diagnosed with MG by internationally recognized diagnostic criteria, not restricted in age, gender, ethnicity, race, and disease stage, met the diagnostic criteria for MG, were treated with VATS, and had complete clinical data, were included.

2.3. Exclusion Criteria. Patients who had malignant tumors, had other immune system diseases, had surgical contraindications or were in lactation period, had mental and other cognitive disorders, and had severe cardiovascular diseases, mental illnesses, etc., will be excluded.

2.4. Methods. In the control group, the patients, after taking supine positions, underwent VATS treatment. During surgery, an approximately 3 cm incision made in the 3rd intercostal space of anterior axillary line on the posterior border of the right pectoralis major muscle was taken as the main operating hole, and an approximately 1.5 cm incision made in the 5 h intercostal space of midaxillary line was taken as the observation hole. Subsequently, after CO_2 pneumothorax was established with appropriate pressure, the medistinal pleura was cut vertically along superior vena cava and anterior phrenic nerve, and then, the pleura was cut parallelly along sternum and posterior arteries and veins in thoracic cage, until the thymus was completely removed [8, 9].

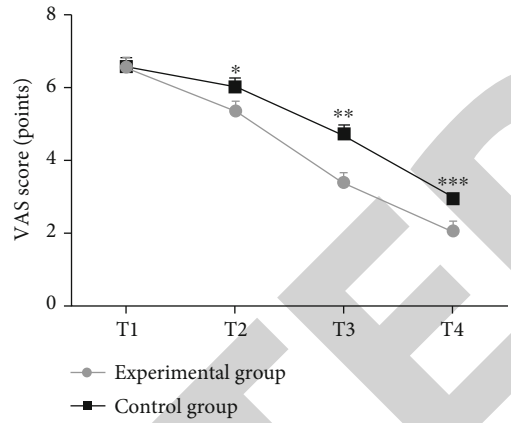

Figure 1: Comparison of VAS scores at different time points after surgery between the two groups ($\bar{x} \pm s$). Note: the abscissa represented T1, T2, T3, and T4, while the ordinate represented VAS score, points. The VAS scores at T1, T2, T3, and T4 in the experimental group were 6.32 ± 0.43 points, 5.17 ± 0.34 points, 3.24 ± 0.28 points, and 1.92 ± 0.23 points, respectively. The VAS scores at T1, T2, T3, and T4 in the control group were 6.35 ± 0.46 points, 5.86 ± 0.32 points, 4.56 ± 0.31 points, and 2.83 ± 0.21 points. * indicated that there were significant differences in VAS score at T2 between the two groups ($t = 10.759$, $P < 0.001$). ** indicated that there were significant differences in VAS score at T3 between the two groups ($t = 23.005$, $P < 0.001$). *** indicated that there were significant differences in VAS score at T4 between the two groups ($t = 21.271$, $P < 0.001$).

On the basis of the treatment in the control group, the patients in the experimental group were treated with high-dose GCS combined with immunosuppressants. The intravenous injection of prednisolone (State Food and Drug Administration approval number: H33020824; manufacturer: Huazhong Pharmaceutical Co., Ltd.; specification: 5 ml: 0.125 g) was performed, 1000 mg/d × 3d, and the dosage was halved every 3 d until the 27th d. At the same time, the patients should take ciclosporin (State Food and Drug Administration approval number: H10960123; manufacturer: Hangzhou Zhongmei Huadong Pharmaceutical Co., Ltd.; specification: 50 mg ∗ 50 s) orally at the dose of 1 mg/(kg · d) for the first 3 d, 2 mg/(kg · d) for 4-6 d, 4 mg/(kg · d) for 7-10 d, and 4 mg/(kg · d) for maintenance, and they also should take mycophenolate mofetil (State Food and Drug Administration approval number: H20031277; manufacturer: Shanghai Roche Pharmaceutical Co., Ltd.; specification: 0.5 g ∗ 20 s) orally, at the dose of 0.5 g/d for the first 3 d, 1 g/d for the first 4-6 d, 1.5 g/d for the first 7-10 d, and 1.5 g/d for maintenance. Additionally, intravenous drip of 10-15 mg/kg cyclophosphamide (State Food and Drug Administration approval number: H32024654;

Table 1: Comparison of therapeutic effect between the two groups [n (%)].

Group	n	Recovery	Markedly effective	Improved	Effective	Ineffective	Overall response rate
Experimental group	53	7 (13.21%)	23 (43.40%)	16 (30.19%)	5 (9.43%)	2 (3.77%)	96.23% (51/53)
Control group	53	2 (3.77%)	14 (26.42%)	12 (22.64%)	16 (30.19%)	9 (16.98%)	83.02% (44/53)
χ^2							4.970
P							0.026

manufacturer: Jiangsu Shengdi Pharmaceutical Co., Ltd.; specification: 0.2 g × 1 vial/box) was also performed, once a week, with the total dose of 10 g.

2.5. Evaluation Indexes. VAS score [10] was adopted to evaluate the degree of limb pain at different time points in the two groups, with the total score of 10 points, and higher scores indicated severer pain. The time points at 1 d, 3 d, 7 d, and 14 d after surgery were set as T1, T2, T3, and T4, respectively.

Quantitative MG score scale [11] was adopted to evaluate patients' limb recovery before and after treatment, with five scoring items and each giving a total score of 10 out of 50, and higher scores indicated better limb recovery.

According to the results of quantitative MG score scale, the treatment effect was categorized as 5 levels, which were summarized as follows. Recovery referred to that patients' total MG score decreased by more than or equal to 95%, compared with the score before treatment; the markedly effective referred to that patients' MG score decreased by 80-94%; the improved referred to that patients' MG score decreased by 60-79%; the effective referred to that patients' MG score decreased by 30-59; the ineffective referred to that patients' MG score decreased by less than or equal to 29%. The total effective rate = recovery rate + markedly effective rate + improved rate + effective rate.

5 ml of fasting venous blood samples were collected from patients in both groups before and after treatment, and the CTLA4 levels in Treg cells were measured by Attune NxT flow cytometer (manufacturer: Beijing Heros Technology Co., Ltd.).

Quality of life of the patients in both groups after treatment was evaluated by the postoperative quality of life scale for MG patients, which was made in our department, with five items in total and each scoring 20 points, and higher scores indicated better quality of life.

The incidence of adverse reactions of the patients was recorded and compared between the two groups.

2.6. Statistical Analysis. All the data were processed for statistical analysis by SPSS21.0 software, and GraphPad Prism 7 (GraphPad Software, San Diego, USA) was used to draw the pictures of the data. Measurement data were expressed by ($\bar{x} \pm s$) and tested by t-test. Enumeration data were expressed as [n (%)] and tested by χ^2 test. The differences had statistical significance when $P < 0.05$.

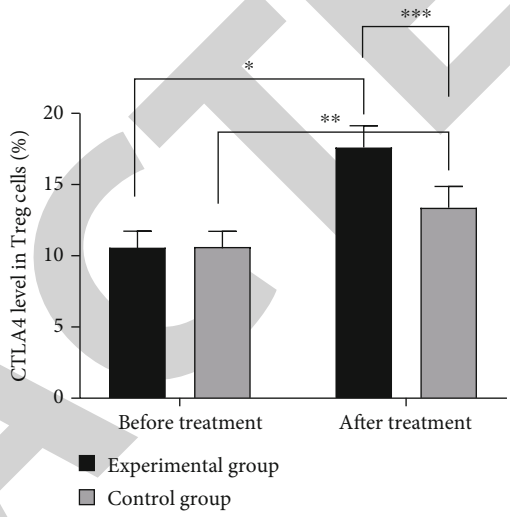

Figure 2: Comparison of CTLA4 levels in Treg cells before and after treatment between the two groups ($\bar{x} \pm s$). Note: the abscissa represented before and after treatment, while the ordinate represented CTLA4 level in Treg cells. The CTLA4 levels in Treg cells in the experimental group before and after treatment were 9.84 ± 1.53% and 16.59 ± 2.17%, respectively, while those in the control group were 9.89 ± 1.55% and 12.36 ± 2.13%, respectively. * indicated that there were significant differences in CTLA4 levels in Treg cells before and after treatment in the experimental group ($t = 18.508$, $P < 0.001$). ** indicated that there were significant differences in CTLA4 levels in Treg cells before and after treatment in the control group ($t = 6.826$, $P < 0.001$); *** indicated that there were significant differences in CTLA4 levels in Treg cells after treatment between the two groups ($t = 10.128$, $P < 0.001$).

3. Results

3.1. Comparison of VAS Scores at Different Time Points after Surgery between the Two Groups. There were no significant differences in VAS scores between the two groups at T1 ($P > 0.05$), and the VAS scores in the experimental group at T2, T3, and T4 were significantly lower than those in the control group ($P < 0.05$), as shown in Figure 1.

3.2. Comparison of Therapeutic Effect between the Two Groups. The overall response rate in the experimental group was significantly higher than that in the control group ($P < 0.05$), as shown in Table 1.

3.3. Comparison of CTLA4 Levels in Treg Cells before and after Treatment between the Two Groups. The CTLA4 levels in Treg cells in both groups after treatment were

Table 2: Comparison of quantitative MG scores before and after treatment between the two groups ($\bar{x} \pm s$, points).

Group	Experimental group ($n = 53$)		Control group ($n = 53$)	
	Before treatment	After treatment	Before treatment	After treatment
Upper limb	3.26 ± 0.42	6.73 ± 0.51	3.28 ± 0.39	4.58 ± 0.49*
Head	2.17 ± 0.24	11.43 ± 0.45	2.19 ± 0.25	7.84 ± 0.42*
Lower limb	3.11 ± 0.24	6.81 ± 0.45	3.09 ± 0.26	4.61 ± 0.48*
Facial muscles	2.63 ± 0.32	7.49 ± 0.36	2.67 ± 0.29	5.02 ± 0.42*
Swallowing	2.04 ± 0.25	8.01 ± 0.33	2.06 ± 0.31	6.04 ± 0.37*
Score	13.21 ± 1.47	40.47 ± 2.10	13.29 ± 1.50	28.09 ± 2.18

Note: each quantitative MG score in the two groups after treatment was significantly higher than that before treatment; * indicated the comparison of each quantitative MG score after treatment between the two groups, $P < 0.05$.

Table 3: Comparison of quality of life scores after treatment between the two groups ($\bar{x} \pm s$, points).

Group	n	Limb function	Linguistic function	Emotional function	Vitality	Cognitive function
Experimental group	53	14.52 ± 2.36	15.27 ± 1.95	14.27 ± 2.36	13.62 ± 2.15	13.83 ± 2.21
Control group	53	9.57 ± 2.47	10.59 ± 2.03	11.35 ± 2.04	9.83 ± 2.11	10.25 ± 1.95
t		10.549	12.104	6.815	9.159	8.843
P		0.001	0.001	0.001	0.001	0.001

Table 4: Comparison of incidence of adverse reactions between the two groups [n (%)].

Group	n	Increased blood glucose	Elevated blood pressure	Pulmonary infection	Infection of digestive canal	Overall incidence
Experimental group	53	1 (1.89%)	0 (0.00%)	1 (1.89%)	1 (1.89%)	5.66% (3/53)
Control group	53	2 (3.77%)	3 (5.66%)	3 (5.66%)	2 (3.77%)	18.87% (10/53)
χ^2						4.296
P						0.038

significantly higher than those before treatment ($P < 0.05$), and the CTLA4 levels in Treg cells in the experimental group after treatment were significantly higher than those in the control group ($P < 0.05$), as shown in Figure 2.

3.4. Comparison of Quantitative MG Scores before and after Treatment between the Two Groups. Each quantitative MG score in the two groups after treatment was significantly higher than that before treatment ($P < 0.05$), and each quantitative MG score in the experimental group after treatment was significantly higher than that in the control group ($P < 0.05$), as shown in Table 2.

3.5. Comparison of Quality of Life Scores after Treatment between the Two Groups. After treatment, the limb function, linguistic function, emotional function, vitality, and cognitive function of the patients in the experimental group were all significantly higher than those in the control group ($P < 0.05$), as shown in Table 3.

3.6. Comparison of Incidence of Adverse Reactions between the Two Groups. The incidence of adverse reactions in the experimental group after treatment was significantly lower than that in the control group ($P < 0.05$), as shown in Table 4.

4. Discussion

MG is an autoimmune antibody-mediated disorder of neuromuscular synaptic transmission. In early stage, patients generally present with weakness of limbs, and with the progress of this disease, they may suffer from dysphagia, low spirits, and even breathing difficulties. MG may either occur as an autoimmune disease with distinct immunogenetic characteristics or as a paraneoplastic syndrome associated with tumors of the thymus. At present, the medical community has not found the specific pathogenesis of MG and has presumed that it may be associated with infection factors, environmental factors, etc. [12–14]. Immunosuppressants combined with GCS is effective for some MG patients, except for a minority of patients. GCS, as a common treatment method for MG including prednisolone, betamethasone, and dexamethasone, plays a key regulatory role in body growth, metabolism, and immune function, and is the most important regulatory hormone in stress response, which can effectively inhibit patients' immune inflammatory response and pathological immune response; however, it is found that long-term adoption also comes with toxic and side effect [15–17]. In addition, long-term administration of hormone drugs can result in adrenal cortex function

decline, osteoporosis, femoral head necrosis, etc. Immunosuppressants can inhibit the proliferation of cells involved in the immune response and reduce the antibody immune response, thereby relieving patients' clinical symptoms [18, 19].

VATS, as a minimally invasive surgery which has been widely applied for the treatment of thoracic diseases, can visualize patients' thorax clearly on a television screen through a high-definition camera, so the surgeon can conduct the surgery by viewing a television screen, with the advantages of wide range of lesion resection and high safety [20, 21]. Some studies reveal that the thymusectomy not only removes the thymus but also effectively clears the fat of anterior mediastinum, but VATS is limited by the surgical field during the resection of the fat of anterior mediastinum, so the surgical procedure should be finished by experienced operators [22, 23]. In this study, after the combination therapy was implemented in MG patients, the overall response rate in the experimental group was significantly higher than that in the control group ($P < 0.05$), demonstrating that the combination therapy has significantly better efficacy than VATS alone in relieving myasthenic symptoms and improving prognosis. Treg cells are T cell subsets that negatively regulate immune responses and maintain immune tolerance, and their number and function defects greatly affect the development and progression of MG. CTLA4, as a critical negative regulator of the T-cell response, maps to chromosome 2q33 and is involved in the negative regulation of immune responses [24, 25]. It has been considered a candidate for many autoimmune diseases. Evidence from Caucasians supported a genetic predisposition of CTLA4 to myasthenia gravis (MG). Several variants of CTLA4 have been extensively tested, indicating an overall influence on the susceptibility of several immune-related diseases [24]. In this study, we found that CTLA4 levels in Treg cells in the experimental group were significantly higher than those in the control group ($P < 0.001$). Chandeze et al. [26] have pointed out in their study that after the implementation of VATS combined with short course of high-dose GCS and immunosuppressants in patients with late-onset and severe MG, the CTLA4 levels in Treg cells of the patients who underwent the treatment were $(16.42 \pm 2.23)\%$, which were significantly higher than $(11.76 \pm 2.15)\%$ of the patients who were treated with VATS alone, illustrating that the combination therapy can enhance the Treg cells levels in the peripheral blood of MG patients and improve therapeutic effect.

In conclusion, the combination therapy can significantly relieve myasthenic symptoms and improve quality of life of patients, with significant therapeutic efficacy and high safety, which is worthy of application and promotion.

Data Availability

The authors confirm that the data supporting the findings of this study are available within the article.

Conflicts of Interest

The authors declare that they have no conflicts of interest.

Authors' Contributions

PL wrote the manuscript. HW and JH conceived and designed the study. PL and XZ were responsible for the collection and analysis of the experimental data. PL and JH interpreted the data and drafted the manuscript. ZG revised the manuscript critically for important intellectual content. All the authors read and approved the final manuscript.

References

[1] J. M. Serrano-Rodríguez, M. Gómez-Díez, M. Esgueva et al., "Pharmacokinetic/pharmacodynamic modeling of benazepril and benazeprilat after administration of intravenous and oral doses of benazepril in healthy horses," *Research in Veterinary Science*, vol. 114, pp. 117–122, 2017.

[2] S. D. Firke, A. S. Patil, R. R. Patil, and A. S. Patil, "Stability-indicating HPTLC method for estimation of benazepril in bulk and tablet dosage form," *Analytical Chemistry Letters*, vol. 8, no. 4, pp. 552–564, 2018.

[3] A. Kumar, S. Dey, A. C. Saxena, and S. Mahajan, "Evaluation of add on effect of carvedilol on standard protocol of digoxin, frusemide and benazepril in the management of dilated cardiomyopathy in dogs," *Indian Journal of Animal Research*, vol. 52, pp. 583–590, 2018.

[4] M. X. Li, L. Zhu, L. Chen, N. Li, and F. Qi, "Assessment of drug-drug interactions between voriconazole and glucocorticoids," *Journal of Chemotherapy*, vol. 30, no. 5, pp. 296–303, 2018.

[5] K. Goto, K. Hiramoto, M. Kawakita, M. Yamaoka, and K. Ooi, "The influence of reactive oxygen species and glucocorticoids on dry skin in a mouse model of arthritis," *Skin Pharmacology and Physiology*, vol. 31, no. 4, pp. 188–197, 2018.

[6] D. D. De Lucena and É. B. Rangel, "Glucocorticoids use in kidney transplant setting," *Expert Opinion on Drug Metabolism & Toxicology*, vol. 14, no. 10, pp. 1023–1041, 2018.

[7] G. Zhao, X. Jiang, F. Wang et al., "Lobectomy with high-position single-intercostal two-port video-assisted thoracoscope for non-small cell lung cancer is a safe and effective surgical procedure," *Journal of Thoracic Disease*, vol. 12, no. 12, pp. 7346–7346, 2020.

[8] N. Peiffer-Smadja, F. Domont, D. Saadoun, and P. Cacoub, "Corticosteroids and immunosuppressive agents for idiopathic recurrent pericarditis," *Autoimmunity Reviews*, vol. 18, no. 6, pp. 621–626, 2019.

[9] T. Zheng, S. Zhu, J. F. Ou et al., "Treatment with corticosteroid and/or immunosuppressive agents before surgery can effectively improve the surgical outcome in patients with Takayasu's arteritis," *Journal of Investigative Surgery*, vol. 32, no. 3, pp. 220–227, 2019.

[10] M. Yang, H. Li, Q. Zhang et al., "Highly diverse cembranoids from the South China Sea soft coral *Sinularia scabra* as a new class of potential immunosuppressive agents," *Bioorganic and Medicinal Chemistry*, vol. 27, no. 15, pp. 3469–3476, 2019.

[11] W.-X. Wang, G.-G. Cheng, Z.-H. Li et al., "Curtachalasins, immunosuppressive agents from the endophytic fungusXylariacf.curta," *Organic & Biomolecular Chemistry*, vol. 17, no. 34, pp. 7985–7994, 2019.

[12] H. Qin, H. Yu, J. Sheng et al., "PI3Kgamma inhibitor attenuates immunosuppressive effect of poly (l-glutamic acid)-

Hindawi
BioMed Research International
Volume 2024, Article ID 9864190, 1 page
https://doi.org/10.1155/2024/9864190

Retraction

Retracted: Expression of lncRNA-ANRIL before and after Treatment and Its Predictive Value for Short-Term Survival in Patients with Coronary Heart Disease

BioMed Research International

Received 12 March 2024; Accepted 12 March 2024; Published 20 March 2024

This article has been retracted by Hindawi following an investigation undertaken by the publisher [1]. This investigation has uncovered evidence of one or more of the following indicators of systematic manipulation of the publication process:

(1) Discrepancies in scope

(2) Discrepancies in the description of the research reported

(3) Discrepancies between the availability of data and the research described

(4) Inappropriate citations

(5) Incoherent, meaningless and/or irrelevant content included in the article

(6) Manipulated or compromised peer review

The presence of these indicators undermines our confidence in the integrity of the article's content and we cannot, therefore, vouch for its reliability. Please note that this notice is intended solely to alert readers that the content of this article is unreliable. We have not investigated whether authors were aware of or involved in the systematic manipulation of the publication process.

Wiley and Hindawi regrets that the usual quality checks did not identify these issues before publication and have since put additional measures in place to safeguard research integrity.

We wish to credit our own Research Integrity and Research Publishing teams and anonymous and named external researchers and research integrity experts for contributing to this investigation.

The corresponding author, as the representative of all authors, has been given the opportunity to register their agreement or disagreement to this retraction. We have kept a record of any response received.

References

[1] J. Sun and S. Qiu, "Expression of lncRNA-ANRIL before and after Treatment and Its Predictive Value for Short-Term Survival in Patients with Coronary Heart Disease," *BioMed Research International*, vol. 2021, Article ID 5431985, 8 pages, 2021.

Hindawi
BioMed Research International
Volume 2021, Article ID 5431985, 8 pages
https://doi.org/10.1155/2021/5431985

Research Article

Expression of lncRNA-ANRIL before and after Treatment and Its Predictive Value for Short-Term Survival in Patients with Coronary Heart Disease

Jinhui Sun and Shi Qiu

Department of Cardiovascular Surgery, The Second Hospital of Shandong University, Jinan 250000, China

Correspondence should be addressed to Shi Qiu; shisha3061@163.com

Received 23 August 2021; Revised 29 October 2021; Accepted 10 November 2021; Published 3 December 2021

Academic Editor: Jianxin Shi

This study aimed at observing the expression of lncRNA-ANRIL (ANRIL) before and after treatment and its predictive value for short-term survival in patients with coronary heart disease (CHD). Altogether, 112 patients with CHD admitted to the hospital were enrolled as a study group (SG), which was divided into a pretreatment study group (preSG) and a posttreatment study group (postSG). Further 72 healthy people undergoing physical examinations during the same period were enrolled as a control group (CG). Peripheral blood was collected from the subjects in the three groups, to detect the expression level of serum ANRIL using quantitative reverse transcription PCR (qRT-PCR). A receiver operating characteristic (ROC) curve was plotted to evaluate the diagnostic value of ANRIL for CHD. Kaplan-Meier survival curves were plotted to analyze 3-year survival rates in high- and low-ANRIL expression groups. Cox regression was conducted to analyze independent risk factors affecting the patients. The expression level of serum ANRIL in preSG was significantly lower than those in CG and postSG ($P < 0.05$). According to the ROC curve, the area under the curve (AUC) of serum ANRIL for diagnosing CHD in CG was 0.894 and the optimal cutoff value was 0.639, with the sensitivity of 86.61% and the specificity of 93.67%. According to the survival curves, the 3-year overall survival rate in the high-ANRIL expression group was significantly lower than that in the low-expression group ($P < 0.05$). History of smoking, high total cholesterol (TC), high triglyceride (TG), high homocysteine (Hcy), and ANRIL expression were independent prognostic factors affecting the overall survival time of the patients ($P < 0.05$). ANRIL is poorly expressed in the peripheral blood of patients with CHD. Its detection has good sensitivity and specificity for diagnosing the disease, and its expression may be related to the poor prognosis of the patients.

1. Introduction

Coronary heart disease (CHD) is a major cause of patient death in developing countries [1] and a main reason for diseases and disabilities [2, 3]. The shortage of blood and oxygen supply or the occlusion or stenosis of coronary arteries leads to myocardial dysfunction, thus resulting in myocardial infarction, unstable angina pectoris, and heart failure [4–6]. CHD has an increasing incidence with the aging of the population [7] and changing disease conditions. Therefore, it is necessary to explore new biomarkers that are helpful for the better diagnosis of the disease.

Long noncoding RNAs (lncRNAs), as a new type of noncoding RNA, play a vital role in chromatin modification, cell differentiation and proliferation, translation, transcription, and other biological processes [8–10]. According to previous studies, many disordered lncRNAs that are found in various tumors can regulate gene transcription and then play an important role in tumorigenesis and they can also act as tumor suppressor genes or oncogenes [11]. Increasing evidences show that lncRNAs play vital roles in regulating the apoptosis of myocardial cells in myocardial ischemia/reperfusion injury [12–14]. Long non-coding RNA antisense noncoding RNA at the INK4 locus (ANRIL), also known as

Table 1: Comparison of general information [n(%)] ($-x \pm$ sd).

Categories	SG ($n = 112$)	CG ($n = 79$)	t/χ^2 value	P value
Gender			0.687	0.408
Male	55 (49.11)	34 (43.04)		
Female	57 (50.89)	45 (56.96)		
Age (years)			0.273	0.601
<60	51 (45.54)	39 (49.37)		
≥60	61 (54.46)	40 (50.63)		
BMI (kg/m^2)			1.521	0.129
	23.4 ± 3.7	22.6 ± 3.4		
Place of residence			0.933	0.334
City	66 (58.93)	52 (65.82)		
Countryside	46 (41.07)	27 (34.18)		
Nationality			0.035	0.851
Han	58 (51.79)	42 (53.16)		
National minorities	54 (48.21)	37 (46.84)		
Educational history			0.984	0.321
≥senior high school	43 (38.39)	36 (45.57)		
<senior high school	69 (61.61)	43 (54.43)		
History of smoking			0.525	0.469
Yes	57 (50.89)	36 (45.57)		
No	55 (49.11)	43 (54.43)		
History of drinking			0.078	0.781
Yes	53 (47.32)	39 (49.37)		
No	59 (52.68)	40 (50.63)		
History of diabetes			1.862	0.172
Yes	58 (51.79)	33 (41.77)		
No	54 (48.21)	46 (58.23)		
History of hypertension			2.889	0.089
Yes	65 (58.04)	36 (45.57)		
No	47 (41.96)	43 (54.43)		
Work history			0.189	0.663
Yes	33 (29.46)	21 (26.58)		
No	79 (70.54)	58 (73.42)		

BMI: body mass index.

lncRNA CDKN2B-AS1, is firstly found in patients with hereditary melanoma and neural system tumor. Studies have shown that abnormally expressed ANRIL is observed in various cancers [10, 11]. Besides, the decrease of ANRIL in intestinal mucosa exhibited a relationship to the increase of inflammation, severity, and risk of Crohn's disease [12]. ANRIL gene has been identified as a genetic susceptibility locus related to type 2 diabetes, CHD, intracranial aneurysm, and cancers in genome-wide association studies of common diseases. Importantly, ANRIL is correlated with atherosclerotic cardiovascular disease by genome-wide association studies [13]. What is more, ANRIL is remarkably upregulated in left ventricle biopsies and peripheral blood mononuclear cells of heart failure patients than control subjects [14], implying that ANRIL was probably involved in heart disease regulation [15]. Zhang et al. reported that overexpressing ANRIL can upregulate vascular endothelial growth factors by activating the nuclear factor κB (NF-κB) signaling pathway in rats to promote angiogenesis [16]. Song et al. found that ANRIL plays a protective role in the treatment of patients with aggravated coronary atherosclerosis. It reduces the apoptosis of vascular endothelial cells and the expression of inflammatory cytokines by reducing its own expression, thereby preventing the development and progression of coronary atherosclerosis [17]. However, there are currently few studies on the predictive value of serum ANRIL in the diagnosis of and the therapeutic effect on CHD.

In this study, the expression of serum ANRIL in patients with CHD was examined and its role in the diagnosis and prognosis of the patients was explored.

2. Materials and Methods

2.1. General Information. A total of 112 patients with CHD admitted to the Department of Cardiology in The Second Hospital of Shandong University from May 2015 to February 2016 were enrolled as the study group (SG), which was divided into a pretreatment study group (preSG) and a posttreatment study group (postSG). These patients met the inclusion criteria stated in our study. The patients in SG consisted of 55 males and 57 females, among whom 51 were <60 years old and 61 were ≥60 years old. Further 72 healthy people undergoing physical examinations during the same period were enrolled as the control group (CG), including 34 males and 45 females, among whom 39 were <60 years old and 40 were ≥60 years old. All participants were informed of this study and signed the informed consent form. Our whole research was approved by the Ethics Committee of The Second Hospital of Shandong University.

2.2. Inclusion and Exclusion Criteria. Inclusion criteria were as follows: patients diagnosed with CHD by coronary angiography at admission [18], patients with stable vital signs, patients with complete general information, patients conforming to indications for PCI, patients whose expected survival time ≥ 1 year, male patients aged 60–82 years, and nonpregnant females. Exclusion criteria were as follows: patients with a stress state; patients with arrhythmia or acute myocardial infarction; patients complicated with valvular disease; patients with hyperthyroidism, infectious diseases, or hematopoietic failure; elderly patients with CHD; patients with mental disorders or a family history of mental diseases; patients with severe hepatic and renal dysfunction; patients with chronic obstructive pulmonary disease; patients who transferred to other hospitals halfway; patients who received other hospitals' treatment without authorization; and patients who withdrew from this experiment halfway.

2.3. Therapeutic Methods. Patients with CHD were treated with aspirin, angiotensin converting enzyme, receptor blockers, nitrates, and other drugs for lowering lipid. All of them were treated for one month according to the doctor's advice.

2.4. Experimental Steps. The serum was collected from the research objects in CG, preSG, and postSG for extracting total RNA using a TRIzol kit (Shanghai Lianshuo Biotechnology Co. Ltd., item no. Invitrogen 15596-026). The concentration and purity of the extracted total RNA were detected with an ultraviolet spectrophotometer (PKUCare Industrial Park Technology Co. Ltd., item no: UV-1100), and its integrity was detected with 1% agarose gel electrophoresis. According to the instruction of the reverse transcription kit (Beijing Protein Innovation Co. Ltd., item no.: BPI01030), the RNA was reversely transcribed into cDNA, which was stored at −80°C for later use. With GAPDH considered as an internal reference, upstream and downstream sequences of ANRIL were 5′-TTATGCTTTGCAGCAC ACTGG-3′ and 5′-GTTCTGCCACAGCTTTGATCT-3′

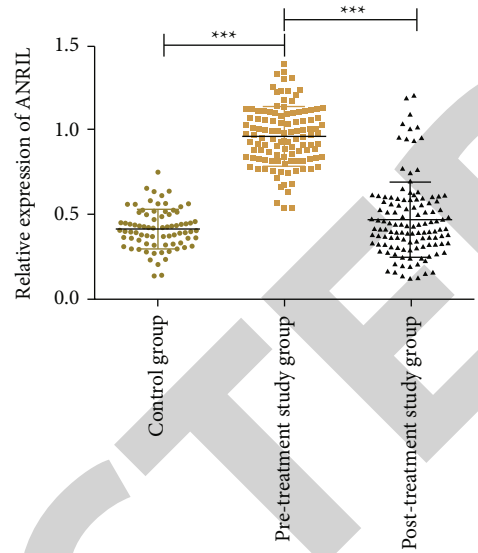

Figure 1: Relative expression of serum ANRIL before treatment. The expression of serum ANRIL in preSG was significantly higher than that in CG and postSG ($P < 0.05$). $^{***}P < 0.05$.

and those of GAPDH were 5′-GGGAAACTGTGGCGTG AT-3′ and 5′-GAGTGGGTGTCGCTGTTGA-3′. The reaction was carried out on the real-time fluorescence quantitative PCR instrument (Shanghai Sunshine Biotech Co. Ltd., item no.: qTOWER3G). Conditions for PCR amplification were as follows: predenaturation at 95°C for 30 s, cycling (denaturation at 95°C for 40 min and annealing) for 40 times, standing at 55°C for 1 min, and then extension at 40°C for 5 min. Three independent experiments were carried out to obtain data, and the relative expression of the genes was expressed after calculated by $2^{-\Delta\Delta CT}$.

2.5. Follow-up. All patients were followed up for 3 years, once every 3 months, up to March 2019. The overall survival time was from the first day after treatment to the last follow-up or patient death.

2.6. Statistical Analysis. SPSS17.0 (IBM Corp., Armonk, NY, USA) was used to statistically analyze the data. GraphPad Prism 6 (GraphPad Software, San Diego, USA) was used to plot figures. Measurement data were expressed by mean ± standard deviation ($-x \pm$ sd), and the comparison of the data between two groups was conducted by independent samples t-test. Count data were expressed by the number of cases/percentage [n(%)]. A receiver operating characteristic (ROC) curve was plotted to evaluate the diagnostic value of serum ANRIL for diagnosing CHD in CG. Independent prognostic factors for the disease were tested by Cox proportional hazards model. $P < 0.05$ indicated a statistically significant difference.

3. Results

3.1. Comparison of General Information. There were no significant differences between SG and CG in gender, age, body mass index (BMI), course of disease, place of residence,

Table 2: Relationship between clinicopathological parameters and relative expression of ANRIL in peripheral blood ($-x \pm$ sd).

Pathological parameters	n	Relative expression of ANRIL	t/F	P
Gender			0.146	0.884
Male	55	0.957 ± 0.15		
Female	57	0.961 ± 0.14		
Age (years)			2.030	0.045
<60	51	0.930 ± 0.13		
≥60	61	0.978 ± 0.12		
Types of CHD			0.001	0.993
Angina pectoris	35	0.958 ± 0.15		
Remote myocardial infarction	33	0.962 ± 0.14		
Acute myocardial infarction	44	0.959 ± 0.14		
History of smoking			0.401	0.689
Yes	57	0.952 ± 0.15		
No	55	0.963 ± 0.14		
History of drinking			0.188	0.852
Yes	53	0.962 ± 0.13		
No	59	0.957 ± 0.15		
History of diabetes			0.127	0.899
Yes	58	0.961 ± 0.12		
No	54	0.958 ± 0.13		
History of hypertension			2.059	0.042
Yes	65	0.984 ± 0.12		
No	47	0.935 ± 0.13		
TC (mmol/L)			2.039	0.044
≥4.34	63	0.987 ± 0.15		
<4.34	49	0.932 ± 0.13		
TG (mmol/L)			1.995	0.049
≤1.93	68	0.941 ± 0.11		
>1.93	44	0.985 ± 0.12		
Hcy (μmol/L)			2.049	0.043
≤16.8	67	0.939 ± 0.12		
>16.8	45	0.988 ± 0.13		

CHD: coronary heart disease (CHD); TC: total cholesterol; TG: triglyceride; Hcy: high homocysteine.

Table 3: Diagnostic value of serum ANRIL in SG.

Diagnostic index	AUC	95% CI	Standard error	Cutoff value	Sensitivity (%)	Specificity (%)
ANRIL	0.894	0.841~0.947	0.027	0.639	86.61	93.67

nationality, educational background, history of smoking, history of drinking, history of diabetes, history of hypertension, types of CHD, and work history ($P > 0.05$). See Table 1.

3.2. Relative Expression of Serum ANRIL before Treatment. The expression of serum ANRIL was (0.409 ± 0.12) ng/mL in CG, (0.959 ± 0.16) ng/mL in preSG, and (0.413 ± 0.13) ng/mL in postSG. The expression in preSG was significantly higher than those in CG and postSG (both $P < 0.05$). See Figure 1.

3.3. Relationship between Pathological Parameters and Expression of ANRIL. There were significant differences in the relative expression of ANRIL between CHD patients with different ages, history of smoking, history of hypertension, high total cholesterol (TC), high triglyceride (TG), and

high homocysteine (Hcy) ($P < 0.05$), not between those with different genders, types of CHD, history of drinking, and history of diabetes ($P > 0.05$). See Table 2.

3.4. Diagnostic Value of Serum ANRIL in SG. According to the ROC curve, ANRIL had a better diagnostic value in SG. The area under the curve (AUC) of serum ANRIL for diagnosing CHD in CG was 0.894, and the optimal cutoff value was 0.639, with the sensitivity of 86.61% and the specificity of 93.67%. See Table 3 and Figure 2.

3.5. Survival of Patients with CHD. With the median relative expression of serum ANRIL as the critical value, there were 57 cases in the high-ANRIL expression group (<0.639) and 55 cases in the low-ANRIL expression group (≥0.639). The 3-year overall survival rate in the high-expression group was 82.46% (47/57), significantly lower than 94.55% (52/55) in the low-ANRIL expression group ($P < 0.05$). See Figure 3.

The 3-year overall survival rate in the high-ANRIL expression group was significantly lower than that in the low-ANRIL expression group ($P < 0.05$).

3.6. Analysis of Prognostic Factors Related to CHD. The univariate analysis was conducted on general and clinicopathological factors. The results showed that gender, types of CHD, history of drinking, and history of diabetes were not prognostic factors affecting the overall survival time of the patients ($P > 0.05$). Different ages, history of smoking, history of hypertension, high TC, high TG, high Hcy, and ANRIL expression may be the prognostic factors ($P < 0.05$). See Table 4. After the significant indicators in the univariate analysis were incorporated into the Cox proportional hazards model, multivariate analysis was conducted through a stepwise regression method. Criteria for variable entry and elimination were 0.05 and 0.1, respectively. The results showed that history of smoking, high TC, high TG, high Hcy, and ANRIL expression were independent prognostic factors affecting the overall survival time ($P < 0.05$). See Table 5.

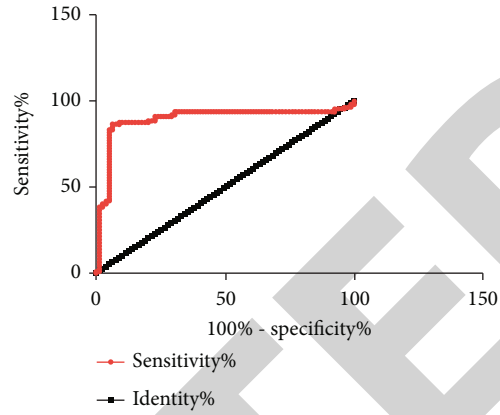

Figure 2: ROC curve of serum ANRIL for diagnosing coronary heart disease.

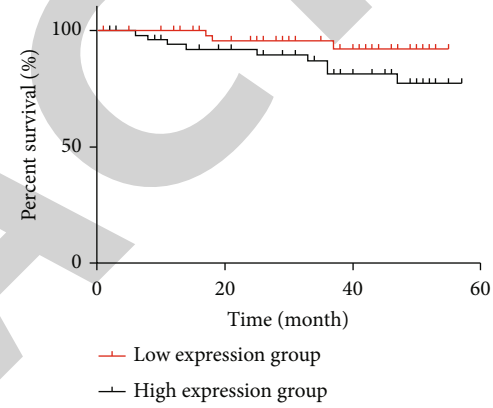

Figure 3: 3-year survival of patients with coronary heart disease.

4. Discussion

CHD is a major cause of pathogenesis and patient death in the world [19, 20] and accounts for 2/3 of the death toll from heart disease [21]. The diagnosis and treatment of CHD have been greatly improved in the past decade, but its incidence and mortality have not significantly decreased [22, 23]. At present, the gold standard for diagnosing the disease is coronary angiography, which has a high risk and an expensive cost and cannot assess microcirculation [24]. Therefore, a noninvasive biomarker with satisfactory sensitivity and specificity should be found to diagnose CHD and monitor its disease activity. Accordingly, it is necessary to further explore a new biomarker that can diagnose the disease and predict its condition more effectively.

At present, the pathogenesis of CHD remains unclear but some scholars have reported the abnormal expression of lncRNA as a tumor suppressor gene or oncogene in patients with CHD. According to Wang et al., interferon-γ and lncRNA-BANCR play a pivotal role in CHD and they may be used as biomarkers for the screening and prevention of the disease in clinical practice [25]. According to Yin et al., lncRNA-CAS5 acts as an upstream regulator in the mTOR signaling pathway to participate in the progression of CHD and its expression is specially downregulated in patients with the disease, so it can be used as a biomarker for the disease [26]. In our study, the relative expression of serum ANRIL in preSG was significantly higher than those in CG and postSG; ANRIL was closely related to different ages, history of smoking, history of hypertension, high TC, high TG, and high Hcy. These findings indicate that ANRIL may become a potential and analytical marker for CHD in the diagnosis of clinical parameters. According to Samanta and others, hypertension, diabetes, drinking, high TC, and tobacco smoke exposure are additive effects leading to heart disease [27]. According to Li et al., smoking, hyperuricemia, drinking, and BMI are risk factors for the increasing pathogenesis and death risks of CHD in the 55–64 age group [28], which is similar to the results of this study. In our further research, after treatment, the expression level of ANRIL significantly decreased; the AUC of serum ANRIL alone for diagnosing CHD was 0.894, and the optimal cutoff value was 0.639, with the sensitivity of 86.61% and the specificity of 93.67%. These findings suggest that the therapeutic effect

Table 4: Univariate analysis of prognostic factors for patients with CHD.

Groups	Number of investigation (cases)	Number of 3-year survival (cases)	χ^2	P
Gender			2.068	0.150
Male	55	33		
Female	57	52		
Age (years)			0.013	0.908
<60	51	38		
≥60	61	47		
Types of CHD			0.565	0.754
Angina pectoris	35	29		
Remote myocardial infarction	33	21		
Acute myocardial infarction	44	35		
History of smoking			4.439	0.035
Yes	57	56		
No	55	29		
History of drinking			0.016	0.899
Yes	53	41		
No	59	44		
History of diabetes			0.028	0.868
Yes	58	43		
No	54	42		
History of hypertension			0.148	0.700
Yes	65	47		
No	47	38		
TC (mmol/L)			4.987	0.026
≥4.34	63	61		
<4.34	49	24		
TG (mmol/L)			5.470	0.019
≤1.93	68	65		
>1.93	44	20		
Hcy (μmol/L)			4.401	0.036
≤16.8	67	63		
>16.8	45	22		
ANRIL expression			3.987	0.046
Low expression	55	52		
High expression	57	47		

CHD: coronary heart disease (CHD); TC: total cholesterol; TG: triglyceride; Hcy: high homocysteine.

on CHD can be predicted by observing changes in the ANRIL expression level. There is currently little research on whether ANRIL affects the therapeutic effect. In our study, patients with high-ANRIL expression had an increasing risk of ineffective treatment. Therefore, observing the expression of ANRIL is helpful to judge the therapeutic effect on patients with CHD. Finally, 112 patients in this study were followed up for 3 years. The overall 3-year survival rate in the high-ANRIL expression group (82.46%) was significantly lower than that in the low-ANRIL expression group (94.55%). According to the univariate analysis of the Cox proportional hazards model, different ages, history of smoking, history of hypertension, high TC, high TG, high Hcy, and ANRIL expression may be prognostic factors affecting the overall survival time. The analysis of

Table 5: Multivariate analysis of prognostic factors for patients with CHD.

Projects	Multivariate HR (95% CI)	P
History of smoking	1.46 (1.04~2.67)	0.035
TC	1.77 (1.13~2.74)	0.012
TG	1.66 (1.12~2.87)	<0.001
Hcy	1.79 (1.21~3.10)	<0.001
ANRIL low expression	2.32 (1.46~3.69)	<0.001

CHD: coronary heart disease (CHD); TC: total cholesterol; TG: triglyceride; Hcy: high homocysteine.

the results shows that the high expression of ANRIL promotes the progression of CHD and that history of smoking, high TC, high TG, and high Hcy are the factors affecting the prognosis of patients with CHD. This reveals that ANRIL is a potential factor for judging the prognosis.

This study confirms the value of serum ANRIL for diagnosing CHD and for evaluating the therapeutic effect on the disease, but it still can be improved. Firstly, the relationship between ANRIL and toxic and side effects during treatment should be further addressed. Secondly, the specific regulatory mechanism of ANRIL in the treatment needs to be discussed. Additionally, the influence of ANRIL on tumor formation in mice can be supplemented. Furthermore, the clinical and molecular mechanism research on rare cases of CHD should be studied.

To sum up, ANRIL is highly expressed in the serum of patients with CHD and it can be used as an effective biomarker for evaluating the therapeutic effect on the disease and the 3-year overall survival rate of the patients.

Data Availability

The datasets used and/or analyzed during the present study are available from the corresponding author on reasonable request.

Ethical Approval

The study was approved by the Ethics Committee of The Second Hospital of Shandong University. Patients who participated in this research signed the informed consent and had complete clinical data.

Consent

Signed written informed consents were obtained from the patients and/or guardians.

Conflicts of Interest

The authors declare that they have no competing interests.

Authors' Contributions

JS wrote the manuscript and analyzed and interpreted the patient general data. SQ performed PCR and was responsible for observation indicator analysis. Both authors read and approved the final manuscript.

References

[1] M. L. Meyer, F. C. Lin, A. Jaensch et al., "Multi-state models of transitions in depression and anxiety symptom severity and cardiovascular events in patients with coronary heart disease," *PLoS One*, vol. 14, no. 3, article e0213334, 2019.

[2] M. G. Marmot and J. F. Mustard, "Coronary heart disease from a population perspective," in *Why are some people healthy and others not?*, pp. 189–214, Routledge, 2017.

[3] A. V. Khera and S. Kathiresan, "Genetics of coronary artery disease: discovery, biology and clinical translation," *Nature Reviews Genetics*, vol. 18, no. 6, pp. 331–344, 2017.

[4] A. K. Shrivastava, H. V. Singh, A. Raizada, and S. K. Singh, "C-reactive protein, inflammation and coronary heart disease," *The Egyptian Heart Journal*, vol. 67, no. 2, pp. 89–97, 2015.

[5] D. Stelzle, A. S. V. Shah, A. Anand et al., "High-sensitivity cardiac troponin I and risk of heart failure in patients with suspected acute coronary syndrome: a cohort study," *European Heart Journal - Quality of Care and Clinical Outcomes*, vol. 4, no. 1, pp. 36–42, 2018.

[6] S. McGlynn and S. Hudson, "Pharmaceutical care (9) coronary heart disease," *Prevention*, vol. 10, 2019.

[7] S. Yamamoto, K. Hotta, E. Ota, R. Mori, and A. Matsunaga, "Effects of resistance training on muscle strength, exercise capacity, and mobility in middle-aged and elderly patients with coronary artery disease: a meta-analysis," *Journal of Cardiology*, vol. 68, no. 2, pp. 125–134, 2016.

[8] Z. Zhang, W. Gao, Q. Q. Long et al., "Increased plasma levels of lncRNA H19 and LIPCAR are associated with increased risk of coronary artery disease in a Chinese population," *Scientific Reports*, vol. 7, no. 1, p. 7491, 2017.

[9] E. Rahimi, A. Ahmadi, M. A. Boroumand, B. Mohammad Soltani, and M. Behmanesh, "Association of ANRIL expression with coronary artery disease in type 2 diabetic patients," *Cell Journal*, vol. 20, p. 41, 2018.

[10] M. M. Kumar and R. Goyal, "LncRNA as a therapeutic target for angiogenesis," *Current Topics in Medicinal Chemistry*, vol. 17, no. 15, pp. 1750–1757, 2017.

[11] Z. W. Zou, C. Ma, L. Medoro et al., "LncRNA ANRIL is up-regulated in nasopharyngeal carcinoma and promotes the cancer progression via increasing proliferation, reprograming cell glucose metabolism and inducing side-population stem-like cancer cells," *Oncotarget*, vol. 7, no. 38, pp. 61741–61754, 2016.

[12] U. Landmesser and P. Jakob, "Noncoding RNAs in Ischemic Cardiovascular Disease and Repair Mechanisms," in *Non-coding RNAs in the Vasculature*, pp. 61–82, Springer, Cham, 2017.

[13] F. Guo, C. Tang, Y. Li et al., "The interplay of LncRNA ANRIL and miR-181b on the inflammation-relevant coronary artery disease through mediating NF-κB signalling pathway," *Journal of Cellular and Molecular Medicine*, vol. 22, no. 10, pp. 5062–5075, 2018.

[14] F. Rühle and M. Stoll, "Long non-coding RNA databases in cardiovascular research," *Genomics, Proteomics & Bioinformatics*, vol. 14, no. 4, pp. 191–199, 2016.

[15] W. Deng, J. Wang, J. Zhang, J. Cai, Z. Bai, and Z. Zhang, "TET2 regulates LncRNA-ANRIL expression and inhibits the growth of human gastric cancer cells," *IUBMB Life*, vol. 68, no. 5, pp. 355–364, 2016.

[16] B. Zhang, D. Wang, T. F. Ji, L. Shi, and J. L. Yu, "Overexpression of lncRNA ANRIL up-regulates VEGF expression and promotes angiogenesis of diabetes mellitus combined with cerebral infarction by activating NF-κB signaling pathway in a rat model," *Oncotarget*, vol. 8, no. 10, pp. 17347–17359, 2017.

[17] C. L. Song, J. P. Wang, X. Xue et al., "Effect of circular ANRIL on the inflammatory response of vascular endothelial cells in a rat model of coronary atherosclerosis," *Cellular Physiology and Biochemistry*, vol. 42, no. 3, pp. 1202–1212, 2017.

[18] S. The, "CT coronary angiography in patients with suspected angina due to coronary heart disease (SCOT-HEART): an

Hindawi
BioMed Research International
Volume 2021, Article ID 5262000, 16 pages
https://doi.org/10.1155/2021/5262000

Research Article

Cystic Fibrosis: Systems Biology Analysis from Homozygous p.Phe508del Variant Patients' Samples Reveals Perturbations in Tissue-Specific Pathways

Joice de Faria Poloni,[1,2] **Thaiane Rispoli**,[3,4] **Maria Lucia Rossetti**,[3,5] **Cristiano Trindade**,[6] **and José Eduardo Vargas**[7]

[1]*Laboratório de Bioinformática Estrutural e Biologia Computacional, Instituto de Informática, Universidade Federal do Rio Grande do Sul, Porto Alegre, RS, Brazil*
[2]*Laboratório de Bioinformática em Bioenergia (LBB), Embrapa Agroenergia Parque Estação Biológica, Brasília, DF, Brazil*
[3]*Programa de Pós-Graduação em Biologia Celular e Molecular, Universidade Federal do Rio Grande do Sul, Porto Alegre, RS, Brazil*
[4]*Centro de Desenvolvimento Científico e Tecnológico (CDCT), Centro Estadual de Vigilância em Saúde (CEVS) Secretaria da Saúde do Estado do Rio Grande do Sul (SES-RS), Porto Alegre, RS, Brazil*
[5]*Programa de Pós-Graduação em Biologia Celular e Molecular Aplicada à Saúde, Universidade Luterana do Brasil, Porto Alegre, RS, Brazil*
[6]*Facultad de Ciencias Básicas y Biomédicas, Universidad Simón Bolívar, Barranquilla, Colombia*
[7]*Programa de Pós-graduação Ciências em Gastroenterologia e Hepatologia, Hospital de Clínicas de Porto Alegre, Porto Alegre, Brazil*

Correspondence should be addressed to Cristiano Trindade; cristiano.trindade@unisimonbolivar.edu.co and José Eduardo Vargas; josevargas@upf.br

Joice de Faria Poloni and Thaiane Rispoli contributed equally to this work.

Received 10 October 2021; Accepted 8 November 2021; Published 2 December 2021

Academic Editor: Chang Gu

Cystic fibrosis (CF) is an autosomal recessive disorder, caused by diverse genetic variants for the CF transmembrane conductance regulator (CFTR) protein. Among these, p.Phe508del is the most prevalent variant. The effects of this variant on the physiology of each tissue remains unknown. This study is aimed at predicting cell signaling pathways present in different tissues of fibrocystic patients, homozygous for p.Phe508del. The study involved analysis of two microarray datasets, E-GEOD-15568 and E-MTAB-360 corresponding to the rectal and bronchial epithelium, respectively, obtained from the ArrayExpress repository. Particularly, differentially expressed genes (DEGs) were predicted, protein-protein interaction (PPI) networks were designed, and centrality and functional interaction networks were analyzed. The study reported that p.Phe508del-mutated CFTR-allele in homozygous state influenced the whole gene expression in each tissue differently. Interestingly, gene ontology (GO) term enrichment analysis revealed that only "neutrophil activation" was shared between both tissues; however, nonshared DEGs were grouped into the same GO term. For further verification, functional interaction networks were generated, wherein no shared nodes were reported between these tissues. These results suggested that the p.Phe508del-mutated CFTR-allele in homozygous state promoted tissue-specific pathways in fibrocystic patients. The generated data might further assist in prediction diagnosis to define biomarkers or devising therapeutic strategies.

1. Introduction

Cystic fibrosis (CF) [OMIM (Online Mendelian Inheritance in Man: #219700)] is a monogenic disease, which is caused by the occurrence of more than 2,000 genetic variants for the protein CF transmembrane conductance regulator (CFTR) [1, 2]. Among these, p.Phe508del is known to be most prevalent CFTR variant. It is responsible for ~70% of CF cases across the globe (http://www.genet.sickkids.on.ca/andhttps://www.cftr2.org/). In particular, this variant involves a three bp deletion in exon 10 that results in the absence of amino acid phenylalanine at position 508 of the final protein (c.1521_1523delCTT, F508del or p.Phe508del) [3].

The CFTR protein is generally located at the apical membrane of polarized epithelial cells present in the respiratory tract, submucosal glands, gastrointestinal tract, exocrine pancreas, liver, sweat ducts, reproductive tract, and other tissues [4]. In particular, this protein functions as a chloride ion channel that controls the movement of ions (Cl^-), water secretion, and absorption in the epithelial tissues. The channel activation is mediated via cycles of phosphorylation of the regulatory domain, ATP-binding to the nucleotide-binding domains, and ATP hydrolysis [5]. Thus, absence or dysfunction of CFTR results in an ionic imbalance, secretion of thick and dehydrated mucus, and fat malabsorption, which further lead to different CF phenotypes [6].

Recently, different CFTR variants were divided into seven classes on the basis of mechanisms that mediated the qualitative and quantitative variations in the expression of CFTR. Additionally, this classification system also considered the availability/applicability of precision medicine [7–10]. Although the morbidity and mortality related to CF are mostly associated to the respiratory system, the researchers have started to explore and understand the implications of CFTR variants on the entire gastrointestinal (GI) system. In fact, several studies have previously shown that inflammation exerts both local and systemic effects [9].

Even though a large number of CFTR variants have been described, very limited information is available regarding the pathway perturbations promoted by the classical and most prevalent CFTR variant, p.Phe508del, and its associated effects. This study is aimed at evaluating and analyzing the gene expression profiles for the bronchial and rectal tissues of CF subjects homozygous for p.Phe508del variant, using systems biology approaches. The findings of the study would assist in improving current understanding regarding the physiology of each tissue, which could further help in devising new and improved therapeutic strategies.

2. Materials and Methods

2.1. Protein-Protein Interaction (PPI) Network Design. To analyze cell signaling pathways for different tissues of CF patients, microarray datasets were collected from the ArrayExpress repository [11]. The inclusion criteria for the study considered gene expression datasets obtained from CF patients' samples homozygous for the p.Phe508del-mutated CFTR-allele. In particular, two datasets fulfilled these requirements, namely, E-GEOD-15568 and E-MTAB-360 that corresponded to the rectal [12] and bronchial epithelium [13], respectively. The rectal epithelium dataset was composed of 13 non-CF and 16 CF patients, whereas the bronchial epithelium dataset was composed of nine non-CF and 19 CF patients. The raw data sets were downloaded using ArrayExpress package and analyzed using the R package arrayQualityMetrics [14, 15]. The analysis for differentially expressed genes (DEGs) was performed using the R package limma, wherein $|\log 2FC| > 0.5$ and adjusted $P < 0.05$ were used as cut-off values [16].

2.2. Protein-Protein Interaction (PPI) Network Design. The DEGs for each dataset were used as input to design the protein-protein interaction (PPI) network, using the meta-search engine STRING 10.5. For each tissue, an individual network was created [17]. For PPI network design, the parameters that were employed involved prediction methods enabled for "experiments," "databases," and "coexpression" and minimum confidence value of interactions to be 0.4, with no more than 20 interactors in the first shell and no more than five interactors in the second shell. According to the aforementioned protocol, the nonconnected nodes were repeatedly provided as an input until no more connections were found. Further, all subnetworks were merged in the software Cytoscape 3.7.2 [18, 19]. An additional network was created using CFTR as input, and the most relevant nodes were obtained from the centrality analysis (see Section 2.3), wherein the parameters involved predictions methods enabled for "experiments," "databases," and "coexpression" and minimum confidence value of interactions of 0.4, with no more than 50 interactors in the first shell and no interactors in the second shell. This network was grown to the saturation, and only interactions between the inputs were retained.

2.3. Centrality Analysis. To assess the topological relevance of the network, the centrality analysis was performed using the Cytoscape plugin CentiScape 2.2 [20, 21]. For centrality analysis, node degree was used to evaluate the node connectivity by calculating adjacent neighbors, betweenness was used to calculate the shortest paths connecting adjacent nodes that pass through each node, and eigenvector was utilized to measure the regulatory potential of a given node based on the relevance of its neighbors. In general, nodes showing above-average scores on the node degree analysis are named "Hub," nodes showing above-average scores for betweenness analysis are denoted as "Bottleneck," and those with above-average scores for eigenvector analysis are termed as "Switch." Thus, nodes combining the three centralities above-average scores are termed as HBS, which denotes a node with a robust regulatory role and a strong influence on the network [21, 22]. Further, the identified HBS nodes were used as input in the Reactome FIViz app to construct a functional interaction network, with the aid of the information obtained from the Reactome database [23].

2.4. Gene Ontology Analysis. Gene Ontology (GO) analysis for DEGs was performed using topGO and clusterProfile, wherein both were performed on R platform [24]. GO results and gene expression data were integrated and plotted

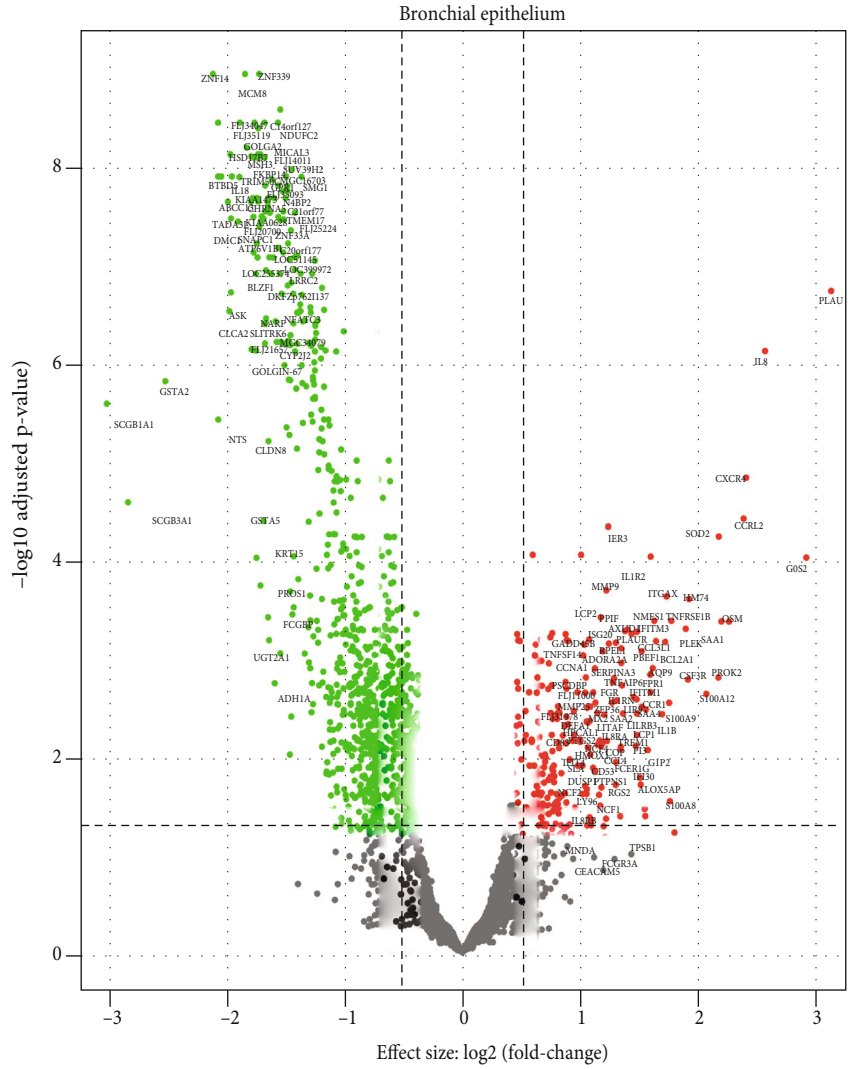

(a)

Figure 1: Continued.

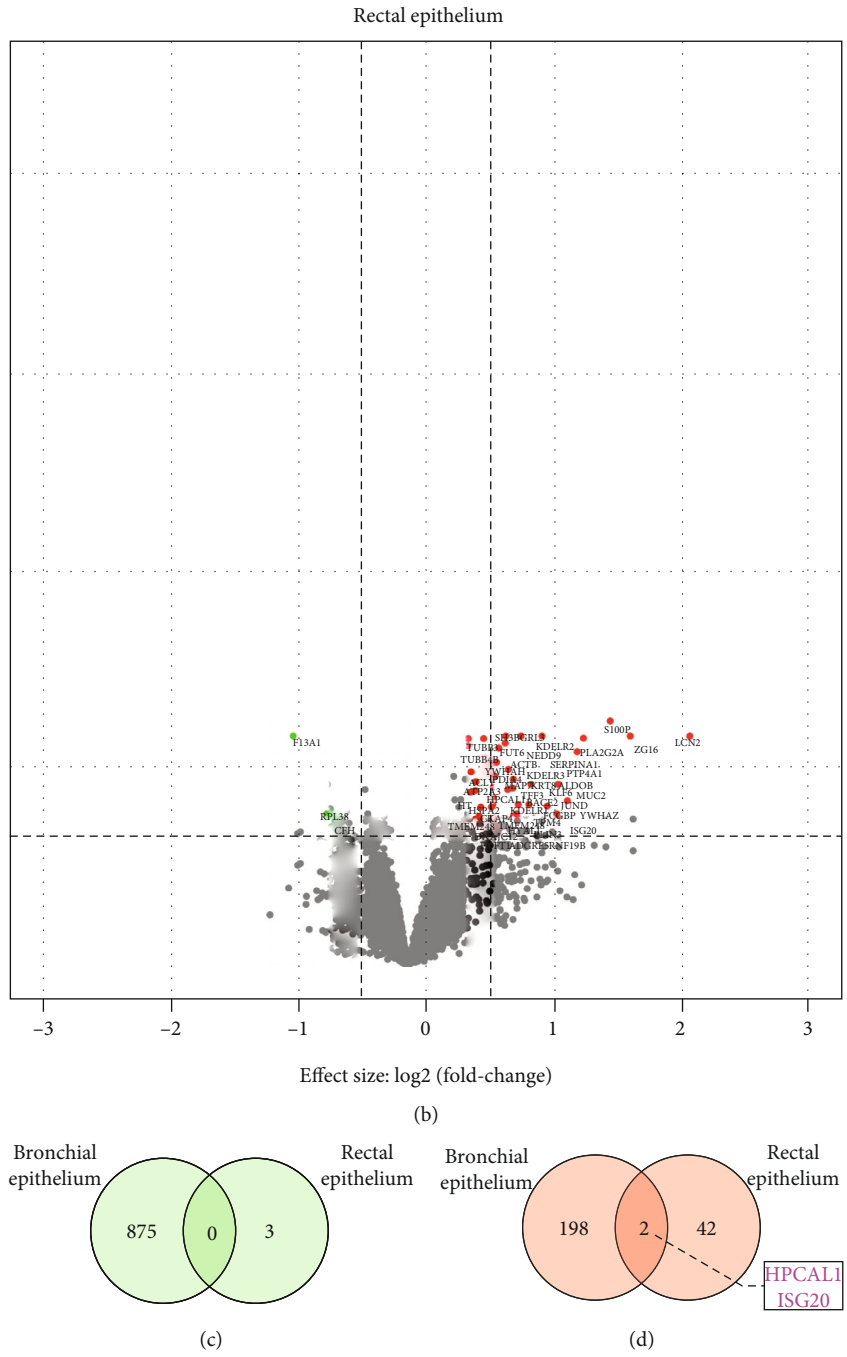

Figure 1: Continued.

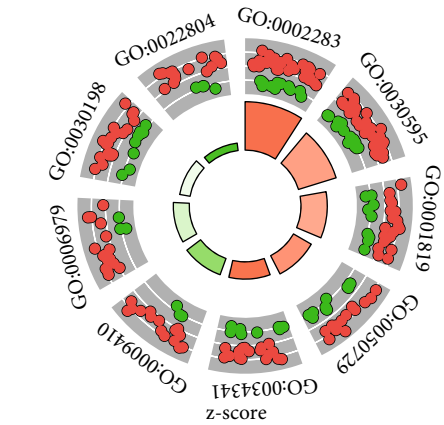

ID	Description
GO:0022804	Active transmembrane transporter activity
GO:0002283	Neutrophil activation involved in immune response
GO:0030595	Leukocyte chemotaxis
GO:0001819	Positive regulation of cytokine production
GO:0050729	Positive regulation of inflammatory response
GO:0034341	Response to interferon-gamma
GO:0009410	Response to xenobiotic stimulus
GO:0006979	Response to oxidative stress
GO:0030198	Extracellular matrix organization

(e)

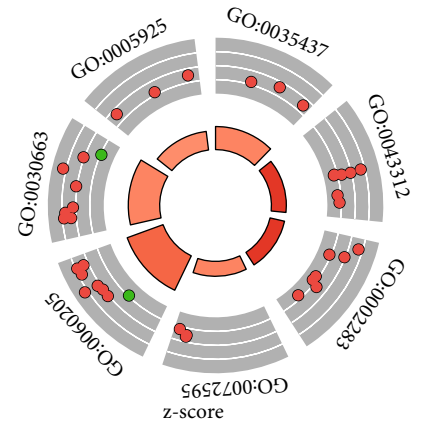

ID	Description
GO:0035437	Maintenance of protein localization in endoplasmic reticulum
GO:0043312	neutrophil degranulation
GO:0002283	Neutrophil activation involved in immune response
GO:0072595	Maintenance of protein localization in organelle
GO:0060205	Cytoplasmic vesicle lumen
GO:0030663	COPI-coated vesicle membrane
GO:0005925	Focal adhesion

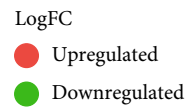

(f)

Figure 1: Summary for the differential expression analysis. Volcano plot for the distribution of over and underexpressed genes in the (a) bronchial epithelium and (b) rectal epithelium. Venn diagram for the underexpressed and overexpressed genes for the (c) bronchial epithelium and (d) rectal epithelium. Visualization of the results for the DEGs enrichment analysis (cut-off FDR < 0.05) obtained from the (e) bronchial epithelium and (f) rectal epithelium. In the inner ring, bar height indicates GO's significance (−log10 adjusted P value), while the color corresponds to the z-score, which is measured according to the gradient of color bar. The outer ring represents the log2FC dispersion value for the DEGs associated with each GO. Green: underexpressed genes; red: overexpressed genes.

using GOplot [25]. GO analysis for DEGs was performed using the default settings, and the results showing FDR < 0.05 were considered to be relevant. Additionally, GO analysis for the PPI network was performed to verify the enriched biological processes related to the DEGs for HBSs (HBS-DEGs), using aforementioned packages, and FDR < 0.001 was applied as cut-off value.

Module discovery and GO analysis for HBS functional interaction network were performed using Reactome FIViz app [23]. The results were recovered by applying filter of FDR < 0.001.

3. Results and Discussion

The comparison of gene expression profiles for the rectal and bronchial epithelium for CF patients, homozygous for the p.Phe508del variant, was compared with non-CF patients. For bronchial epithelium, a total of 1075 DEGs were identified, wherein 200 genes were found to be overexpressed, and 875 genes were underexpressed. The results for these DEGs are depicted in the volcano plot shown in Figure 1(a). In case of the rectal epithelium, 47 DEGs were identified, wherein 44 were overexpressed, while three genes were underexpressed genes (Figure 1(b)).

The discrepant DEGs identified between the rectal and bronchial epithelium showed that CF condition did not promote the expression of similar genes in these tissues. To verify the absence of any similarity between these tissues, DEGs were overlapped between both epithelia (Figures 1(c) and 1(d)).

Interestingly, the results for the analysis showed that only two of the overexpressed genes were shared by both tissues, namely, interferon-stimulated exonuclease gene 20 (ISG20) and hippocalcin-like protein 1 (HPCAL1). With regard to CF, no previous data have directly reported any involvement of ISG20 pathways in CF patients. However, ISG20 could be relevant for CF pathogenesis, wherein broad antiviral properties could have attributed to its expression. In particular, this gene codes for a nuclear $3'$-$5'$ exonuclease, which degrades viral RNAs as part of the interferon- (IFN-) regulated antiviral response [26–28].

In fibrocystic patients, viral respiratory infections are known to promote deterioration of lung functions [29, 30],

which further results in severe respiratory morbidity in children [31]. Additionally, the presence of exacerbated symptoms in the bronchial epithelium of CF patients were found to be associated with the presence of viruses, including respiratory syncytial virus [32], influenza types A and B [32, 33], parainfluenza [34], and human rhinovirus [35]. The results for *in* vitro assessment using human alveolar macrophages showed that H3N2 also promoted the expression of ISG20 [36]. However, it is important to note that the expression of ISG20 was not restricted to the lungs. In fact, this gene was previously shown to be expressed at high levels in the peripheral blood leukocytes, lymphoid tissues (spleen or thymus), and the colon [37]. Additionally, this gene was also expressed in diverse human-tumor types [38, 39].

Hippocalcin-like protein 1 (HPCAL1) is a neuronal calcium sensor (NCS) protein that has been majorly described in the brain [40]. Although its expression has also been reported in different cellular and tumoral models, including the lungs [41], the biological function of HPCAL1 in CF pathogenesis remains unknown.

Importantly, these two DEGs represent only 1% (2/200) of the overexpressed genes for the bronchial epithelium and 4.5% (2/44) for the rectal epithelium of CF samples. In terms of the total number of DEGs, this percentage further reduced to 0.18% (2/1075) and 4.2% (2/47) for the bronchial and rectal epithelia, respectively. This data further supports that the presence of p.Phe508del-mutated CFTR-allele in homozygous state influences the whole gene expression differently in each analyzed tissue.

In contrast to previously established idea, genes can belong to multiple groups at the same level. Thus, a DEG list might be statistically overrepresented in a GO category. To establish the same, GO term enrichment analysis was performed to predict the shared GO terms between the bronchial and rectal epithelia of CF patients (refer to the methods section for more details).

As shown in Figure 1(e), the biological processes for DEGs were found to be associated with immunological responses, namely, inflammatory response (GO:0056729), leukocyte chemotaxis (GO:0030595), and cytokine production (GO:0001819), in case of the bronchial epithelium. In comparison to this, GO terms for the rectal tissue were majorly related to the intracellular transport, involving cytoplasmatic vesicle lumen (GO:0060205), COPI-coated vesicle membrane (GO:0030663), focal adhesion (GO:0005925), and maintenance of protein localization in the endoplasmic reticulum (GO:0035437) and organelles (GO:0072595) (Figure 1(f)). According to this data, the majority of cellular functions were unrelated between these tissues. However, neutrophil activation (GO:0002283) appeared to be shared by the two tissues. Several previous studies have shown that infants with CF exhibited peribronchial neutrophilic infiltration prior to an initial infection [42–44]. In toddlers and older children, the inflammatory response is known to increase gradually, which further stimulates changes in mucus viscosity and affects bronchiolar function [45, 46]. Moreover in older patient, high levels of airway cytokines (e.g., IL−8) were also reported in addition to the neutrophil influx, which aggravated the lung complications [42, 47]. These inflammatory lung conditions facilitate growth of opportunistic and chronic infections at different stages of the lung disease [48].

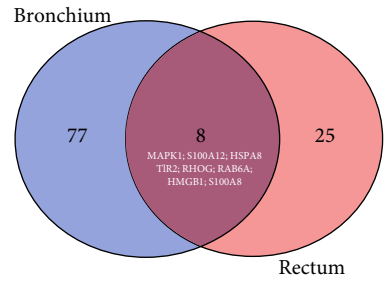

Figure 2: Venn diagram to compare the predicted genes for GO:0002283 between the rectal and bronchial tissues.

In the gastrointestinal tract, neutrophil activation and NETosis have also been reported in the colon mucosa of ulcerative colitis in fibrocystic patients [49]. In general, NETosis refers to the process of cell death that is related to the formation of neutrophil extracellular traps (NETs). The formation of NETs has been previously described in the airways of patients with CF, wherein tissue contamination by different microorganisms can lead to an exacerbated immune response [50]. However, this excessive formation of NETs results in the worsening of patient's condition due to tissue damage caused by the components of NETs [50].

As shown in Figure 2, nonshared DEGs were grouped into the same GO term (GO:0002283) between the bronchial and rectal tissues. A Venn diagram was prepared to compare all the predicted genes for each tissue into this GO term. The results showed that eight genes were shared between these tissues; however, these genes did not show differential expression. This data further suggested that each tissue involved different signaling pathways that contributed to the induction of a similar neutrophil phenotype.

To verify this hypothesis, an interatomic approach was adopted and performed between all DEGs. In general, a network strategy allows application of topological analysis to decipher pathways involved in each tissue. To achieve a systemic perspective for CF, PPI networks were first constructed for the bronchial and rectal tissues (for details refer to the methods section). Consequently, a bronchial PPI network comprising of 1,143 nodes and 8,091 edges was generated (Supplementary Figure 1). In comparison to this, the rectal PPI network was composed of 342 nodes and 2,178 edges (Supplementary Figure 2). Following this, topological centrality analyses were conducted for both networks to define HBSs for each tissue (Supplementary Figure 3a and 3b). In the bronchial PPI network, 175 HBSs were predicted, wherein 30 nodes corresponded to DEGs associated with one or more interrelated ontologies (Figure 3(a)). A similar observation was reported in case of the rectal PPI network, wherein a total of 45 HBSs were predicted. Among these, three nodes, namely, ACTB, TUBB4B, and YWHAZ, showed differential expression. Interestingly, these nodes were also associated with multiple GO for the rectal PPI network (Figure 3(b)).

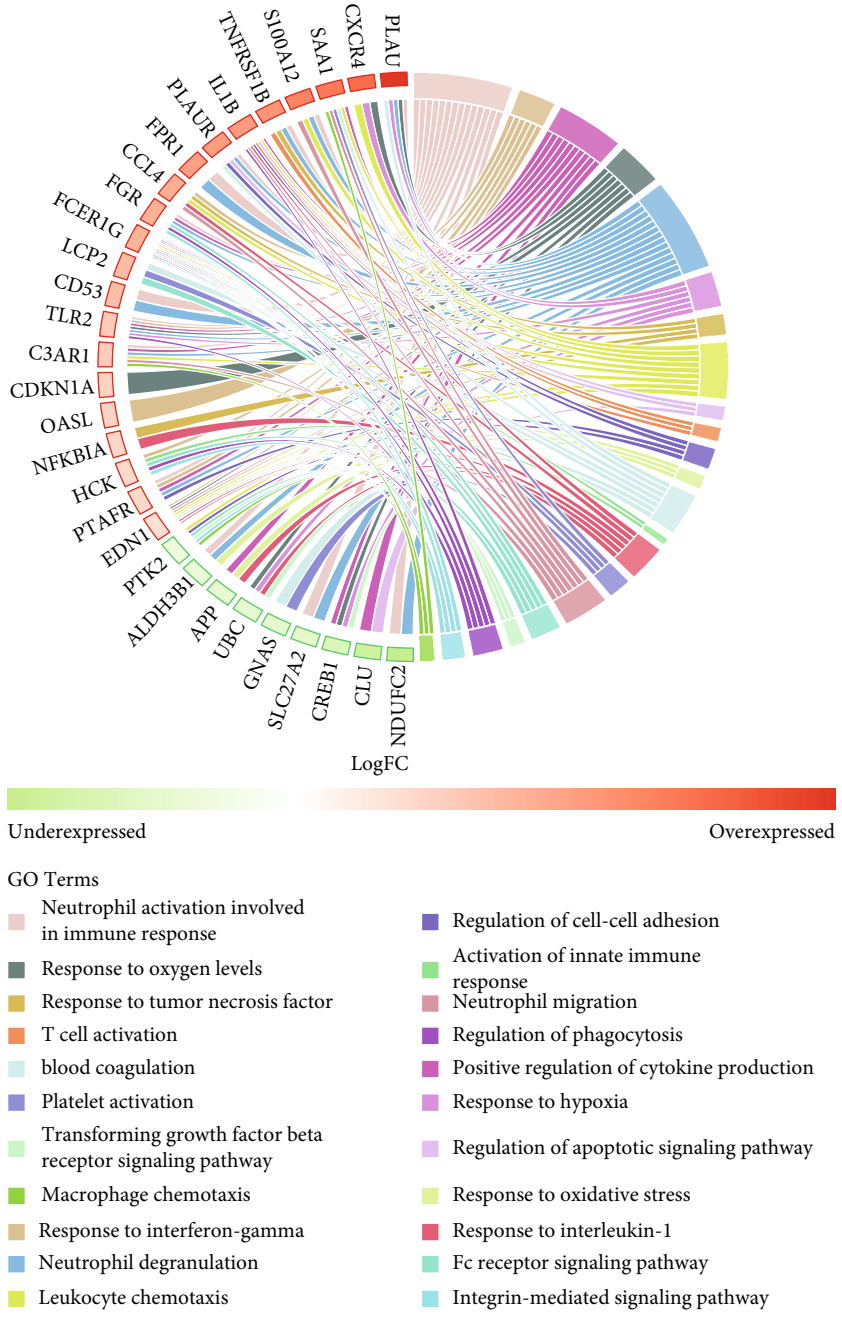

(a)

Figure 3: Continued.

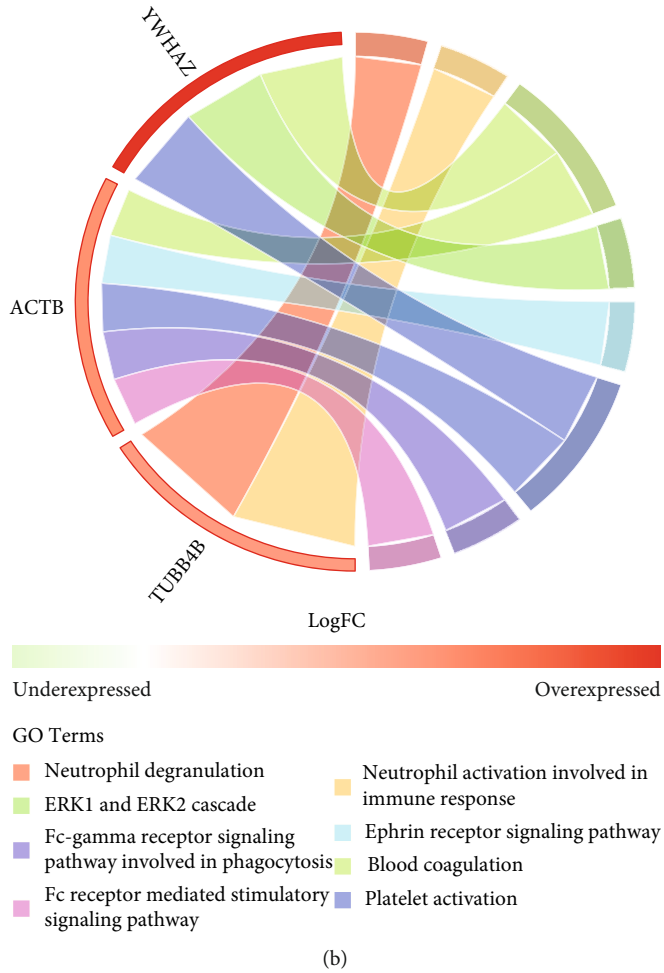

Figure 3: HBS-DEGs were selected from the pool of significant GO terms related to the (a) entire bronchial epithelium and (b) rectal epithelium networks (cut-off FDR < 0.001). These are depicted using the ribbons that link each GO to bronchial and rectal HBS-DEGs, respectively.

Thus, these results suggested that no HBSs were shared between the bronchial and rectal PPI networks, which further confirmed that tissue-specific pathways were associated with the homozygous p.Phe508del variant. Additionally, the terms predicted from GO analysis of DEG (Figures 1(e) and 1(f)) and HBS networks were found to be similar (Figures 3(a) and 3(b)) and shared a GO term that was related to neutrophil activation.

This data highlighted that these HBSs represented relevant biological processes for each tissue; however, no possible regulatory relationships were identified between them at the pathway level. Integrated pathway analyses were employed to capture such tissue-specific signatures.

To gain further insights into the potential relationship between the bronchial and rectal epithelia and tissue-specific response at the pathway level, the HBSs were used to construct functional interaction networks (Figure 4). For bronchial tissue, 20 HBS-DEGs and 35 HBS-non-DEGS were predicted to interconnect the pathways that were majorly composed of activators (Figure 4(a)). Similarly, the rectal epithelium pathways involved only three HBS-DEGs and 27 HBS-non-DEGs (Figure 4(b)). Interestingly, one unique node, MAPK3, a non-DEG, was shared between the pathway-based networks for the two tissues. This observation further confirmed the induction of independent cell signaling processes in each tissue by the homozygous p.Phe508del variant. Moreover, it was possible to discriminate the GO term named neutrophil degranulation at pathway level, where FDR = 1.25×10^{-08} and FDR = 3.08×10^{-05} were used for the bronchial and rectal tissues, respectively. Degranulation from neutrophils has been previously implicated as a significant causative factor in pulmonary disorders, which is dependent of neutrophil activation [51]. Post the analysis of this GO term, no shared HBSs were found between two tissues. In case of the bronchial tissue, CD53, PLAUR, PLAU, S100A12, FGR, and FCER1G were predicted, whereas only TUBB4B was predicted for the rectum. This result verified the initial hypothesis that different tissue-specific pathways could possibly promote a similar neutrophil phenotype.

Interestingly, the other GO term that emerged to be common between the analyzed tissues, obtained from Reactome database, was platelet activation, wherein FDR = 2×10^{-05}

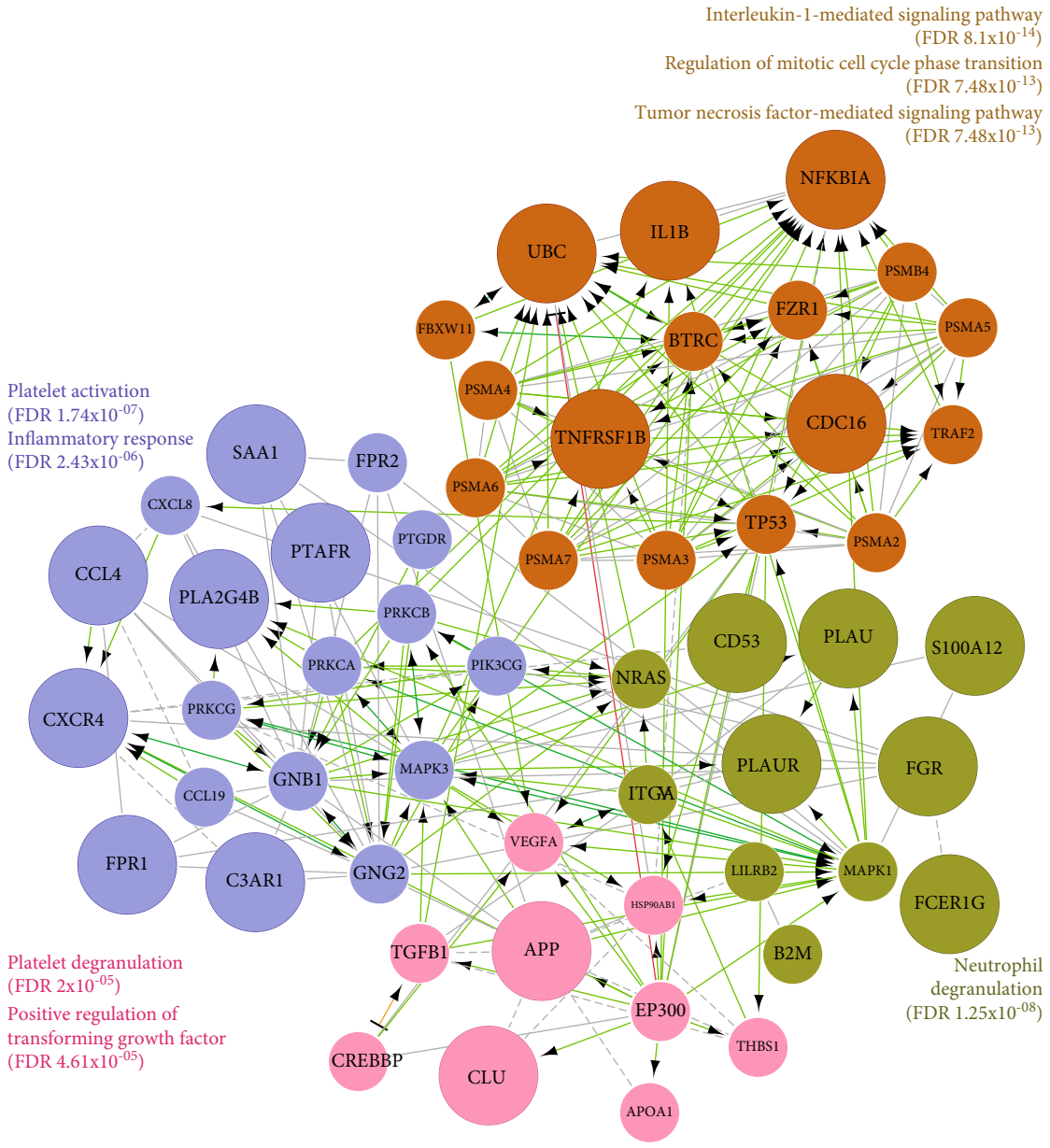

(a)

Figure 4: Continued.

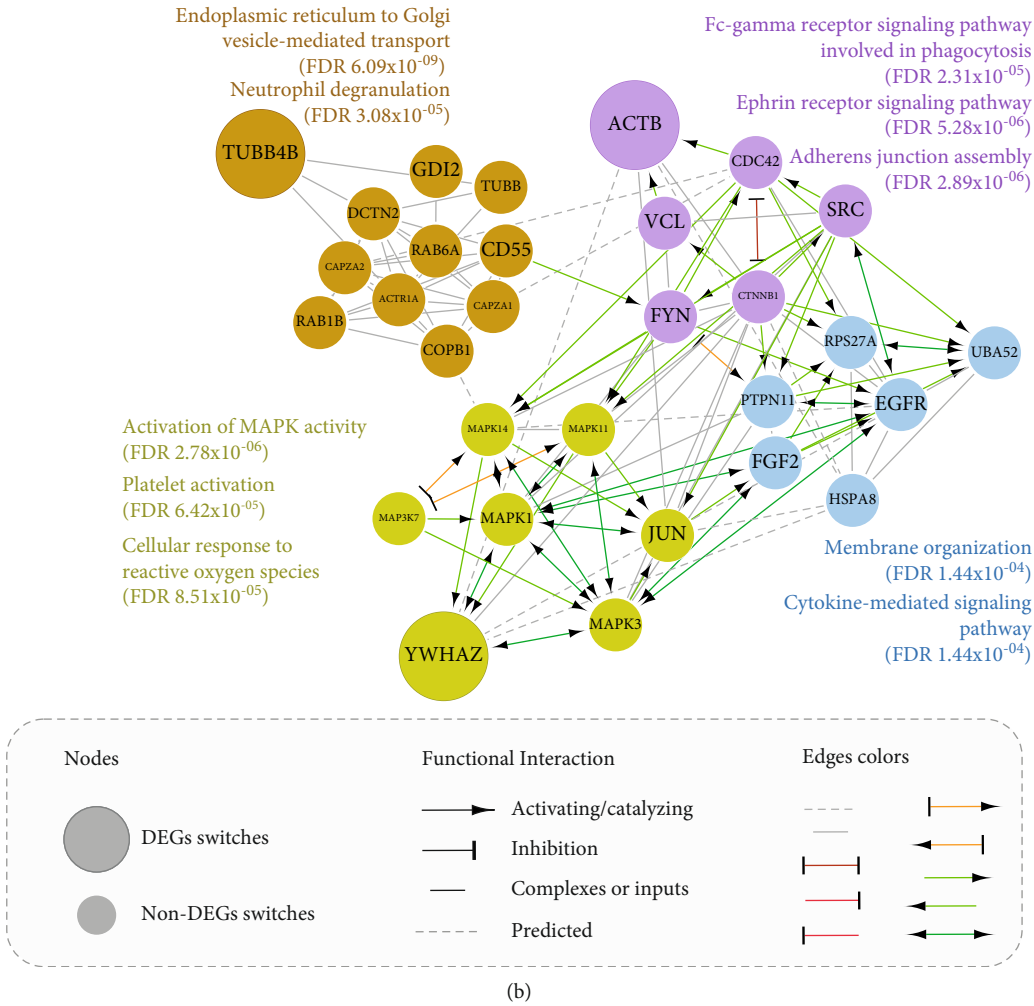

(b)

FIGURE 4: Pathway-based networks with the most significant GOs (cut-off FDR < 0.001) for the HBSs of the (a) bronchial epithelium and (b) rectal epithelium.

and FDR = 6.43×10^{-05} were used for the bronchial and rectal tissue, respectively (Figure 4). Platelets are known to be essential players in the development of inflammatory response, which is attributed to their interaction with leukocytes and their role in the secretion of proinflammatory mediators and migratory behavior cells [52]. In CF patients, increased levels of circulating leukocyte-platelet aggregates have been reported [53–55]. For this GO term, SAA1, CCL4, PTAFR, PLA2G4B, CXCR4, FPR1, and C3AR1 HBSs were predicted for the bronchial epithelium. However, only YWHAZ HBS was found to be associated with this term in case of the rectal tissue. This observation further reinforced the idea that different tissue-specific pathways could induce a similar cellular response.

In the last few year, significant additions have been made to the list of key genes involved in CF [56–61], and the identification of essential disease-related pathways remains a priority, particularly for the development of new treatment strategies. For the first time, the present study defined tissue-specific pathways stratified for the fibrocystic genotype, .p.Phe508del-mutated CFTR-allele in homozygous state. Consequently, the use of in silico strategy in the present study resulted in the identification of putative tissue-specific biomarkers and unraveled their association at the systemic level. To verify this, previous studies were reviewed to find a relationship between each HBS-DEG and CF, based on gene expression data (Table 1).

As shown in Table 1, review of gene expression data reported in previous studies revealed that APP, FPR1, PTFAR1, TNFRSF1B, UBC, and YWHAZ were not reported for CF. An additional network was generated to decipher its tentative functions and predict the interaction between all HBS-DEGs included in Table 1 and CFTR (Figure 5). Interestingly, TNFRSF1B, UBC, and YWHAZ directly modulated this receptor. However, the involvement of these HBS nodes in CF pathogenesis still remains unknown. These three nodes might affect the structural stability of the CF receptor.

TNFRSF1B generally encodes for a high-affinity receptor for tumor necrosis factor (TNF) α. In terms of CF, this protein might influence the trafficking of F508del-CFTR through the Golgi apparatus by regulating the levels of TNF-α in bronchi. In a previous *in vitro* study, F508del-CFTR-transfected HeLa cells and human bronchial cells

Table 1: Literature review and data collection for the predicted HBS-DEGs in the context of CF pathogenesis. Only those studies were considered that explored gene expression data.

Symbol	Gene name	Network	Expression	CF-related	Tissue
APP	Amyloid beta precursor protein	Bronchial	Down	—	—
C3AR1	Complement C3a receptor 1	Bronchial	Up	Yes	Lung [62]
CCL4	C–C motif chemokine ligand 4	Bronchial	Up	Yes	Lung [63], Tear fluid [64]
CD53	CD53 molecule	Bronchial	Up	Yes	Nasal (airway inflammation) [65], Lung [66]
CDC16	Cell division cycle 16	Bronchial	Down	Yes	Blood neutrophils [67]
CLU	Clusterin	Bronchial	Down	Yes	Lung (airway secretions) [68]
CXCR4	C–X–C motif chemokine receptor 4	Bronchial	Up	Yes	Lung [69]
FCER1G	Fc fragment of IgE receptor Ig	Bronchial	Up	Yes	Lung [66, 70], Pancreas [71], Intestine [72]
FGR	FGR protooncogene, Src family tyrosine kinase	Bronchial	Up	Yes	Kidney [73]
FPR1	Formyl peptide receptor 1	Bronchial	Up	—	—
IL1B	Interleukin 1 beta	Bronchial	Up	Yes	Airway mucopurulent secretions [74, 75]
NFKBIA	NFKB inhibitor alpha	Bronchial	Up	Yes	Bronchial gland cells [76], Lung [77]
PLA2G4B	Phospholipase A2 group IVB	Bronchial	Down	Yes	Lung [78]
PLAU	Plasminogen activator, urokinase	Bronchial	Up	Yes	Airway epithelia [79]
PLAUR	Plasminogen activator, urokinase receptor	Bronchial	Up	Yes	Airway epithelia [79]
PTAFR	Platelet activating factor receptor	Bronchial	Up	—	—
S100A12	S100 calcium-binding protein A12	Bronchial	Up	Yes	Lung sputum [80–82]
SAA1	Serum amyloid A1	Bronchial	Up	Yes	Lung fibroblasts [83], Lung [62, 78], Blood [84]
TNFRSF1B	TNF receptor superfamily member 1B	Bronchial	Up	—	—
UBC	Ubiquitin C	Bronchial	Down	—	—
ACTB	Actin beta	Rectal	Up	Yes	Lung [13, 85]
TUBB4B	Tubulin beta 4B class IVb	Rectal	Up	Yes	Airway epithelia [86], ciliated cells [86]
YWHAZ	Tyrosine 3-monooxygenase/tryptophan 5-monooxygenase activation protein zeta	Rectal	Up	—	—

expressing F508del-CFTR in primary culture were exposed to TNF-α (0.5–50 ng/ml) for 10 min [87]. This treatment promoted the maturation of F508del-CFTR via Golgi vesicular transport and induced CFTR chloride currents. According to this evidence, TNF-α and TNFRSF1B balance could be essential for the maturation of CFTR, but this hypothesis still needs to be experimentally tested. At the genomic level, TNFRSF1B polymorphisms have been shown to be associated with severe pulmonary phenotype in CF [88].

In comparison to this, the polyubiquitin gene ubiquitin C (UBC) is considered to be a stress-protective gene, which is upregulated under various stressful conditions, probably as a consequence of the increased demand for ubiquitin for the removal of toxic misfolded proteins [89]. In the context of CF, misfolding of the CFTR proteins has been described for CF patients in several previous studies. In particular, F508del-CFTR mutation is known to be a major cause of 70% of CF cases [90]. In the present study, UBC was downregulated, which further suggested that the degradation of machine-mediated polyubiquitin is also affected in CF patients. Some previous studies have addressed this point, wherein failure in proteasome degradation maintained aberrantly folded CFTR proteins [91, 92].

YWHAZ, a member of 14-3-3 proteins, is a conserved regulatory protein that maintains multiple types of signals via binding to several partner proteins. The binding of 14-3-3 proteins can lead to conformational changes in their partners, masking specific sequences or structural features in the partner proteins that promote the formation of complex [93]. No previous data has reported YWHAZ interaction with CFTR. However, this family of proteins is known to affect a consensus sequence, RXXpS/TXP [94]. It might enforce conformational changes in the binding partner around the phosphorylated docking sites. Future studies are required to explore these conformational changes and elucidate their association with CF phenotypes.

The present study was associated with certain limitations. In this study, gene transcription analysis was performed for a total of 35 CF patients and 22 healthy controls. Complementary studies should be carried out in

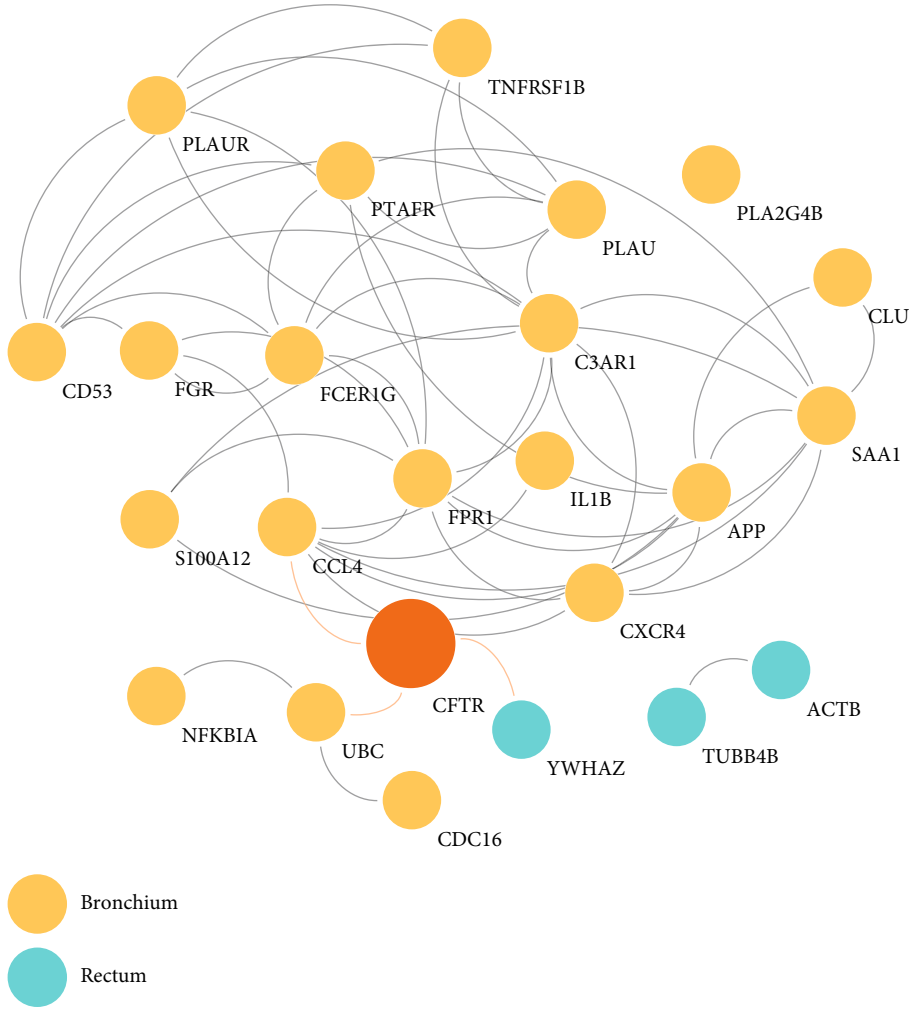

Figure 5: PPI network generated between CFTR and HBSs found in the bronchial and rectal epithelial networks.

independent cohorts with a higher number of tissues. However, this limitation, a low size sample, is recurrent and has been reported in other exploratory works also, which involved different criteria (inclusion/exclusion) for screening of potential markers or key pathways in CF [58, 71, 95, 96]. Additionally, it is crucial to verify whether the p.Phe508del variant in the homozygous state promotes pathways perturbations in several tissues or exclusively in the bronchial and rectal epithelia. Moreover, patients should be followed longitudinally to correlate the genetic expression of the predicted HBSs with the clinical outcomes in the future.

Finally, it is essential to note that choosing an accurate genotyping method for diagnosis and a priori knowledge of population's genetic variations is critical to design putative biomarkers or treatments. For example, the frequency of homozygous p.Phe508del variant changes according to ethnicity [97]. Thus, considering all these points could increase the relevance of our findings.

4. Conclusions

The present study assessed the genetic expression profiles for the bronchial and rectal samples obtained from CF patients homozygous for the p.Phe508del-mutated CFTR-allele and identified certain tissue-specific pathways. The integration of the results of GO analyses for DEGs and network strategies with topological analysis allowed the identification of HBSs for each tissue. Interestingly, each tissue possessed its unique HBSs that were involved in different cell signaling pathways, which promoted a similar cellular phenotype/response. The integrative approach utilized in this study offered comprehensive insights into the molecular networks for the bronchial and rectal epithelia and the underlying regulators involved in CF. The findings of the study might further aid in the development of tissue-specific therapeutics, based on genotypic analysis.

Data Availability

Previously reported gene expression data were used to support this study and are available at doi:10.1038/ejhg.2013.209 and doi:10.1016/j.ygeno.2011.06.008. These prior studies (and datasets) are cited at relevant places within the text as references [11]; [12].

Conflicts of Interest

The authors declare no conflict of interest.

Authors' Contributions

J.E.V is responsible for the conceptualization; J.F.P for the methodology and formal analysis; J.E.V and T.R for the investigation; T.R, J.E.V, and J.F.P for the writing—original draft preparation; M.L.R, C.T, J.E.V, and T.R for the writing—review and editing; J.E.V for the supervision; and C.T for the funding acquisition. All authors have read and agreed to the published version of the manuscript. Joice de Faria Poloni and Thaiane Rispoli contributed equally to this work.

Supplementary Materials

Supplementary Figure 1: bronchial PPI network comprising 1,143 nodes and 8,091 edges. Colored nodes (green to underexpressed genes; red to overexpressed genes) denote differential expression, and diamond shape indicates HBS nodes. Supplementary Figure 2: rectal PPI network comprising 342 nodes and 2,178 edges. Colored nodes denote log2FC of DEGS (green to underexpressed genes; red to overexpressed genes), and diamond shape indicates HBS nodes. Supplementary Figure 3: (a, b) visualization of the subnetworks from the HBS nodes of bronchial epithelium and rectal epithelium networks, respectively. Colored nodes indicate the log2FC of DEGs (green to underexpressed genes; red to overexpressed genes). *(Supplementary Materials)*

References

[1] P. R. Sosnay, K. R. Siklosi, F. van Goor et al., "Defining the disease liability of variants in the cystic fibrosis transmembrane conductance regulator gene," *Nature Genetics*, vol. 45, no. 10, pp. 1160–1167, 2013.

[2] T. Rispoli, S. Martins de Castro, T. Grandi et al., "A low-cost and simple genetic screening for cystic fibrosis provided by the Brazilian public health system," *The Journal of Pediatrics*, vol. 199, pp. 272–277.3, 2018.

[3] X. Meng, J. Clews, A. D. Ciuta, E. R. Martin, and R. C. Ford, "CFTR structure, stability, function and regulation," *Biological Chemistry*, vol. 400, no. 10, pp. 1359–1370, 2019.

[4] N. Derichs, "Targeting a genetic defect: cystic fibrosis transmembrane conductance regulator modulators in cystic fibrosis," *European Respiratory Review : an official journal of the European Respiratory Society*, vol. 22, no. 127, pp. 58–65, 2013.

[5] Z. Zhang, F. Liu, and J. Chen, "Molecular structure of the ATP-bound, phosphorylated human CFTR," *Proceedings of the National Academy of Sciences of the United States of America*, vol. 115, pp. 12757–12762, 2018.

[6] C. Castellani and B. M. Assael, "Cystic fibrosis: a clinical view," *Cellular and Molecular Life Sciences : CMLS*, vol. 74, pp. 129–140, 2017.

[7] F. A. L. Marson, C. S. Bertuzzo, and J. D. Ribeiro, "Classification of CFTR mutation classes," *The Lancet Respiratory Medicine*, vol. 4, pp. e37–e38, 2016.

[8] F. A. L. Marson, C. S. Bertuzzo, and J. D. Ribeiro, "Personalized or precision medicine? The example of cystic fibrosis," *Frontiers in Pharmacology*, vol. 8, p. 390, 2017.

[9] D. M. Bernardi, A. F. Ribeiro, T. N. Mazzola, M. M. Vilela, and V. C. Sgarbieri, "The impact of cystic fibrosis on the immunologic profile of pediatric patients," *Jornal de Pediatria*, vol. 89, pp. 40–47, 2013.

[10] K. De Boeck and M. D. Amaral, "Progress in therapies for cystic fibrosis," *The Lancet Respiratory Medicine*, vol. 4, pp. 662–674, 2016.

[11] A. Athar, A. Füllgrabe, N. George et al., "ArrayExpress update - from bulk to single-cell expression data," *Nucleic Acids Research*, vol. 47, no. D1, pp. D711–D715, 2019.

[12] F. Stanke, A. van Barneveld, S. Hedtfeld, S. Wolfl, T. Becker, and B. Tummler, "The CF-modifying gene *EHF* promotes p.Phe508del-CFTR residual function by altering protein glycosylation and trafficking in epithelial cells," *European Journal of Human Genetics : EJHG*, vol. 22, no. 5, pp. 660–666, 2014.

[13] V. Ogilvie, M. Passmore, L. Hyndman et al., "Differential global gene expression in cystic fibrosis nasal and bronchial epithelium," *Genomics*, vol. 98, no. 5, pp. 327–336, 2011.

[14] A. Kauffmann, T. F. Rayner, H. Parkinson et al., "Importing ArrayExpress datasets into R/Bioconductor," *Bioinformatics*, vol. 25, pp. 2092–2094, 2009.

[15] A. Kauffmann, R. Gentleman, and W. Huber, "arrayQualityMetrics–a bioconductor package for quality assessment of microarray data," *Bioinformatics*, vol. 25, pp. 415-416, 2009.

[16] M. E. Ritchie, B. Phipson, D. Wu et al., "limma powers differential expression analyses for RNA-sequencing and microarray studies," *Nucleic Acids Research*, vol. 43, article e47, 2015.

[17] D. Szklarczyk, A. Franceschini, S. Wyder et al., "STRING v10: protein-protein interaction networks, integrated over the tree of life," *Nucleic Acids Research*, vol. 43, no. D1, pp. D447–D452, 2015.

[18] M. S. Cline, M. Smoot, E. Cerami et al., "Integration of biological networks and gene expression data using Cytoscape," *Nature Protocols*, vol. 2, no. 10, pp. 2366–2382, 2007.

[19] G. Su, J. H. Morris, B. Demchak, and G. D. Bader, "Biological network exploration with Cytoscape 3," *Current Protocols in Bioinformatics*, vol. 47, no. 1, pp. 11–24, 2014.

[20] G. Scardoni, M. Petterlini, and C. Laudanna, "Analyzing biological network parameters with CentiScaPe," *Bioinformatics*, vol. 25, pp. 2857–2859, 2009.

[21] G. Scardoni, G. Tosadori, M. Faizan, F. Spoto, F. Fabbri, and C. Laudanna, "Biological network analysis with CentiScaPe: centralities and experimental dataset integration," *F1000Research*, vol. 3, p. 139, 2014.

[22] G. Scardoni and C. Lau, "Centralities based analysis of complex networks," in *New Frontiers in Graph Theory*, Amazon.com, 2012.

[23] G. Wu, E. Dawson, A. Duong, R. Haw, and L. Stein, "ReactomeFIViz: a Cytoscape app for pathway and network-based data analysis," *F1000Research*, vol. 3, p. 146, 2014.

[24] S. Aibar, C. Fontanillo, C. Droste, and J. De Las Rivas, "Functional gene networks: R/Bioc package to generate and analyse gene networks derived from functional enrichment and clustering," *Bioinformatics*, vol. 31, pp. 1686–1688, 2015.

[25] W. Walter, F. Sanchez-Cabo, and M. Ricote, "GOplot: an R package for visually combining expression data with functional analysis," *Bioinformatics*, vol. 31, pp. 2912–2914, 2015.

[26] L. Espert, G. Degols, C. Gongora et al., "ISG20, a new interferon-induced RNase specific for single-stranded RNA, defines an alternative antiviral pathway against RNA genomic viruses," *The Journal of Biological Chemistry*, vol. 278, pp. 16151–16158, 2003.

[27] C. M. Weiss, D. W. Trobaugh, C. Sun et al., "The interferon-induced exonuclease ISG20 exerts antiviral activity through upregulation of type I interferon response proteins," *mSphere*, vol. 3, 2018.

[28] Z. Zheng, L. Wang, and J. Pan, "Interferon-stimulated gene 20-kDa protein (ISG20) in infection and disease: review and outlook," *Intractable & Rare Diseases Research*, vol. 6, pp. 35–40, 2017.

[29] E. E. Wang, C. G. Prober, B. Manson, M. Corey, and H. Levison, "Association of respiratory viral infections with pulmonary deterioration in patients with cystic fibrosis," *The New England Journal of Medicine*, vol. 311, pp. 1653–1658, 1984.

[30] H. Frickmann, S. Jungblut, T. O. Hirche, U. Gross, M. Kuhns, and A. E. Zautner, "Spectrum of viral infections in patients with cystic fibrosis," *European Journal of Microbiology & Immunology*, vol. 2, pp. 161–175, 2012.

[31] D. Armstrong, K. Grimwood, J. B. Carlin et al., "Severe viral respiratory infections in infants with cystic fibrosis," *Pediatric Pulmonology*, vol. 26, pp. 371–379, 1998.

[32] R. Somayaji, C. H. Goss, U. Khan, M. Neradilek, K. M. Neuzil, and J. R. Ortiz, "Cystic fibrosis pulmonary exacerbations attributable to respiratory syncytial virus and influenza: a population-based study," *Clinical Infectious Diseases : An Official Publication of the Infectious Diseases Society of America*, vol. 64, pp. 1760–1767, 2017.

[33] J. B. Dennis, A. M. Jones, E. A. Davies et al., "Influenza B outbreak at an adult cystic fibrosis centre - clinical impact and factors influencing spread," *Journal of cystic fibrosis : official journal of the European Cystic Fibrosis Society*, vol. 19, pp. 808–814, 2020.

[34] M. R. Kiedrowski and J. M. Bomberger, "Viral-bacterial co-infections in the cystic fibrosis respiratory tract," *Frontiers in Immunology*, vol. 9, p. 3067, 2018.

[35] A. R. Smyth, R. L. Smyth, C. Y. Tong, C. A. Hart, and D. P. Heaf, "Effect of respiratory virus infections including rhinovirus on clinical status in cystic fibrosis," *Archives of Disease in Childhood*, vol. 73, pp. 117–120, 1995.

[36] J. Wang, M. P. Nikrad, E. A. Travanty et al., "Innate immune response of human alveolar macrophages during influenza A infection," *PLoS One*, vol. 7, no. 3, article e29879, 2012.

[37] C. Gongora, G. David, L. Pintard et al., "Molecular cloning of a new interferon-induced PML nuclear body-associated protein," *The Journal of Biological Chemistry*, vol. 272, pp. 19457–19463, 1997.

[38] M. Gao, Y. Lin, X. Liu et al., "ISG20 promotes local tumor immunity and contributes to poor survival in human glioma," *Oncoimmunology*, vol. 8, article e1534038, 2019.

[39] T. Xu, H. Ruan, S. Gao et al., "ISG20 serves as a potential biomarker and drives tumor progression in clear cell renal cell carcinoma," *Aging*, vol. 12, no. 2, pp. 1808–1827, 2020.

[40] K. H. Braunewell, "The darker side of Ca2+ signaling by neuronal Ca2+-sensor proteins: from Alzheimer's disease to cancer," *Trends in Pharmacological Sciences*, vol. 26, pp. 345–351, 2005.

[41] A. Agathanggelou, I. Bieche, J. Ahmed-Choudhury et al., "Identification of novel gene expression targets for the Ras association domain family 1 (RASSF1A) tumor suppressor gene in non-small cell lung cancer and neuroblastoma," *Cancer Research*, vol. 63, pp. 5344–5351, 2003.

[42] M. A. Khan, Z. S. Ali, N. Sweezey, H. Grasemann, and N. Palaniyar, "Progression of cystic fibrosis lung disease from childhood to adulthood: neutrophils, neutrophil extracellular trap (NET) formation, and NET degradation," *Genes*, vol. 10, no. 3, p. 183, 2019.

[43] C. Margaroli, L. W. Garratt, H. Horati et al., "Elastase exocytosis by airway neutrophils is associated with early lung damage in children with cystic fibrosis," *American Journal of Respiratory and Critical Care Medicine*, vol. 199, no. 7, pp. 873–881, 2019.

[44] S. M. Law and R. D. Gray, "Neutrophil extracellular traps and the dysfunctional innate immune response of cystic fibrosis lung disease: a review," *Journal of Inflammation*, vol. 14, no. 1, p. 29, 2017.

[45] J. J. Wine, G. C. Hansson, P. Konig, N. S. Joo, A. Ermund, and M. Pieper, "Progress in understanding mucus abnormalities in cystic fibrosis airways," *Journal of Cystic Fibrosis*, vol. 17, pp. S35–S39, 2018.

[46] D. K. Schlüter, J. S. Ostrenga, S. B. Carr et al., "Lung function in children with cystic fibrosis in the USA and UK: a comparative longitudinal analysis of national registry data," *Thorax*, 2021.

[47] J. E. Vargas, A. A. Souto, P. M. Pitrez, R. T. Stein, and B. N. Porto, "Modulatory potential of resveratrol during lung inflammatory disease," *Medical Hypotheses*, vol. 96, pp. 61–65, 2016.

[48] L. A. Pinto, L. A. de Azeredo Leitão, M. Mocellin et al., "IL-8/IL-17 gene variations and the susceptibility to severe viral bronchiolitis," *Epidemiology and Infection*, vol. 145, no. 4, pp. 642–646, 2017.

[49] Z. Cahilog, H. Zhao, L. Wu et al., "The role of neutrophil NETosis in organ injury: novel inflammatory cell death mechanisms," *Inflammation*, vol. 43, no. 6, pp. 2021–2032, 2020.

[50] S. R. Martinez-Aleman, L. Campos-Garcia, J. P. Palma-Nicolas, R. Hernandez-Bello, G. M. Gonzalez, and A. Sanchez-Gonzalez, "Understanding the entanglement: neutrophil extracellular traps (NETs) in cystic fibrosis," *Frontiers in Cellular and Infection Microbiology*, vol. 7, p. 104, 2017.

[51] P. Lacy, "Mechanisms of degranulation in neutrophils," *Allergy, Asthma, and Clinical Immunology*, vol. 2, no. 3, pp. 98–108, 2006.

[52] Y. Chen, H. Zhong, Y. Zhao, X. Luo, and W. Gao, "Role of platelet biomarkers in inflammatory response," *Biomarker Research*, vol. 8, p. 28, 2020.

[53] I. Tarnow, A. D. Michelson, A. L. Frelinger et al., "Cystic fibrosis heterozygotes do not have increased platelet activation," *Thrombosis Research*, vol. 121, no. 2, pp. 159–162, 2007.

[54] B. P. O'Sullivan, M. D. Linden, A. L. Frelinger et al., "Platelet activation in cystic fibrosis," *Blood*, vol. 105, no. 12, pp. 4635–4641, 2005.

[55] A. Sturm, H. Hebestreit, C. Koenig, U. Walter, and R. Grossmann, "Platelet proinflammatory activity in clinically stable patients with CF starts in early childhood," *Journal of Cystic Fibrosis*, vol. 9, pp. 179–186, 2010.

[56] R. Reilly, M. S. Mroz, E. Dempsey et al., "Targeting the PI3K/Akt/mTOR signalling pathway in cystic fibrosis," *Scientific Reports*, vol. 7, p. 7642, 2017.

[57] J. Gong, F. Wang, B. Xiao et al., "Genetic association and transcriptome integration identify contributing genes and tissues

at cystic fibrosis modifier loci," *PLoS Genetics*, vol. 15, no. 2, article e1008007, 2019.

[58] F. Pineau, D. Caimmi, M. Magalhães et al., "Blood co-expression modules identify potential modifier genes of diabetes and lung function in cystic fibrosis," *PLoS One*, vol. 15, no. 4, article e0231285, 2020.

[59] S. Shanthikumar, M. N. Neeland, R. Saffery, and S. Ranganathan, "Gene modifiers of cystic fibrosis lung disease: a systematic review," *Pediatric Pulmonology*, vol. 54, pp. 1356–1366, 2019.

[60] C. Gu, X. Shi, X. Dang et al., "Identification of common genes and pathways in eight fibrosis diseases," *Frontiers in Genetics*, vol. 11, article 627396, 2020.

[61] M. L. Urban, L. Manenti, and A. Vaglio, "Fibrosis–a common pathway to organ injury and failure," *The New England Journal of Medicine*, vol. 373, pp. 95-96, 2015.

[62] D. Polineni, H. Dang, P. J. Gallins et al., "Airway mucosal host defense is key to genomic regulation of cystic fibrosis lung disease severity," *American Journal of Respiratory and Critical Care Medicine*, vol. 197, no. 1, pp. 79–93, 2018.

[63] S. Brennan, P. D. Sly, C. L. Gangell et al., "Alveolar macrophages and CC chemokines are increased in children with cystic fibrosis," *The European Respiratory Journal*, vol. 34, pp. 655–661, 2009.

[64] M. Mrugacz, "CCL4/MIP-1beta levels in tear fluid and serum of patients with cystic fibrosis," *Journal of Interferon & Cytokine Research : the official journal of the International Society for Interferon and Cytokine Research*, vol. 30, pp. 509–512, 2010.

[65] P. L. Zeitlin, M. Diener-West, K. A. Callahan et al., "Digitoxin for airway inflammation in cystic fibrosis: preliminary assessment of safety, pharmacokinetics, and dose finding," *Annals of the American Thoracic Society*, vol. 14, pp. 220–229, 2017.

[66] N. Joshi, S. Watanabe, R. Verma et al., "A spatially restricted fibrotic niche in pulmonary fibrosis is sustained by M-CSF/M-CSFR signalling in monocyte-derived alveolar macrophages," *The European Respiratory Journal*, vol. 55, no. 1, article 1900646, 2020.

[67] M. Adib-Conquy, T. Pedron, A. F. Petit-Bertron et al., "Neutrophils in cystic fibrosis display a distinct gene expression pattern," *Molecular Medicine*, vol. 14, pp. 36–44, 2008.

[68] J. R. Peters-Hall, K. J. Brown, D. K. Pillai et al., "Quantitative proteomics reveals an altered cystic fibrosis in vitro bronchial epithelial secretome," *American Journal of Respiratory Cell and Molecular Biology*, vol. 53, pp. 22–32, 2015.

[69] M. Carevic, A. Singh, N. Rieber et al., "CXCR4+ granulocytes reflect fungal cystic fibrosis lung disease," *The European Respiratory Journal*, vol. 46, pp. 395–404, 2015.

[70] C. K. Haston, S. Cory, L. Lafontaine, G. Dorion, and M. T. Hallett, "Strain-dependent pulmonary gene expression profiles of a cystic fibrosis mouse model," *Physiological Genomics*, vol. 25, pp. 336–345, 2006.

[71] P. Trouve, E. Genin, and C. Ferec, "In silico search for modifier genes associated with pancreatic and liver disease in cystic fibrosis," *PLoS One*, vol. 12, article e0173822, 2017.

[72] O. Norkina and R. C. De Lisle, "Potential genetic modifiers of the cystic fibrosis intestinal inflammatory phenotype on mouse chromosomes 1, 9, and 10," *BMC Genetics*, vol. 6, p. 29, 2005.

[73] A. Billet, Y. Jia, T. Jensen, J. R. Riordan, and J. W. Hanrahan, "Regulation of the cystic fibrosis transmembrane conductance regulator anion channel by tyrosine phosphorylation," *FASEB Journal : Official Publication of the Federation of American Societies for Experimental Biology*, vol. 29, pp. 3945–3953, 2015.

[74] S. Gallati, "Disease-modifying genes and monogenic disorders: experience in cystic fibrosis," *The Application of Clinical Genetics*, vol. 7, pp. 133–146, 2014.

[75] G. Chen, L. Sun, T. Kato et al., "IL-1β dominates the promucin secretory cytokine profile in cystic fibrosis," *The Journal of Clinical Investigation*, vol. 129, no. 10, pp. 4433–4450, 2019.

[76] O. Tabary, S. Escotte, J. P. Couetil et al., "High susceptibility for cystic fibrosis human airway gland cells to produce IL-8 through the IκB kinase α pathway in response to extracellular NaCl content," *Journal of Immunology*, vol. 164, no. 6, pp. 3377–3384, 2000.

[77] E. Boncoeur, T. Roque, E. Bonvin et al., "Cystic fibrosis transmembrane conductance regulator controls lung proteasomal degradation and nuclear factor-kappaB activity in conditions of oxidative stress," *The American Journal of Pathology*, vol. 172, pp. 1184–1194, 2008.

[78] V. Bezzerri, P. d'Adamo, A. Rimessi et al., "Phospholipase C-β3 is a key modulator of IL-8 expression in cystic fibrosis bronchial epithelial cells," *Journal of Immunology*, vol. 186, no. 8, pp. 4946–4958, 2011.

[79] P. T. Drapkin, C. R. O'Riordan, S. M. Yi et al., "Targeting the urokinase plasminogen activator receptor enhances gene transfer to human airway epithelia," *The Journal of Clinical Investigation*, vol. 105, no. 5, pp. 589–596, 2000.

[80] D. Foell, S. Seeliger, T. Vogl et al., "Expression of S100A12 (EN-RAGE) in cystic fibrosis," *Thorax*, vol. 58, pp. 613–617, 2003.

[81] B. Meijer, R. B. Gearry, and A. S. Day, "The role of S100A12 as a systemic marker of inflammation," *International Journal of Inflammation*, vol. 2012, Article ID 907078, 6 pages, 2012.

[82] E. Lorenz, M. S. Muhlebach, P. A. Tessier et al., "Different expression ratio of S100A8/A9 and S100A12 in acute and chronic lung diseases," *Respiratory Medicine*, vol. 102, pp. 567–573, 2008.

[83] K. Lakota, M. Carns, S. Podlusky et al., "Serum amyloid A is a marker for pulmonary involvement in systemic sclerosis," *PLoS One*, vol. 10, article e0110820, 2015.

[84] T. Simpson, C. Elston, P. Macedo, and F. Perrin, "Amyloidosis in cystic fibrosis," *Paediatric Respiratory Reviews*, vol. 31, pp. 32–34, 2019.

[85] J. M. Wright, C. A. Merlo, J. B. Reynolds et al., "Respiratory epithelial gene expression in patients with mild and severe cystic fibrosis lung disease," *American Journal of Respiratory Cell and Molecular Biology*, vol. 35, pp. 327–336, 2006.

[86] M. Carraro, A. Carrer, A. Urbani, and P. Bernardi, "Molecular nature and regulation of the mitochondrial permeability transition pore(s), drug target(s) in cardioprotection," *Journal of Molecular and Cellular Cardiology*, vol. 144, pp. 76–86, 2020.

[87] S. Bitam, I. Pranke, M. Hollenhorst et al.et al., "An unexpected effect of TNF-alpha on F508del-CFTR maturation and function," *F1000Research*, vol. 4, p. 218, 2015.

[88] M. Hassanzad, P. Farnia, J. Ghanavi, F. Parvini, S. Saif, and A. A. Velayati, "TNFalpha -857C/T and TNFR2 +587 T/G polymorphisms are associated with cystic fibrosis in Iranian patients," *European Journal of Medical Genetics*, vol. 62, article 103584, 2019.

[89] M. Bianchi, R. Crinelli, V. Arbore, and M. Magnani, "Induction of ubiquitin C (UBC) gene transcription is mediated by HSF1: role of proteotoxic and oxidative stress," *FEBS Open Bio*, vol. 8, pp. 1471–1485, 2018.

[90] K. Arora and A. P. Naren, "Pharmacological correction of cystic fibrosis: molecular mechanisms at the plasma membrane to augment mutant CFTR function," *Current Drug Targets*, vol. 17, pp. 1275–1281, 2016.

[91] A. Ahner, X. Gong, and R. A. Frizzell, "Cystic fibrosis transmembrane conductance regulator degradation: cross-talk between the ubiquitylation and SUMOylation pathways," *The FEBS Journal*, vol. 280, pp. 4430–4438, 2013.

[92] E. L. Turnbull, M. F. Rosser, and D. M. Cyr, "The role of the UPS in cystic fibrosis," *BMC Biochemistry*, vol. 8, no. S1, p. S11, 2007.

[93] I. K. Popov, S. M. Hiatt, S. Whalen et al., "A YWHAZ variant associated with cardiofaciocutaneous syndrome activates the RAF-ERK pathway," *Frontiers in Physiology*, vol. 10, p. 388, 2019.

[94] K. L. Pennington, T. Y. Chan, M. P. Torres, and J. L. Andersen, "The dynamic and stress-adaptive signaling hub of 14-3-3: emerging mechanisms of regulation and context-dependent protein-protein interactions," *Oncogene*, vol. 37, pp. 5587–5604, 2018.

[95] K. Jiang, K. E. Poppenberg, L. Wong et al., "RNA sequencing data from neutrophils of patients with cystic fibrosis reveals potential for developing biomarkers for pulmonary exacerbations," *Journal of Cystic Fibrosis*, vol. 18, no. 2, pp. 194–202, 2019.

[96] J. A. Nick, L. A. Sanders, B. Ickes et al., "Blood mRNA biomarkers for detection of treatment response in acute pulmonary exacerbations of cystic fibrosis," *Thorax*, vol. 68, no. 10, pp. 929–937, 2013.

[97] V. Terlizzi, L. Claut, A. Tosco et al., "A survey of the prevalence, management and outcome of infants with an inconclusive diagnosis following newborn bloodspot screening for cystic fibrosis (CRMS/CFSPID) in six Italian centres," *Journal of Cystic Fibrosis*, vol. 20, no. 5, pp. 828–834, 2021.

Hindawi
BioMed Research International
Volume 2024, Article ID 9894720, 1 page
https://doi.org/10.1155/2024/9894720

Retraction

Retracted: Expression of miR-210, miR-137, and miR-153 in Patients with Acute Cerebral Infarction

BioMed Research International

Received 12 March 2024; Accepted 12 March 2024; Published 20 March 2024

This article has been retracted by Hindawi following an investigation undertaken by the publisher [1]. This investigation has uncovered evidence of one or more of the following indicators of systematic manipulation of the publication process:

(1) Discrepancies in scope

(2) Discrepancies in the description of the research reported

(3) Discrepancies between the availability of data and the research described

(4) Inappropriate citations

(5) Incoherent, meaningless and/or irrelevant content included in the article

(6) Manipulated or compromised peer review

The presence of these indicators undermines our confidence in the integrity of the article's content and we cannot, therefore, vouch for its reliability. Please note that this notice is intended solely to alert readers that the content of this article is unreliable. We have not investigated whether authors were aware of or involved in the systematic manipulation of the publication process.

Wiley and Hindawi regrets that the usual quality checks did not identify these issues before publication and have since put additional measures in place to safeguard research integrity.

We wish to credit our own Research Integrity and Research Publishing teams and anonymous and named external researchers and research integrity experts for contributing to this investigation.

The corresponding author, as the representative of all authors, has been given the opportunity to register their agreement or disagreement to this retraction. We have kept a record of any response received.

References

[1] H. Tian, Y. Zhao, C. Du, X. Zong, X. Zhang, and X. Qiao, "Expression of miR-210, miR-137, and miR-153 in Patients with Acute Cerebral Infarction," *BioMed Research International*, vol. 2021, Article ID 4464945, 9 pages, 2021.

Hindawi
BioMed Research International
Volume 2021, Article ID 4464945, 9 pages
https://doi.org/10.1155/2021/4464945

Research Article

Expression of miR-210, miR-137, and miR-153 in Patients with Acute Cerebral Infarction

Hongtao Tian,[1] Yan Zhao,[2] Chao Du,[2] Xiao Zong,[3] Xiuping Zhang,[4] and Xia Qiao[5]

[1]*Department of Neurosurgery, Qingdao Haizi Medical Group, Qingdao, 266000 Shandong Province, China*
[2]*Hemodialysis Room, Qingdao Haizi Medical Group, Qingdao, 266000 Shandong Province, China*
[3]*Qingdao Haizi Medical Group, Qingdao, 266000 Shandong Province, China*
[4]*Department of Ophthalmology, Liaocheng Guangming Eye Hospital, Liaocheng, 252000 Shandong Province, China*
[5]*Department of Neurology, Liaocheng People's Hospital, Liaocheng, 252000 Shandong Province, China*

Correspondence should be addressed to Xia Qiao; xiawoji52950@163.com

Received 29 July 2021; Revised 16 October 2021; Accepted 20 October 2021; Published 2 December 2021

Academic Editor: Jun Yang

Aim. To explore the expression levels of miR-210, miR-137, and miR-153 in patients with acute cerebral infarction. *Material and Methods.* 76 patients with acute cerebral infarction treated in our hospital from April 2016 to October 2017 were enrolled as the observation group. Another 64 normal patients were selected as the control group. The patients were divided into the death and survival groups based on 1-year mortality of patients. qRT-PCR was used to detect the expression of miR-210, miR-137, and miR-153 in the serum of each group. Receiver operating characteristic (ROC) curve was employed to analyze the diagnostic value and predictive value of miR-210, miR-137 and miR-153 death in patients. The correlation between miR-210, miR-137, and miR-153 in the serum of the observation group was analyzed by Pearson's test. *Results.* Levels of miR-210 and miR-137 in the observation group were significantly lower than those in the control group, while levels of miR-153 in the observation group were significantly higher than those in the control group (all $P < 0.05$). The ROC curve of diagnosis of acute cerebral infarction showed that the area under curve of miR-210 was 0.836, that of miR-137 was 0.843, and that of miR-153 was 0.842. The 1-year survival rate was 71.05%. The 1-year survival of the low-expression group of miR-210 and miR-137 was significantly lower than that of the high-expression group, while the 1-year survival of the low-expression group of miR-153 was significantly higher than that of the high-expression group (all $P < 0.05$). The ROC curve for predicting death showed that the area under curve of miR-210 was 0.786, that of miR-137 was 0.824, and that of miR-153 was 0.858. Pearson's correlation analysis showed that the expression of miR-210 was positively correlated with that of miR-137, while miR-137 was negatively correlated with that of miR-153 and miR-210 was negatively correlated with that of miR-153. *Conclusion.* miR-210, miR-137, and miR-153 have a certain value in the diagnosis and prediction of 1-year death of acute cerebral infarction and may be potential diagnostic and predictive indicators.

1. Introduction

Cerebral infarction is a kind of brain injury caused by obstruction of blood supply in the brain. The patients usually have sudden onset and will show symptoms in a short time. The incidence and mortality of cerebral infarction are much higher than those of other brain injury diseases [1, 2]. And most of acute stroke is acute cerebral infarction, which has become the main cause of global disability events [3, 4]. With the development of social aging, its incidence shows an upward trend [5]. The number of cerebral infarction patients worldwide was 33 million in 2010, and it would increase to 77 million by 2030 according to epidemiological speculation [6]. Therefore, we need some indicators to diagnose the disease and predict the prognosis, so that medical staff can carry out targeted and effective treatment according to the predicted situation.

MicroRNA is a class of small-molecule noncoding short-stranded RNA that regulates and influences the occurrence and development of diseases such as cancer and cardiovascular

Table 1: Primer sequences.

Gene	Upstream primer	Downstream primer
miR-210	5′-GTGCAGGGTCCGAGGT-3′	5′-TATCTGTGCGTGTGACAGCGGCT-3′
miR-137	5′-GAAATCCGACAGCTTAAGGAGGTTTGA-3′	5′-CATTGCACAGATAGGATTTGATTTACT-3′
miR-153	5′-UUGCAUAGUCACAAAAGUGAUC-3′	5′-TCCACCACCCAGTTGCTGTA -3′
U6	5′-CTCGCTTCGGCAGCACA-3′	5′-AACGCTTCACGAATTTGCGT-3′

and cerebrovascular diseases by their target proteins [7–9]. However, miR-210 can regulate brain-derived neurotrophic factor (BDNF). When miR-210 is overexpressed, microvessel density and the number of neuronal progenitor cells in the brain of ischemic mice can be increased, thus improving the neurobehaviour of ischemic mice [10]. The research progress of the role of BDNF in neural plasticity, neural protection, and neurogenesis may provide important information for the formulation of new poststroke rehabilitation strategies. It plays a regulatory role in poststroke kinematic learning and rehabilitation. When stroke patients recover, their BDNF will rise and protect the nerve [11–13]. Other miRNAs also regulate BDNF and may play a regulation role in stroke situations. miR-137 is associated with schizophrenia and some neurological disorders. Studies in [14] have suggested that miR-137 regulates the signal pathways related to schizophrenia and the convergence mechanism regulates neuronal responses to Nrg1α and BDNF, so as to alter the neural development, leading to the risk of schizophrenia. miR-153 is closely related to autism. High expression of miR-153 can inhibit the activation of the JAK-STAT signaling pathway by LEPR, thereby enhancing the expression of BDNF and the proliferation of hippocampal neurons and improving the condition of autistic mice [15]. miR-210, miR-137, and miR-153 all have the effect of regulating BDNF, and BDNF also plays a regulatory role in the development of cerebral infarction. However, the clinical effects of the expressions of miR-210, miR-137 and miR-153 in patients with acute cerebral infarction are still unclear.

Therefore, this study explored the clinical value of miR-210, miR-137, and miR-153 in patients with acute cerebral infarction and provided a reference for clinical treatment.

2. Method and Data

2.1. Clinical Data of Patients. 76 patients with acute cerebral infarction treated in our hospital from April 2016 to October 2017 were selected as the observation group in this study, including 45 males and 31 females, with an average age of 57.0 ± 6.4 years. Another 64 patients with normal physical examination were collected as the control group, including 42 males and 22 females, with an average age of 56.4 ± 6.2 years. The study was conducted with the approval of the Medical Ethics Committee. All patients were informed and signed the informed consent.

2.2. Inclusion of Exclusion Criteria

2.2.1. Inclusion Criteria. Acute stroke was diagnosed on the basis of imaging and pathology. The diagnostic criteria were in accordance with the guidelines issued by the American Heart Association Stroke Committee in 2013 [16]. All patients were hospitalized within 6 hours after onset of the disease. The patients could be followed up by telephone with completed clinical data.

2.2.2. Exclusion Criteria. The exclusion criteria are the following: patients with severe liver and kidney dysfunction, patients with malignant tumor history, patients who complicated with other malignant tumors, patients with severe cardiovascular and cerebrovascular diseases, patients with severe inflammation, and pregnant or lactating women.

2.3. Sample Collection. Five milliliters of venous blood was collected from health examinees in the morning and another five milliliters from patients in observation group after admission. The venous blood in the procoagulation tube was centrifuged at 24°C for 10 minutes at the speed of 3000 rpm. The serum was collected for the PCR test and stored at -80°C.

2.4. Major Kits and Instruments. The following are used in the study: hematology analyzer (Siemens, Germany, ADVIA2120i); PCR (ABI Company, USA, 7500); total RNA extraction kit EasyPure microNA Kit and reverse transcription + PCR kit TransScript microNA First-Strand cDNA Synthesis SuperMix (TransGen Biotech Company, Beijing, China, ER601-01, AT351-01); and primers (Shanghai Shenzhen University of Technology). The primers were designed and synthesized by Shanghai Biotechnology Co., Ltd. as shown in Table 1.

2.5. PCR Detection Method. The EasyPure miRNA Kit was used to extract the total RNA from serum, and the total RNA after extraction was tested for its purity, concentration, and integrity by ultraviolet spectrophotometer and agarose gel electrophoresis. Reverse transcription with total RNA using TransScript® miRNA RT Enzyme Mix and 2 × TS miRNA Reaction Mix was operated in strict accordance with the manufacturer's kit. Subsequently, PCR amplification experiments were carried out. The system of PCR reaction was as follows: 1 μL of cDNA, 0.4 μL of upstream and downstream primers, 10 μL of 2 × TransTaq® Tip Green qPCR SuperMix, 0.4 μL of Passive Reference Dye (50x), and finally ddH_2O added to 20 μL. The conditions of PCR reaction were as follows: predenaturation at 94°C for 30 s, denaturation at 94°C for 5 s, annealing at 60°C for 30 s, and a total of 40 cycles were performed. Each sample had three repetitive holes, and the experiment was carried out three times. In this study, U6 was taken as an internal reference and $2^{-\triangle ct}$ was used to analyze the data.

Table 2: Clinical data of patients.

Factors	Observation group ($n = 76$)	Control group ($n = 64$)	$t/\chi^2/Z$ value	P value
Gender				
Male	45 (59.21)	42 (65.63)	0.608	0.436
Female	31 (40.79)	22 (34.38)		
Age	57.0 ± 6.4	56.4 ± 6.2	0.561	0.576
BMI (kg/m^2)	23.65 ± 1.82	24.04 ± 1.97	1.216	0.226
Past medical history				
Hypertension	19 (25.00)	21 (32.81)	1.039	0.308
Diabetes	13 (17.11)	10 (15.63)	0.055	0.814
Hyperlipidemia	8 (10.53)	8 (12.50)	0.134	0.715
History of smoking				
Yes	19 (25.00)	18 (28.13)	0.175	0.676
No	57 (75.00)	46 (71.88)		
History of alcohol abuse				
Yes	9 (11.84)	10 (15.63)	0.424	0.515
No	67 (88.16)	54 (84.38)		
Place of residence				
City	58 (76.32)	50 (78.13)	0.065	0.800
Rural	18 (23.68)	14 (21.88)		
Platelet count (×10^9/L)	152.93 ± 54.41	147.23 ± 51.62	0.632	0.528
Total cholesterol (mmol/L)	6.58 ± 0.87	6.54 ± 0.83	0.782	0.277
Triglyceride (mmol/L)	3.32 ± 0.74	3.47 ± 0.81	1.144	0.255
Location of infarction				
Frontal lobe	12 (15.79)			
Temporal lobe	10 (13.16)			
Parietal lobe	9 (11.84)			
Occipital lobe	9 (11.84)			
Basal ganglia	10 (13.16)			
Thalamus	11 (14.47)			
Cerebellum	10 (13.16)			
Brainstem	5 (6.58)			
Infarct size				
Lacunar infarction	39 (51.32)			
Medium area infarction	23 (30.26)			
Massive infarction	14 (18.42)			

2.6. Follow-Up. A total of 76 patients or their families were followed up by telephone and visited every two months, lasting for one year.

2.7. Observation Indicators

2.7.1. Main Outcome Measure. The levels of miR-210, miR-137, and miR-153 were compared between the observation group and the control group. And 1-year survival of the patients was counted. Then, the receiver ROC was used to analyze the diagnostic value of miR-210, miR-137, and miR-153 in patients with acute cerebral infarction and predictive value of one-year mortality.

2.7.2. Secondary Outcome Measures. The secondary outcome measures following are follows: clinical data of the two groups; miR-210, miR-137, and miR-153 levels in survival patients and death patients; and correlation analysis between miR-210, miR-137, and miR-153 in the observation group.

2.8. Statistical Analysis. This study used SPSS20.0, a medical statistical analysis software (Chicago SPSS Co., Ltd.), to analyze the collected data. And GraphPad Prism 7 (San Diego GraphPad Software Co., Ltd.) was used to draw pictures of the collected data. A chi-square test was used for counting data utilization (%), represented by $X2$. Measurement data were expressed by the means ± standard deviation

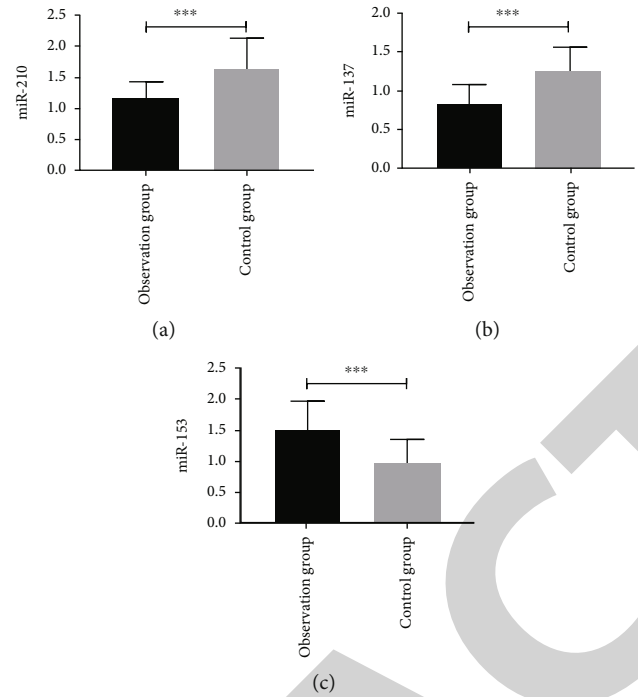

Figure 1: Expression of miR-210, miR-137 and miR-153 in the two groups. (a) Expression of miR-210 in the observation group was significantly lower than that in the control group ($t = 7.197$, $P < 0.001$). (b) miR-137 in the observation group was significantly lower than that in the control group ($t = 9.029$, $P < 0.001$). (c) miR-153 in the observation group was significantly higher than that in the control group ($t = 8.024$, $P < 0.001$). $***$ indicates $P < 0.001$.

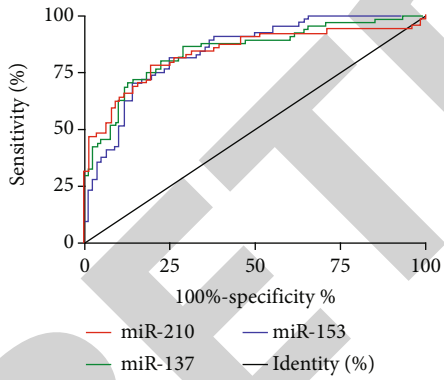

Figure 2: ROC of miR-210, miR-137 and miR-153 in the diagnosis of acute cerebral infarction. The area under curve of miR-210 is 0.836 (95% CI: 0.764-0.907), the area under curve of miR-137 is 0.843 (95% CI: 0.776-0.909), and area under curve of miR-153 is 0.842 (95% CI: 0.778-0.906).

(mean ± SD), which were in a normal distribution. The independent sample t-test was used to compare the two groups, expressed by t. ROC was used to evaluate the diagnostic value of miR-210, miR-137, and miR-153 in patients with acute cerebral infarction and the predictive value of 1-year mortality. K-M survival analysis revealed one-year survival condition of patients and analyzed by a log rank test. Pearson's test was used to analyze the correlation between miR-210, miR-137, and miR-153 in patients. $P < 0.05$ was considered statistically significant.

3. Results

3.1. Clinical Data of Patients. Clinical data of two groups were collected to compare. The results showed that there were no significant differences in gender, age, BMI, past medical history (hypertension, diabetes, hyperlipidemia), smoking history, alcoholism history, residence, platelet count, total cholesterol, and triglyceride between the two groups (all $P > 0.05$), as shown in Table 2.

3.2. Expression of miR-210, miR-137, and miR-153 in Two Groups of Patients. By comparing the expression of miR-210, miR-137, and miR-153, we found that miR-210 in the observation group (1.18 ± 0.26) was significantly lower than that in the control group (1.64 ± 0.48) ($P < 0.05$), and miR-137 in the observation group (0.84 ± 0.24) was significantly lower than that in the control group (1.26 ± 0.31) ($P < 0.05$), but miR-153 in the observation group (1.52 ± 0.45) was significantly higher than that in the control group (0.96 ± 0.36) ($P < 0.05$) (see Figure 1).

3.3. Diagnostic Value of miR-210, miR-137, and miR-153 in Patients with Acute Cerebral Infarction. The diagnostic value of ROC analysis in patients with acute cerebral infarction was drawn by analyzing the expression of miR-210, miR-137, and miR-153 in the observation group and the control group. The area under curve of miR-210 was 0.836 (95% CI: 0.764-0.907); the area under curve of miR-137 was 0.843 (95% CI: 0.776-0.909); and the area under curve of miR-153 was 0.842 (95% CI: 0.778-0.906) (see Figure 2 and Table 3).

Table 3: ROC curve data.

Indicators	AUC	95% CI	Specificity	Sensitivity	Youden index	Cut-off
miR-210	0.836	0.764~0.907	81.58%	71.88%	53.46%	1.401
miR-137	0.843	0.776~0.909	85.53%	70.31%	55.84%	1.121
miR-153	0.842	0.778~0.906	73.68%	81.25%	54.93%	1.299

AUC: area under curve; cut-off: cut point.

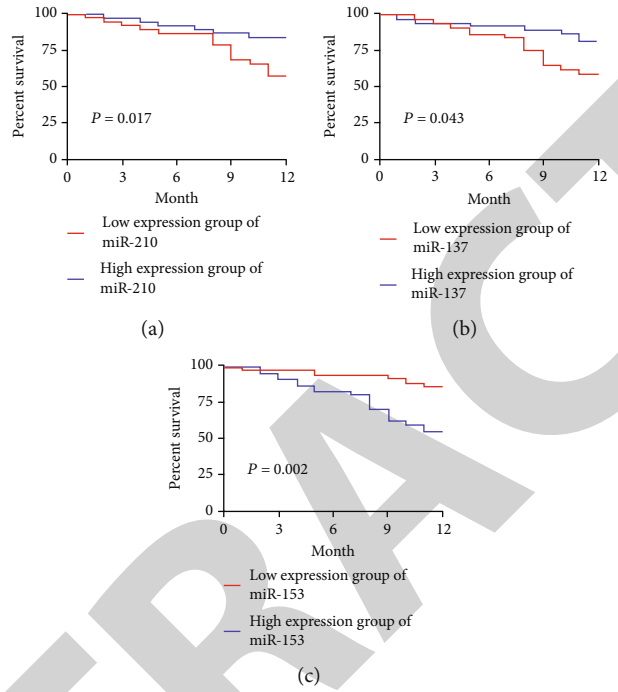

Figure 3: (a) The survival of miR-210 in the low-expression group was significantly lower than that of the high-expression group ($P = 0.017$). (b) The survival of miR-137 in the low-expression group was significantly lower than that of the high-expression group ($P = 0.043$). (c) The survival of miR-153 in the low-expression group was significantly higher than that of the high-expression group ($P = 0.002$).

3.4. One-Year Survival in the Two Groups. According to the one-year survival statistics of the patients in the observation group, 76 patients were followed up, and 0 patient failed to be followed up. 22 patients died, and 54 patients survived within one year, with a survival rate of 71.05%. The patients were divided into the high and low-expression groups based on the median expression of miR-210, miR-137, and miR-153. The K-M curve showed that the one-year survival of miR-210 and miR-137 in the low-expression group was significantly lower than that in the high-expression group ($P < 0.05$) and the one-year survival of miR-153 in the low-expression group was significantly higher than that in the high-expression group ($P < 0.05$, see Figure 3).

3.5. Expression of miR-210, miR-137, and miR-153 in the Survival and Death Groups of Patients. According to the one-year survival condition of the patients in the observation group, the patients were divided into the survival group and the death group. After comparing the expressions of miR-210, miR-137, and miR-153 in the two groups, it was found that miR-210 (1.01 ± 0.13) in the death group was significantly lower than that in the survival group (1.26 ± 0.20) ($P < 0.05$) and miR-137 (0.65 ± 0.15) in the death group was significantly lower than that in the survival group (0.94 ± 0.21) ($P < 0.05$). miR-153 in the death group (1.84 ± 0.23) was significantly higher than that in the survival group (1.39 ± 0.38) ($P < 0.05$, see Figure 4).

3.6. Predictive Value of miR-210, miR-137, and miR-153 in Patients with 1-Year Mortality. The predictive value of ROC analysis in patients with one-year mortality was drawn by analyzing the expression of miR-210, miR-137, and miR-153 in the survival and death groups. It was found that the area under curve of miR-210 was 0.786 (95% CI: 0.680-0.893); the area under curve of miR-137 was 0.824 (95% CI: 0.730-0.918); and the area under curve of miR-153 was 0.858 (95% CI:0.771-0.945) (see Figure 5 and Table 4).

3.7. Correlation Analysis between miR-210, miR-137, and miR-153 in the Observation Group. Through Pearson's analysis of the relationship between miR-210, miR-137, and miR-153 in the observation group, it was found that the expression of miR-210 was positively correlated with miR-

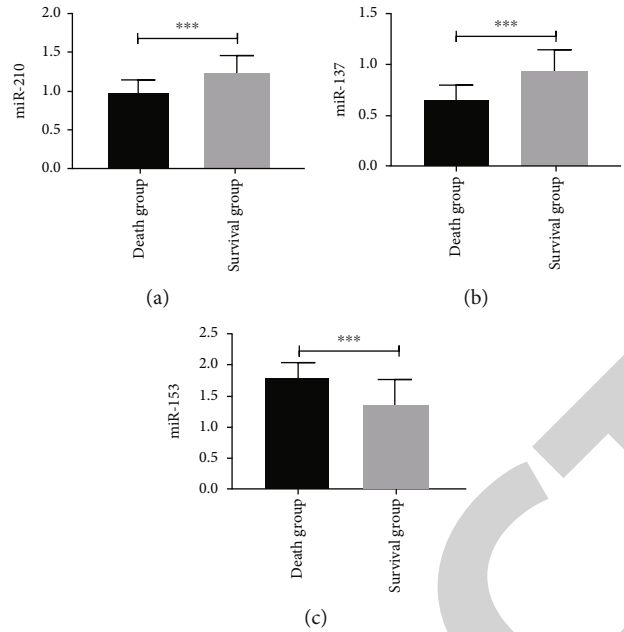

Figure 4: Expression of miR-210, miR-137, and miR-153 in survival and death patients. (a) miR-210 in the death group was significantly lower than that in the survival group ($t = 5.405$, $P < 0.001$). (b) miR-137 in the death group was significantly lower than that in the survival group ($t = 5.884$, $P < 0.001$). (c) miR-153 in the death group was significantly higher than that in the survival group ($t = 5.170$, $P < 0.001$). $***$ indicates $P < 0.001$.

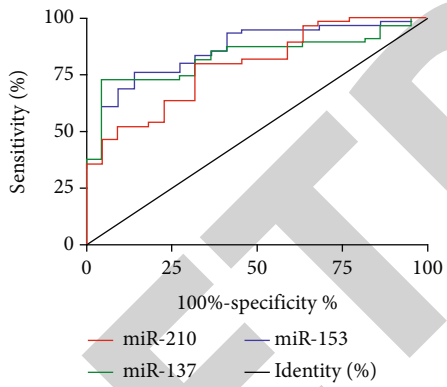

Figure 5: ROC of miR-210, miR-137, and miR-153 predicted patient death. The area under curve of miR-210 was 0.786 (95% CI: 0.680-0.893), the area under curve of miR-137 was 0.824 (95% CI: 0.730-0.918), and area under curve of miR-153 was 0.858 (95% CI: 0.771-0.945).

137, while the expression of miR-137 was negatively correlated with miR-153, and the expression of miR-210 was negatively correlated with miR-153, as shown in Figure 6.

4. Discussion

Acute cerebral infarction can cause severe brain damage [17, 18]. Some of the microRNAs that are proposed to be expressed in the brain will also change. Some of these microRNAs will also change with the severity and alleviation of the disease. And some of them are expected to serve as potential diagnostic and predictive indicators of disease or as a new direction of treatment [19, 20].

MicroRNA-210, a master and pleiotropic hypoxia-miRNA, plays multiple roles in brain ischemia. The current finding that pretreatment with miR-210 inhibitor significantly attenuated hypoxia-ischemia- (HI-) induced brain infarct size suggests that miR-210 has a functional significance in the pathophysiology of HI-induced brain injury in the developing brain. This finding is consistent with the previous study, which found that silencing miR-210 with miR-210-LNA via intracerebroventricular or intranasal delivery induced a neuroprotective effect on neonatal brain HI insult [21]. Wang et al. [22] provide new evidence that miR-210 may be involved in the nicotine-induced epigenetic mechanism. Perinatal nicotine exposure enhances miR-210 expression, but decreases the neurotrophic protein (BDNF/TrkB) expression in neonatal brains and subsequent development of brain hypoxic-ischemia sensitive phenotype in neonates. Thomas et al. reported that miR-137 regulates target proteins within the phosphoinositide 3-kinase-Akt-mechanistic target of rapamycin (PI3K-Akt-mTOR) pathway, which acts downstream of ErbB receptors. Nrg1α increases phospho-S6 (Ser235/236) levels, mRNA translation, AMPA receptor levels, and outgrowth in the dendrites of primary neurons. Chronic inhibition of miR-137 reverses or abolishes the effects of Nrg1α signaling by all measures. Inhibition of miR-137 also abolishes dendritic outgrowth and mRNA translation induced by BDNF [14]. miR-153, an intronic miRNA recognized as a modulator of alpha-synuclein at posttranscription level, has been identified to be a significant component of the brain with an example that reflects synuclein expression in different tissues in the period of neuronal development, indicating that they take coordinated effects in alpha-synuclein. As You et al. described [15], miR-153

Table 4: ROC curve data.

Indicators	AUC	95% CI	Specificity	Sensitivity	Youden index	Cut-off
miR-210	0.786	0.680-0.893	68.18%	77.78%	45.96%	1.115
miR-137	0.824	0.730-0.918	85.53%	95.45%	80.98%	0.867
miR-153	0.858	0.771-0.945	81.82%	75.93%	57.75%	1.609

AUC: area under curve; cut-off: cut point.

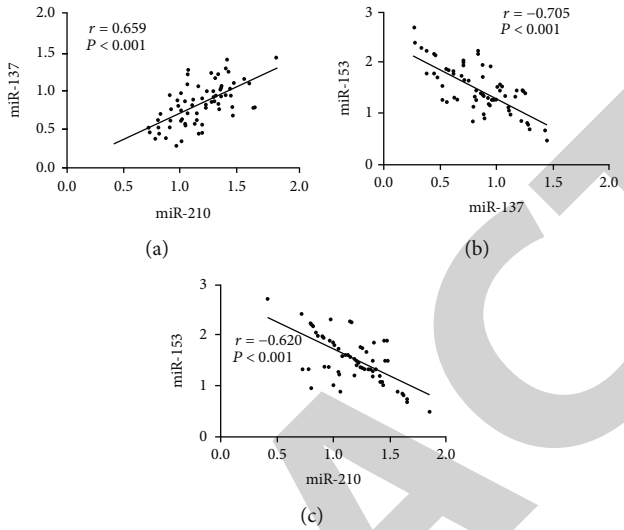

Figure 6: Correlation between miR-210, miR-137, and miR-153 in the observation group. (a) Expression of miR-210 was positively correlated with miR-137 ($r = -0.705, P < 0.001$). (b) Expression of miR-137 was negatively correlated with miR-153 ($r = -0.620, P < 0.001$). (c) Expression of miR-210 was negatively correlated with miR-153 ($r = 0.659, P < 0.001$).

blocked the JAK-STAT signaling pathway through the inhibition of leptin receptor (LEPR), thus regulating BDNF expression and proliferation of hippocampal neurons. Fragkouli and Doxakis also suggested that miR-153 provides protection for neurons against death by downregulating the mTOR signaling pathway [23].

In this study, the expression of miR-210, miR-137, and miR-153 in the observation group and the control group were detected by PCR. The results showed that the expression of miR-210 and miR-137 in the observation group was significantly lower than that in the control group, while the expression of miR-153 was significantly higher than that in the control group. In the study of Jiang et al. [24], it was mentioned that vagus nerve stimulation can exert neuroprotective effects on cerebral ischemia rats, which thus increased expression of miR-210 and decreased antioxidative stress response. The benefits of VNS are weakened after miR-210 knockdown, so they believe that miR-210 mediates antioxidant stress to improve cerebral ischemia. Other studies have also shown that the expression of miR-137 in astrocytes from the hypoxic and glucose-deficient environment to normal environment will also increase [25]. Therefore, we suspect that the expression of miR-210 and miR-137 may decrease with the alleviation of the patient's condition. At the same time, the difference between the two groups also suggests that miR-210, miR-137, and miR-153 may have a potential diagnostic value in acute cerebral infarction. Therefore, we used the ROC curve to find that the area under curve of miR-210 is 0.836. When the cut-off point is 1.401, the best specificity and sensitivity are 81.58% and 71.88%. The area under curve of miR-137 is 0.843. When the cut-off point is 1.121, the best specificity and sensitivity are 70.31% and 55.84%. The area under curve of miR-153 is 0.842. When the cut-off point is 1.299, the best specificity and sensitivity are 73.68% and 81.25%. These results suggest that miR-210, miR-137, and miR-153 may be potential diagnostic indicators for acute cerebral infarction. Yang et al. [26] also compared the expression of miR-153 in cerebral infarction patients and normal people in their study. It was found that the expression of miR-153 in patients with cerebral infarction was also higher than that in normal people. Then, they also found that miR-153 had a good diagnostic ability in the diagnosis of cerebral infarction through ROC curve analysis, which further confirmed our conclusion.

Death has always been a major threat to acute cerebral infarction. Several studies have found that the severity of admission symptoms, insular infarction, and cerebral infarction in patients with acute cerebral infarction are independent predictors of clinical prognosis [27, 28]. We followed up the patients in the observation group for one year and found that the one-year survival rate was 71.05%. The one-year survival of the low-expression group of miR-210 and miR-137 was significantly lower than that of the high-expression group, while the one-year survival of the low-expression group of miR-153 was significantly higher than that of the high-expression group. The results suggest that

the expression of miR-210, miR-137, and miR-153 may predict one-year survival of patients. Therefore, we first compared the expression of miR-210, miR-137, and miR-153 between the death and the survival patients. We found that the expression of miR-210 and miR-137 in the death group was significantly lower than that in the survival group, and the expression of miR-153 was significantly higher than that in the survival group. We then mapped the ROC curves of miR-210, miR-137, and miR-153 predicting death within 1 year based on the expression of survival patients and death patients. We found that the area under curve of miR-210 was 0.786. The optimal specificity and sensitivity were 6.81% and 77.78%, and the area under curve of miR-137 was 0.824. When the cut-off point was 0.867, the best specificity and sensitivity were 85.53% and 95.45%. The area under curve of miR-153 is 0.858. When the cut-off point is 1.609, the best specificity and sensitivity are 81.82% and 75.93%. Therefore, miR-210, miR-137, and miR-153 have a certain predictive value for one-year survival of patients and may become potential predictors.

At the end of the study, we analyzed the relationship between miR-210, miR-137, and miR-153 by Pearson's correlation. It was found that the expression of miR-210 was positively correlated with miR-137, miR-137 was negatively correlated with miR-153, and miR-210 was negatively correlated with miR-153, suggesting that there may be a close relationship between miR-210, miR-137, and miR-153. However, there are still some limitations in this study. Firstly, our study did not include the corresponding treatment research. Whether the indicators before and after the study will change is not clear. Secondly, this study did not collect the expression of miR-210, miR-137, and miR-153 in patients after being discharged from hospital. Finally, this study was only used as a clinical trial. It is not clear what the relationship between miR-17-5p and NLR is. Therefore, we hope to add some basic experiments in future research to explore the relationship between miR-17-5p and NLR and to verify the results of our research.

In summary, miR-210, miR-137, and miR-153 have a certain value in the diagnosis and prediction of 1-year death of acute cerebral infarction and may be potential diagnostic and predictive indicators.

Data Availability

The datasets used and/or analyzed during the current study are available from the corresponding author on reasonable request.

Ethical Approval

The study was approved by the Ethics Committee of People's Hospital of Shouguang City, China.

Consent

Patients who participated in this research signed the informed consent and had complete clinical data. Signed written informed consents were obtained from the patients and/or guardians.

Conflicts of Interest

The authors declare that they have no competing interests.

Authors' Contributions

Hongtao Tian designed the study and drafted the manuscript. Yan Zhao, Chao Du, Xiao Zong, and Xiuping Zhang was responsible for the collection and analysis of the experimental data. Xia Qiao revised the manuscript critically for important intellectual content. All authors read and approved the final manuscript.

References

[1] L. Bozzao, L. M. Fantozzi, S. Bastianello, A. Bozzao, and C. Fieschi, "Early collateral blood supply and late parenchymal brain damage in patients with middle cerebral artery occlusion," *Stroke*, vol. 20, no. 6, pp. 735–740, 1989.

[2] J. Wang, Z. Hu, S. Yang et al., "Inflammatory cytokines and cells are potential markers for patients with cerebral apoplexy in intensive care unit," *Experimental and Therapeutic Medicine*, vol. 16, no. 2, pp. 1014–1020, 2018.

[3] S. Haq, M. Mathur, J. Singh, N. Kaur, R. S. Sibia, and R. Badhan, "Colour Doppler evaluation of extracranial carotid artery in patients presenting with acute ischemic stroke and correlation with various risk factors," *Journal of Clinical and Diagnostic Research*, vol. 11, no. 3, 2017.

[4] J. He, Y. Zhang, T. Xu et al., "Effects of immediate blood pressure reduction on death and major disability in patients with acute ischemic stroke: the CATIS randomized clinical trial," *JAMA*, vol. 311, no. 5, pp. 479–489, 2014.

[5] M. Okon, N. I. Adebobola, S. Julius et al., "Stroke incidence and case fatality rate in an urban population," *Journal of Stroke and Cerebrovascular Diseases*, vol. 24, no. 4, pp. 771–777, 2015.

[6] Y. Béjot, B. Daubail, and M. Giroud, "Epidemiology of stroke and transient ischemic attacks: current knowledge and perspectives," *Revue Neurologique*, vol. 172, no. 1, pp. 59–68, 2016.

[7] H. Schwarzenbach, N. Nishida, G. A. Calin, and K. Pantel, "Clinical relevance of circulating cell-free microRNAs in cancer," *Nature Reviews Clinical Oncology*, vol. 11, no. 3, pp. 145–156, 2014.

[8] B. Dewdney, A. Trollope, J. Moxon, D. Thomas Manapurathe, E. Biros, and J. Golledge, "Circulating microRNAs as biomarkers for acute ischemic stroke: a systematic review," *Journal of Stroke and Cerebrovascular Diseases*, vol. 27, no. 3, pp. 522–530, 2018.

[9] K. Pulkkinen, T. Malm, M. Turunen, J. Koistinaho, and S. Ylä-Herttuala, "Hypoxia induces microRNA miR-210 in vitro and in vivo: ephrin-A3 and neuronal pentraxin 1 are potentially regulated by miR-210," *FEBS Letters*, vol. 582, no. 16, pp. 2397–2401, 2008.

[10] L. L. Zeng, X. S. He, J. R. Liu, C. B. Zheng, Y. T. Wang, and G. Y. Yang, "Lentivirus-mediated overexpression of microRNA-210 improves long-term outcomes after focal cerebral ischemia in mice," *CNS Neuroscience & Therapeutics*, vol. 22, no. 12, pp. 961–969, 2016.

Hindawi
BioMed Research International
Volume 2024, Article ID 9867070, 1 page
https://doi.org/10.1155/2024/9867070

Retraction

Retracted: The Protective Effects of miR-21-Mediated Fibroblast Growth Factor 1 in Rats with Coronary Heart Disease

BioMed Research International

Received 12 March 2024; Accepted 12 March 2024; Published 20 March 2024

This article has been retracted by Hindawi following an investigation undertaken by the publisher [1]. This investigation has uncovered evidence of one or more of the following indicators of systematic manipulation of the publication process:

(1) Discrepancies in scope

(2) Discrepancies in the description of the research reported

(3) Discrepancies between the availability of data and the research described

(4) Inappropriate citations

(5) Incoherent, meaningless and/or irrelevant content included in the article

(6) Manipulated or compromised peer review

The presence of these indicators undermines our confidence in the integrity of the article's content and we cannot, therefore, vouch for its reliability. Please note that this notice is intended solely to alert readers that the content of this article is unreliable. We have not investigated whether authors were aware of or involved in the systematic manipulation of the publication process.

Wiley and Hindawi regrets that the usual quality checks did not identify these issues before publication and have since put additional measures in place to safeguard research integrity.

We wish to credit our own Research Integrity and Research Publishing teams and anonymous and named external researchers and research integrity experts for contributing to this investigation.

The corresponding author, as the representative of all authors, has been given the opportunity to register their agreement or disagreement to this retraction. We have kept a record of any response received.

References

[1] B. Zhang, H. Liu, G. Yang, Y. Wang, and Y. Wang, "The Protective Effects of miR-21-Mediated Fibroblast Growth Factor 1 in Rats with Coronary Heart Disease," *BioMed Research International*, vol. 2021, Article ID 3621259, 9 pages, 2021.

Hindawi
BioMed Research International
Volume 2021, Article ID 3621259, 9 pages
https://doi.org/10.1155/2021/3621259

Research Article

The Protective Effects of miR-21-Mediated Fibroblast Growth Factor 1 in Rats with Coronary Heart Disease

Bin Zhang,[1] Hongguang Liu,[2] Guoping Yang,[3] Yongmei Wang,[4] and Yan Wang[5]

[1]*Department of Cardiology, Affiliated Hospital of Taishan Medical College, China*
[2]*Department of Cardiology, Liaocheng Third People's Hospital, China*
[3]*Department of Cardiology, Zhoucun District People's Hospital of Zibo City, China*
[4]*Department of Cardiology, Tai'an Central Hospital, China*
[5]*Department of Cardiology, Qingdao Central Hospital, China*

Correspondence should be addressed to Yongmei Wang; woyong2982233@163.com

Received 30 September 2021; Revised 23 October 2021; Accepted 25 October 2021; Published 1 December 2021

Academic Editor: Jianxin Shi

Aim. The study is to verify the protective effects of miR-21-mediated fibroblast growth factor 1 (FGF1) against myocardial ischemia in rats with coronary heart disease. *Materials and Methods*. Sprague-Dawley (SD) rat models of myocardial ischemia/reperfusion (MI/R) injury were constructed, and the expression of miR-21 and FGF1 in them was interfered through ischemic postconditioning. The protective effects of miR-21-mediated FGF1 on myocardium of the model rats were analyzed, and the targeted regulatory relationship between miR-21 and FGF1 was verified through myocardial cell experiments to find the mechanism of miR-21. *Results*. MiR-21 and FGF1 with increased expression could protect the cardiac function of model rats and improve their diastolic blood pressure (DBP), systolic blood pressure (SBP), heart rate (HR), coronary flow (CF), bax, and bcl-2 levels, but it would also cause further increase of vascular endothelial growth factor (VEGF) and decreased infarct size (INF). In addition, intervention through both miR-21 mimics and recombinant human FGF1 could highlight the above changes. Pearson correlation analysis revealed that the expression of miR-21 was positively correlated with that of FGF1, and both miR-21 and FGF1 were significantly and linearly correlated with DBP, SBP, HR, CF, INF, bax, and bcl-2, but they were not significantly correlated with the VEGF level. The myocardial cell experiment results revealed that upregulation of miR-21 or FGF1 could alleviate apoptosis caused by hypoxia/reoxygenation of myocardial cells, and inhibition of the FGF1 expression could hinder the effect of miR-21 against apoptosis of myocardial cells. Dual luciferase reporter assay revealed that transfection of miR-21-mimics could effectively raise the fluorescence intensity of pmirGLO-FGF1-3′UTR Wt but had no significant effect on that of pmirGLO-FGF1-3′UTR Mut. *Conclusion*. MiR-21 can specifically mediate the expression of FGF1 to relieve MI/R injury, protect the cardiac function, and resist apoptosis.

1. Introduction

Cardiovascular diseases are the major causes of death and disability worldwide, contributing to 30% of the global mortality and 10% of global burden of disease (1, 2). With the global population increase and population aging, from 1990 to 2013, the number of patients dead for cardiovascular diseases increased by 41% (3), of which about 8,200,000 people died of ischemic heart disease every year (4). Interruption of cardiac blood supply will seriously damage myocardial cells. Although interventional therapy can greatly help to restore cardiac coronary perfusion, but contradictorily, the reperfusion will further damage myocardium, and interventional therapy is unable to rebuild microvascular circulation (5, 6).

MicroRNAs (miRNAs), a kind of short-chain noncoding RNA with 20 bp-long nucleotides, widely exist in animals and plants, which regulates mRNA translation by binding to the 3′ untranslated region targeting mRNA, so it plays an important role in cardiovascular diseases including heart failure (7, 8). miRNAs also play an important role in development of myocardial cells and their survival under stress conditions (9). Previous research results revealed that miR-21 was involved in myocardial ischemia/reperfusion (MI/R) injury, and the protection mechanism of trimetazidine against MI/R injury was its promotion to the expression of miR-21 (10). In addition, the verification results of animal models also revealed that miR-21 could protect the cardiac function of rats with cardiac ischemia injury and reduce

Table 1: Primer sequences.

	Forward primer	Reverse primer
MiR-21	5′-GCGGCAACACCAGTCGATG-3′	5′-TGCGTGTCGTGGAGTC-3′
U6	5′-GCGCGTCGTGAAGCGTTC-3′	5′-GTGCAGGGTCCGAGGT-3′

myocardial cell apoptosis of them (11). It can also protect the endothelial cells through phosphatase gene/vascular endothelial growth factor (VEGF) pathway (12). Fibroblast growth factor 1 (FGF1) is an important regulator of angiogenesis, which directly acts on myocardial cells to maintain the integrity of myocardial function and structure (12). Recently, it was reported that there were targeted binding sites between miR-21 and FGF1, and miR-21 could promote chondrocyte proliferation and suppress apoptosis of them by inhibiting the expression of FGF1 (13).

Whether the interaction between miR-21 and FGF1 in chondrocytes also exists in cardiomyocytes and whether the interaction affects the protective effects of miR-21 and FGF1 against myocardial ischemia injury and reperfusion are still under investigation. In order to find it, this study carried out the following analysis.

2. Materials and Methods

2.1. Establishment of Rat Models of Ischemia-Reperfusion (I/R). A total of 60 mature Sprague-Dawley (SD) rats (strain code: 101; SCXK (Hu): 2017-0011) were all adaptively fed with general nutritious feedstuff (Beijing Zhecheng Technology Co., Ltd.) for one week after being purchased from Beijing Vital River Laboratory Animal Technology Co., Ltd., and the rats were fasted overnight and allowed to drink freely. Among the 60 rats, 40 of them were selected by the random number table method to prepare rat models of MI/R (14), and 10 of them were selected as a control group (CON group) and not intervened through surgery. The rest 10 rats were taken as a Sham operation group (Sham group) and intervened with thoracotomy to separate vessels but no operations about ischemia and perfusion. The 40 rats were intraperitoneally injected with pentobarbital sodium (Sigma, St. Louis, USA, 40 mg/kg) and ventilated with a positive pressure ventilator (ALC-V8, Shanghai, China). Before surgery, the tail clip test was used to check the sufficiency of anesthesia. Thorax was opened at the fourth intercostal space to free the left anterior descending coronary artery (LAD), and ligation was performed at the junction of left auricle and the site 1-2 mm below the boundary of pulmonary cone. The LAD was clamped for 30 minutes and then released for 120 minutes. The 40 model rats were divided into a model group (model group), a miR-21 mimics treatment group (miR-21 group), a FGF1 treatment group (FGF1 group), and a miR-21 mimics+ FGF1 treatment group (combination group) using the random number table method. During the release period of LAD, rats in the miR-21 group were treated with 100 μL of 50 mg/kg miR-21 mimics through intramuscular injection at 10 different sites in the anterior wall of the left heart after being pretreated with liposome 2000, and rats in the FGF1 group were given recombinant human FGF1 through intravenous drip at 10 μg/kg for 10 minutes. The miR-21 mimics was designed and synthesized by Shanghai Gene Pharma Co., Ltd., and recombinant human FGF1 (item number: 13241013) was purchased from the Thermo Fisher Scientific.

2.2. Electrophysiological Measurement of Rats. An electrophysiological signal recorder (Avante Trading (Beijing) Co., Ltd.) was employed to determine the diastolic blood pressure (DBP), systolic blood pressure (SBP), heart rate (HR), and coronary flow (CF) at the left ventricular of each rat in each group.

2.3. Measurement of Infarct Size. The living rats were executed by cervical dislocation after being measured fully, and their myocardial infarct size (INF) was measured based on cardiac tissues sampled from the rats using the computer planimetric method by referring to the method provided by Sodha et al. (15)

2.4. Construction and Transfection of Expression Vectors. All expression vectors were designed and synthesized by Shanghai Gene Pharma Co., Ltd., including miR-21 mimics, si-FGF1, sh-FGF1, pmirGLO-FGF1-3′UTR wild type (Wt), pmirGLO-FGF1-3′UTR mutant type (Mut), and blank vector, pmirGLO-NC. At 24 h before transfection, the cells were digested with trypsin, and then, the cells were transfected with expression vectors when the cell fusion reached about 80% according to specific operation steps in the kit instructions. Subsequently, the cells were cultured in an incubator with 5% CO_2 at 37°C for 48 h, and the culture medium was replaced every 6 h. Quantitative real time polymerase chain reaction (qRT-PCR) was adopted to determine the transfection results. Cells not transfected were used as a control group. The Lipofectamine TM2000 transfection kit (item number: 35050) was purchased from the Invitrogen Company in the United States.

2.5. Grouping and Processing. Myocardial cells were separated from the heart of newborn SD rats (age ≤ 3 days) and cultured by referring to the method proposed by Sadoshima et al. (16), and they were determined using the specific labeling immunofluorescence staining. The cells were divided into a normal cell group, a cell model group, a miR-21 mimic group, a sh-FGF1 group, and a miR-21 mimics+ si-FGF1 group. Myocardial cells in the later three groups were transfected with miR-21 mimics, sh-FGF1, and miR-21 mimics+ si-FGF1, respectively.

2.6. Myocardial Cell Model. Myocardial cells were subject to hypoxic treatment under 3%O_2, 5%CO_2, and 92%N_2 for 24 hours and then were reoxygenated under 5%CO_2 and 95% air for 3 hours.

2.7. qRT-PCR. The total RNA was extracted from myocardial tissues and myocardial cells using TRIzol reagent, respectively,

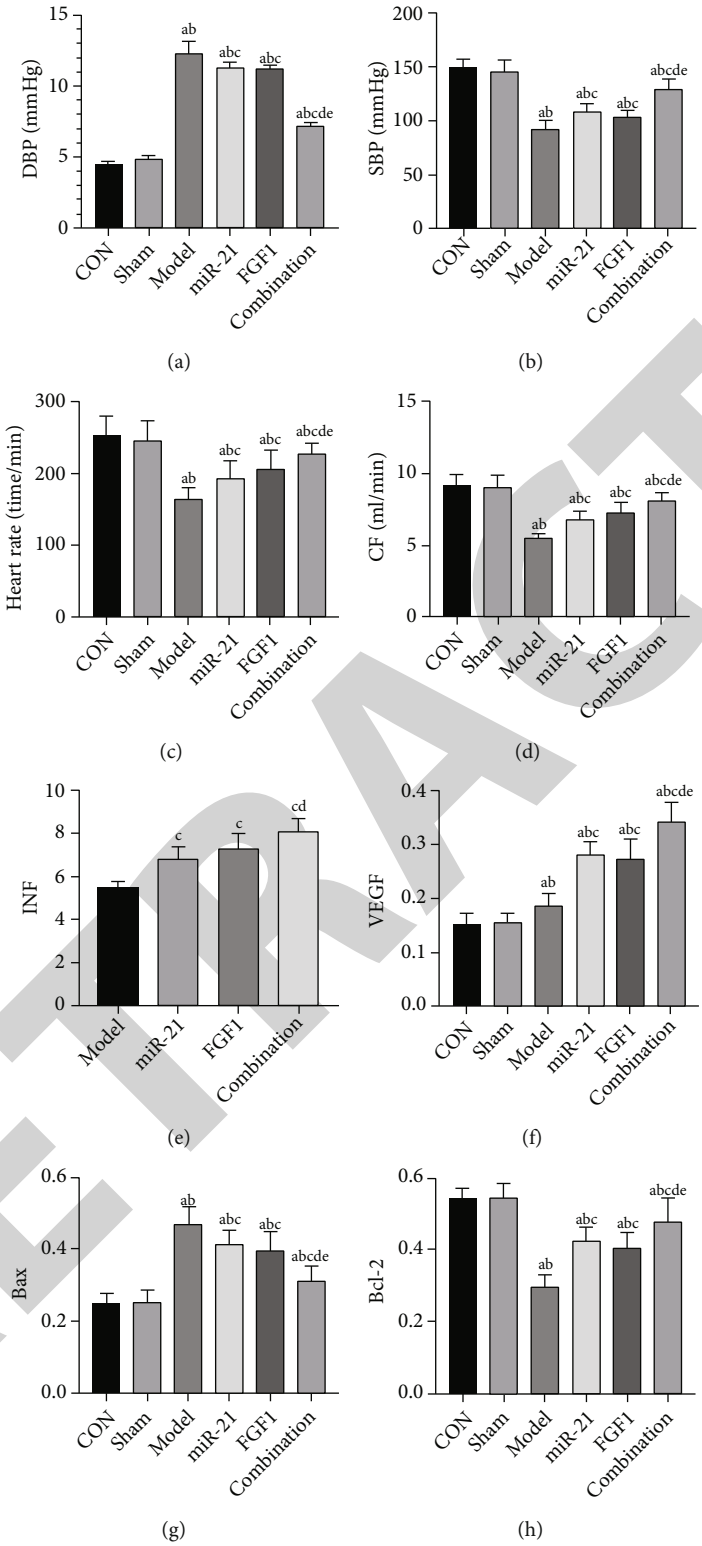

Figure 1: Protective effects of miR-21 and FGF1 against MI/R injury: (a) changes of DBP in rats; (b) changes of SBP in rats; (c) changes in HR in rats; (d) changes of CF in rats; (e) changes of INF in rats; (f) changes of VEGF in rats; (g) changes of bax in rats; (h) changes of bcl-2 in rats. A: in comparison with the CON group, $P < 0.05$; B: in comparison with the Sham group, $P < 0.05$; C: in comparison with the model group, $P < 0.05$; D: in comparison with the miR-21 group, $P < 0.05$; E: in comparison with the FGF1 group, $P < 0.05$. DBP: diastolic blood pressure; SBP: systolic blood pressure; HR: heart rate; CF: coronary flow.

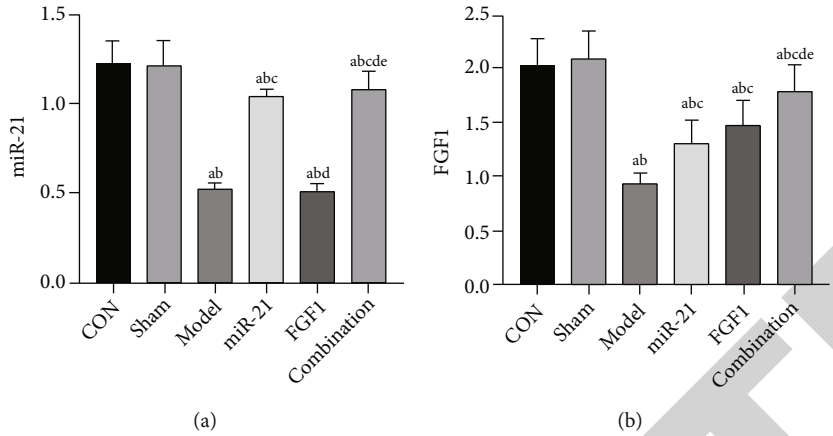

Figure 2: The expression of miR-21 and FGF1 in myocardial tissues: (a) changes of miR-21 in rats; (b) changes of FGF1 in rats. A: in comparison with the CON group, $P < 0.05$; B: in comparison with the Sham group, $P < 0.05$; C: in comparison with the model group, $P < 0.05$; D: in comparison with the miR-21 group, $P < 0.05$; E: in comparison with FGF1, $P < 0.05$. CON: control group.

and the purity, concentration, and integrity of the total RNA were determined using a ultraviolet spectrophotometry and through agarose gel electrophoresis. The A260/A280 value between 1.8 and 2.1 was considered to meet the experimental requirements. The first strand cDNA was synthesized according to the kit instructions, and then, polymerase chain reaction (PCR) amplification was performed through a PCR system that consisted of 20 μL of the total volume containing 0.4 μL of upstream and downstream primers, respectively, 10 μL of 2 × TransTaq® Tip Green qPCR SuperMix, 0.4 μL of Passive Reference Dye (50x), and ddH2O to adjust the volume under predenaturation at 95°C for 30 s followed by 40 cycles of denaturation at 95°C for 5 s, and annealing and extension at 60°C for 30 s. The primer sequences are shown in Table 1.

2.8. Dual Luciferase Reporter Assay. Myocardial cells were transfected with pmirGLO-FGF1-3′UTR Wt, pmirGLO-FGF1-3′UTR Mut, miR-21-mimics, and miR-NC, respectively, after they were cultured to logarithmic growth phase. At 48 h after transfection, the fluorescence intensity of them was detected using the dual luciferase determination system.

2.9. Cell Apoptosis Determination. The cells were digested with 0.25% trypsin. After digestion, the cells were washed with PBS two times and then added with 100 μL of binding buffer to prepare $1 * 10^6$ cells/mL suspension. The suspension was added with AnnexinV-FITC and PI in order, incubated at room temperature for 5 min in the dark, and finally detected using the CytoFLE S flow cytometer system. The experiment was repeated three times, and the average value was taken. Annexin V-FITC/PI apoptosis determination kit (item number: V35113) was purchased from the Invitrogen Company in the United States.

2.10. Statistical Analysis. SPSS19.0 (Asia Analytics Formerly SPSS, China) was adopted for statistical analysis. Comparison between two groups was carried out using the *t*-test, while comparison among multiple groups was performed using the Analysis of Variance. Post hoc analysis was carried out by the LSD test, and correlation analysis was conducted using the Pearson correlation analysis. $P < 0.05$ indicated a significant difference.

3. Results

3.1. Protective Effects of miR-21 and FGF1 against MI/R Injury. As shown in Figure 1, the CON group was not different from the Sham group in the levels of DBP, SBP, HR, CF, VEGF, bax, and bcl-2 (all $P > 0.05$), and both groups showed no myocardial infarction. However, compared with the CON group and the Sham group, the model group showed increased DBP and HR (both $P < 0.05$), decreased SBP and CF (both $P < 0.05$), and large area of myocardial infarction, and it also showed increased VEGF and bax levels and decreased bcl-2 level in myocardial tissues (all $P < 0.05$). Rats intervened with miR-21 mimics, or recombinant human FGF1 showed improved levels of DBP, SBP, HR, bax, and bcl-2 (all $P < 0.05$) and also showed further improvement of VEGF and decrease in INF (both $P < 0.05$). Meantime, the intervention of both miR-21 mimics and recombinant human FGF1 contributed to more significant changes ($P < 0.05$).

3.2. The Expression of miR-21 and FGF1 in Myocardial Tissues. We determined the expression of miR-21 and FGF1 in myocardial tissues of rats in each group to find out whether the intervention was successful. It was turned out that the CON group was not different from the Sham group in the expression of miR-21 and FGF1 (both $P > 0.05$), but compared with the CON group and the Sham group, the model group showed decreased expression of them ($P < 0.05$). In addition, after being intervened with miR-21 mimics, SD rats in the model group showed increased expression of miR-21 and FGF1 in their myocardial tissues (both $P < 0.05$), but after being intervened by recombinant human FGF1, they only showed increased expression of FGF1 ($P < 0.05$), and after being intervened by the two factors meantime, they were not very different from those in the miR-21 group in the expression of miR-21 ($P > 0.05$) but showed significant higher expression of FGF1 than those in the FGF1 group ($P < 0.05$) (Figure 2)

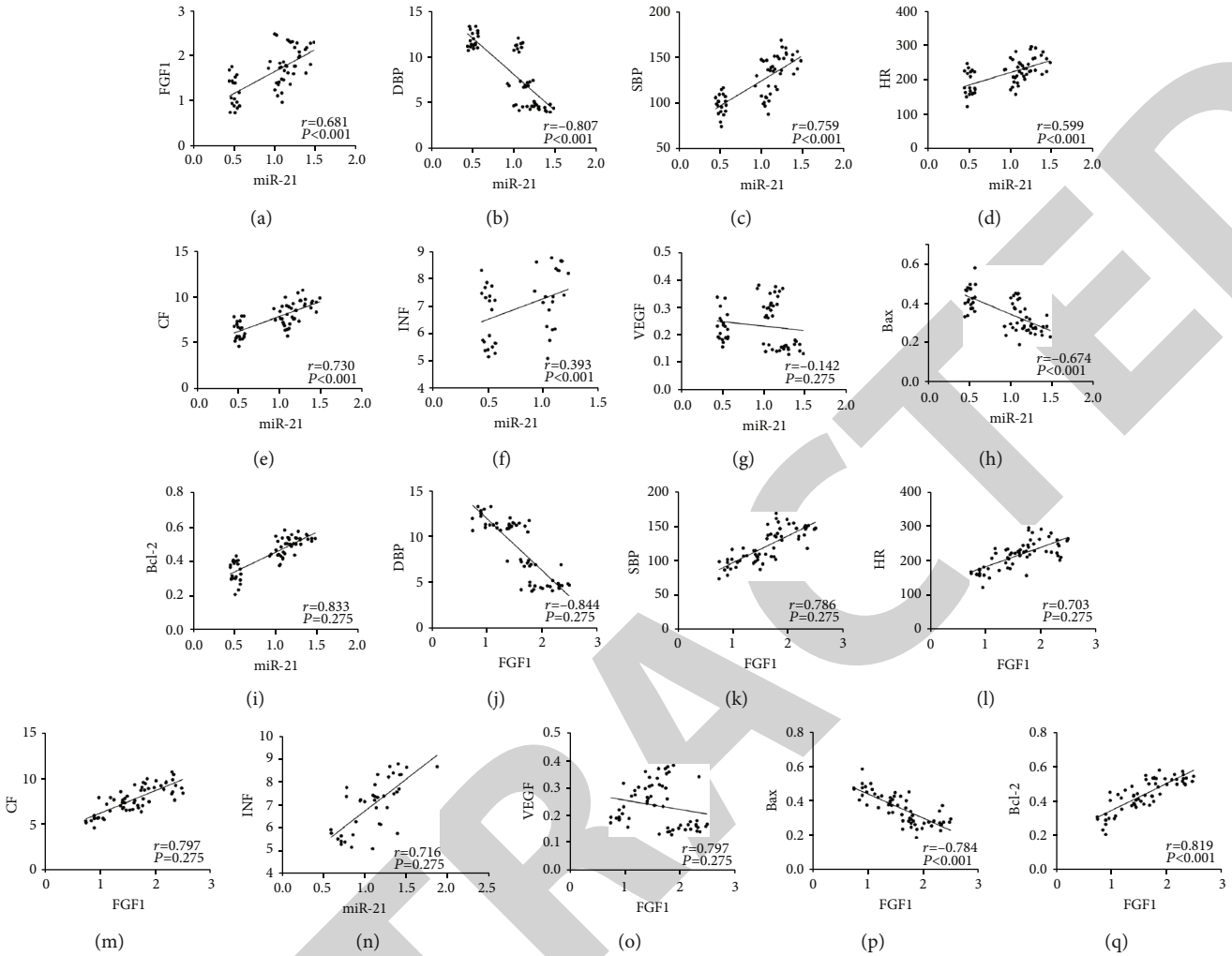

Figure 3: Correlation analysis: (a) analysis of correlation between miR-21 and FGF1; (b) analysis of correlation between miR-21 and DBP; (c) analysis of correlation between miR-21 and SBP; (d) analysis of correlation between miR-21 and HR; (e) analysis of correlation between miR-21 and CF; (f) analysis of correlation between miR-21 and INF; (g) analysis of correlation between miR-21 and VEGF; (h) analysis of correlation between miR-21 and bax; (i) analysis of correlation between miR-21 and bcl-2; (j) analysis of correlation between FGF1 and DBP; (k) analysis of correlation between FGF1 and SBP; (l) analysis of correlation between FGF1 and HR. (m) analysis of correlation between FGF1 and CF; (n) analysis of correlation between FGF1 and INF; (o) analysis of correlation between FGF1 and VEGF; (p) analysis of correlation between FGF1 and bax; (q) analysis of correlation between FGF1 and bcl-2. DBP: diastolic blood pressure; SBP: systolic blood pressure; HR: heart rate; CF: coronary flow.

3.3. Correlation Analysis. Pearson correlation analysis revealed that the expression of miR-21 was positively correlated with that of FGF1 ($P < 0.05$), and miR-21 and FGF1 were significantly and linearly correlated with DBP, SBP, HR, CF, INF, bax, and bcl-2 (all $P < 0.05$) but were not significantly correlated with the VEGF level ($P > 0.05$) (Figure 3)

3.4. The Role of miR-21 in Reducing Myocardial Cell Apoptosis by Targeting FGF1. The myocardial cell experiment results revealed that upregulation of miR-21 or FGF1 could alleviate apoptosis of myocardial cells caused hypoxia/reoxygenation ($P < 0.05$), and inhibition of the FGF1 expression could hinder the effect of miR-21 against apoptosis of myocardial cells ($P < 0.05$) (Figure 4)

3.5. Dual Luciferase Reporter Assay. The results of fluorescence intensity determination revealed that transfection of miR-21-mimics could effectively raise the fluorescence intensity of pmirGLO-FGF1-3′UTR Wt ($P < 0.05$) but had no significant effect on that of pmirGLO-FGF1-3′UTR Mut ($P > 0.05$) (Figure 5)

4. Discussion

Myocardial infarction is one of the five major manifestations of coronary heart disease. Thrombolytic therapy and interventional therapy are currently the main methods to alleviate myocardial ischemia injury in clinical practice. However, myocardial reperfusion will cause more serious injury or death, and MI/R injury is also an important influencing factor

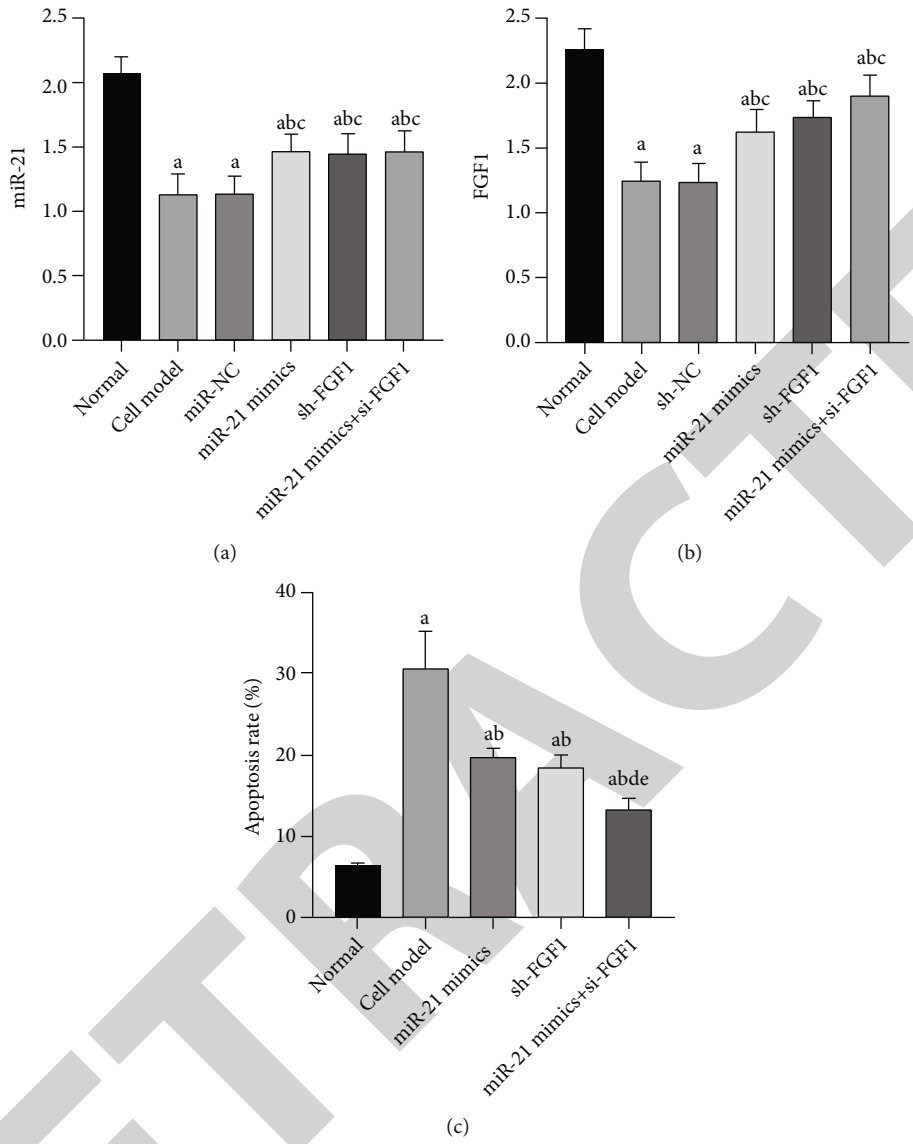

Figure 4: MiR-21 reduces myocardial cell apoptosis by targeting FGF1: (a) changes of miR-21 expression; (b) changes of FGF1 expression; (c) effects of miR-21 and FGF1 on myocardial cell apoptosis. A: in comparison with the normal group, $P < 0.05$; B: in comparison with the cell model group, $P < 0.05$; C: in comparison with the miR-NC group, $P < 0.05$; D: in comparison with the miR-21 minics group, $P < 0.05$; E: in comparison with the sh-FGF1 group, $P < 0.05$.

for poor prognosis of patients with coronary heart disease (17, 18). With the development of therapeutic drugs and methods, myocardial reperfusion has been continuously improved, but there is still a lack of effective means to prevent MI/R injury (19). The results of this study revealed that miR-21 could mediate FGF1 to protect myocardium of rats under ischemia reperfusion and reduce myocardial cell apoptosis, which may become a therapeutic target for preventing MI/R injury in the future.

We constructed rat models of MI/R injury by clamping and then releasing LAD. As we expected, all electrophysiological indexes of the heart of each rat were abnormal, including decreased SBP and CF and increased DBP and HR. Based on dissection of the rats, a large area of myocardial infarction was found, and it was also found that the myocardial tissues of the rats showed significantly lowered expression of miR-21 and FGF1, increased VEGF and bax levels, and lowered expression of bcl-2. It indicated that myocardial cell apoptosis was enhanced, but the rats also underwent ischemic preconditioning, and the VEGF expression promoted angiogenesis and maintained cardiac blood supply. During the recovery of blood supply in rats, we interfered the expression of miR-21 and FGF1 in the rats. The increase in the expression of miR-21 and FGF1 in myocardial cells of the rats suggested that we had successfully intervened it. Meantime, compared with the model rats not intervened, the rats showed some significantly improved cardiac function indexes, decreased myocardial INF, lowered level of the apoptosis factor, bax, and increased levels of antiapoptosis factors, bcl-2, and VEGF. It indicated that both miR-21 and FGF1 could intensity the resistance of myocardium against apoptosis caused by MI/R injury to protect cardiac function, and the simultaneous intervention

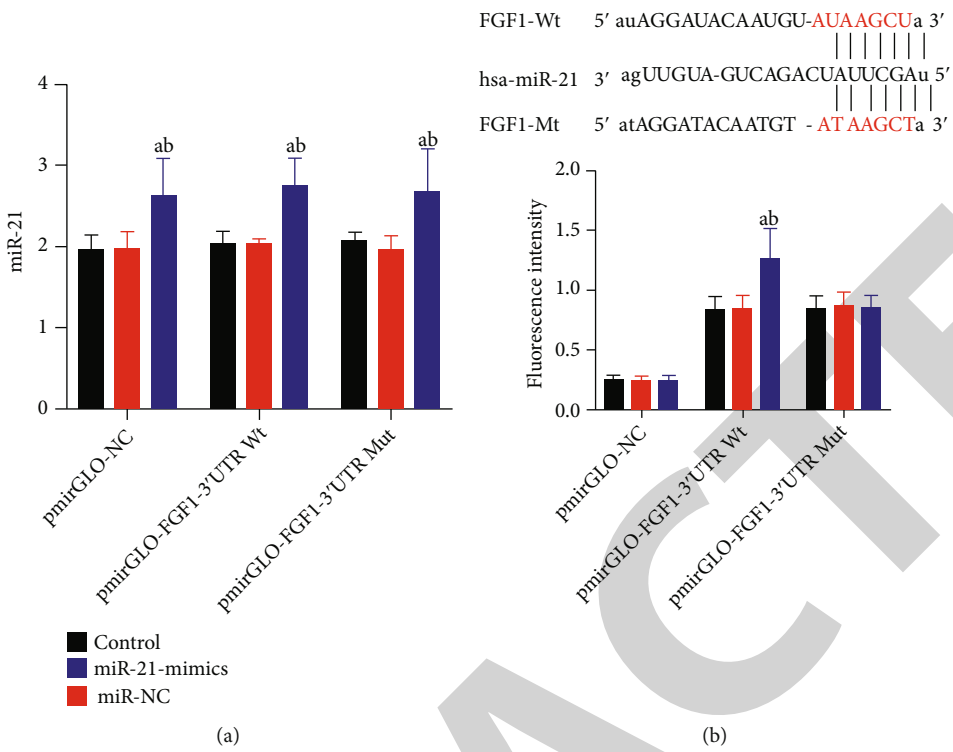

Figure 5: Dual luciferase reporter assay: (a) the expression of miR-21; (b) fluorescence intensity. A: in comparison with the CON group, $P < 0.05$; B: in comparison with the miR-NC group, $P < 0.05$. CON: control group.

of miR-21 and FGF1 could bring a more significant result. Correlation analysis results also revealed that miR-21 and FGF1 were significantly and linearly correlated with cardiac function, INF, bax, and bcl-2 in rats. Although our results showed that both miR-21 and FGF1 could promote the VEGF expression, we did not find any correlation between them. We speculated that it may be related to the self-resistance of rats against I/R injury. In this pathological process, many factors contribute to the increase of VEGF expression level to adapt to myocardial infarction. In addition, we also found that the expression of miR-21 had a significant positive correlation with that of FGF1. In order to verify whether there is an expression regulation relationship between miR-21 and FGF1, we extracted myocardial cells from neonatal rats and cultured them. It was turned out that downregulation of FGF1 expression could inhibit miR-21 from protecting myocardial cells from the injury caused by hypoxia/reoxygenation. Dual luciferase reporter assay revealed that miR-21 could targetedly promote the expression of FGF1 in myocardial cells. Therefore, based on these results, it can be concluded that miR-21 can targetedly mediate the expression of FGF1 to alleviate MI/R injury, protect cardiac function, and resist apoptosis.

Many previous studies reported that miR-21 could protect myocardial tissues from ischemia and reperfusion, and many downstream targets of miR-21 have been found, such as programmed cell death factor 4 (PDCD4). MiR-21/PDCD4 pathway can protect myocardial cells and weaken apoptosis caused by oxidative stress injury (20). In addition, miR-21 can regulate the TLR4/NF-κB pathway to reduce the release of inflammatory factors and relieve myocardial cell injury during MI/R injury in rats (21). In addition to I/R injury in myocardium, miR-21 is also closely related to that in the kidney and brain (22, 23). Generally, miR-21 decreases during I/R injury, but the increase of it can protect organs by mainly reducing apoptosis and inhibiting the release of inflammatory factors. Vascular regeneration and microcirculation reconstruction are very important for the treatment of myocardial infarction. Many studies also reported that miR-21 was related to vascular regeneration, and overexpression of miR-21 could activate hypoxia-inducible factor 1α to promote neovascularization during limb ischemia reperfusion injury (24). FGF1 is also bound up with angiogenesis. Garbayo et al. (25) pointed out that intramyocardial injection of FGF1 could improve the cardiac function of pig models of ischemia reperfusion and promote angiogenesis.

However, miR-21 and FGF1 may play different roles in different cells. As mentioned earlier, Liu et al. (13) concluded that miR-21 suppressed the apoptosis of growth plate chondrocytes and promoted proliferation by targetedly inhibiting FGF1. Moreover, miR-21 may not entirely beneficial against MI/R injury. A study concluded that miR-21 targeted Smad 7 to promote myocardial fibrosis after myocardial infarction, and Smad 7 could regulate tumor necrosis factor beta signal transduction (26, 27). FGF1 is a profibrogenic factor. For example, it promotes pulmonary fibrosis and liver fibrosis (28, 29). However, there is no report on the relationship between FGF1 and myocardial fibrosis, which needs further research and analysis. In addition, the intervention method adopted in this study is ischemic postconditioning, and the role of ischemic preconditioning intervention has not been verified. We will further improve our analysis in future studies. As this is a single/limited region study, a multiregional or

multicentric approach may provide a broad picture which can further enhance the validity of the prospective results. So far, not many efforts have been directed towards establishing a significant association between some of the circulatory candidate miRNAs and the severity of CAD when developing a noninvasive diagnostic method that can help in reducing coronary complications. Considering CAD as a multifactorial and multigenic disease driven by various genetic and nongenetic factors, observations from the current study appear to support the assumption that miRNA signatures have important implications on CAD and its different stages.

To sum up, miR-21 can targetedly mediate the expression of FGF1 to relieve MI/R injury, protect cardiac function, and resist apoptosis.

Data Availability

The authors confirm that the data supporting the findings of this study are available within the article.

Conflicts of Interest

The authors declare that they have no conflicts of interest.

Authors' Contributions

Bin Zhang wrote the manuscript. Bin Zhang and Hongguang Liu conceived and designed the study. Bin Zhang, Hongguang Liu, and Guoping Yang were responsible for the collection and analysis of the experimental data. Yongmei Wang and Yan Wang revised the manuscript critically for important intellectual content. All the authors read and approved the final manuscript.

References

[1] S. Mendis, K. Thygesen, K. Kuulasmaa et al., "World Health Organization definition of myocardial infarction: 2008–09 revision," *International Journal of Epidemiology*, vol. 40, no. 1, pp. 139–146, 2011.

[2] World Health statistics, *Monitoring health for the SDGs sustainable development goals*, WHO, Geneva Switzerland, 2016.

[3] G. A. Roth, M. H. Forouzanfar, A. E. Moran et al., "Demographic and epidemiologic drivers of global cardiovascular mortality," *New England Journal of Medicine*, vol. 372, no. 14, pp. 1333–1341, 2015.

[4] E. J. Benjamin, M. J. Blaha, S. E. Chiuve et al., "Correction to: Heart disease and stroke statistics-2017 update: a report from the American Heart Association," *Circulation*, vol. 135, no. 10, pp. e146–e603, 2017.

[5] H. Li, Y. Liao, L. Gao et al., "Coronary serum exosomes derived from patients with myocardial ischemia regulate angiogenesis through the miR-939-mediated nitric oxide signaling pathway," *Theranostics*, vol. 8, no. 8, pp. 2079–2093, 2018.

[6] I. Díaz, E. Calderón-Sánchez, R. Del Toro et al., "miR-125a, miR-139 and miR-324 contribute to urocortin protection against myocardial ischemia-reperfusion injury," *Scientific Reports*, vol. 7, no. 1, p. 8898, 2017.

[7] M. P. Dragomir, E. Knutsen, and G. A. Calin, "SnapShot: unconventional miRNA functions," *Cell*, vol. 174, no. 4, pp. 1038–1038.e1, 2018.

[8] E. L. Vegter, P. van der Meer, L. J. de Windt, Y. M. Pinto, and A. A. Voors, "MicroRNAs in heart failure:from biomarker to target for therapy," *European Journal of Heart Failure*, vol. 18, no. 5, pp. 457–468, 2016.

[9] M. Notari, J. Pulecio, and A. Raya, "Update on the pathogenic implications and clinical potential of microRNAs in cardiac disease," *BioMed Research International*, vol. 2015, Article ID 105620, 15 pages, 2015.

[10] N. Ma, J. Bai, W. Zhang et al., "Trimetazidine protects against cardiac ischemia/reperfusion injury via effects on cardiac miRNA-21 expression, Akt and the Bcl-2/Bax pathway," *Molecular Medicine Reports*, vol. 14, no. 5, pp. 4216–4222, 2016.

[11] F. Yang, W. Liu, X. Yan et al., "Effects of mir-21 on cardiac microvascular endothelial cells after acute myocardial infarction in rats:role of phosphatase and tensin homolog (PTEN)/vascular endothelial growth factor (VEGF) signal pathway," *Medical Science Monitor:international medical journal of experimental and clinical research*, vol. 22, pp. 3562–3575, 2016.

[12] C. Huang, Y. Liu, A. Beenken et al., "A novel fibroblast growth factor-1 ligand with reduced heparin binding protects the heart against ischemia-reperfusion injury in the presence of heparin co-administration," *Cardiovascular Research*, vol. 113, no. 13, pp. 1585–1602, 2017.

[13] X. Liu, Y. She, H. Wu, D. Zhong, and J. Zhang, "Long non-coding RNA Gas5 regulates proliferation and apoptosis in HCS-2/8 cells and growth plate chondrocytes by controlling FGF1 expression via miR-21 regulation," *Journal of Biomedical Science*, vol. 25, no. 1, p. 18, 2018.

[14] J. Zhang, K. Peng, J. Zhang, X. W. Meng, and F. H. Ji, "Dexmedetomidine preconditioning may attenuate myocardial ischemia/reperfusion injury by down-regulating the HMGB1-TLR4-MyD88-NF-κB signaling pathway," *PLoS One*, vol. 12, no. 2, article e0172006, 2017.

[15] N. R. Sodha, R. T. Clements, J. Feng et al., "The effects of therapeutic sulfide on myocardial apoptosis in response to ischemia–reperfusion injury," *European Journal of Cardio-Thoracic Surgery*, vol. 33, no. 5, pp. 906–913, 2008.

[16] J. Sadoshima, L. Jahn, T. Takahashi, T. J. Kulik, and S. Izumo, "Molecular characterization of the stretch-induced adaptation of cultured cardiac cells. An in vitro model of load-induced cardiac hypertrophy.," *The Journal of Biological Chemistry*, vol. 267, no. 15, pp. 10551–10560, 1992.

[17] E. Ruvinov and S. Cohen, "Alginate biomaterial for the treatment of myocardial infarction: progress, translational strategies, and clinical outlook: from ocean algae to patient bedside," *Advanced Drug Delivery Reviews*, vol. 96, pp. 54–76, 2016.

[18] M. F. Piepoli, U. Corrà, P. Dendale et al., "Challenges in secondary prevention after acute myocardial infarction:a call for action," *European Journal of Preventive Cardiology*, vol. 23, no. 18, pp. 1994–2006, 2016.

[19] D. J. Hausenloy and D. M. Yellon, "Myocardial ischemia-reperfusion injury:a neglected therapeutic target," *The Journal of Clinical Investigation*, vol. 123, no. 1, pp. 92–100, 2013.

[20] J. Xiao, Y. Pan, X. H. Li et al., "Cardiac progenitor cell-derived exosomes prevent cardiomyocytes apoptosis through exosomal miR-21 by targeting PDCD4," *Cell Death & Disease*, vol. 7, no. 6, article e2277, 2016.

[21] Y. Q. Pan, J. Li, X. W. Li, Y. C. Li, J. Li, and J. F. Lin, "Effect of miR-21/TLR4/NF-κB pathway on myocardial apoptosis in rats

Hindawi
BioMed Research International
Volume 2024, Article ID 9760679, 1 page
https://doi.org/10.1155/2024/9760679

Retraction

Retracted: Effect of Dexmedetomidine Combined with Ropivacaine on Cognitive Dysfunction and Inflammatory Response in Patients Undergoing Craniocerebral Surgery

BioMed Research International

Received 12 March 2024; Accepted 12 March 2024; Published 20 March 2024

This article has been retracted by Hindawi following an investigation undertaken by the publisher [1]. This investigation has uncovered evidence of one or more of the following indicators of systematic manipulation of the publication process:

(1) Discrepancies in scope

(2) Discrepancies in the description of the research reported

(3) Discrepancies between the availability of data and the research described

(4) Inappropriate citations

(5) Incoherent, meaningless and/or irrelevant content included in the article

(6) Manipulated or compromised peer review

The presence of these indicators undermines our confidence in the integrity of the article's content and we cannot, therefore, vouch for its reliability. Please note that this notice is intended solely to alert readers that the content of this article is unreliable. We have not investigated whether authors were aware of or involved in the systematic manipulation of the publication process.

Wiley and Hindawi regrets that the usual quality checks did not identify these issues before publication and have since put additional measures in place to safeguard research integrity.

We wish to credit our own Research Integrity and Research Publishing teams and anonymous and named external researchers and research integrity experts for contributing to this investigation.

The corresponding author, as the representative of all authors, has been given the opportunity to register their agreement or disagreement to this retraction. We have kept a record of any response received.

References

[1] Y. Liu, H. Zhang, and W. Zhang, "Effect of Dexmedetomidine Combined with Ropivacaine on Cognitive Dysfunction and Inflammatory Response in Patients Undergoing Craniocerebral Surgery," *BioMed Research International*, vol. 2021, Article ID 4968300, 8 pages, 2021.

Hindawi
BioMed Research International
Volume 2021, Article ID 4968300, 8 pages
https://doi.org/10.1155/2021/4968300

Research Article

Effect of Dexmedetomidine Combined with Ropivacaine on Cognitive Dysfunction and Inflammatory Response in Patients Undergoing Craniocerebral Surgery

Yang Liu, Hongwei Zhang, and Wenhua Zhang

Department of Anesthesiology, The Third Affiliated Hospital of Qiqihar Medical College, Tsitsihar, 161000 Heilongjiang Province, China

Correspondence should be addressed to Yang Liu; liuyang3826@126.com

Received 5 July 2021; Revised 21 October 2021; Accepted 26 October 2021; Published 30 November 2021

Academic Editor: Chang Gu

Objective. To study the effects of dexmedetomidine in combination with ropivacaine in patients undergoing craniocerebral surgery and their efficiency on cognitive function and inflammatory response of patients. *Methods*. 100 patients undergoing craniocerebral surgery in our hospital from November 2018 to September 2020 were randomly selected and divided into a control group and an experimental group by drawing lots, with 50 cases in each group. Patients in the control group received routine anesthesia, while those in the experimental group received 1 μg/kg of dexmedetomidine combined with 0.5% of ropivacaine for anesthesia to compare the anesthesia onset time, analgesic time, postoperative awake time, Social Disability Screening Schedule (SDSS) cognitive function score after waking, visual analogue scale (VAS) pain score, Ramsay sedation score, incidence of adverse reactions, postoperative inflammatory factor expression levels, and changes in heart rate, oxygen saturation, and blood pressure at T0, T1, T2, T3, and T4 between the two groups. *Results*. The anesthesia onset time, SDSS cognitive function score after waking, VAS pain score, Ramsay sedation score, incidence of adverse reactions, and postoperative inflammatory factor expression levels in the experimental group were significantly lower than those in the control group ($P < 0.05$). The analgesic time and postoperative awake time in the experimental group were significantly longer than those in the control group, with statistical significance ($P < 0.05$). There were no statistically significant differences in the changes of heart rate, oxygen saturation, and blood pressure at T0, T1, T2, T3, and T4 between the two groups ($P > 0.05$). *Conclusion*. Dexmedetomidine combined with ropivacaine has high application value in craniocerebral surgery.

1. Introduction

Craniocerebral surgery is a common clinical brain surgery, generally referring to craniotomy, skull repair, etc. This surgery is often required for aneurysm, cerebral hemorrhage, cerebral trauma, and stable circulation during the perioperative period. Patients need anesthesia before surgery, with common anesthesia methods mainly including inhalation anesthesia, intravenous injection of anesthesia drugs, and muscle relaxants. Due to the differences in the patients' condition and physical function, proper anesthetic drugs and anesthesia methods should be selected according to their personal situation [1–3].

Dexmedetomidine is a highly selective α-2 adrenergic receptor agonist. The α-2 receptor agonists have a long track record of use for sedation and analgesia. Animal studies have shown that α-2 agonists are neuroprotective in craniocerebral and subarachnoid injuries. Dexmedetomidine has a significant effect on the central nervous system and decreases the blood flow in the brain and the requirement or needs for cerebral oxygen. It also modifies memory and enhances cognitive ability effects like sedation, analgesic, and anxiolytics. Dexmedetomidine is shown to decrease catecholamine in the brain and improves the perfusion ability in the penumbra. It is a common drug mainly applied in tracheal intubation general anesthesia,

Table 1: Comparison of general data ($x \pm s$).

Group		Experimental group	Control group	t/X^2	P
Gender (male/female)		26/24	25/25	0.04	0.84
Age (years old)		57.34 ± 6.72	57.08 ± 6.52	0.20	0.84
Height (cm)		164.08 ± 10.30	163.77 ± 10.56	0.15	0.88
Weight (kg)		66.52 ± 11.05	65.43 ± 11.67	0.48	0.63
Course of disease (month)		1.36 ± 0.15	1.39 ± 0.11	1.14	0.26
Smoking history (year)		13.75 ± 3.39	14.00 ± 3.34	0.37	0.71
Drinking history (year)		15.37 ± 2.37	15.07 ± 2.55	0.61	0.54
Hypertension (n)		36	33	0.42	0.52
Diabetes mellitus (n)		20	22	0.16	0.69
Hyperlipidemia (n)		13	15	0.20	0.66
Manifestations	Severe trauma	21	20	0.04	0.84
	Encephalorrhagia	13	11	0.22	0.64
	Meningioma	6	8	0.33	0.56
	Intracranial aneurysm	10	11	0.06	0.81

which is also widely used in various types of surgery and often combined with sevoflurane, propofol, and other drugs. In combination, the dosage should be appropriately reduced due to the interaction of multiple drugs and the superposition of efficacy [4–6].

Ropivacaine is a local anesthetic drug commonly used in regional block analgesia and labor analgesia [7–9]. Ropivacaine provides more differential block when given epidurally over bupivacaine allowing for a better separation between sensory and motor block [8, 9]. This advantage of ropivacaine relieved obstetric and postoperative epidural pain. Ropivacaine has a lower systemic toxicity than both racemic mixture and levobupivacaine. In particular, its better cardiotoxic profile has been well documented and is an important advantage when using techniques with a potential for high plasma concentrations [7–9]. In order to study the application effect of dexmedetomidine combined with ropivacaine in craniocerebral surgery, patients undergoing craniocerebral surgery were selected as the research objects in this study and received routine anesthesia as well as anesthesia with dexmedetomidine and ropivacaine, respectively, to observe and compare the anesthesia onset time, analgesic time, postoperative awake time, Social Disability Screening Schedule (SDSS) cognitive function score after waking, visual analogue scale (VAS) pain score, Ramsay sedation score, incidence of adverse reactions, postoperative inflammatory factor expression levels, and changes in heart rate, oxygen saturation, and blood pressure at T0, T1, T2, T3, and T4 between the two groups, with details reported as follows.

2. Materials and Methods

2.1. General Information. 100 patients undergoing craniocerebral surgery in our hospital from November 2018 to September 2020 were randomly selected and divided into a control group and an experimental group by drawing lots, with 50 cases in each group. The age was 47-72 years old in the control group and 45-70 years old in the experimental group. There was no statistical significance in the comparison of general information such as gender, age, and disease types between the two groups ($P > 0.05$), as shown in Table 1.

2.2. Inclusion/Exclusion Criteria

2.2.1. Inclusion Criteria. The patients met the requirements of craniocerebral surgery. The patients were no less than 18 years old. The patients had no other organic diseases or coagulation disorders and did not take coagulation drugs recently. The patients had no history of drug allergy, drug abuse, or bad habits. This study was approved by the Hospital Ethics Committee, and the patients voluntarily participated in the study and signed the informed consent.

2.2.2. Exclusion Criteria. The patients recently (within one year) received other types of surgery. The patients had consciousness disorder and could not cooperate with this study. The patients or family members did not agree to participate in this study.

2.3. Methods. Before surgery, the patients were routinely fasted for 8 h and prohibited from drinking for 4 h. Blood pressure, pulse oxygen saturation, and electrocardiogram were monitored in the room. Mask oxygen-inspiration was maintained, with the oxygen flow of 4 L/min. The right elbow vein of the patients was opened to establish venous access and monitor the invasive venous pressure.

The control group received routine anesthesia, with 2 mg/kg of propofol (manufacturer: Sichuan Guorui Pharmaceutical Co., Ltd.; SFDA approval no. H20040079; specification: 10 mL : 0.1 g), 0.1 mg/kg of cisatracurium (manufacturer: Jiangsu Hengrui Pharmaceutical Co., Ltd.; SFDA approval no. H20060869; specification: 10 mg), and remifentanil at a plasma concentration of 4 ng/(min·kg) (manufacturer: Jiangsu Nhwa Pharmaceutical Co., Ltd.; SFDA approval no. H20143314; specification: 1 mg) for

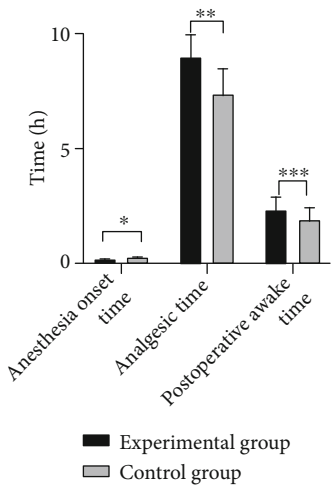

Figure 1: Comparison of anesthesia onset time, analgesic time, and postoperative awake time between the two groups. Note: the abscissa from left to right represents anesthesia onset time, analgesic time, and postoperative awake time, and the ordinate represents time. ∗ indicates the comparison of anesthesia onset time between the experimental group (0.15 ± 0.03 h) and the control group (0.22 ± 0.03 h), with a statistically significant difference ($t = 11.67$, $P < 0.001$). ∗∗ indicates the comparison of analgesic time between the experimental group (8.93 ± 1.00 h) and the control group (7.33 ± 1.12 h), with a statistically significant difference ($t = 7.54$, $P < 0.001$). ∗∗∗ indicates the comparison of postoperative awake time between the experimental group (2.32 ± 0.55 h) and the control group (1.87 ± 0.53 h), with a statistically significant difference ($t = 4.17$, $P < 0.001$).

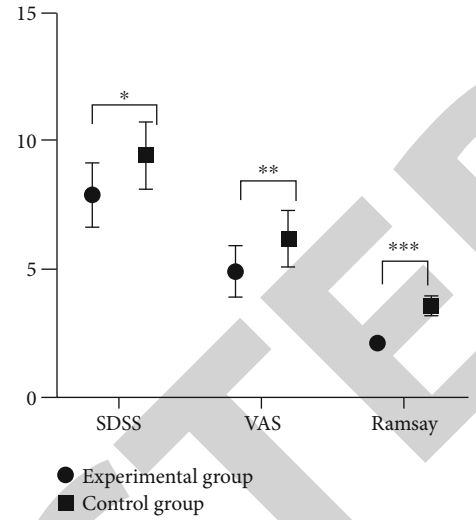

Figure 2: Comparison of SDSS cognitive function score, VAS pain score, and Ramsay sedation score between the two groups after waking. Note: the abscissa from left to right represents SDSS cognitive function score, VAS pain score, and Ramsay sedation score, and the ordinate represents time. ∗ indicates the comparison of SDSS scores between the experimental group (7.93 ± 1.26) and the control group (9.51 ± 1.30), with a statistically significant difference ($t = 6.17$, $P < 0.001$). ∗∗ indicates the comparison of VAS scores between the experimental group (4.95 ± 1.00) and the control group (6.20 ± 1.12), with a statistically significant difference ($t = 5.89$, $P < 0.001$). ∗∗∗ indicates the comparison of Ramsay scores between the experimental group (2.10 ± 0.13 h) and the control group (3.55 ± 0.40 h), with a statistically significant difference ($t = 24.38$, $P < 0.001$). SDSS: social disability screening score; VAS: visual analogue scale.

anesthesia induction, and tracheal intubation was performed after 3 minutes [10–12]. 3 ng/(kg·min) of remifentanil was maintained during surgery, and the minimum target plasma concentration of propofol (2 ng/kg) was ensured for the maintenance of anesthesia. The drugs were discontinued after surgery.

Patients in the experimental group were anesthetized with 1 μg/kg of dexmedetomidine combined with 0.5% of ropivacaine. Based on the control group, dexmedetomidine (manufacturer: Sichuan Guorui Pharmaceutical Co., Ltd.; SFDA approval no. H20143195; specification: 1 mL : 0.1 mg) and ropivacaine (manufacturer: Guangdong Huarunshunfeng Pharmaceutical Co., Ltd.; SFDA approval no. H20050325) were mixed for nerve block, with the block sites at the auriculotemporal nerve, supraorbital nerve, supratrochlear nerve, great occipital nerve, and small occipital nerve. After the block was completed, anesthesia was performed in the same way as in the control group.

2.4. Observation Indexes. The anesthesia onset time, analgesic time, postoperative awake time, Social Disability Screening Schedule (SDSS) cognitive function score after waking, VAS pain score, Ramsay sedation score, incidence of adverse reactions, postoperative inflammatory factor expression levels, and changes in heart rate, oxygen saturation, and blood pressure before surgery (T0), 1 h during surgery (T1), 2 h during surgery (T2), 1 h after surgery (T3), and 2 h after surgery (T4) were compared between the two groups.

Social function was evaluated by SDSS, with a total of 10 items and a total score of 20 points. The SDSS is part of the disability assessment schedule edited by WHO, which is a self-reporting tool for indicating social disability of patients, with higher scores denoting more social disability.

The VAS pain score scale was used to score the postoperative pain of the two groups, with 0 as no pain, 1-3 points as mild and tolerable pain, 4-6 points as the pain that affected sleep but could be tolerated, and 7-10 points as severe and unbearable pain. The score of 2-3 points was good analgesia, and a score more than 3 points indicated incomplete analgesia.

The Ramsay score was used to score the sedative effect of the two groups after surgery. The patients had anxiety, irritability, and other emotions, scoring 1 point. The patients were awake and had cooperative ability, scoring 2 points. The patients were drowsy but could respond to instructions, scoring 3 points. The patients were in a sleeping state but could be woken up, scoring 4 points. The patients were in a sleeping state with slow response to external strong stimulation, scoring 5 points. The patients were in deep sleep with no response to external strong stimulation, scoring 6 points. The score of 2-4 points was satisfactory sedation while that of 5-6 points was excessive sedation.

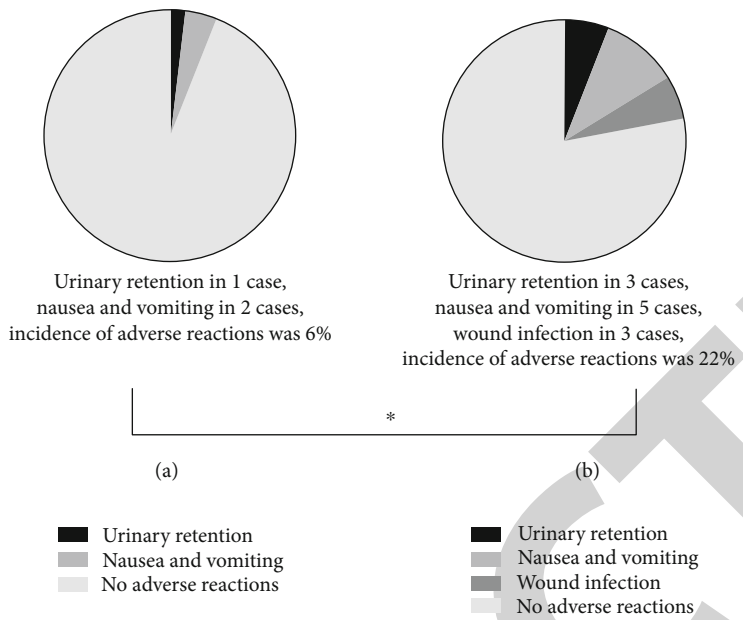

Figure 3: Comparison of the incidence of adverse reactions between the two groups. Note: (a) shows the incidence of adverse reactions in the experimental group, including 1 case of urinary retention and 2 cases of nausea and vomiting, with the incidence of adverse reactions at 6%. (b) shows the incidence of adverse reactions in the control group, including 3 cases of urinary retention, 5 cases of nausea and vomiting, and 3 cases of wound infection, with the incidence of adverse reactions at 22%. ∗ indicates the comparison of the incidence of adverse reactions between the two groups, with a statistically significant difference ($X^2 = 5.32$, $P = 0.02$).

Table 2: Comparison of postoperative inflammatory factor expression levels between the two groups.

Group	CRP (μg/L)	TNF-α (ng/L)	IL-1β (ng/L)	IL-5 (μ/L)	IL-6 (ng/L)
Experimental group	1.65 ± 0.77	3.19 ± 1.03	4.12 ± 1.94	7.00 ± 2.18	3.07 ± 0.80
Control group	4.15 ± 1.13	6.10 ± 2.12	8.05 ± 2.62	11.69 ± 3.46	7.55 ± 3.13
t	12.93	8.73	8.52	8.11	9.81
P	<0.001	<0.001	<0.001	<0.001	<0.001

CRP: C-reactive protein; TNF-α: tumor necrosis factor α; IL: interleukin.

The inflammatory factor expression levels mainly included C-reactive protein (CRP), tumor necrosis factor- (TNF-) α, interleukin- (IL-) 1β, IL-5, and IL-6 expression levels.

2.5. Statistical Processing. SPSS 20.0 was selected as the data processing software, and GraphPad Prism 7 (GraphPad Software, San Diego, USA) was used to draw pictures of the data. The study included count data and measurement data. The measurement data were measured by the t-test, expressed as $\bar{x} \pm s$, and the count data were tested by X^2, expressed as n (%). The difference was statistically significant when $P < 0.05$.

3. Results

3.1. Comparison of Anesthesia Onset Time, Analgesic Time, and Postoperative Awake Time between the Two Groups. The anesthesia onset time, analgesic time, and postoperative awake time during surgery were compared between the two groups. The results showed that the anesthesia onset time in the experimental group was significantly shorter than that in the control group, and the analgesic time and postoperative awake time were significantly longer than those in the control group, with statistically significant differences ($P < 0.05$), as shown in Figure 1.

3.2. Comparison of SDSS Cognitive Function Score, VAS Pain Score, and Ramsay Sedation Score between the Two Groups after Waking. The SDSS cognitive function score, VAS pain score, and Ramsay sedation score were compared between the two groups after waking. The results showed that the SDSS cognitive function score, VAS pain score, and Ramsay sedation score after waking in the experimental group were significantly lower than those in the control group, with statistically significant differences ($P < 0.05$), as shown in Figure 2.

3.3. Comparison of the Incidence of Adverse Reactions between the Two Groups. Adverse reactions in the two groups were compared, and the results showed that the incidence of adverse reactions in the experimental group was significantly lower than that in the control group, with a statistically significant difference ($P < 0.05$), as shown in Figure 3.

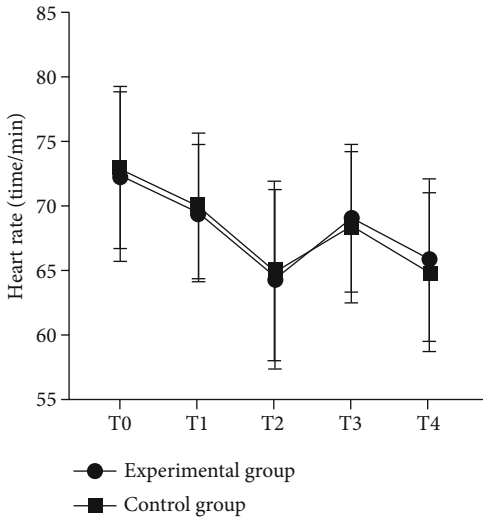

Figure 4: Comparison of heart rate between the two groups at different times. Note: the abscissa from left to right represents T0, T1, T2, T3, and T4, and the ordinate represents heart rate. There was no statistically significant difference in the comparison of the heart rate at T0 between the experimental group (72.36 ± 6.62 times/min) and the control group (73.05 ± 6.29 times/min; $t = 0.53$, $P = 0.59$). There was no statistically significant difference in the comparison of the heart rate at T1 between the experimental group (69.52 ± 5.34 times/min) and the control group (70.11 ± 5.69 times /min; $t = 0.53$, $P = 0.59$). There was no statistically significant difference in the comparison of the heart rate at T2 between the experimental group (64.45 ± 6.96 times/min) and the control group (64.99 ± 7.00 times/min; $t = 0.39$, $P = 0.70$). There was no statistically significant difference in the comparison of the heart rate at T3 between the experimental group (69.13 ± 5.80 times/min) and the control group (68.40 ± 5.94 times/min; $t = 0.62$, $P = 0.54$). There was no statistically significant difference in the comparison of the heart rate at T4 between the experimental group (65.90 ± 6.33 times/min) and the control group (64.89 ± 6.19 times/min; $t = 0.58$, $P = 0.42$).

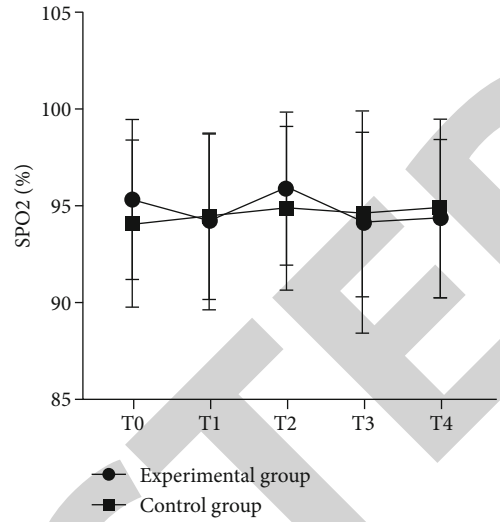

Figure 5: Comparison of oxygen saturation between the two groups at different times. Note: the abscissa from left to right represents T0, T1, T2, T3, and T4, and the ordinate represents oxygen saturation. There was no statistically significant difference in the comparison of the oxygen saturation at T0 between the experimental group (95.33 ± 4.12%) and the control group (94.08 ± 4.36%; $t = 1.47$, $P = 0.14$). There was no statistically significant difference in the comparison of the oxygen saturation at T1 between the experimental group (94.19 ± 4.62%) and the control group (94.41 ± 4.28%; $t = 0.25$, $P = 0.81$). There was no statistically significant difference in the comparison of the oxygen saturation at T2 between the experimental group (95.91 ± 4.00%) and the control group (94.87 ± 4.27%; $t = 1.26$, $P = 0.21$). There was no statistically significant difference in the comparison of the oxygen saturation at T3 between the experimental group (94.15 ± 5.80%) and the control group (94.57 ± 4.29%; $t = 0.41$, $P = 0.68$). There was no statistically significant difference in the comparison of the oxygen saturation at T4 between the experimental group (94.38 ± 4.10%) and the control group (94.89 ± 4.69%; $t = 0.58$, $P = 0.56$).

3.4. Comparison of Postoperative Inflammatory Factor Expression Levels between the Two Groups. The CRP, TNF-α, IL-1β, IL-5, and IL-6 expression levels were compared between the two groups after surgery. The results showed that the CRP, TNF-α, IL-1β, IL-5, and IL-6 expression levels in the experimental group were significantly lower than those in the control group, with statistically significant differences, as shown in Table 2.

3.5. Comparison of the Changes in Heart Rate, Oxygen Saturation, and Blood Pressure at T0, T1, T2, T3, and T4 between the Two Groups. The changes in heart rate, oxygen saturation, and blood pressure at T0, T1, T2, T3, and T4 were compared between the two groups. The results showed that there were no statistically significant differences in the changes of heart rate, oxygen saturation, and blood pressure at T0, T1, T2, T3, and T4 between the two groups, with statistically significant differences, as shown in Figures 4–6.

4. Discussion

Craniocerebral surgery is required for brain tumors, severe brain trauma, cranial deformation, encephalorrhagia, and other diseases, which is a common brain surgery, but with a high risk due to the special surgical sites [13–15]. Before surgery, patients should be routinely examined to select the appropriate anesthesia and surgical methods, mainly including the detection of the cerebral metabolism, intracranial pressure, and cerebral blood flow. Anesthesia is an important prerequisite for the success of surgery. If the anesthesia methods and anesthetic drugs are not suitable, they will seriously or even endanger the life of patients, resulting in surgical failure [16–18]. Common anesthetics mainly include vasoactive agents, inhaled drugs, muscle relaxants, and intravenous drugs, in which some vasoactive agents and inhaled drugs will indirectly increase the cerebral blood flow and intracranial pressure of patients, thereby increasing blood loss during surgery [19–21]. Besides, most intravenous anesthetics reduce intracranial pressure and cerebral blood

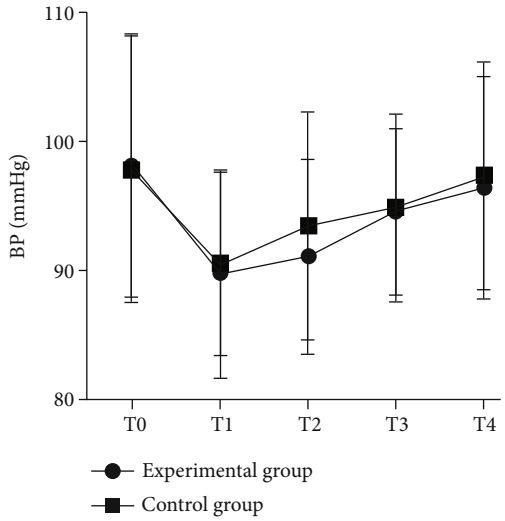

Figure 6: Comparison of blood pressure between the two groups at different times. Note: the abscissa from left to right represents T0, T1, T2, T3, and T4, and the ordinate represents blood pressure (mmHg). There was no statistically significant difference in the comparison of the heart rate at T0 between the experimental group (98.37 ± 10.22 mmHg) and the control group (98.08 ± 10.39 mmHg; $t = 0.14$, $P = 0.89$). There was no statistically significant difference in the comparison of the heart rate at T1 between the experimental group (89.91 ± 8.16 mmHg) and the control group (90.67 ± 7.19 mmHg; $t = 0.49$, $P = 0.62$). There was no statistically significant difference in the comparison of the heart rate at T2 between the experimental group (91.22 ± 7.61 mmHg) and the control group (93.67 ± 8.91 mmHg; $t = 1.48$, $P = 0.15$). There was no statistically significant difference in the comparison of the heart rate at T3 between the experimental group (94.74 ± 6.48 mmHg) and the control group (95.08 ± 7.33 mmHg; $t = 0.25$, $P = 0.81$). There was no statistically significant difference in the comparison of the heart rate at T4 between the experimental group (96.62 ± 8.66 mmHg) and the control group (97.59 ± 8.90 mmHg; $t = 0.55$, $P = 0.58$).

flow, increasing the risk of thrombosis and other diseases. Dexmedetomidine and ropivacaine are two common anesthetics which are used in combination in labor analgesia, epidural surgery, and other types of surgery. Due to their high anesthesia safety and good anesthesia effect, they are widely applied in clinic. In order to further study the application effect of dexmedetomidine combined with ropivacaine in craniocerebral surgery, patients undergoing craniocerebral surgery were selected as the research objects in this study and received routine anesthesia as well as anesthesia with dexmedetomidine and ropivacaine, respectively, to compare the anesthesia onset time, analgesic time, postoperative awake time, SDSS cognitive function score after waking, VAS pain score, Ramsay sedation score, incidence of adverse reactions, postoperative inflammatory factor expression levels, and changes in heart rate, oxygen saturation, and blood pressure at T0, T1, T2, T3, and T4 between the two groups.

The results of this study showed that the anesthesia onset time, SDSS cognitive function score after waking, VAS pain score, Ramsay sedation score, incidence of adverse reactions, and postoperative inflammatory factor expression levels in the experimental group were significantly lower than those in the control group, with statistically significant differences ($P < 0.05$). Some anesthetics can cause cognitive dysfunction and damage the brain nerve and cells of patients. Therefore, the cognitive function score of patients after waking is a means to judge the neurological damage caused by drugs and surgery, which can indirectly confirm the results of anesthesia and surgery. The purpose of anesthesia is to shield the ability of patients to feel pain for a period of time, so that patients cannot feel pain or feel greatly reduced pain when suffering from trauma [22–24]. However, the effect of anesthetics gradually decreases with the passage of time, and patients can gradually clearly feel pain. The stronger the pain of patients, the greater the impact on their psychological state, sleep quality, and other indicators. Drugs with better anesthetic effect will prolong the patients' analgesic time and reduce pain to a certain extent. Some patients have postoperative wound infection mainly due to the inflammatory manifestations caused by significant increase in the inflammatory factor expression levels of patients. The above results show that dexmedetomidine combined with ropivacaine can not only effectively alleviate the pain and improve cognitive function but also significantly reduce the inflammatory factor expression levels, thus improving the inflammatory manifestations and reducing infection risk in patients.

The analgesic time and postoperative awake time in the experimental group were significantly longer than those in the control group, with statistically significant differences ($P < 0.05$). There were no statistically significant differences in the changes of heart rate, oxygen saturation, and blood pressure at T0, T1, T2, T3, and T4 between the two groups ($P > 0.05$). There was no significant difference in blood pressure, oxygen saturation, and heart rate between the two groups before and after surgery, but the results showed that the blood pressure of the two groups decreased at 1 h and 2 h during surgery, and the decrease in the experimental group with dexmedetomidine and ropivacaine was more obvious. This phenomenon was mainly because dexmedetomidine had the effect of lowering blood pressure, and the blood pressure of the two groups gradually recovered after surgery, without affecting the surgical safety. In the study of scholars [25], after the patients undergoing craniocerebral surgery received ropivacaine anesthesia as well as anesthesia with ropivacaine and dexmedetomidine, respectively, the results showed that ropivacaine combined with dexmedetomidine can greatly shorten the onset time of nerve block, prolong the analgesic time, and reduce the pain of patients, which is consistent with the results of this study and fully proves the scientificity of the results in this study.

However, some limitations were still needed to be addressed. Randomized controlled trials require large samples for high-quality analysis of the effects of dexmedetomidine with ropivacaine in different subgroups of patients. The clinical outcomes were not enough to be analyzed due to the short postoperative period. The study did not evaluate effects of sex, age, and the demographical parameters on immune response. Also, clinical and functional recoveries, for example, postoperative pain and behavioral responses, were not evaluated.

In conclusion, dexmedetomidine combined with ropivacaine for anesthesia can significantly improve the anesthetic effect, prolong the analgesic time, and reduce the pain of patients. At the same time, it can also significantly improve the inflammation with little effect on the cognitive function of patients. Therefore, dexmedetomidine combined with ropivacaine has a high application effect in craniocerebral surgery, which is worthy of promotion and application in clinic.

Data Availability

The data used during the present study are available from the corresponding author upon reasonable request.

Conflicts of Interest

The authors declare that they have no conflict of interest.

Acknowledgments

This work was funded by the Tsitsihar Science and Technology Plan Innovation Incentive Project (CSFGG-2020008).

References

[1] Y. Chang, L. Xing, W. Zhou, and W. Zhang, "Up-regulating microRNA-138-5p enhances the protective role of dexmedetomidine on myocardial ischemia-reperfusion injury mice via down-regulating Ltb4r1," *Cell Cycle*, vol. 20, no. 4, pp. 445–458, 2021.

[2] C. Xiaohui, C. Dongtai, L. Qiang et al., "Dexmedetomidine alleviates hypoxia-induced synaptic loss and cognitive impairment via inhibition of microglial NOX2 activation in the hippocampus of neonatal rats," *Oxidative Medicine and Cellular Longevity*, vol. 2021, 18 pages, 2021.

[3] F. Jie, S. Yuncen, D. Fang et al., "The effect of perineural dexamethasone on rebound pain after ropivacaine single-injection nerve block: a randomized controlled trial [J]," *BMC Anesthesiology*, vol. 21, no. 1, 2021.

[4] S. Patrick, P. Michael, and H. Bishr, "Dexmedetomidine and remifentanil as sole anesthetics in infants: questionable hypnosis [J]," *Pediatric Anesthesia*, vol. 31, no. 2, pp. 250-251, 2021.

[5] L. Hu, Q. Cheng, Y. Li, Y. Zhang, J. Chen, and W. Chen, "The protective effects of ropivacaine against high glucose-induced brain microvascular endothelial injury by reducing MMPs and alleviating oxidative stress," *Neurotoxicity Research*, vol. 39, no. 3, pp. 851–859, 2021, (prepublish).

[6] A. DiCesare Michael, M. A. Rech, and M. DeMott Joshua, "Predictors of a response to dexmedetomidine in intubated, critically ill adult patients [J]," *Pharmacotherapy: The Journal of Human Pharmacology and Drug Therapy*, vol. 41, no. 2, pp. 191–197, 2021.

[7] Z. Gao, Z. Li, R. Deng et al., "Dexmedetomidine improves postoperative neurocognitive disorder after cardiopulmonary bypass in rats," *Neurological Research*, vol. 43, no. 2, pp. 164–172, 2021.

[8] C. Liang, Z. Jun, W. He, and L. Wei, "Comparative effects of dexmedetomidine and midazolam on dreaming of patients undergoing flexible bronchoscopy during general anesthesia," *Medical Science Monitor*, vol. 27, 2021.

[9] S. Rao and N. Rajan, "Dexmedetomidine as an adjunct for regional anesthetic nerve blocks [J]," *Current Pain and Headache Reports*, vol. 25, no. 2, 2021.

[10] Z.-G. Song, S.-Y. Pang, G.-Y. Wang, and Z. Zhang, "Comparison of postoperative analgesic effects in response to either dexamethasone or dexmedetomidine as local anesthetic adjuvants: a systematic review and meta-analysis of randomized controlled trials," *Journal of Anesthesia*, vol. 35, no. 2, pp. 270–287, 2021, (prepublish).

[11] Y. J. Wen, L. Jia, R. Y. Min et al., "Dexmedetomidine and Netrin-1 combination therapy inhibits endoplasmic reticulum stress by regulating the ERK5/MEF2A pathway to attenuate cerebral ischemia injury," *Frontiers in Neuroscience*, vol. 15, 2021.

[12] X. Qiang, B. Xu, H. Wang et al., "Analgesic effect of single-shot ropivacaine at different layers of the surgical site in primary total hip arthroplasty: a randomised, controlled, observer-blinded study [J]," *Journal of Orthopaedic Surgery and Research*, vol. 16, no. 1, 2021.

[13] W. C. Tseng, W. L. Lin, H. C. Lai et al., "Adjunctive dexmedetomidine infusion in open living donor hepatectomy: a way to enhance postoperative analgesia and recovery," *International Journal of Clinical Practice*, vol. 75, no. 5, p. e14002, 2021, (prepublish).

[14] Y. S. Jen, F. C. Ning, W. M. Jiuh et al., "Effects of dexmedetomidine on renal microcirculation in ischemia/reperfusion-induced acute kidney injury in rats [J]," *Scientific Reports*, vol. 11, no. 1, p. 11(1), 2021.

[15] X. Wang, R. Guo, X. Chen et al., "The effect of ultrasound-guided erector spinae plane block combined with dexmedetomidine on postoperative analgesia in patients undergoing modified radical mastectomy: a randomized controlled trial," *Pain and therapy*, vol. 10, no. 1, pp. 475–484, 2021, (prepublish).

[16] D. K. H. Chan, R. W. Goh, and C. H. L. Keh, "Continuous wound infusion with ropivacaine alone provides adequate analgesia following laparotomy," *Langenbeck's Archives of Surgery*, vol. 406, no. 2, pp. 413–418, 2021, (prepublish).

[17] K. Teppei, O. Masaki, S. Koji, N. Toru, and T. Takumi, "Suicidal attempt with caffeine overdose treated with dexmedetomidine: a case report [J]," *Journal of Medical Case Reports*, vol. 15, no. 1, 2021.

[18] Y. Liu, Y. Ma, Y. Liu, W. Wang, and F. Liu, "Propofol shows less negative effects on cognitive performances than dexmedetomidine in elderly intensive care unit patients," *Neurological Sciences*, vol. 42, no. 9, pp. 3767–3774, 2021, (prepublish).

[19] T. Xinyi, N. Kaifan, C. Hong et al., "Pruritus after continuous administration of epidural morphine for post-cesarean delivery analgesia: a case control study [J]," *BMC Pregnancy and Childbirth*, vol. 21, no. 1, p. 21(1), 2021.

[20] Z. Zhipeng, L. Xiaoyan, Z. Hongmei, and Z. Caijun, "Dexmedetomidine at a dose of 1 μM attenuates H9c2 cardiomyocyte injury under 3 h of hypoxia exposure and 3 h of reoxygenation through the inhibition of endoplasmic reticulum stress.[J]," *Experimental and Therapeutic Medicine*, vol. 21, no. 2, 2020.

[21] H. Lili, Q. Chuanqi, L. Wang, Z. Tiejun, and L. Jianguo, "Effects of dexmedetomidine on immune response in patients undergoing radical and reconstructive surgery for oral cancer.[J]," *Oncology Letters*, vol. 21, no. 2, 2020.

[22] V. Likhvantsev Valery, L. Giovanni, A. Grebenchikov Oleg et al., "Perioperative dexmedetomidine supplement decreases

Hindawi
BioMed Research International
Volume 2024, Article ID 9783981, 1 page
https://doi.org/10.1155/2024/9783981

Retraction

Retracted: Clinical Effect of Clarithromycin Combined with Tinidazole on Helicobacter pylori-Related Gastritis and Its Influence on COX-2 Expression

BioMed Research International

Received 12 March 2024; Accepted 12 March 2024; Published 20 March 2024

This article has been retracted by Hindawi following an investigation undertaken by the publisher [1]. This investigation has uncovered evidence of one or more of the following indicators of systematic manipulation of the publication process:

(1) Discrepancies in scope

(2) Discrepancies in the description of the research reported

(3) Discrepancies between the availability of data and the research described

(4) Inappropriate citations

(5) Incoherent, meaningless and/or irrelevant content included in the article

(6) Manipulated or compromised peer review

The presence of these indicators undermines our confidence in the integrity of the article's content and we cannot, therefore, vouch for its reliability. Please note that this notice is intended solely to alert readers that the content of this article is unreliable. We have not investigated whether authors were aware of or involved in the systematic manipulation of the publication process.

Wiley and Hindawi regrets that the usual quality checks did not identify these issues before publication and have since put additional measures in place to safeguard research integrity.

We wish to credit our own Research Integrity and Research Publishing teams and anonymous and named external researchers and research integrity experts for contributing to this investigation.

The corresponding author, as the representative of all authors, has been given the opportunity to register their agreement or disagreement to this retraction. We have kept a record of any response received.

References

[1] C. He, F. Kong, X. Zhu et al., "Clinical Effect of Clarithromycin Combined with Tinidazole on Helicobacter pylori-Related Gastritis and Its Influence on COX-2 Expression," *BioMed Research International*, vol. 2021, Article ID 4171019, 9 pages, 2021.

Hindawi
BioMed Research International
Volume 2021, Article ID 4171019, 9 pages
https://doi.org/10.1155/2021/4171019

Research Article

Clinical Effect of Clarithromycin Combined with Tinidazole on Helicobacter pylori-Related Gastritis and Its Influence on COX-2 Expression

Chenxi He,[1] Fanting Kong,[2] Xinying Zhu,[3] Fanlei Kong,[4] Wei Zhao,[1] Yanling Liu,[1] and Kuixiang Wang[4]

[1]*Department of Gastroenterology, Xingtai People's Hospital, Xingtai, 054000 Hebei Province, China*
[2]*Department of Breast Surgery, Xingtai People's Hospital, Xingtai, 054000 Hebei Province, China*
[3]*Department of Gastroenterology, The Third Affiliated Hospital of Hebei Medical University, Shijiazhuang, 050000 Hebei Province, China*
[4]*Department of Orthopedics, Xingtai People's Hospital, Xingtai, 054000 Hebei Province, China*

Correspondence should be addressed to Fanting Kong; fangyu441@163.com

Received 25 July 2021; Revised 21 October 2021; Accepted 25 October 2021; Published 30 November 2021

Academic Editor: Jun Yang

Studies have shown that COX-2 expression is upregulated in gastric cancer (GC) as well as in precancerous lesions and in Helicobacter pylori-induced inflammation, suggesting that cyclooxygenase-2 (COX-2) may play an important role in gastric carcinogenesis. We attempted to investigate the role of clarithromycin with tinidazole on Helicobacter pylori-related gastritis from the aspects of clinical effect and COX-2 expression. From January 2016 to January 2019, 130 patients with Helicobacter pylori-related chronic gastritis were collected and grouped into the observation group (OG) and the control group (CG). Altogether, 80 patients in the OG were treated with clarithromycin with tinidazole, while 50 patients in the CG were treated with amoxicillin with metronidazole. Clinical symptom improvement time, content of COX-2 and B cell lymphoma-2 (BCL-2), content of inflammatory factors interleukin-1 (IL-1), IL-4, and C-reactive protein (CRP), expression level of nutritional indicators serum albumin (ALB), realbumin (PA), and transferrin (TF), clearance of Helicobacter pylori, total effective rate, and incidence of adverse reactions were detected. Compared with the CG, the OG had shorter clinical symptom improvement time, lower COX-2 and Bcl-2, lower expression of inflammatory factors IL-1, IL-4, and CRP, higher expression of nutritional indicators ALB, TF, and PA, higher clearance rate of Helicobacter pylori, higher total effective rate, and lower incidence of adverse reactions. Clarithromycin combined with tinidazole can effectively improve the clinical effect of Helicobacter pylori-related gastritis and reduce the expression level of COX-2.

1. Introduction

Helicobacter pylori, a gram-negative bacterium, exists in the stomach, and its infection rate is as high as 90% all over the world, and about 20%-30% of infected people will undergo some kinds of diseases, including peptic ulcer, gastric carcinoma, or mucosa-related lymphoid tissue lymphoma [1–3]. In both developed and developing countries, Helicobacter pylori infection is closely related to the cross-living environment and hereditary susceptibility [4, 5]. The gastritis induced by it is chronic and can develop into atrophic gastritis, intestinal metaplasia, and dysplasia. At the same time, cyclooxygenase-2 (COX-2), an important factor in Helicobacter pylori-associated gastritis, angiogenesis, and inhibition of apoptosis in gastric carcinoma are evidently related to infiltration [6–8]. Recently, studies have shown that COX-2 expression is upregulated in GC as well as in precancerous lesions and in Helicobacter pylori-induced inflammation, suggesting that COX-2 may play an important role in gastric carcinogenesis [8, 9]. Chronic atrophic gastritis

caused by Helicobacter pylori activates synthesis of growth factors and cytokines leading to elevated COX-2 expression [6, 8]. Studies in vitro find that Helicobacter pylori was correlated with an upregulation of the expression of COX-2 mRNA/protein 2 in gastric cancer (GC) cell line. Therefore, the relatively early role of COX-2 in gastric carcinogenesis makes it an attractive target for cancer chemoprevention [6–11].

Clarithromycin interacts with peptidyl transferases of partial RNA of bacteria, which can effectively inhibit the activity of bacterial ribosomes and hinder the synthesis of proteins [12]. But the problem is that bacterial RNA is easy to mutate, which will lead to bacterial resistance to clarithromycin [13]. Tinidazole is a relatively new nitroimidazole derivative, which has strong antibacterial activity, good pharmacokinetic characteristics, and less side effects and is a good antibacterial drug [13]. Because of their good antibacterial properties, these two drugs are often used alone or in combination in various bacterial diseases [14–16]. In this study, we intended to explore the effects of clarithromycin and tinidazole on Helicobacter pylori and inflammation elimination. However, the effect of the combined use of the two drugs in Helicobacter pylori-related gastritis is still unclear. In this study, we studied the combination of two drugs and its influence on COX-2.

2. Method

2.1. Data. From January 2016 to January 2019, 130 Helicobacter pylori-related chronic gastritis patients were collected and grouped into the observation group (OG) and the control group (CG). The OG consisted of 43 men and 37 women, aged 32-57 years with an average age of 42.13 ± 1.21 years. The CG consisted of 28 men and 22 women, aged 31-58 years with an average age of 41.87 ± 1.53 years. There was no evident difference in general data between the CG and the OG ($p > 0.05$), but it was comparable. This research has been approved by the ethics committee. The family members and the patients have signed the informed consent form.

Inclusion criteria include patients have abdominal discomfort, burning pain, fullness, pantothenic acid, belching, and other symptoms; patients were confirmed as superficial gastritis or atrophic gastritis by gastroscopy; after 13C breath test, bacterial culture, and urease test, the results were positive, and there was direct evidence of Helicobacter pylori infection. Exclusion criteria include patients with severe hepatic and renal insufficiency and tumors; patients have contraindications to the drugs used in this study; patients were unconscious or suffered from mental illness; patients had communication barriers; patients did not cooperate with clinical treatment.

2.2. Methods. Patients in the CG were given amoxicillin combined with metronidazole for Helicobacter pylori-related gastritis, in which amoxicillin [manufacturer: Shanghai Haihong Group Chaohu C-Dragon Pharmaceutical Co., Ltd., SFDA Approval No. H34023991; specification: 125 mg (calculated by C16H199N3O5S)] was taken with warm water, three times a day, and each time was applied according to the patient's body mass, 5 mg/kg. Combined use of metronidazole (manufacturer: Fujian Yoshida Huamin Antibiotics Co., Ltd., SFDA Approval No. H35020323; specification: 200 mg) was applied with warm water, 3 times a day, 7 mg/kg. Fourteen days indicated a course, and a total of two courses were performed.

Patients in the OG were treated with clarithromycin and tinidazole, among which clarithromycin (manufacturer: Hainan Hewlett-Packard Medical Biotechnology Co., Ltd., SFDA Approval No. H20040649; specification: 125 mg) was taken with warm water, 3 times a day, and each amount was taken according to the patient's body mass, 0.5 mg/kg. At the same time, tinidazole was used in combination (manufacturer: Guangzhou Baiyunshan Pharmaceutical Holdings Co., Ltd., Baiyunshan Pharmaceutical General Factory, SFDA Approval No. H44021435; specification: 500 mg) and taken with warm water once a day, and each time was measured according to the patient's body mass, 15 mg/kg. Fourteen days indicated a course, and a total of two courses were performed.

2.3. Detection Indicators

2.3.1. Improvement Time of Clinical Symptoms. The improvement of clinical symptoms was observed and compared, including belch improvement time, epigastric pain improvement time, acid reflux improvement time, and abdominal distension improvement time.

2.3.2. Content of Cox-2 and Bcl-2. Before treatment and 14 days and 30 days after treatment, the mRNA contents of COX-2 and Bcl-2 were detected and compared. Before treatment and 14 days and 30 days after treatment, 3 ml of fasting venous blood was taken from a vacuum nonanticoagulation tube, placed at room temperature for 30 min, and centrifuged at $1500 \times g$ at 4°C for 10 min. Then, the upper serum was taken and detected by qPCR. First, total RNA in the blood was extracted: about 50 mg of plasma was moved into a 1.5 ml RNAse-free centrifuge tube, and 0.5 ml of TRIzol was added. After shaking, 0.5 ml of TRIzol was put in, and then, the whole process was lasted for about 30 minutes. A total of 200 μl chloroform was added to every 1 ml TRIzol, which was quickly shaken and mixed for 30 s, then placed on ice for 5 min, and then centrifuged at $1500 \times g$ at 4°C for 10 min. A pipette was applied to transfer about 400-600 μl of supernatant to a new centrifuge tube; then, 500 μl/1 ml TRIzol isopropanol was added, covered, mixed upside down repeatedly, then placed for 10 min, put into a centrifuge, and centrifuged at $1500 \times g$ at 4°C for 10 min. The supernatant was discarded, isopropyl alcohol was absorbed, and 1 ml of 75% ethanol was added and mixed well. It was centrifuged at $1500 \times g$ at 4°C for 10 min, and RNA was washed. The supernatant was discarded and dried naturally for 5-10 min, and 20 μl DEPC water was applied to dissolve the total RNA. Then, qPCR was carried out in ABI7500 fluorescence quantitative PCR instrument in the USA, and the steps were as follows: 95°C for 5 min, 95°C for 15 s, and 60°C for 30 s, for a total of 40 cycles, and

Table 1: Related primers.

Factor	Upstream primer	Downstream primer
COX-2	5′-TGAAACCCACTCCAAACACAG-3′	5′-TCATCAGGCACAGGAGGAAG-3′
Bcl-2	5′-TGGGATGCCTTTGTGGAACTAT-3′	5′-AGAGACAGCCAGGAGAAATCAAAC-3′
GAPDH	5′-TGCGAGTACTCAACACCAACA-3′	5′-GCATATCTTCGGCCCACA-3′

60~95°C. Compared with internal reference, Bcl-2/GAPDH and COX-2/GAPDH were obtained. The ratio represents the relative expression level (Table 1).

Before treatment and 14 days and 30 days after treatment, COX-2 and Bcl-2 were detected and compared. Cox-2 and Bcl-2 protein, Bcl-2/GAPDH, and COX-2/GAPDH in serum of the CG and the OG were tested by Western blot. The ratio represents the relative expression level.

2.3.3. Level of Inflammatory Factors. Before treatment and 14 days and 30 days after treatment, COX-2 and Bcl-2 in the blood of the two groups were detected and compared. Interleukin-1 (IL-1), interleukin-4 (IL-4), and serum C-reactive protein (CRP) were compared by ELISA.

2.3.4. Nutritional Indicators. Before treatment and 14 days and 30 days after treatment, the nutritional indexes in the blood of the CG and the OG were detected and compared. The nutritional indexes of the patients were detected by ELISA, and some plasma samples were collected to detect the serum albumin (ALB), prealbumin (PA), and transferrin (TF).

2.3.5. Clearance of Helicobacter pylori. After treatment, the clearance of Helicobacter pylori was examined. The two groups were examined by gastroscopy, and Hp was detected by 14C-urea breath test. If the bacteriological examination results are negative after treatment, the patients who are reinfected by the same pathogenic bacteria are counted as the number of reinfected cases. If the results are positive for two consecutive times after treatment, it is counted as the number of uncleaned cases. If the results are negative for two consecutive times after treatment, it is counted as the number of clearance cases. After that, the bacterial clearance rate of the two groups of patients was calculated, bacterial clearance rate = (cleared cases/total cases) × 100%.

2.3.6. Total Effective Rate. After treatment, the total effective rate of patients was counted. The criteria are as follows: symptoms such as fullness, loss of appetite, and stomachache disappeared after meals, and gastroscopy showed that the ulcer surface healed, which was cured; symptoms such as fullness, loss of appetite, and stomachache after meals were evidently improved, and gastroscopy showed that the ulcer surface was reduced by >80%, which was markedly effective; after dinner, symptoms such as fullness, loss of appetite, and stomachache were alleviated, and gastroscopy showed that the ulcer surface was reduced by 50%~80%, which was effective; symptoms and signs were not improved, and gastroscopy showed that the ulcer surface was reduced by <50%, which was ineffective. Total effective rate = [(effective cases + markedly effective cases + cured cases)/total cases] × 100%.

Table 2: General data.

Group	OG ($n = 80$)	CG ($n = 50$)	t/X^2	p
Gender			0.06	0.802
Male	43 (55.00)	28 (56.00)		
Female	37 (45.00)	22 (43.00)		
Average age (years)	42.13 ± 1.21	41.87 ± 1.53	1.08	0.284
BMI (kg/m^2)	26.82 ± 2.75	27.17 ± 2.93	0.69	0.493
Years of education	10.23 ± 1.47	9.97 ± 1.69	0.93	0.356
Patient's family residence			0.31	0.575
Rural	36 (45.00)	20 (40.00)		
Urban	44 (55.00)	30 (60.00)		
Patient's family type			0.07	0.785
Other	16 (20.00)	11 (22.00)		
Core family	64 (80.00)	39 (78.00)		
Drinking			0.81	0.367
Yes	66 (82.50)	38 (76.00)		
No	14 (17.50)	12 (24.00)		
History of hypertension				
Yes	52 (77.50)	41 (82.00)		
No	28 (22.50)	9 (18.00)		
History of hyperlipidemia			0.01	0.952
Yes	62 (77.50)	41 (82.00)		
No	18 (22.50)	9 (18.00)		
History of diabetes			0.09	0.759
Yes	58 (72.50)	35 (70.00)		
No	22 (27.50)	15 (30.00)		

2.3.7. Adverse Reactions. The total incidence of adverse reactions of the CG and the OG after treatment was analyzed. The related indicators were nausea, dizziness, and vomiting.

2.4. Statistical Methods. SPSS 22.0 was applied for comprehensive data statistical analysis, and the measurement data were represented as $X \pm S$ and tested by t-test. The counting data were represented as X^2. When $p < 0.05$, the difference is obvious and has statistical significance.

3. Results

3.1. General Information. There was no evident difference in general information such as gender, average age, average course of disease, and average weight between the CG and the OG ($p > 0.05$). See Table 2 for details.

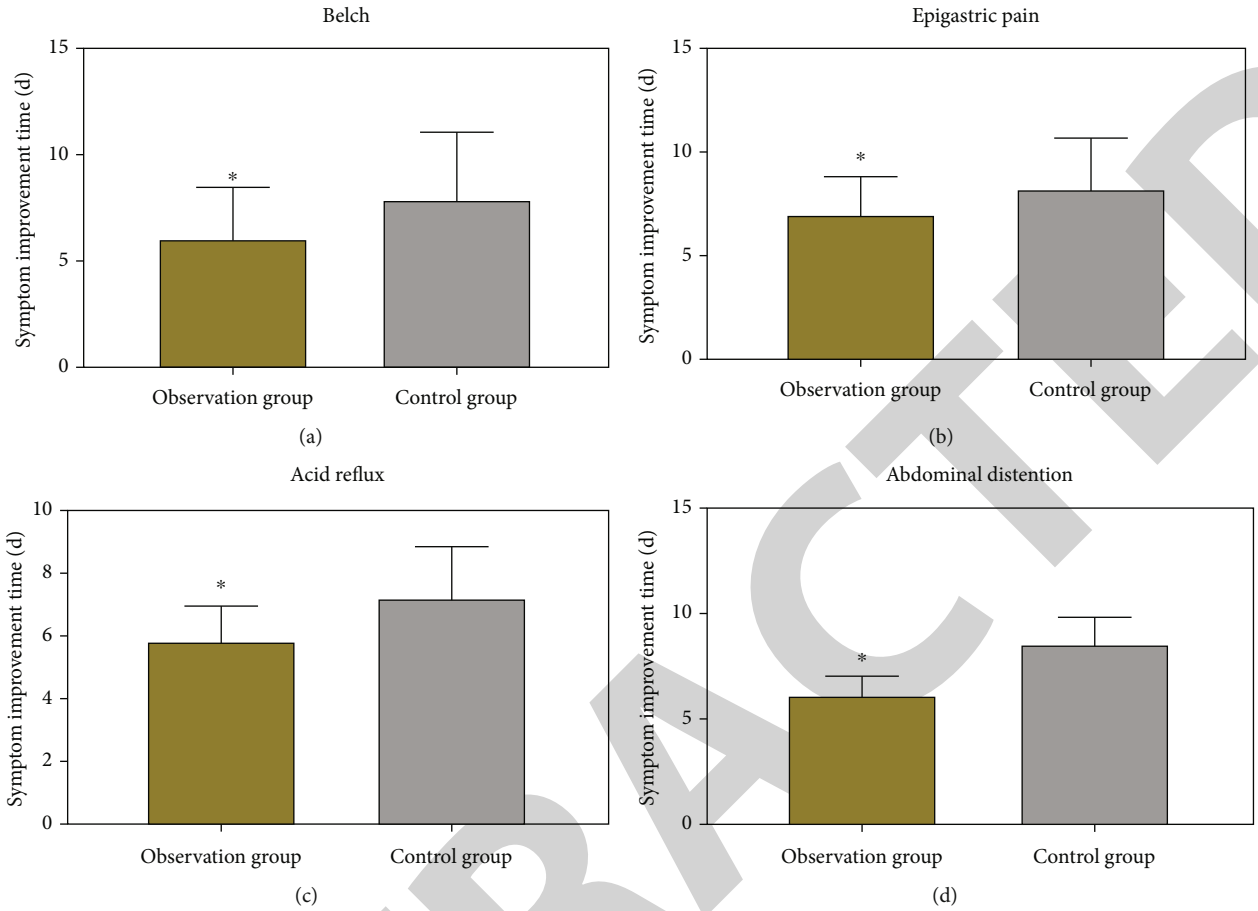

Figure 1: Improvement time of clinical symptoms of the two groups of patients: (a) improvement time of belch: the improvement time of belching in the OG was shorter than that in the CG ($p < 0.05$); (b) improvement time of epigastric pain: the improvement time of epigastric pain in the OG was shorter than that in the CG ($p < 0.05$); (c) improvement time of acid reflux: the improvement time of acid reflux in the OG was shorter than that in the CG ($p < 0.05$); (d) improvement time of abdominal distension: the improvement time of abdominal distension in the OG was shorter than that in the CG ($p < 0.05$). $*$ means compared with the CG, $p < 0.05$.

3.2. The Improvement Time of Clinical Symptoms in the OG Was Shorter Than That in the CG. The belch improvement time, epigastric pain improvement time, acid reflux improvement time, and abdominal distension improvement time in the OG were shorter than those in the CG ($p < 0.05$). See Figure 1 for details.

3.3. Cox-2 and Bcl-2 in the OG after Treatment Were Lower Than Those in the CG. There was no evident difference in COX-2, Bcl-2 mRNA, and protein levels between the CG and the OG before treatment ($p > 0.05$). The mRNA and protein levels of Cox-2 and Bcl-2 in the OG were lower than those in the CG after 14 days of treatment ($p < 0.05$), but there was no difference between the CG and the OG after 30 days of treatment ($p > 0.05$). See Figure 2 for details.

3.4. The Level of Inflammatory Factors in the OG after Treatment Was Lower Than That in the CG. Comparing IL-2, IL-4, and CRP before treatment and 14 d and 30 d after treatment, it was found that there was no evident difference in IL-1, IL-4, and CRP between the CG and the OG before treatment ($p > 0.05$), but after treatment for 14 d and 30 d, IL-1, IL-4, and CRP in the CG and the OG decreased evidently. See Figure 3 for details.

3.5. After Treatment, the Nutritional Indexes of the OG Were Higher Than Those of the CG. Comparing the levels of nutritional indexes before treatment and after 14 days and 30 days of treatment, it was found that there was no evident difference in ALB, Tf, and PA levels between the CG and the OG before treatment ($p > 0.05$), but after 14 days and 30 days of treatment, the levels of ALB, Tf, and PA in the OG were evidently higher than those in the CG ($p > 0.05$). See Figure 4 for details.

3.6. The Clearance of Helicobacter pylori in the OG Was Better Than That in the CG. The clearance rate of Helicobacter pylori in the OG was evidently higher than that in the CG ($p < 0.05$). See Table 3 for details.

3.7. The Total Effective Rate of the OG Was Higher Than That of the CG. The total effective rates of the CG and the OG were compared. The total effective rate of the OG was evidently higher than that of the CG ($p < 0.05$). See Table 4 for details.

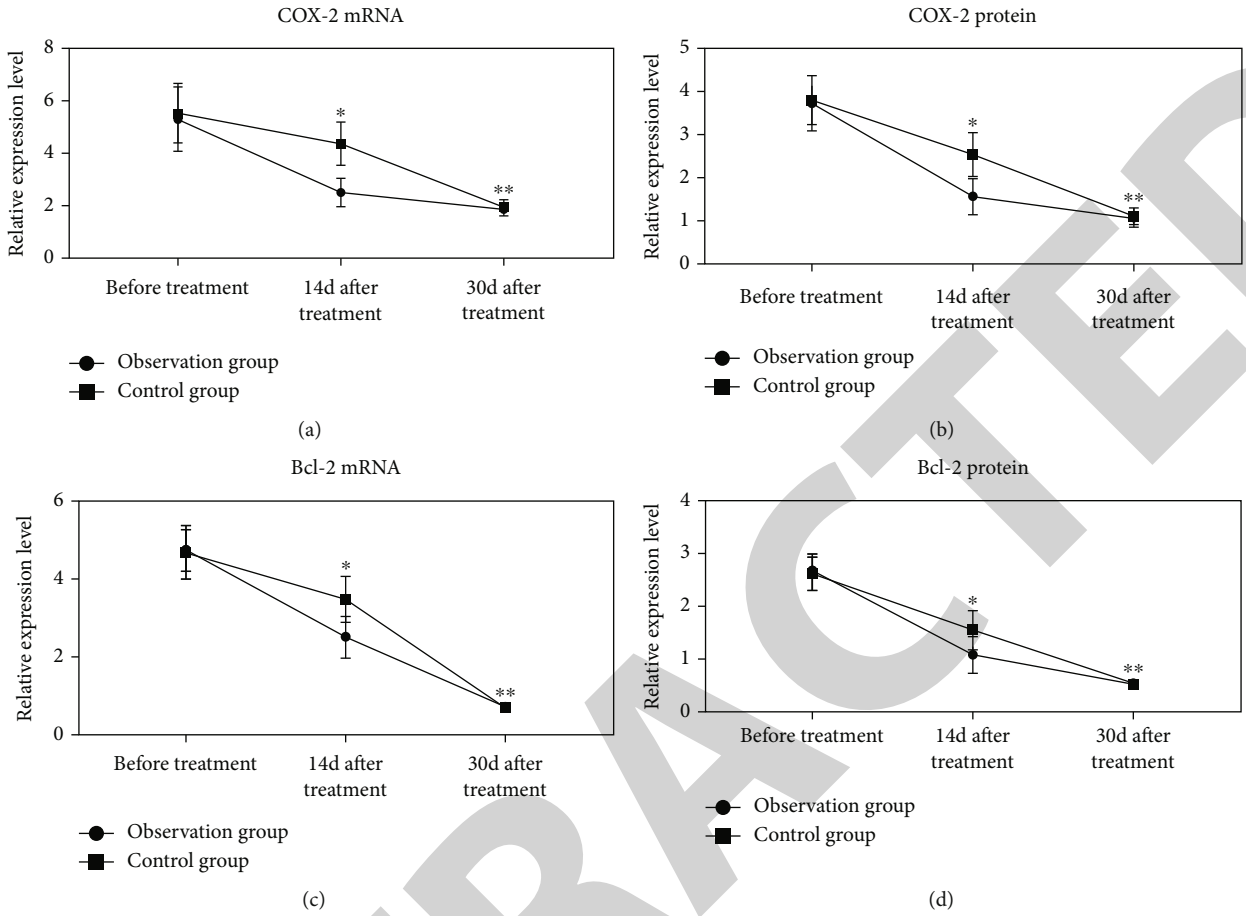

Figure 2: Relative expression levels of COX-2 and Bcl-2 in the two groups: (a) COX-2 mRNA: after treatment for 14 d and 30 d, COX-2 mRNA levels in the two groups decreased evidently, and Cox-2 mRNA levels in the OG were lower than those in the CG after treatment for 14 d ($p < 0.05$), but there was no difference between the two groups after treatment for 30 d ($p > 0.05$); (b) COX-2 protein: after 14 days and 30 days of treatment, the COX-2 protein level in the OG was evidently lower than that in the CG ($p < 0.05$), but there was no difference between the CG and the OG after 30 days of treatment ($p > 0.05$); (c) Bcl-2 mRNA: after treatment for 14 d and 30 d, the Bcl-2 mRNA level in the OG was evidently lower than that in the CG ($p < 0.05$), but there was no difference between the CG and the OG after treatment for 30 d ($p > 0.05$); (d) Bcl-2 protein: after 14 days and 30 days of treatment, the protein level of Bcl-2 in the OG was evidently lower than that in the CG ($p < 0.05$), but there was no difference between the CG and the OG after 30 days of treatment ($p > 0.05$). $*$ means compared with before treatment, $p < 0.05$; $**$ means compared with 14 days after treatment, $p < 0.05$.

3.8. The Incidence of Adverse Reactions in the OG Was Higher Than That in the CG. Comparing the incidence of adverse reactions between the CG and the OG, it was found that the incidence of adverse reactions in the OG was evidently lower than that in the CG ($p < 0.05$). See Table 5 for details.

4. Discussion

Nowadays, Helicobacter pylori is the leading cause of a series of stomach diseases [17, 18]. For the treatment of Helicobacter pylori-related gastritis, it is necessary to use a treatment method with good antibacterial effect. In this study, we studied the effect of clarithromycin and tinidazole on C gastritis. In the discussion, we will discuss the combination of these two drugs on patients from the aspects of Helicobacter pylori, COX-2, and inflammatory factors.

In this experiment, the clearance rate of Helicobacter pylori in the OG was higher than that in the CG. In superficial gastritis caused by Helicobacter pylori, lymphocytes, polymorphonuclear leukocytes, and macrophages in gastric mucosa will be infected. With the passage of time, gastric mucosa will undergo further loss of glandular cells, which will eventually deteriorate into atrophic gastritis. Helicobacter pylori does not usually interact directly with immune cells in the stomach, yet components of the bacterium can exert their effects on these cells, leading to modulation of host inflammation [6, 12, 19]. Indeed, studies in an Helicobacter pylori mouse infection model showed that Helicobacter pylori vacuolating cytotoxin A (VacA) targets gastric lamina propria myeloid cells, thereby suppressing interleukin-23 (IL-23) expression by dendritic cells and inducing IL-10 and transforming growth factor-β (TGF-β) expression in macrophages. It was suggested that Helicobacter pylori uses VacA to promote tolerogenesis in the host [19]. Helicobacter pylori bacterial factors can also upregulate proinflammatory responses in immune cells thus leading to an exacerbation of inflammation. An example of

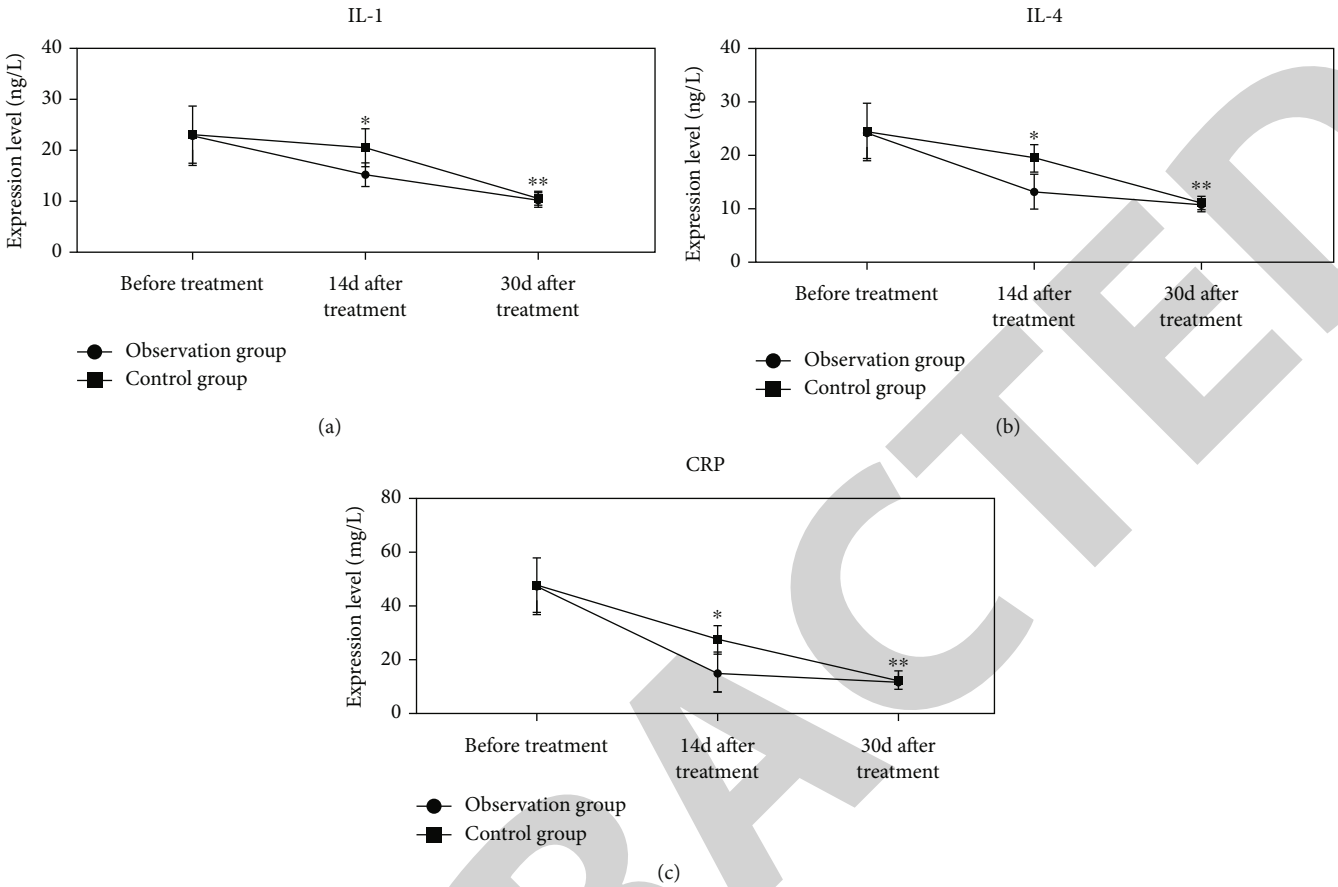

Figure 3: Levels of inflammatory factors in the two groups: (a) IL-1: after 14 days and 30 days of treatment, IL-1 levels in the two groups decreased evidently, IL-1 levels in the OG were lower than those in the CG after 14 days of treatment ($p < 0.05$), but there was no difference between the two groups after 30 days of treatment ($p > 0.05$); (b) IL-4: after 14 days and 30 days of treatment, the levels of IL-4 in the OG were evidently lower than those in the CG ($p < 0.05$), but there was no difference between the CG and the OG after 30 days of treatment ($p > 0.05$); (c) CRP: after 14 days and 30 days of treatment, the levels of CRP in the OG were evidently lower than those in the CG ($p < 0.05$), but there was no difference between the CG and the OG after 30 days of treatment ($p > 0.05$). $*$ means compared with before treatment, $p < 0.05$; $**$ means compared with 14 days after treatment, $p < 0.05$.

this is the uncharacterized Helicobacter pylori protein HP1173 whose secretion levels vary significantly among strains. Recombinant HP1173 (rHP1173) was able to bind to THP-1 monocyte-derived macrophages, resulting in the production of the proinflammatory cytokines, tumor necrosis factor (TNF), and IL-1β, as well as the C-X-C motif chemokine ligand 8 (CXCL8), in a dose- and time-dependent manner [19].

In our study, in view of the results of this experiment on inflammatory factors, the level of inflammatory factors in the OG decreased faster, indicating that clarithromycin combined with tinidazole is more effective in eliminating Helicobacter pylori, and better pathogen elimination can alleviate the inflammatory reaction caused by this bacterium. In some studies, it was found that amoxicillin and metronidazole have poor clearance effect on Helicobacter pylori, and it is easy to cause bacterial drug resistance when they are combined with metronidazole [20, 21]. Clarithromycin is a good drug, but it can easily cause bacterial resistance. Tinidazole has been proved to be effective in the treatment of Helicobacter pylori infection and can be used as the first-line treatment drug for eradication of Helicobacter pylori. Its combination with clarithromycin can reduce the drug resistance of Helicobacter pylori caused by clarithromycin [22]. To sum up, it can be proved that clarithromycin combined with tinidazole has a better cleaning effect on Helicobacter pylori, thus reducing the inflammatory reaction.

According to the results of COX-2 and Bcl-2 in the CG and the OG, the mRNA and protein levels of COX-2 and Bcl-2 in the OG were lower after operation. Cox-2 is highly induced by various inflammatory cytokines in the site where inflammation occurs. Therefore, when gastritis occurs, inflammatory cytokines rise, leading to an increase in their levels. Upregulating of Cox-2 can even stimulate cell division and angiogenesis, inhibit apoptosis, and lead to the occurrence of gastric carcinoma [23]. Bcl-2 is another factor caused by inflammatory factors, which plays a promoting role in the carcinogenesis mediated by Helicobacter pylori infection [24]. Therefore, combined with the previous clearance results, we found that Helicobacter pylori can cause severe inflammatory reaction in the stomach, with the increase of inflammatory factors, COX-2, Bcl-2, and other factors, and then induce carcinoma in the stomach. Clarithromycin combined with tinidazole has a better bacterial

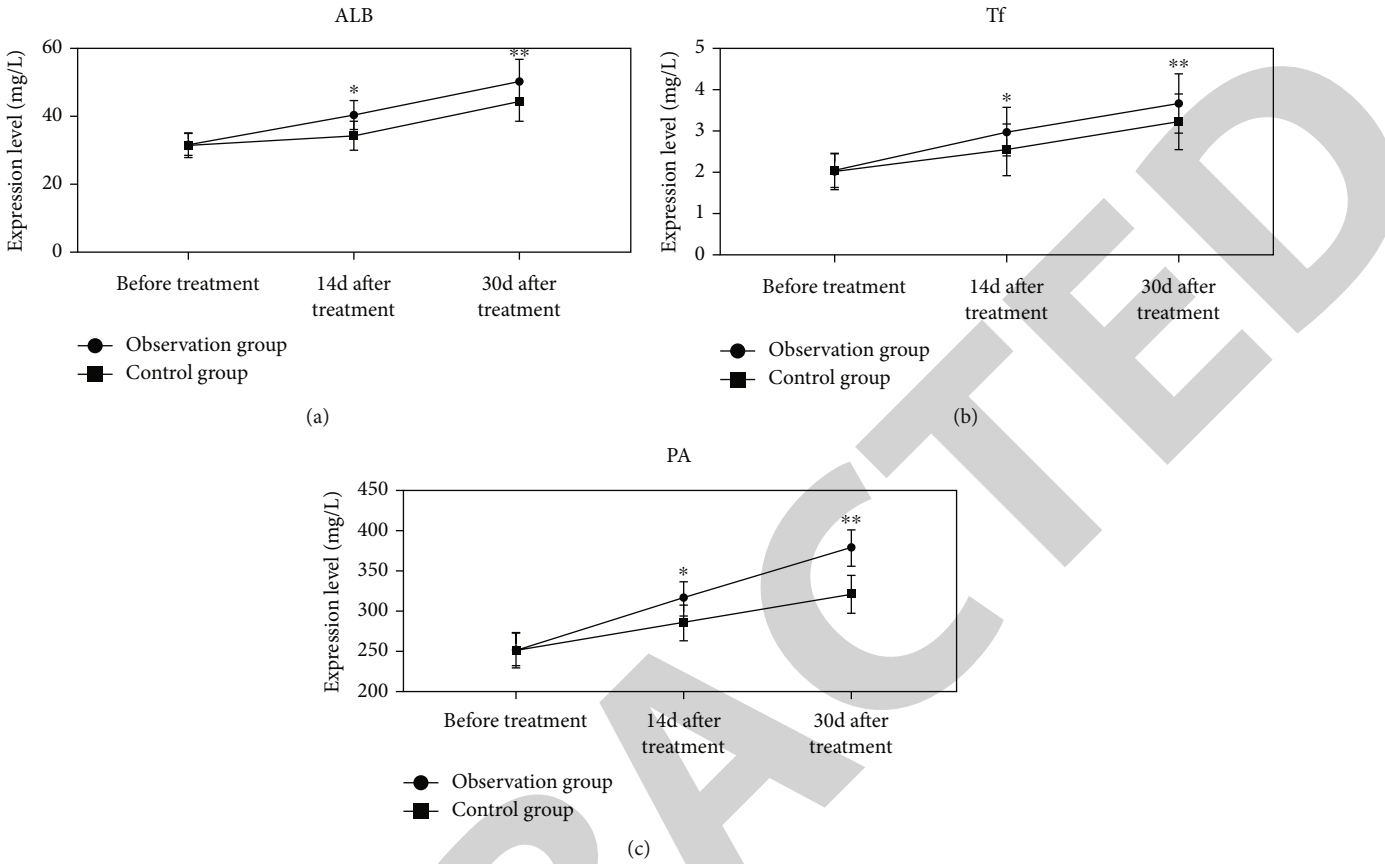

Figure 4: Nutritional index levels of patients in the two groups: (a) ALB: after treatment for 14 d and 30 d, the ALB levels of patients in the two groups increased evidently, and the ALB levels in the OG were lower than those in the CG after treatment for 14 d and 30 d ($p < 0.05$); (b) Tf: after 14 days and 30 days of treatment, the Tf level in the OG was evidently higher than that in the CG ($p < 0.05$); (c) PA: after treatment for 14 days and 30 days, the PA level in the OG was evidently higher than that in the CG ($p < 0.05$). $*$ means compared with before treatment, $p < 0.05$; $**$ means compared with 14 days after treatment, $p < 0.05$.

Table 3: Total effective rate.

Classification	OG ($n = 80$)	CG ($n = 50$)	X^2	p
Number of reinfection cases	4 (5.00)	7 (14.00)	—	—
Number of uncleared cases	2 (2.50)	5 (10.00)	—	—
Number of cleared cases	74 (92.50)	38 (76.00)	—	—
Clearance rate (%)	76 (92.50)	38 (76.00)	7.02	0.008

Table 4: Total effective rate.

Classification	OG ($n = 80$)	CG ($n = 50$)	X^2	p
Cured	34 (42.50)	17 (34.00)	—	—
Markedly effective	44 (55.00)	15 (30.00)		
Effective	20 (25.00)	11 (22.00)	—	—
Ineffective	2 (2.50)	7 (14.00)	—	—
Total effective rate (%)	78 (97.50)	43 (86.00)	6.32	0.012

Table 5: Incidence of complications.

Classification	OG ($n = 80$)	CG ($n = 50$)	X^2	p
Nausea	1 (1.25)	5 (10.00)	—	—
Dizzy	3 (3.75)	4 (8.00)	—	—
Vomiting	1 (1.25)	1 (2.00)	—	—
Incidence of adverse reactions (%)	5 (6.25)	10 (20.00)	5.70	0.017

clearance effect, and its role in treating Helicobacter pylori is to clean up Helicobacter pylori which induced diseases and then reduce the inflammation, reduce inflammatory factors, and inhibit the increase of COX-2 and Bcl-2 levels caused by inflammatory factors, thus effectively alleviating various symptoms caused by stomach inflammation. Therefore, we can see that some clinical symptoms in the OG have a shorter improvement time. The decrease of adverse

reactions in the OG may be that there are fewer inflammatory factors and the symptoms are relieved better, so the incidence of adverse reactions is greatly reduced.

There are still some shortcomings in this experiment. We failed to investigate the satisfaction and dissatisfaction of patients by questionnaire when they were discharged from hospital. In the future research, we will pay attention to the treatment methods. At the same time, we should pay more attention to molecular mechanisms and the relationship between gastric carcinoma induced by Helicobacter pylori and these drugs.

To sum up, clarithromycin combined with tinidazole can better eliminate Helicobacter pylori, reduce the expression of COX-2 and other molecules, and play a better clinical effect.

Data Availability

The authors confirm that the data supporting the findings of this study are available within the article.

Conflicts of Interest

No conflict of interest exists.

Authors' Contributions

Chenxi He and Fanting Kong contributed equally to this study as co-first authors.

Acknowledgments

This study was supported by the Youth Science and Technology Project of Hebei Health Department (No. 20210237).

References

[1] T. Tongtawee, T. Bartpho, S. Kaewpitoon et al., "Genetic polymorphisms in TLR1, TLR2, TLR4, and TLR10 of Helicobacter pylori-associated gastritis: a prospective cross-sectional study in Thailand," *European Journal of Cancer Prevention*, vol. 27, no. 2, pp. 118–123, 2018.

[2] Y. Qing, M. Wang, Y. M. Lin et al., "Correlation between Helicobacter pylori-associated gastric diseases and colorectal neoplasia," *World Journal of Gastroenterology*, vol. 22, no. 18, pp. 4576–4584, 2016.

[3] S. F. Zaidi, "Helicobacter pylori associated Asian enigma: does diet deserve distinction?," *Journal of Gastrointestinal Oncology*, vol. 8, no. 4, pp. 341–350, 2016.

[4] V. Misra, R. Pandey, S. P. Misra, and M. Dwivedi, "Helicobacter pylori and gastric cancer: Indian enigma," *World Journal of Gastroenterology*, vol. 20, no. 6, pp. 1503–1509, 2014.

[5] T. Tongtawee, S. Kaewpitoon, N. Kaewpitoon et al., "Characteristics and risk factors of Helicobacter pylori associated gastritis: a prospective cross-sectional study in Northeast Thailand," *Gastroenterology Research and Practice*, vol. 2016, Article ID 9130602, 8 pages, 2016.

[6] R. Mejias-Luque, J. Zoller, F. Anderl et al., "Lymphotoxin β receptor signalling executes Helicobacter pylori-driven gastric inflammation in a T4SS-dependent manner," *Gut*, vol. 66, no. 8, pp. 1369–1381, 2017.

[7] Y. Teng, B. Cang, F. Mao et al., "Expression of ETS1 in gastric epithelial cells positively regulate inflammatory response in Helicobacter pylori-associated gastritis," *Cell Death & Disease*, vol. 11, no. 7, p. 498, 2020.

[8] F. Han, J. Ren, J. Zhang et al., "JMJD2B is required for Helicobacter pylori-induced gastric carcinogenesis via regulating COX-2 expression," *Oncotarget*, vol. 7, no. 25, pp. 38626–38637, 2016.

[9] H. J. Lee, J. M. Park, Y. M. Han et al., "The role of chronic inflammation in the development of gastrointestinal cancers: reviewing cancer prevention with natural anti-inflammatory intervention," *Expert Review of Gastroenterology & Hepatology*, vol. 10, no. 1, pp. 129–139, 2016.

[10] M. Jeong, J. M. Park, Y. M. Han et al., "Dietary prevention of Helicobacter pylori-associated gastric cancer with kimchi," *Oncotarget*, vol. 6, no. 30, pp. 29513–29526, 2015.

[11] Y. M. Han, K. J. Kim, M. Jeong et al., "Suppressed Helicobacter pylori-associated gastric tumorigenesis in fat-1 transgenic mice producing endogenous ω-3 polyunsaturated fatty acids," *Oncotarget*, vol. 7, no. 41, pp. 66606–66622, 2016.

[12] F. Mégraud, L. Bénéjat, E. N. Ontsira Ngoyi, and P. Lehours, "Molecular approaches to identify Helicobacter pylori antimicrobial resistance," *Gastroenterology Clinics of North America*, vol. 44, no. 3, pp. 577–596, 2015.

[13] B. S. Sanches, G. M. Martins, K. Lima et al., "Detection of Helicobacter pylori resistance to clarithromycin and fluoroquinolones in Brazil: a national survey," *World Journal of Gastroenterology*, vol. 22, no. 33, pp. 7587–7594, 2016.

[14] M. A. B. Petrina, L. A. Cosentino, L. K. Rabe, and S. L. Hillier, "Susceptibility of bacterial vaginosis (BV)-associated bacteria to secnidazole compared to metronidazole, tinidazole and clindamycin," *Anaerobe*, vol. 47, pp. 115–119, 2017.

[15] R. Brindle, O. M. Williams, P. Davies et al., "Adjunctive clindamycin for cellulitis: a clinical trial comparing flucloxacillin with or without clindamycin for the treatment of limb cellulitis," *BMJ Open*, vol. 7, no. 3, article e013260, 2017.

[16] J. Albrecht, P. A. Baine, B. Ladizinski, G. B. Jemec, and M. Bigby, "Long-term clinical safety of clindamycin and rifampicin combination for the treatment of hidradenitis suppurativa. A critically appraised topic," *The British Journal of Dermatology*, vol. 180, no. 4, pp. 749–755, 2019.

[17] Q. Hu, Y. Zhang, X. Zhang, and K. Fu, "Gastric mucosa-associated lymphoid tissue lymphoma and Helicobacter pylori infection: a review of current diagnosis and management," *Biomarker Research*, vol. 4, no. 1, p. 15, 2016.

[18] M. R. Nair, D. Chouhan, S. Sen Gupta, and S. Chattopadhyay, "Fermented foods: are they tasty medicines for Helicobacter pylori associated peptic ulcer and gastric cancer?," *Frontiers in Microbiology*, vol. 7, p. 1148, 2016.

[19] H. Yin, A. Chu, S. Liu, Y. Yuan, and Y. Gong, "Identification of DEGs and transcription factors involved in H. pylori-associated inflammation and their relevance with gastric cancer," *PeerJ*, vol. 8, article e9223, 2020.

[20] A. Shiotani, H. Lu, M. P. Dore, and D. Y. Graham, "Treating Helicobacter pylori effectively while minimizing misuse of antibiotics," *Cleveland Clinic Journal of Medicine*, vol. 84, no. 4, pp. 310–318, 2017.

[21] D. Y. Graham, "Vonoprazan Helicobacter pylori eradication therapy: ethical and interpretation issues," *Gut*, vol. 66, no. 2, pp. 384–386, 2017.

Hindawi
BioMed Research International
Volume 2024, Article ID 9793809, 1 page
https://doi.org/10.1155/2024/9793809

Retraction

Retracted: The Expression of miR-23a And miR-146a in the Saliva of Patients with Periodontitis and Its Clinical Significance

BioMed Research International

Received 12 March 2024; Accepted 12 March 2024; Published 20 March 2024

This article has been retracted by Hindawi following an investigation undertaken by the publisher [1]. This investigation has uncovered evidence of one or more of the following indicators of systematic manipulation of the publication process:

(1) Discrepancies in scope

(2) Discrepancies in the description of the research reported

(3) Discrepancies between the availability of data and the research described

(4) Inappropriate citations

(5) Incoherent, meaningless and/or irrelevant content included in the article

(6) Manipulated or compromised peer review

The presence of these indicators undermines our confidence in the integrity of the article's content and we cannot, therefore, vouch for its reliability. Please note that this notice is intended solely to alert readers that the content of this article is unreliable. We have not investigated whether authors were aware of or involved in the systematic manipulation of the publication process.

Wiley and Hindawi regrets that the usual quality checks did not identify these issues before publication and have since put additional measures in place to safeguard research integrity.

We wish to credit our own Research Integrity and Research Publishing teams and anonymous and named external researchers and research integrity experts for contributing to this investigation.

The corresponding author, as the representative of all authors, has been given the opportunity to register their agreement or disagreement to this retraction. We have kept a record of any response received.

References

[1] L. Kang, N. Li, and L. Wang, "The Expression of miR-23a and miR-146a in the Saliva of Patients with Periodontitis and Its Clinical Significance," *BioMed Research International*, vol. 2021, Article ID 5135278, 8 pages, 2021.

Hindawi
BioMed Research International
Volume 2021, Article ID 5135278, 8 pages
https://doi.org/10.1155/2021/5135278

Research Article

The Expression of miR-23a and miR-146a in the Saliva of Patients with Periodontitis and Its Clinical Significance

Lanhua Kang,[1] Ning Li,[2] and Lexiu Wang[3]

[1]*Department of Stomatology, The First Affiliated Hospital of Shandong First Medical University (Shandong Qianfo Hospital), China*
[2]*Department of Prosthodontics, Taian Stomatological Hospital, Shandong Province, China*
[3]*Department of Stomatology, Jinan Jigang Hospital, Shandong Province, China*

Correspondence should be addressed to Lexiu Wang; muxie3848@163.com

Received 23 July 2021; Revised 5 October 2021; Accepted 7 October 2021; Published 30 November 2021

Academic Editor: Jianxin Shi

Background. This study is aimed at exploring the significance of the expression of miR-23a and miR-146a in patients with periodontitis and their correlations with inflammatory factors. *Methods*. A total of 120 patients with chronic periodontitis admitted to the department of stomatology in Yantai Yuhuangding Hospital from August 2017 to December 2018 were enrolled as a study group, and 80 healthy volunteers in physical examination during the same period were enrolled as a control group. The expression of miR-23a, miR-146a, interleukin-1β (IL-1β), interleukin-6 (IL-6), and interleukin-17 (IL-17) in the saliva of people in the two groups was determined using the quantitative real-time polymerase chain reaction (qRT-PCR) and enzyme-linked immunosorbent assay (ELISA). *Results*. The study group showed significantly higher relative expression of saliva miR-23a and miR-146a than the control group. The area under the curve (AUC) of saliva miR-23a and miR-146a for diagnosing periodontitis was 0.857 and 0.886, respectively. The expression of saliva miR-23a and miR-146a increased with the deterioration of periodontitis in the patients. After basic treatment, the study group showed significantly decreased expression of saliva miR-23a and miR-146a. Patients in the study group showed significantly higher levels of saliva IL-1β, IL-6, and IL-17 than those in the control group, and their saliva miR-23a and miR-146a were positively correlated with their saliva IL-1β, IL-6, and IL-17, respectively. *Conclusion*. Saliva miR-23a and miR-146a can be used as biomarkers for the diagnosis and assessment of periodontitis, and they may have regulatory relationships with IL-1β, IL-6, and IL-17.

1. Introduction

Periodontitis is a chronic destructive disease of periodontal tissues caused by oral flora disorder [1]. It is a common disease. According to statistics, 10-15% of the global population suffers from severe periodontitis [2]. It not only has negative effects on patients' oral health, emotion, speech, and nutrition but also increases the risks of systemic diseases such as cardiovascular disease, diabetes, and disease of the respiratory system. It may also affect pregnancy outcomes [3, 4]. Because the symptoms of early periodontitis are not obvious and oral endoscopy is relatively costly and difficult to be widely carried out, the diagnosis level of early periodontitis is relatively low, and most patients have already suffered from tooth loss at the time of diagnosis and are already under serious negative impacts of it on their life quality. Therefore, it is of great clinical value to find easily detectable and economic biomarkers for patients with periodontitis.

MicroRNA (miR) is a short-chain noncoding RNA, with the ability to regulate physiological and pathological processes by blocking protein translation or inhibiting target gene expression through inducing mRNA degradation [5]. Because miR can be involved in cell growth, proliferation, apoptosis, and other biological functions, it has become a research hotspot [6]. miR is a major regulator of inflammation, and the imbalance of molecular processes involved in its induced inflammatory pathway has been proved to conduce to the development of inflammatory diseases [7]. miR-23a and miR-146a, major members of miR, are abnormally expressed in many inflammatory diseases. For example, a study by Hu et al. revealed that miR-23a showed

Table 1: Primer sequences.

Group	Upstream (5′-3′)	Downstream (5′-3′)
miR-23a	GGGGATCACATTGCCAGG	AGTGCGTGTCGTGGAGTC
miR-146a	TGTTGCTGAAGAGCTCTGGTAC	TCGTCTGATGATGTCGAATGTAC
U6	CTTCGGCAGCACATATACTAAAAT	CGCTTCACGAATTTGCGTGTCAT

downregulated expression in articular cartilage tissues of patients with rheumatoid arthritis, and it could inhibit the interleukin-17- (IL-17-) mediated expression of proinflammatory mediators by targeting IKKα [8], and a study by Wade et al. pointed out that miR-23a decreased in synovial tissues of patients with psoriatic arthritis, and its decreased expression can induce activation of synovial fibroblasts [9]. A study by Zeng et al. concluded that upregulation of miR-146a expression was helpful to inhibit inflammatory responses in rats with acute lung injury induced by lipopolysaccharide [10]. In addition, a study by Zhou et al. revealed that in terms of rheumatoid arthritis, miR-146a promoted the proinflammatory phenotypes that regulate T cells by intensifying the activation of STAT1, thus contributing to the pathogenesis of rheumatoid arthritis [11]. All the above studies revealed that miR-23a and miR-146a were closely related to inflammatory diseases. However, there are few reports on miR-23a and miR-146a in periodontitis. Therefore, we selected miR-23a and miR-146a as research factors for this study.

This study explored the expression of saliva miR-23a and miR-146a in patients and healthy people and the correlations of the two factors with inflammatory factors so as to find an easily detectable and economical biomarker for the diagnosis and prognosis of periodontitis.

2. Materials and Methods

2.1. Patients. A total of 120 patients with chronic periodontitis admitted to the department of stomatology in Yantai Yuhuangding Hospital from August 2017 to December 2018 were enrolled as a study group. The inclusion criteria were as follows: patients meeting the diagnostic criteria of periodontitis [12], patients with detailed clinical data, patients with more than 16 remaining teeth in their oral cavities, patients who had not taken any antibiotics or immunoregulation drugs within 6 months before participating in this study and had not received any drugs for periodontitis or surgical treatment for it within 6 months before it, and patients with normal communication ability. In addition, 80 healthy volunteers undergoing physical examination in Yantai Yuhuangding Hospital at the same time were selected as a control group. The exclusion criteria were as follows: patients with pneumonia, osteoarthritis, or other inflammatory diseases; patients with infectious diseases or tumor diseases; women in pregnancy, lactation, or menstruation; or patients who had received orthodontic treatment. This study was approved by the Medical Ethics Committee of Yantai Yuhuangding Hospital, and each person in the two groups signed an informed consent form after understanding the study.

2.2. Main Instruments and Reagents. The materials used in this study include the following: TRIzol extraction kit (Wuhan Chundu Biotechnology Co., Ltd., China, CDLG-4396); reverse transcription kit (Tiangen Biotech (Beijing) Co., Ltd., China, FP209); real-time fluorescence ration PCR instrument (ABI Companies, United States, 7300); spectrophotometer (Hach Company, United States, DR5000); enzyme-linked immunosorbent assay (ELISA) kits for human interleukin-1β (IL-1β), human interleukin-6 (IL-6), and human interleukin-17 (IL-17) (Elabscience, China, E-EL-H0149C, E-EL-H102C, and E-EL-H105km-1); and multifunctional enzyme marking instrument (Shanghai Flash Spectrum Biotechnology Co., Ltd., China, SuPerMax 3100). All primers were designed and synthesized by Takara Bioengineering Co., Ltd. (China). See Table 1.

2.3. Severity Grading. The severity of periodontitis was evaluated according to the periodontal probing depth (PD), gingival index (GI), attachment loss (AL), and X-ray film as follows: mild periodontitis: GI > 1, AL: 1-2 mm, alveolar bone resorption length < 1/3 root length, and PD ≤ 4 mm; moderate periodontitis: GI > 1, AL: 3-4 mm, alveolar bone resorption length: 1/3-1/2 root length, and PD ≤6 mm; and severe periodontitis: GI > 1, AL ≥ 5 mm, alveolar bone resorption length ≥ 1/2 root length, and PD > 6 mm.

2.4. Basic Periodontal Treatment and Reexamination. Before treatment, patients in the study group were given guidance about oral hygiene and diet before being treated with oral prophylaxis, gingival flap operation, or others. At 21 d after treatment, they were reexamined.

2.5. Specimen Collection. The swab test on premises was employed to collect saliva specimens from people in the two groups as follows [13]. They were prohibited from eating and overexercising 2 h before specimen collection. Their oral cavities were wiped with cotton swab stained with 2% citric acid to stimulate saliva secretion, and their saliva was collected with RNA enzyme-free centrifuge tubes, centrifuged at 3000 r/min for 15 min at 4°C, and the upper layer of them was taken and stored in a -80°C refrigerator.

2.6. Determination of the Expression of miR-23a and miR-146a (qRT-PCR). The total RNA was extracted with a TRIzol extraction kit, and the concentration and purity of it were determined using a DR5000 ultraviolet spectrophotometer. Reverse transcription of it was carried out using the reverse transcription kit in strict accordance with the instructions of the kit. Subsequently, a polymerase chain reaction (PCR) amplification experiment was performed, with U6 as the internal reference. The PCR reaction system consisted

Table 2: Comparison between the two groups in general data (n (%), $x \pm$ sd).

Group	Control group ($n = 80$)	Study group ($n = 120$)	χ^2/t	P value
Sex			2.222	0.136
Male	49 (61.25)	70 (58.33)		
Female	31 (38.75)	50 (41.67)		
Age (years)	48.34 ± 3.54	47.72 ± 4.98	0.963	0.337
Weight (kg)	63.24 ± 8.33	65.56 ± 9.78	1.742	0.083
Educational level			1.770	0.183
<Senior high school	33 (41.25)	61 (50.83)		
≥Senior high school	47 (58.75)	59 (49.17)		
Dietary favor			0.589	0.443
Light	51 (63.75)	70 (58.33)		
Heavy	29 (36.25)	50 (41.67)		
Place of residence			1.337	0.248
Urban area	34 (42.50)	61 (50.83)		
Rural area	46 (57.50)	59 (49.17)		
Having exercise habit or not			0.575	0.448
Yes	37 (46.25)	49 (40.83)		
None	43 (53.75)	71 (59.17)		
Marital status			1.561	0.458
Married	74 (92.50)	106 (88.33)		
Unmarried	5 (6.25)	9 (7.50)		
Divorced	1 (1.25)	5 (4.17)		
Smoking history			1.871	0.171
Yes	45 (56.25)	79 (65.83)		
None	35 (43.75)	41 (34.17)		
Drinking history			0.124	0.725
Yes	48 (60.00)	69 (57.50)		
None	32 (40.00)	51 (42.50)		

of 20 μl of the total volume containing 10 μl of 2x Talent qPCR PreMix, 1.25 μl of upstream and downstream primers, respectively, 100 ng of cDNA, and water to adjust the volume. PCR was carried out under predenaturation at 95°C for 3 min, followed by 40 cycles of denaturation at 95°C for 5 s, and annealing and extension at 60°C for 15 s. Data in this study were analyzed using $2^{-\Delta\Delta ct}$ [14].

2.7. Determination of the Expression of Inflammatory Factors (ELISA). ELISA was employed to determine the expression levels of three inflammatory factors in the saliva of the two groups, namely, IL-1β, IL-6, and IL-17, in strict accordance with instructions of ELISA kits for IL-1β, IL-6, and IL-17. A blank well, a standard well, and a well for specimens to be determined were set. A total of 50 μl of standards with different concentrations were added into the standard well, and 10 μl of specimens to be determined and 40 μl of diluent were added into the well for specimens to be determined successively. Then, 100 μl of the horseradish peroxidase-labeled detection antibody was added into the standard well and the well for specimens to be determined, respectively. Each well was blocked with a microplate sealer and incubated in a 37°C incubator for 1 h. After incubation, the microplate sealer was removed. The liquid in each well was

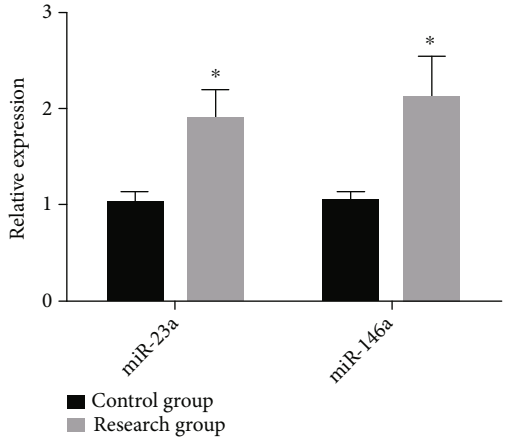

Figure 1: Comparison between the two groups in the expression of saliva miR-23a and miR-146a. The study group showed significantly higher relative expression of saliva miR-23a and miR-146a than the control group (all $P < 0.05$). Note: * indicates that in comparison with the control group, $P < 0.05$.

Table 3: Diagnostic value of saliva miR-23a and miR-146a for periodontitis.

Group	AUC	95% CI	Standard error	Cutoff value	Sensitivity (%)	Specificity (%)
miR-23a	0.857	0.802-0.912	0.028	1.429	81.67	83.75
miR-146a	0.886	0.838-0.934	0.025	1.589	82.50	86.25

discarded, and each well was washed with washing solution for 1 min and patted to dry. This step was repeated 5 times. Each well was added with 50 μl of chromogenic reagent A and 50 μl of chromogenic reagent B, respectively, and the liquid in each well was mixed well. Subsequently, each well was developed in the dark at 37°C for 10-15 min and then added with 50 μl of sulfuric acid to terminate the reaction. The optical density of each well was detected using an enzyme marking instrument at 450 nm, on which the levels of IL-1β, IL-6, and IL-17 were calculated.

2.8. Statistical Analysis. In this study, the data were statistically analyzed using SPSS 21.0 (EASY BIO Company) and visualized to figures using GraphPad Prism 7. Enumeration data were expressed by the number of cases/percentage (n (%)), and comparison between the two groups in terms of them was performed using the chi-squared test. Measurement data were expressed by the mean ± standard deviation ($x \pm$ sd), and comparison between the two groups in terms of them was performed using the independent-samples t-test. Comparison of one same group before and after treatment was performed using the paired t-test. Receiver operating characteristic (ROC) curves were drawn to evaluate the diagnostic value of saliva miR-23a and miR-146a in diagnosing periodontitis, and correlation analysis was performed using the Pearson correlation method. $P < 0.05$ indicated a significant difference.

3. Results

3.1. Comparison between the Two Groups in General Data. There were no significant differences between the two groups in general data including sex, age, weight, educational level, dietary favor, place of residence, exercise habit, marital status, smoking history, and drinking history (all $P > 0.05$). See Table 2.

3.2. Comparison between the Two Groups in the Expression of Saliva miR-23a and miR-146a. The relative expression of saliva miR-23a and miR-146a in the control group was 1.02 ± 0.12 and 1.06 ± 0.15, respectively, while that in the study group was 1.89 ± 0.49 and 2.12 ± 0.56, respectively, so it was apparent that the study group showed significantly higher relative expression of saliva miR-23a and miR-146a than the control group (both $P < 0.05$). See Figure 1.

3.3. Diagnostic Value of Saliva miR-23a and miR-146a for Periodontitis. We drew receiver operating characteristic (ROC) curves of saliva miR-23a and miR-146a for diagnosing periodontitis, finding that the area under the curve (AUC) of saliva miR-23a for diagnosing periodontitis was 0.857 (95% CI: 0.802-0.912), and its cutoff value, diagnostic sensitivity, and diagnostic specificity were 1.429, 81.67%, and 83.75%, respectively. It was also revealed that the AUC of saliva miR-146a for diagnosing periodontitis was 0.886 (95% CI: 0.838-0.934), and its cutoff value, diagnostic sensitivity, and diagnostic specificity were 1.589, 82.50%, and 86.25%, respectively. See Table 3 and Figure 2.

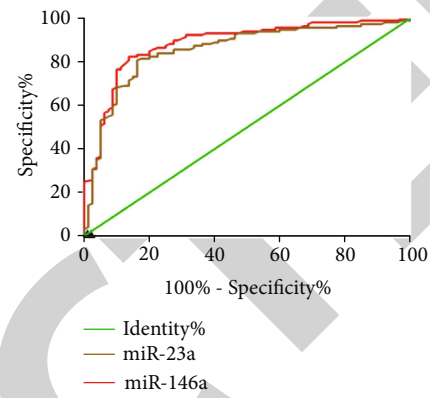

Figure 2: ROC curves of saliva miR-23a and miR-146a for diagnosing periodontitis. The AUCs of saliva miR-23a and miR-146a were 0.857 and 0.886, respectively. Their diagnostic sensitivities were 81.67% and 82.50%, respectively, and their diagnostic specificities were 83.75% and 86.25%, respectively.

3.4. Changes of the Expression of miR-23a and miR-146a in Patients under Different Severities. The relative expression of saliva miR-23a in patients with mild periodontitis, patients with moderate periodontitis, and patients with severe periodontitis was 1.69 ± 0.08, 1.88 ± 0.12, and 2.04 ± 0.10, while the relative expression of saliva miR-146a in them was 1.87 ± 0.09, 2.08 ± 0.11, and 2.342 ± 0.13, respectively, so it was apparent that the expression of miR-23a and miR-146a increased with the deterioration of periodontitis, and the two groups had significant differences in the expression of them (both $P < 0.05$). See Figure 3.

3.5. Changes of miR-23a and miR-146a in the Study Group before and after Treatment. The expression of saliva miR-23a and miR-146a in the study group was significantly lower than that after treatment (1.45 ± 0.33 vs. 1.89 ± 0.49; 1.59 ± 0.38 vs. 2.12 ± 0.56) (both $P < 0.05$). See Figure 4.

3.6. Comparison between the Two Groups in the Expression of Saliva IL-1β, IL-6, and IL-17. The levels of saliva IL-1β, IL-6, and IL-17 in the control group were 1.88 ± 0.63, 3.24 ± 0.85, and 7.57 ± 1.58 ng/l, respectively, and those in the study group were 3.35 ± 0.94, 6.14 ± 1.32, and 12.57 ± 2.68 ng/l, respectively, so it was apparent that the study group showed significantly higher levels of IL-1β, IL-6, and IL-17 than the control group (all $P < 0.05$). See Figure 5.

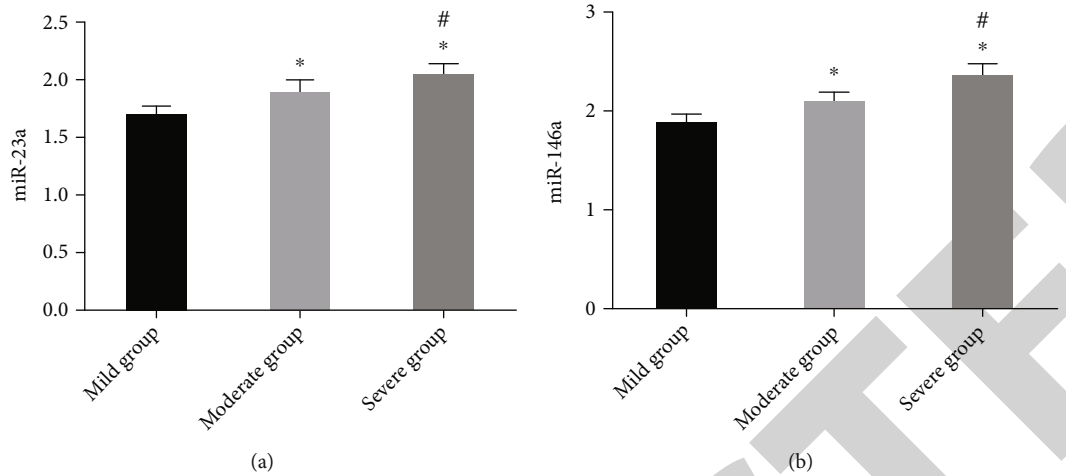

Figure 3: Changes of the expression of miR-23a and miR-146a in patients at different stages. The expression of miR-23a increased with the deterioration of the disease, and there were significant differences between the two groups in it ($P < 0.05$) (a). The expression of miR-146a increased with the deterioration of the disease, and there were significant differences between the two groups in it ($P < 0.05$) (b). Notes: ∗ indicates that in comparison with the situation of the mild periodontitis group, $P < 0.05$; # indicates that in comparison with the situation of the moderate periodontitis group, $P < 0.05$.

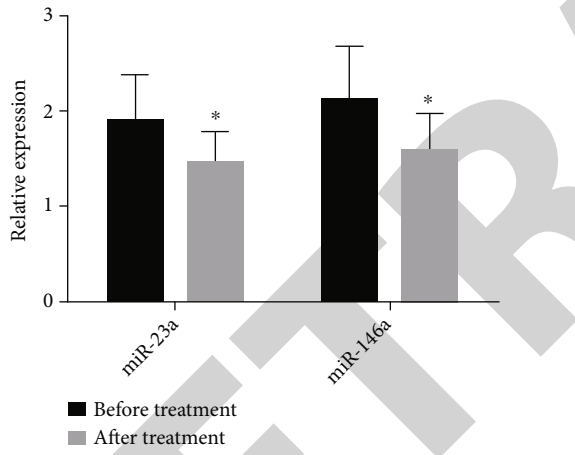

Figure 4: Changes of the expression of miR-23a and miR-146a in the study group before and after treatment. After treatment, the expression of saliva miR-23a and miR-146a decreased significantly ($P < 0.05$). Note: ∗ indicates that in comparison with the situation of the same group before treatment, $P < 0.05$.

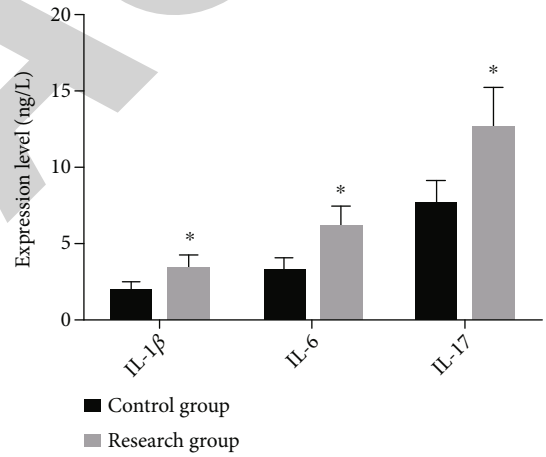

Figure 5: Comparison between the two groups in the levels of saliva IL-1β, IL-6, and IL-17. The study group showed significantly higher levels of saliva IL-1β, IL-6, and IL-17 than the control group (all $P < 0.05$). Note: ∗ indicates that in comparison with the control group, $P < 0.05$.

3.7. Analysis of the Correlation of miR-23a and miR-146a with IL-1β, IL-6, and IL-17. Pearson correlation analysis revealed that in the study group, saliva miR-23a was obviously and positively correlated with saliva IL-1β, IL-6, and IL-17, respectively ($r = 0.542$, $P < 0.001$; $r = 0.638$, $P < 0.001$; and $r = 0.606$, $P < 0.001$), and saliva miR-146a was also obviously and positively correlated with them, respectively ($r = 0.606$, $P < 0.001$; $r = 0.639$, $P < 0.001$; and $r = 0.646$, $P < 0.001$). See Figure 6.

4. Discussion

Early diagnosis and observation of periodontitis can provide important information for periodontitis treatment and facilitate the selection of an appropriate treatment plan, so they are a key step to alleviate patients' symptoms and improve their life quality [15]. At present, the diagnosis level for early periodontitis is unsatisfactory. Although imaging evaluation can provide information about the severity of periodontitis based on its results in terms of exploration depth, attachment level, bleeding detection, and loss of alveolar bone, it is relatively costly and unable to detect disease activity, resulting in certain limitations [16]. Therefore, it is of great significance to find biological factors closely related to the diagnosis and assessment of periodontitis.

Saliva is a biological fluid with abundant clinical information, which is easy to collect and store, so it is an ideal choice for the early detection of diseases [17]. At present,

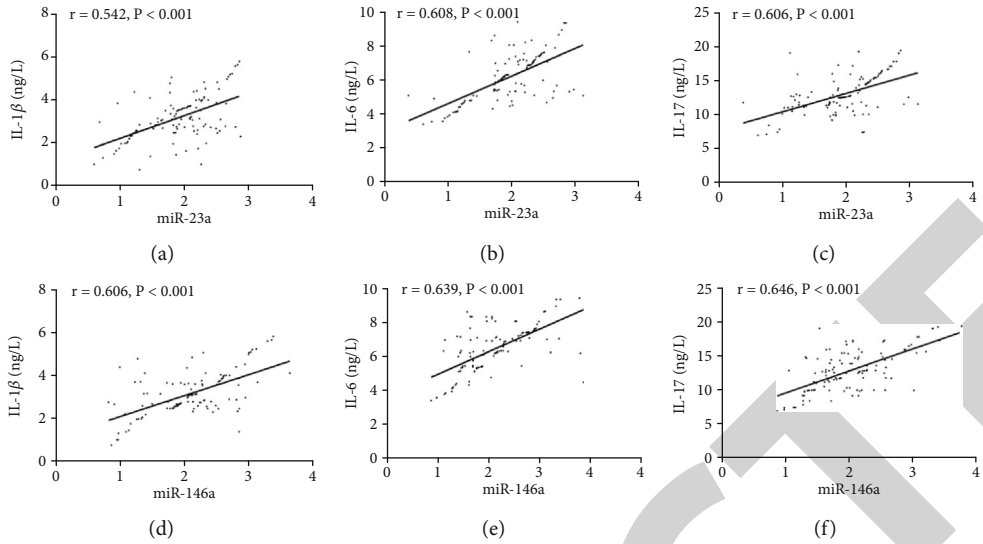

Figure 6: Analysis of the correlation of saliva miR-23a and miR-146a with IL-1β, IL-6, and IL-17. Pearson correlation analysis revealed that in the study group, saliva miR-23a was obviously and positively correlated with saliva IL-1β, IL-6, and IL-17, respectively ($r = 0.542$, $P < 0.001$; $r = 0.638$, $P < 0.001$; and $r = 0.606$, $P < 0.001$) (a–c), and saliva miR-146a was also obviously and positively correlated with them, respectively ($r = 0.606$, $P < 0.001$; $r = 0.639$, $P < 0.001$; and $r = 0.646$, $P < 0.001$) (d–f).

saliva miR is proved to be feasible as a disease diagnosis method [18]. A study showed that saliva miR-21 could be used as a biomarker for diagnosing colorectal cancer, and its sensitivity was higher than that of serum miR-21 (65% vs. 97%) [19]. One other study concluded that miR-1246 and miR-4644 in the saliva exosome could be used as biomarkers of identifying patients with pancreatic cancer or cholangiocarcinoma [20]. In addition, a study by Humeau et al. revealed that miR-23a showed significantly upregulated expression in the saliva of patients with pancreatic cancer, and its sensitivity and specificity for diagnosing pancreatic cancer were 85.7% and 100%, respectively [21]. We determined the expression of miR-23a and miR-146a in the saliva of patients with periodontitis and healthy volunteers, finding that patients in the study group showed significantly higher expression of saliva miR-23a and miR-146a than healthy people in the control group. It indicated that saliva miR-23a and miR-146a may be used as biomarkers for periodontitis diagnosis. To verify it, we drew ROC curves of saliva miR-23a and miR-146a for periodontitis diagnosis, which showed that the AUCs of saliva miR-23a and miR-146a for periodontitis diagnosis were 0.857 and 0.886, respectively; their diagnostic sensitivities were 81.67% and 82.50%, respectively, and their diagnostic specificities were 83.75% and 86.25%, respectively. It suggested that saliva miR-23a and miR-146a had certain diagnostic value for periodontitis. We also determined the expression of miR-23a and miR-146a in the saliva of patients with periodontitis at different stages and patients in the study group, finding that the expression of saliva miR-23a and miR-146a increased with the deterioration of the disease, and patients in the study group showed significantly decreased expression of saliva miR-23a and miR-146a after treatment. It indicated that saliva miR-23a and miR-146a were expected to be biomarkers of periodontitis.

Periodontitis is one of the most common infection-driven inflammatory diseases characterized by gingival inflammation and bone loss [22]. The occurrence of periodontitis may lead to increases in local proinflammatory cytokines and mediators and thus cause specific local host responses [23]. IL-1β, IL-6, and IL-17 are three common inflammatory factors involved in the occurrence and development of various inflammatory diseases including periodontitis. Fine et al. longitudinally evaluated periodontal disease progression in children at risk for aggressive periodontitis and reported that IL-1β demonstrated high specificity and sensitivity to predict alveolar bone loss [24]. IL-1β stimulated endothelial cells to induce selectins, which facilitate the recruitment of leukocytes, activate macrophage IL-1 production, and stimulate the production of inflammatory mediators. A study pointed out that IL-1β and IL-6 were highly expressed in the saliva of patients with periodontitis and had diagnostic value for periodontitis [25]. A previous systematic review and meta-analysis indicated that macrophage inflammatory protein- (MIP-) 1α had excellent diagnostic accuracy while IL-1β and IL-6 had acceptable diagnostic values [26]. One other study revealed that IL-6 and IL-17 were highly expressed in the saliva of patients with periodontitis, and they increased with the deterioration of periodontitis in the patients [27]. Ozçaka et al. state that there is an emerging understanding of the role of T helper 17 and IL-17 cytokines in periodontal diseases, and little is known about their main role in disease pathogenesis and host conservation [28]. Pradeep et al. reported in their study that the GCF concentration of IL-17 is near to zero. Since the results of their research indicated a lack of IL-17 in GCF, they recognized that it cannot be considered a biomarker in periodontal disease development [29]. Isaza-Guzmán et al. also found no relationship between IL-17 salivary concentrations and chronic periodontitis and stated

that it is futile to decide on the role of this cytokine in periodontal disease or its severity detection [30]. Our study also revealed that the expression of IL-1β, IL-6, and IL-17 was high in the saliva of the patients with periodontitis, which was similar to the above research results. In addition, we also used the Pearson correlation method to analyze the correlation of saliva miR-23a and miR-146a with saliva IL-1β, IL-6, and IL-17, finding that saliva miR-23a and miR-146a were obviously and positively correlated with saliva IL-1β, IL-6, and IL-17, which suggested that miR-23a and miR-146a had regulatory relationships with IL-1β, IL-6, and IL-17.

Although this study has confirmed that saliva miR-23a and miR-146a can be used as biomarkers for the diagnosis and assessment of periodontitis, it still has some deficiencies. For example, firstly, there were no basic experiments, so the correlations of miR-23a and miR-146a with periodontitis and inflammatory factors were not explored deeply. Secondly, the subjects in the study group and control group were from the same area, resulting in certain limitations in the results. In future research, we will add more experiments to address these deficiencies.

5. Conclusion

To sum up, saliva miR-23a and miR-146a can be used as biomarkers for the diagnosis and assessment of periodontitis, and they may have regulatory relationships with IL-1β, IL-6, and IL-17.

Data Availability

The authors confirm that the data supporting the findings of this study are available within the article.

Conflicts of Interest

The authors declare that they have no conflicts of interest.

Authors' Contributions

Lanhua Kang and Ning Li performed the experiments, analyzed the data, and wrote the manuscript. Lexiu Wang designed the study. All the authors agreed to be accountable for the accuracy and integrity of all aspects of the research. Lanhua Kang and Lexiu Wang contributed equally to this work as co-first authors.

References

[1] A. Z. Kalea, R. Hoteit, J. Suvan et al., "Upregulation of gingival tissue miR-200b in obese periodontitis subjects," *Journal of Dental Research*, vol. 94, 3_suppl, pp. 59S–69S, 2015.

[2] D. Joshi, T. Garg, A. K. Goyal, and G. Rath, "Advanced drug delivery approaches against periodontitis," *Drug Delivery*, vol. 23, no. 2, pp. 363–377, 2016.

[3] I. L. C. Chapple, F. Van der Weijden, C. Doerfer et al., "Primary prevention of periodontitis: managing gingivitis," *Journal of Clinical Periodontology*, vol. 42, pp. S71–S76, 2015.

[4] S. Yost, A. E. Duran-Pinedo, R. Teles, K. Krishnan, and J. Frias-Lopez, "Functional signatures of oral dysbiosis during periodontitis progression revealed by microbial metatranscriptome analysis," *Genome Medicine*, vol. 7, no. 1, p. 27, 2015.

[5] Y. Huang, Y. Liu, L. Li et al., "Involvement of inflammation-related miR-155 and miR-146a in diabetic nephropathy: implications for glomerular endothelial injury," *BMC Nephrology*, vol. 15, no. 1, 2014.

[6] R. Rupaimoole and F. J. Slack, "MicroRNA therapeutics: towards a new era for the management of cancer and other diseases," *Nature Reviews. Drug Discovery*, vol. 16, no. 3, pp. 203–222, 2017.

[7] M. Kebschull and P. N. Papapanou, "Mini but mighty: microRNAs in the pathobiology of periodontal disease," *Periodontology*, vol. 69, no. 1, pp. 201–220, 2015.

[8] J. Hu, C. Zhai, J. Hu et al., "miR-23a inhibited IL-17-mediated proinflammatory mediators expression via targeting IKKα in articular chondrocytes," *International Immunopharmacology*, vol. 43, pp. 1–6, 2017.

[9] S. M. Wade, M. Trenkmann, T. McGarry et al., "Altered expression of microRNA-23a in psoriatic arthritis modulates synovial fibroblast pro-inflammatory mechanisms via phosphodiesterase 4B," *Journal of Autoimmunity*, vol. 96, pp. 86–93, 2019.

[10] Z. Zeng, H. Gong, Y. Li et al., "Upregulation of miR-146a contributes to the suppression of inflammatory responses in LPS-induced acute lung injury," *Exp Lung Res*, vol. 39, no. 7, pp. 275–282, 2013.

[11] Q. Zhou, S. Haupt, J. T. Kreuzer et al., "Decreased expression of miR-146a and miR-155 contributes to an abnormal Treg phenotype in patients with rheumatoid arthritis," *Annals of the Rheumatic Diseases*, vol. 74, no. 6, pp. 1265–1274, 2015.

[12] G. C. Armitage, "Periodontal diagnoses and classification of periodontal diseases," *Periodontology*, vol. 34, no. 1, pp. 9–21, 2004.

[13] J. H. Bahn, Q. Zhang, F. Li et al., "The landscape of microRNA, piwi-interacting RNA, and circular RNA in human saliva," *Clinical Chemistry*, vol. 61, no. 1, pp. 221–230, 2015.

[14] K. J. Livak and T. D. Schmittgen, "Analysis of relative gene expression data using real-time quantitative PCR and the $2^{-\Delta\Delta\_C\_}{}_T$ method," *Methods*, vol. 25, no. 4, pp. 402–408, 2001.

[15] I. L. C. Chapple, B. L. Mealey, T. E. Van Dyke et al., "Periodontal health and gingival diseases and conditions on an intact and a reduced periodontium: consensus report of workgroup 1 of the 2017 World Workshop on the Classification of Periodontal and Peri-Implant Diseases and Conditions," *Journal of Periodontology*, vol. 89, pp. S74–S84, 2018.

[16] P. B. Patil and B. R. Patil, "Saliva:a diagnostic biomarker of periodontal diseases," *J Indian Soc Periodontol*, vol. 15, no. 4, pp. 310–317, 2011.

[17] D. Malamud, "Saliva as a diagnostic fluid," *Dental Clinics of North America*, vol. 55, no. 1, pp. 159–178, 2011.

[18] G. Schmalz, S. Li, R. Burkhardt et al., "MicroRNAs as Salivary Markers for Periodontal Diseases: A New Diagnostic Approach?," *BioMed Research International*, vol. 2016, Article ID 1027525, 14 pages, 2016.

[19] A. A. Sazanov, E. V. Kiselyova, A. A. Zakharenko, M. N. Romanov, and M. I. Zaraysky, "Plasma and saliva miR-21 expression in colorectal cancer patients," *Journal of Applied Genetics*, vol. 58, no. 2, pp. 231–237, 2017.

[20] T. Machida, T. Tomofuji, T. Maruyama et al., "miR-1246 and miR-4644 in salivary exosome as potential biomarkers for

Hindawi
BioMed Research International
Volume 2024, Article ID 9894363, 1 page
https://doi.org/10.1155/2024/9894363

Retraction

Retracted: Study on the Efficacy and Safety of Ambroxol Combined with Methylprednisolone in Patients with Acute Lung Injury

BioMed Research International

Received 12 March 2024; Accepted 12 March 2024; Published 20 March 2024

This article has been retracted by Hindawi following an investigation undertaken by the publisher [1]. This investigation has uncovered evidence of one or more of the following indicators of systematic manipulation of the publication process:

(1) Discrepancies in scope

(2) Discrepancies in the description of the research reported

(3) Discrepancies between the availability of data and the research described

(4) Inappropriate citations

(5) Incoherent, meaningless and/or irrelevant content included in the article

(6) Manipulated or compromised peer review

The presence of these indicators undermines our confidence in the integrity of the article's content and we cannot, therefore, vouch for its reliability. Please note that this notice is intended solely to alert readers that the content of this article is unreliable. We have not investigated whether authors were aware of or involved in the systematic manipulation of the publication process.

Wiley and Hindawi regrets that the usual quality checks did not identify these issues before publication and have since put additional measures in place to safeguard research integrity.

We wish to credit our own Research Integrity and Research Publishing teams and anonymous and named external researchers and research integrity experts for contributing to this investigation.

The corresponding author, as the representative of all authors, has been given the opportunity to register their agreement or disagreement to this retraction. We have kept a record of any response received.

References

[1] W. Su, Q. Dong, and F. Jiao, "Study on the Efficacy and Safety of Ambroxol Combined with Methylprednisolone in Patients with Acute Lung Injury," *BioMed Research International*, vol. 2021, Article ID 5771101, 8 pages, 2021.

Hindawi
BioMed Research International
Volume 2021, Article ID 5771101, 8 pages
https://doi.org/10.1155/2021/5771101

Research Article

Study on the Efficacy and Safety of Ambroxol Combined with Methylprednisolone in Patients with Acute Lung Injury

Weiwei Su, Qinglian Dong, and Fangfang Jiao

Department of Critical Care Medicine, Dongying People's Hospital of Shandong Provincial Hospital Group, Dongying, Shandong Provincial, China

Correspondence should be addressed to Fangfang Jiao; fangyue8573101154@163.com

Received 28 July 2021; Accepted 18 October 2021; Published 28 November 2021

Academic Editor: Jun Yang

Background. There is no better treatment method towards paraquat-induced acute lung injury (ALI) at present. Ambroxol combined with methylprednisolone exhibits a significant improvement effect on ALI treatment, whereas their mechanism in ALI is still unclear. *Methods*. 64 patients with ALI caused by paraquat poisoning brought to our hospital from January 2015 to January 2018 were selected. They were separated into a combined treatment group (CTG) and a routine treatment group (RTG) on the basis of different treatment methods. The survival of patients was observed after 7 days of treatment. Arterial blood gas, oxygen partial pressure (PaO_2), partial pressure of carbon dioxide ($PaCO_2$), oxygenation index (PaO_2/FiO_2), patient's spontaneous respiratory rate (RR), tidal volume (VT), and positive end-expiratory pressure (PEEP) were observed before and after treatment for 7 days. Interleukin 6 (IL-6) and tumor necrosis factor α (TNF-α) were analyzed. The differences of indexes between the dead patients and the survivors were observed, and the potential predictive value of death was analyzed. *Results*. After treatment, the indexes of patients were significantly improved in both groups compared with those before therapy. Further comparison showed that the improvement of PaO_2, $PaCO_2$, and PaO_2/FiO_2 in CTG was obviously higher than that in RTG ($p < 0.05$). The improvement of RR, PEEP, and VT in CTG was obviously higher than that in RTG ($p < 0.05$). The decreased degree of IL-6 and TNF-α in CTG was higher than that in RTG ($p < 0.05$). The 7-day mortality rate of 64 patients was 39.06%, and there was no obvious difference in the 7-day survival rate in both groups ($p = 0.649$). IL-6 and TNF-α were expected to be potential prediction indexes of paraquat-induced ALI. *Conclusion*. Ambroxol combined with methylprednisolone significantly improved the oxygen partial pressure and oxygenation index of patients with paraquat-induced ALI and inhibited the inflammatory response of patients.

1. Introduction

Paraquat belongs to bipyridyliums. Because of its broad-spectrum activity, high-efficiency, limited environmental pollution, and ease of use, it is widely applied in agriculture production all over the world, especially in developing countries [1]. However, it is also highly toxic to human beings and animals, mainly because its redox activity generates reactive oxygen species (ROS) [2]. Although paraquat is extremely toxic to human beings and livestock at present, there is no specific toxinicide [3].

After paraquat poisoning, it accumulates in human lungs and is prone to acute lung injury (ALI) and pulmonary fibrosis [4, 5]. Currently, a patient is mainly treated clinically by dialysis combined with drug therapy after paraquat poisoning [6]. Ambroxol is a new mucolytic agent. In recent years, many reports reveal that ambroxol plays a vital role in protecting the respiratory system [7]. Methylprednisolone has strong anti-inflammatory and anti-immune effects. Early application of methylprednisolone can improve the body's tolerance to harmful factors, reduce severe inflammatory reaction caused by paraquat poisoning, reduce inflammatory exudation, and has an antifibrosis effect [8, 9]. Previous studies have found that [10] high-dose ambroxol has an objective effect in the treatment of ALI caused by paraquat poisoning. However, there are few studies on the treatment

Table 1: Comparison of baseline data.

Factors		RTG ($n = 34$)	CTG ($n = 30$)	p value
Age	≥35 years old ($n = 38$)	21	17	0.679
	<35 years old ($n = 26$)	13	13	
Gender	Male ($n = 48$)	28	20	0.148
	Female ($n = 16$)	6	10	
BMI (kg/m^2)		22.41 ± 1.82	21.94 ± 1.58	0.277
Smoking history	Yes ($n = 45$)	26	19	0.251
	No ($n = 19$)	8	11	
Place of residence	City ($n = 20$)	11	9	0.839
	Rural ($n = 44$)	23	21	
Educational level	≥Junior high school ($n = 29$)	16	13	0.765
	<Junior high school ($n = 35$)	18	17	
LIS score		2.15 ± 0.48	2.10 ± 0.58	0.707

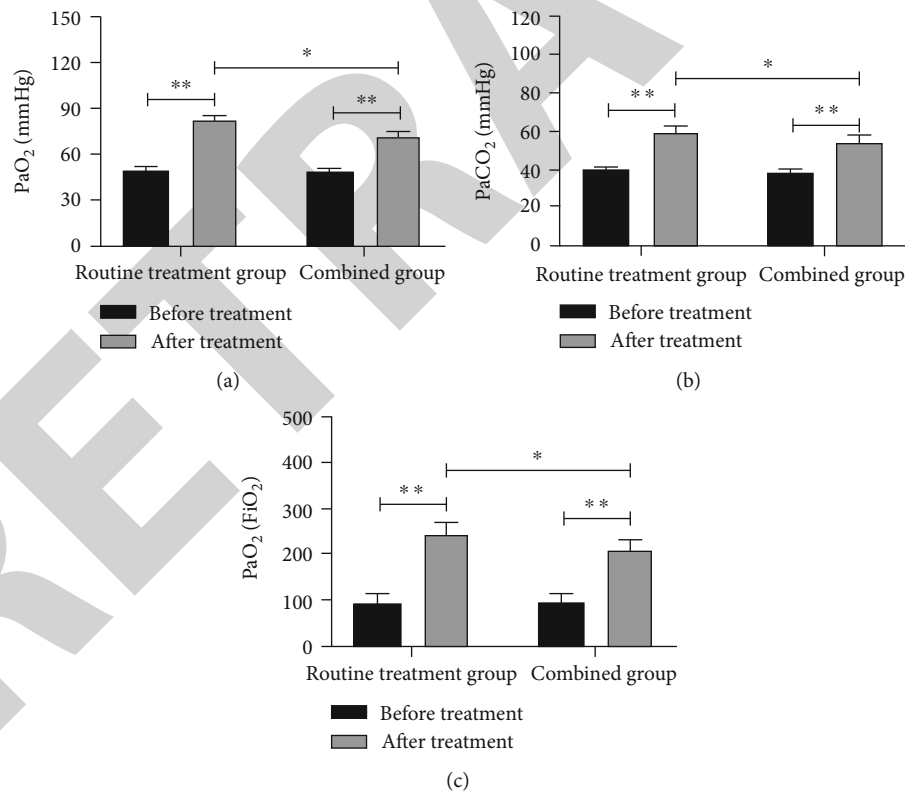

Figure 1: Changes of blood gas indexes before and after treatment. (a) Changes of PaO_2 before and after treatment were detected by blood gas analysis. (b) Changes of $PaCO_2$ before and after treatment were detected by blood gas analysis. (c) Changes of PaO_2/FiO_2 before and after treatment were detected by blood gas analysis. $^*p < 0.05$ and $^{**}p < 0.01$.

of paraquat-induced ALI by high-dose ambroxol combined with methylprednisolone. It is not clear whether large doses of combined drugs can improve the patient's disease.

Therefore, this research was aimed at exploring the effect of high-dose ambroxol combined with methylprednisolone on the improvement of patients with ALI caused by

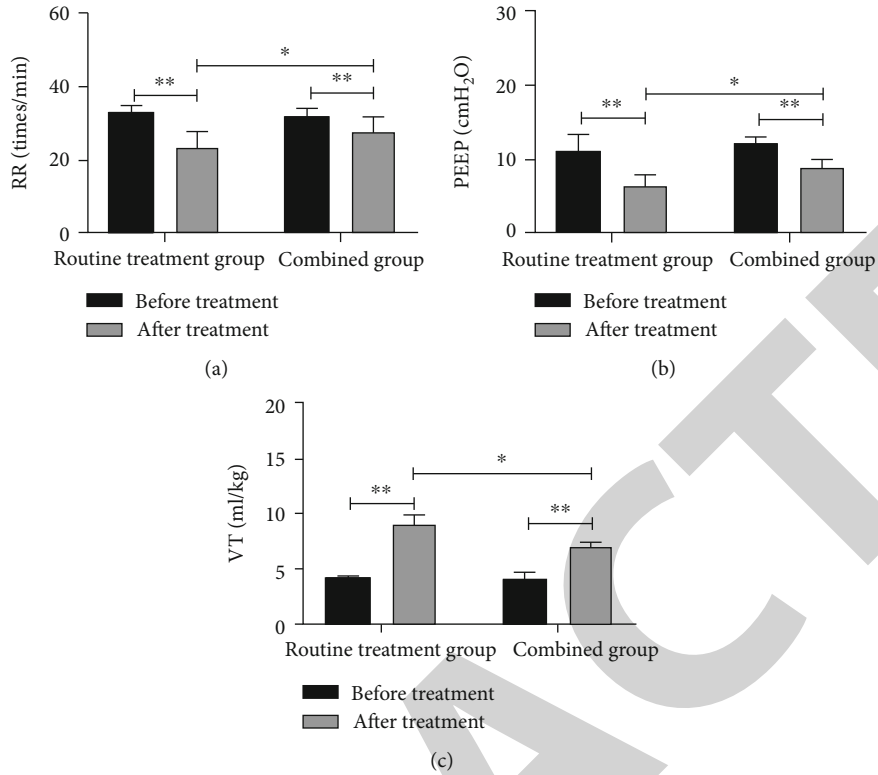

Figure 2: Changes of respiratory parameters before and after treatment. (a) Analysis on the changes of RR before and after treatment. (b) Analysis on the changes of PEEP before and after treatment. (c) Analysis on the changes of VT before and after treatment. $^{*}p < 0.05$ and $^{**}p < 0.01$.

paraquat and its influence on survival, hoping to furnish reference for clinical treatment.

2. Methods and Data

2.1. Clinical Data. From January 2015 to January 2018, 64 patients with ALI caused by paraquat poisoning brought to our hospital were selected, including 48 men and 16 women, with an average age of 35.6 ± 8.4 years old. Patients were separated into a high-dose treatment group ($n = 34$) and RTG ($n = 30$) on the basis of different treatment schemes.

Inclusion criteria were as follows: all patients were poisoned by paraquat and did not take other pesticides. The patients were confirmed to have ALI within 0-6 hours after taking paraquat during admission, and their families signed informed consent.Exclusion criteria were as follows: comorbid with tumor, cardiovascular, and cerebrovascular diseases; patients who died within 1 day after admission.

This research was ratified by the Medical Ethics Committee of our hospital.

2.2. Methods of Treatment. In this research, patients underwent gastric lavage and catharsis first in the two groups, and then, hemoperfusion and hemodialysis were used to treat patients for 4~6 h, once/d, for 3~4 d in succession. In addition, the patients were ventilated by ventilator (SIMV+PsV+PEEP mode). In RTG, the patients were injected intravenously with 500 mg/d methylprednisolone for 3 days, followed by a dose reduction. It was supplemented by antioxidation, liver protection, myocardial nutrition, maintenance of water electrolyte, acid-base balance, etc. On this basis, patients in CTG were given 20 mg/kg/d ambroxol hydrochloride injection by intravenous infusion for 12 h for 3-5 days.

2.3. ELISA Test. The expressions of IL-6 and TNF-α were detected through ELISA (Shanghai Enzyme-Linked Biotechnology Co., Ltd., PI330, PT518). The blank hole, standard sample hole, and sample hole to be tested were set up. 50 μL of standard product was added into the standard sample hole with different concentrations. The 10 μL sample to be tested was first put in the sample well, and then, the 40 μL sample diluent was added. Nothing was added to the blank well. In addition to the blank well, 100 μL of HRP-labeled detection antibody was put in each of the standard hole and the sample hole. The reaction holes were sealed with a sealing plate membrane and cultivated in a water bath at 37°C for 65 min. The liquid was discarded, and absorbent paper was used to pat dry. Each hole was filled with washing liquid and allowed to stand for 2 min, the washing liquid was thrown out, and absorbent paper was used to pat dry. This was repeated 6 times. Each 50 μL of substrates A and B was put in each hole and cultivated at 37°C in the dark for 10 min. The 50 μL of terminal liquid was added to each hole, and OD values of each hole were tested at the wavelength of 450 nm within 15 min to calculate the concentration.

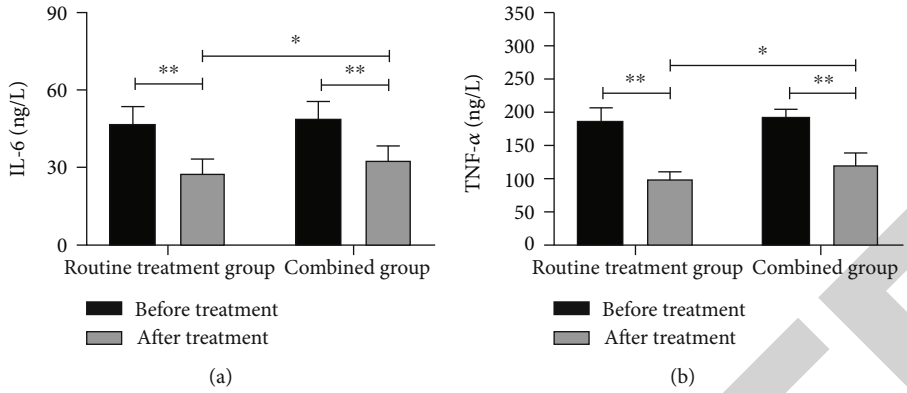

Figure 3: Changes of IL-6 and TNF-α before and after treatment. (a) ELISA was used to detect changes of IL-6 before and after treatment. (b) ELISA was used to detect the changes of TNF-α before and after treatment. $^{*}p < 0.05$ and $^{**}p < 0.01$.

2.4. Outcome Measures. Main outcome measures were as follows: to observe the survival of patients after 7 days of treatment; to observe the arterial blood gas, PaO_2, $PaCO_2$, and oxygenation index (PaO_2/FiO_2) before and after treatment for 7 days; to observe the spontaneous RR, VT, and PEEP before and after treatment for 7 days; and to observe the IL-6 and TNF-α before and after treatment for 7 days.

The secondary observation index is as follows: to compare the baseline data of patients in the two groups and to observe the differences of various indexes between the dead patients and the survivors and analyze the potential predictive value of death.

2.5. Statistical Analysis. In this research, SPSS20.0 was applied to make statistical analysis on the collected data, and GraphPad 7 was applied to draw the required pictures. The general data of patients were analyzed by the chi-square test. The biological indexes of patients were analyzed by t-test, in which the normal distribution data was represented by mean number ± standard deviation (mean ± SD). The independent sample t-test was used for intergroup comparisons. The data that did not accord with the normal distribution was represented by quartile. ROC was applied to plot the potential predicting value of each index of dead patients and survivors. K-M survival curve was applied to analyze the 7-day survival of patients in the two groups. $p < 0.05$ indicated that there was statistical difference.

3. Results

3.1. Comparison of Baseline Data. In this study, we first compared the baseline data of patients in RTG and CTG. Through analysis, we found that there were no statistical differences in the age, gender, BMI (body mass index), history of smoking, place of residence, educational level, and LIS score in both groups ($p > 0.05$) (Table 1).

3.2. Changes of Blood Gas Indexes before and after Treatment. In this study, the changes of blood gas indexes were compared in both groups before and after treatment. By comparing, we found that there was no significant difference in PaO_2, $PaCO_2$, and PaO_2/FiO_2 in both groups before therapy ($p > 0.05$). Further comparing the changes before and after treatment, we found that PaO_2, $PaCO_2$, and PaO_2/FiO_2 increased significantly in both groups after therapy ($p < 0.01$). By further comparing, we found that the improvement of PaO_2, $PaCO_2$, and PaO_2/FiO_2 in CTG was obviously higher than that in RTG ($p < 0.05$) (Figure 1).

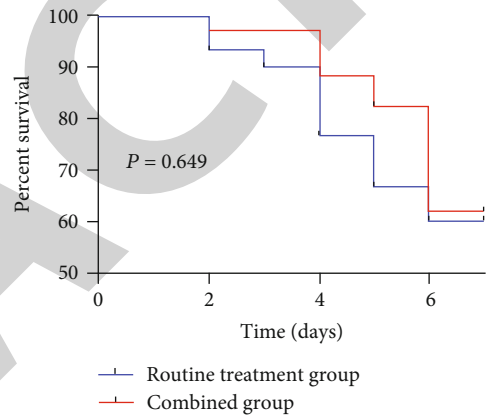

Figure 4: Effect of different treatment methods on patients' 7-day survival.

3.3. Changes of Respiratory Parameters before and after Treatment. In this study, the changes of respiratory parameters were compared in both groups before and after treatment. By comparing, we found that there was no obvious difference in RR, PEEP, and VT in both groups before treatment ($p > 0.05$). Further comparing the changes before and after treatment, we found that RR and PEEP reduced obviously in the two groups after therapy ($p < 0.01$), while VT increased significantly. By further comparing, we found that the improvement of RR, PEEP, and VT in CTG was obviously higher than that in RTG ($p < 0.05$) (Figure 2).

3.4. Changes of Inflammatory Factors before and after Treatment. In addition, we also detected the levels of IL-6 and TNF-α in patients' serum before and after therapy. Through comparison, we found that there were no statistical differences in the levels of IL-6 and TNF-α in patients' serum before treatment ($p > 0.05$), while after therapy, the levels of

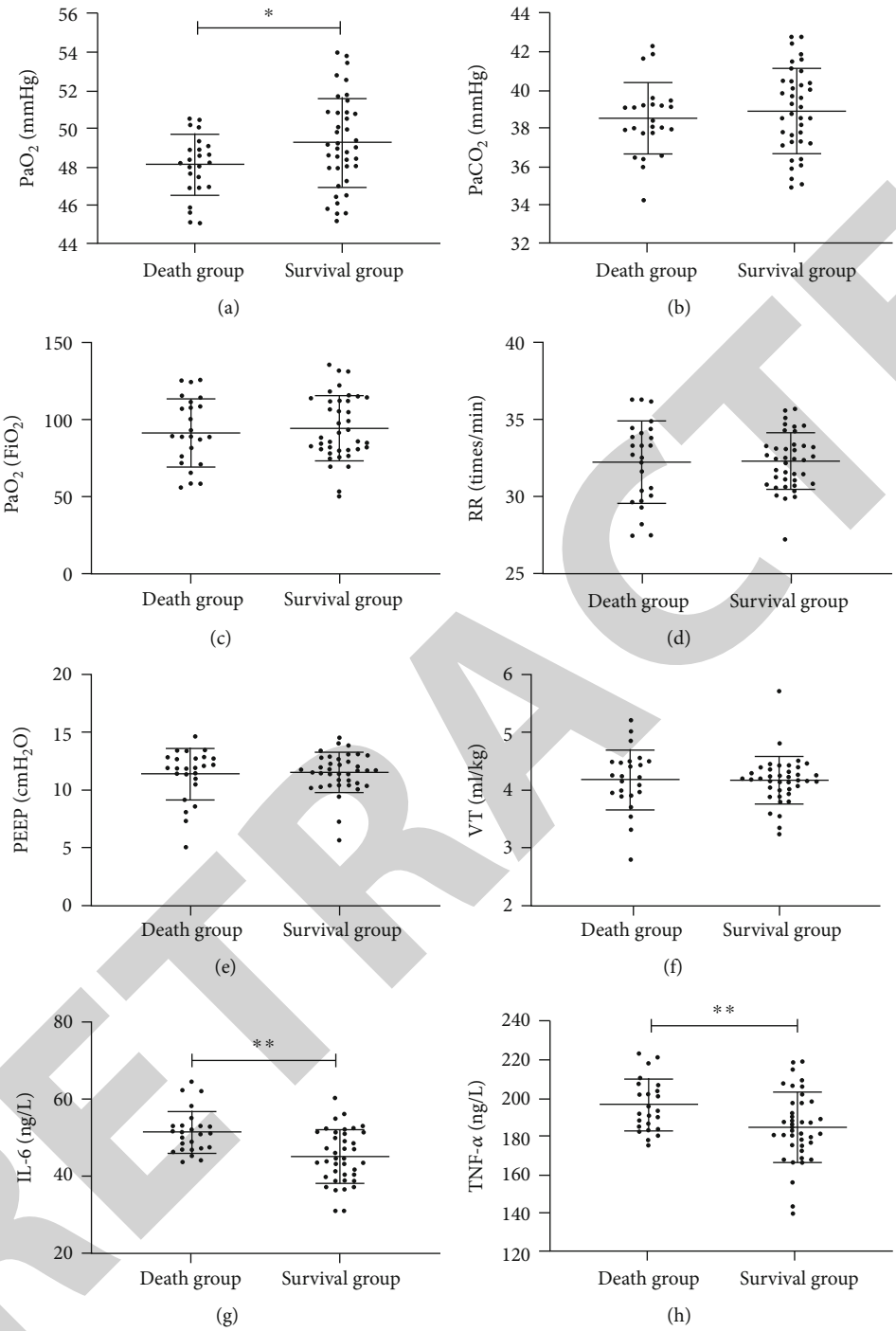

Figure 5: Expressions of blood gas index, respiratory parameters, and inflammatory factor before treatment in patients with death and survival. (a) PaO_2 expression before treatment in patients with death and survival. (b) $PaCO_2$ expression before treatment in patients with death and survival. (c) PaO_2/FiO_2 expression before treatment in patients with death and survival. (d) RR expression before treatment in patients with death and survival. (e) PEEP expression before treatment in patients with death and survival. (f) VT expression before treatment in patients with death and survival. (g) IL-6 expression before treatment in patients with death and survival. (h) TNF-α expression before treatment in patients with death and survival.

IL-6 and TNF-α in patients' serum were obviously lower than before treatment ($p < 0.01$). Further analysis, we found that the decreasing degrees of IL-6 and TNF-α of patients in CTG were higher than those in RTG ($p < 0.05$) (Figure 3).

3.5. Survival of Patients. We have made statistics on the 7-day survival of patients. The 7-day mortality rate of 64 patients was 39.06%. Based on further analysis of the survival in the two groups, it showed that the mortality rate of patients in RTG was 40.00% and that in CTG was 38.23%.

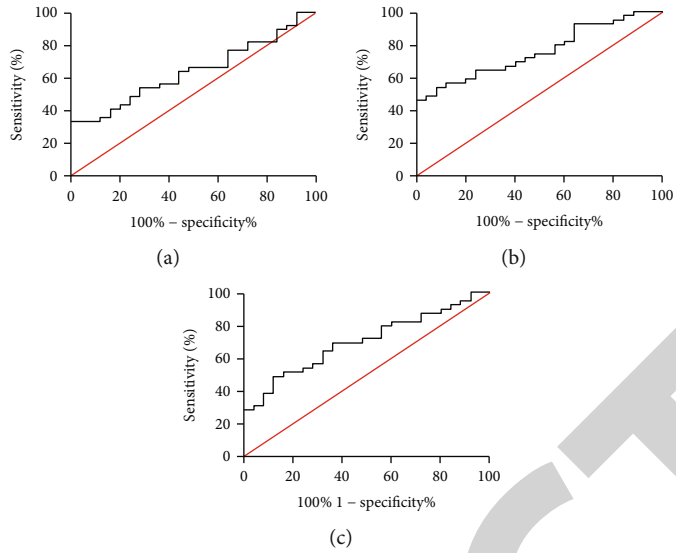

Figure 6: ROC curve area of PaO_2, IL-6, and TNF-α. (a) PaO_2 was used to predict the area under the curve of paraquat-induced ALI. (b) IL-6 was used to predict the area under the curve of paraquat-induced ALI. (c) TNF-α was used to predict the area under the curve of paraquat-induced ALI.

Table 2: ROC parameters of PaO_2, IL-6, and TNF-α.

Indicators	AUC	p value	Specificity	Sensitivity	Youden index	Cut-off
PaO_2	0.641	0.059	100.00%	33.33%	33.33%	>50.52
IL-6	0.757	0.001	100.00%	46.15%	46.15%	<43.67
TNF-α	0.701	0.007	88.00%	48.71%	36.72%	<182.11

There were no statistical differences in the 7-day survival rate in both groups ($p = 0.649$) (Figure 4).

3.6. Predictive Value of Each Index on the Death of Patients before Treatment. At the end of the study, we analyzed the value of each index in predicting the death of patients, and patients were separated into the death group ($n = 25$) and the survival group ($n = 39$) on the basis of the death situation of patients. The changes of blood gas index, respiratory parameters, and inflammatory factors were further compared before treatment. Through analysis, we found that there was no statistical difference in $PaCO_2$, PaO_2/FiO_2, RR, PEEP, and VT of patients between the death group and the survival group ($p > 0.05$). PaO_2 in the death group was obviously lower than that in the survival group, and IL-6 and TNF-α in the death group were obviously higher than those in the survival group, and there was statistical difference ($p < 0.05$). Then, we drew an ROC curve according to the different indexes. The results showed that the area under the PaO_2 curve was 0.641, the area under the IL-6 curve was 0.757, and the area under the TNF-α curve was 0.701. Among them, IL-6 and TNF-α were expected to be potential prediction indexes of ALI caused by paraquat (Figures 5 and 6 and Table 2).

4. Discussion

Paraquat is a common herbicide in developing countries due to its remarkable herbicidal effect and low cost [11]. At present, the main treatment schemes for paraquat poisoning clinically include gastric lavage, catharsis, activated carbon adsorption, hemoperfusion, antioxidant free radical drugs, and immunosuppressive agents [12–14]. Although the survival time of the patients is prolonged, the prognosis of the patients is still not significantly improved. The main cause of death is ALI [15]. In this study, we found that ambroxol combined with methylprednisolone had improved the inflammatory response and disease condition in patients with paraquat-induced ALI. We also found that IL-6 and TNF-α had high clinical value in predicting the 7-day survival of patients and were expected to become potential clinical predictors.

In this study, we found that ambroxol combined with methylprednisolone on the basis of conventional treatment significantly improved the oxygen partial pressure and oxygenation index of patients, suggesting that combined medication might improve pulmonary hyperemia/exudation, regulate lung compliance, and inhibit the development of ALI. Ambroxol, as a mucus drainage promoter, can cleave acidic mucopolysaccharide fibers in sputum, inhibit the synthesis process of acidic mucopolysaccharide fibers in goblet cells and glands, form obvious stimulation to mucous cells, enhance adhesion of small molecules of mucus, and increase protein secretion, thereby reducing mucus and sputum viscosity, realizing effective sputum dilution, reducing sputum cough difficulty, reducing incidence of cilia adhesion, and further improving the respiratory condition of patients [16,

17]. Methylprednisolone, as a glucocorticoid, has rapid onset and anti-inflammatory effects in the treatment of ALI, and it has therapeutic effects on many links of inflammatory reaction. In addition, it can increase local blood flow and inhibit the release of the proteolytic enzyme [18, 19]. The combined use of the two drugs further improved the patient's inflammatory reaction and increased the patient's oxygen partial pressure and oxygenation index.

Previous reports have shown that [20] ambroxol alleviates ventilator-induced lung injury by inhibiting c-Jun, and it also plays an inhibitory role on the occurrence of inflammatory reactions in the body of patients. In the studies of Theroux et al. [21], it has shown that preventive methylprednisolone can reduce inflammation in children and improve the result of one-time lung ventilation. In our study, it was found that the expression of IL-6 and TNF-α in patients' peripheral venous blood was further reduced after the combination of drugs, suggesting that the combination of drugs reduced the inflammatory reaction of patients, which was similar to the results of the above study. It also suggested that ambroxol combined with methylprednisolone played a positive effect in improving ALI caused by paraquat.

At the end of the research, we made a short-term observation on the survival of the patients, and it was found that the two treatment schemes had no obvious influence on the patients' 7-day survival. In addition, patients were further separated into groups on the basis of their survival conditions. To observe the connection of various indexes with the patients' survival, the results showed that PaO_2 in the dead group was obviously lower than that in the survival group, while the expression of IL-6 and TNF-α in the dead group was higher than that in the survival group. Then, we further drew an ROC curve and found that IL-6 and TNF-α had higher clinical value in calculating the patients' short-term survival. However, we still need to further explore its potential mechanism.

There are still some limitations in this study. First of all, we have not conducted a long-term follow-up survey on patients. In addition, due to the small sample size, deviation may be caused to the data results. Therefore, we hope to increase our sample size in future studies and conduct long-term follow-up of patients, so as to supplement our research conclusions. Different doses of ambroxol might have negative effects on host defenses. Therefore, more work will be necessary in clinics to find an optimal therapeutic dosage of ambroxol with minimal side effects.

To sum up, ambroxol combined with methylprednisolone significantly improved the oxygen partial pressure and oxygenation index of patients with paraquat-induced ALI and inhibited the inflammatory response of patients.

Data Availability

The authors confirm that the data supporting the findings of this study are available within the article.

Conflicts of Interest

There is no conflict of interest.

Authors' Contributions

Weiwei Su and Qinglian Dong performed the experiments, analyzed the data, and wrote the manuscript. Fangfang Jiao designed the study. All the authors agreed to be accountable for the accuracy and integrity of all aspects of the research. Weiwei Su and Qinglian Dong contributed equally to this study as co-first authors.

References

[1] T. S. Kumar, M. R. Ranjan, and D. Smita, "Paraquat poisoning," *The Journal of the Association of Physicians of India*, vol. 67, no. 11, pp. 70-71, 2019.

[2] B. Sun and Y. He, "Paraquat poisoning mechanism and its clinical treatment progress," *Zhonghua Wei Zhong Bing Ji Jiu Yi Xue*, vol. 29, no. 11, pp. 1043–1046, 2017.

[3] R. J. Dinis-Oliveira, J. A. Duarte, A. Sanchez-Navarro, F. Remiao, M. L. Bastos, and F. Carvalho, "Paraquat poisonings: mechanisms of lung toxicity, clinical features, and treatment," *Critical Reviews in Toxicology*, vol. 38, no. 1, pp. 13–71, 2008.

[4] F. Zhang, L. Hu, Y. X. Wu et al., "Doxycycline alleviates paraquat-induced acute lung injury by inhibiting neutrophil-derived matrix metalloproteinase 9," *International Immunopharmacology*, vol. 72, pp. 243–251, 2019.

[5] L. Zhang, Q. Li, W. Liu, Z. Liu, H. Shen, and M. Zhao, "Mesenchymal stem cells alleviate acute lung injury and inflammatory responses induced by paraquat poisoning," *Medical Science Monitor*, vol. 25, pp. 2623–2632, 2019.

[6] H. Shen, N. Wu, Y. Wang et al., "Chloroquine attenuates paraquat-induced lung injury in mice by altering inflammation, oxidative stress and fibrosis," *International Immunopharmacology*, vol. 46, pp. 16–22, 2017.

[7] D. Cazan, L. Klimek, A. Sperl, M. Plomer, and S. Kolsch, "Safety of ambroxol in the treatment of airway diseases in adult patients," *Expert Opinion on Drug Safety*, vol. 17, no. 12, pp. 1211–1224, 2018.

[8] G. W. Tu, Y. Shi, Y. J. Zheng et al., "Glucocorticoid attenuates acute lung injury through induction of type 2 macrophage," *Journal of Translational Medicine*, vol. 15, no. 1, p. 181, 2017.

[9] G. Zhang, X. Zhang, H. Huang, Y. Ji, D. Li, and W. Jiang, "Saquinavir plus methylprednisolone ameliorates experimental acute lung injury," *Brazilian Journal of Medical and Biological Research*, vol. 51, no. 10, p. e7579, 2018.

[10] X. Wu, S. Li, J. Zhang et al., "Meta-analysis of high doses of ambroxol treatment for acute lung injury/acute respiratory distress syndrome based on randomized controlled trials," *The Journal of Clinical Pharmacology*, vol. 54, no. 11, pp. 1199–1206, 2014.

[11] S. Kumar, "Paraquat tongue," *Indian Journal of Gastroenterology*, vol. 35, no. 4, p. 321, 2016.

[12] A. de Pont and M. Volbeda, "Extracorporeal treatment for paraquat poisoning," *Critical Care Medicine*, vol. 46, no. 10, pp. e1015–e1016, 2018.

[13] G. Dorooshi, S. Zolfaghari, N. Eizadi-Mood, and F. Gheshlaghi, "A new treatment approach for acute paraquat poisoning," *Journal of Research in Pharmacy Practice*, vol. 7, no. 2, pp. 115-116, 2018.

[14] Z. Oghabian, J. Williams, M. Mohajeri et al., "Clinical features, treatment, prognosis, and mortality in paraquat poisonings: a

Hindawi
BioMed Research International
Volume 2024, Article ID 9793607, 1 page
https://doi.org/10.1155/2024/9793607

Retraction

Retracted: The Influence of ICAM1 3′UTR Gene Polymorphism on the Occurrence and Metastasis of Primary Liver Cancer

BioMed Research International

Received 12 March 2024; Accepted 12 March 2024; Published 20 March 2024

This article has been retracted by Hindawi following an investigation undertaken by the publisher [1]. This investigation has uncovered evidence of one or more of the following indicators of systematic manipulation of the publication process:

(1) Discrepancies in scope

(2) Discrepancies in the description of the research reported

(3) Discrepancies between the availability of data and the research described

(4) Inappropriate citations

(5) Incoherent, meaningless and/or irrelevant content included in the article

(6) Manipulated or compromised peer review

The presence of these indicators undermines our confidence in the integrity of the article's content and we cannot, therefore, vouch for its reliability. Please note that this notice is intended solely to alert readers that the content of this article is unreliable. We have not investigated whether authors were aware of or involved in the systematic manipulation of the publication process.

Wiley and Hindawi regrets that the usual quality checks did not identify these issues before publication and have since put additional measures in place to safeguard research integrity.

We wish to credit our own Research Integrity and Research Publishing teams and anonymous and named external researchers and research integrity experts for contributing to this investigation.

The corresponding author, as the representative of all authors, has been given the opportunity to register their agreement or disagreement to this retraction. We have kept a record of any response received.

References

[1] L. He, S. Wang, and X. Ma, "The Influence of ICAM1 3′UTR Gene Polymorphism on the Occurrence and Metastasis of Primary Liver Cancer," *BioMed Research International*, vol. 2021, Article ID 7377299, 11 pages, 2021.

Hindawi
BioMed Research International
Volume 2021, Article ID 7377299, 11 pages
https://doi.org/10.1155/2021/7377299

Research Article

The Influence of ICAM1 3′UTR Gene Polymorphism on the Occurrence and Metastasis of Primary Liver Cancer

Li He,[1] Suwen Wang,[2] and Xusheng Ma[1]

[1]*Houbo College of Xinjiang Medical University, No. 12 of Shengli Road, Karamay, Xinjiang, China*
[2]*Shihezi University School of Medicine, Beier Road, Shihezi, Xinjiang, China*

Correspondence should be addressed to Suwen Wang; sunxia0608@163.com

Li He and Suwen Wang contributed equally to this work.

Received 12 June 2021; Revised 25 July 2021; Accepted 27 July 2021; Published 26 November 2021

Academic Editor: Chang Gu

Objective. In this study, we explored the influence of single nucleotide polymorphism (SNP) in the noncoding region of intercellular adhesion molecule 1 (ICAM1) gene on the occurrence and metastasis of primary hepatocellular carcinoma (PHC). *Methods*. Sanger sequencing was used to analyze the genotypes of rs3093032, rs923366, and rs281437 locus in the 3′ untranslated region (UTR) of the *ICAM1* gene. The level of plasma ICAM1 was analyzed by enzyme-linked immunosorbent assay (ELISA). *Results*. After adjusting for risk factors such as BMI, smoking, drinking, family history of tumors, and hepatitis B virus test results, the CT genotype at rs3093032 of the *ICAM1* gene (OR = 0.19, 95% CI: 0.08-0.44, $P < 0.01$), dominance model (OR = 0.23, 95% CI: 0.11-0.48, $P < 0.01$), and T allele (OR = 0.27, 95% CI: 0.14-0.53, $P < 0.01$) were related to the reduced risk of PHC susceptibility. rs923366 locus CT genotype (OR = 0.63, 95% CI: 0.44-0.90, $P = 0.01$), TT genotype (OR = 0.23, 95% CI: 0.10-0.53, $P < 0.01$), dominant model (OR = 0.55, 95% CI: 0.39-0.77, $P < 0.01$), recessive model (OR = 0.28, 95% CI: 0.12-0.62, $P < 0.01$), and T allele (OR = 0.55, 95% CI: 0.42-0.73, $P < 0.01$) were related to a reduction in the risk of PHC susceptibility. rs281437 locus CT genotype (OR = 2.08, 95% CI: 1.40-3.09, $P < 0.01$), TT genotype (OR = 5.20, 95% CI: 2.22-12.17, $P < 0.01$), dominant model (OR = 2.45, 95% CI: 1.69-3.54, $P < 0.01$), recessive model (OR = 4.32, 95% CI: 1.86-10.06, $P < 0.01$), and T allele (OR = 2.46, 95% CI: 1.79-3.38, $P < 0.01$) were significantly related to the increased risk of PHC susceptibility. SNPs at rs3093032, rs923366, and rs281437 of the *ICAM1* gene were significantly correlated with TNM stage and tumor metastasis of PHC patients ($P < 0.05$). *Conclusion*. SNPs at rs3093032, rs923366, and rs281437 in the 3′UTR region of the *ICAM1* gene are related to the occurrence and metastasis of PHC.

1. Introduction

Primary hepatocellular carcinoma (PHC) is one of the most common malignant tumors in the world, and its morbidity and mortality are among the top malignant tumors in the world [1, 2]. The treatment of PHC mainly includes radical surgery, hepatic artery embolization chemotherapy, radiotherapy, and local radiofrequency ablation, but it is easy to relapse after treatment and the prognosis is poor [3–5].

The cause and pathogenesis of hepatocellular carcinoma have not yet been fully elucidated. With the progress of molecular biology, virology, and genetics, researchers have found that the occurrence of hepatocellular carcinoma is related to the interaction of environmental and genetic factors [6, 7]. Important risk factors for hepatocellular carcinoma include chronic hepatitis B virus and chronic hepatitis C virus infection, alcohol abuse, chromosomal instability, oxidative damage, DNA methylation genetic signal transduction pathway obstacles, and gene polymorphisms. Therefore, to study the molecular pathological mechanism of PHC and to find new treatment methods at the gene level are of great significance for the prevention and treatment of PHC.

Intercellular adhesion molecule 1 (ICAM1) is a transmembrane single-chain glycoprotein with a molecular weight of 90-115 kD. It belongs to the immunoglobulin superfamily. It has five immunoglobulin structures and a

transmembrane structure. It is expressed in leukocytes, fibroblasts, epithelial cells, and other cells [8, 9]. The *ICAM1* gene is located on the human chromosome 19p13.2, which consists of 7 exons, 6 introns, 2.4 kb upstream sequence, and 1.5 kb 3′ noncoding RNA sequence. The rs3093032 site is located at 10285660 bp, the rs923366 site is located at 10286547 bp, and the rs281437 site is located at 10286562 bp, all located in the 3′UTR region of the *ICAM1* gene.

In this study, rs3093032 locus, rs923366 locus, and rs281437 locus were selected for research to explore their correlation with the occurrence and metastasis of PHC and provide clinical value for the prevention and treatment of PHC.

2. Methods

2.1. Ethics Statement. This study followed the "Declaration of Helsinki" and was carried out with the approval of the ethics committee. The subjects signed a written informed consent.

2.2. Subjects. A collection of 290 PHC patients who were clinically admitted in the National Human Genetic Resources Sharing Service Platform from 2013 to 2016 were used as the research objects. All patients included in the study were diagnosed as PHC through clinical, imaging, and pathology. Among them, there were 163 male PHC patients and 127 female patients. Inclusion criteria are as follows: (1) the diagnostic criteria of PHC conformed to practice guidelines for the pathological diagnosis of primary liver cancer [10]; (2) no adjuvant treatment was performed before surgery. Exclusion criteria are as follows: (1) patients who had received radiotherapy and chemotherapy; (2) patients with a history of blood transfusion; (3) patients with other vital organ diseases such as heart, lung, and kidney; (4) patients with hyperlipidemia; (5) patients with hypertension; and (6) patients with diabetes. Two hundred and ninety non-PHC patients with no history of blood transfusion, no heart, lung, or kidney disease, no hyperlipidemia, and no hypertension or diabetes were recruited as the control group, including 166 males and 124 females. A questionnaire was designed to collect the basic information of the subjects; the content of the questionnaire included the patient's age, gender, body mass index (BMI), smoking, drinking, tumor family history, hepatitis B virus, and other information.

2.3. Selection of SNP Sites. According to the variation tool in the National Center for Biotechnology Information (NCBI) database, the minor allele frequency (MAF) > 0.05 in the 3′UTR region of the *ICAM1* gene was selected for research.

2.4. Genotype Analysis of SNP Locus of the ICAM1 Gene. We collected 5 mL of peripheral venous blood from each subject, and genomic DNA was extracted from peripheral blood leukocytes using TIANamp Blood DNA Kit (Tiangen Biotech, Beijing, China). According to the sequence information of 100 bp upstream and downstream of the SNP site in the database of dbSNP (https://www.ncbi.nlm.nih.gov/snp/), primer sequences were designed using Primer-BLAST. The rs3093032 site primer sequence was 5′-ACA TAG CCC CAC CAT GAG GA-3′ (forward) and 5′-ACA TGT CTA TGG AGG GCC AC-3′ (reverse). The rs923366 site primer sequence was 5′-CAG CTT TGG AAG CCT CAT CCG-3′ (forward) and 5′-GTG ACA CCT CCC CTC AAC TC-3′ (reverse). The rs281437 site primer sequence was 5′-GCC TCA GCC TTG TGT GAG TTG-3′ (forward) and 5′-GAT CAG GCT GTG GCT GCT TAG-3′ (reverse). The primers were synthesized by Shanghai Sijia Biotechnology Co., Ltd. (Shanghai, China), and then, PCR reaction was performed. The PCR reaction system consists of 2.5 μL 10x buffer, 0.5 μL dNTP (10 mmol/L), 5 μL each of forward primer and reverse primer, 5 μL DNA template, 2 U Taq enzyme, and ddH_2O to keep the total volume at 25 μL. The PCR reaction conditions were 94°C predenaturation for 2 minutes and then 94°C, 30 s, 60°C, 35 s, 72°C, 45 s, and repeated 30 cycles. After the PCR amplification was completed, the products were sequenced by Shanghai Sijia Biotechnology Co., Ltd. (Shanghai, China) and compared with the dbSNP database based on the sequencing results, and the subject's genotype was determined based on the comparison results.

2.5. Enzyme-Linked Immunosorbent Test (ELISA). The ICAM1 (soluble) Human ELISA Kit (Thermo Fisher Scientific, Waltham, USA) was used to detect the plasma ICAM1 level of the subjects. Using the detected OD_{450} as the ordinate and the concentration of the standard as the abscissa, we drew a standard curve and calculated the concentration of soluble ICAM1 in the plasma sample according to the OD_{450} value, and each sample was tested 3 times.

2.6. Statistical Analysis. The χ^2 test was used to evaluate the differences between groups of categorical variables [n (%)], and the t -test and one-way ANOVA were used to evaluate the differences between groups of continuous variables (mean ± SD). Whether the genotype frequency accords with Hardy-Weinberg equilibrium was evaluated by the χ^2 test. Logistic regression was used to analyze the correlation between SNPs at rs3093032, rs923366, and rs281437 in the *ICAM1* gene and PHC susceptibility, the odds ratio (OR) and 95% confidence interval (CI) were calculated, and the risk factors of PHC in the single factor logistic regression analysis were adjusted. SPSS 26.0 (SPSS, Chicago, IL, USA) was used for statistical analysis. All statistical tests were two-sided tests. $P < 0.05$ indicated that the difference was statistically significant.

3. Results

3.1. Clinical Characteristics of Patients with Primary Liver Cancer and the Control Group. The clinical characteristics of 290 PHC patients and the control group are compared in Table 1. The results of one-way ANOVA showed that body mass index (BMI), smoking, drinking, family history of tumors, and hepatitis B virus test results were related to PHC susceptibility, including BMI ≥ 25 kg/m^2, smoking,

Table 1: Comparison of clinical characteristics between PHC patients and controls.

Characteristics	PHC ($n = 290$)	Control ($n = 290$)	OR (95% CI)	P value
Age [n (%)]				
<60	136 (46.90%)	140 (48.28%)	1.00 (reference)	
≥60	154 (53.10%)	150 (51.72%)	1.06 (0.76-1.46)	0.80
Gender [n (%)]				
Male	163 (56.21%)	166 (57.24%)	1.00 (reference)	
Female	127 (43.79%)	124 (42.76%)	1.04 (0.75-1.45)	0.87
BMI [kg/m^2, n (%)]				
<25	147 (50.69%)	175 (60.34%)	1.00 (reference)	
≥25	143 (49.31%)	115 (39.66%)	1.48 (1.07-2.06)	0.02
Smoking [n (%)]				
No	125 (43.10%)	174 (60.00%)	1.00 (reference)	
Yes	165 (56.90%)	116 (40.00%)	1.98 (1.42-2.76)	<0.01
Drinking [n (%)]				
No	118 (40.69%)	156 (53.79%)	1.00 (reference)	
Yes	172 (59.31%)	134 (46.21%)	1.70 (1.22-2.36)	<0.01
Family history of tumors [n (%)]				
No	236 (81.38%)	278 (95.86%)	1.00 (reference)	
Yes	54 (18.62%)	12 (4.14%)	5.30 (2.77-10.15)	<0.01
Hepatitis B virus [n (%)]				
Positive	53 (18.28%)	255 (87.93%)	1.00 (reference)	
Negative	237 (81.72%)	35 (12.07%)	5.06 (4.12-6.17)	<0.01
TNM staging [n (%)]				
I	42 (14.48%)			
II	75 (25.86%)			
III	86 (29.66%)			
IV	87 (30.00%)			
Metastasis				
Yes	168 (57.93%)			
No	122 (42.07%)			

PHC: primary hepatocellular carcinoma; OR: odds ratio; CI: confidence interval; BMI: body mass index; TNM: tumor-node-metastasis.

drinking, family history of tumors, and hepatitis B virus positive which were risk factors for PHC ($P < 0.05$) (Table 1).

3.2. ICAM1 Gene Polymorphism Was Associated with PHC Susceptibility. First, we analyzed the genotype frequencies of *ICAM1* gene rs3093032, rs923366, and rs281437 locus in the control group. The results showed that the control group *ICAM1* gene rs3093032, rs923366, and rs281437 locus genotype frequencies were in accordance with the Hardy-Weinberg equilibrium ($P = 0.11$, $P = 0.23$, and $P = 0.07$) (data not listed in Table 2). According to ICAM1 gene rs3093032 locus, rs923366 locus, and rs281437 locus allele frequency, the minimum sample size of the PHC and control groups was 63 cases/63 cases, 108 cases/108 cases, and 89 cases/89 cases, respectively.

The analysis results showed that taking the CC genotype at rs3093032 as a reference, after adjusting for risk factors such as BMI, smoking, drinking, family history of tumors, and hepatitis B virus test results, the CT genotype (OR = 0.19, 95% CI: 0.08-0.44, $P < 0.01$) and the dominant model (OR = 0.23, 95% CI: 0.11-0.48, $P < 0.01$) were related to the reduced risk of PHC susceptibility, and the PHC susceptibility risk of T allele carriers was 0.27 times than that of C allele carriers (95% CI: 0.14-0.53, $P < 0.01$).

Taking the CC allele at rs923366 as a reference, after adjusting for risk factors such as BMI, smoking, drinking, family history of tumors, and hepatitis B virus test results, the CT genotype (OR = 0.63, 95% CI: 0.44-0.90, $P = 0.01$), TT genotype (OR = 0.23, 95% CI: 0.10-0.53, $P < 0.01$), dominant model (OR = 0.55, 95% CI: 0.39-0.77, $P < 0.01$), recessive model (OR = 0.28, 95% CI: 0.12-0.62, $P < 0.01$), and the risk of PHC susceptibility was reduced. The PHC susceptibility risk of T allele carriers was 0.55 times than that of C allele carriers (95% CI: 0.42-0.73, $P < 0.01$).

Compared with the CC genotype at rs281437, CT genotype (OR = 2.08, 95% CI: 1.40-3.09, $P < 0.01$), TT genotype (OR = 5.20, 95% CI: 2.22-12.17, $P < 0.01$), the dominant model (OR = 2.45, 95% CI: 1.69-3.54, $P < 0.01$), and the recessive model (OR = 4.32, 95% CI: 1.86-10.06, $P < 0.01$) were associated with increased risk of PHC susceptibility,

Table 2: *ICAM1* gene rs3093032 locus, rs923366 locus, rs281437 locus genotype, genetic model, allele frequency, and PHC susceptibility.

	PHC ($n = 290$)	Control ($n = 290$)	OR (95% CI)*	P value
rs3093032				
CC	281 (96.90%)	254 (87.59%)	1.00 (reference)	
CT	7 (2.41%)	33 (11.38%)	0.19 (0.08-0.44)	<0.01
TT	2 (0.69%)	3 (1.03%)	0.60 (0.10-3.64)	0.91
CT+TT	9 (3.10%)	36 (12.41%)	0.23 (0.11-0.48)	<0.01
CC+CT	288 (99.31%)	287 (98.97%)	1.00 (reference)	
TT	2 (0.69%)	3 (1.03%)	0.66 (0.11-4.01)	0.65
C	569 (98.10%)	541 (93.28%)	1.00 (reference)	
T	11 (1.90%)	39 (6.72%)	0.27 (0.14-0.53)	<0.01
rs923366				
CC	195 (67.24%)	154 (53.10%)	1.00 (reference)	
CT	87 (30.00%)	109 (37.59%)	0.63 (0.44-0.90)	0.01
TT	8 (2.76%)	27 (9.31%)	0.23 (0.10-0.53)	<0.01
CT+TT	95 (32.76%)	136 (46.90%)	0.55 (0.39-0.77)	<0.01
CC+CT	282 (97.24%)	263 (90.69%)	1.00 (reference)	
TT	8 (2.76%)	27 (9.31%)	0.28 (0.12-0.62)	<0.01
C	477 (82.24%)	417 (71.90%)	1.00 (reference)	
T	103 (17.76%)	163 (28.10%)	0.55 (0.42-0.73)	<0.01
rs281437				
CC	177 (61.03%)	230 (79.31%)	1.00 (reference)	
CT	85 (29.31%)	53 (18.28%)	2.08 (1.40-3.09)	<0.01
TT	28 (9.66%)	7 (2.41%)	5.20 (2.22-12.17)	<0.01
CT+TT	113 (38.97%)	60 (20.69%)	2.45 (1.69-3.54)	<0.01
CC+CT	262 (90.34%)	283 (97.59%)	1.00 (reference)	
TT	28 (9.66%)	7 (2.41%)	4.32 (1.86-10.06)	<0.01
C	439 (75.69%)	513 (88.45%)	1.00 (reference)	
T	141 (24.31%)	67 (11.55%)	2.46 (1.79-3.38)	<0.01

*Adjust factors such as BMI, smoking, drinking, family history of tumors, and hepatitis B virus. OR: odds ratio; CI: confidence interval.

and the PHC susceptibility risk of T allele carriers was 2.46 times than that of the C allele (95% CI: 1.79-3.38, $P < 0.01$) (Table 2).

3.3. Stratified Analysis. In order to further refine the relationship between genetic factors and PHC susceptibility in different populations, we conducted a stratified analysis for the population's age, gender, body mass index (BMI), smoking, drinking, family history of tumors, and hepatitis B virus test results. The analysis results showed that only young people (age < 60 years), elderly people (age ≥ 60 years), male, BMI < 25 kg/m^2, BMI ≥ 25 kg/m^2, smokers, nonsmokers, drinkers, nondrinkers, no family history of cancer, and carriers of CT+TT genotype at rs3093032 had a lower risk of susceptibility to PHC than CC genotype ($P < 0.05$) (Table 3).

Young people (age < 60 years), elderly people (age ≥ 60 years), female, BMI < 25 kg/m^2, BMI ≥ 25 kg/m^2, nonsmokers, drinkers, nondrinkers, no family history of cancer, hepatitis B virus-positive people, and carriers of CT+TT genotype at rs923366 had a lower risk of susceptibility to PHC than CC genotype ($P < 0.05$) (Table 4).

Young people, elderly people, female, BMI < 25 kg/m^2, BMI ≥ 25 kg/m^2, smokers, nonsmokers, drinkers, nondrinkers, no family history of cancer, hepatitis B virus-positive people, hepatitis B virus-negative people, and carriers of rs281437 CT +TT genotype had higher risk of susceptibility to PHC than CC genotype ($P < 0.05$) (Table 5).

3.4. Correlation between ICAM1 Gene Polymorphism and TNM Stage. SNPs at rs3093032, rs923366, and rs281437 of the *ICAM1* gene were significantly correlated with TNM stage ($P < 0.05$) (Table 6). The progress of PHC patients with CT+TT genotype and CC genotype at rs3093032 was low, the progress of PHC patients with CT+TT genotype and CC genotype at rs923366 was low, and PHC patients with CT+TT genotype and CC genotype at rs281437 had a high degree of progression. This showed that the SNPs at rs3093032, rs923366, and rs281437 of the *ICAM1* gene were associated with tumor progression in PHC patients.

3.5. The Correlation between ICAM1 Gene Polymorphism and Tumor Metastasis. ICAM1 gene rs3093032 locus and rs923366 locus CT+TT genotype had lower risk of tumor

Table 3: Stratified analysis of the correlation between SNP at rs3093032 of the *ICAM1* gene and PHC susceptibility risk.

	PHC ($n = 290$)	Control ($n = 290$)	OR (95% CI)*	P value
Age [years, n (%)]				
<60				
CC	133 (97.79%)	122 (87.14%)	1.00 (reference)	
CT+TT	3 (2.21%)	18 (12.86%)	0.15 (0.04-0.53)	<0.01
≥60				
CC	148 (96.10%)	132 (88.00%)	1.00 (reference)	
CT+TT	6 (3.90%)	18 (12.00%)	0.30 (0.12-0.77)	0.02
Gender [n (%)]				
Male				
CC	157 (96.32%)	139 (83.73%)	1.00 (reference)	
CT+TT	6 (3.68%)	27 (16.27%)	0.20 (0.08-0.49)	<0.01
Female				
CC	124 (97.64%)	115 (92.74%)	1.00 (reference)	
CT+TT	3 (2.36%)	9 (7.26%)	0.31 (0.08-1.17)	0.13
BMI [kg/m^2, n (%)]				
<25				
CC	144 (97.96%)	153 (87.43%)	1.00 (reference)	
CT+TT	3 (2.04%)	22 (12.57%)	0.15 (0.04-0.49)	<0.01
≥25				
CC	137 (95.80%)	101 (87.83%)	1.00 (reference)	
CT+TT	6 (4.20%)	14 (12.17%)	0.32 (0.12-0.85)	0.03
Smoking [n (%)]				
No				
CC	123 (98.40%)	151 (86.78%)	1.00 (reference)	
CT+TT	2 (1.60%)	23 (13.22%)	0.11 (0.03-0.46)	<0.01
Yes				
CC	158 (95.76%)	103 (88.79%)	1.00 (reference)	
CT+TT	7 (4.24%)	13 (11.21%)	0.35 (0.14-0.91)	0.04
Drinking [n (%)]				
No				
CC	118 (99.16%)	139 (89.10%)	1.00 (reference)	
CT+TT	1 (0.84%)	17 (10.90%)	0.07 (0.01-0.53)	<0.01
Yes				
CC	163 (95.32%)	115 (85.82%)	1.00 (reference)	
CT+TT	8 (4.68%)	19 (14.18%)	0.30 (0.13-0.70)	<0.01
Family history of cancer [n (%)]				
No				
CC	229 (97.45%)	243 (87.41%)	1.00 (reference)	
CT+TT	6 (2.55%)	35 (%)	0.18 (0.08-0.44)	<0.01
Yes				
CC	52 (94.55%)	11 (91.67%)	1.00 (reference)	
CT+TT	3 (5.45%)	1 (8.33%)	0.64 (0.06-6.69)	0.70
Hepatitis B virus [n (%)]				
Negative				
CC	51 (96.23%)	222 (87.06%)	1.00 (reference)	
CT+TT	2 (3.77%)	33 (12.94%)	0.26 (0.06-1.14)	0.09
Positive				
CC	230 (97.05%)	32 (91.43%)	1.00 (reference)	
CT+TT	7 (2.95%)	3 (8.57%)	0.33 (0.08-1.32)	0.24

*Adjust factors such as BMI, smoking, drinking, family history of tumors, and hepatitis B virus. OR: odds ratio; CI: confidence interval.

Table 4: Stratified analysis of the correlation between SNP at rs923366 of the *ICAM1* gene and PHC susceptibility risk.

	PHC ($n = 290$)	Control ($n = 290$)	OR (95% CI)*	P value
Age [years, n (%)]				
<60				
CC	90 (66.18%)	75 (53.57%)	1.00 (reference)	
CT+TT	46 (33.82%)	65 (46.43%)	0.59 (0.36-0.96)	0.04
≥60				
CC	105 (68.18%)	79 (52.67%)	1.00 (reference)	
CT+TT	49 (31.82%)	71 (47.33%)	0.52 (0.33-0.83)	<0.01
Gender [n (%)]				
Male				
CC	99 (60.74%)	96 (57.83%)	1.00 (reference)	
CT+TT	64 (39.26%)	70 (42.17%)	0.89 (0.57-1.38)	0.67
Female				
CC	96 (75.59%)	58 (46.77%)	1.00 (reference)	
CT+TT	31 (24.41%)	66 (53.23%)	0.28 (0.17-0.49)	<0.01
BMI [kg/m^2, n (%)]				
<25				
CC	108 (73.47%)	92 (52.57%)	1.00 (reference)	
CT+TT	39 (26.53%)	83 (47.43%)	0.40 (0.25-0.64)	<0.01
≥25				
CC	87 (60.84%)	62 (53.91%)	1.00 (reference)	
CT+TT	56 (39.16%)	53 (46.09%)	0.75 (0.46-1.24)	0.32
Smoking [n (%)]				
No				
CC	93 (74.40%)	93 (53.45%)	1.00 (reference)	
CT+TT	32 (25.60%)	81 (46.55%)	0.40 (0.24-0.65)	<0.01
Yes				
CC	102 (61.82%)	61 (52.59%)	1.00 (reference)	
CT+TT	63 (38.18%)	55 (47.41%)	0.69 (0.42-1.11)	0.16
Drinking [n (%)]				
No				
CC	83 (69.75%)	90 (57.69%)	1.00 (reference)	
CT+TT	36 (30.18%)	66 (42.31%)	0.59 (0.36-0.98)	0.04
Yes				
CC	112 (65.50%)	64 (47.76%)	1.00 (reference)	
CT+TT	59 (34.50%)	70 (52.24%)	0.48 (0.30-0.77)	<0.01
Family history of cancer [n (%)]				
No				
CC	158 (67.23%)	146 (52.52%)	1.00 (reference)	
CT+TT	77 (32.77%)	132 (47.48%)	0.54 (0.38-0.77)	<0.01
Yes				
CC	37 (67.27%)	8 (66.67%)	1.00 (reference)	
CT+TT	18 (32.77%)	4 (33.33%)	0.97 (0.26-3.66)	0.97
Hepatitis B virus [n (%)]				
Negative				
CC	36 (67.92%)	139 (54.51%)	1.00 (reference)	
CT+TT	17 (32.08%)	116 (45.49%)	0.57 (0.30-1.06)	0.10
Positive				
CC	159 (67.09%)	15 (42.86%)	1.00 (reference)	
CT+TT	78 (32.91%)	20 (57.14%)	0.37 (0.18-0.76)	<0.01

*Adjust factors such as BMI, smoking, drinking, family history of tumors, and hepatitis B virus. OR: odds ratio; CI: confidence interval.

Table 5: Stratified analysis of the correlation between SNP at rs281437 locus of the *ICAM1* gene and PHC susceptibility risk.

	PHC ($n = 290$)	Control ($n = 290$)	OR (95% CI)*	P value
Age [years, n (%)]				
<60				
CC	82 (60.29%)	114 (81.43%)	1.00 (reference)	
CT+TT	54 (39.71%)	26 (18.57%)	2.89 (1.67-4.99)	<0.01
≥60				
CC	95 (61.69%)	116 (77.33%)	1.00 (reference)	
CT+TT	59 (38.31%)	34 (22.67%)	2.12 (1.28-3.50)	<0.01
Gender [n (%)]				
Male				
CC	111 (68.10%)	127 (76.51%)	1.00 (reference)	
CT+TT	52 (31.90%)	39 (23.49%)	1.53 (0.94-2.48)	0.11
Female				
CC	66 (1.97%)	103 (83.06%)	1.00 (reference)	
CT+TT	61 (48.03%)	21 (16.94%)	4.53 (2.53-8.13)	<0.01
BMI [kg/m^2, n (%)]				
<25				
CC	85 (57.82%)	136 (77.71%)	1.00 (reference)	
CT+TT	62 (42.18%)	39 (22.29%)	2.54 (1.57-4.13)	<0.01
≥25				
CC	92 (64.34%)	94 (81.74%)	1.00 (reference)	
CT+TT	51 (35.66%)	21 (18.26%)	2.48 (1.38-4.45)	<0.01
Smoking [n (%)]				
No				
CC	72 (57.60%)	129 (71.14%)	1.00 (reference)	
CT+TT	53 (42.40%)	45 (25.86%)	2.11 (1.29-3.45)	<0.01
Yes				
CC	105 (63.64%)	101 (87.07%)	1.00 (reference)	
CT+TT	60 (36.36%)	15 (12.93%)	3.85 (2.05-7.21)	<0.01
Drinking [n (%)]				
No				
CC	79 (66.39%)	127 (81.41%)	1.00 (reference)	
CT+TT	40 (33.61%)	29 (18.59%)	2.22 (1.27-3.86)	<0.01
Yes				
CC	98 (57.31%)	103 (76.87%)	1.00 (reference)	
CT+TT	73 (42.69%)	31 (23.13%)	2.48 (1.50-4.09)	<0.01
Family history of cancer [n (%)]				
No				
CC	141 (60.00%)	220 (79.14%)	1.00 (reference)	
CT+TT	94 (40.00%)	58 (20.86%)	2.53 (1.71-3.73)	<0.01
Yes				
CC	36 (65.45%)	10 (83.33%)	1.00 (reference)	
CT+TT	19 (34.55%)	2 (16.67%)	2.64 (0.52-13.29)	0.39
Hepatitis B virus [n (%)]				
Negative				
CC	31 (58.49%)	202 (79.22%)	1.00 (reference)	
CT+TT	22 (41.51%)	53 (20.78%)	2.71 (1.45-5.05)	<0.01
Positive				
CC	146 (61.60%)	28 (80.00%)	1.00 (reference)	
CT+TT	91 (38.40%)	7 (20.00%)	2.49 (1.05-5.94)	0.03

*Adjust factors such as BMI, smoking, drinking, family history of tumors, and hepatitis B virus. OR: odds ratio; CI: confidence interval.

Table 6: The correlation between the different genotypes at rs3093032, rs923366, and rs281437 of the *ICAM1* gene and TNM stage.

	III/IV ($n = 173$)	I/II ($n = 117$)	OR (95% CI)*	P value
rs3093032				
CC	171 (98.84%)	110 (94.02%)	1.00 (reference)	
CT+TT	2 (1.16%)	7 (5.98%)	0.18 (0.04-0.90)	0.04
rs923366				
CC	130 (75.14%)	65 (55.56%)	1.00 (reference)	
CT+TT	43 (24.86%)	52 (44.44%)	0.41 (0.25-0.68)	<0.01
rs281437				
CC	78 (45.09%)	99 (84.62%)	1.00 (reference)	
CT+TT	95 (54.91%)	18 (15.38%)	6.70 (3.73-12.02)	<0.01

*Adjust factors such as BMI, smoking, drinking, family history of tumors, and hepatitis B virus. OR: odds ratio; CI: confidence interval.

Table 7: Correlation between different genotypes at rs3093032, rs923366, and rs281437 of the *ICAM1* gene and metastasis.

	Metastasis ($n = 168$)	Nonmetastasis ($n = 122$)	OR (95% CI)*	P value
rs3093032				
CC	166 (98.81%)	115 (94.26%)	1.00 (reference)	
CT+TT	2 (1.19%)	7 (5.74%)	0.20 (0.04-0.97)	0.03
rs923366				
CC	126 (75.00%)	69 (56.56%)	1.00 (reference)	
CT+TT	42 (25.00%)	53 (43.44%)	0.43 (0.26-0.72)	<0.01
rs281437				
CC	74 (44.05%)	103 (84.43%)	1.00 (reference)	
CT+TT	94 (55.95%)	19 (15.57%)	6.89 (3.87-12.26)	<0.01

*Adjust factors such as BMI, smoking, drinking, family history of tumors, and hepatitis B virus. OR: odds ratio; CI: confidence interval.

metastasis than CC genotype PHC patients ($P < 0.05$). The risk of tumor metastasis in patients with CT+TT genotype PHC at rs281437 was significantly higher than that of patients with CC genotype PHC ($P < 0.05$) (Table 7).

3.6. Plasma ICAM1 Levels in PHC Patients Were Abnormally Elevated, and ICAM1 Gene Polymorphisms Were Related to Plasma ICAM1 Levels. The plasma ICAM1 level of subjects was detected by ELISA, and the results showed that the plasma ICAM1 level of PHC patients was abnormally increased ($P < 0.01$, Figure 1(a)). We observed that the differences in plasma ICAM1 levels of *ICAM1* gene rs3093032, rs923366, and rs281437 in plasma of PHC patients and the control group were statistically significant ($P < 0.05$). The plasma ICAM1 level of subjects with CT +TT genotype at rs3093032 was significantly lower than that of subjects with CC genotype ($P < 0.01$, Figure 1(b)). The plasma ICAM1 level of subjects with CT+TT genotype at rs923366 locus was significantly lower than that of subjects with CC genotype ($P < 0.01$, Figure 1(c)). The plasma ICAM1 level of subjects with CT+TT genotype at rs281437 locus was significantly higher than that of subjects with CC genotype ($P < 0.05$, Figure 1(d)).

3.7. Correlation between Plasma ICAM1 Level and Tumor Progression and Metastasis in PHC Patients. We further analyzed the correlation between plasma ICAM1 level in PHC patients and tumor progression and metastasis, and the results showed that plasma ICAM1 levels in PHC patients with tumor progression were higher ($P < 0.01$, Figure 2(a)). Compared with PHC patients without tumor metastasis, we detected higher levels of ICAM1 in the plasma of patients with tumor metastasis ($P < 0.01$, Figure 2(b)).

4. Discussion

At present, surgical resection was still the most effective treatment for liver cancer, but due to the multifocality of liver cancer, vascular invasion, combined with liver cirrhosis, a small number of patients were suitable for surgical treatment [11, 12]. With the improvement of surgery, chemotherapy, and radiotherapy, the survival rate of liver cancer patients had been greatly improved, but distant metastasis was the most important factor affecting their prognosis [13]. Therefore, research on the pathogenesis of liver cancer and a correct understanding of the mechanism and mode of liver cancer metastasis were essential for formulating a reasonable treatment plan and adopting targeted intervention measures to improve survival.

ICAM1 belongs to the immunoglobulin superfamily. It is a single-transmembrane single-chain glycoprotein. There are 5 immunoglobulin structural regions in the extracellular region, of which the I region binds to LFA-1 and the III

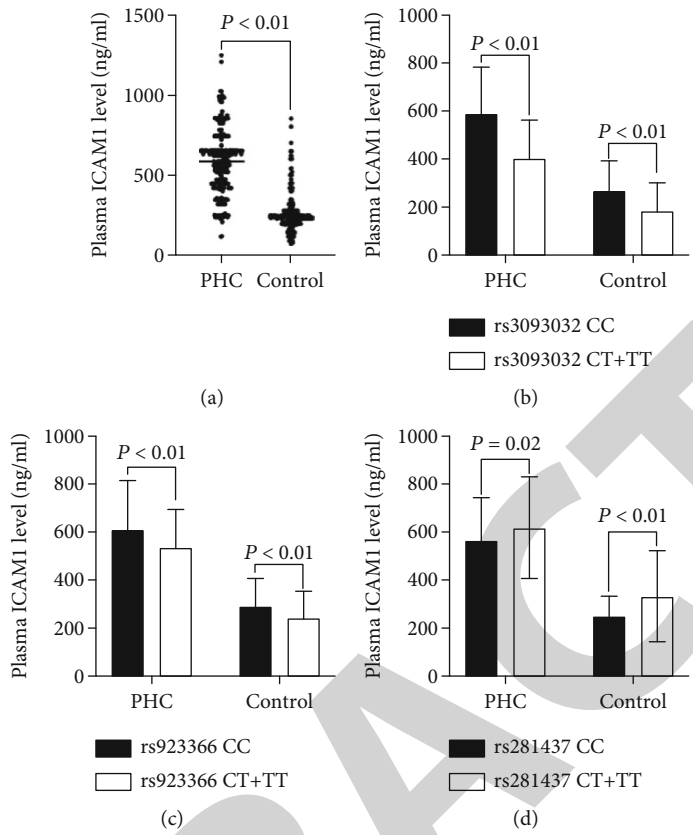

Figure 1: Results of plasma ICAM1 level detection: (a) plasma ICAM1 level of PHC patients compared with control subjects; (b) comparison of plasma ICAM1 levels between subjects with CT+TT genotype at rs3093032 and subjects with CC genotype; (c) comparison of plasma ICAM1 levels in subjects with CT+TT genotype at rs923366 locus and subjects with CC genotype; (d) comparison of plasma ICAM1 levels in subjects with CT+TT genotype at rs281437 locus and subjects with CC genotype.

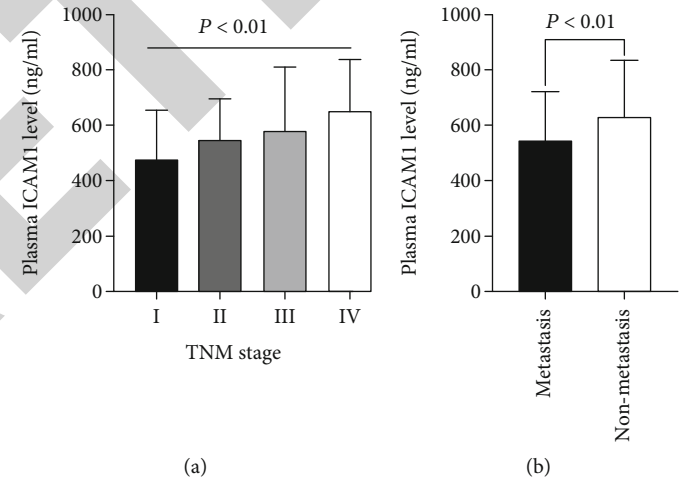

Figure 2: The correlation between plasma ICAM1 level and tumor progression and metastasis in PHC patients: (a) comparison of plasma ICAM1 levels in PHC patients with different TNM stages; (b) comparison of plasma ICAM1 levels between PHC patients with tumor metastasis and without tumor metastasis.

region and complement receptor-3 (CR3 or Mac-1), and ICAM1 works by combining with LFA-1 and Mac-1 [14–16]. ICAM1 is widely present in white blood cells, monocytes, peripheral blood lymphocytes, vascular endothelial cells, etc. [17]. Studies had found that ICAM1 could bind to LFA-1 and Mac-1 to inhibit the activation and transmission of the second signal system of CTL and NK and made cytotoxic T cells, natural killer cells, and macrophages lost

their ability to kill tumor cells, which escaped the body's cellular immune surveillance [14, 18, 19].

In this study, we found that the plasma ICAM1 level of PHC patients was significantly higher than that of the control group, and the plasma ICAM1 level of PHC patients with tumor progression and metastasis was higher, which was consistent with the results of Zhu et al. [20]. The researcher found that ICAM1 may be a potential serum biomarker for liver cancer diagnosis in 236 patients with hepatocellular carcinoma (HCC) undergoing hepatectomy. It was also an independent predictor of DFS and OS after surgical resection and is expected to provide important reference value for the prediction of intrahepatic and extrahepatic metastasis. In addition, Guo et al. [21] found that the increase of ICAM1 expression level was related to the development of HCC complication portal vein tumor thrombosis (PVTT) and poor prognosis. It reminded us that ICAM1 played an important role in the occurrence and development of PHC.

We knew that the occurrence and development of PHC were closely related to genetic factors and environmental factors. At present, there was little research on ICAM1 gene polymorphism and the occurrence and development of PHC. Chen et al. [22] studied 305 HCC patients and 613 controls and found that the interaction between *ICAM1* gene rs5498 site SNP and the environment was related to the susceptibility of liver cancer, which could be used as a marker of the risk of vascular invasion in smokers with liver cancer. In this study, we found that SNPs at rs3093032, rs923366, and rs281437 in the 3′UTR region of the *ICAM1* gene were significantly related to the risk of PHC susceptibility, tumor progression, and metastasis. Combined with the bioinformatics prediction, we speculated that the rs3093032 locus was located at the predicted junction of hsa-miR-4648 and the 3′UTR of the *ICAM1* gene, the rs923366 site was located at the predicted binding site of hsa-miR-1299 and hsa-miR-875-3p with the 3′UTR of the *ICAM1* gene, and the rs281437 site was located at the predicted binding site of hsa-miR-3667-5p, hsa-miR-4684-3p, and hsa-miR-4696 and *ICAM1* gene 3′UTR. Whether these SNPs affected the expression of ICAM1 and the role of microRNAs in it needed further study.

In conclusion, SNPs at rs3093032, rs923366, and rs281437 in the 3′UTR region of the *ICAM1* gene are related to the occurrence and metastasis of PHC and may be new targets for PHC prevention and treatment.

Data Availability

The data used during the present study are available from the corresponding author upon reasonable request.

Conflicts of Interest

The authors declare no conflict of interest.

Authors' Contributions

Suwen Wang and Li He collected and analyzed the clinical data of patients. Xusheng Ma and Chao Ning conceived and designed the experiments. All authors read and approved the final manuscript. Li He and Xusheng Ma contributed equally to this work.

Acknowledgments

This work was supported by the Karamay City Innovative Talent Project 2018RC001A-01.

References

[1] N. N. Massarweh and H. B. El-Serag, "Epidemiology of hepatocellular carcinoma and intrahepatic cholangiocarcinoma," *Cancer Control*, vol. 24, no. 3, p. 1073274817729245, 2017.

[2] M. C. Wallace, D. Preen, G. P. Jeffrey, and L. A. Adams, "The evolving epidemiology of hepatocellular carcinoma: a global perspective," *Expert Review of Gastroenterology & Hepatology*, vol. 9, no. 6, pp. 765–779, 2015.

[3] M. S. Grandhi, A. K. Kim, S. M. Ronnekleiv-Kelly, I. R. Kamel, M. A. Ghasebeh, and T. M. Pawlik, "Hepatocellular carcinoma: from diagnosis to treatment," *Surgical Oncology*, vol. 25, no. 2, pp. 74–85, 2016.

[4] C. Q. Ling, J. Fan, H. S. Lin et al., "Clinical practice guidelines for the treatment of primary liver cancer with integrative traditional Chinese and Western medicine," *J Integr Med*, vol. 16, no. 4, pp. 236–248, 2018.

[5] C. Y. Liu, K. F. Chen, and P. J. Chen, "Treatment of liver cancer," *Cold Spring Harbor Perspectives in Medicine*, vol. 5, no. 9, article a021535, 2015.

[6] J. L. Petrick, P. T. Campbell, J. Koshiol et al., "Tobacco, alcohol use and risk of hepatocellular carcinoma and intrahepatic cholangiocarcinoma: the Liver Cancer Pooling Project," *British Journal of Cancer*, vol. 118, no. 7, pp. 1005–1012, 2018.

[7] P. Pancoska and B. I. Carr, "Macro- and micro-environmental factors in clinical hepatocellular cancer," *Seminars in Oncology*, vol. 41, no. 2, pp. 185–194, 2014.

[8] A. van de Stolpe and P. T. van der Saag, "Intercellular adhesion molecule-1," *Journal of Molecular Medicine (Berlin, Germany)*, vol. 74, no. 1, pp. 13–33, 1996.

[9] S. Liu, N. Li, X. Yu et al., "Expression of intercellular adhesion molecule 1 by hepatocellular carcinoma stem cells and circulating tumor cells," *Gastroenterology*, vol. 144, no. 5, pp. 1031–1041.e10, 2013.

[10] W. M. Cong, H. Bu, J. Chen et al., "Practice guidelines for the pathological diagnosis of primary liver cancer: 2015 update," *World Journal of Gastroenterology*, vol. 22, no. 42, pp. 9279–9287, 2016.

[11] D. Zamora-Valdes, T. Taner, and D. M. Nagorney, "Surgical treatment of hepatocellular carcinoma," *Cancer Control*, vol. 24, no. 3, p. 1073274817729258, 2017.

[12] M. Omata, A. L. Cheng, N. Kokudo et al., "Asia-Pacific clinical practice guidelines on the management of hepatocellular carcinoma: a 2017 update," *Hepatology International*, vol. 11, no. 4, pp. 317–370, 2017.

[13] F. Piñero, M. Dirchwolf, and M. G. Pessôa, "Biomarkers in hepatocellular carcinoma: diagnosis, prognosis and treatment response assessment," *Cells*, vol. 9, no. 6, p. 1370, 2020.

[14] M. S. Diamond, D. E. Staunton, S. D. Marlin, and T. A. Springer, "Binding of the integrin Mac-1 (CD11b/CD18) to the third immunoglobulin-like domain of ICAM-1 (CD54)

Hindawi
BioMed Research International
Volume 2024, Article ID 9808357, 1 page
https://doi.org/10.1155/2024/9808357

Retraction

Retracted: PFNA-II Internal Fixation Helps Hip Joint Recovery and Improves Quality of Life of Patients with Lateral-Wall Dangerous Type of Intertrochanteric Fracture

BioMed Research International

Received 12 March 2024; Accepted 12 March 2024; Published 20 March 2024

This article has been retracted by Hindawi following an investigation undertaken by the publisher [1]. This investigation has uncovered evidence of one or more of the following indicators of systematic manipulation of the publication process:

(1) Discrepancies in scope

(2) Discrepancies in the description of the research reported

(3) Discrepancies between the availability of data and the research described

(4) Inappropriate citations

(5) Incoherent, meaningless and/or irrelevant content included in the article

(6) Manipulated or compromised peer review

The presence of these indicators undermines our confidence in the integrity of the article's content and we cannot, therefore, vouch for its reliability. Please note that this notice is intended solely to alert readers that the content of this article is unreliable. We have not investigated whether authors were aware of or involved in the systematic manipulation of the publication process.

Wiley and Hindawi regrets that the usual quality checks did not identify these issues before publication and have since put additional measures in place to safeguard research integrity.

We wish to credit our own Research Integrity and Research Publishing teams and anonymous and named external researchers and research integrity experts for contributing to this investigation.

The corresponding author, as the representative of all authors, has been given the opportunity to register their agreement or disagreement to this retraction. We have kept a record of any response received.

References

[1] W. Mu and J. Zhou, "PFNA-II Internal Fixation Helps Hip Joint Recovery and Improves Quality of Life of Patients with Lateral-Wall Dangerous Type of Intertrochanteric Fracture," *BioMed Research International*, vol. 2021, Article ID 5911868, 6 pages, 2021.

Hindawi
BioMed Research International
Volume 2021, Article ID 5911868, 6 pages
https://doi.org/10.1155/2021/5911868

Research Article

PFNA-II Internal Fixation Helps Hip Joint Recovery and Improves Quality of Life of Patients with Lateral-Wall Dangerous Type of Intertrochanteric Fracture

Weilu Mu[1,2] **and Junlin Zhou**[1]

[1]*Department of Orthopedics, Beijing Chaoyang Hospital, Capital Medical University, China*
[2]*Department of Orthopedics, The Third Hospital of Shijiazhuang, China*

Correspondence should be addressed to Junlin Zhou; zhudao51499203@163.com

Received 23 July 2021; Revised 13 October 2021; Accepted 18 October 2021; Published 23 November 2021

Academic Editor: Chang Gu

Objective. To analyze the effect of PFNA-II internal fixation on hip joint recovery and quality of life (QOL) in patients with lateral-wall dangerous type of intertrochanteric fracture. *Methods*. One hundred and twelve patients with lateral-wall dangerous type of intertrochanteric fracture who underwent surgical treatment in our hospital from May 2017 to May 2019 were selected as the participants of the study. Based on the treatment method, all the enrolled patients were divided into two groups: proximal femoral nail antirotation (PFNA group; $n = 59$) who received closed reduction and minimally invasive PFNA internal fixation and dynamic hip screw group (DHS; $n = 53$) who received internal fixation. The clinical indicators, curative effect, hip function score, pain degree, postoperative QOL score, and complications were compared between the two groups. *Results*. The operation time, intraoperative blood loss, postoperative drainage volume, and the incidence of postoperative complications in PFNA group were statistically lower than those in DHS group ($P < 0.05$). The curative effect in PFNA group was notably better than that in DHS group. There were no significant differences in scores of hip function, visual analogue scale (VAS), and QOL between the two groups before operation ($P > 0.05$). However, the hip function score and QOL score increased in both groups after surgery, and the increase was more significant in the PFNA group, while the VAS score decreased in both groups, and the decrease in PFNA group was more significant ($P < 0.05$). *Conclusion*. PFNA internal fixation for the treatment of lateral-wall dangerous type of intertrochanteric fracture has the advantages of short operation time, less intraoperative blood loss, effective improvement of hip joint function, and fewer postoperative complications, which is worthy of clinical application.

1. Introduction

As a common type of clinical hip fracture, femoral intertrochanteric fracture (FIF) refers to the fracture between the base of the femoral neck and the lesser trochanter, which is mostly related to osteoporosis and commonly seen in the elderly caused by the direct impact between the femoral trochanter due to falls of the elderly or by indirect torsion of the femoral trochanter [1, 2]. The incidence of FIF increases with age, and the increasing aging population in recent years has driven it to become a serious traumatic disease that threatens the health of the elderly [3], coupled with the fact that elderly patients are always complicated with a variety of concurrent diseases such as diabetes and hypertension, which makes the condition more complicated, the treatment more trickier, and the prognosis generally poor, enormously affecting the short-term and long-term quality of life (QOL) of the patients [4, 5].

Clinical practice suggests that conservative treatment can easily lead to hip varus, limb external rotation, shortening deformity, disuse osteoporosis, and muscle atrophy, and meanwhile, patients are prone to complications like pulmonary infection, urinary system infection, bedsores, joint contracture, and deep vein thrombosis due to long-term bed rest, resulting in an increase in mortality [4, 6]. Most scholars believe that as long as patient's physical conditions

allow, internal fixation surgery should be adopted to ensure a timely and stable reduction after FIF, so as to prompt patients to recover their mobility as soon as possible and reduce serious complications caused by long-term bed rest, thereby reducing mortality and improving the prognosis of patients [7, 8]. At present, there are many surgical methods for the clinical treatment of FIF, and the choice of internal fixation covers nail plate system (DHS, DCS, PCCP), PFNA (Proximal femoral nail antirotation), and artificial joint replacement [9]. As the condition of FIF is more complicated, and the choice of different internal fixation methods varies according to patient's age, condition, physical condition, and clinical type of fracture, how to choose internal fixation for timely treatment and maximize recovery of patient's health has become the key to clinical work [10].

Therefore, this study retrospectively analyzed 112 cases of elderly patients with lateral-wall dangerous type of intertrochanteric fracture who were treated with PFNA or DHS (dynamic hip screw) surgery and compared the clinical indicators of the two surgical methods and the recovery of limb function of the patients, so as to provide reference for the clinical treatment of FIF in the elderly.

2. Materials and Methods

2.1. General Information. One hundred and twelve patients with lateral-wall dangerous type of intertrochanteric fracture who underwent surgical treatment in our hospital from May 2017 to May 2019 were selected as the participants and divided into PFNA group and DHS group according to the treatment methods. In PFNA group, 59 patients were treated with closed reduction and minimally invasive PFNA internal fixation, among which 25 were males and 34 were females, aged 54-83 years old, with an average age of 67.43 ± 5.32 years old, and the course of disease was 2-8 d, with an average disease course of 5.23 ± 1.41 d. In DHS group, 53 patients were treated with DHS internal fixation, among which 23 were males and 30 were females, aged 53-82 years old, with an average age of 68.26 ± 6.24 years old, and the course of disease was 2-6 d, with an average disease course of 4.87 ± 1.39 d. Inclusion criteria: all the FIF patients were confirmed as the dangerous type of lateral wall by X-ray and CT, with complete medical records and operation tolerance, and signed the informed consent. Exclusion criteria: patients with old or pathological FIF, fractures caused by bone and joint tuberculosis/bone tumor secondary, or heart, liver, and kidney complications; patients with blood diseases, coagulation disorders, immune system diseases, or surgical contraindications; patients with other fractures; patients with a history of lower limb surgery; patients with existing consciousness, communication or mental disorders; and patients with poor coordination or compliance.

2.2. Treatment. All the patients were placed in a supine position for traction after general anesthesia. DHS group was treated with DHS internal fixation. A straight incision of 10-14 cm was made on the lateral side of the greater trochanter to expose the proximal lateral side of the femur. Then, the neck stem angle locator was used, the guide pin was drilled in the appropriate position, and the nails of appropriate length were implanted. For patients with more fractured fractures, lag screws and steel wires can be used to fix the fractures, and the screws were placed on the outside of the steel plate. Finally, the incisions were sutured, and routine negative pressure drainage was performed postoperatively. PFNA group was treated with PFNA internal fixation. A 3-4 cm surgical incision was made at the apex of the femoral trochanter. With the aid of X-ray, the guide needle was drilled and confirmed to enter the medullary cavity, and reamed along the opening of the guide needle to the proximal end of the femur. Then, an appropriate PFNA nail was inserted and tilted forward 15° to measure and determine the length of the spiral blade. After expanding the channel along the guide pin, the screw blade was inserted and locked, and with the aid of the sight, a distal locking pin was placed, and the tail cap was installed. Finally, the incision was closed.

2.3. Evaluation Indicators. (1) The excellent and good rate and various surgical indexes (including the time of operation, postoperative bed rest, and the time from the completion of operation to the weight-bearing time of the affected limb) of hip joint function recovery were observed in the two groups after treatment. (2) The recovery of hip joint function was assessed based on the Harris Hip Score (HHS) [11], which was evaluated from four aspects: function, pain, deformity, and motion. The total score was 100 points, and the score and corresponding evaluation were as follows: excellent: ≥90; good: 80-89 points; fair: 70-79 points; poor: <70 points. (3) The adverse reactions were observed in the two groups before and after treatment. (4) The hip pain degree in the two groups was evaluated by visual analogue scale (VAS) before and after operation. The higher the degree of hip pain, the higher the VAS score [12]. (5) The QOL of the patients was evaluated with the Short-Form 36 Item Health Survey (SF-36) from the dimensions of pain, physiology and social function, body, and overall health. The higher the score, the better the patient's QOL [13]

2.4. Statistical Methods. All the data in this study were processed by SPSS22.0 statistical software. The measurement data were expressed as "$x \pm s$", and the comparison between groups was done by t-test. The counting data were expressed as % and tested with χ^2. $P < 0.05$ indicated a statistically significant difference.

3. Results

3.1. Comparison of General Data between PFNA Group and DHS Group. There was no statistical difference between the two groups of patients in terms of age, gender, fracture type, cause of injury, and underlying comorbidities ($P > 0.05$) (Table 1).

3.2. Comparison of Various Clinical Indicators between PFNA Group and DHS Group. The operation time, intraoperative blood loss, and postoperative drainage volume of patients in PFNA group were evidently less than those in DHS group ($P < 0.05$) (Table 2).

Table 1: Comparison of general data between PFNA group and DHS group.

Factors	PFNA group ($n = 59$)	DHS group ($n = 53$)	t/χ^2 value	P
Age (years old)	67.43 ± 5.32	68.26 ± 6.24	0.760	0.449
Gender			0.012	0.913
Male	25 (42.37)	23 (43.4)		
Female	34 (57.63)	30 (56.6)		
Cause of injury			1.983	0.159
Fall	42 (71.19)	31 (58.49)		
Collision	17 (28.81)	22 (41.51)		
Time between operation and injury (day)	5.23 ± 1.41	4.87 ± 1.39	1.358	0.177
Fracture type			0.304	0.581
Open	14 (23.73)	15 (28.3)		
Closed	45 (76.27)	38 (71.7)		
AO classification of fracture			0.373	0.830
A1	14 (23.73)	19 (35.85)		
A2	23 (38.98)	22 (41.51)		
A3	12 (20.34)	12 (22.64)		
Tronzo-Evans classification			1.439	0.837
I	5 (8.47)	6 (11.32)		
II	16 (27.12)	13 (24.53)		
III	13 (22.03)	18 (33.96)		
IV	10 (16.95)	9 (16.98)		
V	5 (8.47)	7 (13.21)		
Underlying comorbidities			0.168	0.682
Hypertension	10 (16.95)	13 (24.53)		
Coronary heart disease	7 (11.86)	12 (22.64)		
Diabetes mellitus	6 (10.17)	7 (13.21)		
Chronic lung disease	3 (5.08)	3 (5.66)		
Others	4 (6.78)	5 (9.43)		

Abbreviation: PFNA: proximal femoral nail antirotation; DHS: dynamic hip screw group.

Table 2: Comparison of clinical indicators between the two groups ($x \pm$ sd).

Groups	n	Operation time	Intraoperative blood loss (mL)	Postoperative drainage volume (mL)
PFNA group	59	54.94 ± 7.29	119.69 ± 19.43	72.10 ± 14.12
DHS group	53	61.17 ± 6.45	130.64 ± 18.75	81.13 ± 15.76
t	—	4.767	3.027	3.198
P	—	<0.001	0.003	0.002

Abbreviation: PFNA: proximal femoral nail antirotation; DHS: dynamic hip screw group.

3.3. Comparison of the Incidence of Postoperative Complications between the Two Groups. In PFNA group, there were 2 cases of adverse reactions, which were 1 case of bedsore and 1 case of pulmonary infection, and the total incidence of adverse reactions was 3.38%, while there were 9 cases of total adverse reactions in DHS group, including 1 case each of incision infection, delayed fracture healing, deep vein thrombosis, urinary infection, 3 cases of bedsore, and 2 cases of pulmonary infection, with a total incidence of adverse reactions of 16.99%. The χ^2 test showed that compared with DHS group, the incidence of postoperative complications in the PFNA group was remarkably lower ($P < 0.05$) (Table 3).

3.4. Patient Efficacy. In PFNA group, the treatment effect was excellent in 20 cases, and good in 29 cases, with an excellent and good rate of treatment effect of 83.05%. In DHS group, there were 12 cases with excellent therapeutic effect, 17 cases with good therapeutic effect, with an excellent and good therapeutic effect rate of 54.72% The χ^2 test showed that the treatment effect was obviously better in PFNA group than in DHS group ($P < 0.05$) (Table 4).

3.5. Hip Function Scores before and after Operation in the Two Groups. There was no significant difference in the hip function score between PFNA group and DHS group before operation, but the hip function score increased significantly after different treatments. Meanwhile, it was found that the hip function score of PFNA group was remarkably higher than that of DHS group, which meant that the hip function

Table 3: Incidence of postoperative complications in PFNA group and DHS group (n (%)).

Groups	n	Incision infection	Bedsore	Delayed fracture healing	Deep vein thrombosis	Lung infection	Urinary infection	Total adverse reactions
PFNA group	59	0 (0.00)	1 (1.69)	0 (0.00)	0 (0.00)	1 (1.69)	0 (0.00)	2 (3.38)
DHS group	53	1 (1.89)	3 (5.66)	1 (1.89)	1 (1.89)	2 (3.77)	1 (1.89)	9 (16.99)
χ^2	—	—	—	—	—	—	—	5.823
P	—	—	—	—	—	—	—	0.016

Abbreviation: PFNA: proximal femoral nail antirotation; DHS: dynamic hip screw group.

Table 4: Comparison of therapeutic effect between the two groups ($x \pm$ sd).

Groups	n	Excellent	Good	Fair	Poor	Excellent and good
PFNA group	59	20 (33.90)	29 (49.15)	6 (10.17)	4 (6.78)	49 (83.05)
DHS group	53	12 (22.64)	17 (32.08)	13 (24.53)	11 (20.75)	29 (54.72)
χ^2	—	—	—	—	—	10.600
P	—	—	—	—	—	0.001

Abbreviation: PFNA: proximal femoral nail antirotation; DHS: dynamic hip screw group.

score in PFNA group increased more significantly than that in DHS group (Table 5, Figure 1).

3.6. Comparison of VAS Scores of Hip Pain before and after Operation between PFNA Group and DHS Group. The VAS score of hip pain did not differ markedly between the two groups before operation ($P > 0.05$), while the postoperative VAS score decreased dramatically in both groups ($P < 0.05$). Meanwhile, it was found that the postoperative VAS score of hip pain in PFNA group was remarkably lower than that in DHS group ($P < 0.05$), so the VAS score of hip pain in PFNA group decreased more significantly after operation (Table 6).

3.7. Comparison of QOL Scores before and after Operation between the Two Groups. There was no significant difference in the QOL score before operation between PFNA group and DHS group ($P > 0.05$), but the QOL score increased dramatically after different operations ($P < 0.05$), and the postoperative QOL score in PFNA group was statistically higher than that in DHS group ($P < 0.05$). Therefore, compared with before operation, the score of QOL in PFNA group increased more significantly after operation (Figure 2).

Table 5: Comparison of hip function scores before and after operation in the two groups ($x \pm$ sd).

Groups	n	Before operation	After operation
PFNA group	59	45.50 ± 6.49	$80.73 \pm 9.20^*$
DHS group	53	44.73 ± 7.89	$64.19 \pm 8.12^*$
t	—	0.566	10.040
P	—	0.572	<0.001

Note: * indicated $P < 0.05$ compared with that before operation. PFNA: proximal femoral nail antirotation; DHS: dynamic hip screw group.

4. Discussion

With the acceleration of aging in recent years, the incidence of FIF has been on the rise [14]. Anatomically, the trochanter is very rich in blood supply, so it can generally heal after fracture, but hip varus is easy to occur without intervention [14]. As to hip varus, it is a serious complication of FIF, which seriously affects the limb function of patients, and in serious cases, it can lead to paralysis [15]. With good effect, traction treatment has been applied in clinical practice; however, the healing was slow. In addition, the majority of elderly patients with this disease are often complicated with other diseases, resulting in long bed time, so it is easy to be complicated with infections, pressure sores, and other diseases [16].

The lateral wall refers to the proximal lateral femoral cortex above the lateral femoral crest. It can prop up the bone of the head and neck, and effectively resist its varus, rotation, and diaphysis displacement, which can avoid the cutting out of the screw. For the selection of internal fixation materials, the thickness of the lateral wall and whether it is ruptured or not are important reference indexes [17]. For FIF, whether treated with the extramedullary roof or medullary nail, it is necessary to place the spiral blade into the head and neck of the femur through the lateral wall and ensure the integrity of the lateral wall is the key to the stability of the internal fixation of FIF [18]. In addition, compared with the general intertrochanteric fractures, lateral-wall dangerous type of intertrochanteric fracture is more serious, and the fracture reduction difficulty is increased due to the severe comminuted fracture and the involvement of the small trochanter. Although the integrity of the lateral wall can be maintained, it is too thin and brittle. Considering from the perspective of stability, it is very important to choose the appropriate fixation treatment, but there is still a lot of controversy over which surgical treatment is more effective [19]. PFNA and DHS, which we discussed in this study, are the mainstream surgical methods for the treatment of unstable

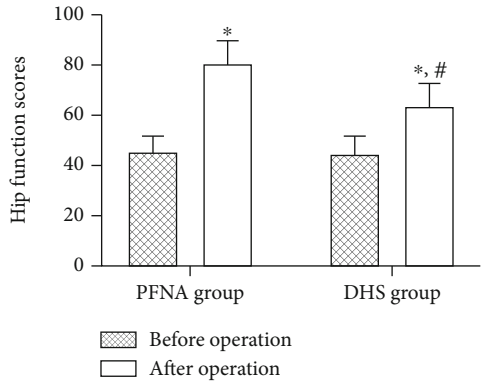

Figure 1: Hip joint function scores before and after operation in PFNA group and DHS group. There was no significant difference in the hip function score between PFNA group and DHS group before operation ($P > 0.05$), but the hip function score increased significantly after different operations ($P < 0.05$), and the increase in PFNA group was more significant. Note: * indicated $P < 0.05$ compared with that before operation; # indicated $P < 0.05$ compared with PFNA group after operation. PFNA: proximal femoral nail antirotation; DHS: dynamic hip screw group.

Table 6: VAS scores of hip pain before and after operation in the two groups ($x \pm$ sd).

Groups	n	Before operation	After operation
PFNA group	59	6.24 ± 2.86	1.80 ± 0.27*
DHS group	53	6.43 ± 2.45	2.59 ± 0.21*
t	—	0.375	17.140
P	—	0.708	<0.001

Note: * indicated $P < 0.05$ compared with that before operation. PFNA: proximal femoral nail antirotation; DHS: dynamic hip screw group.

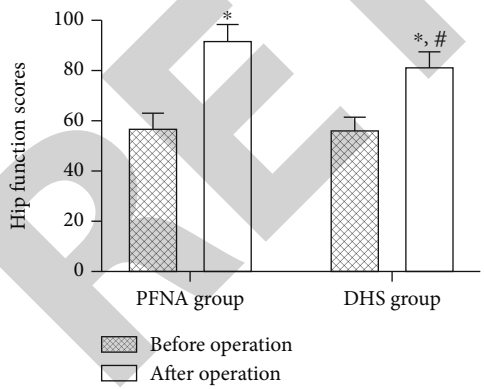

Figure 2: Comparison of preoperative quality of life scores between PFNA group and DHS group. There was no statistically significant difference in the quality of life score between PFNA group and DHS group before operation ($P > 0.05$). After different operations, the quality of life score increased significantly in both groups ($P < 0.05$), and compared with those before surgery, the quality of life score in PFNA group increased more significantly after operation. Note: * indicated $P < 0.05$ compared with that before operation; # indicated $P < 0.05$ compared with PFNA group after operation. PFNA: proximal femoral nail antirotation; DHS: dynamic hip screw group.

intertrochanteric fractures caused by osteoporosis. PFNA, a minimally invasive internal fixation approach, enjoys the advantage of less trauma and can achieve second-stage dynamic fixation [20, 21]. In addition, the spiral blade enters the bone in a self-rotating manner, which can play a good role in filling the bone. Foreign scholars Mereddy et al. [22] performed PFNA surgery on 62 patients with unstable intertrochanteric fractures, and they found that the femoral head resection rate was only 3.6%, while the remaining patients had good therapeutic effect. This study compared the curative effect of DHS internal fixation and minimally invasive PFNA internal fixation on patients with FIF. Compared with DHS group, the effect of PFNA group was statistically better, suggesting the feasibility of the treatment in both groups. However, in contrast, PFNA has more obvious advantages in minimally invasive operation and is more conducive to the recovery of hip joint. Observing the clinical indicators, it was found that compared with DHS group, the operative time and fracture healing time in PFNA group were shorter, the intraoperative blood loss was less, the hip joint function and QOL were higher, and the incidence of complications was lower, with statistically significant differences. These results have proved the feasibility and effectiveness of closed reduction and minimally invasive internal fixation of PFNA in the treatment of lateral-wall dangerous type of intertrochanteric fracture. PFNA internal fixation can promote rapid fracture healing and improve the function of hip joint with higher safety. DHS can maintain the stability of the fracture end by sliding pressure and increase the stability through the pressure system, but there is no support on the medial side, so it lacks resistance to the inside rotation force. Moreover, DHS is easy to loosen after fixation and cannot control rotation, so it is often necessary to fix it again. For the lateral-wall dangerous type of intertrochanteric fracture with high stability requirements, this method is not effective.

To sum up, PFNA internal fixation for the treatment of lateral-wall dangerous type of intertrochanteric fracture has the advantages of short operation time, less intraoperative blood loss, effective improvement of hip joint function, and fewer postoperative complications, which is worthy of clinical application.

Data Availability

The authors confirm that the data supporting the findings of this study are available within the article.

Conflicts of Interest

The authors declare that they have no conflicts of interest.

Authors' Contributions

Weilu Mu and Junlin Zhou performed the experiments, analyzed data, and wrote the manuscript. Weilu Mu designed the study. All the authors agreed to be accountable for the accuracy and integrity of all aspects of the research.

Hindawi
BioMed Research International
Volume 2024, Article ID 9893040, 1 page
https://doi.org/10.1155/2024/9893040

Retraction

Retracted: Investigation on Risk Stratification and the Prognostic Value of hs-TnT Combined with MMP-2 in Patients with Acute Coronary Syndrome

BioMed Research International

Received 12 March 2024; Accepted 12 March 2024; Published 20 March 2024

This article has been retracted by Hindawi following an investigation undertaken by the publisher [1]. This investigation has uncovered evidence of one or more of the following indicators of systematic manipulation of the publication process:

(1) Discrepancies in scope

(2) Discrepancies in the description of the research reported

(3) Discrepancies between the availability of data and the research described

(4) Inappropriate citations

(5) Incoherent, meaningless and/or irrelevant content included in the article

(6) Manipulated or compromised peer review

The presence of these indicators undermines our confidence in the integrity of the article's content and we cannot, therefore, vouch for its reliability. Please note that this notice is intended solely to alert readers that the content of this article is unreliable. We have not investigated whether authors were aware of or involved in the systematic manipulation of the publication process.

Wiley and Hindawi regrets that the usual quality checks did not identify these issues before publication and have since put additional measures in place to safeguard research integrity.

We wish to credit our own Research Integrity and Research Publishing teams and anonymous and named external researchers and research integrity experts for contributing to this investigation.

The corresponding author, as the representative of all authors, has been given the opportunity to register their agreement or disagreement to this retraction. We have kept a record of any response received.

References

[1] Y. Li, L. Li, K. Wang, P. Wu, and Y. Cui, "Investigation on Risk Stratification and the Prognostic Value of hs-TnT Combined with MMP-2 in Patients with Acute Coronary Syndrome," *BioMed Research International*, vol. 2021, Article ID 1040171, 5 pages, 2021.

Hindawi
BioMed Research International
Volume 2021, Article ID 1040171, 5 pages
https://doi.org/10.1155/2021/1040171

Research Article

Investigation on Risk Stratification and the Prognostic Value of hs-TnT Combined with MMP-2 in Patients with Acute Coronary Syndrome

Ying Li,[1] Li Li,[1] Kun Wang,[1] Pengtao Wu,[2] and Yijie Cui[3]

[1]*The No.2 Hospital of Baoding Physical Medicine and Rehabilitation Department, Baoding, 071000 Hebei, China*
[2]*The No.2 Hospital of Baoding Internal Medicine and Cardiovascular Department, Baoding, 071000 Hebei, China*
[3]*The No.2 Hospital of Baoding Computerized Tomography Scan Room, Baoding, 071000 Hebei, China*

Correspondence should be addressed to Yijie Cui; cuifu330861@163.com

Received 19 July 2021; Revised 20 October 2021; Accepted 22 October 2021; Published 23 November 2021

Academic Editor: Jianxin Shi

Objective. The aim of this study was at investigating the risk stratification and prognostic value of hypersensitive troponin T (hs-TnT) combined with matrix metalloproteinase 2 (MMP-2) in patients with acute coronary syndrome (ACS). *Methods*. 80 patients with coronary syndrome admitted to our hospital from January 2019 to January 2020 and 40 healthy people (control group) in the same period were selected. According to different types of diseases, the patients were divided into an acute group ($n = 40$) and stable group ($n = 40$). Besides, they all were monitored by the hs-TnT value, serum MMP-2, and coronary angiography at admission and the comparative analysis was carried out. The patients in both groups were followed up for 30 days, and the incidence of adverse cardiovascular events in the patients during this period was recorded. *Results*. Compared with those in the control group, the MMP-2 and hs-TnT levels in the acute group and the stable group were significantly higher and the MMP-2 and hs-TnT levels in the acute group were significantly higher than those in the stable group, with statistically significant differences ($P < 0.05$). The 30-day follow-up results showed that the incidence of adverse cardiovascular events in the acute group was significantly higher than that in the stable group, with statistically significant differences ($P < 0.05$). The hs-TnT and MMP-2 levels in the acute myocardial infarction (AMI) group were significantly higher than those in the unstable angina pectoris (UAP) group, with statistically significant differences ($P < 0.01$). The hs-TnT and MMP-2 levels in the non-single-vessel group were significantly higher than those in the single-vessel group, with statistically significant differences ($P < 0.01$). *Conclusion*. The hs-TnT and MMP-2 high expression levels are closely associated with myocardial injury, and they can effectively predict the severity of patients' disease. In addition, the hs-TnT and MMP-2 elevated levels can be considered as an important index to judge the short-term treatment efficacy and the risk stratification of early ACS, playing an important role in clinical treatment and rehabilitation in the later stage.

1. Introduction

Acute coronary syndromes (ACS) represent a major cause of mortality in our country. Currently, there is a very wide spectrum of clinical presentation since the actual classification of ACS is based on electrocardiographic presentation, that is, to say based on the absence or presence of ST segment elevation. Most patients with acute coronary syndrome (ACS) present with chest pain and a few with upper abdominal pain [1]. Medically, ACS is divided into non-ST-segment elevation ACS and ST-segment elevation ACS [2–4]. This disease is caused by increased blood viscosity and myocardial oxygen consumption, as well as sympathetic excitation, thus resulting in the rupture or erosion of unstable atherosclerotic plaque, massive platelet aggregation, and even thrombosis. Non-ST-segment elevation ACS mostly occurs at night or at rest and lasts for more than 20 minutes. A diagnosis of ACS should be considered in all patients presenting with ischemic symptoms. Clinical signs and symptoms of ischemia include various combinations of chest

pain; upper extremity, mandibular, or epigastric discomfort; dyspnea; diaphoresis; nausea; fatigue; or syncope. The pain and discomfort associated with an ACS event may occur with exertion or at rest and are often diffuse rather than localized [5].

Besides, the manifestation of this disease is radiation chest pain, accompanied by burning and a sense of pressure, and some patients also present with chest distress and sense of being close to death [6]. Generally speaking, ACS has the characteristics of acute onset and rapid progress, which seriously endangers patients' health and life. Therefore, when the patients have the above suspected symptoms, they should see a doctor immediately to avoid delaying treatment. With the advancement of the medical level, it has been found that hypersensitive troponin has a significant clinical value for the diagnosis of ACS [7]. At present, the main diagnostic criteria for this disease are the global definition of myocardial infarction whose core is the elevation of myocardial markers, namely, the elevation of troponin.

As one of the matrix metalloproteinase genes, MMP-2 is widely distributed in the human body and most of the cells including endothelial cells, epithelial cells, and stromal cells are expressed. MMP-2 causes the rupture of plaque cells to a certain extent mainly by degrading the extracellular matrix of plaque, as well as digesting and destroying the fibrous structure, and finally leads to ACS [8]. Therefore, in order to further investigate the risk stratification and prognostic values of hypersensitive troponin T (hs-TnT) combined with MMP-2 in patients with ACS, 80 patients with coronary syndromes admitted to our hospital from January 2019 to January 2020 and 40 healthy people in the same period were selected as study objects and the summary report is as follows.

2. Materials and Methods

2.1. General Information. In this study, 80 patients with coronary syndromes admitted to our hospital from January 2019 to January 2020 and 40 healthy people in the same period were selected as study objects. According to different types of diseases, patients were divided into the acute group and stable group. Among them, there were 19 males and 21 females both aging from 37 to 73 years in the acute group, with an average age of 53.27 ± 1.45 years, and their course of disease ranged from 1 to 6 years, with an average course of disease of 3.05 ± 0.56 years. The coronary angiography showed that 18 patients had single-vessel disease and 22 patients had non-single-vessel (two or more) disease. Among them, 26 patients had acute myocardial infarction (AMI) and 14 patients had unstable angina pectoris (UAP). There were 18 males and 22 females aging from 39 to 71 years in the stable group, with an average age of 53.04 ± 1.38 years, and their course of disease ranged from 2 to 8 years, with an average course of disease of 3.21 ± 0.63 years. The coronary angiography also revealed that 23 patients had single-vessel disease and 17 patients had non-single-vessel disease. Among them, 25 patients had AMI and 15 patients had UAP. There were 20 males and 20 females aging from 37 to 68 years in the control group, with the average age of 52.85 ± 1.46 years. There were no significant differences in age, sex ratio, and other general data among the three groups ($P > 0.05$), with research significance. This study was approved by the Hospital Ethics Committee, and the patients and their families were informed of the purpose and process of this study and signed the informed consent.

2.2. Inclusion Criteria. According to the classification criteria of International Society of Federation of Cardiology and World Health Organization on acute myocardial infarction and stable angina pectoris, the patients were divided into the acute group, stable group, and control group. Among them, the control group with healthy people undergoing physical examination in the same period had normal results of electrocardiogram (ECG) and coronary angiography without coronary heart disease.

2.3. Exclusion Criteria. Patients had renal and hepatic dysfunction, were allergic to iodine, had myocardial infarction and trauma or underwent surgery recently, had malignant tumors, and had arrhythmia and atrial fibrillation.

2.4. Methods

2.4.1. Clinical Data Collection. The age, gender, drinking and smoking history, triglyceride, hyperlipidemia, and hypertension of patients were included.

2.4.2. Sample Collection, Processing, and Preservation. Serum samples were collected from all the patients. 10 ml of fasting venous blood was collected from the three groups and placed in anticoagulant tubes. Blood centrifuge (manufacturer: Guangzhou Jidi Instrument Co. Ltd.; model type: JIDI-4D-WS) was adopted to centrifuge at 3000 r/min for 10–15 min. Then, the supernatants were taken and stored at −75°C for use. Enzyme-linked immunosorbent assay was adopted by an experienced technician to detect the MMP-2 expression levels in serum, and chemiluminescence immunoassay was also carried out to determine the hs-TnT expression levels of patients. The serum MMP-2 kit was provided by Shanghai Bairui Biological Technology Co. Ltd., and the hs-TnT kit was provided by Shanghai Kalang Biotechnology Co. Ltd. All operations strictly followed the experimental standards.

2.5. Evaluation Indexes. The MMP-2 and hs-TnT levels in serum of the three groups, patients with different types of ACS, and patients with different numbers of diseased coronary vessels were compared and analyzed.

Adverse cardiovascular events included myocardial infarction, cardiac arrest, sudden cardiac death, and angina.

2.6. Statistical Methods. SPSS 21.0 statistical software was adopted to process the clinical data of the two groups, and the measurement data were expressed as $(\bar{x} \pm s)$. The data between multiple groups were compared by one-way ANOVA and tested by t^2. The enumeration data were expressed as $[n(\%)]$ and tested by x^2, with statistically significant differences ($P < 0.05$).

Table 1: Comparison of clinical data of patients in each group ($n = 40$).

Factors	Acute group	Stable group	Control group	$t_1^2(x^2)/p_1$	$t_2^2(x^2)/p_2$	$t_3^2(x^2)/p_3$
Age (years old)	53.27 ± 1.45	53.04 ± 1.38	52.85 ± 1.46	0.73/0.47	1.29/0.20	0.58/0.56
Course of disease (year)	3.05 ± 0.56	3.21 ± 0.63	/	1.20/0.23	/	/
Male/female (case)	19/21	18/22	20/20	0.015/0.90	0.11/0.74	0.20/0.65
Drinking (%)	55% (22/40)	50% (20/40)	7.5% (3/40)	0.20/0.65	21.00/0	17.64/0
Smoking (%)	52.5% (21/40)	47.5% (19/40)	5% (2/40)	0.20/0.66	22.03/0	22.03/0
Triglyceride (mmol/l)	2.05 ± 0.43	1.86 ± 0.26	0.92 ± 0.19	2.39/0.02	15.20/0	18.46/0
Hyperlipidemia (case)	22	19	0	0.45/0.50	30.34/0	24.92/0
Hypertension (case)	24	173	3	2.45/0.12	24.65/0	13.07/0

$t_1^2(x^2)/p_1$ represents a comparison between the acute group and the stable group. $t_2^2(x^2)/p_2$ represents a comparison between the acute group and the control group. $t_3^2(x^2)/p_3$ represents a comparison between the stable group and the control group.

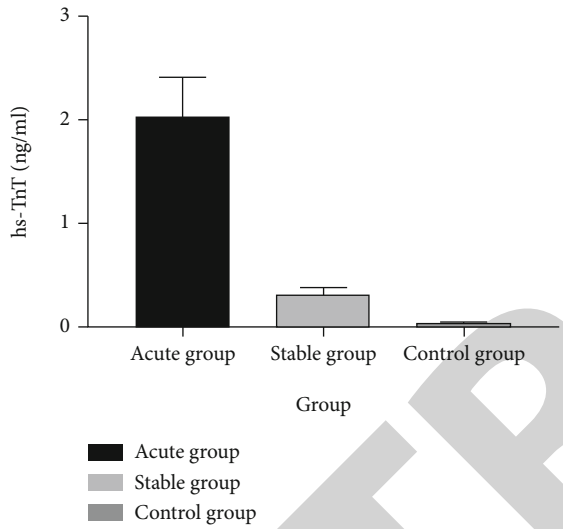

Figure 1: Comparison of hs-TnT levels of three groups of experimental subjects. The abscissa represents the acute group, the stable group, and the control group, while the ordinate represents the hs-TnT level. As shown in Figure 1, the hs-TnT level was the highest in the acute group and the lowest in the control group. hs-TnT: hypersensitive troponin T.

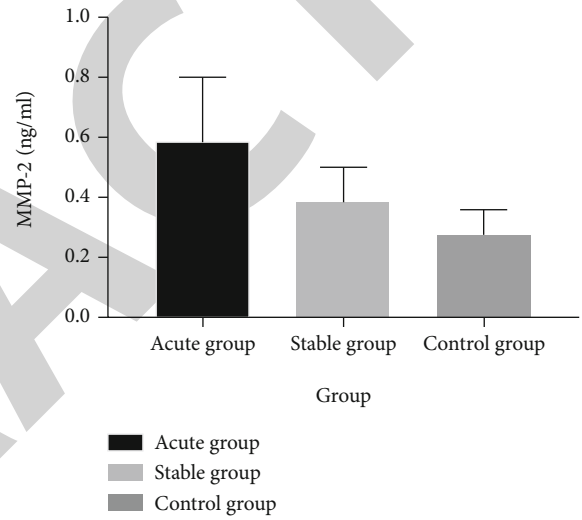

Figure 2: Comparison of MMP-2 levels of three groups of experimental subjects. The abscissa represents the acute group, the stable group, and the control group, while the ordinate represents the MMP-2 level. As shown in Figure 2, the MMP-2 level was the highest in the acute group and the lowest in the control group. MMP-2: matrix metalloproteinase 2.

3. Results

3.1. Comparison of Clinical Data of Patients in Each Group. The study results showed that the number of patients with smoking and drinking history in the acute group and the stable group was significantly higher than that in the control group ($P < 0.05$). The triglyceride levels in the acute group and the stable group were significantly higher than that in the control group ($P < 0.05$). The number of patients with hyperesteremia and hypertension in the acute group and the stable group was significantly higher than that in the control group ($P < 0.05$), as detailed in Table 1.

3.2. Comparison of hs-TnT and MMP-2 Levels of Three Groups of Experimental Subjects. The study results showed that the hs-TnT and MMP-2 levels in the acute group were significantly higher than those in the stable group and the control group and the hs-TnT and MMP-2 levels in the stable group were significantly higher than those in the control group, with statistically significant differences ($P < 0.05$), as detailed in Figures 1 and 2.

3.3. Comparison of the Incidence of Adverse Cardiovascular Events between the Two Groups after 30 Days. The study results showed that the incidence of cardiovascular events after 30 days in the acute group was significantly higher than that in the stable group, with statistically significant differences ($P < 0.05$), as detailed in Table 2.

3.4. Comparison of the hs-TnT and MMP-2 Levels in Patients with Different Types of ACS. The study results showed that the hs-TnT and MMP-2 levels in the AMI group were significantly higher than those in the UAP group, with statistically significant differences ($P < 0.01$), as detailed in Table 3.

Table 2: Comparison of the incidence of adverse cardiovascular events between the two groups after 30 days.

Group	n	Myocardial infarction	Cardiac arrest	Sudden cardiac death	Angina pectoris	Incidence
Acute group	40	7.5% (3/40)	10% (4/40)	7.5% (3/40)	10% (4/40)	32.5%
Stable group	40	0	2.5%(1/40)	0	5% (2/40)	7.5%
x^2		3.1117	1.920	2.051	0.721	8.669
p		0.077	0.166	0.152	0.396	0.003

Table 3: Comparison of the hs-TnT and MMP-2 levels in patients with different types of ACS.

Group	N	Hs-TnT (ng/ml)	MMP-2 (ng/ml)
AMI group	51	1.79 ± 0.32	0.52 ± 0.17
UAP group	29	0.48 ± 0.11	0.37 ± 0.13
t		21.292	4.113
p		<0.01	<0.01

hs-TnT: hypersensitive troponin T; AMI: acute myocardial infarction.

Table 4: Comparison of hs-TnT and MMP-2 levels in patients with different numbers of diseased coronary vessels.

Group	n	hs-TnT (ng/ml)	MMP-2 (ng/ml)
Single-vessel group	41	0.67 ± 0.18	0.27 ± 0.14
Non-single-vessel group	39	1.91 ± 0.37	0.54 ± 0.22
t		19.207	6.582
p		<0.01	<0.01

MMP-2:matrix metalloproteinase 2; hs-TnT: hypersensitive troponin T; UAP: unstable angina pectoris.

3.5. Comparison of the hs-TnT and MMP-2 Levels in Patients with Different Numbers of Diseased Coronary Vessels. The study results showed that the hs-TnT and MMP-2 levels in the non-single-vessel group were significantly higher than those in the single-vessel group, with statistically significant differences ($P < 0.05$), as detailed in Table 4.

4. Discussion

ACS is mainly characterized by acute onset, severe illness, and high mortality. According to the survey results of the World Health Organization, about 15 million people worldwide die from cardiovascular and cerebrovascular diseases every year and more than half of them die from ACS [8]. With the change of daily lifestyle, the patients with ACS in China are on the rise year by year. It has become a consensus that early diagnosis and treatment can save more patients' lives. The cardiovascular biomarker is a kind of biochemical substance associated with the generation, development, diagnosis, clinical treatment, prognosis, and rehabilitation of patients' diseases, which is of great significance for disease treatment, diagnosis, and prevention. The sensitivity of hs-TnT is higher than that of cardiac troponin I (cTn I) and cardiac troponin T (cTn T) which are currently widely used as diagnostic biomarkers for myocardial injury caused by ischemic heart diseases in clinical and forensic medicine.

With the application of hs-TnT in the study, the increase of the hs-TnT level in patients with ACS can be measured at the time of onset and visit, which plays an important role in disease diagnosis. A large number of studies have shown that hs-TnT is a more common troponin [10], which only exists in human myocardium. When myocardial injury occurs in patients, the level of troponin concentration will show a rising trend, which is long lasting and the earliest increasing indicator in various physical indicators of patients. Therefore, this indicator can be used for the diagnosis and treatment of myocardial injury [11]. hs-TnT is also a sensitive inflammatory indicator which is synthesized by the liver and can effectively reflect the systemic inflammation of patients. Inflammation will occur in the rupture of plaque. The coagulation mechanism is affected by cytokines, which stimulates the human liver, promotes the production of a large amount of hs-TnT, and releases hs-TnT in the blood. MMP-2 can be formed in human fibroblasts, endothelial cells, macrophages, and other cells and have a joint effect with calcium and zinc ions, having a degradation effect on the human extracellular matrix. Relevant information showed that [12] the MMP-2 level in serum is an important cytokine for judging the prognosis of ACS and can be used as an important parameter for clinical risk prediction. Additionally, the MMP-2 level in serum plays an important role in the early diagnosis and treatment of acute high-risk coronary syndrome and in identifying potential risk factors.

The study results are consistent with the results of the "*Application Value of Serum Hypersensitivity Troponin T and Myoglobin Detection in Acute Myocardial Infarction*" by Yimei and Weipeng [9]. Compared with those in the stable group, hs-TnT and MMP-2 levels in the acute group remarkably increased, with statistically significant differences ($P < 0.05$). In [13] and others' studies, the dynamic follow-up survey of patients with ACS showed that the incidence of adverse cardiovascular events was 28%, the hs-TnT in serum was 2.08 ± 0.29 ng/ml, and the MMP-2 in serum was 0.52 ± 0.17 ng/ml. Relevant foreign data [14] showed that the hs-TnT high expression level is positively correlated with cardiovascular disease. It has been fully demonstrated that the hs-TnT and MMP-2 high expression levels in serums of the patients with ACS can effectively predict poor prognosis and increased incidence of cardiovascular events. In addition, attention should be paid to the prevention of cardiovascular events in such patients at a later stage [15].

However, there are some limitation here. It was conducted on a relatively small number of participants; a large number of population should be included in the following

Hindawi
BioMed Research International
Volume 2021, Article ID 9485273, 12 pages
https://doi.org/10.1155/2021/9485273

Research Article

Analysis of the Expression and Prognostic Value of MSH2 in Pan-Cancer Based on Bioinformatics

Wenli Qiu,[1] **Ke Ding**,[2] **Lusheng Liao**,[3] **Yongchang Ling**,[4] **Xiaoqiong Luo**,[1] **and Junli Wang**[1,3]

[1]*Medical Reproduction Center, Affiliated Hospital of Youjiang Medical University for Nationalities, Baise, Guangxi, China*
[2]*Department of Sports Medicine, Affiliated Hospital of Youjiang Medical University for Nationalities, Baise, Guangxi, China*
[3]*School of Medical Laboratory Science, Youjiang Medical University for Nationalities, Baise, Guangxi, China*
[4]*Department of Obstetrics, Affiliated Hospital of Youjiang Medical University for Nationalities, Baise, Guangxi, China*

Correspondence should be addressed to Junli Wang; baisewangjunli@163.com

Received 1 September 2021; Accepted 6 November 2021; Published 23 November 2021

Academic Editor: Jianxin Shi

Background. MutS homolog 2 (MSH2), with the function of identifying mismatches and participating in DNA repair, is the "housekeeping gene" in the mismatch repair (MMR) system. MSH2 deficiency has been reported to enhance cancer susceptibility for the association of hereditary nonpolyposis colorectal cancer. However, the expression and prognostic significance of MSH2 have not been studied from the perspective of pan-cancer. *Methods*. The GTEx database was used to analyze the expression of MSH2 in normal tissues. The TCGA database was used to analyze the differential expression of MSH2 in pan-cancers. The prognostic value of MSH2 in pan-cancer was assessed using Cox regression and Kaplan-Meier analysis. Spearman correlations were used to measure the relationship between the expression level of MSH2 in pan-cancer and the level of immune infiltration, tumor mutational burden (TMB), and microsatellite instability (MSI). *Results*. MSH2 is highly expressed in most type of cancers and significantly correlated with prognosis. In COAD, KIRC, LIHC, and SKCM, the expression of MSH2 was significantly positively correlated with the abundance of B cells, CD4+ T cells, CD8+ T cells, dendritic cells, macrophages, and neutrophils. In THCA, MSH2 expression correlated with CD8+T Cell showed a significant negative correlation. MSH2 had significantly negative correlations with stromal score and immune score in a variety of cancers and significantly correlated with TMB and MSI of a variety of tumors. *Conclusions*. MSH2 may play an important role in the occurrence, development, and immune infiltration of cancer. MSH2 can emerge as a potential biomarker for cancer diagnosis and prognosis.

1. Introduction

Cancer has seriously endangered global public health. The incidence and mortality of cancer are increasing rapidly every year, which has gradually become the primary killer threatening human health [1, 2]. Despite continuing improvements in diagnosis and treatment methods of cancers, a series of problems such as cancer recurrence and drug resistance still lead to the low survival [3]. Therefore, it is urgent to find novel methods for cancer diagnostics and treatments. With the continuous development and improvement of public databases for example The Cancer Genome Atlas (TCGA), new immunotherapy targets have been discovered through pan-cancer expression analysis of genes and evaluation of their relationship with clinical prognosis and immunity [4]. Autophagy-related protein 5 is a protein related to autophagosome formation. Studies using public database analysis have found that autophagy-related protein 5 plays an important role in tumor metabolism and tumor immunity through pan-cancer analysis and is a promising tumor predictive biomarker in most solid tumors [5].

MutS homolog 2 (MSH2) is homologous to the *E. coli* MutS gene and participates in DNA mismatch repair (MMR) [6, 7]. Human MSH2/6 can form a complex with BLM-p53-RAD51 in response to DNA damage repair [8]. When DNA is damaged, MSH2 promotes cell apoptosis by

regulating ATR/Chk2/p53 signal transduction [9]. In addition, MSH2 is not only closely associated with the autophagy pathway. MSH2 deficiency can also cause accelerated telomere shortening in normal human cells [10, 11].

MSH2 gene is intimately linked to the occurrence and development of cancer, whose expression ratios is different in various types of malignant lymphoproliferative diseases derived from B cells [12]. MSH2 missense mutations affect splicing, which may regulate the occurrence and development of cancer in a tissue-specific manner [13]. MSH2-deficient tumor cell lines have lost most of the ability to accurately repair plasmid DNA double-strand breaks through homologous recombination and increased susceptibility to cancer by promoting deletions or insertion mutations associated with DNA double-strand break repair [14]. Recent studies have indicated that the MSH2 is closely related to the occurrence of Lynch syndrome (Lynch), whose new splicing site mutation (c.1661+2 T>G) can cause Lynch [15, 16]. Lynch is an autosomal dominant genetic disease. Lynch patients have a significantly increased risk of breast and multiple gastric cancer [17, 18]. It is reported that the abnormal expression of MSH2 is related to cancers such as oral squamous cell carcinoma, primary prostate cancer, breast cancer, and gastric cancer [18–21]. However, MSH2 is currently being investigated in specific cancer types rather than analyzed from the perspective of pan-cancer. In this study, we evaluated the expression and prognostic value of MSH2 in pan-cancer and analyzed the association in the MSH2 expression levels and tumor microenvironment, tumor mutational burden (TMB), and microsatellite instability (MSI) in 33 cancer types.

2. Materials and Methods

2.1. Sample Information. The Cancer Genome Atlas (TCGA; https://portal.gdc.cancer.gov/) contains clinical data of 33 cancer types, allowing cancer researchers to search and download cancer data for analysis. Download data of 33 different cancer types in the TCGA database through UCSC Xena (https://xena.ucsc.edu/). Genotype-Tissue Expression (GTEx; https://gtexportal.org/) studied more than 7,000 autopsy samples from 449 healthy human donors, covering 44 tissues. We obtained 31 different normal tissue MSH2 expression matrix and clinical information data through GTEx database. The TIMER database (https://cistrome.shinyapps.io/timer/) is a comprehensive resource for systematically analyzing the immune infiltration of different cancer types. It can analyze the correlation between the expression of the MSH2 gene and the abundance of immune infiltration in pan-cancer. We downloaded score data of six immune infiltrating cells from 33 cancers from the timer database and analyzed the correlation between MSH2 gene expression and the score of these immune cells. The full name and abbreviation of cancer are given as follows: adrenocortical carcinoma (ACC); bladder urothelial carcinoma (BLCA); breast invasive carcinoma (BRCA); cervical squamous cell carcinoma and endocervical adenocarcinoma (CESC); cholangiocarcinoma (CHOL); colon adenocarcinoma (COAD); lymphoid neoplasm diffuse large B-cell lymphoma (DLBC); esophageal carcinoma (ESCA); glioblastoma multiforme (GBM); head and neck squamous cell carcinoma (HNSC); kidney chromophobe (KICH); kidney renal clear cell carcinoma (KIRC); kidney renal papillary cell carcinoma (KIRP); acute myeloid leukemia (LAML); brain lower grade glioma (LGG); liver hepatocellular carcinoma (LIHC); lung adenocarcinoma (LUAD); lung squamous cell carcinoma (LUSC); mesothelioma (MESO); ovarian serous cystadenocarcinoma (OV); pancreatic adenocarcinoma (PAAD); pheochromocytoma and paraganglioma (PCPG); prostate adenocarcinoma (PRAD); rectum adenocarcinoma (READ); sarcoma (SARC); skin cutaneous melanoma (SKCM); stomach adenocarcinoma (STAD); testicular germ cell tumors (TGCT); thyroid carcinoma (THCA); thymoma (THYM); uterine corpus endometrial carcinoma (UCEC); uterine carcinosarcoma (UCS); uveal melanoma (UVM).

2.2. Expression Analysis of MSH2 Gene in Pan-Cancer. The differential expression of MSH2 in tumor and adjacent normal tissues was analyzed by Wilcoxon's test. The R package "ggpubr" was used to visualize pictures ($^{***}P < 0.001$; $^{**}P < 0.01$; $^{*}P < 0.05$).

2.3. Survival Analysis of MSH2 Gene in Pan-Cancer. Each sample downloaded from the TCGA database extracts survival-related data, was selected overall survival (OS) to study the relationship between MSH2 expression and patient survival, and analyzed by univariate survival to study the relationship between MSH2 expression and patient survival. According to the median value of MSH2 expression level, patients were divided into high-expression group and low-expression group. The Kaplan-Meier method was used to compare the survival rate of patients in the groups mentioned above. The R packages "survival" and "forestplot" were used to draw forest plots. Kaplan-Meier curves were drawn by the R package "survival" and "survminer."

2.4. The Relationship between MSH2 Gene Expression and Immune Cells. The TIMER database "Gene" module was used to evaluate the correlation between the expression of MSH2 and the level of immune infiltrating cells in pan-cancer. Six types of immune infiltrating cells include B cells, CD4+ T cells, CD8+ T cells, dendritic cells, macrophages, and neutrophils. Use R-package "estimate" to calculate the immune score and stromal score in each tumor sample calculated by R-package "estimate."

2.5. Association Analysis of MSH2 Gene Expression with Tumor Mutation Burden and Microsatellite Instability. Tumor mutation burden (TMB) refers to the number of base mutations per million bases. The Spearman method was used to calculate the correlation between TMB and MSH2 expression. Microsatellite instability (MSI) refers to the phenomenon that new microsatellite alleles appear at a certain microsatellite site in tumors due to the insertion or deletion of repeat units compared with normal tissues. The Spearman method was used to calculate the correlation between MSI and MSH2 expression. R package "fmsb" was applied for image visualization ($^{***}P < 0.001$; $^{**}P < 0.01$; $^{*}P < 0.05$).

2.6. Statistical Analysis. All the data of gene expression were normalized by log2 transformation. The differential expression of MSH2 in pan-cancer was tested by Wilcox test. The Kaplan-Meier curve and Cox proportional hazards model were used for survival analysis. The Spearman method was used to study the correlation between two variables. P value < 0.05 was considered as significant. The visualization of the data is processed by R software (version 4.1.0).

3. Results

3.1. MSH2 Is Highly Expressed in Pan-Cancer. The MSH2 expression level in bone marrow tissue was the highest among 31 kinds of normal tissues through database search of the GTEx, while lower in most other normal tissues (Figure 1(a)). Subsequently, we evaluated the expression level of MSH2 in 33 cancer types in the TCGA database. The results showed that MSH2 was widely expressed in all cancer types. Among them, MSH2 expression was highest in TGCT and lowest in CHOL (Figure 1(b)). Compared with the corresponding normal tissues based on the TCGA database, MSH2 is significantly higher expressed in BLCA, BRCA, CESC, CHOL, COAD, ESCA, HNSC, LIHC, LUAD, LUSC, PRAD, READ, STAD, and UCEC, while significantly lower expressed only in KICH (Figure 1(c)).

3.2. The Prognostic Value of MSH2 in Pan-Cancer. Univariate Cox regression analysis was used to evaluate the correlation between MSH2 expression levels in 33 different tumor types in the TCGA database and the overall survival (OS) of patients. Forest plots in 33 different types of tumors showed that the expression of MSH2 in ACC (HR = 3.183, $P < 0.001$), KICH (HR = 3.071, $P = 0.009$), KIRC (HR = 0.654, $P = 0.009$), KIRP (HR = 2.307, $P = 0.008$), LGG (HR = 2.287, $P < 0.001$), LIHC (HR = 1.821, $P < 0.001$), PAAD (HR = 2.276, $P = 0.001$), READ (HR = 0.466, $P = 0.017$), SARC (HR = 1.722, $P < 0.001$), THYM (HR = 0.298, $P = 0.009$), and UCEC (HR = 1.563, $P = 0.003$) was significantly correlated with overall survival. MSH2 was a high-risk gene in ACC, KICH, KIRP, LGG, LIHC, PAAD, SARC, and UCEC; however, MSH2 was a low-risk gene in KIRC, READ, and THYM (Figure 2). Kaplan-Meier survival analysis also demonstrated that among patients with KIRC ($P = 0.002$), STAD ($P = 0.003$), and THYM ($P = 0.019$), those with high levels of MSH2 had longer survival times, while in patients with ACC ($P = 0.025$), LGG ($P = 0.006$), LIHC ($P < 0.001$), MESO ($P = 0.037$), PAAD ($P < 0.002$), SARC ($P = 0.007$), and UCEC ($P = 0.005$), high MSH2 expression was associated with poor OS (Figure 3).

3.3. MSH2 Is Associated with Tumor Immune Infiltrating Cells in Pan-Cancer. We obtained the correlation coefficient between MSH2 expression level and immune cell infiltration level in 39 cancer types through TIMER database and selected MSH2 expression level and B cells, CD4+ T cells, CD8+ T cells, dendritic cells, macrophages, and neutrophils which related to cancers for analysis. The results showed that in COAD, the expression of MSH2 and B cells ($R = 0.234$, $P < 0.001$), CD4+ T cells ($R = 0.199$, $P < 0.001$), CD8+ T cells ($R = 0.27$, $P < 0.001$), macrophages ($R = 0.228$, $P < 0.001$), neutrophils ($R = 0.25$, $P < 0.001$), and dendritic cells ($R = 0.222$, $P < 0.001$) infiltration levels was significantly positively correlated; in KIRC, the expression of MSH2 and B cells ($R = 0.261$, $P < 0.001$), CD4+ T cells ($R = 0.298$, $P < 0.001$), CD8+ T cells ($R = 0.275$, $P < 0.001$), macrophages ($R = 0.386$, $P < 0.001$), neutrophils ($R = 0.428$, $P < 0.001$), and dendritic cells ($R = 0.357$, $P < 0.001$) infiltration levels was significantly positively correlated; in LIHC, the expression of MSH2 related to B cells ($R = 0.388$, $P < 0.001$), CD4+ T cells ($R = 0.413$, $P < 0.001$), CD8+ T cells ($R = 0.29$, $P < 0.001$), macrophages ($R = 0.499$, $P < 0.001$), neutrophils ($R = 0.460$, $P < 0.001$), and dendritic cells ($R = 0.443$, $P < 0.001$) infiltration levels was significantly positively correlated; in SKCM, the expression of MSH2 related to B cells ($R = 0.117$, $P = 0.013$), CD4+T cells ($R = 0.103$, $P = 0.030$), CD8+T cells ($R = 0.412$, $P < 0.001$), macrophages ($R = 0.231$, $P < 0.001$), neutrophils ($R = 0.469$, $P < 0.001$), and dendritic cells ($R = 0.247$, $P < 0.001$) infiltration levels was significantly positively correlated; in THCA, the expression of MSH2 related to B cells ($R = 0.626$, $P < 0.001$), CD4+T cells ($R = 0.499$, $P < 0.001$), macrophages ($R = 0.519$, $P < 0.001$), neutrophils ($R = 0.271$, $P < 0.001$), and dendritic cells ($R = 0.282$, $P < 0.001$) infiltration levels was significantly positively correlated, and CD8+ T cell ($R = -0.408$, $P < 0.001$) infiltration levels were significantly negatively correlated (Figure 4).

3.4. MSH2 Is Associated with Tumor Microenvironment in Pan-Cancer. We use the R software package estimate to calculate the stromal score and immune score of 33 cancers and analyze the relationship between the expression level of MSH2 and these two scores. The results of the study showed that the top six tumors with the most significant correlation between MSH2 and stromal score were GBM ($R = -0.45$, $P < 0.001$), LUSC ($R = -0.3$, $P < 0.001$), SARC ($R = -0.56$, $P < 0.001$), BRCA ($R = -0.31$, $P < 0.001$), STAD ($R = -0.36$, $P < 0.001$), and TGCT ($R = -0.58$, $P < 0.001$) (Figures 5(a)–5(f)); the top six tumors with the most significant correlation between MSH2 and immune score are CESC ($R = -0.37$, $P < 0.001$), LAML ($R = -0.44$, $P < 0.001$), GBM ($R = -0.50$, $P < 0.001$), KIRP ($R = -0.32$, $P < 0.001$), SARC ($R = -0.46$, $P < 0.001$), and UCEC ($R = -0.37$, $P < 0.001$) (Figure 5(g)–5(l)).

3.5. The Expression of MSH2 in Pan-Cancer Is Related to Tumor Mutation Burden and Microsatellite Instability. TMB and MSI are considered as important factors inducing tumor occurrence and development. The analysis of correlation between MSH2 expression and TMB and MSI in 33 common cancers reflected that the expression of MSH2 in ACC, BLCA, BRCA, HNSC, LGG, LUAD, LUSC, MESO, OV, PRAD, READ, SKCM, STAD, and UCEC was significantly positively correlated with TMB. However, in CHOL, KIRP, THCA, and THYM, the expression of MSH2 was significantly negatively correlated with TMB (Figure 6(a)). The expression of MSH2 in STAD and UCEC was significantly positively correlated with MSI. On the contrary, the

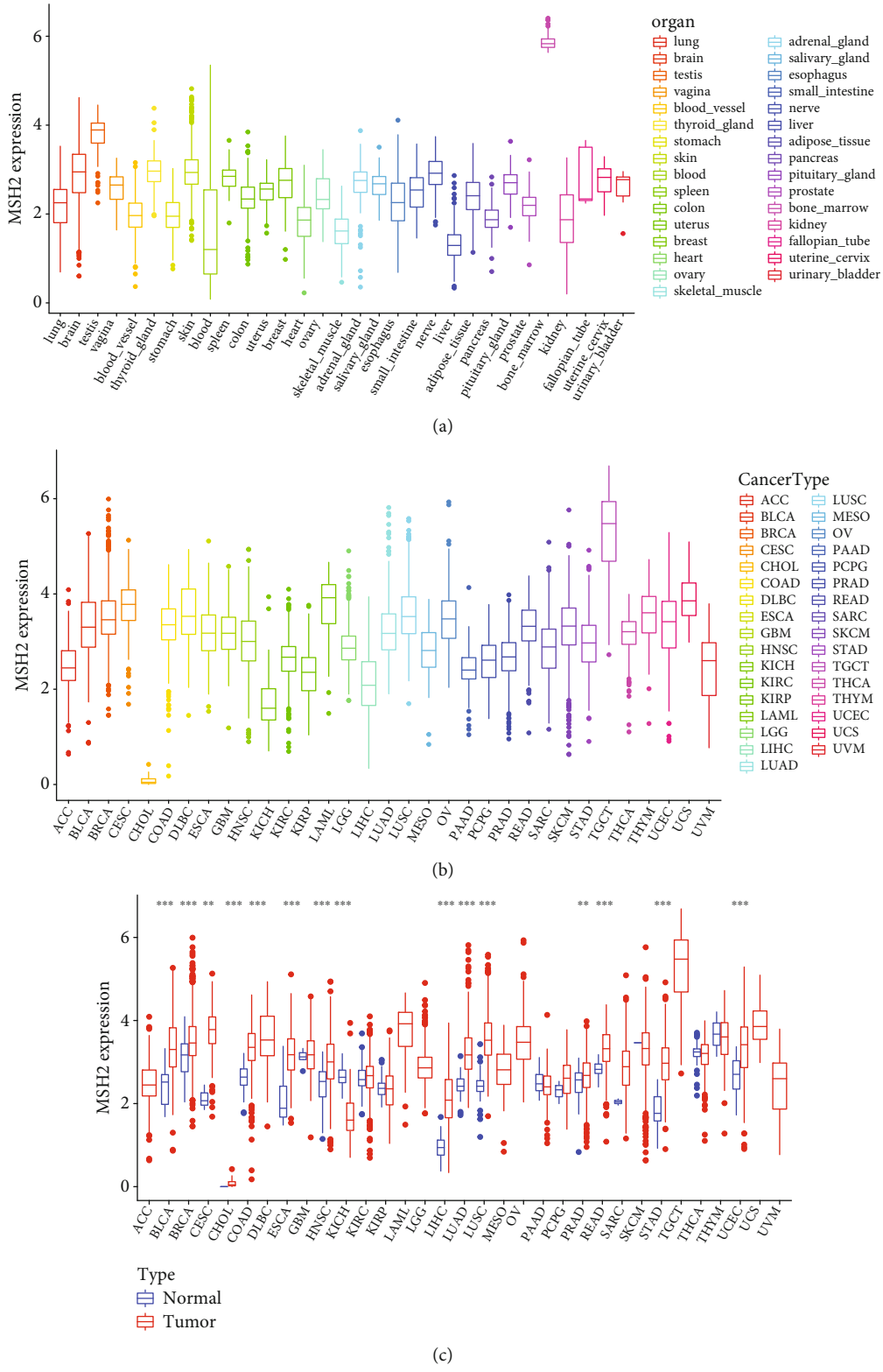

Figure 1: The expression of MSH2 in pan-cancer. (a) The expression of MSH2 in normal tissues. (b) The expression of MSH2 in tumor tissues. (c) Differential expression of MSH2 in normal tissues and tumor tissues. $^{*}P < 0.05$, $^{**}P < 0.01$, $^{***}P < 0.001$.

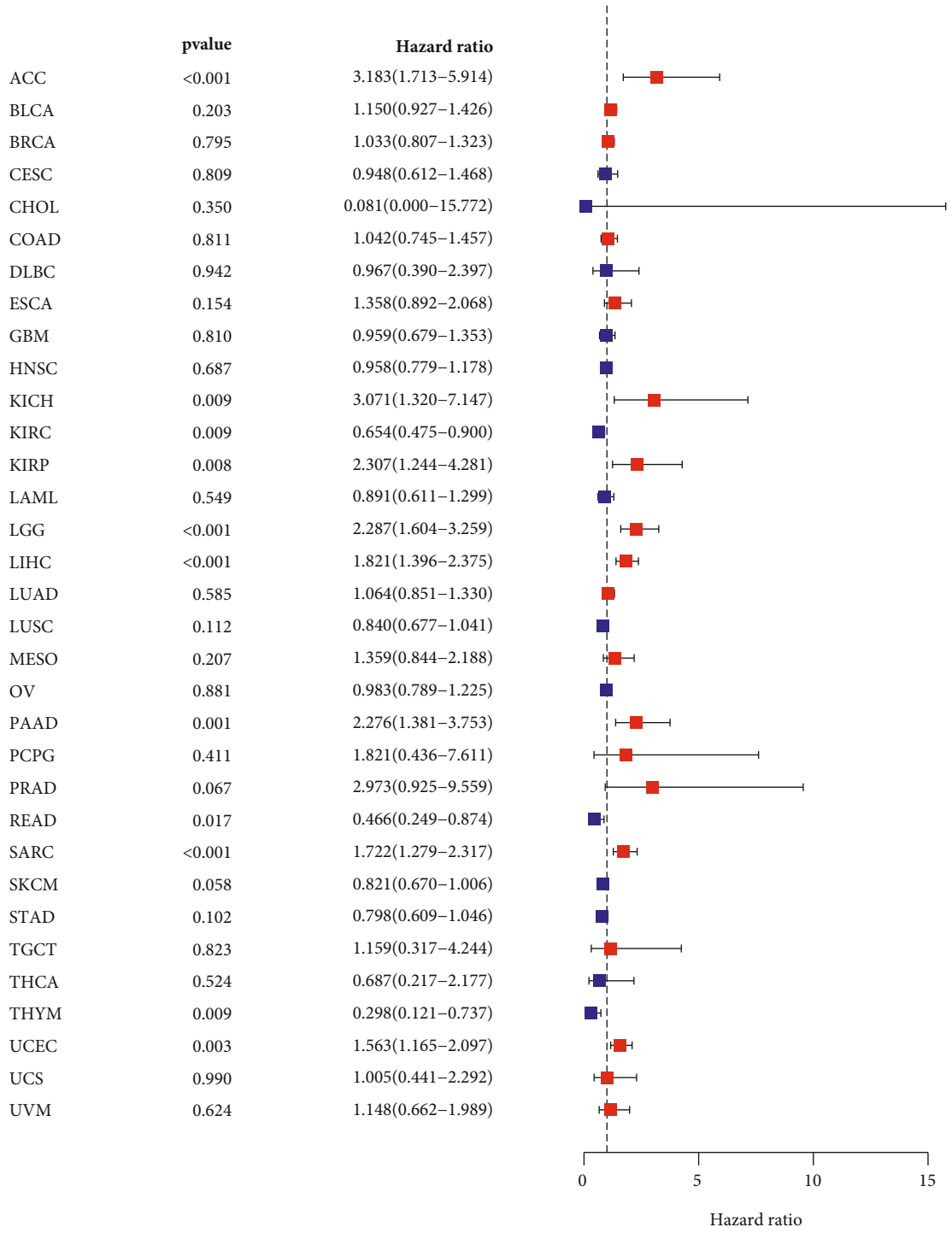

Figure 2: Forest plot of the correlation between MSH2 expression level and overall survival in 33 tumor types.

expression of MSH2 in THCA, PRAD, and DLBC showed significantly negative correlation with MSI (Figure 6(b)).

4. Discussion

Mismatch repair proteins are composed of multiple DNA base mismatch proteins that specifically repair DNA bases, which play an important role in maintaining the fidelity and stability of the genome and avoiding or reducing mutations in the process of gene coding [22]. MSH2 is an essential part of the DNA mismatch repair system for DNA damage repairment [23, 24]. According to the previous reports, the expression MSH2 was increased in oral squamous cell carcinoma and decreased in breast and gastric cancer [19, 25, 26]. MSH2 may have a functional consequence in different types of cancer, which is worthy of our further study.

The results of this study showed that compared with other tissues, MSH2 expression level is the highest in bone

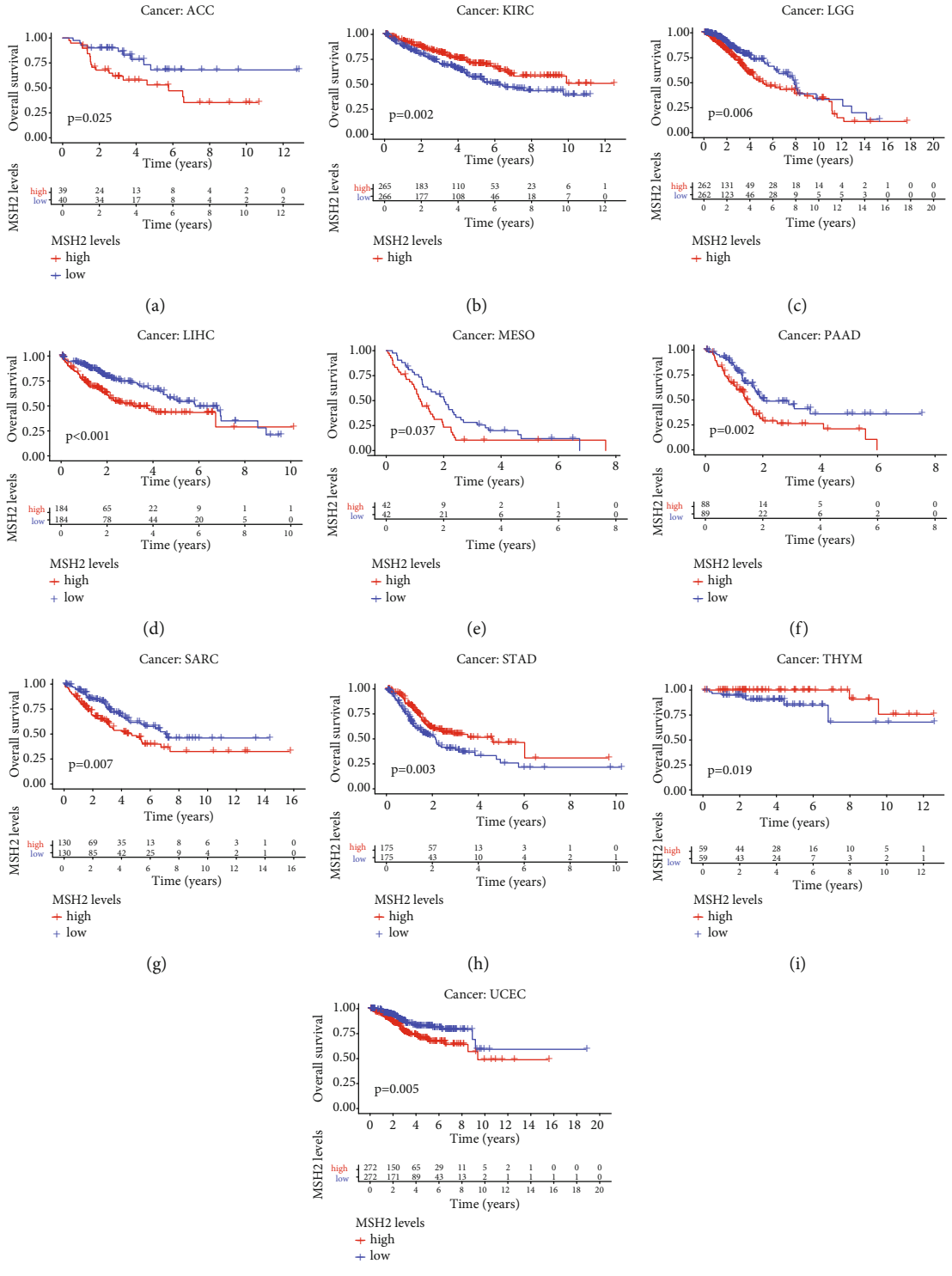

Figure 3: Kaplan-Meier OS curves of MSH2 expression in the ten most significantly associated tumors. (a) KM curves of high and low MSH2 expression in ACC patients. (b) KM curves of high and low MSH2 expression in KIRC patients. (c) KM curves of high and low MSH2 expression in LGG patients. (d) KM curves of high and low MSH2 expression in LIHC patients. (e) KM curves of high and low MSH2 expression in MESO patients. (f) KM curves of high and low MSH2 expression in PAAD patients. (g) KM curves of high and low MSH2 expression in SARC patients. (h) KM curves of high and low MSH2 expression in STAD patients. (i) KM curves of high and low MSH2 expression in THYM patients. (j) KM curves of high and low MSH2 expression in UCEC patients.

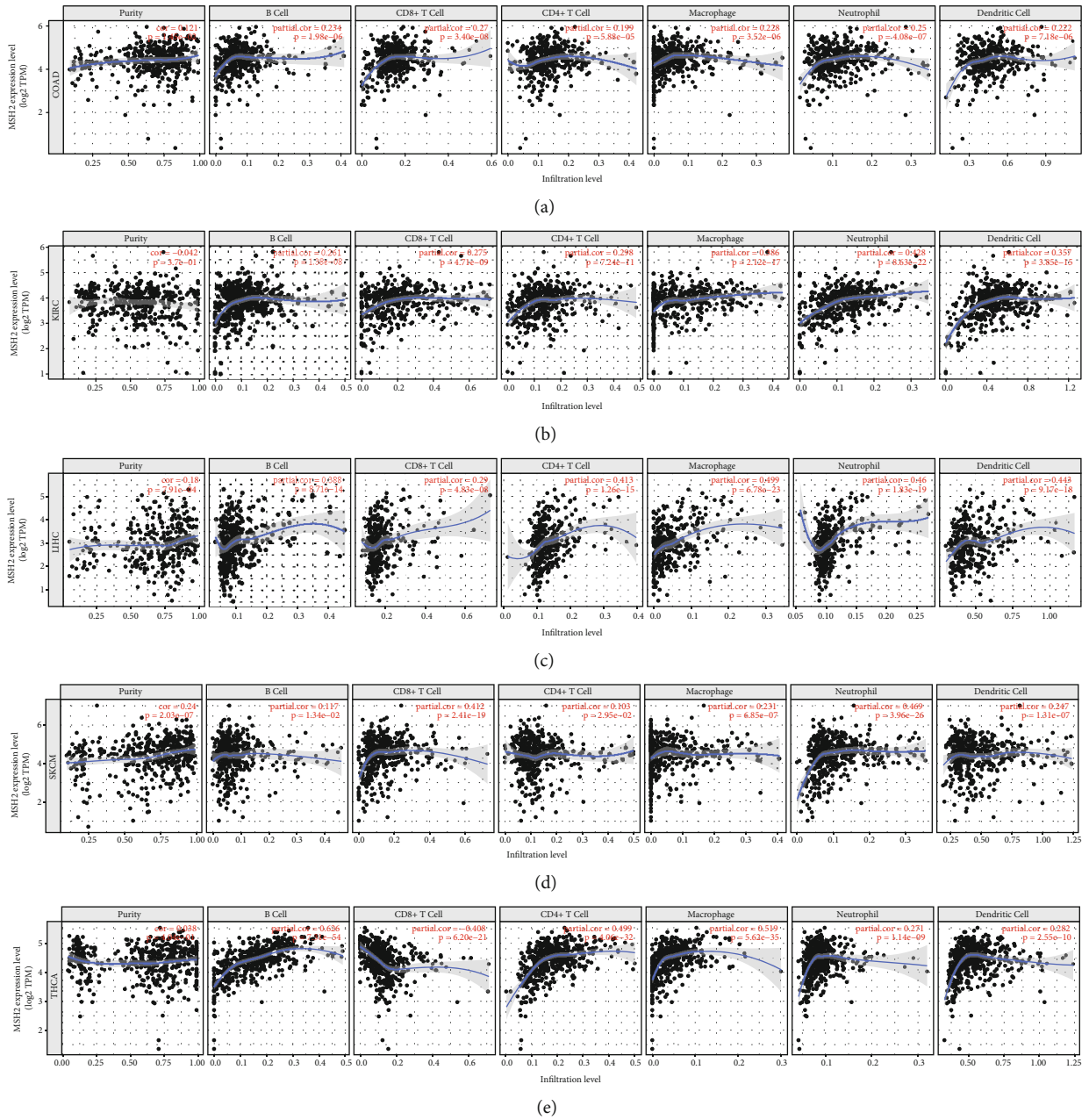

Figure 4: Correlation analysis between MSH2 expression and tumor immune infiltrating cells in pan-cancer. (a) Correlation analysis between expression levels of MSH2 and tumor immune infiltrating cells in COAD. (b) Correlation analysis between expression levels of MSH2 and tumor immune infiltrating cells in KIRC. (c) Correlation analysis between the expression level of MSH2 and tumor immune infiltrating cells in LIHC. (d) Correlation analysis between expression levels of MSH2 and tumor immune infiltrating cells in SKCM. (e) Correlation analysis between the expression level of MSH2 and tumor immune infiltrating cells in THCA.

marrow tissue. Normally, bone marrow hyperplasia is active, which may lead to relatively high levels of MSH2 expression. Through analysis of the TCGA database, we found that MSH2 is highly expressed in a variety of cancer types when compared with the corresponding normal tissues. It has been reported that MSH2 expression is increased in low-grade and high-grade urothelial malignancy [27]. In addition, MSH2 was overexpressed in patients with colon cancer and oral squamous cell carcinoma [19, 28]. The research results showed above agreeing with our conclusions. Malik et al. proposed that in the Pakistani population, MSH2 deficiency may lead to the occurrence and development of breast cancer [25]. This result was inconsistent with our current results. The current study demonstrated that the expression of MSH2 in gastric cancer tissues was significantly reduced, especially in poorly differentiated gastric cancer when compared with normal gastric mucosal tissue [26]. The expression of MSH2 may indicate the advanced stages and negative prognosis of gastric cancer. This result may also be of relevance for different sample sources or the heterogeneity of the tumor. In this study, we demonstrated the prognostic value of MSH2 in pan-cancer. Kaplan-Meier

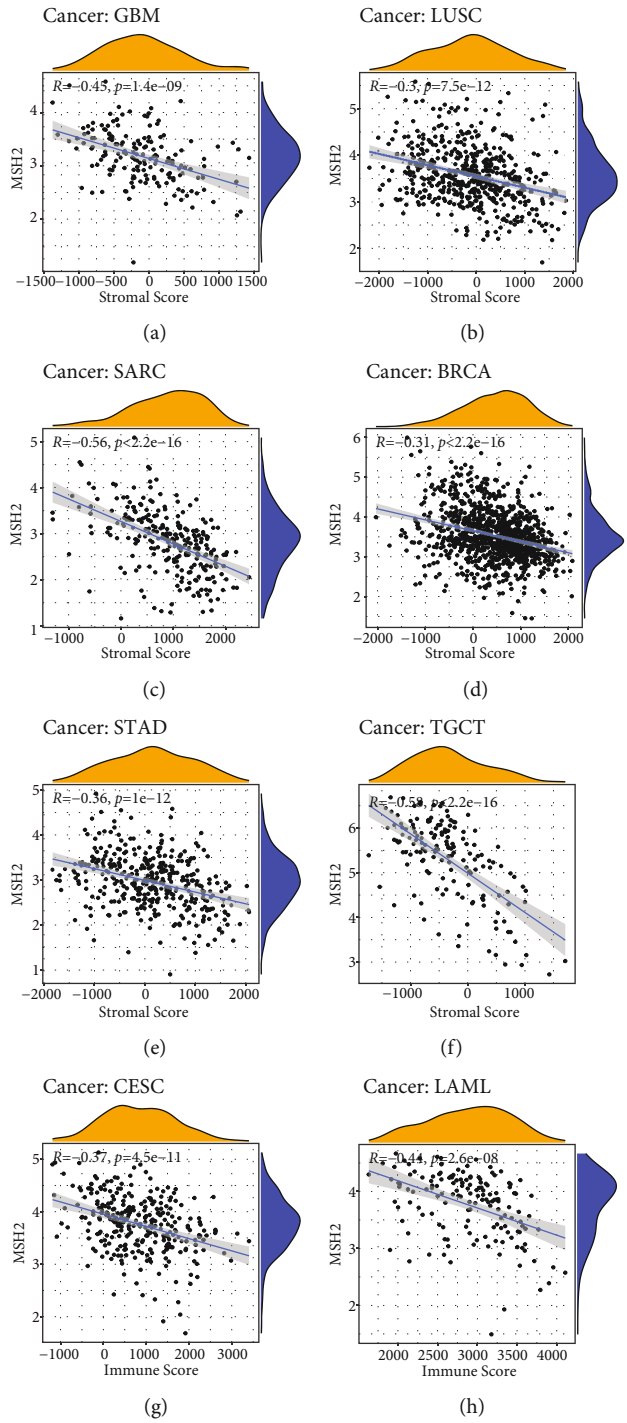

Figure 5: Continued.

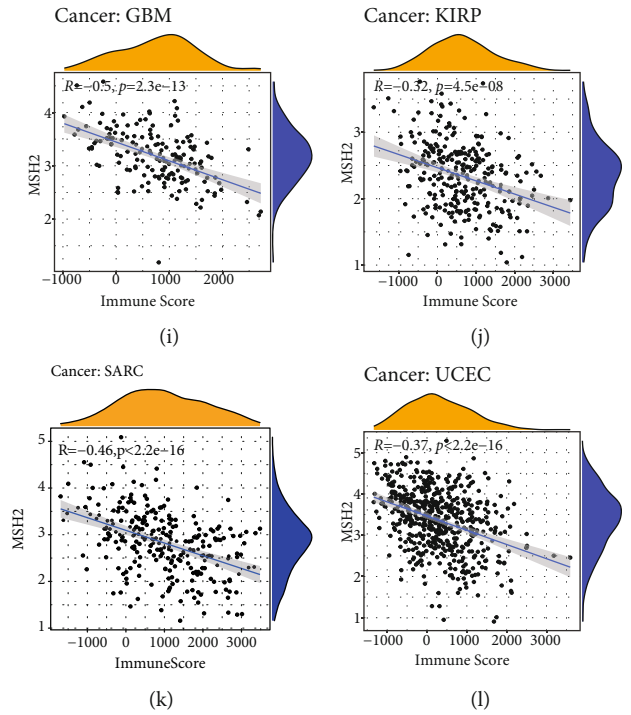

Figure 5: Correlation analysis of MSH2 expression and tumor microenvironment in pan-cancer. (a) Correlation between MSH2 expression and stromal score in GBM. (b) Correlation between MSH2 expression and stromal score in LUSC. (c) Correlation between MSH2 expression and stromal score in SARC. (d) Correlation between MSH2 expression and stromal score in BRCA. (e) Correlation between MSH2 expression and stromal score in STAD. (f) Correlation between MSH2 expression and stromal score in TGCT. (g) Correlation between MSH2 expression and immune score in CESC. (h) Correlation between MSH2 expression and immune score in LAML. (i) Correlation between MSH2 expression and immune score in GBM. (j) Correlation between MSH2 expression and immune score in KIRP. (k) Correlation between MSH2 expression and immune score in SARC. (l) Correlation between MSH2 expression and immune score in UCEC.

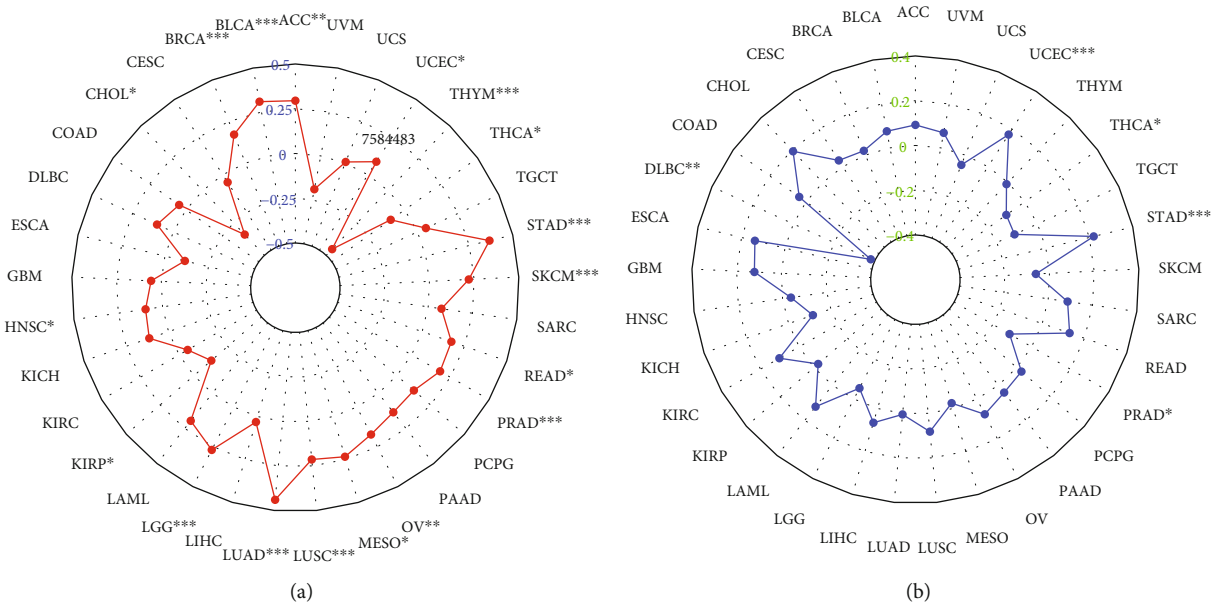

Figure 6: The correlation of MSH2 expression with TMB and MSI in pan-cancer. (a) Correlation between TMB and MSH2 expression. (b) Correlation between MSI and MSH2 expression.

analysis showed that high expression of MSH2 is associated with poorer OS in patients with ACC, LGG, LIHC, MESO, PAAD, SARC, and UCEC. In contrast, high expression of MSH2 was associated with a positive prognosis for patients with KIRC, STAD, and THYM. MLH1/MSH2 served as an independent prognostic and predictive factor for outcome of stage II/III sporadic colorectal cancer [29]. When receiving platinum-based chemotherapy, patients with low-expressing MSH2 bladder cancer had an inferior survival [30]. In short, these findings indicated that MSH2 can potentially work as a prognostic biomarker for pan-cancer.

Tumor cells, fibroblasts, immune cells, and the extracellular matrix are important components of the tumor microenvironment, which significantly affect the diagnosis and treatment of tumors. According to reports, tumor-infiltrating immune cells have an important impact on the occurrence and development of tumors which antagonizing or promoting the occurrence and development of tumors [31]. This study found that contrary to the negative correlation between the expression of MSH2 and CD8+T Cell in THCA, the expression of MSH2 was significantly positively correlated with the infiltration of six immune cells in COAD, KIRC, LIHC, and SKCM. MSH2 protein stimulated the proliferation of $\gamma\delta$ T cells in peripheral blood mononuclear cells. $\gamma\delta$ T cells were a small part of T lymphocytes and played an important role in tumor surveillance [32]. Existing evidence showed that MSH2 is overexpressed in pancreatic cancer cells and can be used as a CD4+ helper T cell antigens for the immunotherapy of patients with pancreatic cancer [33]. In LUAD, high expression of MSH2 was significantly correlated with CD8+ T cell infiltration [34]. In addition, the loss of MMR protein expression was related to the selective downregulation of human leukocyte antigen class I antigens, which contributes to the immune escape of endometrial carcinomas [35]. We also found that in GBM, LUSC, SARC, BRCA, STAD, and TGCT, MSH2 expression was significantly negatively correlated with stromal score; in CESC, LAML, GBM, KIRP, SARC, and UCEC, MSH2 expression and immune score were significantly negatively related. In short, these results indicate that the abnormal expression of MSH2 is closely related to the immune infiltration of tumor cells, which may change the immune microenvironment of tumor and patients outcome.

TMB is a promising biomarker for pan-cancer prediction, leading immunotherapy into the era of precision medicine [36]. In LUAD, the increase in MSH2 expression was significantly positively correlated with TMB [34]. Studies have shown that high nonsynonymous TMB was a good prognostic factor for patients with non-small-cell lung cancer [37]. TMB was associated with the survival rate of patients with various cancer types treated with immune checkpoint inhibitor (ICI) [38]. TMB and MSI are important biomarkers of ICI, and there is a certain correlation between the two. Studies have shown that high MSI and high TMB occur simultaneously in gastrointestinal cancers such as stomach adenocarcinoma, duodenum adenocarcinoma, and small intestine adenocarcinoma [39]. Our research showed that the expression level of MSH2 was significantly correlated with TMB in ACC, BLCA, BRCA, HNSC, LGG, LUAD, LUSC, MESO, OV, PRAD, READ, SKCM, STAD, UCEC, CHOL, KIRP, THCA, and THYM; the expression level of MSH2 was significantly correlated with STAD, UCEC, THCA, PRAD, and DLBC. This indicated that the expression level of MSH2 may affect the response of patients with immune checkpoint suppression therapy by affecting the TMB and MSI of cancer. However, further research need to determine whether MSH2 can be used as a predictor of the efficacy of immunotherapy in related cancer types. In conclusion, the results of this study provide clues to the link between MSH2 and cancer immunity.

5. Conclusion

This study revealed the role of abnormal expression of MSH2 in the occurrence and development of pan-cancer through comprehensive by bioinformatics methods and indicated that MSH2 expression may mediate immune infiltration and affect the prognosis of pan-cancer patients. MSH2 can emerge as a potential biomarker for cancer diagnosis and prognosis, providing a new direction for exploring the pathogenesis of pan-cancer. However, this study still has certain limitations. First of all, this research is relying on public databases and short of verification by experiments. Secondly, MSH2 is highly expressed in a variety of cancers and related to poor prognosis, but the specific mechanism of this effect still needs further investigation. The expression of MSH2 also has a certain correlation with tumor microenvironment, TMB, and MSI, however lack of data to verify its correlation. In the future, we will continue to explore the mechanism of action of MSH2 in different cancer types at the cellular or molecular level based on the results of this study.

Data Availability

The data used to support the findings of this study are available from the corresponding author upon request.

Conflicts of Interest

The authors declare that they have no conflicts of interest.

Authors' Contributions

Wenli Qiu and Ke Ding contributed equally to this work.

References

[1] F. Bray, J. Ferlay, I. Soerjomataram, R. L. Siegel, L. A. Torre, and A. Jemal, "Global cancer statistics 2018: GLOBOCAN estimates of incidence and mortality worldwide for 36 cancers in 185 countries," *CA: a Cancer Journal for Clinicians*, vol. 68, no. 6, pp. 394–424, 2018.

[2] J. Tang, L. Pearce, J. O'Donnell-Tormey, and V. M. Hubbard-Lucey, "Erratum: trends in the global immuno-oncology landscape," *Nature Reviews Drug Discovery*, vol. 17, no. 12, p. 922, 2018.

[3] J. Ferlay, M. Colombet, I. Soerjomataram et al., "Cancer incidence and mortality patterns in Europe: estimates for 40

countries and 25 major cancers in 2018," *European Journal of Cancer*, vol. 103, pp. 356–387, 2018.

[4] A. Blum, P. Wang, and J. C. Zenklusen, "SnapShot: TCGA-analyzed tumors," *Cell*, vol. 173, no. 2, p. 530, 2018.

[5] C. Xu, Y. Zang, Y. Zhao et al., "Comprehensive pan-cancer analysis confirmed that ATG5 promoted the maintenance of tumor metabolism and the occurrence of tumor immune escape," *Frontiers in Oncology*, vol. 11, pp. 652211–652211, 2021.

[6] R. Fishel, M. K. Lescoe, M. R. S. Rao et al., "The human mutator gene homolog _MSH2_ and its association with hereditary nonpolyposis colon cancer," *Cell*, vol. 75, no. 5, pp. 1027–1038, 1993.

[7] R. Fishel, A. Ewel, S. Lee, M. K. Lescoe, and J. Griffith, "Binding of mismatched microsatellite DNA sequences by the human MSH2 protein," *Science*, vol. 266, no. 5189, pp. 1403–1405, 1994.

[8] Q. Yang, R. Zhang, X. W. Wang et al., "The mismatch DNA repair heterodimer, hMSH2/6, regulates BLM helicase," *Oncogene*, vol. 23, no. 21, pp. 3749–3756, 2004.

[9] N. Pabla, Z. Ma, M. A. McIlhatton, R. Fishel, and Z. Dong, "hMSH2 Recruits ATR to DNA Damage Sites for Activation during DNA Damage- induced Apoptosis," *The Journal of Biological Chemistry*, vol. 286, no. 12, pp. 10411–10418, 2011.

[10] X. Zeng and T. J. Kinsella, "A novel role for DNA mismatch repair and the autophagic processing of chemotherapy drugs in human tumor cells," *Autophagy*, vol. 3, no. 4, pp. 368–370, 2007.

[11] A. Mendez-Bermudez and N. J. Royle, "Deficiency in DNA mismatch repair increases the rate of telomere shortening in normal human cells," *Human Mutation*, vol. 32, no. 8, pp. 939–946, 2011.

[12] V. Kotoula, P. Hytiroglou, V. Kaloutsi, S. Barbanis, S. Kouidou, and C. S. Papadimitriou, "Mismatch repair gene expression in malignant lymphoproliferative disorders of B-cell origin," *Leukemia & Lymphoma*, vol. 43, no. 2, pp. 393–399, 2002.

[13] P. Lastella, N. C. Surdo, N. Resta, G. Guanti, and A. Stella, "In silico and in vivo splicing analysis of MLH1 and MSH2 missense mutations shows exon- and tissue-specific effects," *BMC Genomics*, vol. 7, no. 1, 2006.

[14] J. F. Villemure, C. Abaji, I. Cousineau, and A. Belmaaza, "MSH2-deficient human cells exhibit a defect in the accurate termination of homology-directed repair of DNA double-strand breaks," *Cancer Research*, vol. 63, no. 12, pp. 3334–3339, 2003.

[15] X. Jia, B. B. Burugula, V. Chen et al., "Massively parallel functional testing of _MSH2_ missense variants conferring Lynch syndrome risk," *American Journal of Human Genetics*, vol. 108, no. 1, pp. 163–175, 2021.

[16] J. Li, Y. Li, H. Ni et al., "A novel splice-site mutation in MSH2 is associated with the development of lynch syndrome," *Frontiers in Oncology*, vol. 10, p. 983, 2020.

[17] A. G. Nikitin, D. A. Chudakova, R. F. Enikeev et al., "Lynch syndrome germline mutations in breast cancer: next generation sequencing case-control study of 1,263 participants," *Frontiers in Oncology*, vol. 10, 2020.

[18] A. Wang, Z. Li, M. Wang et al., "Molecular characteristics of synchronous multiple gastric cancer," *Theranostics*, vol. 10, no. 12, pp. 5489–5500, 2020.

[19] S. P. Donís, A. P. González, M. G. O. Alves et al., "MLH1, MSH2, MRE11, and XRCC1 in oral leukoplakia and oral squamous cell carcinoma," *Applied Immunohistochemistry & Molecular Morphology*, vol. 29, no. 8, pp. 613–618, 2021.

[20] L. B. Guedes, E. S. Antonarakis, M. T. Schweizer et al., "MSH2 loss in primary prostate cancer," *Clinical Cancer Research*, vol. 23, no. 22, pp. 6863–6874, 2017.

[21] S. S. Malik, N. Masood, M. Asif, P. Ahmed, Z. U. Shah, and J. S. Khan, "Expressional analysis of MLH1 and MSH2 in breast cancer," *Current Problems in Cancer*, vol. 43, no. 2, pp. 97–105, 2019.

[22] S. M. Mirkin, "Expandable DNA repeats and human disease," *Nature*, vol. 447, no. 7147, pp. 932–940, 2007.

[23] C. D. Heinen, "Translating mismatch repair mechanism into cancer care," *Current Drug Targets*, vol. 15, no. 1, pp. 53–64, 2014.

[24] P. Pitsikas, D. Lee, and A. J. Rainbow, "Reduced host cell reactivation of oxidative DNA damage in human cells deficient in the mismatch repair gene hMSH2," *Mutagenesis*, vol. 22, no. 3, pp. 235–243, 2007.

[25] S. S. Malik, S. Mubarik, A. Aftab et al., "Correlation of MSH2 exonic deletions and protein downregulation with breast cancer biomarkers and outcome in Pakistani women/patients," *Environmental Science and Pollution Research International*, vol. 28, no. 3, pp. 3066–3077, 2021.

[26] Q. X. Zhang, Y. Ding, X. P. Le, and P. Du, "Studies on microsatellite instability in p16 gene and expression of hMSH2 mRNA in human gastric cancer tissues," *World Journal of Gastroenterology*, vol. 9, no. 3, pp. 437–441, 2003.

[27] F. S. Leach, J. T. Hsieh, K. Molberg, M. H. Saboorian, J. D. McConnell, and A. I. Sagalowsky, "Expression of the human mismatch repair gene hMSH2," *Cancer*, vol. 88, no. 10, pp. 2333–2341, 2000.

[28] R. Liccardo, A. Nolano, M. Lambiase et al., "MSH2 overexpression due to an unclassified variant in 3'-untranslated region in a patient with colon cancer," *Biomedicine*, vol. 8, no. 6, p. 167, 2020.

[29] S. M. Wang, B. Jiang, Y. Deng, S. L. Huang, M. Z. Fang, and Y. Wang, "Clinical significance ofMLH1/MSH2for stage II/III sporadic colorectal cancer," *World journal of gastrointestinal oncology*, vol. 11, no. 11, pp. 1065–1080, 2019.

[30] A. Goodspeed, A. Jean, and J. C. Costello, "A whole-genome CRISPR screen identifies a role of MSH2 in cisplatin-mediated cell death in muscle-invasive bladder cancer," *European Urology*, vol. 75, no. 2, pp. 242–250, 2019.

[31] X. Lei, Y. Lei, J. K. Li et al., "Immune cells within the tumor microenvironment: biological functions and roles in cancer immunotherapy," *Cancer Letters*, vol. 470, pp. 126–133, 2020.

[32] H. Chen, X. Ji, L. Cui, J. Zhang, and W. He, "Characterization of complementary determinant region 3δ in human MutS homologue 2-specific $\gamma\delta$ T cells," *Scandinavian Journal of Immunology*, vol. 81, no. 2, pp. 121–128, 2015.

[33] T. Okada, S. Noji, Y. Goto et al., "Immune responses to DNA mismatch repair enzymes hMSH2 and hPMS1 in patients with pancreatic cancer, dermatomyositis and polymyositis," *International Journal of Cancer*, vol. 116, no. 6, pp. 925–933, 2005.

[34] M. Jia, L. Yao, Q. Yang, and T. Chi, "Association of MSH2 expression with tumor mutational burden and the immune microenvironment in lung adenocarcinoma," *Frontiers in Oncology*, vol. 10, pp. 168–168, 2020.

[35] R. A. de Jong, A. Boerma, H. M. Boezen, M. J. Mourits, H. Hollema, and H. W. Nijman, "Loss of HLA class I and mismatch repair protein expression in sporadic endometrioid

endometrial carcinomas," *International Journal of Cancer*, vol. 131, no. 8, pp. 1828–1836, 2012.

[36] J. D. Fumet, C. Truntzer, M. Yarchoan, and F. Ghiringhelli, "Tumour mutational burden as a biomarker for immunotherapy: current data and emerging concepts," *European Journal of Cancer*, vol. 131, pp. 40–50, 2020.

[37] S. Devarakonda, F. Rotolo, M. S. Tsao et al., "Tumor mutation burden as a biomarker in resected non-small-cell lung cancer," *Journal of Clinical Oncology*, vol. 36, no. 30, pp. 2995–3006, 2018.

[38] R. M. Samstein, C. H. Lee, A. N. Shoushtari et al., "Tumor mutational load predicts survival after immunotherapy across multiple cancer types," *Nature Genetics*, vol. 51, no. 2, pp. 202–206, 2019.

[39] Z. R. Chalmers, C. F. Connelly, D. Fabrizio et al., "Analysis of 100,000 human cancer genomes reveals the landscape of tumor mutational burden," *Genome Medicine*, vol. 9, no. 1, 2017.

Hindawi
BioMed Research International
Volume 2024, Article ID 9821414, 1 page
https://doi.org/10.1155/2024/9821414

Retraction

Retracted: Long-Term Carbohydrate-Containing Late-Evening Snack Significantly Improves the Ratio of Branched Chain Amino Acids to Aromatic Amino Acids in Adults with Liver Cirrhosis due to Hepatitis B

BioMed Research International

Received 12 March 2024; Accepted 12 March 2024; Published 20 March 2024

This article has been retracted by Hindawi following an investigation undertaken by the publisher [1]. This investigation has uncovered evidence of one or more of the following indicators of systematic manipulation of the publication process:

(1) Discrepancies in scope

(2) Discrepancies in the description of the research reported

(3) Discrepancies between the availability of data and the research described

(4) Inappropriate citations

(5) Incoherent, meaningless and/or irrelevant content included in the article

(6) Manipulated or compromised peer review

The presence of these indicators undermines our confidence in the integrity of the article's content and we cannot, therefore, vouch for its reliability. Please note that this notice is intended solely to alert readers that the content of this article is unreliable. We have not investigated whether authors were aware of or involved in the systematic manipulation of the publication process.

Wiley and Hindawi regrets that the usual quality checks did not identify these issues before publication and have since put additional measures in place to safeguard research integrity.

We wish to credit our own Research Integrity and Research Publishing teams and anonymous and named external researchers and research integrity experts for contributing to this investigation.

The corresponding author, as the representative of all authors, has been given the opportunity to register their agreement or disagreement to this retraction. We have kept a record of any response received.

References

[1] W. Hou, Z. Lv, J. Yang, J. Wu, Z.-y. Wang, and Q.-h. Meng, "Long-Term Carbohydrate-Containing Late-Evening Snack Significantly Improves the Ratio of Branched Chain Amino Acids to Aromatic Amino Acids in Adults with Liver Cirrhosis due to Hepatitis B," *BioMed Research International*, vol. 2021, Article ID 1074565, 11 pages, 2021.

Hindawi
BioMed Research International
Volume 2021, Article ID 1074565, 11 pages
https://doi.org/10.1155/2021/1074565

Research Article

Long-Term Carbohydrate-Containing Late-Evening Snack Significantly Improves the Ratio of Branched Chain Amino Acids to Aromatic Amino Acids in Adults with Liver Cirrhosis due to Hepatitis B

Wei Hou, Zheng Lv, Jing Yang, Jing Wu, Zhong-ying Wang, and Qing-hua Meng

Department of Critical Care Medicine of Liver Disease, Beijing Youan Hospital, Capital Medical University, Beijing 100069, China

Correspondence should be addressed to Qing-hua Meng; huazailiao539177@163.com

Received 23 July 2021; Revised 5 October 2021; Accepted 7 October 2021; Published 22 November 2021

Academic Editor: Jianxin Shi

Background. The liver is the primary organ for amino acid metabolism, and metabolic disorder of amino acids is common in liver disease. However, the characteristics of plasma amino acid profiles in patients with HBV-related cirrhosis and the impacts of late-evening snack (LES) on cirrhosis are unclear. *Objectives*. To investigate the characteristics of plasma amino acid profiles in patients with HBV-related chronic hepatitis, cirrhosis, and the effects of late-evening snacks on plasma amino acid profiles. *Methods*. 86 patients with HBV-related cirrhosis and eighty patients with chronic hepatitis B were included in this study. The plasma amino acid profiles were measured by the amino acid analyzer. Patients were randomly divided into two groups, of which the liver cirrhosis group was to receive daily LES ($n = 43$) or non-LES ($n = 43$) for 6 months. Plasma amino acid profiles and biochemical parameters were measured in both groups at baseline and after 1, 3, and 6 months. *Results*. Compared to healthy controls, the plasma concentration in the liver cirrhosis group of threonine, serine, glycine, glutamine, cysteine, tyrosine, phenylalanine, arginine, and methionine increased significantly ($P < 0.05$), while the ratio of branched chain amino acids (BCAA) to aromatic amino acids (AAA) decreased significantly ($P < 0.05$). A carbohydrate-predominant LES treatment resulted in a significant increase in BCAA/AAA and decrease in the level of ammonia and glutamine compared with baseline after 6 months of supplementation ($P < 0.05$). Patients with Child-Pugh B and C are more responsive to changes in amino acid profiles than those with Child-Pugh A. *Conclusions*. The application of an LES carbohydrate module for six months in liver cirrhosis patients was associated with increased BCAA/AAA and decreased level of ammonia. Patients with Child-Pugh B and C grades were the most beneficial population.

1. Introduction

Liver cirrhosis is the result of chronic liver injury caused by various etiologies. According to the World Health Organization in July 2015, more than 240 million people worldwide are chronically infected with hepatitis B, amid which 20%-30% develop cirrhosis or liver cancer, and more than 780,000 annual deaths due to hepatitis B-related cirrhosis and liver cancer [1]. Protein-energy malnutrition is one of the most common comorbidities related to cirrhosis in adults, which is characterized by increased fat and protein oxidation and decreased carbohydrate utilization in the fasted state [2–4]. Protein wasting is the most typical feature of the alterations in nutrient utilization, which is manifested with muscle mass loss, hypoalbuminemia, and abnormal amino acid profile [5–8].

The normal metabolism of amino acids is an important basis for life activities, and it plays an indispensable role in various fundamental biological processes. The changes of plasma amino acid profiles were also associated with the severity of liver injury. The use of BCAA as a nutritional supplementation may contribute to the positive effects of LES on survival in patients with cirrhosis. We, therefore, compared the survival rates between patients treated with LES and those given daytime BCAA supplementation and found that LES supplementation, compared to daytime

supplementation, clearly improves prognosis in patients with cirrhosis. The characteristics were that aromatic amino acids (AAA; phenylalanine, tyrosine, and tryptophan) increased, branched chain amino acids (BCAA; valine, leucine, and isoleucine) decreased, and the ratio of BCAA to AAA decreased [9]. Apart from perturbations in BCAA and AAA levels, changes in plasma concentrations of other amino acids were also observed in previous studies.

Current guidelines from both the American Society for Parenteral and Enteral Nutrition [10] and the European Society for Clinical Nutrition and Metabolism recommend nutritional support through night time for energy requirement and thus further preventing the increased utilization of lean body stores because of overnight fasting in cirrhotic patients. Late-evening snacks (LES) containing multiple nutrients, usually rich in BCAA and/or carbohydrates, are reported to be beneficial not only in reducing the oxidation of fat and nitrogen for energy supplementation in the fasted state but also in maintaining overall nitrogen balance and improving these patients' quality of life [11–13]. An LES has been shown to improve the nutritional status, liver function reserves, and sarcopenia in patients with cirrhosis, each of which raises the potential to improve the survival of these patients; however, little is known about the survival benefit of LES thus far. To date, few studies have investigated the impact of an LES on amino acid profiles especially the ratio of BCAA to AAA in HBV-related cirrhotic patients. The goal of the current study is to investigate the effect of a carbohydrate-containing late-evening snack on plasma amino acid profiles in adults with hepatitis B-related cirrhosis.

2. Subjects and Methods

2.1. Subjects. 86 inpatients (68 males and 18 females, mean age: 51.47 ± 11.78 years) with HBV-related cirrhosis and eighty inpatients (42 males and 38 females, mean age: 38.33 ± 10.16 years) with chronic hepatitis B were included in the study (2017 March–2019 March). A total of 30 healthy controls were obtained from the staff of the Department, during the same period. The diagnosis is hepatitis B viral infection according to serology results (COBAS AmpliPrep/COBAS TaqMan HBV test, Roche Molecular Systems Inc, Branchburg, NJ, USA). HBV-related chronic hepatitis and cirrhosis definitions referred to the guidelines of prevention and treatment for chronic hepatitis B (2015). Inclusion criteria include all HBV-related cirrhosis and chronic hepatitis B patients hospitalized in our department, aged between 18 and 65 years. Patients were excluded from the study if they had a known history of hepatitis C virus infection, alcoholic liver disease, severe infection, malignant tumor such as liver cancer, active gastrointestinal bleeding within 2 weeks, intravenous or oral amino acid or protein preparations within 2 weeks, diabetes mellitus, and thyroid dysfunction or were infected with human immunodeficiency virus. The study complies with the ethical guidelines of the 1975 Declaration of Helsinki and was approved by the Human Research Committee of Capital Medical University. All participants signed written informed consent prior to study enrollment.

2.2. Study Design. Eighty-six consecutive patients with HBV-related cirrhosis were classified into three groups based on the Child-Pugh grades; 28 patients were considered Child's grade A, 28 patients were grade B, and 30 patients were grade C. Eighty consecutive patients with chronic hepatitis B were selected as the chronic hepatitis B group. Thirty subjects were recruited as the healthy control. The blood samples were collected to analyze the laboratory values (hematologic, biochemical) and the amino acid profiles by the automatic amino acid analyzer (membraPure GmbH, Berlin, GER) on the first morning after admission.

According to random numbers generated in advance, all the 86 cirrhotic patients were randomly divided into two groups, the study group (with LES supplementation; $n = 43$) and the control group ($n = 43$). The patients with the study group received the nutritional intervention of 200 kcal late-evening snacks for six months; the patients in the control group were not supplemented with the LES. The blood samples were collected to examine the laboratory values (hematologic, biochemical) and the amino acid profiles before and 1, 3, and 6 months after LES intervention, respectively. All patients received standard antiviral treatment (entecavir 0.5 mg/day; Squibb Pharmaceuticals Ltd., Shanghai, China). All patients' dietary intake was required to be recorded weekly. And energy and nutrient intake were evaluated through referring to the collected food intake records. To minimize the difference in energy and macronutrient intake between both groups, two full-time staffs were responsible for the follow-up of both groups and provided weekly telephone diet guidance. Seven patients were lost to follow-up, with four in the study group and three in the control group. No adverse reactions were observed in either group.

2.3. Testing of Plasma Amino Acid Profiles. Venous blood was drawn from each patient after overnight fasting. Plasma was centrifuged at a speed of 2000 r/min at normal atmospheric temperature for 5 min. Plasma was separated and stored in a refrigerator at -80°C for reserve. Amino acid analysis was performed at the Beijing Institute of Hepatology using the A300 Amino Acid Analyzer (membraPure GmbH, Berlin, GER). Twenty amino acid concentrations in total were measured. These include essential amino acids (histidine, isoleucine, leucine, lysine, methionine, phenylalanine, threonine, and valine) that cannot be synthesized by humans, nonessential amino acids (glutamic acid, alanine, glycine, aspartate, cystine, proline, serine, and tyrosine), branched chain amino acids (leucine, isoleucine, and valine) which are critical to muscle metabolism, aromatic amino acids (tyrosine, phenylalanine, and tryptophan), and sulfur amino acids (cysteine and methionine) which are critical for redox metabolism, among other functions.

2.4. LES Snack. Patients in the study group were given an LES in the form of lotus-root starch, which is a traditional snack in China. Traditionally, lotus-root starch is usually used as a thickening agent in sauces in mixed food dishes and/or served as a constituent in pudding making. The nutritional composition of the LES includes 200 kcal energy

Table 1: Basic characteristics of patients with cirrhosis and chronic hepatitis B ($\bar{X} \pm$ s.d.).

	Cirrhosis group	Chronic hepatitis B group	Healthy control group	F	P
N	86	80	30		—
Age	51.5 ± 11.5	39.9 ± 6.6*	47.7 ± 8.2	13.81	<0.001
Gender (M/F)	68/18	10/8	7/3	—	0.108
WBC ($\times 10^9$/L)	5.1 ± 1.7	7.5 ± 1.7*	7.6 ± 1.7*	21.38	<0.001
HB (g/L)	107.1 ± 22.6	120.8 ± 10.3*	127.9 ± 4.3*	34.44	<0.001
PLT ($\times 10^9$/L)	65.7 ± 21.0	173.5 ± 39.3*	253.2 ± 48.2*	284.22	<0.001
ALT (U/L)	45.6 ± 19.3	39.2 ± 8.7	35.6 ± 7.2	2.20	0.116
AST (U/L)	74.8 ± 30.0	26.6 ± 8.0*	26.3 ± 6.1*	35.35	<0.001
TBIL (μmol/L)	48.0 ± 23.4	16.3 ± 4.2*	14.8 ± 3.3*	26.01	<0.001
ALB (g/L)	28.6 ± 4.4	41.4 ± 3.3*	41.7 ± 3.0*	100.86	<0.001
PALB (mg/L)	95.4 ± 27.0	199.8 ± 23.2*	181.9 ± 22.1*	150.11	<0.001
CHE (U/L)	3925.7 ± 1241.2	8113.6 ± 656.8*	9938.1 ± 1531.5*	179.72	<0.001
CR (μmol/L)	61.3 ± 16.7	56.5 ± 11.5	49.5 ± 10.0*	2.97	0.056
CHOL (mmol/L)	4.3 ± 0.8	4.1 ± 0.5	4.6 ± 0.9	1.04	0.356
TG (mmol/L)	1.4 ± 0.7	1.2 ± 0.4	1.1 ± 0.4	2.55	0.083
PT (s)	16.7 ± 2.3	13.5 ± 1.0*	13.3 ± 0.8*	25.52	<0.001
INR	1.3 ± 0.2	1.2 ± 0.1*	1.1 ± 0.1*	10.10	<0.001
NH_3 (μmol/L)	79.6 ± 27.5	44.3 ± 17.1*	27.2 ± 11.6*	52.38	<0.001
GLU (mmol/L)	5.1 ± 2.3	6.2 ± 2.3	5.9 ± 2.6	1.175	0.279

Abbreviations: WBC: white blood cell count; HB: hemoglobin; PLT: platelet count; ALT: alanine aminotransferase; AST: aspartate transferase; TBIL: total bilirubin; ALB: albumin; PALB: prealbumin; CHE: cholinesterase; CR: creatinine; CHOL: total cholesterol; TG: triglyceride; PT: prothrombin time; INR: international normalized ratio; NH_3: ammonemia; GLU: blood glucose; BCAA: branched chain amino acids; AAA: aromatic amino acids. *$P < 0.01$ compared with the cirrhosis group.

in total, 50 g of carbohydrate, 0.1 g protein, and 0.05 g fiber with a GI of 30 [14, 15].

2.5. Laboratory Parameters. Biochemical parameters including cholesterol, triglyceride, aspartate aminotransferase, alanine aminotransferase, prealbumin, albumin, creatinine, total bilirubin, and cholinesterase were measured using a chemistry analyzer (Olympus 5421, Olympus, Tokyo, Japan). The automatic coagulation analyzer (TOP700, ACL, American) was applied to analyze prothrombin time (PT) and international normalized ratio (INR). The automated hematology analyzer (XE-5000 analyzer, Hissen Meikang, Kōbe, Japan) was used to evaluate levels of white blood cells, hemoglobin, and platelets.

2.6. Statistical Analysis. SPSS 19.0 statistical software (SPSS Inc., Chicago, IL, USA) was used for data analysis. All data were analyzed for normality and were described as the mean ± s.d. Baseline characteristics between groups were compared using one-way ANOVA, independent group t-test, and χ^2 test. The effects of LES were evaluated by repeated measures analysis of variance. $P < 0.05$ was considered statistically significant.

3. Results

3.1. Basic Characteristics of Research Objects. Demographic characteristics (age and gender) and laboratory values (hematologic, biochemical) were compared between the cirrhosis group, the chronic hepatitis B group, and the healthy control group. The mean age of patients in the chronic hepatitis B group was significantly lower than the mean age of patients in the other two groups ($P < 0.01$, respectively). The difference in gender was not statistically significant. The level of white blood cells, hemoglobin, platelets, albumin, prealbumin, and cholinesterase in patients with cirrhosis was significantly lower than those in patients with chronic hepatitis B and healthy controls ($P < 0.01$, respectively), and the level of aspartate transferase, total bilirubin, prothrombin time, and INR was significantly higher than those in the chronic hepatitis B group and the healthy control group ($P < 0.01$, respectively). These three groups demonstrated no significant difference in alanine aminotransferase, creatinine, and triglyceride (Table 1).

3.2. Characteristics of Plasma Amino Acid Profiles in Patients with Chronic Hepatitis and Cirrhosis. Compared with the healthy control group, the concentrations of taurine, aspartic acid, threonine, serine, glycine, glutamine, cysteine, tyrosine, phenylalanine, arginine, and methionine in the cirrhosis group were significantly increased, while the concentrations of glutamic acid, valine, leucine, and the BCAA/AAA ratio were significantly decreased; the concentration of aspartic acid, threonine, serine, valine, and phenylalanine in the chronic hepatitis B group increased, the concentrations of

Table 2: Comparison of plasma amino acid profiles between cirrhosis group, chronic hepatitis B group, and healthy control group ($\bar{X} \pm$ s.d.).

Amino acid (μmol/L)	Cirrhosis group $n = 86$	Chronic hepatitis B group $n = 80$	Healthy control group $n = 30$	F	P
TAU	428.4 ± 283.3	388.0 ± 37.7	197.5 ± 48.9*	3.89	0.023
ASP	16.7 ± 11.4	28.5 ± 16.4**	12.9 ± 8.7**	10.00	<0.001
THR	165.6 ± 66.9	178.0 ± 40.4	117.6 ± 19.1**	3.40	0.037
SER	161.8 ± 6.96	152.3 ± 66.5	95.8 ± 25.7**	4.40	0.014
GLU	38.2 ± 12.8	50.9 ± 13.7**	50.3 ± 15.7**	9.44	<0.001
GLY	279.4 ± 105.0	246.5 ± 170.0	184.3 ± 67.2*	3.34	0.038
ALA	401.4 ± 156.7	397.1 ± 175.1	441.7 ± 189.2	0.296	0.744
GLN	847.1 ± 78.8	733.3 ± 101.7	683.5 ± 98.2*	2.49	0.046
CYS	106.2 ± 21.8	58.1 ± 11.3*	63.7 ± 10.1*	57.64	<0.001
VAL	204.1 ± 94.2	285.0 ± 84.0**	213.3 ± 61.6	5.97	0.003
ILE	92.9 ± 31.2	102.7 ± 31.7	101.6 ± 31.0	0.93	0.396
LEU	135.1 ± 32.9	157.5 ± 37.8**	184.0 ± 18.5*	18.74	<0.001
TYR	142.4 ± 37.1	82.5 ± 22.6**	58.0 ± 22.4**	44.21	<0.001
PHE	88.3 ± 18.2	62.7 ± 11.1**	45.2 ± 11.9**	42.26	<0.001
HIS	72.6 ± 15.8	72.1 ± 16.3	68.0 ± 13.5	0.37	0.688
TRP	52.4 ± 19.6	44.7 ± 9.3	42.8 ± 6.7	2.40	0.096
ORN	435.8 ± 83.3	439.8 ± 104.4	477.4 ± 96.3	1.00	0.371
LYS	215.1 ± 55.1	204.3 ± 45.3	180.8 ± 35.8	2.06	0.132
ARG	88.1 ± 23.2	76.5 ± 15.5*	72.2 ± 16.5*	4.05	0.020
PRO	189.5 ± 42.6	186.6 ± 41.1	194.3 ± 34.7	0.11	0.897
MET	27.3 ± 5.4	18.9 ± 4.7**	21.5 ± 5.1**	7.25	0.007
BCAA/AAA	1.59 ± 0.52	2.98 ± 0.62*	3.41 ± 0.68*	83.91	<0.001

Abbreviations: TAU: taurine; ASP: aspartic acid; THR: threonine; SER: serine; GLU: glutamic acid; GLY: glycine; ALA: alanine; GLN: glutamine; CYS: cysteine; VAL: valine; LEU: leucine; ILE: isoleucinetyrosine; TYR: tyrosine; PHE: phenylalanine; HIS: histidine; TRP: tryptophan; ORN: ornithine; LYS: lysine; ARG: arginine; PRO: proline; MET: methionine. *$P < 0.05$ compared with cirrhosis group; **$P < 0.01$ compared with cirrhosis group.

leucine decreased, and the difference was statistically significant. No significant differences were found with respect to the concentration of other amino acids between the healthy control group and the cirrhosis group and the chronic hepatitis B group. Compared with the chronic hepatitis B group, the concentration of aspartic acid, glutamic acid, valine, and leucine and the ratio of BCAA to AAA in the cirrhosis group were significantly decreased, while the concentration of cysteine, tyrosine, phenylalanine, arginine, and methionine was increased, and the differences were statistically significant. No significant difference was detected in the concentration of other amino acids between the chronic hepatitis B group and the cirrhosis group (Table 2).

3.3. Characteristics of Plasma Amino Acid Profiles in Cirrhosis Patients with Hyperammonemia and Normal Ammonemia. According to the level of ammonia, sixty-four patients with Child-Pugh class B and C cirrhosis were divided into two groups: hyperammonemia group and normal ammonemia group. Compared with the normal ammonemia group, the concentrations of taurine, glycine, glutamine, tyrosine, tryptophan, and arginine in the hyperammonemia group were increased, while the concentrations of aspartic acid, leucine, and isoleucinetyrosine and the ratio of BCAA to AAA were decreased, and the difference was statistically significant (Table 3).

3.4. Effect of Late-Evening Snacks on Biochemical Parameters and Plasma Amino Acid Profiles in Patients with Liver Cirrhosis

3.4.1. Basic Characteristics and Macronutrient Intake of the Study and Control Groups. The basic characteristics of the two groups are shown in Table 4. No significant difference was found in age, gender, anthropometry data, and laboratory values between the study and control groups ($P > 0.05$). Macronutrient intake of the two groups at baseline and 3rd month and 6th month is shown in Table 4. These two groups demonstrated no significant difference in macronutrient intake.

3.4.2. Laboratory Values. Changes of laboratory values in patients with cirrhosis before and after late-evening snacks are shown in Table 5. No significant differences in laboratory values at baseline were observed between the study group

Table 3: Comparison of plasma amino acid profiles in cirrhosis patients with hyperammonemia and normal ammonemia ($\bar{X} \pm$ s.d.).

Amino acid (μmol/L)	Patients with normal ammonemia $n = 28$	Patients with hyperammonemia $n = 36$	t	P
TAU	317.9 ± 181.3	706.5 ± 242.5	47.63	<0.001
ASP	22.6 ± 13.3	8.4 ± 3.5	18.01	<0.001
THR	167.5 ± 102.5	154.0 ± 39.1	0.81	0.449
SER	158.2 ± 90.1	141.3 ± 65.2	3.39	0.038
GLU	39.1 ± 11.0	38.3 ± 13.0	0.15	0.864
GLY	233.5 ± 77.9	300.0 ± 140.0	4.28	0.017
ALA	373.9 ± 103.8	384.0 ± 166.2	1.89	0.158
GLN	701.3 ± 88.6	889.3 ± 75.9	3.18	0.047
CYS	101.2 ± 26.4	110.4 ± 17.6	1.31	0.277
VAL	221.4 ± 100.6	190.9 ± 90.6	0.78	0.462
ILE	105.5 ± 40.0	85.8 ± 25.0	3.55	0.033
LEU	149.2 ± 29.9	122.8 ± 29.1	5.16	0.008
TYR	130.9 ± 31.4	158.3 ± 33.1	4.77	0.011
PHE	83.6 ± 17.6	92.7 ± 17.4	1.92	0.154
HIS	70.1 ± 15.8	74.4 ± 16.2	0.54	0.586
TRP	40.6 ± 10.5	61.8 ± 19.7	10.68	<0.001
ORN	418.8 ± 85.4	443.2 ± 89.6	0.86	0.425
LYS	217.1 ± 40.4	204.7 ± 54.4	0.94	0.396
ARG	79.0 ± 19.9	93.6 ± 21.4	3.51	0.034
PRO	196.0 ± 46.5	186.7 ± 41.6	0.47	0.625
MET	25.8 ± 6.2	30.9 ± 4.6	2.58	0.059
BCAA/AAA	1.94 ± 0.58	1.31 ± 0.34	14.33	<0.001

Abbreviations: TAU: taurine; ASP: aspartic acid; THR: threonine; SER: serine; GLU: glutamic acid; GLY: glycine; ALA: alanine; GLN: glutamine; CYS: cysteine; VAL: valine; LEU: leucine; ILE: isoleucinetyrosine; TYR: tyrosine; PHE: phenylalanine; HIS: histidine; TRP: tryptophan; ORN: ornithine; LYS: lysine; ARG: arginine; PRO: proline; MET: methionine; BCAA: branched chain amino acids; AAA: aromatic amino acids.

and the control group ($P < 0.05$). Compared with baseline, the levels of ALB and PALB in the study group were significantly increased, while the level of NH_3 was significantly decreased both at the 3rd month and the 6th month ($P < 0.05$).

The potential impact of LES supplementation on ALB, PALB, and NH_3 was explored through dividing the treatment group (+LES) into three groups based on the Child-Pugh grade with the Child-Pugh A group ($n = 11$), the Child-Pugh B group ($n = 12$), and the Child-Pugh C group ($n = 20$). In spite of the obvious difference in the levels of ALB, PALB, and NH_3 in the Child-Pugh A group after 6 months of LES supplementation, LES treatment contributed to a significant increase in levels of ALB and PALB and a significant decrease in NH_3 in patients with Child-Pugh B and C at the 6th month (Table 6).

3.4.3. Plasma Amino Acid Profiles. No significant differences in plasma amino acid concentration at baseline were noted between the study and control groups ($P < 0.05$). Compared with baseline, the concentration of leucine and isoleucine and the ratio of BCAA to AAA in the study group increased gradually at the 1st month, 3rd month, and 6th month, and significant statistical differences were observed at the 6th month ($P < 0.05$). In the meantime, the concentration of threonine and tryptophan in the study group decreased gradually, the lowest concentration of which was observed at the 6th month ($P < 0.05$). Meanwhile, there are no significant differences in plasma amino acid concentration at the 6th month compared with baseline in the control group ($P < 0.05$). However, comparing with the control group, a significant increase in VAL ($P < 0.05$) and BCAA/AAA ratio ($P < 0.01$) and an obvious decrease in MET ($P < 0.01$) were observed in patients in the study group after 6 months of LES supplementation (Table 7).

Compared with baseline, LES treatment at the 6th month resulted in a significantly higher increase in the ratio of BCAA/AAA in patients with Child-Pugh B (1.86 vs. 2.38; $P = 0.027$) and C (1.72 vs. 2.18; $P = 0.046$), while the impact of LES supplementation was not obvious in the Child-Pugh A group (2.03 vs. 2.39; $P = 0.268$) (Figure 1).

4. Discussion

Our discovery showed that there was a significant amino acid imbalance in patients with chronic hepatitis, especially

Table 4: Basic characteristics of study and control group ($\bar{X} \pm$ s.d.).

	Study group	Control group	t	P
N	43	43	—	—
Age	51.0 ± 10.3	50.2 ± 11.7	0.251	0.803
Gender (M/F)	19/7	22/4	—	0.202
Height (cm)	171.5 ± 8.1	170.8 ± 7.2	0.496	0.627
Weight (kg)	69.8 ± 12.5	68.2 ± 13.7	0.112	0.955
BMI	23.8 ± 3.8	23.3 ± 4.0	0.173	0.867
Macronutrient intake at baseline				
Carbohydrate (g/day)	247.6 ± 42.4	246.3 ± 46.9	0.974	0.381
Fat (g/day)	41.4 ± 14.2	42.7 ± 14.7	0.136	0.883
Protein (g/day)	68.9 ± 12.9	69.3 ± 13.1	0.132	0.886
Energy (kcal/day)	1652.1 ± 251.7	1649.0 ± 267.5	0.175	0.862
Macronutrient intake after 3 months				
Carbohydrate (g/day)	250.6 ± 49.0	248.1 ± 48.2	0.978	0.379
Fat (g/day)	40.3 ± 13.8	41.5 ± 14.0	0.140	0.879
Protein (g/day)	70.1 ± 9.5	69.6 ± 12.5	0.136	0.884
Energy (kcal/day)	1644.6 ± 257.7	1643.2 ± 252.9	0.181	0.858
Macronutrient intake after 6 months				
Carbohydrate (g/day)	251.0 ± 42.7	250.3 ± 47.1	0.977	0.380
Fat (g/day)	42.1 ± 12.9	40.2 ± 13.6	0.151	0.876
Protein (g/day)	69.4 ± 13.2	71.2 ± 14.7	0.147	0.877
Energy (kcal/day)	1655.5 ± 248.8	1653.8 ± 258.1	0.164	0.869

in patients with cirrhosis, which was manifested by the decreased level of branched chain amino acid, the increased level of aromatic amino acid level, and the decrease of BCAA to AAA ratio. Daily consumption of carbohydrate-predominant late-evening snacks for 6 months significantly increased the ratio of BCAA to AAA and improved the imbalance of amino acids in patients with hepatitis B-related cirrhosis, especially for those with Child-Pugh B and C stages.

In this study, we compared the concentrations of plasma amino acid in patients with cirrhosis and chronic hepatitis B and healthy subjects. The plasma levels of branched chain amino acids (leucine, valine, and isoleucine) in patients with cirrhosis and chronic hepatitis B were significantly lower than those in the healthy control group, while the level of glutamine was significantly higher in patients with cirrhosis and chronic hepatitis B. Recently, increasing studies have shown that hyperammonemia and hyperglutaminemia could exert an effect on the reduction of branched chain amino acids. Current studies suggest that intestinal bacteria are not the major source of ammonia in cirrhosis patients, but intestinal catabolism of glutamine in blood [16, 17]. It has been proved that the close relationship between glutamine and ammonia metabolism plays a central role in the pathogenesis of hyperammonemia, hyperglutaminemia, and BCAA reduction in patients with liver cirrhosis [18]. Our study also confirmed that patients with hyperammonemia have higher glutamine levels. Another characteristic of plasma amino acid profiles in patients with chronic hepatitis and cirrhosis is elevated levels of aromatic amino acids. Plasma levels of AAA increase partially due to the deficient function in liver detoxification, portal-systemic shunting, and increased protein catabolism [19]. In addition to the changes of branched chain amino acids and aromatic amino acids, our study also showed that the plasma concentration of taurine, aspartic acid, threonine, serine, glycine, glutamine, cysteine, arginine, and methionine in patients with cirrhosis or chronic hepatitis B was significantly higher than that in healthy control groups. These phenomenons may be related to many factors, such as decreased protein synthesis, metabolic dysfunction, and increased muscle decomposition in patients with liver disease.

Convergent evidence suggested that nutritional supplementation is an effective vehicle to improve overall nutritional status in patients with cirrhosis [20]. Most of these studies have focused on BCAA supplementation, which exerts beneficial effect on the nutritional status and substrate utilization in adults with liver disease [12, 21]. However, gastrointestinal upset resulting from BCAA supplementation limits patients' long-term adherence to BCAA supplementation, which to some extent challenged the research with a long time of follow-up. Our previous study found that a carbohydrate-predominant late-evening snack is responsible for the increase in fasting carbohydrate oxidation, resting

Table 5: Changes of laboratory values in patients with cirrhosis before and after late-evening snacks ($\bar{X} \pm$ s.d.).

	Study group						Control group						Treatment effects
	Baseline ($n = 43$)	1st month ($n = 43$)	3rd month ($n = 41$)	6th month ($n = 39$)	F	P	Baseline ($n = 43$)	1st month ($n = 43$)	3rd month ($n = 42$)	6th month ($n = 40$)	F	P	P
WBC ($\times 10^9$/L)	4.2 ± 1.8	4.3 ± 1.9	4.5 ± 1.8	5.0 ± 1.7	1.449	0.242	4.8 ± 1.8	4.6 ± 1.9	4.2 ± 1.9	4.2 ± 1.7	1.076	0.346	0.108
HB (g/L)	89.9 ± 24.2	90.3 ± 27.4	94.8 ± 24.8	101.5 ± 29.7	1.234	0.297	90.9 ± 21.4	93.5 ± 25.8	97.0 ± 22.8	92.0 ± 22.4	0.534	0.589	0.218
PLT ($\times 10^9$/L)	84.4 ± 16.8	83.1 ± 22.0	80.1 ± 32.2	79.5 ± 20.1	0.316	0.730	78.4 ± 25.6	80.6 ± 24.0	87.1 ± 14.1	80.0 ± 19.0	1.487	0.233	0.924
ALT (U/L)	54.6 ± 20.3	53.8 ± 21.6	49.8 ± 17.3	46.3 ± 18.0	1.279	0.284	56.2 ± 17.1	54.7 ± 18.9	51.3 ± 18.6	50.5 ± 20.0	0.698	0.501	0.447
AST (U/L)	65.0 ± 28.1	66.9 ± 24.7	68.2 ± 21.6	66.6 ± 19.1	0.124	0.883	76.6 ± 32.1	74.3 ± 30.6	63.8 ± 18.2	70.6 ± 17.9	1.777	0.177	0.448
TBIL (μmol/L)	44.0 ± 15.2	45.5 ± 18.1	44.6 ± 18.2	39.8 ± 17.1	0.591	0.556	40.1 ± 12.8	41.4 ± 17.2	44.5 ± 16.1	42.8 ± 18.0	0.487	0.617	0.564
ALB (g/L)	29.8 ± 4.0	32.0 ± 3.2	31.8 ± 5.7	33.8 ± 4.2*	4.614	0.013	29.4 ± 5.7	29.9 ± 6.0	30.0 ± 5.8	30.8 ± 5.5	0.386	0.681	0.036
PALB (mg/L)	105.9 ± 25.1	110.4 ± 28.7	122.3 ± 30.5*	126.9 ± 30.2*	3.779	0.027	102.9 ± 23.4	108.2 ± 21.7	107.8 ± 25.4	106.8 ± 33.0	0.229	0.796	0.031
CHE (U/L)	4524.3 ± 1275.8	4324.3 ± 1319.6	4332.7 ± 1471.4	4459.3 ± 1414.8	0.118	0.889	4399.9 ± 1416.7	4310.9 ± 1428.2	4159.3 ± 1425.7	4310.3 ± 1471.1	0.177	0.838	0.730
CR (μmol/L)	60.0 ± 17.2	61.7 ± 18.2	62.1 ± 15.0	60.5 ± 18.7	0.105	0.901	60.8 ± 18.4	52.4 ± 15.5	58.3 ± 14.3	58.4 ± 14.8	0.199	0.820	0.663
CHOL (mmol/L)	4.4 ± 0.8	4.5 ± 0.9	4.8 ± 1.1	4.6 ± 1.1	1.085	0.343	4.5 ± 0.9	4.8 ± 0.8	5.0 ± 1.0	4.9 ± 1.0	1.643	0.201	0.501
TG (mmol/L)	1.7 ± 0.7	1.8 ± 0.8	1.9 ± 0.6	1.7 ± 0.6	0.776	0.464	1.6 ± 0.8	1.7 ± 0.9	1.8 ± 0.7	1.9 ± 0.6	1.161	0.319	0.281
PT (S)	15.3 ± 1.7	15.1 ± 1.9	15.1 ± 1.8	15.0 ± 1.4	0.186	0.831	15.2 ± 1.6	15.9 ± 1.9	15.1 ± 1.5	14.3 ± 1.5	2.145	0.125	0.100
INR	1.2 ± 0.3	1.2 ± 0.4	1.2 ± 0.2	1.3 ± 0.1	0.178	0.837	1.2 ± 0.1	1.3 ± 0.2	1.3 ± 0.1	1.2 ± 0.2	0.185	0.164	0.458
NH_3 (μmol/L)	68.6 ± 25.6	66.1 ± 27.4	55.5 ± 22.5*	47.6 ± 20.7*	2.467	0.031	65.4 ± 24.7	62.7 ± 26.1	57.4 ± 20.2	60.6 ± 21.2	1.089	0.345	0.045
GLU (mmol/L)	5.1 ± 2.3	5.5 ± 2.9	6.0 ± 2.3	5.5 ± 2.6	0.342	0.693	5.8 ± 3.1	5.9 ± 3.8	5.2 ± 3.9	6.0 ± 1.7	0.217	0.728	0.469

Abbreviations: WBC: white blood cell count; HB: hemoglobin; PLT: platelet count; ALT: alanine aminotransferase; AST: aspartate transferase; TBIL: total bilirubin; ALB: albumin; PALB: prealbumin; CHE: cholinesterase; CR: creatinine; CHOL: total cholesterol; TG: triglyceride; PT: prothrombin time; INR: international normalized ratio; NH_3: ammonemia; GLU: blood glucose. *$P < 0.05$ compared with baseline.

Table 6: Changes of ALB, PALB, and NH_3 before and after late-evening snacks in patients with cirrhosis of different Child-Pugh grades ($\bar{X} \pm$ s.d.).

	Baseline	1st month	3rd month	6th month	F	P
Child-Pugh A ($n = 11$)						
ALB (g/L)	33.5 ± 4.7	34.3 ± 3.8	35.1 ± 4.1	35.8 ± 4.4	1.082	0.348
PALB (mg/L)	128.8 ± 26.9	126.2 ± 27.4	130.0 ± 28.1	132.1 ± 28.4	0.131	0.832
NH_3 (μmol/L)	39.6 ± 24.8	33.8 ± 24.4	32.4 ± 23.0	32.1 ± 22.7	0.358	0.672
Child-Pugh B ($n = 12$)						
ALB (g/L)	29.1 ± 4.4	32.7 ± 5.1	33.5 ± 3.9	34.2 ± 4.6	3.742	0.015
PALB (mg/L)	106.4 ± 29.1	112.3 ± 28.4	125.6 ± 27.3	127.4 ± 26.6	3.782	0.026
NH_3 (μmol/L)	68.0 ± 25.6	60.1 ± 25.4	55.5 ± 22.1	47.6 ± 23.3	2.118	0.044
Child-Pugh C ($n = 20$)						
ALB (g/L)	24.2 ± 4.8	27.0 ± 4.2	30.0 ± 3.9	32.4 ± 5.0	5.782	0.006
PALB (mg/L)	87.7 ± 25.8	102.3 ± 26.7	116.3 ± 27.7	120.7 ± 28.0	5.438	0.007
NH_3 (μmol/L)	91.1 ± 24.8	88.7 ± 24.0	78.3 ± 25.2	60.5 ± 25.8	3.784	0.023

Abbreviations: ALB: albumin; PALB: prealbumin; NH_3: ammonemia.

energy expenditure (REE), and reductions in fat oxidation in adults with chronic liver disease [13]. The use of a carbohydrate-based (low glycemic index) nutritional module that is absorbed more slowly overnight promoted carbohydrate utilization for energy supplementation and decreased fat and protein mobilization from the adipocyte and lean tissue.

With six-month nutritional intervention by carbohydrate-predominant late-evening snack, we can observe that the level of ALB and PALB in the study group significantly increased, and the level of NH_3 significantly decreased. We reasoned that LES-treated patients demonstrated a significantly higher overall survival than PS-matched patients who did not receive LES therapy. More importantly, this survival benefit was more significant in patients with Child-Pugh C cirrhosis than in those with Child-Pugh A or B cirrhosis. In the 6th month, unbalanced amino acid profiles improved gradually; the ratio of BCAA to AAA increased significantly. Hepatic encephalopathy is one of the most common complications of severe liver disease. Its pathogenesis has not yet been fully elucidated. The main theories include hyperammonemia and amino acid imbalance [22, 23]. It was shown that cirrhosis patients exhibited more pronounced clearance of BCAA from plasma compared to healthy subjects [24]. Most authors believe that BCAA levels are decreased partially because of their support in muscle ammonia clearance [25]. Studies have implied that BCAA is effective in the treatment of hepatic encephalopathy complicated in cirrhosis and liver failure [26, 27]. Increased BCAA concentrations in the blood and muscles can stimulate ammonia removal from the blood and promote the recovery of muscle strength. Phenylalanine and tyrosine are not synthesized in vivo, and they are not converted into other metabolites in skeletal muscle. Proteolysis leads to an increase in plasma concentration of phenylalanine and tyrosine. Patients with cirrhosis are catabolic, and AAA release from muscle tissue may contribute to the higher AAA blood concentrations in cirrhosis patients. Our previous study found that carbohydrate-predominant LES could potentially improve the status of protein-energy malnutrition which occurs in patients with liver cirrhosis and promote the improvement of liver function [13]. These factors may result in a reduction of skeletal muscle decomposition catabolism; therefore, the release of AAA is reduced. On the other hand, recovery of liver function contributes to the degradation of ammonia and reduces the consumption of BCAA. LES not only help to improve the ratio of BCAA to AAA but also decrease the level of ammonia and glutamine and increase the level of albumin and prealbumin. The most beneficial population was patients with Child-Pugh B and C grades.

This study has several limitations. The retrospective nature of our study limits the assessment of variables including dietary intake, daily physical activity or exercise, and weight change, all of which may affect outcomes in patients with chronic liver disease. Limitations in this study design include carbohydrate which is the main component of LES; for better taste, branched amino acids are not added. With the continuous research and development of functional food, the addition of special functional ingredients may be able to improve the amino acid imbalance in a shorter time. The detection method of amino acids is another limitation in this study. The method used in this study is an automatic amino acid analyzer. Currently, the more accurate detection method is high-performance liquid chromatography (HPLC). The sensitivity (minimum detection limit) of the automatic amino acid analyzer is slightly lower than that of HPLC (automatic amino acid analyzer vs. HPLC: <3 pmol vs. <0.5 pmol). But it has little influence on the results of this study. If possible, the choice of HPLC is more accurate. The advantage of this study is that most patients in the LES group were followed up effectively. Our team has enough full-time staff to follow up and conduct weekly guidance by telephone to ensure a low drop-off rate and credibility of the results. In addition, none of the patients experienced any adverse side effects. A prospective study should be performed to validate the findings of the present study. Finally, our study is based on a single-

Table 7: Changes of plasma amino acid profiles in patients with cirrhosis before and after late-evening snacks ($\bar{X} \pm$ s.d.).

Amino acid (μmol/L)	Study group						Control group				Treatment effects
	Baseline ($n = 43$)	1st month ($n = 43$)	3rd month ($n = 41$)	6th month ($n = 39$)	F	P	Baseline ($n = 43$)	6th month ($n = 40$)	t	P	P
TAU	296.6 ± 147.0	255.8 ± 103.2	270.9 ± 112.0	288.8 ± 110.7	0.605	0.613	315.7 ± 145.7	309.1 ± 118.2	0.176	0.861	0.537
ASP	20.7 ± 12.7	19.7 ± 6.6	19.8 ± 7.0	20.8 ± 7.7	0.105	0.957	19.3 ± 8.8	22.7 ± 11.5	1.182	0.243	0.497
THR	172.8 ± 25.0	157.0 ± 68.3	165.3 ± 63.8	133.1 ± 57.9*	2.368	0.075	181.5 ± 32.1	159.5 ± 57.5	1.683	0.099	0.115
SER	157.0 ± 93.5	183.9 ± 59.4	181.8 ± 63.0	162.5 ± 67.2	0.908	0.440	162.3 ± 41.7	167.3 ± 41.8	0.366	0.716	0.783
GLU	38.9 ± 11.4	37.7 ± 12.9	39.9 ± 12.5	36.2 ± 11.0	0.476	0.700	38.0 ± 14.7	41.9 ± 12.0	1.015	0.315	0.081
GLY	235.4 ± 80.1	252.8 ± 90.9	251.9 ± 93.0	270.1 ± 96.5	0.628	0.599	250.9 ± 67.2	275.0 ± 76.8	1.184	0.242	0.844
ALA	377.1 ± 106.7	387.5 ± 130.8	420.8 ± 135.1	372.6 ± 135.1	0.722	0.541	372.5 ± 159.7	396.1 ± 128.8	0.572	0.570	0.545
GLN	808.3 ± 107.5	797.4 ± 92.1	789.1 ± 128.3	766.6 ± 120.9	1.038	0.375	812.6 ± 147.4	802.7 ± 115.0	0.198	0.856	0.369
CYS	100.3 ± 27.1	109.0 ± 24.2	102.8 ± 21.9	97.2 ± 18.6	1.205	0.312	106.9 ± 20.2	104.5 ± 24.8	0.368	0.714	0.246
VAL	228.1 ± 101.0	205.7 ± 92.1	215.0 ± 94.0	258.1 ± 66.2	1.647	0.183	211.0 ± 94.1	210.8 ± 82.6	0.008	0.994	0.032
ILE	92.8 ± 27.8	98.8 ± 35.6	107.5 ± 33.8	112.2 ± 33.6*	1.748	0.155	95.4 ± 24.4	98.6 ± 34.0	0.390	0.698	0.167
LEU	141.8 ± 28.1	145.3 ± 42.9	161.2 ± 36.7	164.3 ± 37.8*	2.382	0.074	145.2 ± 34.0	139.4 ± 61.3	0.424	0.673	0.092
TYR	131.1 ± 31.5	123.2 ± 45.8	132.5 ± 46.7	126.4 ± 35.7	0.287	0.834	139.2 ± 41.8	132.2 ± 47.3	0.553	0.583	0.631
PHE	84.6 ± 17.9	80.6 ± 32.0	81.0 ± 30.4	75.7 ± 24.1	0.472	0.703	89.5 ± 19.8	80.4 ± 29.2	1.291	0.203	0.542
HIS	70.8 ± 15.8	68.1 ± 20.2	71.5 ± 15.9	72.3.7 ± 19.1	0.268	0.848	71.0 ± 17.9	70.3 ± 16.1	0.144	0.886	0.701
TRP	46.5 ± 14.0	46.4 ± 19.4	45.5 ± 16.4	37.1 ± 16.0*	1.894	0.136	46.2 ± 18.0	46.3 ± 16.8	0.010	0.992	0.057
ORN	418.8 ± 85.6	459.0 ± 117.6	475.5 ± 104.4	431.8 ± 107.1	1.546	0.208	445.7 ± 77.0	403.2 ± 136.0	1.373	0.176	0.416
LYS	215.6 ± 41.6	226.9 ± 58.2	218.7 ± 56.7	223.1 ± 61.2	0.211	0.889	221.1 ± 69.1	226.0 ± 63.8	0.264	0.793	0.872
ARG	85.8 ± 23.7	82.9 ± 23.7	86.5 ± 25.8	80.4 ± 24.4	0.339	0.797	84.5 ± 25.3	85.8 ± 25.0	0.193	0.848	0.445
PRO	193.5 ± 46.7	192.9 ± 58.7	181.3 ± 44.0	174.9 ± 45.4	0.873	0.458	188.7 ± 40.2	179.3 ± 40.6	0.823	0.415	0.721
MET	24.9 ± 7.9	24.4 ± 6.7	23.1 ± 8.1	21.2 ± 6.8	1.223	0.305	23.4 ± 7.0	26.5 ± 6.5	1.621	0.112	0.008
BCAA/AAA	1.81 ± 0.50	1.95 ± 0.85	2.05 ± 0.63	2.32 ± 0.60**	2.819	0.043	1.77 ± 0.43	1.80 ± 0.61	1.807	0.424	0.003

Abbreviations: TAU: taurine; ASP: aspartic acid; THR: threonine; SER: serine; GLU: glutamic acid; GLY: glycine; ALA: alanine; GLN: glutamine; CYS: cysteine; VAL: valine; LEU: leucine; ILE: isoleucinetyrosine; TYR: tyrosine; PHE: phenylalanine; HIS: histidine; TRP: tryptophan; ORN: ornithine; LYS: lysine; ARG: arginine; PRO: proline; MET: methionine. BCAA: branched chain amino acids; AAA: aromatic amino acids. *$P < 0.05$ compared with baseline; **$P < 0.01$ compared with baseline.

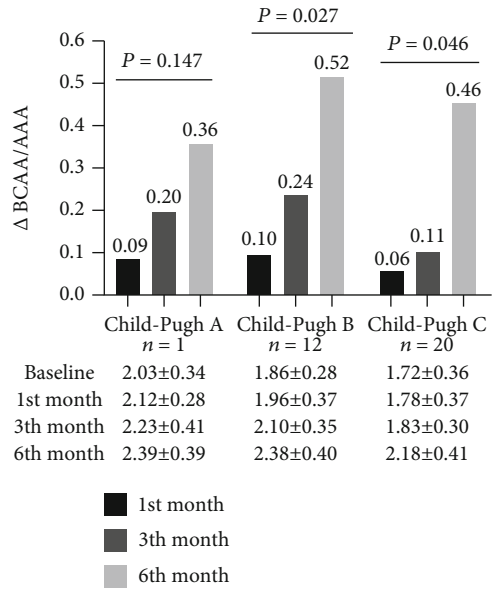

Figure 1: The impact of disease severity on the ratio of BCAA to AAA in cirrhosis patients due to hepatitis B infection supplemented with a late-evening snack. Notes: compared with baseline, for LES treatment at 6th month, the ratio of BCAA to AAA in patients with Child-Pugh B and C increased; the difference was statistically significant, while the impact of LES supplementation was not obvious in Child-Pugh A group. BCAA: branched chain amino acids; AAA: aromatic amino acids.

center cohort of patients, which has a potential limitation to generalize our findings to other populations and regions. Therefore, further multicenter and prospective cohort studies are warranted to clarify the causal relationship between LES and survival.

In conclusion, there was significant amino acid imbalance in patients with chronic hepatitis, especially cirrhosis, which was manifested by the decreased level of branched chain amino acid and BCAA to AAA ratio and the increased level of aromatic amino acid level. The application of an LES carbohydrate module (lotus-root starch) for six months in liver cirrhosis patients was beneficial in increasing the ratio of BCAA to AAA and decreasing the level of ammonia. The most beneficial population was patients with Child-Pugh B and C grades.

Abbreviations

AAA: Aromatic amino acids
ALA: Alanine
ALB: Albumin
ALT: Alanine aminotransferase
ARG: Arginine
ASP: Aspartic acid
AST: Aspartate transferase
BCAA: Branched chain amino acids
CHE: Cholinesterase
CHOL: Total cholesterol
CR: Creatinine
CYS: Cysteine
GLN: Glutamine
GLU: Blood glucose
GLU: Glutamic acid
GLY: Glycine
HB: Hemoglobin
HBV: Hepatitis B virus
HIS: Histidine
ILE: Isoleucinetyrosine
INR: International normalized ratio
LES: Late-evening snack
LEU: Leucine
LYS: Lysine
MET: Methionine
NH_3: Ammonemia
ORN: Ornithine
PALB: Prealbumin
PHE: Phenylalanine
PLT: Platelet count
PRO: Proline
PT: Prothrombin time
REE: Resting energy expenditure
SER: Serine
TAU: Taurine
TBIL: Total bilirubin
TG: Triglyceride
THR: Threonine
TRP: Tryptophan
TYR: Tyrosine
VAL: Valine
WBC: White blood cell count.

Data Availability

The authors confirm that the data supporting the findings of this study are available within the article.

Conflicts of Interest

There is no conflict of interest.

Authors' Contributions

Qing-hua Meng, Zheng Lv, and Wei Hou designed research; Zheng Lv, Jing Yang, Jing Wu, and Zhong-ying Wang conducted research; Wei Hou analyzed data and wrote the paper. Qing-hua Meng had primary responsibility for the final content. All authors read and approved the final manuscript. Wei Hou and Zheng Lv contributed equally to this article as co-first authors.

Acknowledgments

The study was funded by the Capital Foundation of Medical Development (2016-1-2181). Youan Liver Disease and AIDS Fund, Beijing Youan Hospital, Capital Medical University (BJYAYY-GG2019-02).

References

[1] Organization WH, *Guidelines for the prevention, care and treatment of persons with chronic hepatitis B infection*, World

Hindawi
BioMed Research International
Volume 2024, Article ID 9850985, 1 page
https://doi.org/10.1155/2024/9850985

Retraction

Retracted: Treatment of Severe Ptosis by Conjoint Fascial Sheath Suspension

BioMed Research International

Received 12 March 2024; Accepted 12 March 2024; Published 20 March 2024

This article has been retracted by Hindawi following an investigation undertaken by the publisher [1]. This investigation has uncovered evidence of one or more of the following indicators of systematic manipulation of the publication process:

(1) Discrepancies in scope

(2) Discrepancies in the description of the research reported

(3) Discrepancies between the availability of data and the research described

(4) Inappropriate citations

(5) Incoherent, meaningless and/or irrelevant content included in the article

(6) Manipulated or compromised peer review

The presence of these indicators undermines our confidence in the integrity of the article's content and we cannot, therefore, vouch for its reliability. Please note that this notice is intended solely to alert readers that the content of this article is unreliable. We have not investigated whether authors were aware of or involved in the systematic manipulation of the publication process.

Wiley and Hindawi regrets that the usual quality checks did not identify these issues before publication and have since put additional measures in place to safeguard research integrity.

We wish to credit our own Research Integrity and Research Publishing teams and anonymous and named external researchers and research integrity experts for contributing to this investigation.

The corresponding author, as the representative of all authors, has been given the opportunity to register their agreement or disagreement to this retraction. We have kept a record of any response received.

References

[1] P. Sang, M. Fang, X. Li, C. Liu, and Q. Xi, "Treatment of Severe Ptosis by Conjoint Fascial Sheath Suspension," *BioMed Research International*, vol. 2021, Article ID 1837458, 6 pages, 2021.

Hindawi
BioMed Research International
Volume 2021, Article ID 1837458, 6 pages
https://doi.org/10.1155/2021/1837458

Research Article

Treatment of Severe Ptosis by Conjoint Fascial Sheath Suspension

Pengfei Sang, Mingsong Fang, Xuan Li, Chang Liu, and Qingchun Xi

Department of Plastic Surgery, Hefei Second People's Hospital, China

Correspondence should be addressed to Qingchun Xi; xqc981101@163.com

Received 23 July 2021; Revised 30 September 2021; Accepted 20 October 2021; Published 19 November 2021

Academic Editor: Jianxin Shi

Objective. To explore the role of conjoint fascial sheath (CFS) suspension in the treatment of severe ptosis. *Methods*. A total of 110 patients with severe ptosis who were admitted to our hospital from May 2018 to December 2020 were included. Fifty-seven patients treated with frontalis suspension were assigned into group A, and the remaining 53 patients treated with CFS suspension were assigned into group B. The curative effect, ocular surface alterations, complications, and satisfaction in the two groups were compared. *Results*. Patients in group B suffered from severe upper eyelid retraction and lid lag than those in group A, as well as more limited range of motion (ROM) ($P < 0.05$). The curative effect and patient satisfaction in group B were higher than those in group A ($P < 0.05$). Postsurgical complications in group B were fewer than those in group A ($P < 0.05$). *Conclusion*. CFS suspension is effective in the treatment of severe ptosis.

1. Introduction

Blepharoptosis is common in ocular plastic surgery and may be induced by multiple mechanisms, for example, congenital ptosis caused by low function of fibroadipose tissue in levator palpebrae superioris (LPS) muscle, myogenic ptosis caused by dysgenesis-induced weakness of LPS muscle, and neurogenic ptosis caused by complete or partial loss of cranial nerve III [1, 2]. Blepharoptosis refers to the drooping of either or both sides of the upper eyelid, resulting in narrow palpebral fissure and covering the eyes [3], which may also be associated with other eye diseases or systemic diseases [4, 5]. Aponeurosis repair and levator myectomy are preferred options for its treatment. Frontalis suspension, a common surgical treatment for patients with severe ptosis and poor levator function [6], establishes a connection between frontalis and tarsus, thus correcting the position of eyelid through the elevatory force of the frontalis [7]. However, it cannot fully meet the normal physiological requirements and is commonly associated with postoperative keratitis, and vulnerable patients are prone to corneal complications [8]. Conjoint fascia sheath (CFS) has been histologically confirmed to be a kind of fascial tissue membrane with elasticity and toughness. It is widely used in ptosis correction by connecting the special muscle sheath of the levator in the CFS with levator muscle to suspend eyelid [9]. This study is aimed at exploring the role of CSF suspension in the treatment of severe ptosis.

2. Data and Methods

2.1. General Data. A total of 110 patients with severe ptosis who were admitted to our hospital from May 2018 to December 2020 were included. Fifty-seven patients treated with frontalis suspension were assigned into group A, and the remaining 53 patients treated with CFS suspension were assigned into group B.

2.2. Exclusion and Inclusion Criteria

2.2.1. Inclusion Criteria. The criteria include patients with upper eyelid covering the cornea of about 2/3 or more and upper eyelid levator muscle strength > 4.0 mm [10]. This study was approved by the Ethics Committee of our hospital, and all participants signed informed consent forms.

2.2.2. Exclusion Criteria. The criteria include patients with communication disorders, relevant treatment history, oculomotor nerve dysfunction, ocular myasthenia gravis, strabismus, or jaw-winking syndrome.

Table 1: General data ($x \pm SD$) [n(%)].

Classification	Group A ($n = 57$)	Group B ($n = 53$)	t/χ^2	P
Sex			1.182	0.277
Male	33 (57.89)	36 (67.92)		
Female	24 (42.11)	17 (32.08)		
Age (years)	24.58 ± 7.29	25.15 ± 7.40	0.406	0.685
Height (cm)	171.57 ± 5.68	172.32 ± 6.31	0.656	0.513
Weight (kg)	54.21 ± 8.38	55.43 ± 7.65	0.795	0.428
Residence			0.616	0.251
Rural	21 (36.84)	22 (41.51)		
Urban	36 (63.16)	31 (58.49)		
Nationality			0.275	1.191
Han nationality	40 (70.18)	42 (79.25)		
Ethnic minorities	17 (29.82)	11 (20.75)		
Economic level			1.413	0.493
Poor	12 (21.05)	8 (15.09)		
Well-off	26 (45.61)	30 (56.60)		
Wealthy	19 (33.33)	15 (28.30)		
Staying up late			1.695	0.193
Yes	35 (61.40)	26 (49.06)		
No	22 (38.60)	27 (50.94)		
Exercise			0.344	0.557
Yes	28 (49.12)	29 (54.72)		
No	29 (50.88)	24 (45.28)		
Obesity			0.257	0.611
Yes	13 (22.81)	10 (18.87)		
No	44 (77.19)	43 (81.13)		
Smoking			1.674	0.195
Yes	21 (36.84)	26 (49.06)		
No	36 (63.16)	27 (50.94)		
Drinking			0.018	0.891
Yes	24 (42.11)	23 (43.40)		
No	33 (57.89)	30 (56.60)		
Type			1.169	0.279
Congenital	42 (73.68)	34 (64.15)		
Acquired	15 (26.32)	19 (35.85)		

2.3. Methods. Patients in group A underwent frontalis suspension: two to three drops of tetracaine gel were used for topical anesthesia, and 20 g/L lidocaine was used for subcutaneous and subconjunctival infiltration anesthesia. Skin and subcutaneous tissue were incised to expose orbicularis oculi, and the frontalis muscle was separated through an incision above the eyebrow arch. A tunnel was made on each pedicel of muscle flaps through a 5 mm incision, and mattress sutures of two muscle flaps were pull out from the eyebrow incision through the tunnel. The frontalis muscle and subcutaneous tissue were bluntly dissected upwards to 15-20 mm above the eyebrow arch, with a width of 25-35 mm.

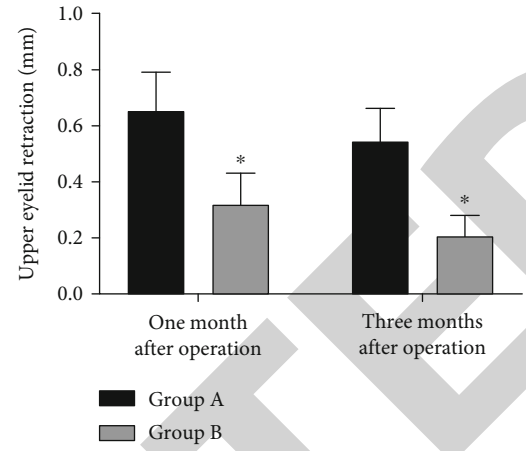

Figure 1: Comparison of upper eyelid retraction after surgery. Upper eyelid retraction length in group B is shorter than that in group A at 1 month and 3 months after surgery ($P < 0.05$). $^*P < 0.05$ *vs.* group A.

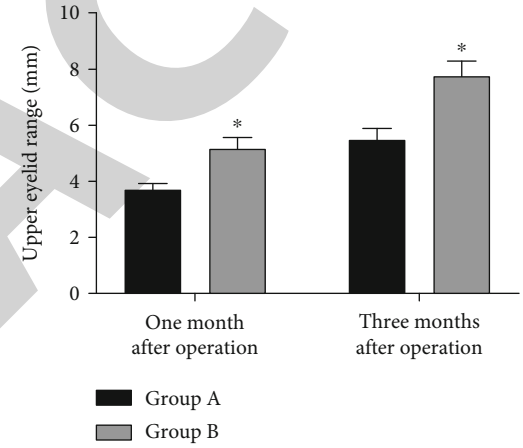

Figure 2: Comparison of ROM of upper eyelid after surgery. ROM of upper eyelid in group B is larger than that in group A at 1 month and 3 months after surgery ($P < 0.05$). $^*P < 0.05$ *vs.* group A.

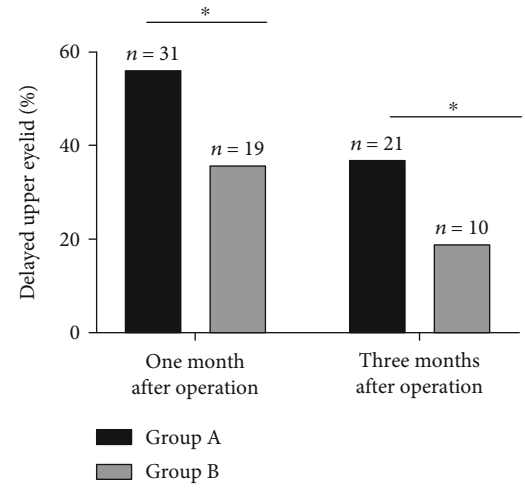

Figure 3: Comparison of lid lag after surgery. Lid lag in group B is lower than that in group A at 1 month and 3 months after surgery ($P < 0.05$). $^*P < 0.05$ between the two groups.

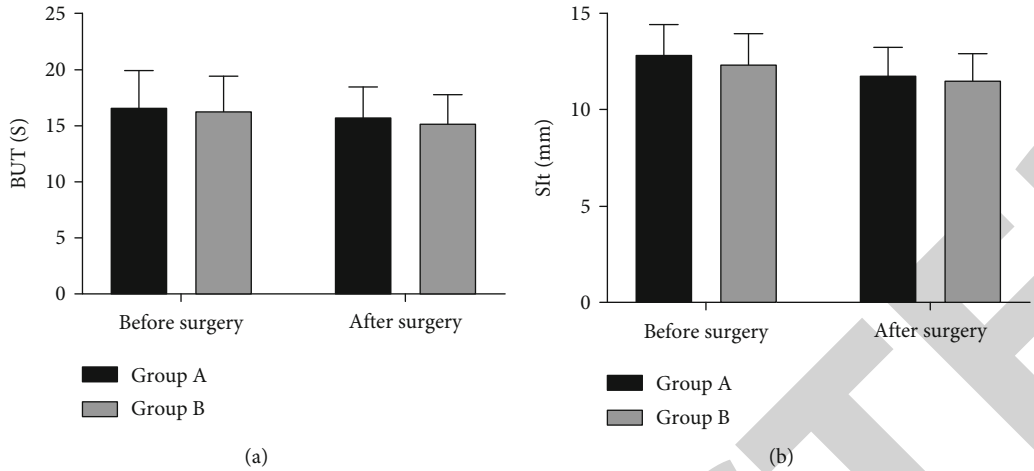

Figure 4: Comparison of ocular surface before and after surgery. (a) Comparison of BUT: there is no significant difference in BUT between the two groups both before and after surgery ($P > 0.05$). (b) Comparison of SIt: there is no significant difference in SIt between the two groups both before and after surgery ($P > 0.05$).

Table 2: Comparison of corrective effect [n(%)].

Corrective effect	Group A ($n = 57$)	Group B ($n = 53$)	χ^2	P
Well corrected	20 (35.09)	36 (67.92)	—	—
Overcorrected	17 (29.82)	8 (15.09)	—	—
Undercorrected	11 (19.30)	6 (11.32)	—	—
Relapse	9 (15.79)	3 (5.66)	—	—
Correction rate	20 (35.09)	36 (67.92)	11.851	<0.001

The frontalis muscle and periosteum were separated to the same plane as subcutaneous separation layer, separating the frontalis muscle from the skin at the top and separating the frontalis muscle from the periosteum at the bottom. The inner, middle, and outer points were fixed at the anterior one-third of tarsus. Curvature and height of sutures were adjusted to ensure the normal head-up of patients, and the height of palpebral fissure was controlled to ensure the complete separation of eyelid and eyeball. Afterwards, the incision was sutured to form a double eyelid.

Patients in group B were treated with CFS suspension: all patients were supine anesthetized in the same way as group A. They were operated under the microscope. The marking line was designed, and eyelid infiltration anesthesia was carried out. Skin was cut along the line, and orbicular muscle at the lower edge of the incision was removed to expose tarsus. The incision was separated upward to 5 mm above the fornix along the space between Muller's muscle and levator aponeurosis, in order to fully expose CFS. Three pairs of mattress sutures were made with 5-0 absorbable suture to fix CFS at the anterior one-third of tarsus so that the upper eyelid margin of the affected eye was located at the upper edge of the cornea when looking straight ahead in a sitting position. Suturing height was adjusted to make the margin of eyelid smooth and natural. 5-0 silk thread was used to lift levator aponeurosis, and the incision was sutured intermittently.

2.4. Outcome Measures

2.4.1. Corrective Effect Assessment [11]. Upper eyelid located 1~2 mm below the upper corneal margin was considered to be well corrected; upper eyelid located at or above the upper corneal margin was considered to be overcorrected; upper eyelid located >2 mm below the upper corneal margin was considered to be undercorrected; no changes in the position of upper eyelid were considered a relapse.

2.4.2. Upper Eyelid Retraction, Lid Lag, and Range of Motion (ROM) at 1 Month and 3 Months after Surgery. ROM determination: the thumb pressed the eyebrow arch to block the traction of the frontalis muscles to upper eyelid. Patients were instructed to look down and then look up to measure the distance of the lowest point of the upper eyelid margin moved.

2.4.3. Ocular Surface. Tear film break-up time (BUT) and Schirmer I test (SIt) were monitored before and one week after surgery. BUT was continuously tested for 3 times, and tear film instability was identified at BUT < 10 s; SIt was tested for 5 min, and a length of filter paper wetted less than 5 mm indicated low secretion.

3. Statistical Analysis

SPSS 21.0 (SPSS Inc., Chicago, IL, USA) was employed for statistical analysis. The measurement data were expressed by $x \pm \mathrm{SD}$, and the intergroup comparison adopted t-test. The counting data were expressed by [n(%)], and the intergroup comparison adopted chi-square test. Difference was considered statistically significant at $P < 0.05$.

4. Results

4.1. General Data. There was no difference in general data between the two groups ($P > 0.05$), as shown in Table 1.

Table 3: Comparison of postsurgical complications [n(%)].

Complication	Group A ($n = 57$)	Group b ($n = 53$)	χ^2	P
Lagophthalmos	2 (3.51)	1 (1.89)	—	—
Upper eyelid entropion	1 (1.75)	0 (0.00)	—	—
Exposure conjunctivitis	3 (5.26)	0 (0.00)	—	—
Hematoma in the eyebrow area	4 (7.02)	2 (3.77)	—	—
Trichiasis	4 (7.02)	2 (3.77)	—	—
Conjunctival prolapse	0 (0.00)	0 (0.00)	—	—
Total incidence rate	14 (24.56)	5 (9.43)	4.398	0.036

4.2. Upper Eyelid Retraction after Surgery. Upper eyelid retraction in group A and group B at 1 month after surgery was 0.65 ± 0.14 mm and 0.32 ± 0.11 mm, respectively, and those values were 0.54 ± 0.12 mm and 0.21 ± 0.07 mm at 3 months after surgery. It is suggested that the upper eyelid retraction in group B was shorter than that in group A at 1 month and 3 months after surgery ($P < 0.05$), as shown in Figure 1.

4.3. ROM of Upper Eyelid after Surgery. ROM of upper eyelid in group A and group B was 3.68 ± 0.24 mm and 5.21 ± 0.35 mm, respectively, at 1 month after surgery, and those values were 5.45 ± 0.42 mm and 7.78 ± 0.48 mm at 3 months after surgery. The ROM of upper eyelid in group B was larger than that in group A at 1 month and 3 months after surgery ($P < 0.05$), as shown in Figure 2.

4.4. Lid Lag after Surgery. Lid lag in group A and group B was 56.14% and 35.85%, respectively, at 1 month after surgery, and those values were 36.84% and 18.87% at 3 months after surgery. The lid lag in group B was lower than that in group A at 1 month and 3 months after surgery ($P < 0.05$), as shown in Figure 3.

4.5. Ocular Surface before and after Surgery. The BUT in group A and group B was 16.68 ± 3.29 s and 16.33 ± 3.18 s, respectively, before surgery, while after surgery, the values were 15.74 ± 2.78 s and 15.26 ± 2.59 s. The SIt in group A and group B was 12.84 ± 1.54 mm and 12.46 ± 1.48 mm, respectively, before surgery, while after surgery, the values were 11.76 ± 1.46 mm and 11.54 ± 1.32 mm. There was no difference in BUT and SIt between the two groups both before and after surgery ($P < 0.05$), as shown in Figure 4.

4.6. Comparison of Corrective Effect. Corrective effect in group B was better than that in group A after surgery ($P < 0.05$); see Table 2.

4.7. Comparison of Complications. Postsurgical complications in group B were fewer than those in group A ($P < 0.05$), as shown in Table 3.

4.8. Comparison of Patient Satisfaction. Patient satisfaction in group B was higher than that in group A ($P < 0.05$), as shown in Table 4.

Table 4: Comparison of patient satisfaction [n(%)].

Satisfaction	Group A ($n = 57$)	Group B ($n = 53$)	χ^2	P
Highly satisfied	12 (21.05)	24 (45.28)	—	—
Satisfied	21 (36.84)	19 (35.85)	—	—
Generally satisfied	16 (28.07)	8 (15.09)	—	—
Dissatisfied	8 (14.04)	2 (3.77)	—	—
Overall satisfaction	33 (57.89)	43 (81.13)	6.944	0.008

5. Discussion

Ptosis, a common disease encountered in ocular plastic surgery [12], refers to drooping or displacement of the upper eyelid, accompanied by narrowing of vertical palpebral fissure. Ptosis is generally mild and insignificant, but it may cause visual impairment in a few patients whose pupil is completely covered [13–15], affecting the quality of life and increasing the burden. In this study, we compared the efficacy of CFS suspension and frontalis suspension, and it turned out that the upper eyelid retraction, lid lag, and ROM of patients undergoing CFS suspension improved better than those undergoing frontalis suspension. This may be due to the long relaxation time of elastic materials used in frontalis suspension leads to unstable results and upper eyelid retraction. In frontalis suspension, excessive movement of the frontalis muscle may induce inflammation, infection, extravasation, extrusion of materials, eyelid deformation, and involuntary paroxysmal movement of eyelids in the upward direction [16]. In comparison, CFS is less invasive and harmful to tissues and blood vessels and does not change the movement direction of the upper eyelid, thereby reducing lid lag. This may be one of the reasons why CFS suspension is better than frontalis suspension. Tear film is a protective coating lining the outermost layer of corneal epithelium that plays a pivotal role in maintaining eye health [17, 18]. It prevents excessive evaporation and entry of dust and other foreign particles, resists bacterial infection, lubricates eyelids, and maintains optimal visual performance [19, 20]. SIt is the most commonly used method to evaluate the production of aqueous tears [21], and BUT has been widely used to measure tear film stability and diagnose common tear issues [22]. Generally, plastic surgery or repair of the upper eyelid may lead to decreased corneal sensation

and increased tear production in the early stage after surgery. However, in this study, there was no difference in ocular surface alterations between the two groups. Frontalis suspension has no effect on the lacrimal and accessory lacrimal glands and can control tear secretion [23]. Therefore, it is suggested that both CFS suspension and frontalis suspension have no significant influence on the ocular surface of patients.

Our findings demonstrated that CFS resulted in fewer postsurgical complications. In frontalis suspension, materials are used to connect the eyelid to the eyebrow, and dysfunctional eyelid is lifted through the frontalis muscle [24], whereas CFS suspension connects the special muscle sheath of levator in CFS with levator muscle to suspend the eyelid, thus reducing complications such as infection, extrusion, breakage, and granuloma formation. This may also be one of the reasons for higher satisfaction of patients undergoing CFS suspension. There is evidence that CFS suspension has good and lasting efficacy and short recovery time in ptosis, which is worth popularizing [25].

There are several limitations in this study. We have not yet evaluated the effects of the two surgical methods on inflammatory factors nor on the quality of life and revision rates.

To sum up, CFS suspension is effective in the treatment of severe ptosis, with fewer complications and long-lasting efficacy.

Data Availability

The authors confirm that the data supporting the findings of this study are available within the article.

Conflicts of Interest

No conflict of interest exists.

Authors' Contributions

Pengfei Sang, Xun Li, and Mingsong Fang performed the experiments, analyzed the data, and wrote the manuscript. Qingchun Xi and Chang Liu designed the study. All the authors agreed to be accountable for the accuracy and integrity of all aspects of the research.

Acknowledgments

The work was supported by the Clinical Application Study of Upper Eyelid Combined Fascial Sheath (CFS) in Patients with Severe Ptosis (hwk2018yb004).

References

[1] S. M. Jacobs, A. J. Tyring, and A. J. Amadi, "Traumatic ptosis: evaluation of etiology, management and prognosis," *Journal of ophthalmic & vision research.*, vol. 13, pp. 447–452, 2018.

[2] M. A. Elsamkary and M. M. Roshdy, "Clinical trial comparing autogenous fascia lata sling and Gore-Tex suspension in bilateral congenital ptosis," *Clinical Ophthalmology*, vol. 10, pp. 405–409, 2016.

[3] Y. Wang, Y. Xu, X. Liu, L. Lou, and J. Ye, "Amblyopia, strabismus and refractive errors in congenital ptosis: a systematic review and meta-analysis," *Scientific Reports*, vol. 8, p. 8320, 2018.

[4] M. Marenco, I. Macchi, I. Macchi, E. Galassi, M. Massaro-Giordano, and A. Lambiase, "Clinical presentation and management of congenital ptosis," *Clinical Ophthalmology*, vol. 11, pp. 453–463, 2017.

[5] A. J. Park, B. Eliassi-Rad, and M. A. Desai, "Ptosis after glaucoma surgery," *Clinical Ophthalmology*, vol. 11, pp. 1483–1489, 2017.

[6] Y. Takahashi, I. Leibovitch, and H. Kakizaki, "Frontalis suspension surgery in upper eyelid blepharoptosis," *The open ophthalmology journal*, vol. 4, pp. 91–97, 2010.

[7] A. Naik, A. Patel, N. Bothra, L. Panda, M. N. Naik, and S. Rath, "Endoscope-assisted harvest of autogenous fascia lata in frontalis suspension surgery: a minimally invasive approach revisited," *Indian Journal of Ophthalmology*, vol. 66, pp. 440–444, 2018.

[8] K. P. Shah and B. Mukherjee, "Efficacy of frontalis suspension with silicone rods in ptosis patients with poor Bell's phenomenon," *Taiwan journal of ophthalmology*, vol. 7, pp. 143–148, 2017.

[9] B. Li, J. Yang, W. Wu et al., "Anatomical and histological study of the conjoint fascial sheath of the levator and superior rectus for ptosis surgery," *Ophthalmic Plastic and Reconstructive Surgery*, vol. 36, no. 6, pp. 617–620, 2020.

[10] J. Finsterer, "Ptosis: causes, presentation, and management," *Aesthetic Plastic Surgery*, vol. 27, pp. 193–204, 2003.

[11] L. Zuo, X. X. Wang, X. Y. Huang, J. L. Zhang, and Y. Y. Du, "A modified levator resection technique involving retention of the levator palpebrae superioris muscle suspension system for treatment of congenital ptosis," *Aesthetic Plastic Surgery*, vol. 41, pp. 856–862, 2017.

[12] J. W. Yang, "Modified levator muscle resection using Putterman Muller's muscle-conjunctival resection-ptosis clamp," *Aesthetic Surgery Journal*, vol. 38, pp. 480–487, 2018.

[13] P. Pavone, S. Y. Cho, A. D. Pratico, R. Falsaperla, M. Ruggieri, and D. K. Jin, "Ptosis in childhood: a clinical sign of several disorders: case series reports and literature review," *Medicine*, vol. 97, article e12124, 2018.

[14] J. S. Paik, S. A. Kim, S. H. Park, and S. W. Yang, "Refractive error characteristics in patients with congenital blepharoptosis before and after ptosis repair surgery," *BMC Ophthalmology*, vol. 16, p. 177, 2016.

[15] R. A. Harrad, C. M. Graham, and J. R. Collin, "Amblyopia and strabismus in congenital ptosis," *Eye*, vol. 2, Part 6, pp. 625–627, 1988.

[16] W. Chen, Z. Liu, Q. Tian et al., "Levator resection with suspensory ligament of the superior fornix suspension for correction of pediatric congenital ptosis with poor levator function," *Eye*, vol. 30, pp. 1490–1495, 2016.

[17] M. Patterson, H. J. Vogel, and E. J. Prenner, "The effect of repeated lateral compression and expansions mimicking blinking on selected tear film polar lipid monofilms," *Biochimica et Biophysica Acta - Biomembranes*, vol. 1859, pp. 319–330, 2017.

[18] M. S. Milner, K. A. Beckman, J. I. Luchs et al., "Dysfunctional tear syndrome: dry eye disease and associated tear film disorders - new strategies for diagnosis and treatment," *Current Opinion in Ophthalmology*, vol. 27, Supplement 1, pp. 3–47, 2017.

Hindawi
BioMed Research International
Volume 2024, Article ID 9873517, 1 page
https://doi.org/10.1155/2024/9873517

Retraction

Retracted: LncRNA PVT1 Promotes Hypoxia-Induced Cardiomyocyte Injury by Inhibiting miR-214-3p

BioMed Research International

Received 12 March 2024; Accepted 12 March 2024; Published 20 March 2024

This article has been retracted by Hindawi following an investigation undertaken by the publisher [1]. This investigation has uncovered evidence of one or more of the following indicators of systematic manipulation of the publication process:

(1) Discrepancies in scope

(2) Discrepancies in the description of the research reported

(3) Discrepancies between the availability of data and the research described

(4) Inappropriate citations

(5) Incoherent, meaningless and/or irrelevant content included in the article

(6) Manipulated or compromised peer review

The presence of these indicators undermines our confidence in the integrity of the article's content and we cannot, therefore, vouch for its reliability. Please note that this notice is intended solely to alert readers that the content of this article is unreliable. We have not investigated whether authors were aware of or involved in the systematic manipulation of the publication process.

Wiley and Hindawi regrets that the usual quality checks did not identify these issues before publication and have since put additional measures in place to safeguard research integrity.

We wish to credit our own Research Integrity and Research Publishing teams and anonymous and named external researchers and research integrity experts for contributing to this investigation.

The corresponding author, as the representative of all authors, has been given the opportunity to register their agreement or disagreement to this retraction. We have kept a record of any response received.

References

[1] C. Liu, J. Zhang, X. Lun, and L. Li, "LncRNA PVT1 Promotes Hypoxia-Induced Cardiomyocyte Injury by Inhibiting miR-214-3p," *BioMed Research International*, vol. 2021, Article ID 4604883, 9 pages, 2021.

Hindawi
BioMed Research International
Volume 2021, Article ID 4604883, 9 pages
https://doi.org/10.1155/2021/4604883

Research Article

LncRNA PVT1 Promotes Hypoxia-Induced Cardiomyocyte Injury by Inhibiting miR-214-3p

Chuanliang Liu,[1] **Jieqiong Zhang**,[2] **Xuejie Lun**,[3] **and Lei Li**[2]

[1]*The First Department of Health Care, Weifang People's Hospital, China*
[2]*The Third Department of Health Care of Weifang People's Hospital, 151 Guangwen Street, Kuiwen District, Weifang City, 261041 Shandong Province, China*
[3]*Department of Internal Medicine, Weifang Municipal Hospital, China*

Correspondence should be addressed to Lei Li; leshun5878@163.com

Received 27 July 2021; Revised 6 October 2021; Accepted 8 October 2021; Published 15 November 2021

Academic Editor: Chang Gu

Objective. To explore the effect and related mechanism of LncRNA PVT1 on hypoxia-induced cardiomyocyte injury. *Methods*. PVT1RNA and miR-214-3p levels were detected by quantitative real-time polymerase chain reaction (qRT-PCR). Cell vitality and apoptosis were, respectively, evaluated by Cell Counting Kit-8 (CCK-8) and flow cytometry analysis. Starbase and Dual luciferase reporter (DLR) gene assay was employed to validate the interaction between miR-214-3p and PVT1. *Results*. PVT1 was statistically upregulated, and miR-214-3p was statistically downregulated in hypoxia-induced H9c2 cells. The survival rate of H9c2 cells induced by hypoxia decreased statistically, while the apoptosis rate increased statistically ($P < 0.05$). PVT1 knockdown upregulated the hypoxia-induced H9c2 cell viability and inhibited apoptosis. DLR assay verified the targeting relationship between PVT1 and miR-214-3p. In addition, miR-214-3p inhibitors reversed the viability of H9c2 cells with PVT1 knockout and promoted apoptosis. *Conclusion*. Silencing PVT1 can enhance the hypoxia-induced H9c2 cell viability and inhibit apoptosis, providing a potential target for the treatment of cardiovascular diseases.

1. Introduction

As a common disease, the incidence of cardiovascular diseases (CVDs) keeps increasing as the social environment and living habits change, which hazards human life safety [1, 2]. Today, along with the advances in science and technology and the development of medical technology, people's understanding of CVDs is also constantly making breakthroughs [3]. While for CVDs, it is of the essence to explore the mechanism of its occurrence and development and to find effective therapeutic drugs or targets.

In CVDs, cardiomyocyte injury is among the key factors leading to the occurrence and development of the disease [4]. For example, in acute myocardial infarction, myocardial ischemia/reperfusion is among the most pervasive types of myocardial injury in clinical practice [5]. Previous studies [6] have pointed out that cardiomyocyte apoptosis is the main form of cardiomyocyte injury; so, exploring the mechanism of cardiomyocyte apoptosis and how to prevent it is vital for the treatment of CVDs patients. LncRNA, as a non-coding long strand RNA, plays a biological role in cells mainly through regulating protein transcription and has been found to be essential in a wide spectrum of diseases in recent years, including CVDs [7]. For example, a study [8] found that inhibition of lncRNA MALAT1 statistically increased miR-558, decreased the survival rate, and increased the apoptosis rate of isoproterenol-treated H9c2 cells. LncRNA PVT1 is an oncogene that exerts marked effects on multiple tumors, and studies in recent years have found that it also plays a key role in some CVDs [9, 10]. For instance, a study [11] found that lncRNA PVT1 was statistically increased in cardiac tissues of mice with cardiac hypertrophy. However, up to now, the mechanism of PVT1 in cardiomyocyte injury remains poorly understood.

Therefore, through the establishment of cardiomyocyte injury model, we inquired into the effect of lncRNA PVT1

on cardiomyocyte injury and its related mechanism, in order to provide more target directions for CVD prevention and treatment.

2. Materials and Methods

2.1. Culture and Modeling of Cells. At 37°C, cardiomyocyte H9c2 cells (Shanghai Cell Bank of Chinese Academy of Sciences) were placed in DMEM (Dulbecco's Modified Eagle Medium; Thermo Fisher Science, Inc., Waltham, MA, USA) with 10% FBS (fetal bovine serum; Gibco, Gran Island, NY, USA) and 100 μg/mL penicillin/streptomycin (Invitrogen, Thermo Fisher Scientific) and 5%CO_2 for incubation. Then, the cardiomyocytes were collected for transfection when the adherent growth reached 80% and classified into the hypoxia group and control group. In the hypoxia group, H9c2 cells were cultured with a mixture of 1% O_2, 94% N_2, and 5% CO_2 within a specified time, and those in control group shared the same culture conditions besides that the O_2 concentration was 21%.

2.2. Transfection of Cells. As to the small interfering RNAs (si-PVT1-#1, si-PVT1-#2, si-PVT1-#3) and the control siRNA (si-NC) of PVT1, they were all obtained from Shanghai GenePharma (Shanghai, China). MiR-214-3p mimic sequence (miR-214-3p-mimics), miR-214-3p targeted inhibition sequence (miR-214-3p-inhibitor), and miR negative control (miR-NC) were constructed by FitGene Co., Ltd. (Guangzhou, Guangdong, China). Strictly following the manufacturer's instructions, cells' transfection was performed with Lipofectamine™ 2000 kit (Invitgen, Carlsbad, CA, USA).

2.3. qRT-PCR. From tissues and cells, total RNA was separated with the aid of Trizol Reagent, and 5 μg of it was subjected to reverse transcriptional cDNA as instructed by the instructions. Finishing transcription, synthetic cDNA (1 μL) was processed for amplification. PCR reaction conditions (40 cycles) are as follows: 60 s predenaturation at 95°C, 40 s denaturation at 95°C, and 40 s extension anneal at 60°C. MiR-214-3p used U6 as a control, PVT1 used GAPDH as an internal reference, and $2^{-\triangle\triangle ct}$ was responsible for data analysis. See Table 1 for primer sequences.

2.4. Cell Proliferation Test. H9c2 cell viability was evaluated by CCK-8. 48 h after transfection, the cells were diluted to 3×10^5cells/mL and inoculated into 96-well plates (3000 cells/well) with 100 μL cells per well for culture in normal or hypoxic medium. Then, at 48 hours of culture, 10 μL CCK8 solution (10 μL, Sigma, SF, USA) was added for another 2 h of culture in the incubator at 37°C and 5% CO_2. With the aid of a microplate reader (Bio-Rad, Cal, USA), OD value at 450 nm was measured for cell proliferation determination and growth curve plotting. The experiment was conducted in triplicate.

2.5. Apoptosis Test. Finishing digestion with 0.25% trypsin, the cells were rinsed with PBS twice, immersed in binding buffer (100 μL) to rearrange to 1×10^6 cells/mL, and added with Annexin V-FITC and PI with 10 μL each successively for 5-minute culture at indoor temperature in dark place. Flow cytometry system was used for detection, and the experiment was conducted in triplicate to average the value.

2.6. Western Blotting. The total protein of HUVEC was obtained by using a RIPA lysis buffer (Cell Signal Technology, Danvers, MA, USA) containing protease inhibitors. The proteins were then separated by SDS-PAGE (10%) with sodium dodecyl sulfate-polyacrylamide gel electrophoresis and transferred to a PVDF membrane (MilliPore, Bilerika, Ma, USA). After sealing with 5% skimmed milk and TBST, it was cultivated all night long at 4°C with anti-Bcl-2 (1 : 500), Bax (1 : 500), cle-caspase-3 (1 : 500), or GAPDH(1 : 1000) (Abcam, Cambridge, Massachusetts, USA). Then, at indoor temperature, it was immersed in horseradish peroxidase-labeled goat anti-rabbit secondary antibody (1 : 1000; Wuhan Boster Biological Technology Co., Ltd.) for 1-hour culture, followed by 3 times of rinsing with PBS, 5 min each. In a dark room, development was carried out under the prerequisite that the excess liquid on the film was blotted with a filter paper and then illuminated by ECL to develop.

2.7. DLR Assay. The potential miRNAs that could bind to PVT1 was screened through the bioinformatics database starBase v2.0. Oligonucleotides containing PVT1 target sequences were then amplified and cloned into pmirGLO plasmid (WT). The wild type (Wt) and mutant (Mut) of pmirGLO-PVT1-3′UTR were established, respectively, and transferred to the downstream of the luciferase reporter gene for sequencing and identification of the constructed plasmids. By referring to the manufacturer's instructions, Lipofectamine 2000 (Invitrogen, Thermo Fisher Scientific, USA) was used to cotransfect the plasmids constructed above with miR-214-3p-mimcs and miR-NC into H9c2 cells. The luciferase activity after 48 hours of incubation was determined by dual luciferase assay system.

2.8. RIP Detection. As instructed by the guidelines, EZ-Magna RIP kit (Shanghai Advantage Biological Co., Ltd.) was utilized for RNA immunoprecipitation. From the culture plate, H9c2 cells were scraped and lysed in 100% RIP Lysis Buffer. Then, the cell extracts were left in the RIP buffer supplemented with magnetic beads, which could adsorb human anti-AGO2 antibody (1 : 2000, Abcam, USA). Finally, protease K was used for sample digestion and RNA extraction for WB analysis. Immunoglobulin G (IgG) (1 : 1000, Abcam, USA) was used as a negative control. Acquired from Thermo Fisher Scientific, NanoDrop spectrophotometer was used to detect RNA concentration, while RNA quality was analyzed by a Bioanalyzer obtained from Agilent Corporation, Santa Clara, California, USA. The experimental samples were repeated three times.

2.9. RNA Pull-down Assay. Biotin-labeled PVT1 (1 μg) was loaded into the Eppendorf (EP) test tube using magnetic RNA protein pull-down kit (Pierce, Rockford, IL, USA). Then, structural buffer was added for a 2-minute bath at 95°C and a 3-minute ice bath successively. After incubating 50 μL fully resuspended beads overnight in EP tube at 4°C,

Table 1: Primer sequences.

Gene	Upstream primer (5′-3′)	Downstream primer (5′-3′)
miR-214-3p	ACAGCAGGCACAGACAGG	GTGCAGGGTCCGAGGT
U6	AAAATTTCTCACGCCGGTATTC	CCTGCAGACCGTTCGTCAA
PVT1	GCCCCTTCTATGGGAATCACTA	GGGGCAGAGATGAAATCGTAAT
GAPDH	GGAGCGAGATCCCTCCAAAA	GGCTGTTGTCATACTTCTCATGG

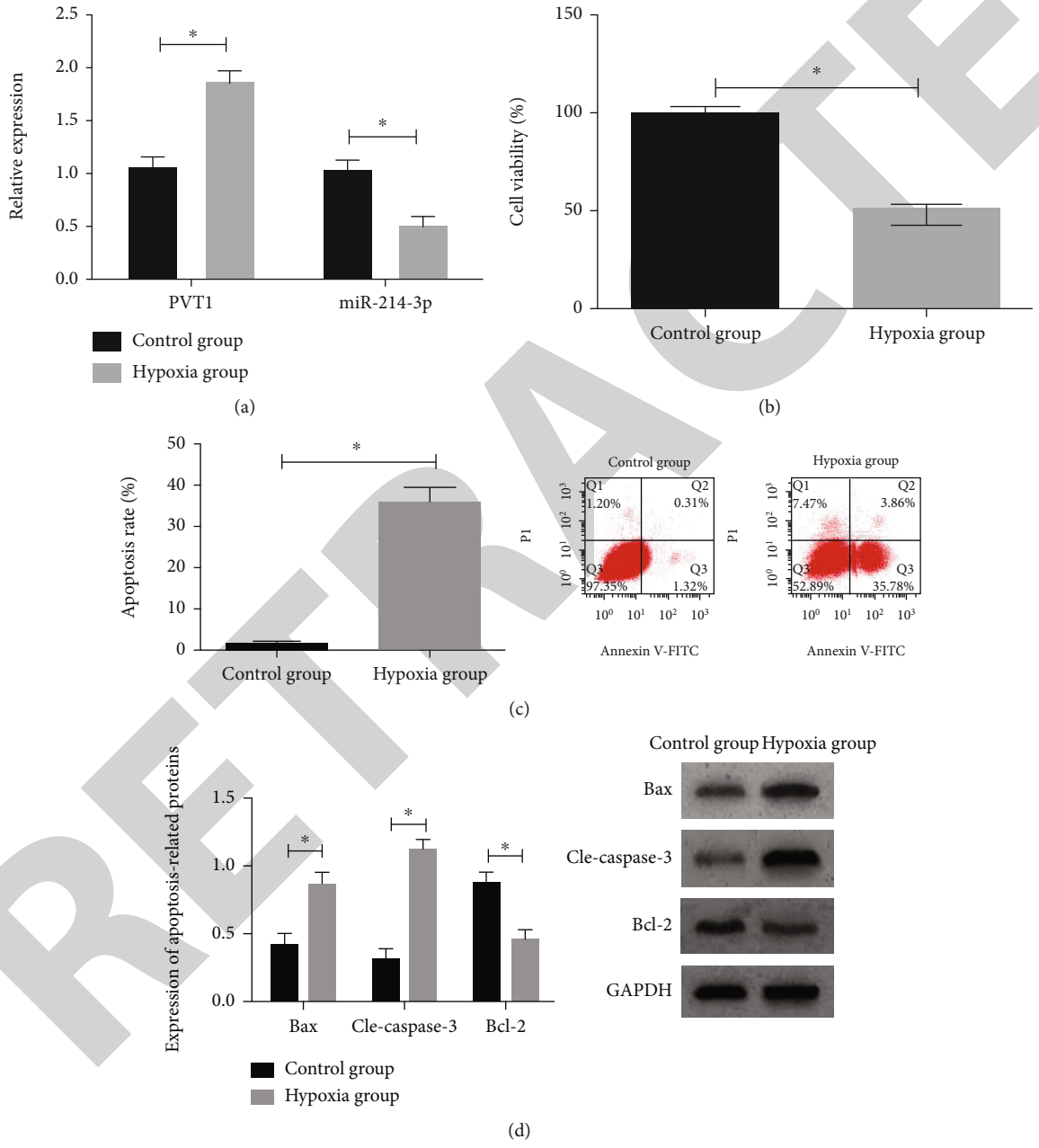

Figure 1: Hypoxia induced PVT1 upregulation in cardiomyocyte H9c2 cells. (a) PVT1 and miR-214-3p expression in H9c2 cells induced by hypoxia. (b) Survival rate of H9c2 cells induced by hypoxia. (c) Apoptosis rate of H9c2 cells induced by hypoxia. (d) Expression of apoptosis-related proteins in H9c2 cells induced by hypoxia. * indicated $P < 0.05$.

the beads were centrifuged at the speed of 1500 × g for 3 minutes to discard the supernatant and then rinsed with 500 μL RNA binding protein immunoprecipitation (RIP) washing solution for 3 times. After washing, they were added with 10 μL cell lysis buffer and left to stand for 1 h at indoor temperature. At low speed, the cultured bead-RNA-protein

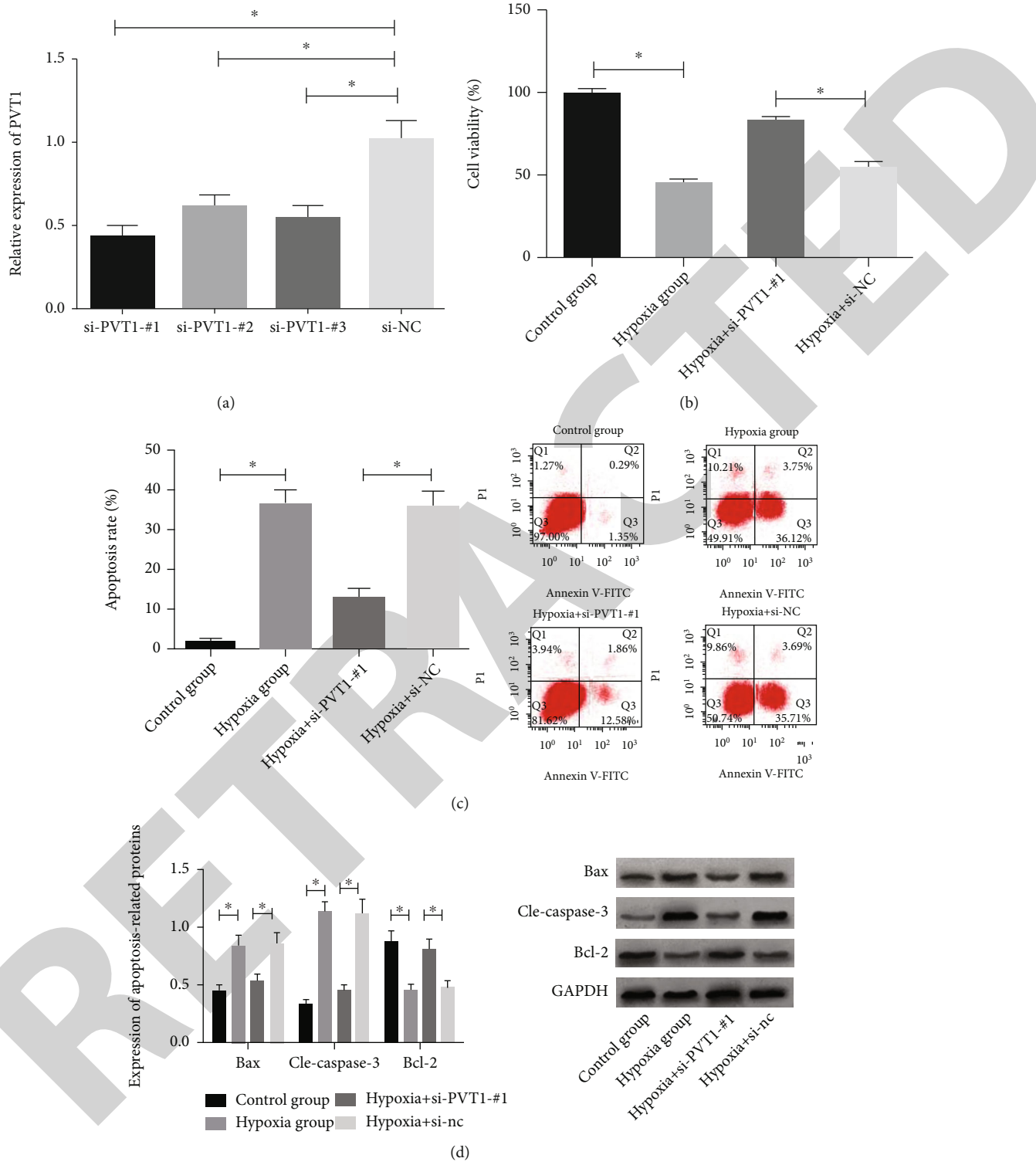

Figure 2: Knockdown of PVT1 alleviated hypoxia-induced cardiomyocyte injury. (a) Knockdown efficiency of PVT1 in cardiomyocytes. (b) Effects of PVT1 knockdown on the survival rate of hypoxic-induced cardiomyocytes. (c) Effects of PVT1 knockdown on the apoptosis rate of hypoxic-induced cardiomyocytes. (d) Effects of PVT1 knockdown on apoptosis-related proteins in hypoxic-induced cardiomyocytes. * indicated $P < 0.05$.

mixture was centrifuged, and the obtained supernatant was rinsed with 500 μL RIP washing buffer for three times after centrifugation. Finally, taking 10 μL cell lysate supernatant as the input protein, the protein expression profiles were determined by WB. The experiment was carried out in triplicate.

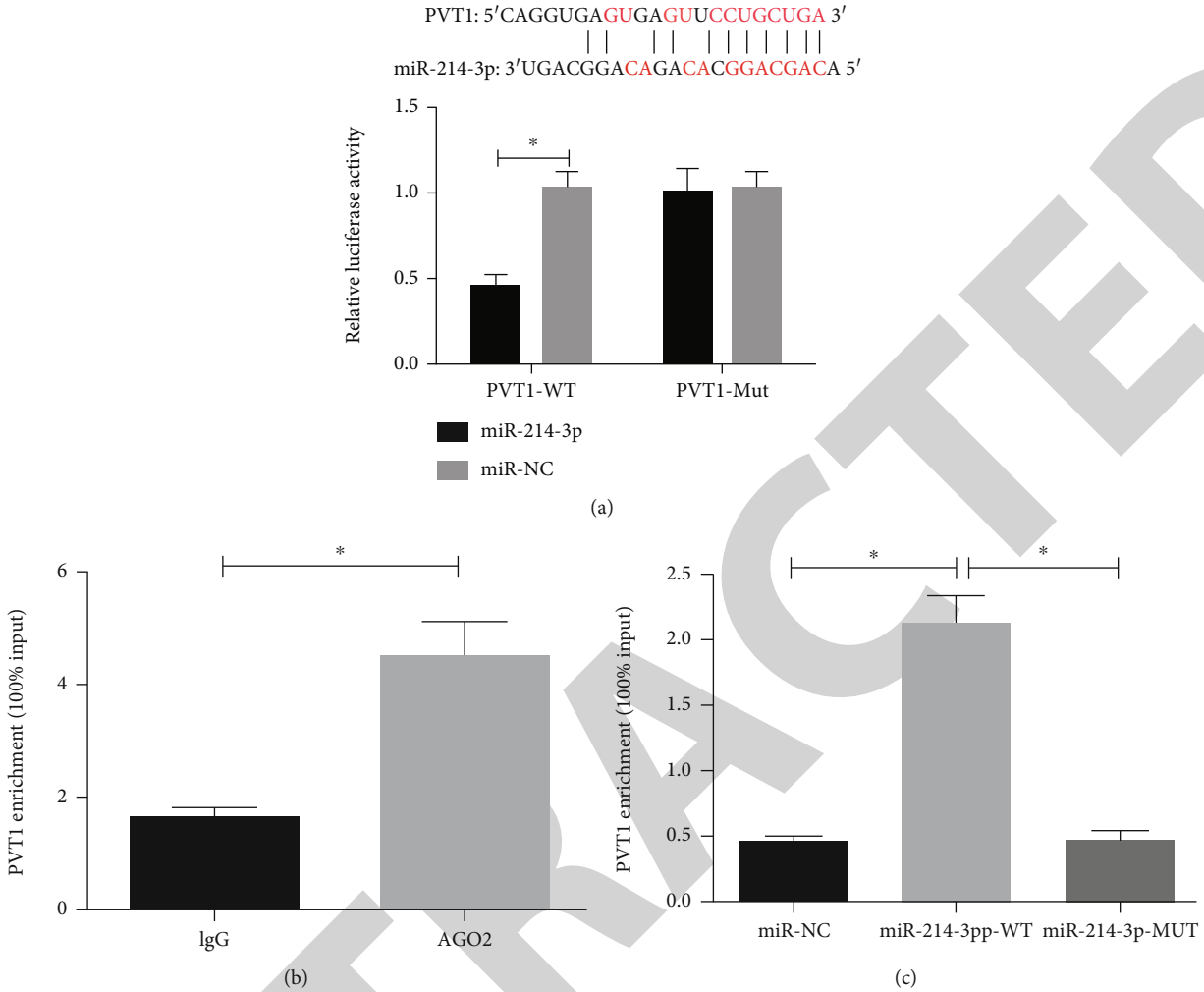

Figure 3: Relationship between PVT1 and miR-214-3p. (a) DLR confirmed that there was a binding relationship between PVT1 and miR-214-3p. (b) Enrichment ability of PVT1 and AGO2 evaluated by RIP assay. (c) Enrichment ability of PVT1 and miR-214-3p determined by RNA pull-down. * indicated $P < 0.05$.

2.10. Statistical Processing. SPSS19.0 and GraphPad 7 were employed for analysis and image rendering of the experimental data, respectively. Comparison between groups was performed by independent *t*-test, those among multiple groups were done by one-way ANOVA, and postpairwise comparisons were done by LSD-t. Multitime expression profiles were analyzed by repeated measures ANOVA, and post-hoc tests were conducted by Bonferroni. $P < 0.05$ indicated a statistically significant difference.

3. Results

3.1. Hypoxia Induced PVT1 Upregulation in Cardiomyocyte H9c2 Cells. When we established a model of H9c2 cell injury using hypoxia induction, PVT1 was found to be enhanced, and miR-214-3p was statistically declined in H9c2. The effect of hypoxia induction was evaluated by measuring the cell survival rate and the proportion of apoptotic cells. The survival rate of H9c2 cells was statistically reduced, and the apoptosis rate was statistically increased after hypoxia compared with control group. We further found that in hypoxia-induced H9c2 cells, apoptotic proteins Bax and CLE-Caspade-3 increased, while antiapoptotic protein Bcl-2 decreased. It is suggested that PVT1 may be related to H9c2 cell damage induced by hypoxia (Figure 1).

3.2. Knocking Down PVT1 Attenuated Hypoxia-Induced Cardiomyocyte Injury. Si-PVT1 was used to downregulate PVT1 to study PVT1's role in hypoxia-induced injury of H9c2 cells. According to transfection efficiency, the inhibition efficiency of si-PVT1-#1 transfection was the highest. Downregulation of PVT1 evidently lowered hypoxia-induced cell injury through increasing cell survival rate and reducing apoptosis rate. In addition, PVT1 downregulation suppressed apoptotic proteins Bax and cle-caspase-3 and elevated Bcl-2. It shows that downregulation of PVT1 can reduce hypoxic-induced cardiomyocyte injury (Figure 2).

3.3. PVT1 Could Sponge miR-214-3p. With the aim of further exploring the mechanism of the action of PVT1 on H9c2 cells, we predicted the potential miRs of PVT1 through starbase online and found that there were potential binding

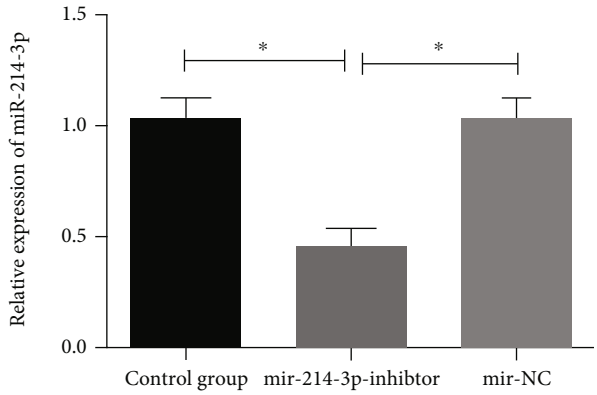

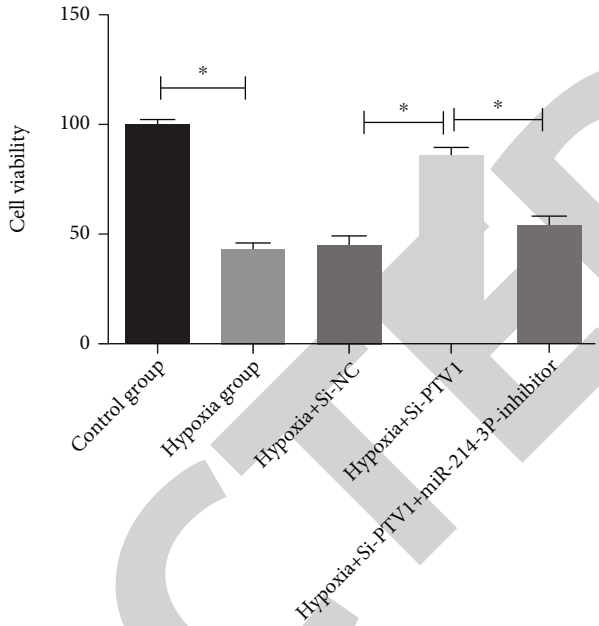

(a) (b)

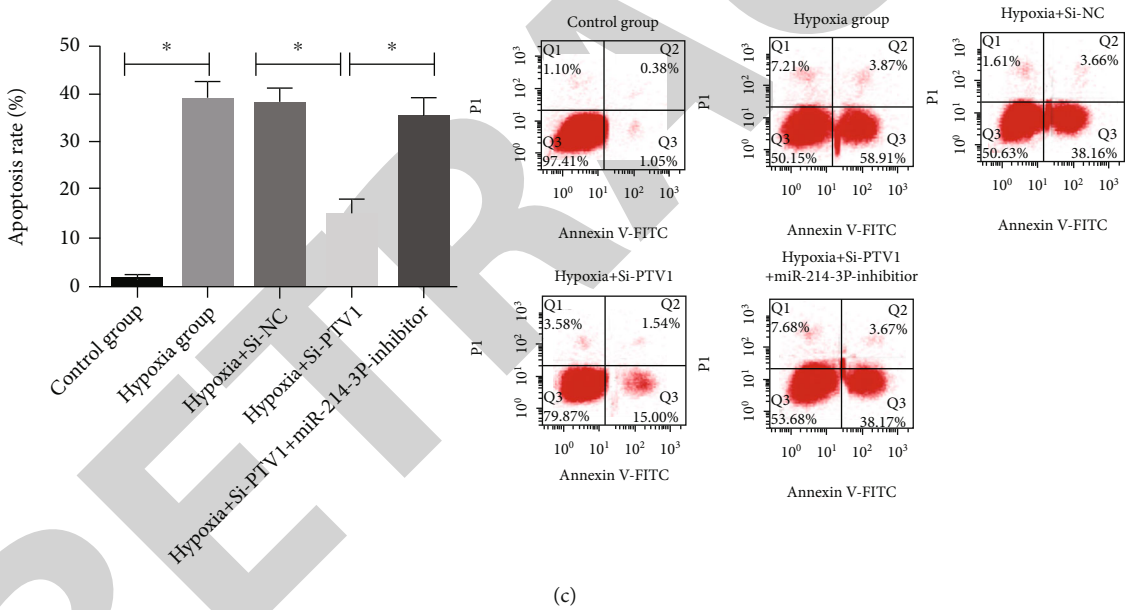

(c)

Figure 4: Continued.

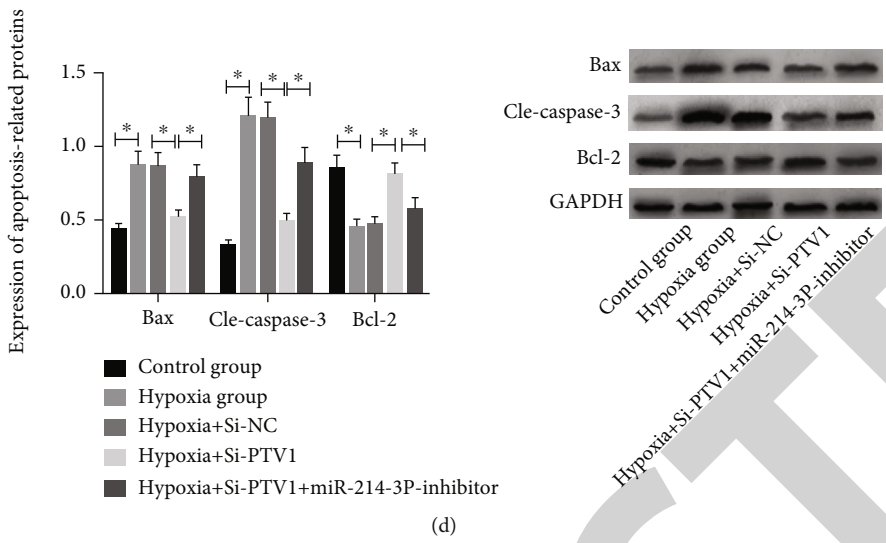

Figure 4: PVT1 sponge adsorption of miR-214-3p aggravated hypoxia-induced cardiomyocyte injury. (a) Inhibition efficiency of miR-214-3p in cardiomyocytes. (b) Effects of cotransfection of miR-214-3p-inhibitor and Si-PVT1 on viability of cardiomyocytes induced by hypoxia. (c) Effects of cotransfection of miR-214-3p-inhibitor and Si-PVT1 on the apoptosis rate of cardiomyocytes induced by hypoxia. (d) Effects of cotransfection of miR-214-3p-inhibitor and Si-PVT1 on apoptosis-related proteins in cardiomyocytes induced by hypoxia. * indicated $P < 0.05$.

targets between PVT1 and miR-214-3p, which were further verified by DLR, RIP test, and pull-down test. The dual luciferase reporter assay revealed miR-214-3p-mimics markedly suppressed PVT1-WT fluorescence activity. RIP assay identified that PVT1 and miR-214-3p levels precipitated by Ago2 antibody were statistically increased compared with IgG (Figure 3).

3.4. PVT1 Sponge Adsorption of miR-214-3p Aggravated Hypoxia-Induced Cardiomyocyte Injury. With the purpose of confirming whether PVT1 affected hypoxia-induced cardiotoxicity through sponge adsorption of miR-214-3p, we transfected miR-214-3p inhibitor into H9c2 cells and found that miR-214-3p was statistically inhibited. MiR-214-3p inhibitor statistically decreased the viability of H9c2 cells with PVT1 knockout and promoted apoptosis after cotransfecting miR-214-3p inhibitor plus Si-PVT1 into hypoxia-induced H9c2 cells. Similarly, miR-214-3p inhibitors downregulated Bcl-2 and promoted Bax and cle-caspase-3. It suggests that by sponging miR-214-3p, PVT1 aggravates hypoxia-induced cardiomyocyte injury. (Figure 4).

4. Discussion

The pathomechanism of CVD is a complex and multifactorial process. The primary mechanism of CVD is atherosclerosis. Inflammation in atherogenesis raises the risk of hypoxia, which will activate hypoxia-inducible factor-1α (HIF1A) [12, 13]. Tissue hypoxia seems to be one of the common features in cardiovascular disorders including atherosclerosis, vascular remodeling, and heart failure. In the hypoxic environment, each cell exhibits several types of responses at transcriptional, translational, or posttranslational levels. Most of the gene expressions are, at the transcriptional level, significantly suppressed in the hypoxic environment. In contrast, the expression of a group of genes is significantly enhanced in hypoxia, including hypoxia-inducible genes [12]. At present, how to improve hypoxia-induced cardiomyocyte injury is also a hot research direction. It has been proposed that some intracellular proteins, such as protein kinase [14] and heat stress protein [15], can be used to provide endogenous myocardial protection against hypoxia induced cardiomyocyte injury, whereas clinically understanding the mechanism of hypoxic cardiomyocytes injury is of the essence for the treatment of CVDs.

LncRNA, as a popular noncoding RNA in recent years, has also been extensively studied in the treatment of CVDs [16]. For example, a study [17] found that inhibiting lncRNA NEAT1 could reduce hypoxia-induced cardiomyocyte injury through sponging miR-378a-3p. However, few studies have investigated the role and mechanism of lncRNA PVT1 in hypoxic cardiomyocyte injury. In our study, we first observed a significant decrease in survival rate of hypoxic-induced cardiomyocytes and a significant increase in apoptosis rate, suggesting that PVT1 may be related to hypoxia-induced cardiomyocyte injury. In the study of Sun et al. [18], PVT1 was highly expressed in patients with heart failure, which was in line with our results. Then, for the purpose of further analyzing PVT1's effect on hypoxia-induced cardiomyocytes, we knocked down PVT1. The results showed that when PVT1 in hypoxia-induced injury cardiomyocytes was knocked down, the cell survival rate was statistically improved, and the apoptosis rate was statistically decreased, suggesting that the injury of cardiomyocytes was improved. Currently, the role of PTV1 in hypoxia-induced cardiomyocyte injury has not been explored. Although here we have found for the first time that inhibition of PTV1 can improve hypoxia-induced cardiomyocyte injury, the specific downstream mechanism remains unknown.

It is well known that LncRNA may play a role of molecular sponge in regulating miRNA expression and biological function [19]. This also provides new insights into exploring the downstream molecular mechanism of PVT1 on hypoxia-induced cardiomyocyte injury. Increasing evidence has confirmed the role of miRNAs in CVDs. Zhang et al. [20] revealed that miR-27 reduced hypoxia/reoxygenation induced cardiomyocyte injury by targeting TGFBR1 and inhibiting NF-κB pathway. Ma et al. [21] found that by targeting PDCD4, miR-532-5p could reduce hypoxia-induced cardiomyocyte apoptosis. Subsequently, we found through the prediction of biological information that there were shared sites between PTV1 and miR-214-3p. It is reported [22] that the lack of miR-214-3p aggravates cardiac fibrosis. There is also evidence [23] showing that miR-214-3p is linked with cardiomyocyte apoptosis in diabetic cardiomyopathy. In our study, miR-214-3p declined statistically in hypoxia-induced cardiomyocytes, and subsequently, DLR, RIP, and pull-down experiments verified that PVT1 can directly bind miR-214-3p, which suggested that PVT1 played its role in hypoxia-induced cardiomyocyte injury through sponging miR-214-3p. Finally, to further prove the targeting effect of PVT1 on miR-214-3p, cotransfection of miR-214-3p inhibitor and Si-PVT1 was conducted on hypoxia-induced H9c2 cells. It was observed that miR-214-3p inhibitor statistically inhibited the viability of PVT1 knock-out H9c2 cells and promoted apoptosis, which further proved that PVT1 could affect hypoxia-induced cardiomyocyte by through sponging miR-214-3p.

Recently, the crosstalk between miRNAs and long noncoding RNA (lncRNA) has attracted increasing attention leading to the identification of new regulatory networks (reviewed by Ballantyne et al. and Yoon et al. [24]). An example of such crosstalk is the interaction between lncRNA MiR143HG and miR-143/145: the focus of this review. Mir-143/145 is a vascular-enriched miRNA cluster, fairly extensively studied in vascular biology and in the pathophysiology of cardiovascular disease [25–30]. This microRNA cluster was shown to be encoded in a bicistronic unit [30] located downstream of the lncRNA MiR143HG, host gene of the miR-143 miRNA. Notably, the structure, the expression, and the function of lncRNAs have gained increasing attention, resulting in rapid progression in the understanding of their potential importance.

In addition, previous findings suggested that silencing of PVT1 improved spatial learning and memory, decreased neuronal loss, the number of TUNEL-positive cell, and the expression of cleaved-caspase-3 and Bax while increased the procaspase-3 and Bcl-2 expression in hippocampus tissues in epileptic rats. Furthermore, silencing of PVT1 decreased the expression of axin and cyclin D1 in hippocampus tissues in epileptic rats [31].

In summary, lncRNA PVT1 can play a role in hypoxia-induced cardiomyocyte injury by sponging miR-214-3p, which is a feasible biological biomarker for diagnosing and treating CVDs. However, our study is limited by the small sample size. In addition, the function of PVT1 in CKD and the molecular mechanism remain unclear. Further study is necessary to find the optimal hypoxic pattern of different cell types. Understanding the mechanism of lncRNA PVT1 would undoubtedly provide important insight into its role in CVDs and provide potential approaches to regulate its expression, including sirRNA or gene editing.

Data Availability

The authors confirm that the data supporting the findings of this study are available within the article.

Conflicts of Interest

The authors declare that they have no conflict of interest.

Authors' Contributions

Chuanliang Liu and Jieqiong Zhang performed the experiments, analyzed data, and wrote the manuscript. Xuejie Lun and Lei Li designed the study. All the authors agreed to be accountable for the accuracy and integrity of all aspects of the research.

References

[1] L. Johnson Jason, "Elucidating the contributory role of microRNA to cardiovascular diseases (a review)," *Vascular Pharmacology*, vol. 114, pp. 31–48, 2019.

[2] I. Rabinovich-Nikitin, B. Lieberman, T. A. Martino, and L. A. Kirshenbaum, "Circadian-Regulated Cell Death in Cardiovascular Diseases," *Circulation*, vol. 139, no. 7, pp. 965–980, 2019.

[3] S. E, M. C. Costa, S. Kurc, A. Drożdż, N. Cortez-Dias, and F. J. Enguita, "The circulating non-coding RNA landscape for biomarker research: lessons and prospects from cardiovascular diseases," *Acta Pharmacologica Sinica*, vol. 39, no. 7, pp. 1085–1099, 2018.

[4] Q. Cheng, J. Gu, B. K. Adhikari, L. Sun, and J. Sun, "Is CD47 a potentially promising therapeutic target in cardiovascular diseases? – Role of CD47 in cardiovascular diseases," *Life Sciences*, vol. 247, 2020.

[5] P. J. Hohensinner, N. Takacs, C. Kaun et al., "Urokinase plasminogen activator protects cardiac myocytes from oxidative damage and apoptosis via hOGG1 induction," *Apoptosis*, vol. 22, no. 8, pp. 1048–1055, 2017.

[6] J. Zhao, M. Yin, H. Deng et al., "Cardiac Gab1 deletion leads to dilated cardiomyopathy associated with mitochondrial damage and cardiomyocyte apoptosis," *Cell Death & Differentiation*, vol. 23, no. 4, pp. 695–706, 2016.

[7] Y.-W. Hu, F.-X. Guo, Y.-J. Xu et al., "Long noncoding RNA NEXN-AS1 mitigates atherosclerosis by regulating the actin-binding protein NEXN," *The Journal of Clinical Investigation*, vol. 129, no. 3, pp. 1115–1128, 2019.

[8] X. Guo, X. Wu, Y. Han, E. Tian, and J. Cheng, "LncRNA MALAT1 protects cardiomyocytes from isoproterenol-induced apoptosis through sponging miR-558 to enhance ULK1-mediated protective autophagy," *Journal of Cellular Physiology*, vol. 234, no. 7, pp. 10842–10854, 2019.

[9] C. Feng, Q. Sun, W. Chen, Y. Bai, D. Hu, and X. Xie, "The neuroprotective mechanisms of ginkgolides and bilobalide in cerebral ischemic injury: a literature review," *Molecular Medicine*, vol. 25, no. 1, 2019.

Hindawi
BioMed Research International
Volume 2021, Article ID 8171236, 9 pages
https://doi.org/10.1155/2021/8171236

Research Article

Screening of Parkinson's Differential MicroRNA Based on GEO Database and Its Clinical Verification

Xuping Jiang,[1] Lili Xiao,[1] Xumei Jiang,[2] Guangsheng Li,[1] and Zhijuan Lu[1]

[1]*Department of Neurology, Ganzhou People's Hospital, Ganzhou 341000, Jiangxi Province, China*
[2]*Department of Pharmacy, Ganzhou Fifth People's Hospital, Ganzhou 341000, Jiangxi Province, China*

Correspondence should be addressed to Zhijuan Lu; luannai076930266@163.com

Received 2 July 2021; Revised 18 October 2021; Accepted 19 October 2021; Published 13 November 2021

Academic Editor: Jun Yang

Objective. This study is set out to explore the potential difference of miR in PD through GEO data and provide diagnostic indicators for clinical practice. *Methods*. In this study, differential miR was screened through the Gene Expression Omnibus (GEO) database, 68 PD patients treated in our hospital from May 2017 to March 2018 were collected as the research group (RG), and 50 normal subjects who underwent physical examination in our hospital during the same period were collected as the control group (CG). Quantitative real-time polymerase chain reaction (qRT-PCR) was used to detect the expression and diagnostic value of miR-374a-5p in serum of patients. The potential target genes of miR-374a-5p were predicted, and Kyoto Encyclopedia of Genes and Genomes (KEGG) analysis and Gene Ontology Consortium (GO) were carried out. *Results*. GEO2R analysis revealed that 193 miRs are expressed differentially, of which 78 were highly expressed and 115 were poorly expressed. The miR-374a-5p expression in the serum of the RG was reduced markedly and had a diagnostic value. Targetscan and miRDB online websites were used to predict their target genes, with 415 common target genes. miR-374a-5p may participate in 27 functional pathways and 8 signal pathways. *Conclusion*. miR-335-5p has low expression in PD and is expected to be a potential diagnostic indicator.

1. Introduction

Parkinson's disease (PD) is the second clinically common neurodegenerative disease after Alzheimer's disease, characterized by gradual loss of dopaminergic neurons in the substantia nigra [1, 2]. Statistics reveal that [3, 4] patients over 60 years old have one PD patient per 800-1000 people, and the incidence of that line is higher than that of women. At present, the relevant mechanism of PD is not clear. Studies have found that [3] PD may be caused by deletion of SNCA and PINK1 genes. However, this disease is sporadic, and its pathogenesis involves environment, epigenetic, etc. In addition, it has a long latent period, the early stage of the disease has no great influence on patients, and the lack of medical knowledge leads to their admission to enter the middle and late stages [5, 6]. With the continuous improvement of the medical level in recent years, PD prevention has been popularized, but patients' daily life will be seriously affected in the middle and late stages of the disease [7].

MicroRNA (miR) is a short-chain noncoding RNA with a length of 20-25 nucleotides [8]. Studies show that [9, 10] miR can regulate downstream target genes by regulating the $3'$ untranslated region of downstream target gene mRNA. Previous studies have found that miR is involved in the occurrence and development of various diseases such as tumors, cardiovascular diseases, and neurological diseases [11–13]. Some studies have revealed that there are differential expression levels of various miRs in PD. For example, some studies have found that the miR-221 expression in the serum of [14] PD patients reduces, which is expected to become a potential diagnostic indicator of PD. Other studies have found that [15] miR-155 can regulate the inflammatory response of the Parkinson's disease model induced by α-synuclein. The GEO database is one of the largest public chip databases in the world [16], which

contains gene chips for various diseases. We have found that there are many differences in miR through analysis of the chips in the database this time, but it has not been clinically verified.

Therefore, in this research, we explored the differential genes in expression profile dataset GSE16658 and carried out clinical verification to find potential observation indicators for clinical use.

2. Materials and Methods

2.1. Patient Data. Sixty-eight PD patients treated in our hospital from May 2017 to March 2018 were collected as the research group (RG), and another 50 normal patients who underwent physical examination in our hospital during the same period were collected as the control group (CG). There was no statistical difference between the two groups in age and gender. This study was approved by the Medical Ethics Committee of our hospital. Inclusion criteria include patients who met Parkinson's diagnostic criteria and those who met Hoehn and Yahr (H&Y) staging criteria [17]. Patients and their families were informed, and they all signed an informed consent form. Exclusion criteria include patients who were secondary or iatrogenic PD, who passed the mini-mental state examination (MMSE) score, and who had renal insufficiency, multiple tumors, and stroke.

MMSE refers to the test that measures global cognitive functioning on domains that include memory, attention, language, praxis, and visuospatial ability. The summed scores of MMSE ranged from 0 to 30, with higher values denoting better cognitive function.

2.2. GEO Chip Analysis. We checked Parkinson's disease microRNA-related chips by logging into the Gene Expression Omnibus (GEO) database (https://www.ncbi.nlm.nih.gov/gds) and selected GSE16658 for analysis. The miRNA expression dataset GSE16658 was downloaded from the National Center for Biotechnology Information GEO database (http://www.ncbi.nlm.nih.gov/geo). In the GSE16658 dataset, expression profiles were obtained from peripheral blood mononuclear cells from patients with PD and normal controls and were quantified using the miRCURY LNA microRNA Array, v.10.0-hsa, mmu & rno (Exiqon A/S, Vedbæk, Denmark). The analysis was performed by GEO2R software built in the GEO database. miRs with the top 10 differences were selected for heat mapping. The chip data are shown in Table 1.

2.3. Collection of Test Samples. We collected 5 mL of peripheral venous blood from people in the two groups and then subpacked it to the blood collection tube (5 mL) of inert separation gel and coagulant. Then, it was centrifuged at 3000 rpm for 10 min at 24°C to collect part of serum for subsequent experiments, and the surplus part was placed in an EP tube without RNA enzyme for later use at -80°C.

2.4. Quantitative Real-Time Polymerase Chain Reaction (qRT-PCR) Detection. Total RNA was extracted from the collected serum by the TRIzol kit (Invitrogen Company, USA), and its purity, concentration, and integrity were detected by ultraviolet spectrophotometer and agarose gel electrophoresis. Subsequently, reverse transcription was carried out using the TaqMan™ reverse transcription kit (Invitrogen Company, USA), and the transcription steps were strictly operated according to the kit instructions. The obtained cDNA was subjected to subsequent research. PCR amplification was carried out using the PrimeScript RT Master Mix kit (Takarabo Company, Japan). The amplification system was as below: 10 μL SYBR qPCR Mix, 0.8 μL for upstream and downstream primers, 2 μL cDNA product, 0.4 μL 50x ROX reference dye, and RNase-free water supplemented to 20 μL. PCR reaction conditions were as below: 95°C predenaturation for 60 s, 95°C denaturation for 30 s, and 60°C annealing extension for 40 s, with a total of 40 cycles. In the experiment, three parallel repeating holes were designed, and all specimens were repeatedly tested 3 times. miR used U6 as the internal reference and used $2^{-\Delta\Delta ct}$ to analyze the data [18]. The PCR instrument was 7500PCR instrument from ABI Company.

Table 1: Baseline data.

Data	GSE16658
Time	
Submission date	Jun 17, 2009
Last update date	Jan 13, 2016
Contact name	Sofia A Oliveira
Address	
Organization name	Instituto de Medicina Molecular
Department	Edificio Egas Moniz
Street address	Av. Prof Egas Moniz
City	Lisbon
Country	Portugal
ZIP/postal code	1649-028
Organism	Homo sapiens
Experiment type	Noncoding RNA profiling by array
Platforms	GPL7722, miRCURY LNA microRNA Array, v.10.0-hsa, mmu & rno

2.5. Bioinformatics Analysis. The online target gene prediction website was used to predict the target gene, and then, the clusterProfiler package in R software was used to carry out Kyoto Encyclopedia of Genes and Genomes (KEGG) analysis and Gene Ontology Consortium (GO) and draw pictures.

2.6. Statistical Analysis. In this study, the SPSS20.0 software package was used to carry out statistical analysis on the collected data. GraphPad Prism 7 was used to draw the data picture. The usage (%) of the counting data was confirmed by the chi-squared test and expressed by χ^2. The K-S test was employed to analyze the data distribution. The measurement data were expressed by the mean ± standard deviation (means ± SD). The comparison of normal distribution data between the two groups was conducted by the independent-samples t-test, which was expressed by t. ROC was used to

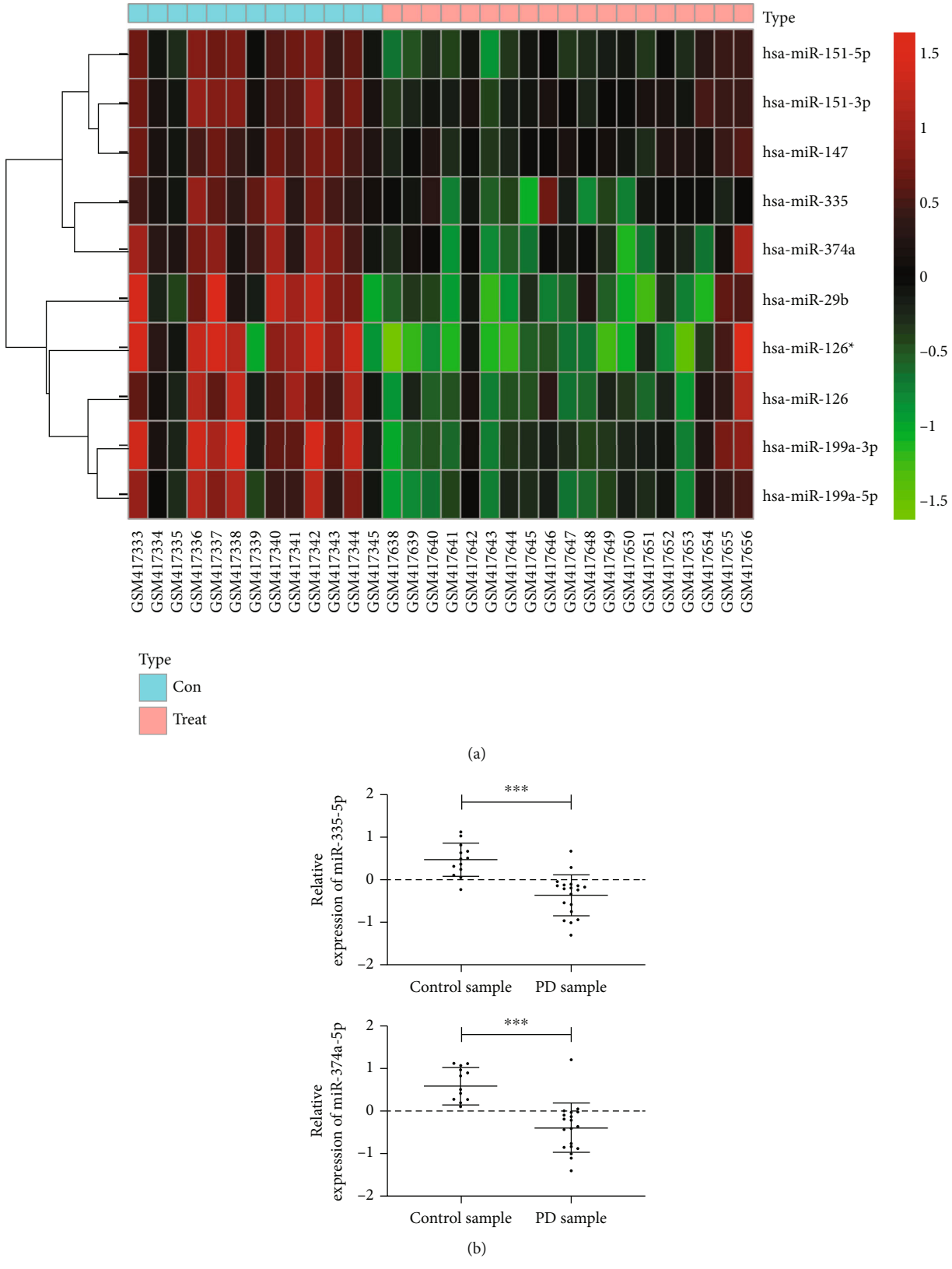

Figure 1: miR with top 10 differences in GSE16658 chip. (a) miR with significant differences in the top 10. (b) Expression of miR-335-5p and miR-374a-5p. *** indicates $p < 0.001$. A p value lower than 0.001 was statistically different.

Table 2: Top 10 differences of miR.

miRNA	Adjusted p value	p value	t value	β	log FC
miR-335	$1.730E-03$	$8.720E-06$	-5.261	3.540	-0.831
miR-374a	$1.730E-03$	$9.140E-06$	-5.245	3.498	-0.978
miR-199a-3p	$1.750E-03$	$1.650E-05$	-5.044	2.961	-1.126
miR-126*	$1.750E-03$	$2.234E-05$	-4.941	2.686	-1.593
miR-151-3p	$1.750E-03$	$2.320E-05$	-4.928	2.652	-0.614
miR-199a-5p	$1.750E-03$	$2.769E-05$	-4.868	2.491	-0.951
miR-151-5p	$2.070E-03$	$4.702E-05$	-4.687	2.010	-0.719
miR-126	$2.070E-03$	$4.713E-05$	-4.686	2.008	-0.985
miR-29b	$2.070E-03$	$4.915E-05$	-4.672	1.969	-1.236
miR-147	$2.130E-03$	$6.340E-05$	-4.584	1.738	-0.496

Note: log FC: fold change.

analyze the diagnostic value of miR-374a-5p in PD. A p value lower than 0.05 was statistically different.

3. Results

3.1. Analysis of Chip Results. Through analysis by online analysis software GEO2R, we found 193 miRs with differences, including 78 with high expression and 115 with low expression. We selected the top 10 miRs for display and combined the references and adjusted differences. Finally, we selected miR-335-5p and miR-374a-5p for further research. More details are shown in Figure 1 and Table 2.

3.2. Expression of miR-335-5p and miR-374a-5p in PD Patients. We detected the miR-335 and miR-374a-5p expression in the serum of patients. The results revealed that the miR-335-5p expression in the serum of the RG was not different from that in the CG, while the miR-374a-5p expression in the serum of patients reduced remarkably. Furthermore, we found that miR-374a-5p had a certain clinical value in the diagnosis of PD by drawing ROC curve analysis, and the area under the curve was 0.820. More details are shown in Figure 2.

3.3. Relationship between miR-374a-5p and H&Y Stage. We divided patients into three stages according to the H&Y stage, namely, the first stage (H&Y stage: 1-2, $n = 30$), the second stage (H&Y stage: 3-4, $n = 25$), and the third stage (H&Y stage: 5, $n = 13$). We further detected the miR-374a-5p expression in patients of different stages and explored that miR-374a-5p was differentially expressed in the three stages. The ROC curve analysis displayed that miR-374a-5p had high clinical value in distinguishing patients at different stages. More details are shown in Figure 3 and Table 3.

3.4. Bioinformatics Analysis. In order to further explore the relevant mechanism of miR-374a-5p, we predicted its target genes through the online websites of Targetscan and miRDB. The results demonstrated that 415 common target genes existed. To further determine its potential mechanism, we employed the R software clusterProfiler package for GO and KEGG enrichment analysis. The results exhibited that miR-374a-5p might participate in 27 functional pathways and 8 signal pathways. More details are shown in Figure 4 and Tables 4 and 5.

4. Discussion

PD is a serious nervous system disease. The gradual loss of dopaminergic neurons in substantia nigra is one of the primary causes of PD [19]. What is more, due to the long incubation period of PD, patients are not clear about its early symptoms, which leads to PD patients being in the middle and late stages, thus causing them to miss the best treatment period [20]. Therefore, we urgently need to explore the relevant mechanism of PD.

In recent years, more and more studies have found a close relationship between miR and PD. For instance, Ma and others [21] pointed out that serum miR-221 could be used as a biomarker of Parkinson's disease. Other studies have discovered that [22] inhibition of miR-34b and miR-34c enhances the α-synuclein expression in Parkinson's disease, thus improving the disease condition. All the above studies signify that miR is involved in the occurrence and development of PD. In order to better screen potential PD differences of miR, we analyzed based on PD chips in the GEO database and found significant differences between miR-335-5p and miR-374a-5p, and the differences between the two after correction were the same, so we chose them for research.

Previous studies on miR-335-5p, miR-374a-5p, and PD are very few. To verify the expression and value of the two miRs in PD, we tested them. As a result, we found that there was no difference in the miR-335-5p expression in the serum of PD patients, while the miR-374a-5p slashed. Moreover, we also plotted the ROC curve and verified that miR-374a-5p had a high clinical value in distinguishing PD from normal people. Previous studies have found that miR-374a-5p is expressed in breast cancer, esophageal cancer, colon cancer, and other tumors and participates in the occurrence and development of tumors through relevant mechanisms [23–25]. This study was the first time we found that miR-374a-5p was differentially expressed in PD. To

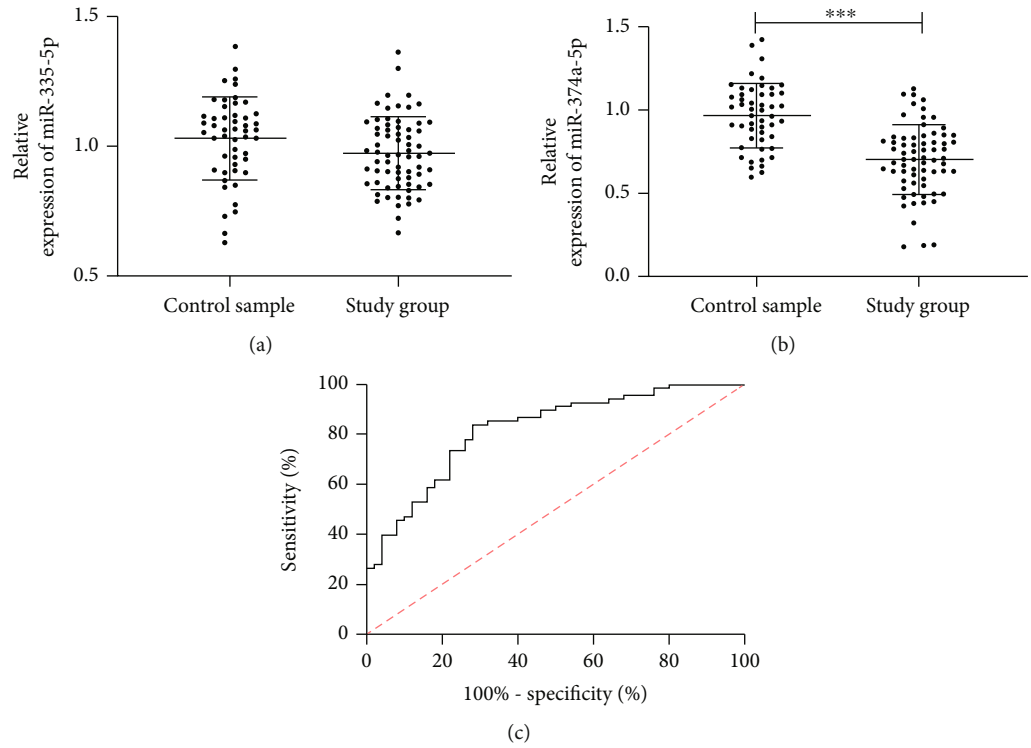

Figure 2: Expression and diagnostic value of miR-335-5p and miR-374a-5p in PD. (a) Expression of miR-335-5p in PD patients. (b) Expression of miR-374a-5p in PD patients. (c) ROC curve of miR-374a-5p in diagnosis of PD. *** indicates $p < 0.001$. A p value lower than 0.001 was statistically different.

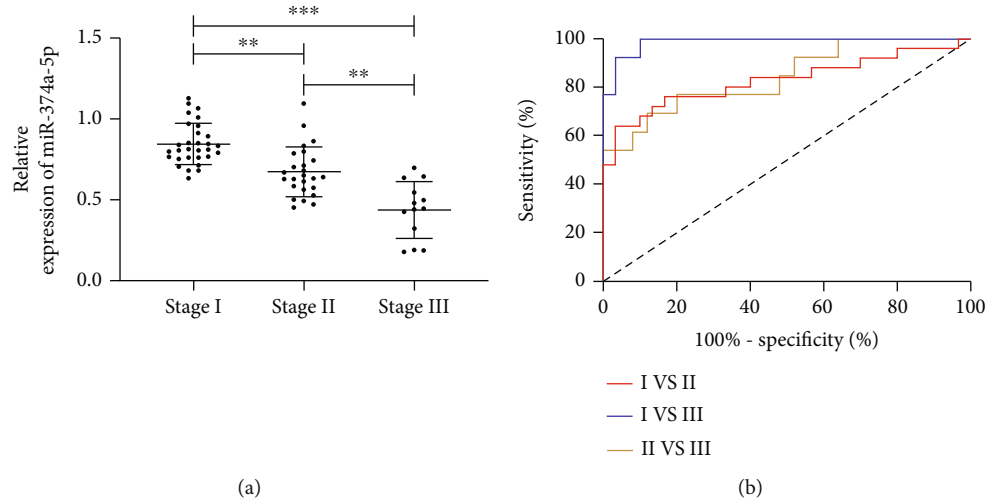

Figure 3: Relationship between miR-374a-5p and H&Y stage. (a) Expression of miR-374a-5p in different stages. (b) Diagnostic value of miR-374a-5p in distinguishing different stages.

Table 3: ROC parameters.

Factor	AUC	95% CI	Specificity	Sensitivity	Youden index	Cut-off
I vs. II	0.828	0.709-0.947	96.67%	64.00%	60.67%	0.680
I vs. III	0.987	0.963-1.000	90.00%	100.00%	90.00%	0.700
II vs. III	0.843	0.705-0.981	88.00%	69.23%	57.23%	0.498

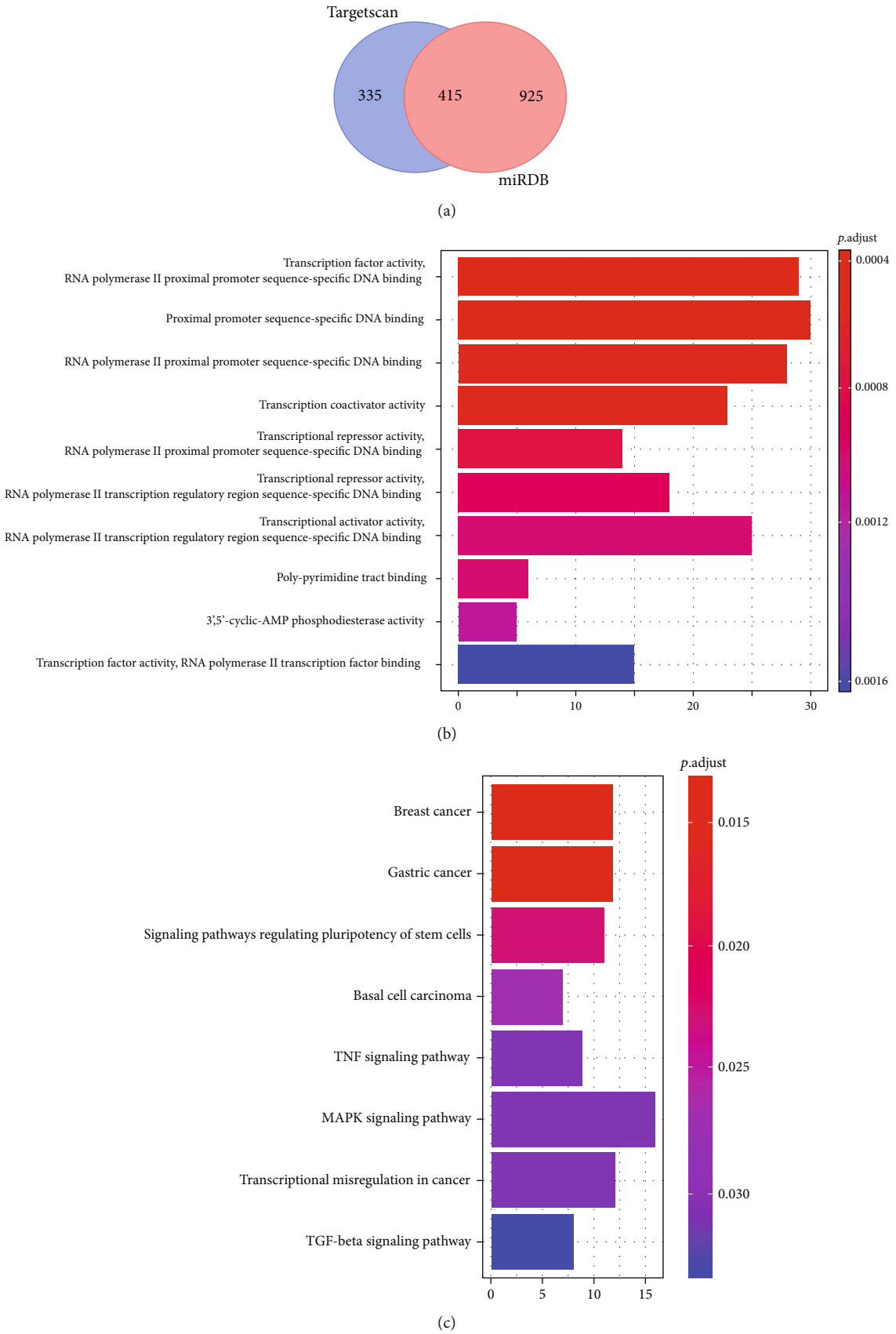

Figure 4: Prediction and functional analysis of miR-374a-5p target gene. (a) miR-374a-5p target genes were predicted jointly by Targetscan and miRDB. (b) Top 10 functional pathways for GO enrichment. (c) Signal pathway for KEGG enrichment.

Table 4: Top 10 terms for GO enrichment.

ID	Description	p value	Gene ID	Count
GO:0000982	Transcription factor activity, RNA polymerase II proximal promoter sequence-specific DNA binding	$2.872E-05$	MEF2D, MECP2, HES1, DACH1, EN1, NFIL3, ZBTB20, NR3C1, PITX2, RORB, ZNF281, HOXA10, NEUROD1, NR4A3, BCL11B, GABPA, GATA3, KLF8, SP1, MYT1L, ATF2, MSX1, BHLHE40, SP3, FOSB, RFX4, ASCL1, CEBPB, ONECUT2	29
GO:0000987	Proximal promoter sequence-specific DNA binding	$2.872E-05$	MEF2D, HES1, RFX3, EN1, NFIL3, NR3C1, PITX2, RORB, ZNF281, ZNF516, HOXA10, NEUROD1, NR4A3, BCL11B, GABPA, GATA3, CHD7, KLF8, SP1, ATF2, NEUROG2, BHLHE40, SP3, FOSB, RFX4, ASCL1, NKX2-2, CEBPB, ONECUT2, SMAD6	30
GO:0000978	RNA polymerase II proximal promoter sequence-specific DNA binding	$1.024E-04$	MEF2D, HES1, RFX3, EN1, NFIL3, NR3C1, PITX2, RORB, ZNF281, HOXA10, NEUROD1, NR4A3, BCL11B, GABPA, GATA3, CHD7, KLF8, SP1, ATF2, NEUROG2, BHLHE40, SP3, FOSB, RFX4, ASCL1, CEBPB, ONECUT2, SMAD6	28
GO:0003713	Transcription coactivator activity	$1.024E-04$	ACTN4, TAF5L, TAF4B, RNF14, HCFC1, PPARGC1A, PITX2, RORB, NEUROD1, KAT6A, SP4, GABPA, GATA3, RORA, TFDP1, JMY, ATF2, TCERG1, MED13, NCOA1, MED12L, ACTN1, NKX2-2	23
GO:0001078	Transcriptional repressor activity, RNA polymerase II proximal promoter sequence-specific DNA binding	$3.497E-04$	MECP2, HES1, DACH1, EN1, NFIL3, ZBTB20, ZNF281, GATA3, KLF8, MYT1L, BHLHE40, SP3, ASCL1, CEBPB	14
GO:0001227	Transcriptional repressor activity, RNA polymerase II transcription regulatory region sequence-specific DNA binding	$4.575E-04$	MECP2, HES1, DACH1, EN1, FOXD3, NFIL3, ZBTB20, ZNF281, MLX, GATA3, KLF8, ZC3H8, MYT1L, MSX1, BHLHE40, SP3, ASCL1, CEBPB	18
GO:0001228	Transcriptional activator activity, RNA polymerase II transcription regulatory region sequence-specific DNA binding	$5.664E-04$	MEF2D, HOXA1, HCFC1, NR3C1, PITX2, RORB, HOXA10, PKNOX1, NEUROD1, NR4A3, BCL11B, GBX2, GABPA, FOXD2, GATA3, RORA, TFDP1, SP1, ATF2, MSX1, ETV5, FOSB, RFX4, CEBPB, ONECUT2	25
GO:0008187	Poly-pyrimidine tract binding	$5.664E-04$	PNPT1, UHMK1, IFIT5, MSI2, ATXN1, PABPC1	6
GO:0004115	$3',5'$-Cyclic-AMP phosphodiesterase activity	$7.791E-04$	PDE4D, PDE3A, PDE7B, PDE10A, PDE8B	5
GO:0001076	Transcription factor activity, RNA polymerase II transcription factor binding	$1.373E-03$	NR3C1, PPARGC1A, PITX2, RORB, NEUROD1, GBX2, RORA, ATF2, TCERG1, MED13, NCOA1, BHLHE40, ARHGAP5, CDC73, MED12L	15

Table 5: KEGG enrichment terms.

ID	Description	p value	Gene ID	Count
hsa05224	Breast cancer	0.013	HES1, WNT3, WNT5A, WNT16, GADD45A, SP1, FZD5, FGF18, NCOA1, FGF5, AKT1, APC	12
hsa05226	Gastric cancer	0.013	WNT3, FGFR2, WNT5A, WNT16, GADD45A, FZD5, FGF18, CCNE2, FGF5, AKT1, APC, HGF	12
hsa04550	Signaling pathways regulating pluripotency of stem cells	0.020	WNT3, FGFR2, WNT5A, KAT6A, INHBB, WNT16, FZD5, ACVR2B, AKT1, SMARCAD1, APC	11
hsa05217	Basal cell carcinoma	0.025	WNT3, WNT5A, BMP2, WNT16, GADD45A, FZD5, APC	7
hsa04668	TNF signaling pathway	0.028	MAP2K6, VEGFC, MAP2K4, CCL2, MMP14, ATF2, AKT1, CEBPB, BIRC3	9
hsa04010	MAPK signaling pathway	0.028	MAP2K6, VEGFC, FGFR2, MAP2K4, DUSP6, GADD45A, MAP3K2, RASA2, ATF2, FGF18, STK4, NTF3, TGFA, FGF5, AKT1, HGF	16
hsa05202	Transcriptional misregulation in cancer	0.028	AFF1, HOXA10, NR4A3, BCL11B, WNT16, DUSP6, GADD45A, SP1, ETV5, HOXA11, CEBPB, BIRC3	12
hsa04350	TGF-beta signaling pathway	0.031	PITX2, BMP2, INHBB, TFDP1, SP1, NEO1, ACVR2B, SMAD6	8

further determine the clinical value of miR-374a-5p in PD, we also analyzed the diagnostic value of miR-374a-5p in different H&Y stages. The H&Y stage is an important clinical score used to distinguish PD, which is divided into 5 stages. In this study, we further divided the patients into 3 stages based on the H&Y stage. Previously, Zhang and others divided them into groups according to this scheme. After grouping patients, we further detected the miR-374a-5p expression in patients' serum. At last, we confirmed that miR-374a-5p was differentially expressed in those at different stages through Figure 3(a), and its expression decreased with the increase of stages, which indicated that PD was tied to the miR-374a-5p expression in the serum of severe patients. In addition, through ROC curve analysis, we found that miR-335-5p had a high clinical value in distinguishing patients of different stages, and the area under the curve was more than 0.8. Through the above research, we preliminarily confirmed the clinical value of miR-335-5p in PD, but we are still unclear about its relevant mechanism.

To further determine the relevant mechanism of miR-335-5p, we predicted its downstream target genes. Through the joint prediction of two online websites, we found 415 potential target genes downstream of miR-335-5p. Further enrichment analysis discovered that miR-335-5p participated in many functional pathways and signal pathways. Among them, the TNF signaling pathway, MAPK signaling pathway, and TGF-beta signaling pathway are important signal pathways for PD occurrence [26–28]. For instance, previous studies have found that [29] TNF signal inhibition in the central nervous system has an impact on normal brain function and neurodegenerative diseases. Other studies have verified that [30] activation of the MAPK signal pathway aggravates the condition of PD patients. Besides, studies have found that [31] TGF-β plays a role in the development, maintenance, and neuroprotection of dopamine neurons. Nevertheless, the analysis of this life letter provides us with the direction for future research.

There are still some limitations in this study. First of all, we only collected patient serum samples, and the samples were single. Some studies have found that differential expression of miR has also been detected in cerebrospinal fluid and peripheral blood mononuclear cells (PBMC). Moreover, the number of samples is relatively small, which may affect the data. Last but not least, we have not conducted in-depth research on the mechanism of miR-335-5p. Although we have conducted the credibility analysis to provide ideas for our research, we have not conducted experiments to confirm it. Hence, we hope to add more experiments and samples in future research to improve our research results.

To summarize, miR-335-5p has low expression in PD and is expected to become a potential diagnostic indicator.

Data Availability

The data used during the present study are available from the corresponding author upon reasonable request.

Conflicts of Interest

The authors declare that they have no conflicts of interest.

References

[1] S. Sveinbjornsdottir, "The clinical symptoms of Parkinson's disease," *Journal of Neurochemistry*, vol. 139, Supplement 1, pp. 318–324, 2016.

[2] R. B. Schneider, J. Iourinets, and I. H. Richard, "Parkinson's disease psychosis: presentation, diagnosis and management," *Neurodegenerative Disease Management*, vol. 7, no. 6, pp. 365–376, 2017.

[3] L. M. Bekris, I. F. Mata, and C. P. Zabetian, "The genetics of Parkinson disease," *Journal of Geriatric Psychiatry and Neurology*, vol. 23, no. 4, article 20938043, pp. 228–242, 2010.

[4] M. K. Lin and M. J. Farrer, "Genetics and genomics of Parkinson's disease," *Genome Medicine*, vol. 6, no. 6, p. 48, 2014.

[5] A. Ascherio and M. A. Schwarzschild, "The epidemiology of Parkinson's disease: risk factors and prevention," *Lancet Neurology*, vol. 15, no. 12, pp. 1257–1272, 2016.

[6] M. Grayson, "Parkinson's disease," *Nature*, vol. 538, no. 7626, article S1, 2016.

[7] S. Lotankar, K. S. Prabhavalkar, and L. K. Bhatt, "Biomarkers for Parkinson's disease: recent advancement," *Neuroscience Bulletin*, vol. 33, no. 5, pp. 585–597, 2017.

[8] A. M. Mohr and J. L. Mott, "Overview of microRNA biology," *Seminars in Liver Disease*, vol. 35, no. 1, pp. 3–11, 2015.

[9] V. Agarwal, G. W. Bell, J. W. Nam, and D. P. Bartel, "Predicting effective microRNA target sites in mammalian mRNAs," *eLife*, vol. 4, 2015.

[10] J. Fernandes, A. S. Vieira, J. C. Kramer-Soares et al., "Hippocampal microRNA-mRNA regulatory network is affected by physical exercise," *Biochimica et Biophysica Acta - General Subjects*, vol. 1862, no. 8, pp. 1711–1720, 2018.

[11] C. K. Chou, R. T. Liu, and H. Y. Kang, "MicroRNA-146b: a novel biomarker and therapeutic target for human papillary thyroid cancer," *International Journal of Molecular Sciences*, vol. 18, no. 3, 2017.

[12] A. Wojciechowska, A. Braniewska, and K. Kozar-Kaminska, "MicroRNA in cardiovascular biology and disease," *Advances in Clinical and Experimental Medicine*, vol. 26, no. 5, pp. 865–874, 2017.

[13] D. S. Greenberg and H. Soreq, "MicroRNA therapeutics in neurological disease," *Current Pharmaceutical Design*, vol. 20, no. 38, pp. 6022–6027, 2014.

[14] S. E. Oh, H. J. Park, L. He, C. Skibiel, E. Junn, and M. M. Mouradian, "The Parkinson's disease gene product DJ-1 modulates miR-221 to promote neuronal survival against oxidative stress," *Redox Biology*, vol. 19, pp. 62–73, 2018.

[15] A. D. Thome, A. S. Harms, L. A. Volpicelli-Daley, and D. G. Standaert, "MicroRNA-155 regulates alpha-synuclein-induced inflammatory responses in models of Parkinson disease," *The Journal of Neuroscience*, vol. 36, no. 8, pp. 2383–2390, 2016.

[16] T. Barrett, S. E. Wilhite, P. Ledoux et al., "NCBI GEO: archive for functional genomics data sets–update," *Nucleic Acids Research*, vol. 41, no. Database issue, pp. D991–D995, 2013.

[17] X. Bai, Y. Tang, M. Yu et al., "Downregulation of blood serum microRNA 29 family in patients with Parkinson's disease," *Scientific Reports*, vol. 7, no. 1, p. 5411, 2017.

[18] K. J. Livak and T. D. Schmittgen, "Analysis of relative gene expression data using real-time quantitative PCR and the 2(-delta delta C(T)) method," *Methods*, vol. 25, no. 4, pp. 402–408, 2001.

[19] P. M. Antony, N. J. Diederich, R. Kruger, and R. Balling, "The hallmarks of Parkinson's disease," *The FEBS Journal*, vol. 280, no. 23, pp. 5981–5993, 2013.

[20] A. Schrag, L. Horsfall, K. Walters, A. Noyce, and I. Petersen, "Prediagnostic presentations of Parkinson's disease in primary care: a case-control study," *Lancet Neurology*, vol. 14, no. 1, pp. 57–64, 2015.

[21] W. Ma, Y. Li, C. Wang, F. Xu, M. Wang, and Y. Liu, "Serum miR-221 serves as a biomarker for Parkinson's disease," *Cell Biochemistry and Function*, vol. 34, no. 7, pp. 511–515, 2016.

[22] S. Kabaria, D. C. Choi, A. D. Chaudhuri, M. M. Mouradian, and E. Junn, "Inhibition of miR-34b and miR-34c enhances alpha-synuclein expression in Parkinson's disease," *FEBS Letters*, vol. 589, no. 3, pp. 319–325, 2015.

[23] D. Son, Y. Kim, S. Lim et al., "miR-374a-5p promotes tumor progression by targeting ARRB1 in triple negative breast cancer," *Cancer Letters*, vol. 454, pp. 224–233, 2019.

[24] W. Chen, Y. Zhang, H. Wang, T. Pan, Y. Zhang, and C. Li, "LINC00473/miR-374a-5p regulates esophageal squamous cell carcinoma via targeting SPIN1 to weaken the effect of radiotherapy," *Journal of Cellular Biochemistry*, vol. 120, no. 9, pp. 14562–14572, 2019.

[25] M. L. Slattery, A. J. Pellatt, F. Y. Lee et al., "Infrequently expressed miRNAs influence survival after diagnosis with colorectal cancer," *Oncotarget*, vol. 8, no. 48, pp. 83845–83859, 2017.

[26] Q. S. Zhang, Y. Heng, Y. H. Yuan, and N. H. Chen, "Pathological alpha-synuclein exacerbates the progression of Parkinson's disease through microglial activation," *Toxicology Letters*, vol. 265, pp. 30–37, 2017.

[27] Y. Dong, L. L. Han, and Z. X. Xu, "Suppressed microRNA-96 inhibits iNOS expression and dopaminergic neuron apoptosis through inactivating the MAPK signaling pathway by targeting CACNG5 in mice with Parkinson's disease," *Molecular Medicine*, vol. 24, no. 1, p. 61, 2018.

[28] J. H. Koo, Y. C. Jang, D. J. Hwang et al., "Treadmill exercise produces neuroprotective effects in a murine model of Parkinson's disease by regulating the TLR2/MyD88/NF-kappaB signaling pathway," *Neuroscience*, vol. 356, pp. 102–113, 2017.

[29] P. C. Tiwari and R. Pal, "The potential role of neuroinflammation and transcription factors in Parkinson disease," *Dialogues in Clinical Neuroscience*, vol. 19, no. 1, pp. 71–80, 2017.

[30] S. K. Jha, N. K. Jha, R. Kar, R. K. Ambasta, and P. Kumar, "p38 MAPK and PI3K/AKT signalling cascades inParkinson's disease," *International Journal of Molecular and Cellular Medicine*, vol. 4, no. 2, pp. 67–86, 2015.

[31] R. Calvello, A. Cianciulli, G. Nicolardi et al., "Vitamin D treatment attenuates neuroinflammation and dopaminergic neurodegeneration in an animal model of Parkinson's disease, shifting M1 to M2 microglia responses," *Journal of NeuroImmune Pharmacology*, vol. 12, no. 2, pp. 327–339, 2017.

Hindawi
BioMed Research International
Volume 2024, Article ID 9823071, 1 page
https://doi.org/10.1155/2024/9823071

Retraction

Retracted: Clinical Efficacy of Methotrexate Combined with Iguratimod on Patients with Rheumatoid Arthritis and Its Influence on the Expression Levels of HOTAIR in Serum

BioMed Research International

Received 12 March 2024; Accepted 12 March 2024; Published 20 March 2024

This article has been retracted by Hindawi following an investigation undertaken by the publisher [1]. This investigation has uncovered evidence of one or more of the following indicators of systematic manipulation of the publication process:

(1) Discrepancies in scope

(2) Discrepancies in the description of the research reported

(3) Discrepancies between the availability of data and the research described

(4) Inappropriate citations

(5) Incoherent, meaningless and/or irrelevant content included in the article

(6) Manipulated or compromised peer review

The presence of these indicators undermines our confidence in the integrity of the article's content and we cannot, therefore, vouch for its reliability. Please note that this notice is intended solely to alert readers that the content of this article is unreliable. We have not investigated whether authors were aware of or involved in the systematic manipulation of the publication process.

Wiley and Hindawi regrets that the usual quality checks did not identify these issues before publication and have since put additional measures in place to safeguard research integrity.

We wish to credit our own Research Integrity and Research Publishing teams and anonymous and named external researchers and research integrity experts for contributing to this investigation.

The corresponding author, as the representative of all authors, has been given the opportunity to register their agreement or disagreement to this retraction. We have kept a record of any response received.

References

[1] J. Tan, J. Dan, and Y. Liu, "Clinical Efficacy of Methotrexate Combined with Iguratimod on Patients with Rheumatoid Arthritis and Its Influence on the Expression Levels of HOTAIR in Serum," *BioMed Research International*, vol. 2021, Article ID 2486617, 7 pages, 2021.

Hindawi
BioMed Research International
Volume 2021, Article ID 2486617, 7 pages
https://doi.org/10.1155/2021/2486617

Research Article

Clinical Efficacy of Methotrexate Combined with Iguratimod on Patients with Rheumatoid Arthritis and Its Influence on the Expression Levels of HOTAIR in Serum

Jingya Tan,[1] Jiaqiang Dan,[2] and Yi Liu[1]

[1]*Department of Rheumatology and Immunology, The People's Hospital of Wenjiang, Chengdu 611130, China*
[2]*Department of Breast and Thyroid Surgery, Chengdu Fifth People's Hospital, Chengdu 611130, China*

Correspondence should be addressed to Yi Liu; kebipa4355@163.com

Received 29 July 2021; Revised 13 October 2021; Accepted 18 October 2021; Published 12 November 2021

Academic Editor: Chang Gu

Objective. This study was designed to explore the clinical efficacy of methotrexate combined with iguratimod on patients with rheumatoid arthritis (RA) and its influence on the expression levels of HOTAIR in serum. *Methods*. A total of 268 RA patients were selected as research objects, 145 patients received methotrexate alone were used as a control group (CG), 123 patients received methotrexate combined with iguratimod were taken as a research group (RG), and serum of 60 healthy people undergoing physical examination was selected as a healthy control group (HCG). The therapeutic value of two therapeutic methods for RA was compared, and the HOTAIR expression in serum was detected by qRT-PCR. *Results*. Compared with methotrexate used alone, the joint use of methotrexate and iguratimod could provide better clinical efficacy for RA patients and would not increase the incidence of adverse events. HOTAIR was highly expressed in the serum of RA patients, and its expression decreased after treatment. *Conclusion*. Combination therapy of methotrexate and iguratimod is a safe and effective way to treat RA patients, which can be popularized clinically.

1. Introduction

Rheumatoid arthritis (RA) is a systemic autoimmune disease characterized by inflammatory synovitis and progressive joint destruction [1]. RA is the most common connective tissue disease, with a prevalence rate of 0.5% to 2% in the general population, and the incidence in women is higher than that in men, with a ratio of 3 : 1 [2]. RA itself and treatment can lead to a variety of complications, such as increased risk of cardiovascular diseases, diabetes, and osteoporotic fracture, which have a serious negative impact on life and health of patients [3, 4]. Therefore, it has become a hot research topic to explore treatment methods that can provide effective therapeutic effects and improve prognosis.

Methotrexate has been used to treat RA since the 1980s, and it is still the first-line drug for RA treatment to this day [5]. Therapy based on methotrexate is the core of rheumatoid arthritis. For most patients with rheumatoid arthritis, methotrexate is recommended as the first antirheumatic drug to improve diseases [6], but its long-term use will lead to increased drug resistance. Methotrexate and other antirheumatic drugs were recommended in the 2012 guidelines of the American College of Rheumatology (ACR) to treat RA [7]. Iguratimod is an orally active small molecule compound, which is approved in Japan as an antirheumatic drug to improve diseases [8]. In a 52-week multicenter study of more than 2000 RA patients, iguratimod was shown to be safe and effective in treating RA [9]. A clinical study conducted in China found that, compared with methotrexate, iguratimod showed no less efficacy and less side effects [10]. Long noncoding RNA (lncRNA) refers to RNA 200 nucleotides in length and does not participate in protein production [11]. Hox transcript antisense intergenic RNA (HOTAIR), the first lncRNA to be identified, exists on chromosome 12 and has been proved to have a role in the regulation of chromatin state and epigenetic mechanisms within

its different target transcripts. HOTAIR has been found to be expressed differentially in RA. HOTAIR is a 2,158 bp lncRNA located at the boundary of HOXC gene cluster, which is involved in the occurrence and development of various diseases [12]. However, little is known about the downstream signaling pathway of lncRNAs in regulating autoimmunity and inflammation. More studies are warranted to elucidate this issue in future. It is also prospective to investigate novel diagnostic and therapeutic strategies for RA by targeting lncRNAs.

Increased inflammatory mediator levels were linked to autoimmune diseases accompanied by chronic or repeated inflammation. Many cytokines, such as interleukin- (IL-) 6 and tumor necrosis factor- (TNF-) a, play a significant role in RA pathogenesis. TNF-α is a protein mainly produced by activated macrophages and monocytes. It participates in human inflammatory response and immune response and is essential to maintain homeostasis [13].

At present, there are few and incomplete researches on the efficacy and safety of methotrexate combined with iguratimod in treating RA. Therefore, this study mainly explored the efficacy and safety of the combination therapy of methotrexate and iguratimod and analyzed its influence on the expression levels of HOTAIR and TNF-α, which is aimed at providing a safe and effective treatment method for RA patients.

2. Materials and Methods

2.1. General Information. A total of 268 RA patients admitted to the People's Hospital of Wenjiang from July 2017 to January 2019 were selected as the research objects. Among them, 145 patients received methotrexate alone were selected as the control group (CG), and the remaining 123 patients received methotrexate combined with iguratimod were selected as the research group (RG). Inclusion criteria were as follows: patients all conformed to RA-like diagnostic criteria [14], those who signed an informed consent, and patients who received no drugs for rheumatoid arthritis and anti-inflammatory drugs in the first two months. Exclusion criteria were as follows: patients with communication barriers, incomplete clinical data, education level less than or equal to primary school, complications of heart, liver, kidney, and other important organs, malignant tumors and blood diseases, or drug allergy involved in this study and patients in pregnancy and lactation.

2.2. Treatment Methods. Patients in the CG were treated by methotrexate (China Tonghua Maoxiang Pharmaceutical Co., Ltd., SFDA Approval No.: H22022674). The method of use is as follows: 10 mg/time, once a week; 12.5 mg/time after two weeks, twice a week; and 15 mg/time after four weeks, once a week until the end of the experiment. And it was taken orally. On the basis of the CG, those in the RG were treated by iguratimod (China Simcere Pharmaceutical Co., Ltd., SFDA Approval No.: H20110084), twice a day, 25 mg/dose. Every 12 weeks is one course of treatment, and patients from both groups continue to treat for two courses of treatment.

2.3. Outcome Measures. After the treatment, the efficacy was evaluated: markedly effective: symptoms disappeared completely, physical signs improved by more than 75%, and C-reactive protein (CRP) and erythrocyte sedimentation rate decreased significantly and fell to the normal range; effective: symptoms partially improved, physical signs improved by more than 30%, and CRP and ESR decreased to some extent, but did not fall within the normal range; ineffective: symptoms and signs did not improve, and CRP and ESR did not significantly decrease. Total effective = markedly effective + effective.

The clinical symptoms of the two groups were observed and recorded, including the number of joint swelling, joint tenderness, and morning stiffness time before and after treatment.

DAS28 evaluation standard [15] was used to evaluate the disease activity of patients before and after treatment: >5.1 was high disease activity, <3.2 was low disease activity, and <2.6 was disease remission.

Visual analogue scale (VAS) [16] was used to evaluate the pain degree of patients before and after treatment, with painless score of 0. The higher the score was, the more severe the pain was.

Barthel index [17] was used to score the self-care ability of patients before and after treatment, including 10 items such as decoration, walking on flat ground, dressing, eating, and bathing, with a total score of 100 points. The higher the score was, the better the self-care ability was.

Adverse events. The incidence of adverse events after treatment between the two groups was compared, mainly including transaminase elevation, leukopenia, renal function and liver function damage, dizziness, diarrhea, nausea and vomiting, hypertension, and infection.

QLQ-C30 [18] was used to evaluate the quality of life of patients six months after treatment, including four items of disease control, life behavior, exercise, and psychological and emotional changes. Each item scored 100 points, and the higher the score was, the better the quality of life was.

The serum of patients in the CG and the RG was collected, respectively, before and after treatment. qRT-PCR and ELISA were used to detect the expression levels of HOTAIR and TNF-α in patients' serum before and after treatment. The experimental process was strictly carried out in accordance with the kit instructions of TRIzol extraction kit (Wuhan Chundu Biotechnology Co., Ltd., China, CDLG-4396), reverse transcription kit (Tiangen Biochemical Technology (Beijing) Co., Ltd., China, FP209), human TNF-α ELISA kit (Biolake, China, ECA0020), etc.

2.4. Statistical Treatment. SPSS 21.0 (IBM Corp, Armonk, NY, USA) was used for statistical analysis, and GraphPad Prism 7 was used to draw the data picture. The counting data were under chi-square test, comparison of the measurement data between the two groups was under independent-samples t test, and paired t test was used for comparison before and after treatment in the group. Comparison of the measurement data from more than two groups was conducted by one-way analysis of variance, correctness of statistical value was verified by post hoc test (Tukey HSD

method), and Pearson method was used for correlation analysis. $P < 0.05$ means differences were statistically significant.

3. Results

3.1. Comparison of General Data between Patients in the Two Groups. There was no significant difference between the CG and the RG in general data such as gender, age, weight, education level, dietary preference, place of residence, exercise habits, marital status, history of smoking, and history of drinking ($P > 0.05$) (Table 1).

3.2. Comparison of Clinical Efficacy between Patients in the Two Groups. The total effective rate of the RG was 86.18%, significantly higher than that of the CG (70.34%), with statistically significant difference ($P > 0.05$) (Table 2).

3.3. Comparison of Improvement of Clinical Symptom of Patients between the Two Groups before and after Treatment. There was no significant difference in the number of joint swelling, joint tenderness, and morning stiffness time between the CG and the RG before treatment ($P > 0.05$). After treatment, the three abovementioned symptoms in the two groups significantly improved compared with those before treatment, and the improvement in the RG was more significant than that in the CG ($P < 0.05$) (Table 3).

3.4. Comparison of VAS, DAS28, and Barthel Scores of Patients between the Two Groups before and after Treatment. There was no significant difference in VAS, DAS28, and Barthel scores of patients between the two groups before treatment ($P > 0.05$). After treatment, VAS and DAS28 scores of those in both groups decreased significantly, and the decrease in the RG was more significant than that in the CG, while Barthel score was opposite ($P < 0.05$) (Table 4).

3.5. Comparison of Adverse Events of Patients between the Two Groups. After treatment, adverse events occurred in patients from both groups, but there was no significant difference in the incidence of adverse events such as transaminase elevation, leukopenia, renal and liver function damage, dizziness, diarrhea, nausea, vomiting, hypertension, and infection between both groups ($P > 0.05$) (Table 5).

3.6. Comparison of QLQ-C30 Score of Patients between the Two Groups. The QLQ-C30 scale in the RG was significantly higher than that in the CG ($P < 0.05$), as shown in Table 6.

3.7. Comparison of the Expression Levels of Serum HOTAIR and TNF-α in Each Group. Before treatment, the expression levels of HOTAIR and TNF-α in serum of patients in the CG and the RG were significantly higher than those in the HCG ($P < 0.05$), while there was no significant difference between the CG and the RG ($P > 0.05$). After treatment, the expression levels of HOTAIR and TNF-α in serum of patients in the two groups decreased significantly, and their expression in the RG was lower than that in the CG ($P < 0.05$) (Figure 1).

Table 1: Comparison of general data of patients in the two groups ((*n*(%)), $x \pm$ sd).

Group	Control group ($n = 145$)	Research group ($n = 123$)	χ^2/t	P
Gender			2.072	0.150
Male	40 (27.59)	44 (35.77)		
Female	105 (72.41)	79 (64.23)		
Age (years)	55.27 ± 8.21	56.23 ± 9.89	0.868	0.386
Weight (kg)	65.34 ± 8.33	64.77 ± 7.78	0.575	0.566
Education level			2.901	0.089
<high school	77 (53.10)	78 (63.41)		
≥high school	68 (46.90)	45 (36.59)		
Dietary preference			0.673	0.412
Light	97 (66.90)	88 (71.54)		
Greasy	48 (33.10)	35 (28.46)		
Place of residence			0.080	0.778
Cities and towns	85 (58.62)	70 (56.91)		
Countryside	60 (41.38)	53 (43.09)		
Exercise habits			0.983	0.321
Yes	90 (62.07)	69 (56.10)		
No	55 (37.93)	54 (43.90)		
Marital status			1.153	0.562
Married	129 (88.96)	114 (92.68)		
Unmarried	8 (5.52)	4 (3.25)		
Divorce	8 (5.52)	5 (4.07)		
History of smoking			0.010	0.920
Yes	84 (57.93)	72 (58.54)		
No	61 (42.07)	51 (41.46)		
History of drinking			1.054	0.305
Yes	68 (46.90)	50 (40.65)		
No	77 (53.10)	73 (59.35)		

3.8. Correlation Analysis between HOTAIR and TNF-α. The correlation between serum HOTAIR and TNF-α in 268 RA patients before treatment was analyzed by Pearson analysis. The results showed that HOTAIR was positively correlated with TNF-α ($r = 0.643$, $P < 0.001$) (Figure 2).

4. Discussion

Methotrexate mainly inhibits the synthesis of thymine and purine by inhibiting dihydrofolate reductase, thus inhibiting the activity of immune cells and achieving the therapeutic purpose [19]. Iguratimod is a new antirheumatic drug with

Table 2: Comparison of clinical efficacy of patients between the two groups (n(%)).

Group	Markedly effective	Effective	Ineffective	Total effective rate
Control group ($n = 145$)	44 (30.34)	58 (40.00)	43 (29.66)	102 (70.34)
Research group ($n = 123$)	70 (56.91)	36 (29.27)	17 (13.82)	106 (86.18)
χ^2	-	-	-	9.602
P	-	-	-	0.002

Table 3: Comparison of improvement of clinical symptoms in patients between the two groups before and after treatment ($x \pm s$).

Group	Time	Control group ($n = 145$)	Research group ($n = 123$)	t	P
Number of joint swelling (pieces)	Before treatment	15.57 ± 4.25	14.81 ± 5.03	1.341	0.181
	After treatment	$8.56 \pm 3.52^{\#}$	$4.34 \pm 2.69^{\#}$	10.872	<0.001
Number of joint tenderness (months)	Before treatment	8.54 ± 1.35	8.23 ± 1.42	1.829	0.069
	After treatment	$5.45 \pm 0.74^{\#}$	$3.01 \pm 0.56^{\#}$	29.998	<0.001
Morning stiffness time (h)	Before treatment	3.38 ± 0.66	3.31 ± 0.56	0.927	0.355
	After treatment	$2.67 \pm 0.53^{\#}$	$1.64 \pm 0.33^{\#}$	18.695	<0.001

Note: Compared with before treatment, $^{\#}P$ was less than 0.05.

Table 4: Comparison of VAS, DAS28, and Barthel scores of patients before and after treatment between the two groups (score, $x \pm$ s).

Group	Time	Control group ($n = 145$)	Research group ($n = 123$)	t	P
VAS score	Before treatment	8.21 ± 1.75	8.11 ± 1.87	0.452	0.652
	After treatment	$5.14 \pm 1.42^{\#}$	$3.19 \pm 0.81^{\#}$	13.480	<0.001
DAS28 score	Before treatment	6.53 ± 1.45	6.34 ± 1.61	1.016	0.311
	After treatment	$3.77 \pm 0.64^{\#}$	$2.61 \pm 0.59^{\#}$	15.323	<0.001
Barthel score	Before treatment	64.24 ± 8.24	65.56 ± 7.65	1.350	0.178
	After treatment	$81.34 \pm 6.35^{\#}$	$88.24 \pm 5.52^{\#}$	9.407	<0.001

Note: Compared with before treatment, $^{\#}P$ was less than 0.05.

Table 5: Comparison of adverse events of patients in the two groups after treatment (n(%)).

Group	Control group ($n = 145$)	Research group ($n = 123$)	χ^2	P
Transaminase elevation	23 (15.86)	16 (13.01)	0.436	0.509
Leukopenia	12 (8.28)	14 (11.38)	0.733	0.392
Renal and liver function damage	9 (6.21)	11 (8.94)	0.722	0.396
Dizziness	27 (18.62)	24 (19.51)	0.034	0.853
Diarrhea	19 (13.10)	23 (18.70)	1.577	0.209
Nausea and vomiting	23 (15.86)	29 (23.58)	2.533	0.112
Hypertension	7 (4.83)	5 (4.07)	0.090	0.764
Infection	15 (10.34)	10 (8.13)	0.386	0.534

Table 6: Comparison of QLQ-C30 score of patients between the two groups (score, $x \pm s$).

Group	Control group ($n = 145$)	Research group ($n = 123$)	t	P
Disease control	80.24 ± 6.25	85.24 ± 5.56	6.863	<0.001
Life behavior	81.24 ± 5.34	89.56 ± 4.87	13.231	<0.001
Exercise	74.21 ± 4.45	79.78 ± 4.67	9.982	<0.001
Psychological emotion	77.24 ± 7.67	86.32 ± 5.33	11.057	<0.001

anticytokine ability [20]. It can suppress the production of immunoglobulin and various inflammatory cytokines, promote the differentiation of bone cells, inhibit the generation of osteoclasts, and reduce bone absorption and joint destruction [21]. Some research results revealed that the joint use of methotrexate and iguratimod was superior to iguratimod or

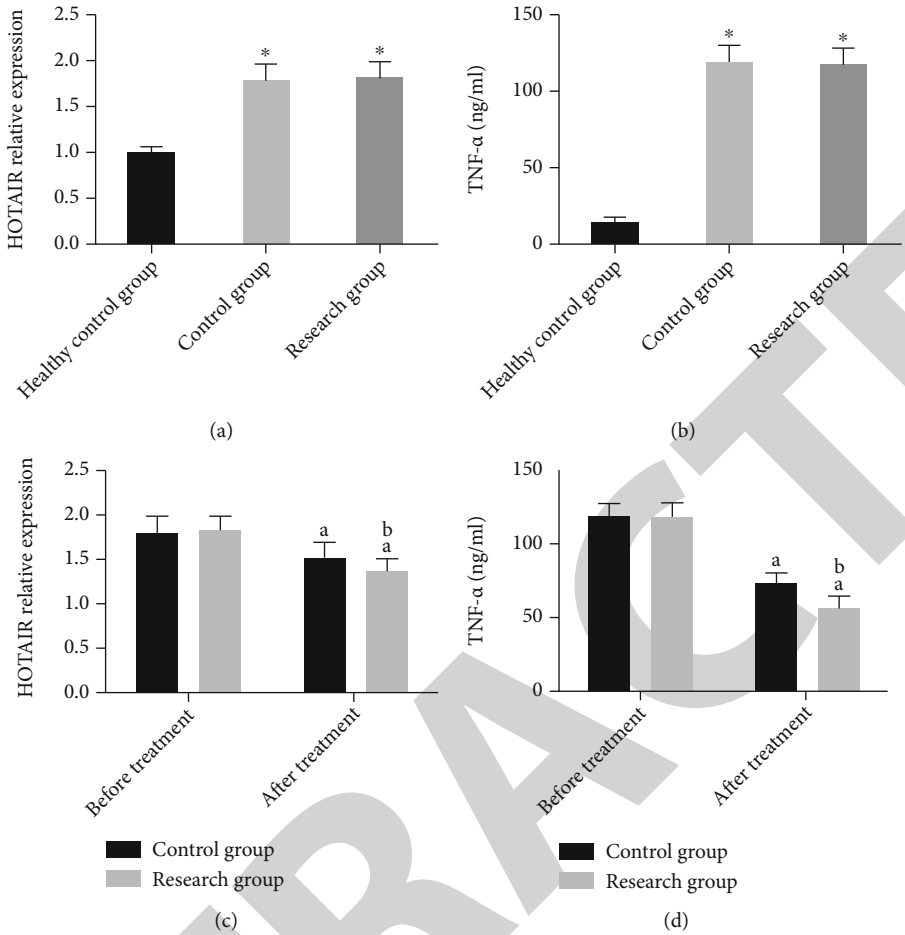

Figure 1: Comparison of the expression levels of serum HOTAIR and TNF-α in each group. (a, b) The expression levels of HOTAIR and TNF-α in serum of patients in the CG and the RG were significantly higher than those in the HCG ($P < 0.05$). (c, d) Compared with before treatment, the expression levels of serum HOTAIR and TNF-α of patients in the two groups decreased significantly after treatment, and their expression in the RG was lower than that in the CG ($P < 0.05$). Note: Compared with the HCG, $^{*}P$ was less than 0.05. Compared with before treatment, ^{a}P in the group was less than 0.05. Compared with the CG, ^{b}P was less than 0.05.

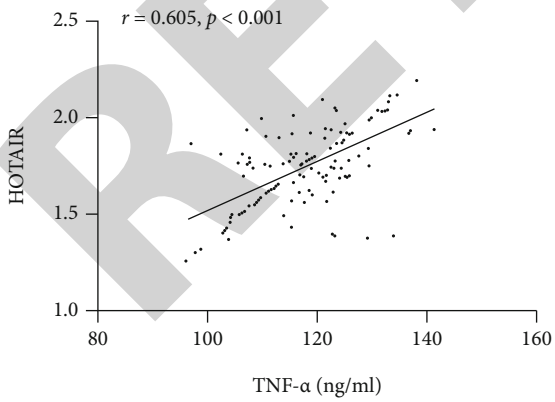

Figure 2: Correlation analysis between HOTAIR and TNF-α. Pearson analysis showed that there was a significant positive correlation between HOTAIR and TNF-α ($r = 0.643$, $P < 0.001$).

methotrexate monotherapy for RA patients and was also effective for patients with poor response to previous antirheumatic drug therapy [22]. Other research results showed that the joint use of methotrexate and iguratimod had better efficacy on active RA than methotrexate alone and did not increase the incidence of adverse events [23]. Our results indicated that the total effective rate of the RG was significantly higher than that of the CG. After treatment, the clinical symptoms, VAS score, DAS28 score, Barthel score, and QLQ-C30 score of the RG were all better than those of the CG, and there was no significant difference in the incidence of adverse events between the two groups. This represented that methotrexate combined with iguratimod was a more effective way to treat RA. The reason we suspected might be that the joint use of the two might jointly inhibit the production of inflammatory factors, thus reducing the inflammatory response. Subsequently, we detected the TNF-α level in serum of both groups and found that its level of the RG was significantly lower than that of the CG after treatment, which indicated that methotrexate combined with iguratimod could jointly inhibit the production of inflammatory factors.

lncRNA is considered to be a universal regulator of gene expression, and thousands of lncRNAb have been discovered

at present [24]. HOTAIR is an important member of lncRNAb, which has been discovered. It is involved in the occurrence of many diseases, such as gastric cancer, esophageal squamous cell carcinoma, and nasopharyngeal carcinoma [25–27]. Recently, some researches have found that HOTAIR has certain connection with arthritis diseases, for example, some research results have indicated that HOTAIR is highly expressed in osteoarthritis cartilage [28]. Other research results showed that the HOTAIR expression level is upregulated in blood monocytes and serum exosomes of RA patients but downregulated in differentiated osteoclasts and rheumatoid synovial cells, and its overexpression can reduce the expression of matrix metalloproteinase 2 (MMP-2) and MMP-13 [29]. MMP may play a role in many pathological processes, including inflammation, cardiovascular diseases, pulmonary diseases, and cancer. MMP-9 is implicated in the development of a variety of autoimmune diseases, including systemic lupus erythematosus, Sjogren's syndrome, systemic sclerosis, RA, and multiple sclerosis [30]. It was detected that downregulated HOTAIR significantly suppressed MMP-9 secretion. Furthermore, in RA patients, the serum level of HOTAIR had a significantly positive correlation with MMP-9 level, erythrocyte sedimentation rate (ESR), hemoglobin (Hb), and platelets count. This agrees partially with the work of Wang and others who found that downregulated HOTAIR leads to suppression of MMP-2 and MMP-9 secretion. They also demonstrated that HOTAIR knockdown in vitro and in vivo significantly decreased the levels of MMP-2 and MMP-9 [31–33].

According to our research results, the HOTAIR expression in serum of patients in the CG and the RG was significantly higher than that in the HCG. After treatment, its expression decreased markedly, and there was a remarkable positive correlation between serum HOTAIR and TNF-α in patients in the CG before treatment, suggesting that HOTAIR might participate in the pathogenesis of RA, and methotrexate, iguratimod, and HOTAIR might have certain regulatory relationships. Inflammatory cytokines, especially TNF-α, and two interleukins, IL-1β and IL-6, are key in driving inflammation and joint damage. Cytokines such as IL-23, IL-17A, as discussed above, and interferon gamma (IFN-γ) also play crucial roles in the pathogenesis of RA. IL-4 and IL-10, on the other hand, have been suggested to improve arthritis. While there is overall consensus on the inflammatory role of IL-6 in the pathogenesis of RA, there are some studies pointing out that its role is not clear-cut. It has emerged that IL-1 signaling reduces IL-6 signaling in RA, overall worsening patients' conditions [34].

There are some shortcomings in this study. For instance, the optimal dosage of the joint use of methotrexate and iguratimod and the relationship between HOTAIR and RA, as well as methotrexate and iguratimod, have not been deeply explored. Future studies are needed to explain how the immune cell functions are regulated by methotrexate and iguratimod. The participation of methotrexate and iguratimod and its dysregulation in RA pathogenesis are needed to be investigated on a larger scale. Exploring the role of them in RA pathogenesis is essential for the deep understanding and, therefore, effective treatment of this disease.

5. Conclusion

In conclusion, compared with methotrexate used alone, the joint use of methotrexate and iguratimod can provide better clinical efficacy for RA patients, improve their symptoms and life treatment, and will not increase the occurrence of adverse events. Besides, HOTAIR may participate in the pathogenesis of RA.

Data Availability

The authors confirm that the data supporting the findings of this study are available within the article.

Ethical Approval

Ethical issues (including plagiarism, informed consent, misconduct, data fabrication and/or falsification, double publication and/or submission, and redundancy) have been completely observed by the authors.

Conflicts of Interest

The authors declare that they have no conflicts of interest.

Authors' Contributions

Jingya Tan and Jiaqiang Dan performed the experiments, analyzed data and wrote the manuscript. Yi Liu designed the study. All the authors agreed to be accountable for the accuracy and integrity of all aspects of the research. Jingya Tan and Jiaqiang Dan contributed equally to this study as co-first authors.

References

[1] P. C. Taylor, E. C. Keystone, D. van der Heijde et al., "Baricitinib versus placebo or adalimumab in rheumatoid arthritis," *The New England Journal of Medicine*, vol. 376, no. 7, pp. 652–662, 2017.

[2] Z. X. Yunt and J. J. Solomon, "Lung disease in rheumatoid arthritis," *Rheumatic Diseases Clinics of North America*, vol. 41, no. 2, pp. 225–236, 2015.

[3] A. Boonen and J. L. Severens, "The burden of illness of rheumatoid arthritis," *Clinical Rheumatology*, vol. 30, no. S1, pp. 3–8, 2011.

[4] L. Hartman, L. A. Rasch, T. Klausch et al., "Harm, benefit and costs associated with low-dose glucocorticoids added to the treatment strategies for rheumatoid arthritis in elderly patients (GLORIA trial): study protocol for a randomised controlled trial," *Trials*, vol. 19, no. 1, p. 67, 2018.

[5] B. Friedman and B. Cronstein, "Methotrexate mechanism in treatment of rheumatoid arthritis," *Joint, Bone, Spine*, vol. 86, no. 3, pp. 301–307, 2019.

[6] G. S. Hazlewood, C. Barnabe, G. Tomlinson, D. Marshall, D. J. Devoe, and C. Bombardier, "Methotrexate monotherapy and methotrexate combination therapy with traditional and biologic disease modifying anti-rheumatic drugs for rheumatoid arthritis: a network meta-analysis," *Cochrane Database of Systematic Reviews*, vol. 2016, article CD010227, 2016.

Hindawi
BioMed Research International
Volume 2024, Article ID 9758259, 1 page
https://doi.org/10.1155/2024/9758259

Retraction

Retracted: miR-1226-3p Promotes eNOS Expression of Pulmonary Arterial Endothelial Cells to Mitigate Hypertension in Rats via Targeting Profilin-1

BioMed Research International

Received 12 March 2024; Accepted 12 March 2024; Published 20 March 2024

This article has been retracted by Hindawi following an investigation undertaken by the publisher [1]. This investigation has uncovered evidence of one or more of the following indicators of systematic manipulation of the publication process:

(1) Discrepancies in scope

(2) Discrepancies in the description of the research reported

(3) Discrepancies between the availability of data and the research described

(4) Inappropriate citations

(5) Incoherent, meaningless and/or irrelevant content included in the article

(6) Manipulated or compromised peer review

The presence of these indicators undermines our confidence in the integrity of the article's content and we cannot, therefore, vouch for its reliability. Please note that this notice is intended solely to alert readers that the content of this article is unreliable. We have not investigated whether authors were aware of or involved in the systematic manipulation of the publication process.

Wiley and Hindawi regrets that the usual quality checks did not identify these issues before publication and have since put additional measures in place to safeguard research integrity.

We wish to credit our own Research Integrity and Research Publishing teams and anonymous and named external researchers and research integrity experts for contributing to this investigation.

The corresponding author, as the representative of all authors, has been given the opportunity to register their agreement or disagreement to this retraction. We have kept a record of any response received.

References

[1] J. Jian and L. Xia, "miR-1226-3p Promotes eNOS Expression of Pulmonary Arterial Endothelial Cells to Mitigate Hypertension in Rats via Targeting Profilin-1," *BioMed Research International*, vol. 2021, Article ID 1724722, 7 pages, 2021.

Hindawi
BioMed Research International
Volume 2021, Article ID 1724722, 7 pages
https://doi.org/10.1155/2021/1724722

Research Article

miR-1226-3p Promotes eNOS Expression of Pulmonary Arterial Endothelial Cells to Mitigate Hypertension in Rats via Targeting Profilin-1

Jie Jian[1] and Liang Xia[2]

[1]*Department of Cardiac Surgery, Guangdong Cardiovascular Institute, Guangdong Provincial People's Hospital, Guangdong Academy of Medical Sciences, Guangzhou 51000, Guangdong Province, China*
[2]*Department of Critical Care Medicine, The First Affiliated Hospital of Chongqing Medical University, 400016 Chongqing, China*

Correspondence should be addressed to Liang Xia; jiao96426867@163.com

Received 23 July 2021; Revised 6 October 2021; Accepted 8 October 2021; Published 3 November 2021

Academic Editor: Chang Gu

In pulmonary arterial hypertension (PAH), microRNAs (miRNAs) are related with dysfunction of pulmonary arterial endothelial cells. miR-1226-3p was found to be downregulated in the serum of PAH patients, while few studies have illustrated the regulation mechanism of miR-1226-3p on PAH. In this study, we aimed to systematically investigate the role of miR-1226-3p in PAH. Sprague-Dawley (SD) rats were treated with monocrotaline (MCT) to establish the PAH models. The right ventricular systolic pressure (RVSP), ratio of the right ventricle to the left ventricle with septum (RV/(LV+S) ratio), and nitric oxide (NO) content were used to reflect the symptom of the rats. The rat models were used to observe the regulation mechanism of miR-1226-3p on PAH, and dual-luciferase reporter assay was used to verify the binding effect of miR-1226-3p to Pfn1. Besides, the qRT-PCR and western blot were used to measure the expression levels of miR-1226-3p and some keys proteins such as eNOS and Pfn1, respectively. The results showed that the PAH models were established successfully. The RVSP levels and the RV/(LV+S) ratio of the PAH rats were higher than those indexes in normal rats, while the NO content showed the opposite trends. Besides, the decreased miR-1226-3p and eNOS were, respectively, found in the PAH rats and rPAECs, and overexpressed miR-1226-3p could reverse the disadvantages of the PAH rats including increased RVSP, high RV/(LV+S) ratio, and decreased NO content. Furthermore, miR-1226-3p could directly target the 3′-UTR of Profilin-1 (Pfn1). Overexpressed Pfn1 led to decreased eNOS, while miR-1226-3p could partly inhibit the expression of Pfn1 and increase the expression level of eNOS in rPAECs. In summary, this study suggests miR-1226-3p as a protector to increase eNOS, improve NO content in rPAECs of the PAH rats via targeting Pfn, and finally protect the rats from the injury induced by PAH.

1. Introduction

Pulmonary arterial hypertension (PAH) is characterized by increased pulmonary vascular resistance, right heart failure, and high mortality [1, 2]. Even with the current medical conditions, the 5-year survival of patients remains unsatisfactory [3, 4]. Furthermore, the pathological changes of the tissues such as inflammation and pulmonary vasoconstriction had already happened by the time patients were diagnosed with PAH. As a potential interventional point, consideration has been given to the increased arterial pressure induced by nitric oxide (NO) deficiency in endothelial cells, which is a hallmark event of PAH. The synthesis dysfunction of vasodilator NO is well considered a major reason of PAH [5, 6]. Abnormal expression and dysfunction of the endothelial NO synthase (eNOS) in the human pulmonary arterial endothelial cells (HPAECs) leads to decreased NO content and thus contributes to the development and progression of PAH [7, 8].

MicroRNAs (miRNAs) are small, highly conserved, noncoding RNA molecules involved in regulating gene expression. They target mRNA molecules for cleavage or

translational repression, resulting in the degradation of mRNA and/or the inhibition of mRNA translation [9, 10]. Abnormal expression of miRNAs is implicated in several diseases including some cancers and multiple cardiovascular diseases. Moreover, modulating the expression level of some factors has been thought as a promising therapeutic strategy of miRNAs in clinical intervention [11, 12]. Consequently, highlighting the usefulness of miRNAs as diagnostic and prognostic targets is necessary [13]. In PAH, miRNAs are related with dysfunction of pulmonary arterial endothelial cells [14, 15]. One study has found that miR-1226-3p was downregulated in the serum of patients with PAH, while few studies have illustrated the regulation mechanism of miR-1226-3p on PAH [16].

Recently, profilin 1(Pfn1), a regulator of actin dynamics, emerged as a potential new player in the field. Pfn1 is abundant in stable atherosclerotic plaques and in thrombi extracted from infarct-related arteries in patients with acute myocardial infarction. In this study, the expression level of miR-1226-3p in a rat model was determined to analyze its effect in PAH pathologies. Furthermore, the potential target gene of miR-1226-3p was investigated to illustrate its regulation mechanism on PAH.

2. Materials and Methods

2.1. Animal Models. 50 male Sprague-Dawley (SD) rats (weight: 210 ± 10 g, average age: 6-8weeks) were purchased from Betterbiotechnology Co., Ltd. (Nanjing, China). All animals were given freedom to obtain food and water at any time. The rats ($n = 20$) were randomly divided into the control and PAH groups. Monocrotaline (MCT) was purchased from MedChem Express (New Jersey, USA), and the rats in the PAH groups were injected with MCT at 60 mg/kg to establish the pulmonary hypertension models, while rats in the control group were injected with normal saline.

Rats ($n = 30$) were randomly divided into three groups, including a PAH+saline group, a PAH+miR-NC group, and a PAH+miR-1226-3p group. In addition, at the time points of 48 hours before MCT treatment and 7 and 14 days after MCT treatment, the rats in the MCT+miR-1226-3p group and in the MCT-miR-NC group were infected with miR-1226-3p overexpressed lentivirus and negative control miRNA (miR-NC) lentivirus (2×10^8 TU/ml per rat), respectively. All lentivirus were constructed by Hanbio Biotechnology Co., Ltd. (Shanghai, China).

After 21 days of MCT treatment, rats were anesthetized and then used to measure the hemodynamics. The biological data acquisition and analysis system (BL-420s, Techman Sorfware Co., Ltd., Chengdu, China) was used to measure the right ventricular systolic pressure (RVSP) and ratio of the right ventricle to the left ventricle with septum (RV/(LV+S) ratio) of rats. After that, the lung tissues of rats were collected for the following experiments.

2.2. Measurement of the Level of NO. The level of NO in the homogenate of lung tissues was determined as described previously. NO was detected with a Sievers chemiluminescence nitric oxide analyzer (Model 280; Sievers, Boulder, USA). Standard curves with $NaNO_3$ were performed daily.

2.3. Cells Culture. The pulmonary arteries obtained from normal rats were used to isolate the rat arterial endothelial cells (rPAECs). The cells were cultured in DMEM (Thermo Fisher Scientific, Massachusetts, USA) which included 10% fetal bovine serum (FBS, Hyclone, South Logan, UT, USA). All cells were incubated in incubator at 37°C.

2.4. Cell Transfection. When the rRAECs were cultured at 70% confluence, the miR-1226-3p mimic, miR-NC or Pfn1 overexpression plasmid (pCMV-Pfn1) were transfected into cells with Lipofectamine 2000 (Invitogen, California, USA), and then, cells were incubated in incubator at 37°C for 48 h. In addition, all of miR-1226-3p mimic, miR-NC, and pCMV-Pfn1 were purchased from Beijing Generay Biotech Co., Ltd (Beijing, China).

2.5. qRT-PCR. Total RNAs of the tissues or cells were extracted by a TRIzol reagent. After that, the extracts were transcribed into cDNA by a PrimeScript® RT reagent Kit (Thermo Fisher, Massachusetts, USA). The primers of miR-1226-3p were synthesized and purified by Synbio Technology (Suzhou, China). According to the operation instruction of the KAPA qRT-PCR kit (Sigma-Aldrich, Missouri, USA), the reaction systems (10 μl) were prepared for qRT-PCR, and the reaction conditions included predenaturation at 95°C for 30 s, 95°C for 5 s, and 60°C for 30s for a total of 40 cycles. U6 was used as the control of miR-1226-3p. The sequences of forward and reverse primer of miR-612 and U6 have been shown in Table 1.

2.6. Western Blot. The total protein of the tissues or cells were extracted by RIPA buffer (containing 1% PMSF for keep stability of proteins), and the concentration of total proteins was measured by BCA protein assay kit (Beyotime, Shanghai, China). All proteins were separated by 10% SDS-PAGE, and then, they were transferred from SDS-PAGE onto the PVDF membranes. After that, the nonfat milk with concentration at 5% was used to block membranes for 1 hour, and then, the membranes were incubated with the primary antibodies of target proteins at 4°C overnight, and the β-actin was used for quantification of target proteins. After washing three times with TBST, the membranes were incubated with the secondary antibodies for 1.5 hours at 25°C. Finally, a chemiluminescence detection system was used to observe protein expression level.

2.7. Dual-Luciferase Reporter Assay. The 3′-UTR fragments of Pfn1 and the mutant one were synthesized and inserted into the pmirGLO luciferase reporter vector (Promega, Wisconsin, USA). The reporter constructs were named as Pfn1-Wt and Pfn1-Mut, respectively. After that, the vectors of Pfn1-Wt and Pfn1-Mut were cotransfected into 293T cells with miR-1226-3p mimic or miR-NC, respectively. In addition, both miR-1226-3p mimic and miR-NC were purchased from Beijing Generay Biotech Co., Ltd. (Beijing, China).

Table 1: Primer sequence of miR-1226-3p and U6.

Name of primer	Sequences
miR-1226-3p-F	5′-GCGGCTCACCAGCCCTGTGT-3′
miR-1226-3p-R	5′-CAGCCACAAAAGAGCACAAT-3′
U6-F	5′-CTCGCTTCGGCAGCACA-3′
U6-R	5′-AACGCTTCACGAATTTGCGT-3′

2.8. In Vivo Experiment. Rats ($n = 30$) were randomly divide into three groups, including a PAH+saline group, a PAH +miR-NC group, and a PAH+miR-1226-3p group. In addition, at the time points of 48 hours before MCT treatment and 7 and 14 days after MCT treatment, the rats in the MCT+miR-1226-3p group and in the MCT-miR-NC group were infected with miR-1226-3p overexpressed lentivirus and negative control miRNA (miR-NC) lentivirus (2×10^8 TU/ml per rat), respectively. All lentivirus were constructed by Hanbio Biotechnology Co., Ltd. (Shanghai, China).

After 21 days of MCT treatment, rats were anesthetized and then used to measure the hemodynamics. The biological data acquisition and analysis system (BL-420s, Techman Sorfware Co., Ltd., Chengdu, China) was used to measure the right ventricular systolic pressure (RVSP) and ratio of the right ventricle to the left ventricle with septum (RV/(LV+S) ratio) of rats. After that, the lung tissues of rats were collected for following experiments.

2.9. Statistical Analysis. All the experiments were performed at least three times, and the data were analyzed by SPSS 20.0, and the figures were charted by GraphPad Prism 8.0. The difference between the groups was calculated through Chi-squared test or ANOVA with Tukey's post hoc test. $P < 0.05$ means that it is statistically significant between two groups.

3. Results

3.1. The PAH Rat Models Were Established Successfully. To verified the utilizability of models after treating with MCT, the RVSP level and RV/(LV+S) ratio of the rats were detected. The results showed that the RVSP level and RV/(LV+S) ratio of the PAH rats were significantly higher than those indexes in the rats injected with normal saline (Figures 1(a) and 1(b), $P < 0.05$). Besides, it was observed that the content of NO in the lung tissue of the PAH rats significantly decreased compared with the normal rats (Figure 2(b), $P < 0.05$).

3.2. Decreased miR-1226-3p and Downregulated eNOS Were Observed in the Lungs of the PAH Rats and rPAECs, Respectively. To analyze the connection between miR-1226-3p and PAH, qRT-PCR was used to measure the expression level of miR-1226-3p in the lung tissues of the PAH rats. The results showed that miR-1226-3p was significantly downregulated in lungs of the PAH rats (Figure 2(a), $P < 0.05$). Besides, overexpressed miR-1226-3p increased the expression level of eNOS in rPAECs (Figures 2(c) and 2(d), $P < 0.05$).

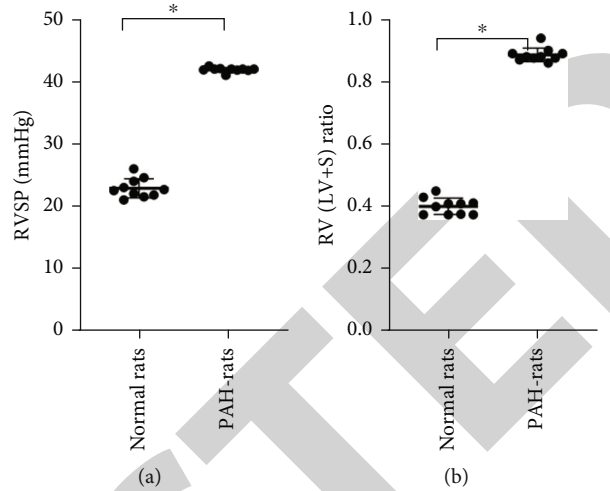

Figure 1: The PAH rats were established successfully. (a) The RVSP level of the rats. (b) The RV/(LV+S) ratio of the rats. Statistical analysis is by one-way ANOVA with Turkey's post hoc analysis. $^*P < 0.05$.

3.3. miR-1226-3p Can Directly Target the 3′-UTR of Pfn1. To make sure the regulation mechanism of miR-1226-3p on PAH, the miRWalk, an online database, was used to predict the downstream targets of miR-1226-3p. The results showed that Pfn1 was one of potential factors, which had low binding energy with miR-1226-3p compared with the most of others. Based on this, dual-luciferase reporter assay was used to further confirm the accuracy of the forecast results. The results showed that miR-1226-3p can directly target the 3′-UTR of Pfn1-wt and inactivate the luciferase activity of the Pfn1-wt rather than Pfn1-mut (Figure 3(a), $P < 0.05$). Besides, the significantly increased expression level of BNF1 was observed in the rRAECs when miR-1226-3p was downregulated (Figures 3(b) and 3(c), $P < 0.05$).

3.4. miR-1226-3p Upregulated eNOS via Inhibiting the Expression of Pfn1. To explore the relationship of miR-1226-3p and Pfn1, the miR-1226-3p mimic and Pfn1 were cotransfected into rRAECs, and western blot and qRT-PCR were used to observe the expression levels of Pfn1 and miR-1226-3p, respectively. The results showed that the Pfn1 inhibited the expression of eNOS in rRAECs, while miR-1226-3p could reverse this phenomenon (Figures 4(a)–4(d), $P < 0.05$).

3.5. miR-1226-3p Alleviated the Symptom of the PAH Rats. To verify the function of miR-1226-3p in protecting rats away from the injury induced by PAH, the lentivirus of miR-1226-3p were used to infect the PAH rats, and the RVSP level, RV/(LV+S) ratio, and NO content of the PAH rats were detected. The results showed that the RVSP level and RV/(LV+S) ratios significantly decreased in the PAH rats infected with lentivirus of miR-1226-3p compared with the PAH rats infected with lentivirus of miR-NC

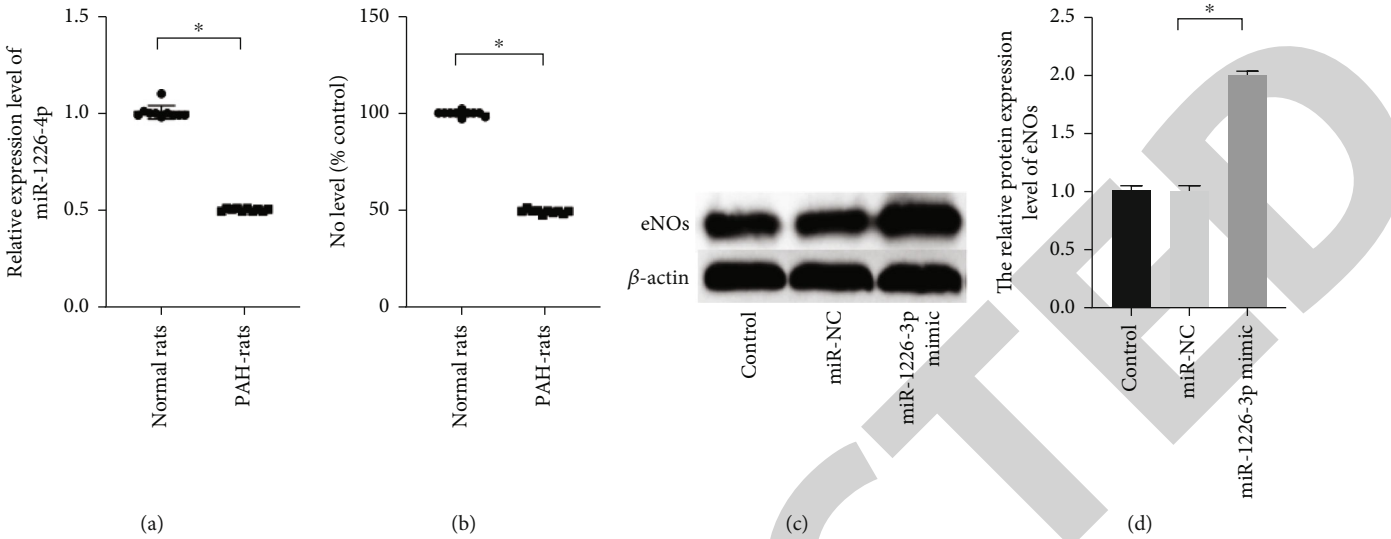

FIGURE 2: miR-1226-3p was downregulated in the lung tissues of the PAH rats. The NO content in the lung tissues of the PAH rats decreased significantly, and eNOS was upregulated in rPAECs when miR-1226-3p was overexpressed. (a) The relative expression level of miR-1226-3p in the lung tissue of the PAH rats. (b) The NO level in the lung tissue of the PAH rats. (c, d) The relative protein expression level of eNOS in rPAECs. $^*P < 0.05$.

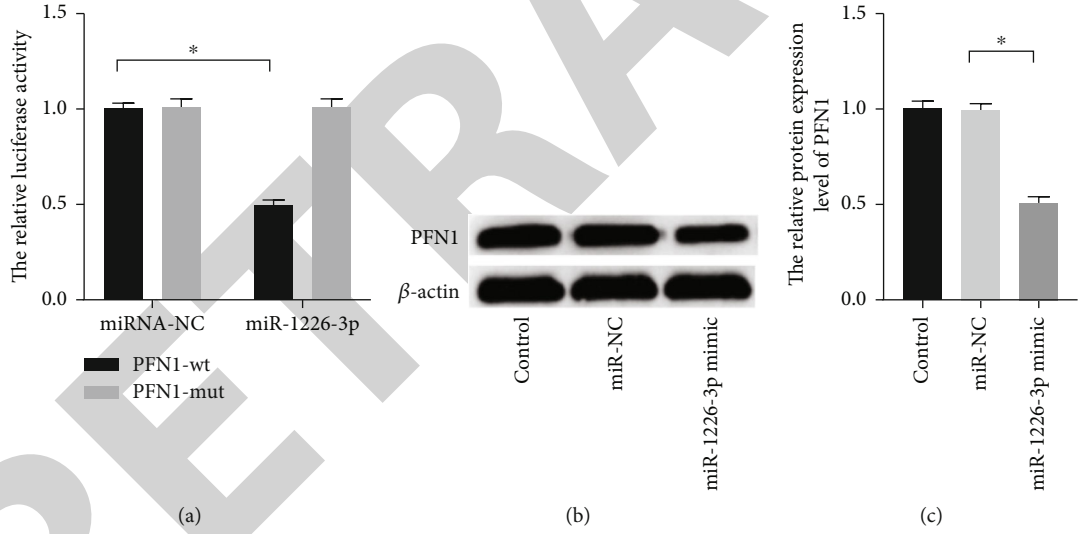

FIGURE 3: miR-1226-3p directly targeted the 3′-URT of Pfn1, and overexpressed miR-1226-3p inhibits the expression of Pfn1. (a) miR-1226-3p reduced the luciferase activity of Pfn1-wt. (b, c) The relative protein expression level of Pfn1 in HPAECs transfected with miR-1226-3p mimic. $^*P < 0.05$.

(Figures 5(a) and 5(b), $P < 0.05$). Besides, the NO content in lung tissues of the PAH rats infected with lentivirus of miR-1226-3p increased significantly (Figure 5(c), $P < 0.05$).

4. Discussion

It is confirmed that the increased NO content in the blood is a pathway of regulating blood pressure in mammals, which could prevent and improve the symptom of PAH [17]. One study has indicated that the expression level of miR-1226-3p is significantly decreased in the peripheral blood of patients with PAH [16]. Therefore, this study has focused on the connection between miR-1226-3p and PAH. We demonstrated that the expression level of miR-1226-3p decreased significantly in lungs of the PAH rats, and overexpressed miR-1226-3p could alleviate the symptom of the PAH rats including high RVSP level, high RV/(LV+S) ratio, and low NO content in the lung tissues. It was found that the synthesis progression of NO in the blood of the PAH rats could be attenuated when the rats were treated with MCT, and the level of miR-1226-3p could influence the protein level of eNOS in rPAECs. Furthermore, we confirmed that miR-1226-3p directly targeted the 3′-UTR of Pfn1 which was an upstream regulator of eNOS, and miR-1226p

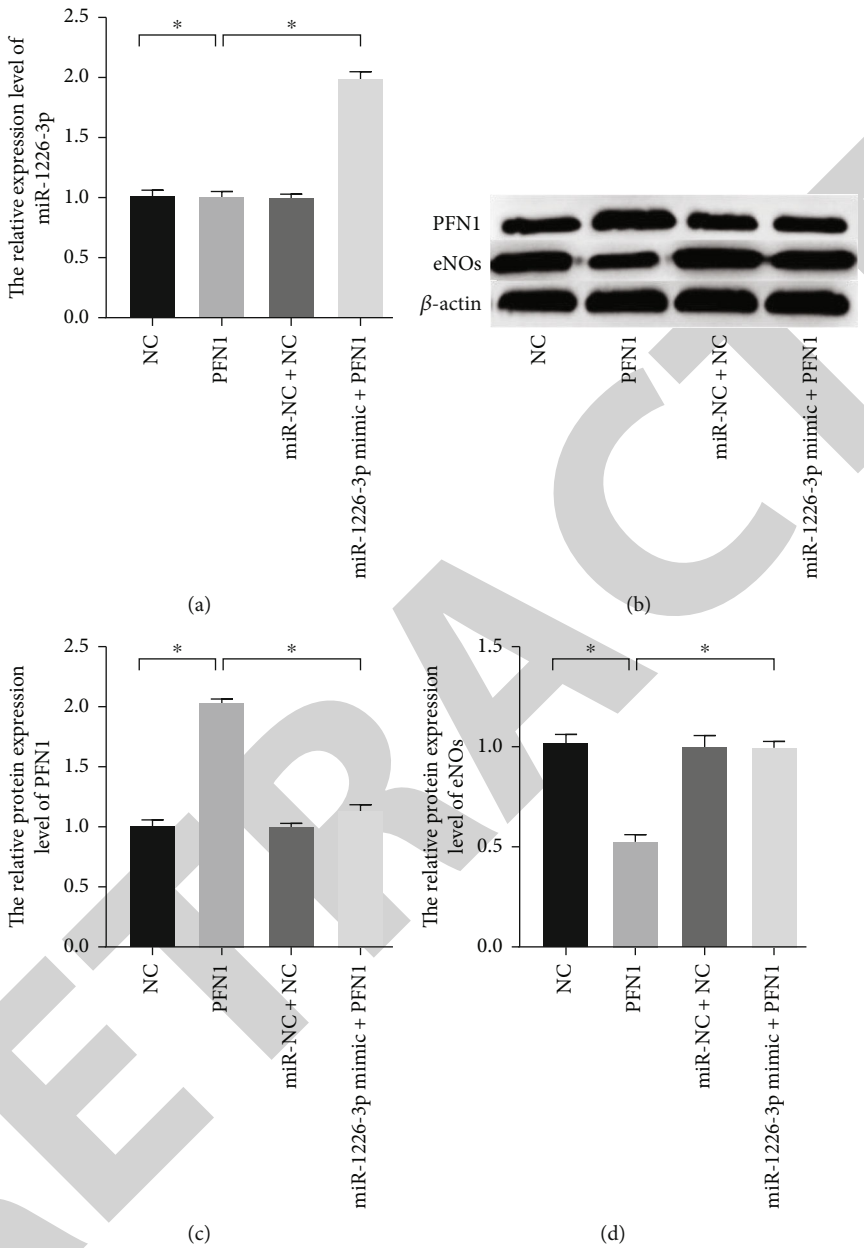

Figure 4: Pfn1 inhibited the expression of eNOS, while miR-1226-3p reversed the effect of Pfn1 on eNOS. (a) The relative expression level of miR-1226-3p. (b–d) The relative protein expression levels of PFN1 and eNOS. $^{*}P < 0.05$.

reversed the phenomenon of decreased eNOS in rPAECs induced by overexpressed Pfn1. Those observations suggest that miR-1226-3p could alleviate the symptoms of the PAH rats through activating the eNOS/NO pathway via targeting Pfn1.

MCT exposure is a common method used in rats to establish the models to imitate the symptoms of the patients with PAH [18, 19]. In this study, MCT was also used to induce to the formation of PAH in normal rats, and the pathological changes of the PAH rats proved by several experiments, including the RVSP level and RV/(LV+S) ratio, suggested that the models were established successfully. Based on this, we found that miR-1226-3p was downregulated in the lung tissues of the rats treated with MCT, which suggests that miR-1226-3p may have a potential connection with the PAH. Besides, it was also captured that overexpressed miR-1226-3p could diminish the alterations of the PVSP level, RV/(LV+S) ratio, and NO content in the lung tissues of the PAH rats induced by MCT treatment. Those observations suggest that the deficiency of miR-1226-3p, and eNOS is a potential reason to contribute the formation of PAH in the rats treated with MCT.

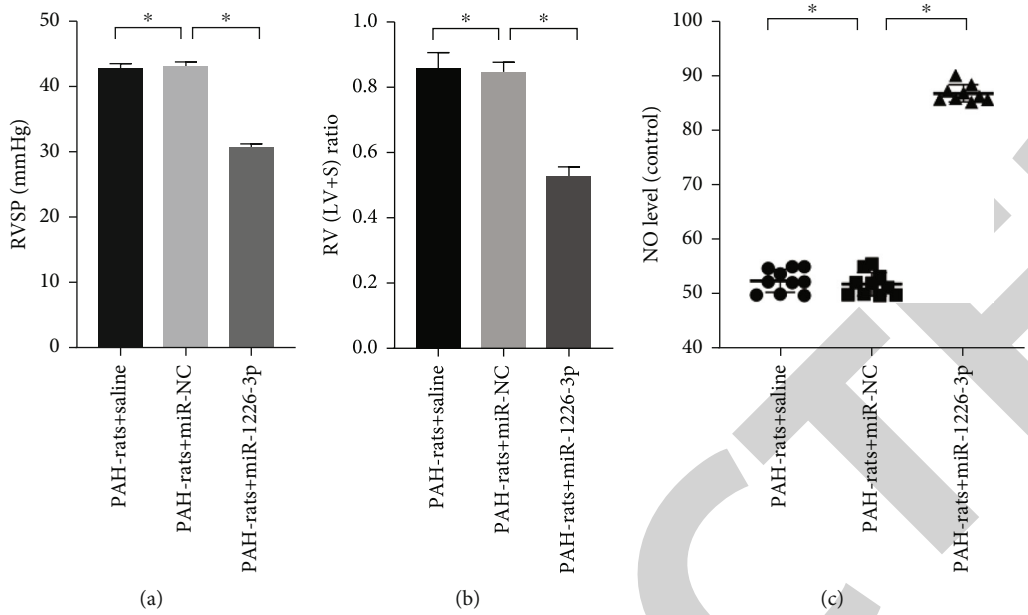

Figure 5: miR-1226-3p protected the PAH rats away from the injury induced by MCT. (a) The RVSP level of the PAH rats in the groups of saline, miR-NC, and miR-1226-3p. (b) The RV/(LV+S) ratio of the PAH rats in the groups of saline, miR-NC, and miR-1226-3p. (c) The NO level of the PAH rats in the groups of saline, miR-NC, and miR-1226-3p. $^*P < 0.05$.

There are many factors causing pulmonary hypertension, including hypoxia, oxidative stress, and the pathological changes in pulmonary vascular structure [20–22]. As a key substance, NO is synthesized by eNOS and can improve the symptom of PAH in patients via alleviating the pressure of arterial artery [23]. In the PAH rats, the decreased NO level in lung tissues of the PAH rats was observed, and the expression level of eNOS was also found to be downregulated in rPAECs, significantly. Those observations support that eNOS deficiency and decrease of NO may be the major reasons in formation of PAH.

Recently, some studies have indicated that eNOS is downregulated in human pulmonary artery endothelial cells, and its expression level is modulated by many factors [24]. The functions of regulating in translation of mRNAs is a common mechanism of miRNAs in taking parts in cellular life activities, and some miRNAs can directly involve in the progression of hypertension via mediating the expression level of eNOS in vascular endothelial cells [25, 26]. In this study, we found that eNOS was upregulated in rRAECs when miR-1226-3p was overexpressed. At present, few studies have illustrated the regular mechanism between miR-1226-3p and eNOS. For miR-1226-3p, it has been found to take a part in regulations of several diseases via targeting the key factors in pathways [27]. A growing amount of data associate Pfn 1, a protein crucial for cell biology, with the pathogenesis of coronary artery disease. It is increasingly clear that Pfn1 functions far beyond its well-known role as an actin dynamic regulator. In this study, Pfn1 was predicted as a potential target of miR-1226-3p by miRWalk, and miR-1226-3p could reduce the luciferase activity of Pnf1 via directly targeting with 3′-UTR of Pnf1. Pfn1 has connected with many diseases of human, and its overexpression contributes to the decreased eNOS in the vascular endothelial cell [28, 29]. We also confirmed that overexpressed Pfn1 induced the downregulation of eNOS, while miR-1226-3p could partly reverse the effect of Pfn1 on the expression of eNOS.

5. Conclusion

In summary, our study suggests that miR-1226-3p plays a protector role in alleviating the symptoms of the PAH rats though promoting the eNOS expression in HPAECs via targeting Pfn1.

Data Availability

The authors confirm that the data supporting the findings of this study are available within the article.

Conflicts of Interest

The authors declare that they have no conflicts of interest.

Authors' Contributions

Jie Jian and Liang Xia performed the experiments, analyzed data, and wrote the manuscript. Jie Jian designed the study. All the authors agreed to be accountable for.

References

[1] H. H. Leuchte, H. ten Freyhaus, H. Gall et al., "Risk stratification strategy and assessment of disease progression in patients with pulmonary arterial hypertension: updated recommendations from the Cologne Consensus Conference 2018," *International Journal of Cardiology*, vol. 272, pp. 20–29, 2018.

Hindawi
BioMed Research International
Volume 2024, Article ID 9859240, 1 page
https://doi.org/10.1155/2024/9859240

Retraction

Retracted: Disorder Genes Regulate the Progression of Ischemic Stroke through the NF-κB Signaling Pathway

BioMed Research International

Received 12 March 2024; Accepted 12 March 2024; Published 20 March 2024

This article has been retracted by Hindawi following an investigation undertaken by the publisher [1]. This investigation has uncovered evidence of one or more of the following indicators of systematic manipulation of the publication process:

(1) Discrepancies in scope

(2) Discrepancies in the description of the research reported

(3) Discrepancies between the availability of data and the research described

(4) Inappropriate citations

(5) Incoherent, meaningless and/or irrelevant content included in the article

(6) Manipulated or compromised peer review

The presence of these indicators undermines our confidence in the integrity of the article's content and we cannot, therefore, vouch for its reliability. Please note that this notice is intended solely to alert readers that the content of this article is unreliable. We have not investigated whether authors were aware of or involved in the systematic manipulation of the publication process.

Wiley and Hindawi regrets that the usual quality checks did not identify these issues before publication and have since put additional measures in place to safeguard research integrity.

We wish to credit our own Research Integrity and Research Publishing teams and anonymous and named external researchers and research integrity experts for contributing to this investigation.

The corresponding author, as the representative of all authors, has been given the opportunity to register their agreement or disagreement to this retraction. We have kept a record of any response received.

References

[1] W. Wei, W. Xin, Y. Tang et al., "Disorder Genes Regulate the Progression of Ischemic Stroke through the NF-κB Signaling Pathway," *BioMed Research International*, vol. 2021, Article ID 2464269, 11 pages, 2021.

Hindawi
BioMed Research International
Volume 2021, Article ID 2464269, 11 pages
https://doi.org/10.1155/2021/2464269

Research Article

Disorder Genes Regulate the Progression of Ischemic Stroke through the NF-κB Signaling Pathway

Wei Wei,[1] Wenqiang Xin,[2] Yufeng Tang,[1] Zhonglun Chen,[1] Yue Heng,[1] Mingjun Pu,[1] Bufan Yang,[1] Jiacai Zuo,[1] and Jingfeng Duan[1]

[1]*Department of Neurology, Mianyang Central Hospital, Mianyang 621000, China*
[2]*Department of Neurosurgery, Tianjin Medical University General Hospital, Tianjin 300052, China*

Correspondence should be addressed to Jingfeng Duan; pengcaiduan122823@163.com

Received 10 July 2021; Revised 7 September 2021; Accepted 8 September 2021; Published 27 October 2021

Academic Editor: Jianxin Shi

Stroke is an acute cerebrovascular disease, including ischemic and hemorrhagic stroke. Stroke is the second leading cause of death after ischemic heart disease, which accounts for 9% of the global death toll. To explore the molecular mechanisms of the effects of the dysregulated factors, in the GEO database, we obtained transcriptome data from 24 h/72 h of mice with ischemic stroke and 24 h/72 h of normal mice. We then performed differential gene analysis, coexpression analysis, enrichment analysis, and regulator prediction bioinformatics analysis to identify the potential genes. We made a comparison between the ischemic stroke 72 h and the ischemic stroke for 24 h, and 5103 differential genes were obtained ($p < 0.05$). Four functional barrier modules were obtained by weighted gene coexpression network analysis. The critical genes of each module were ASTL, Zfp472, Fmr1 gene, and Nap1l1. The results of the enrichment analysis showed ncRNA metabolism, microRNAs in cancer, and biosynthesis of amino acids. These three functions and pathways have the most considerable count value. The regulators of the regulatory dysfunction module were predicted by pivotal analysis of TF and noncoding RNA, and critical regulators including NFKB1 (NF-κB1), NFKBIA, CTNNB1, and SP1 were obtained. Finally, the pivotal target gene found that CTNNB1, NFKB1, NFKBia, and Sp1 are involved in 18, 32, 2, and 60 target genes, respectively. Therefore, we believe that NFKB1 and Sp1 have a potential role in the progression of ischemic stroke. The NFKB signaling pathway promotes inflammatory cytokines and regulates the progression of ischemic stroke.

1. Introduction

Ischemic stroke is the second leading cause of death after ischemic heart disease, accounting for 9% of the global death toll. According to the World Health Organization, 15 million people worldwide suffer from stroke each year, of which more than 6 million die and another 5 million are permanently disabled. Evidence suggests that after ischemic stroke, ROS production rapidly increases overwhelming antioxidant defenses, causing further tissue damage [1].

According to statistics, there are about 25.7 million stroke survivors in the world, and ischemic stroke is still the most common type of stroke. Risk factors include hypertension, hyperlipidemia, and atrial fibrillation as well as bad habits [2]. Ischemic stroke is a multifactorial disease that causes a severe burden of noncommunicable diseases in developing countries. Diabetes, obesity, high blood pressure, and heart disease are prone to ischemic stroke, and the incidence of ischemic stroke is also proportional to body weight. It is mainly because the brain is the tissue that stores energy and it is an active endocrine organ that secretes many humoral factors [3]. Cerebral ischemia activates a cascade of multiple cell type-specific pathological mechanisms. In the central nervous system, ischemic stroke is caused by ischemia that consists of platelets, endothelial cells, and neutrophils. Damage to cell diversity after ischemia can induce cell death or tissue damage in the brain. According to this principle, studies have been conducted to block ASK1 by pharmacological and genetic manipulation to enhance neuroprotection. It thus prevents ischemic stroke [4]. Some studies suggest that blood-brain barrier protection can be used as a treatment strategy for ischemic stroke. The

blood-brain barrier (BBB) is an essential component of the neurovascular unit (NVU), which contains tight junction (TJ) proteins, nutrient transporters, and various ions to maintain healthy brain physiology. The destruction of BBB is the primary pathological marker in the process of ischemic stroke [5], which will regulate matrix metalloproteinases and inflammatory regulators after stimulation. Recent studies have found that ischemic stroke is also associated with lipoprotein A (LPA). It has the potential to cause arteriosclerosis, but there are conflicts in gender-related risk differences [6]. Further studies have also shown that ischemic stroke weight aortic stiffness is also associated with AHR.

In ischemic stroke, studies suggest that the underlying pathophysiological mechanism is impaired baroreceptor function in rigid arteries, leading to impaired BP self-regulation [7]. The study also believes that high heart rate is a strong predictor of poor prognosis in patients with ischemic stroke and can be used to improve their prognosis [8]. A large number of studies have shown that the main progress of ischemic stroke is related to proinflammatory cytokines, including plasma tumor necrosis factor-α (TNF-α) and interleukin (IL-1β, IL-6, IL-8, IL-10, and IL-17). The levels of proinflammatory cytokines were determined by enzyme-linked immunosorbent assay (ELISA). The National Institutes of Health Stroke Scale (NIHSS) can also be used to assess the severity of stroke in patients with ischemic stroke. The results indicate that the severity of the disease is associated with increased inflammation [9]. Currently, the drugs for the treatment of ischemic stroke are perillyl alcohol (PA), probenecid, minocycline, and shikonin. Perillo (PA) has antioxidant and anti-inflammatory properties that protect the nerve by mitigating oxidative stress and inflammation [10]. Probenecid is a potent pannexin 1-channel inhibitor that prevents ischemic brain damage by inhibiting brain inflammation and edema [11, 12]. Minocycline can alleviate the glial cell production of proinflammatory cytokines on neural stem cells [13]. Shikonin effectively protects the brain from damage by regulating the inflammatory response and improving BBB permeability [14]. Studies have shown that embryonic stem cells, induced pluripotent stem cells, neural stem cells, and mesenchymal stem cells may be beneficial for cell replacement and beneficial for neuroprotection, regulating inflammation and immune response [15]. The purpose of this study was to understand the mechanism of proinflammatory cytokines in the regulation of ischemic stroke and provide a reference for the clinical treatment of ischemic stroke.

2. Materials and Methods

2.1. Data Resource. All data in this study were from GEO, the microarray data of the database numbered GSE102558 was selected, and the data of the probe in the experiment was GPL20710. In this dataset, induced ischemic stroke (middle cerebral artery occlusion) in wild-type animals was applied. After 24 and 72 hours, the isolated cardiac RNA were extracted. For both time points, we generated and analyzed sham operated control animals. The Gene Expressions Comprehensive Database is an international public knowledge base. With advances in bioinformatics, GEO can now accept high-throughput sequencing data for other data applications, including detection of genomic methylation, chromosome structure, and genomic and proteome interactions. We downloaded the transcriptome data of cardiac samples of 24 h/72 h ischemic stroke mice (6 each) and 24 h/72 h normal mice (6 each) in GEO for differential analysis of gene differential expression [16].

2.2. Difference Analysis. We analyzed the processing of the GEO specimens and the sample microarray data obtained in the R language. The difference analysis of the gene expression map data in this study is mainly realized by using the R language limma package [17–19], which contains preliminary screening and correction of data. We used the correct background function to calibrate and standardize the data, setting the threshold of $p < 0.05$ and $|\log FC| > 2$, which is exceptionally significant. We then used the quantile normalization method in the normalizeBetweenArrays function to filter out the control probes in the GPL20710 data and the low-expressed probes. We used the eBayes and lmfit functions to identify differentially expressed genes in the dataset, with default parameters.

2.3. Coexpression Analysis. To explore the molecular mechanisms of gene expression during the progression of ischemic stroke, we performed a differential analysis between 24 h/72 h (6 each) of ischemic stroke mice and 24 h/72 h (6 each) of normal mice. Thus, the expression profile of the differential gene was made based on the obtained 5103 differential genes. We used a weighted gene coexpression network analysis (WGCNA) [20] to analyze the differential expression profile matrix obtained from the study. The aim is to explore the synergistic expression of differential genes, thereby clustering to form gene modules with the same/similar expression function, which we also call functional disorder modules. We used the correlation coefficient weighting method to take the N-th power of the correlation coefficient between genes and then obtained the correlation coefficient between any two genes. Before the results of the correlation coefficients were clustered, the links between the genes in the network need to be subject to the scale-free network distribution to be more biologically significant. After obtaining the weighted correlation coefficients, we clustered them and constructed a clustering tree by correlation coefficients between different genes. The different branches of the cluster tree represented different functional barrier modules. Contrasting colors represented different modules, and there was a high correlation between the genes in the same branch. Based on the ability of the gene to regulate in each dysfunction module, we unearthed the essential genes that cause the dysfunction of the functional modules.

2.4. Enrichment Analysis. After obtaining the functional disorder module, it is necessary to understand the function and signaling pathway of the critical genes involved in the module, in order to better understand the molecular mechanism of ischemic stroke healing. The enrichment analysis of the function and pathway of the gene of the dysfunctional

module is an effective means to explore the potential mechanism of gene expression of ischemic stroke healing for myocarditis. In this study, we took acute wound specimens and samples on the third postoperative day.

On the 3rd and seventh day after surgery, we obtained 14 functional disorder modules by coexpression analysis. We used the Bioconductor's clusterProfiler package [21] in the R language for enrichment analysis of functions and pathways. With the clusterProfiler package, we can perform statistical analysis and visualization of functional clustering of genes or gene clusters.

GlueGO was used to enrich the functions and paths of each module and build a corresponding function and access network. We identified modules that participate in the ratio of corresponding functions and pathways to find the highest channel. In this study, the function of participating in neutrophils and vesicles was found to have a higher count value.

2.5. Regulator Analysis. Gene transcription and posttranscriptional regulation are often centered on noncoding RNA (ncRNA) and transcription factor (TF). Therefore, we also believe that ncRNA and TF are regulators of the entire molecular mechanism, so we need to analyze its regulators to understand the molecular mechanism of ischemic stroke healing better. We scientifically predict and test the role of dysfunction modules for skin posthealing by bioinformatics, thereby improving the accuracy and efficiency of the experiment. During the ncRNA pivot analysis, we screened the control lines between each regulator and each module to be greater than or equal to 6 plots, and for the significance of the abdominal muscle targets between each module, p value < 0.01. In the course of TF pivot analysis, we calculated the target significance of enrichment in each module based on the hypergeometric test (p value < 0.01). The data is finally entered into Cytoscape to make a pivot-module network diagram.

2.6. Back to Target Genes. Based on the obtained ncRNA and TF that drive ischemic stroke, the target genes are traced back. A single regulator can involve several target genes. We used the interaction pairs in the raid database to backtrack the obtained ncRNA and TF. The interactions between humans and mice were screened separately, and then, score > 0.5 was selected for combined deduplication. We finally obtained ncRNA and TF target genes.

3. Results

3.1. Determining the Expression of Dysregulated Molecules in Ischemic Stroke. We performed differential gene analysis by comparing transcriptome data from cardiac samples. A broad threshold $p < 0.05$ was set, and 5103 differential genes were obtained (Table S1). Among the differential genes, we believe that there are expression disorders that regulate the progression of ischemic stroke.

3.2. Identify Ischemic Stroke-Related Functional Disorder Modules. Biological networks can characterize the underlying pathogenic mechanisms of biological disease and clusters form modules, each of which characterizes a potential mechanism of action. Each module also contains the core genes for its function, and core genetic disorders will drive the module to dysregulate, causing abnormalities in a global function, leading to disease. In order to study the functional disorder module related to the progression of ischemic stroke, it is necessary to construct the expression profile matrix in the sample for the above 5103 differential genes and their interaction genes. Based on the weighted gene coexpression network analysis (WGCNA), we observed that these genes showed significant grouping expression in the samples, and the genes with similar behavioral expression formed a module for coexpression clustering. In this study, we aggregated gene expression behavior into modules. It helps us to observe the complex collaborative relationships between these genes from the perspective of expression behavior. Among the four functional disorder modules (Figures 1(a) and 1(b)), based on the functional disorder module, we further identified the essential genes of each module and obtained the four core genes Astl, Zfp472, Fmr1, and Napl1l1 (Table 1). We associated the module with the phenotype data and plotted it (Figure 1(c)). In the sample, the turquoise module was associated with gene expression 24 h of ischemic stroke. In the 72 h sample of ischemic stroke, MEblue, MEbrown, and yellow were associated with gene expression 72 h of ischemic stroke.

3.3. Functions and Pathways Involved in the Gene of Interest. Function and pathway are essential mediators of the physiological response of the disease. We performed functional and pathway enrichment analysis on the four functional barrier modules and obtained a total of 22056 biological processes, 2693 cells, 4840 molecular functions, and 993 KEGG pathways (Table S2). The highest function of count is ribosomal large subunit assembly, and the highest path of count is steroid biosynthesis. We extracted some of the functions and pathways of interest from the table for analysis and bubble diagrams (Figures 2(a) and 2(b)). The results showed that the ncRNA metabolic process, microRNAs in cancer, and biosynthesis of amino acids had the most substantial count value. From the figure, we can see that ncRNA and miRNA are related to the whole process of ischemic stroke, mainly to regulate the biosynthesis of amino acids and affect the expression of proteins and the proinflammatory cytokines. The endogenous polypeptide produced by the immune system cells with many powerful biological effects can mediate a variety of immune responses. Therefore, we believe that critical genes mainly affect the progression of ischemic stroke by regulating the production of proinflammatory cytokines.

3.4. ncRNA and TF That Drive the Development of Ischemic Stroke. Through the above analysis, we obtained functional and critical genes that are associated with the progression of ischemic stroke. From the perspective of systems biology and systems genetics, transcription and posttranscriptional regulation of genes have long been recognized as a critical regulator of disease development and progression. Transcription factors and ncRNA are conventional regulators.

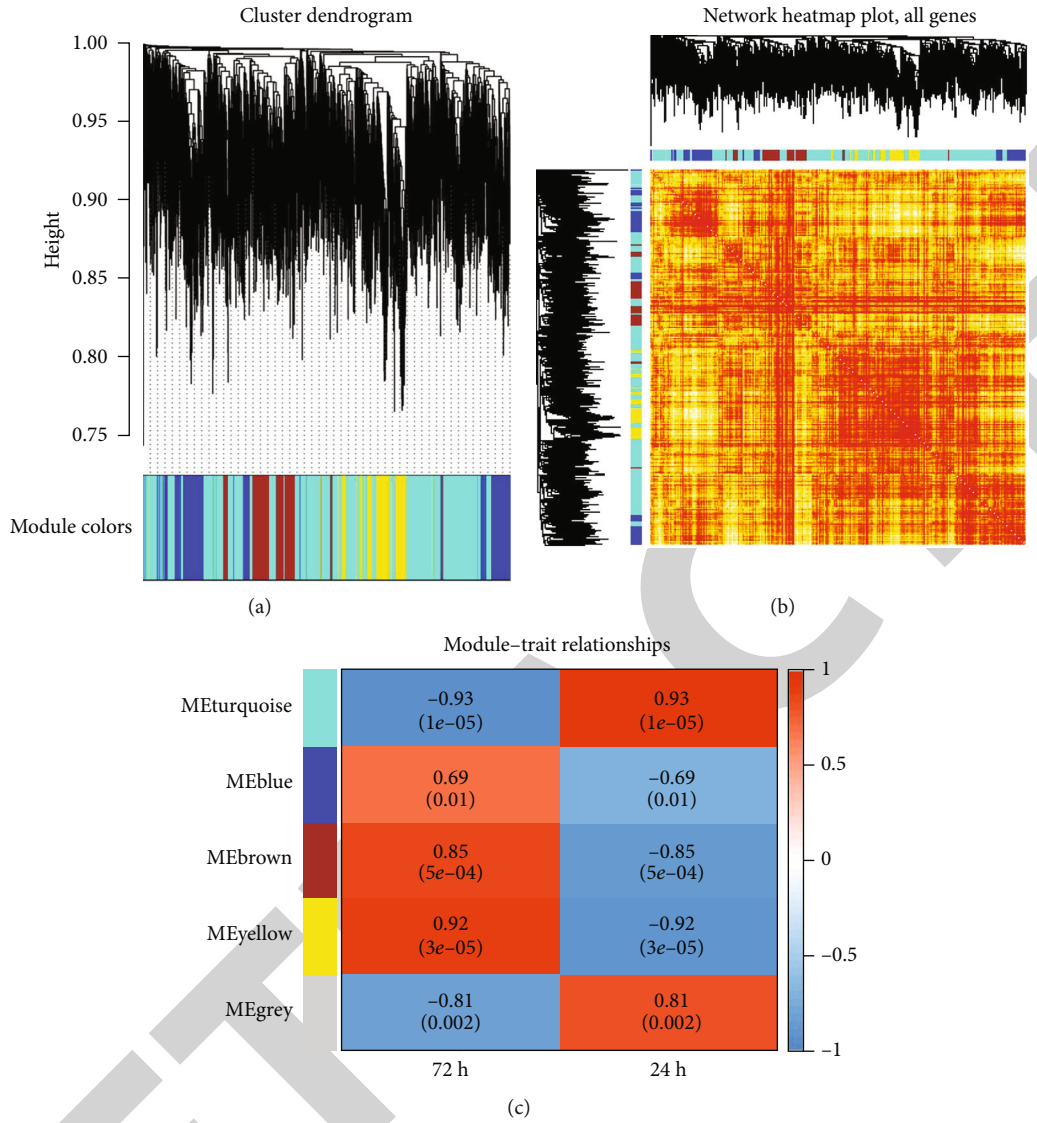

Figure 1: Synergistic expression of differential genes between acute wound specimens and postoperative wounds on days 3 and 7. (a) The 14 coexpression panels obtained by clustering were identified as modules, and 14 colors represent 14 coexpression modules. (b) Expression heat map of all genes in the sample, whose expression behavior is clustered into 14 coexpression modules. (c) Each row represents a module, each column represents a phenotype, the color of each cell is mapped by the corresponding correlation coefficient, the value is from -1 to 1, the color transitions from blue to white, and then transitions to red.

Table 1: Hub gene of modules.

Color	Hudgens	Module
Blue	Astl	m4
Brown	Zfp472	m3
Turquoise	Fmr1	m1
Yellow	Nap1l1	m2

We performed a pivotal analysis of coexpressed modular genes to explore critical transcriptional regulators in the progression of ischemic stroke. Pivot analysis was performed based on the targeted regulation of the TF and ncRNA on the module gene, and a network diagram of the relationship between TF and ncRNA was obtained (Figures 3(a) and 3(b)). The results showed a total of 53 ncRNAs involving 56 ncRNA-module pairs. There are 17 TFs involving 19 TF-module pairs (Tables S3 and S4). In the ncRNA pivot assay, miR-10b-5p was most ligated to ncRNA. In the analysis, the modules and TF connections are more NFKB1, Ctnnb1. NFKB1 has shown its pivotal role in the analysis of the functions and pathways in which our genes of interest are involved. Therefore, we believe that NFKB1 has a potential regulatory role in the progression of ischemic stroke. The mechanism of action may be that proinflammatory cytokines regulate the progression of ischemic stroke through the NFKB signaling pathway.

3.5. Backtracking the Target Gene of the Pivot. After analyzing the ncRNA and TF that drive ischemic stroke, we

(a)

Figure 2: Continued.

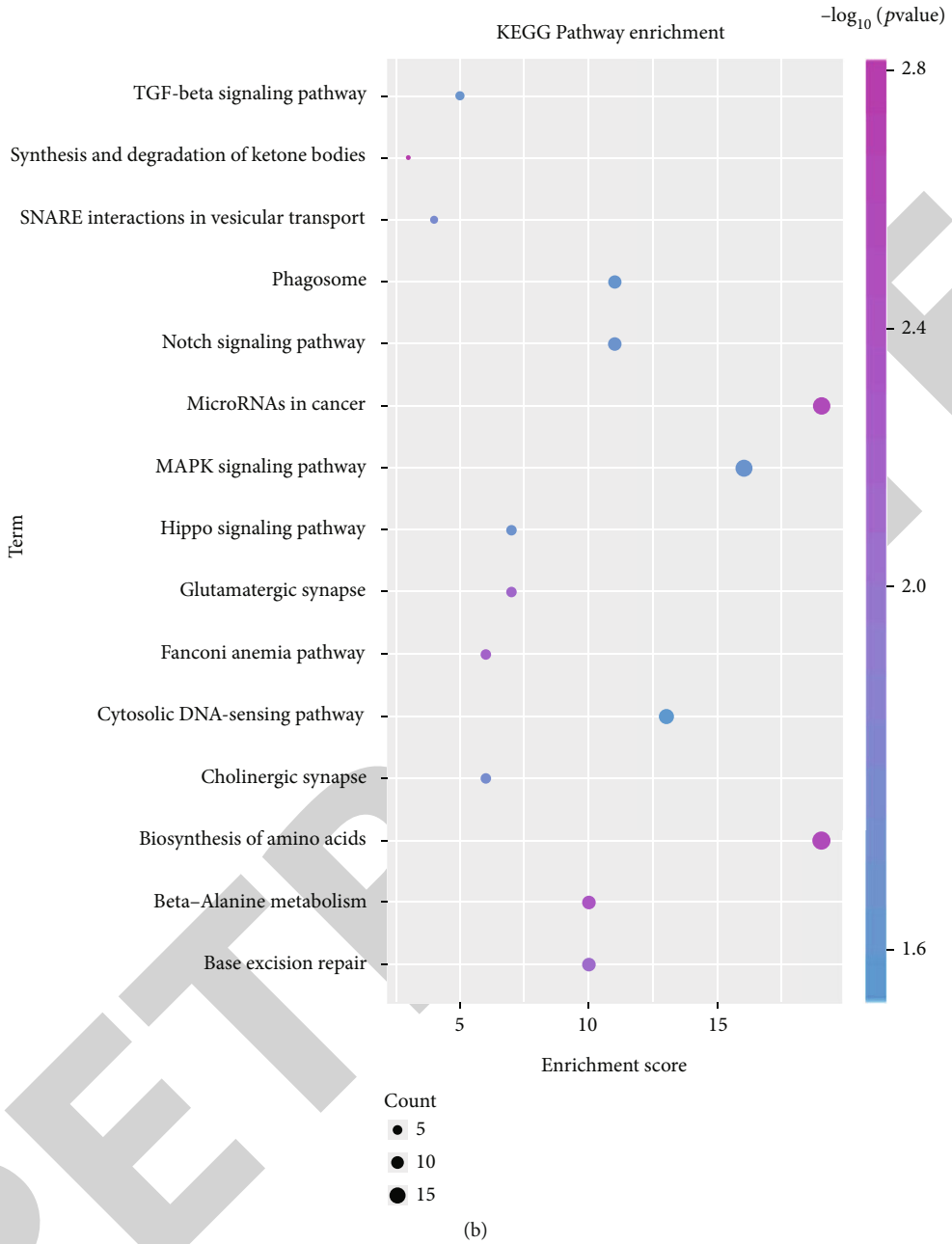

Figure 2: Functional and pathway enrichment analysis excerpts of the module gene. (a) Module gene GO function enrichment analysis excerpt. The color increases from blue to purple, and the enrichment increases significantly. The larger the circle, the more significant the proportion of the gene in the module that accounts for the GO function. (b) Module gene KEGG pathway enrichment analysis excerpt. The color increases from blue to purple, and the enrichment increases significantly. The larger the circle, the more significant the proportion of the gene in the KEGG pathway entry.

obtained a network diagram of their interactions. The ncRNA or TF-related target genes are not represented in the network diagram, so we need to backtrack the obtained ncRNA pivot and TF pivot (Tables S5 and S6). The results of retrospective target genes showed that G730013B05Rik and mmu-miR-362-3p involved 103 and 92 target genes, respectively, and Ctnnb1, NFKB1, NFKBia, and Sp1 involved 18, 32, 2, and 60 target genes, respectively. Therefore, we believe that G730013B05Rik, mmu-miR-362-3p, NFKB1, and Sp1 have potential roles in the progression of ischemic stroke. The mechanism of action may be that proinflammatory cytokines regulate the progression of ischemic stroke through the NFKB signaling pathway.

4. Discussion

Ischemic stroke is considered to be one of the major health problems in the world with high mortality and morbidity. Studies have found that it is associated with inflammation, oxidative stress, and excitotoxicity. Ischemic stroke is often

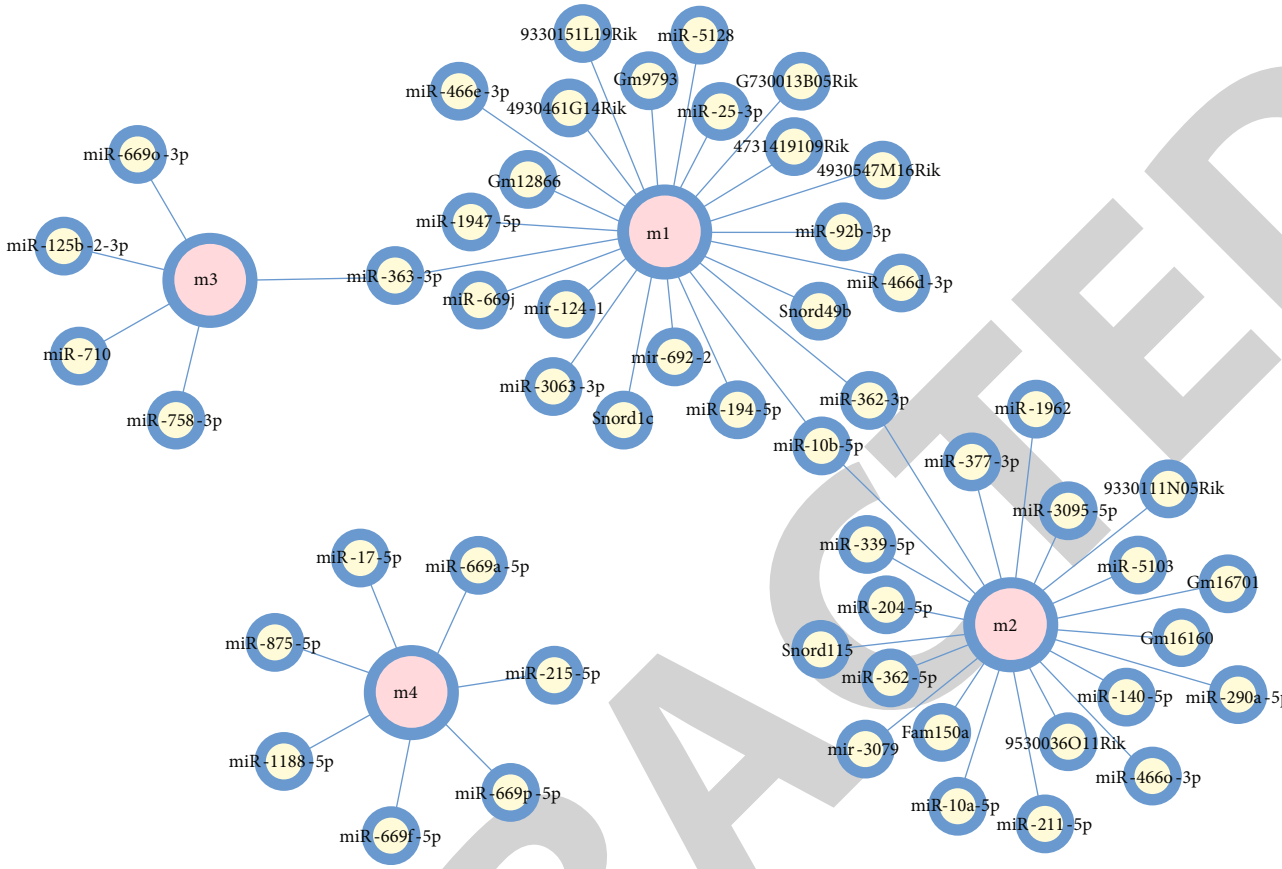

(a)

Figure 3: Continued.

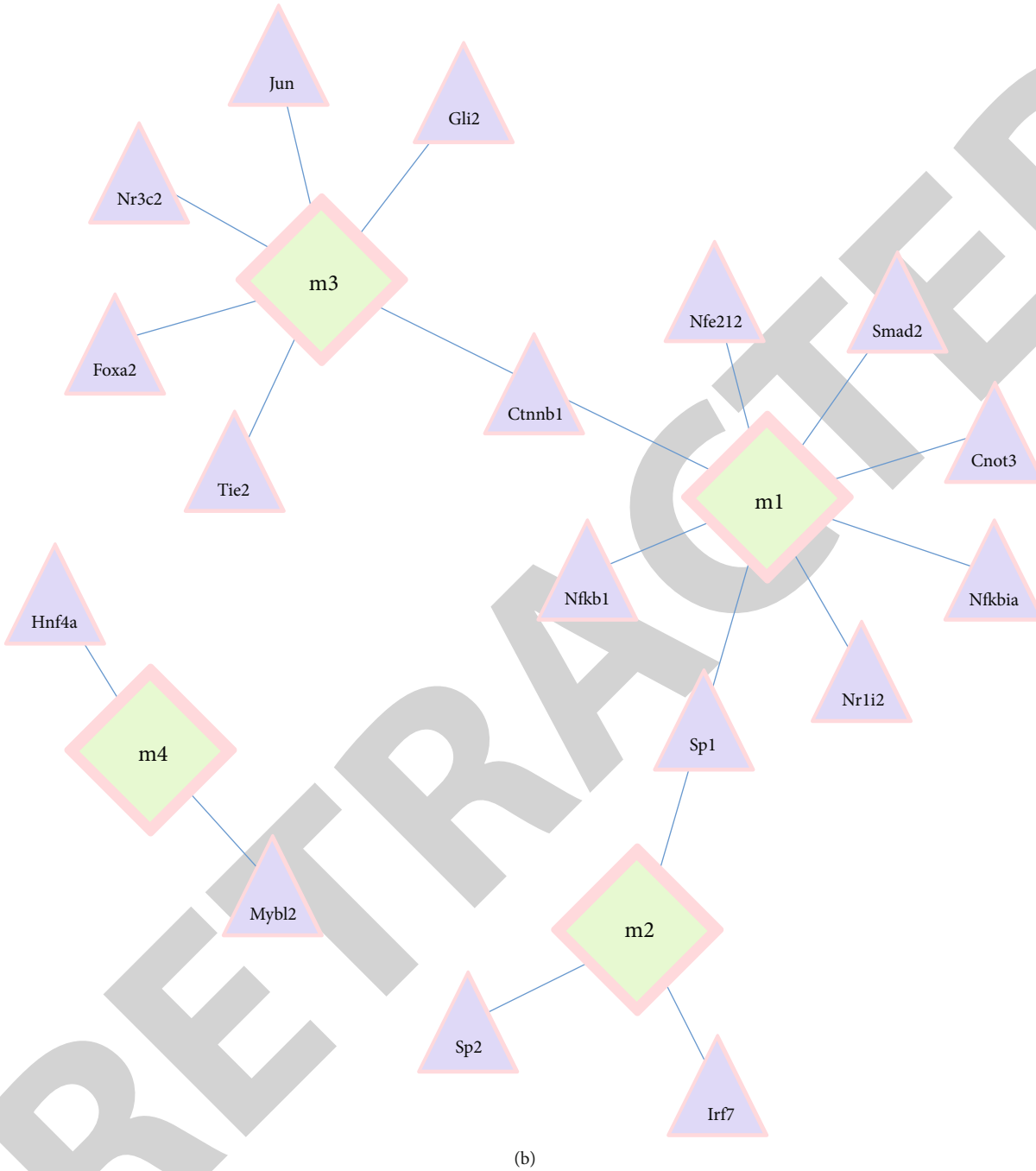

Figure 3: Regulatory effect of the regulator on the dysfunction module. (a) Orange circles represent modules and yellow circles represent ncRNA. (b) The green circle represents the module, and the purple circle represents the TF.

required to be treated in a short period, so it is needed to developing a more effective neuroprotective agent in the direction of treatment. For targeted treatment and prevention of ischemic stroke, we need to understand the mechanisms of dysfunction. Recent studies have shown that both endogenous basic fibroblast growth factor (bFGF), apolipoprotein E gene (APOE), BET 2, and remote ischemic preconditioning (RIPerC) are significantly reduced with ischemic related to stroke. bFGF is not only related to neuroprotection and neurotrophic effects but also excessive astrocyte proliferation and glial scar formation after neuronal injury. The presence of the E4 allele is a risk factor for ischemic cerebrovascular disease. RIPerC prevents collateral collapse from having neuroprotective effects [22–25]. In order to study its mechanism of action, we need to analyze its differential genes. We collected transcriptome data from 24 h/72 h in ischemic stroke mice and 24 h/72 h in normal mice (GSE102558). Difference analysis and coexpression analysis were performed after standardization [26]. After WGCNA coexpression network analysis, a total of 5103

differential genes were obtained. Due to a large number of differential genes, we need to further cluster these differential genes. We clustered similarly expressed genes to obtain four related functional disorder modules, including the four core genes Astl, Zfp472, Fmr1, and Nap1l1. Also, other studies have shown that single-nucleotide polymorphisms (SNPs) are associated with ischemic stroke, mainly affected by ZNF208 and HNF1A [27, 28]. ADAMTS-4 has an anti-inflammatory effect mainly in the CNS. There are more and more studies on promoting ischemic stroke [29, 30], but we still need to continue to analyze how proinflammatory cytokines work. We analyzed the functions and pathways involved in differential genes, and the highest function of count was ribosomal large subunit assembly, and the highest path of count was steroid biosynthesis. Analysis of the functions and pathways of interest revealed that the larger count values were mainly focused on the regulation of amino acid biosynthesis. Proinflammatory cytokines are endogenous polypeptides produced by the immune system cells with many powerful biological effects. Therefore, we believe that the gene of interest mainly affects the progression of ischemic stroke by regulating the production of proinflammatory cytokines. The main proinflammatory cytokines in the study were tumor necrosis factor alpha (TNF-alpha) and interleukins. Studies on TNF-alpha have shown that the immune system can affect brain function quickly and adversely. TNF-α signaling may be a target of neuroprotection, which may be involved in the pathogenesis of ischemic stroke [30, 31]. Interleukins are also typical proinflammatory cytokines, and the level of interleukins after ischemia is increased [32–34], suggesting a potential mechanism of action with ischemic stroke. It is noteworthy that studies have shown that IL-6, IL-1β, and TNFα are both inhibited by TLR4/NF-κB [35]. In this study, the ncRNA and TF were analyzed by pivotal analysis. The module and TF were more connected with NFKB1. The NF-κB signaling pathway acts as a "molecular switch" in ischemic stroke. When it is on, numerous proinflammatory cytokines, cellular adhesion molecules, and immunologic mediators are expressed or synthesized and secreted, promoting an inflammatory response. Studies have shown that NFKB1 (NF-κB1) is significantly involved in the progression of ischemic stroke. We have learned that NFKB1 (NF-κB1) can be cotranslated by the 26S proteasome to produce 105KD protein. Proinflammatory cytokines are precisely peptides, so we believe that the mechanism of action may be that proinflammatory cytokines regulate the progression of ischemic stroke through the NFKB signaling pathway. Comparing the studies done by other scholars, we found that the genes of the NFKB family do significantly regulate the progression of ischemic stroke. The TLR4/MyD88/NF-κB signaling pathway and the ROS/TLR4/NF-κB inflammatory signaling pathway [36, 37] have all shown their regulatory mechanisms. Proinflammatory and anti-inflammatory effects, as well as neuroprotection, are associated with the NF-κB signaling pathway [38, 39]. However, the major limitation is there is no further experimental validation for our results, which will be performed soon. In summary, the study suggests that the NFKB signaling pathway mainly regulates the role of proinflammatory cytokines in ischemic stroke.

Data Availability

The datasets used and/or analyzed during the present study are available from the corresponding author on reasonable request.

Ethical Approval

The study was approved by the Ethics Committee of Mianyang Central Hospital.

Consent

Consent is not applicable in this paper.

Conflicts of Interest

The authors declare that they have no competing interests.

Authors' Contributions

WW, WX, YT, ZC, and JD led the conception and design of this study. WW, WX, YT, YH, MP, BY, and JZ were responsible for the data collection and analysis. WW, ZC, and JD were in charge of interpreting the data and drafting the manuscript. WX, YT, and ZC made revision from critical perspective for important intellectual content. The final version was read and adopted by all the authors.

Supplementary Materials

Supplementary 1. Table S1: DEG of genes (p value < 0.05).

Supplementary 2. Table S2: enrichment_all.

Supplementary 3. Table S3: ncRNA pivot that regulates modular genes.

Supplementary 4. Table S4: TF pivot that regulates modular genes.

Supplementary 5. Table S5: ncRNA_target_gene.

Supplementary 6. Table S6: TF_target_gene.

References

[1] R. Rodrigo, R. Fernandez-Gajardo, R. Gutierrez et al., "Oxidative stress and pathophysiology of ischemic stroke: novel therapeutic opportunities," *CNS & Neurological Disorders Drug Targets*, vol. 12, no. 5, pp. 698–714, 2013.

[2] J. F. Meschia and T. Brott, "Ischaemic stroke," *European Journal of Neurology*, vol. 25, no. 1, pp. 35–40, 2018.

[3] J. Gairolla, R. Kler, M. Modi, and D. Khurana, "Leptin and adiponectin: pathophysiological role and possible therapeutic target of inflammation in ischemic stroke," *Reviews in the Neurosciences*, vol. 28, no. 3, pp. 295–306, 2017.

[4] S. Y. Cheon, E. J. Kim, J. M. Kim, and B. N. Koo, "Cell type-specific mechanisms in the pathogenesis of ischemic stroke: the role of apoptosis signal-regulating kinase 1," *Oxidative Medicine and Cellular Longevity*, vol. 2018, Article ID 2596043, 9 pages, 2018.

[5] A. E. Sifat, B. Vaidya, and T. J. Abbruscato, "Blood-brain barrier protection as a therapeutic strategy for acute ischemic

stroke," *The AAPS Journal*, vol. 19, no. 4, pp. 957–972, 2017.

[6] A. H. Nave, K. S. Lange, C. O. Leonards et al., "Lipoprotein (a) as a risk factor for ischemic stroke: a meta-analysis," *Atherosclerosis*, vol. 242, no. 2, pp. 496–503, 2015.

[7] M. Kwarciany, D. Gasecki, K. Kowalczyk et al., "Acute hypertensive response in ischemic stroke is associated with increased aortic stiffness," *Atherosclerosis*, vol. 251, pp. 1–5, 2016.

[8] Z. Zhu, C. Zhong, T. Xu et al., "Effect of renal function status on the prognostic value of heart rate in acute ischemic stroke patients," *Atherosclerosis*, vol. 263, pp. 1–6, 2017.

[9] L. Feng, J. Guo, and F. Ai, "Circulating long noncoding RNA ANRIL downregulation correlates with increased risk, higher disease severity and elevated pro-inflammatory cytokines in patients with acute ischemic stroke," *Journal of Clinical Laboratory Analysis*, vol. 33, no. 1, article e22629, 2019.

[10] R. Tabassum, K. Vaibhav, P. Shrivastava et al., "Perillyl alcohol improves functional and histological outcomes against ischemia-reperfusion injury by attenuation of oxidative stress and repression of COX-2, NOS-2 and NF-κB in middle cerebral artery occlusion rats," *European Journal of Pharmacology*, vol. 747, pp. 190–199, 2015.

[11] X. X. Xiong, L. J. Gu, J. Shen et al., "Probenecid protects against transient focal cerebral ischemic injury by inhibiting HMGB1 release and attenuating AQP4 expression in mice," *Neurochemical Research*, vol. 39, no. 1, pp. 216–224, 2014.

[12] M. Freitas-Andrade, J. F. Bechberger, B. A. MacVicar, V. Viau, and C. C. Naus, "Pannexin1 knockout and blockade reduces ischemic stroke injury in female, but not in male mice," *Oncotarget*, vol. 8, no. 23, pp. 36973–36983, 2017.

[13] S. U. Vay, S. Blaschke, R. Klein, G. R. Fink, M. Schroeter, and M. A. Rueger, "Minocycline mitigates the gliogenic effects of proinflammatory cytokines on neural stem cells," *Journal of Neuroscience Research*, vol. 94, no. 2, pp. 149–160, 2016.

[14] L. Wang, Z. Li, X. Zhang et al., "Protective effect of shikonin in experimental ischemic stroke: attenuated TLR4, p-p38MAPK, NF-κB, TNF-α and MMP-9 expression, up-regulated claudin-5 expression, ameliorated BBB permeability," *Neurochemical Research*, vol. 39, no. 1, pp. 97–106, 2014.

[15] L. Hao, Z. Zou, H. Tian, Y. Zhang, H. Zhou, and L. Liu, "Stem cell-based therapies for ischemic stroke," *BioMed Research International*, vol. 2014, Article ID 468748, 17 pages, 2014.

[16] E. Clough and T. Barrett, "The gene expression omnibus database," *Methods in Molecular Biology*, vol. 1418, pp. 93–110, 2016.

[17] M. E. Ritchie, B. Phipson, D. Wu et al., "limma powers differential expression analyses for RNA-sequencing and microarray studies," *Nucleic Acids Research*, vol. 43, no. 7, article e47, 2015.

[18] C. W. Law, Y. Chen, W. Shi, and G. K. Smyth, "voom: precision weights unlock linear model analysis tools for RNA-seq read counts," *Genome Biology*, vol. 15, no. 2, p. R29, 2014.

[19] G. K. Smyth, "Linear models and empirical Bayes methods for assessing differential expression in microarray experiments," *Statistical Applications in Genetics and Molecular Biology*, vol. 3, no. 1, pp. 1–25, 2004.

[20] P. Langfelder and S. Horvath, "WGCNA: an R package for weighted correlation network analysis," *BMC Bioinformatics*, vol. 9, no. 1, p. 559, 2008.

[21] G. Yu, L. G. Wang, Y. Han, and Q. Y. He, "clusterProfiler: an R package for comparing biological themes among gene clusters," *OMICS*, vol. 16, no. 5, pp. 284–287, 2012.

[22] L. Ye, Y. Yang, X. Zhang et al., "The role of bFGF in the excessive activation of astrocytes is related to the inhibition of TLR4/NFκB signals," *International Journal of Molecular Sciences*, vol. 17, no. 1, p. 37, 2016.

[23] C. Konialis, K. Spengos, P. Iliopoulos et al., "The APOE E4 allele confers increased risk of ischemic stroke among Greek carriers," *Advances in Clinical and Experimental Medicine*, vol. 25, no. 3, pp. 471–478, 2016.

[24] J. Jane, R. Lo, and C. A. Graham, "BET 2: blood biomarkers as an alternative to imaging in diagnosing acute ischaemic stroke," *Emergency Medicine Journal*, vol. 35, no. 5, pp. 336–338, 2018.

[25] J. Ma, Y. Ma, B. Dong, M. V. Bandet, A. Shuaib, and I. R. Winship, "Prevention of the collapse of pial collaterals by remote ischemic perconditioning during acute ischemic stroke," *Journal of Cerebral Blood Flow and Metabolism*, vol. 37, no. 8, pp. 3001–3014, 2017.

[26] R. Veltkamp, S. Uhlmann, M. Marinescu et al., "Experimental ischaemic stroke induces transient cardiac atrophy and dysfunction," *Journal of Cachexia, Sarcopenia and Muscle*, vol. 10, no. 1, pp. 54–62, 2019.

[27] J. Yu, F. Zhou, D. Luo et al., "ZNF208polymorphisms associated with ischemic stroke in a southern Chinese Han population," *The Journal of Gene Medicine*, vol. 19, no. 1-2, 2017.

[28] Y. J. Zhou, R. X. Yin, S. C. Hong, Q. Yang, X. L. Cao, and W. X. Chen, "Association of the HNF1A polymorphisms and serum lipid traits, the risk of coronary artery disease and ischemic stroke," *The Journal of Gene Medicine*, vol. 19, no. 1-2, p. e2941, 2017.

[29] S. Lemarchant, H. Dunghana, Y. Pomeshchik et al., "Anti-inflammatory effects of ADAMTS-4 in a mouse model of ischemic stroke," *Glia*, vol. 64, no. 9, pp. 1492–1507, 2016.

[30] S. H. Baik, M. Fane, J. H. Park et al., "Pin1 promotes neuronal death in stroke by stabilizing Notch intracellular domain," *Annals of Neurology*, vol. 77, no. 3, pp. 504–516, 2015.

[31] G. Cui, H. Wang, R. Li et al., "Polymorphism of tumor necrosis factor alpha (TNF-alpha) gene promoter, circulating TNF-alpha level, and cardiovascular risk factor for ischemic stroke," *Journal of Neuroinflammation*, vol. 9, no. 1, p. 235, 2012.

[32] P. Kumar, A. K. Yadav, A. Kumar, R. Sagar, A. K. Pandit, and K. Prasad, "Association between interleukin-6 (G174C and G572C) promoter gene polymorphisms and risk of ischaemic stroke: a meta-analysis," *Annals of Neurosciences*, vol. 22, no. 2, pp. 61–69, 2015.

[33] B. Silva, L. Sousa, A. Miranda et al., "Memory deficit associated with increased brain proinflammatory cytokine levels and neurodegeneration in acute ischemic stroke," *Arquivos de Neuro-Psiquiatria*, vol. 73, no. 8, pp. 655–659, 2015.

[34] R. Zhou, Z. Yang, X. Tang, Y. Tan, X. Wu, and F. Liu, "Propofol protects against focal cerebral ischemia via inhibition of microglia-mediated proinflammatory cytokines in a rat model of experimental stroke," *PLoS One*, vol. 8, no. 12, article e82729, 2013.

[35] P. Zhang, Z. F. Guo, Y. M. Xu, Y. S. Li, and J. G. Song, "_N_ -Butylphthalide (NBP) ameliorated cerebral ischemia reperfusion-induced brain injury via HGF-regulated TLR4/NF-κB signaling pathway," *Biomedicine & Pharmacotherapy*, vol. 83, pp. 658–666, 2016.

Hindawi
BioMed Research International
Volume 2024, Article ID 9852462, 1 page
https://doi.org/10.1155/2024/9852462

Retraction

Retracted: Protein Arginine Methyltransferase 5 Promotes the Migration of AML Cells by Regulating the Expression of Leukocyte Immunoglobulin-Like Receptor B4

BioMed Research International

Received 12 March 2024; Accepted 12 March 2024; Published 20 March 2024

This article has been retracted by Hindawi following an investigation undertaken by the publisher [1]. This investigation has uncovered evidence of one or more of the following indicators of systematic manipulation of the publication process:

(1) Discrepancies in scope

(2) Discrepancies in the description of the research reported

(3) Discrepancies between the availability of data and the research described

(4) Inappropriate citations

(5) Incoherent, meaningless and/or irrelevant content included in the article

(6) Manipulated or compromised peer review

The presence of these indicators undermines our confidence in the integrity of the article's content and we cannot, therefore, vouch for its reliability. Please note that this notice is intended solely to alert readers that the content of this article is unreliable. We have not investigated whether authors were aware of or involved in the systematic manipulation of the publication process.

Wiley and Hindawi regrets that the usual quality checks did not identify these issues before publication and have since put additional measures in place to safeguard research integrity.

We wish to credit our own Research Integrity and Research Publishing teams and anonymous and named external researchers and research integrity experts for contributing to this investigation.

The corresponding author, as the representative of all authors, has been given the opportunity to register their agreement or disagreement to this retraction. We have kept a record of any response received.

References

[1] L. Zhao, B. Cheng, J. Xiong et al., "Protein Arginine Methyltransferase 5 Promotes the Migration of AML Cells by Regulating the Expression of Leukocyte Immunoglobulin-Like Receptor B4," *BioMed Research International*, vol. 2021, Article ID 7329072, 18 pages, 2021.

Hindawi
BioMed Research International
Volume 2021, Article ID 7329072, 18 pages
https://doi.org/10.1155/2021/7329072

Research Article

Protein Arginine Methyltransferase 5 Promotes the Migration of AML Cells by Regulating the Expression of Leukocyte Immunoglobulin-Like Receptor B4

Lu Zhao,[1,2] **Bingqing Cheng**,[3,4] **Jie Xiong**,[3,4] **Dan Ma**,[3,4] **Xin Liu**,[1] **Li Wang**,[1] **Xi Zhang**,[2] **and Jishi Wang**[1,3,4]

[1]*School of Clinical Medicine, Guizhou Medical University, Guiyang 550004, China*
[2]*Medical Center of Hematology, Xinqiao Hospital, State Key Laboratory of Trauma, Burn and Combined Injury, Army Medical University, Chongqing 400037, China*
[3]*Department of Hematology, Affiliated Hospital of Guizhou Medical University, Guiyang 550004, China*
[4]*Key Laboratory of Hematological Disease Diagnostic and Treat Centre of Guizhou Province, Guiyang 550004, China*

Correspondence should be addressed to Jishi Wang; wjs1025373217@163.com

Received 12 August 2021; Accepted 24 September 2021; Published 19 October 2021

Academic Editor: Jun Yang

Acute myeloid leukemia (AML) is the most common type of acute leukemia in adults with poor prognosis. Especially for AML-M5 type, due to the strong cell migration ability, the possibility of extramedullary invasion is large and widespread, which leads to poor therapeutic effect. Previous studies have found that protein arginine methyltransferase 5 (PRMT5) could promote the proliferation and differentiation of leukemic cells in AML, but its regulation on the invasive ability of AML cells remains unclear. This study was designed to explore the role of PRMT5 in regulating the invasion of AML cells and to investigate the mechanisms. Patient samples were collected for detection of PRMT5 expression level. AML cells were used for exploring the function of PRMT5. The results of clinical samples showed that the expression of PRMT5 was significantly increased in newly diagnosed and recurrent AML patients, and the expression of leukocyte immunoglobulin-like receptor B4 (LILRB4) was positively correlated with the level of PRMT5. In the cell experiment in vitro, we found that when PRMT5 was knocked down, the invasion, migration, and adhesion capacities of MV-4-11 cells and THP-1 cells were decreased, and the mRNA and protein levels of LILRB4 were also decreased. Moreover, we screened related signaling pathways and found that PRMT5 affected the expression of downstream LILRB4 by activating mTOR pathway, which in turn enhanced the invasive ability of AML cells. Taken together, PRMT5 plays an important role in the invasion of AML, which acts via regulating the expression of LILRB4. PRMT5 could act as a potential therapeutic candidate for AML.

1. Background

Acute myeloid leukemia (AML) is the most common type of acute leukemia in adults. Despite the various therapeutic discoveries on AML with the deepening research [1–4], the "anthracycline-cytarabine" regimen remains the commonly used chemotherapeutic regimen. AML is still definitely a catastrophic disease [1, 5–7]. In recent years, it has been proven that acute leukemia is often accompanied by extramedullary infiltration (EMI). The incidence of EMI in AML is approximately 20%-40%, mostly in M5 (acute monocytic leukemia) and M4 (acute myelomonocytic leukemia) types according to French-American-British (FAB) classification system. For the majority of these patients, the remission rate after induction chemotherapy is low, with poor prognosis [1, 8]. Therefore, it is of great significance to study the EMI mechanism of AML and to explore the therapeutic targets for AML.

Protein arginine methyltransferases (PRMTs) are a type of enzymes that transfer methyl from cofactor S-Adenosylmethionine (SAM) to substrate protein arginine omega-nitrogen. According to its specificity, PRMTs can

be divided into three subgroups: I, II, and III, which are asymmetric dicarboxylic esters, symmetric dicarboxylic esters, and monomethylated substrates, respectively [9]. Protein arginine methyltransferase 5 (PRMT5), a kind of type II PRMT, catalyzes the symmetrical dimethylation of protein arginine residues, which is involved in diverse cellular processes, including transcription, DNA damage response, splicing, translation, and cellular signal transduction [10, 11]. Some studies have shown that PRMT5 is not only involved in the development of normal human immune system, but also participates in the regulation of tumor invasion, migration, and T cell-mediated immune response as well as pathological process of AML [12–15]. The overexpression of PRMT5 is detected in various types of AML cell lines [10, 16, 17]. Functionally, PRMT5 can inactivate p53 by methylation, affect mixed lineage leukemia rearrangement, or promote the growth of leukemia through microRNA (miR)/protein network, thereby promoting cell differentiation and proliferation [17–20]. In addition, PRMT5 can alter the transcriptional process of multiple essential genes through the methylation of splice regulators, which is necessary to maintain the survival of leukemic cells [16, 17, 21, 22]. Therefore, suppressing PRMT5 represents an exciting anticancer strategy. At present, three types of PRMT5 inhibitors are available to treat solid cancers and blood malignancies. However, the role of PRMT5 in AML has not been completely clarified, and the role and mechanism of PRMT5 in tumor invasion and migration also remain unclear.

Leukocyte Ig-like receptor subfamily B (LILRB) is a group of type I transmembrane glycoproteins with ligand-bound extracellular Ig-like domain and intracellular immune receptor tyrosine inhibitory motif (ITIMs) and can recruit tyrosine phosphatase SHP-1, SHP-2, or inositol phosphatase SHIP, with immunosuppressive function [23–26]. Thus, leukocyte immunoglobulin-like receptor B4 (LILRB4) is considered as an immune checkpoint protein [27, 28]. Moreover, LILRB4 could act as a tumor maintenance factor, but it may not affect normal development, which is an attractive target for cancer treatment [26, 28, 29]. Monocyte AML is a subtype of AML. Extramedullary diseases, including gingival infiltration and involvement of skin and cerebrospinal fluid, are common in monocyte AML [28]. The latest findings show the low expression of LILRB4 in normal monocytes [24, 25] and high expression of LILRB4 in monocytes of acute monocytic leukemia, which is a marker of monocyte AML [30]. It can inhibit immune activation, promote tumor infiltration and invasion, and affect the invasive ability in AML [28, 29, 31]. Some studies have suggested that PRMT5 plays important roles in the regulation of immune response, migration, and invasion in tumorigenesis [12–15, 20]. In addition, PRMT5 can regulate the downstream factors of LILRB4 [31–33].

In this study, we investigated the changes of PRMT5 expression in AML-M5 patients, MV-4-11, and THP-1 and further explored the effects of PRMT5 on the invasion and migration in AML. Moreover, we also examined the correlation between PRMT5 and LILRB4 in relation with AML infiltration and additionally assessed the pathway underlying the effects of PRMT5 methylation on the expression of LILRB4, aiming to provide experimental evidence for the treatment of AML.

2. Methods and Materials

2.1. Patient Samples. Bone marrow samples were collected from 30 (AML-M5 or AML-M4) patients from the Affiliated Hospital of Guiyang Medical University (Guiyang City, Guizhou Province) from May 2018 to April 2020 (Table 1). All AML samples were collected from bone marrow of untreated patients. In addition, 20 hematopoietic stem cell transplantation donors were collected from Guizhou hematopoietic stem cell laboratory as the normal control. All patients were diagnosed by FAB and confirmed by clinical laboratory examination, blood routine examination, and bone marrow examination. These AML samples were from bone marrow of untreated patients. And in all patient samples, the number of bone marrow blasts is ≥80%. We collected individual bone marrow nuclear cells from AML patients and the hematopoietic stem cell transplant donor by Ficoll gradient centrifugation. According to the Helsinki Declaration, AML patients who provided primary AML samples signed written informed consent. The study protocol was approved by the Medical Science Ethics Review Committee of the University Hospital of Guizhou Medical University (2019 Ethical Review No. 123).

2.2. Cell Culture. Human THP-1 (AML-M5), kasumi-1 (AML-M2), HL-60 (human promyelocytic leukemia cell), and MV-4-11 (AML-M4) cells were cultured in RPMI1640 medium and IMDM medium containing 10% fetal bovine serum (FBS), respectively. The primordial cells of patients with AML were taken from the blood samples of patients from the Affiliated Hospital of Guizhou Medical University and stored in the leukemia cell bank of the Affiliated Hospital of Guizhou Medical University. All cells were incubated at 37°C and 5% CO_2.

2.3. Reagents and Antibodies. EPZ015666 and mTOR inhibitor-3 were purchased from MCE (China). Antibody against PRMT5 (YN3030) was purchased from Immunoway (Suzhou, China). Anti-LILRB4 (K004989P), anti-PI3K (K106692P), anti-phosph-PI3K (K006379P), anti-AKT (K101311P), anti-phosph-AKT (K006214P), anti-NF-κB (K002162P), anti-phosph-NF-κB (K006209P), anti-mTOR (K003351P), and anti-phosph-mTOR (K006205P) antibodies were purchased from Solei Bao Technology (Beijing). Anti-ERK (4695T) and anti-phosph-ERK(4370T) were purchased from Cell Signaling Technology (Danvers, MA, USA).

2.4. Western Blot Analysis. After washing with saline twice, cells were lysed in RIPA buffer containing PMSF and proteasome inhibitor to extract the total protein (Solarbio Life Sciences Technology Co., Ltd., Beijing, China), followed by quantification of protein concentration by BCA protein concentration assay kit (Solei Bao Technology Co., Ltd., Beijing, China). The same amount of protein (20 μg) was separated by 10% SDS-PAGE gel and transferred to the PVDF

Table 1: The characteristics of the AML patients.

Patients	Sex	Age (years)	BM/PB	FAB	WBC (10^9L)	HB (g/L)	PLT (10^9L)	%blasts (BM)	Evaluation
AML1	M	50	BM	M5	145.19	60	17	67.92	Initial
AML2	F	51	BM	M4	1.89	85	10	46	Initial
AML3	M	53	BM	M5	10.11	80	65	43	Initial
AML4	F	61	BM	M5	2.51	61	183	73	Initial
AML5	F	73	BM	M5	17.68	80	80	26	Initial
AML6	F	42	BM	M5	4.76	123	108	87	Relapse
AML7	M	35	BM	M4	8.68	84	21	58.6	Relapse
AML8	F	50	BM	M5	1.27	51	34	89	Initial
AML9	M	73	BM	M4	1.21	59	44	31	Initial
AML10	F	39	BM	M5	36.05	106	23	39	Initial
AML11	F	77	BM	M5	196.96	77	32	91	Initial
AML12	F	22	BM	M5	39.9	97	180	84	Relapse
AML13	M	59	BM	M5	1.97	128	91	57	Initial
AML14	F	49	BM	M5	1.3	57	113	93	Relapse
AML15	F	61	BM	M5	25.5	56	20	39	Initial
AML16	M	53	BM	M5	66.12	71	10	80	Initial
AML17	F	66	BM	M5	4.27	119	56	21	Relapse
AML18	M	23	BM	M4	95.29	135	52	89	Initial
AML19	F	47	BM	M5	1.19	68	46	38	Initial
AML20	M	56	BM	M5	14.53	72	104	85	Relapse
AML21	F	49	BM	M5	2.05	82	21	15	Relapse
AML22	M	50	BM	M5	103.76	113	58	79	Relapse
AML23	F	73	BM	M5	19.05	26	24	14	Relapse
AML24	M	39	BM	M4	6.31	71	198	39	Initial
AML25	M	73	BM	M4	5.2	105	108	27-35	Relapse
AML26	F	21	BM	M4	127.64	74	143	23	Relapse
AML27	F	39	BM	M5	5.7	78	32	50	Relapse
AML28	M	40	BM	M4	38.36	89	11	36	Relapse
AML29	M	23	BM	M4	2.41	112	211	27	Relapse
AML30	M	59	BM	M5	0.18	61	60	54	Relapse

membrane (Millipore Company, Milford, Massachusetts, USA). Membranes were subsequently blocked with 5% skim milk diluted in TBST for 2 h and incubated with primary antibody (1 : 1000) overnight, followed by incubation with fluorescent coupled secondary antibody (1: 2000). β-Actin was used as the loading control and for normalization. The signal strength of the film was measured by Tanon (Shanghai, China).

2.5. RT-qPCR. Total RNA was extracted from MV-4-11, THP-1, and bone marrow blood samples of patients by the Trizol method. Afterwards, reverse transcription was performed with Single strand cDNA synthesis kit. qRT-PCR was performed using an SYBR Green PCR Master Mix (TianGen Biotech, Beijing, China) and a PRISM 7500 real-time PCR detection system (ABI, USA). The expression level of target gene was normalized to that of β-actin. The primer sequences for qRT-PCR were as follows: PRMT5F: 5′-GGGAAGAGGATGGGAAAC-3′ and PRMT5R: 5′-TGATTGACAACAACCGCTAT-3′; LILRB4F: 5′-TCAGTACCTCCCAGTGCC-3′ and LILRB4R: 5′-CCACAAGGTCCGTCTCAA-3′; and β-actinF: 5′-CTACCTCATGAAGATCCTCACCGA-3′ and β-actinR: 5′-TTCTCCTTAATGTCACGCACGATT-3′.

2.6. Small Interference with RNA-Transfected Cells. siRNA against PRMT5 (si-PRMT5) was used to suppress the expression of PRMT5 in cells. Sasastic siRNA (si-NC) was used as the negative control. The siRNA sequence was designed and synthesized by Quan yang Biotechnology Co., Ltd. (Shanghai, China).

The sequence is as follows: si-PRMT5: 5′-GGGACUGGAAUACGCUAAUTT—3′.

The final concentration per siRNA was 2.5 nmol. According to the commodity specification, Lipo8000TM transdye reagent and siRNA raw solution (250 μl/hole) were mixed and further added to the ThP-1 and MV-4-11 cells,

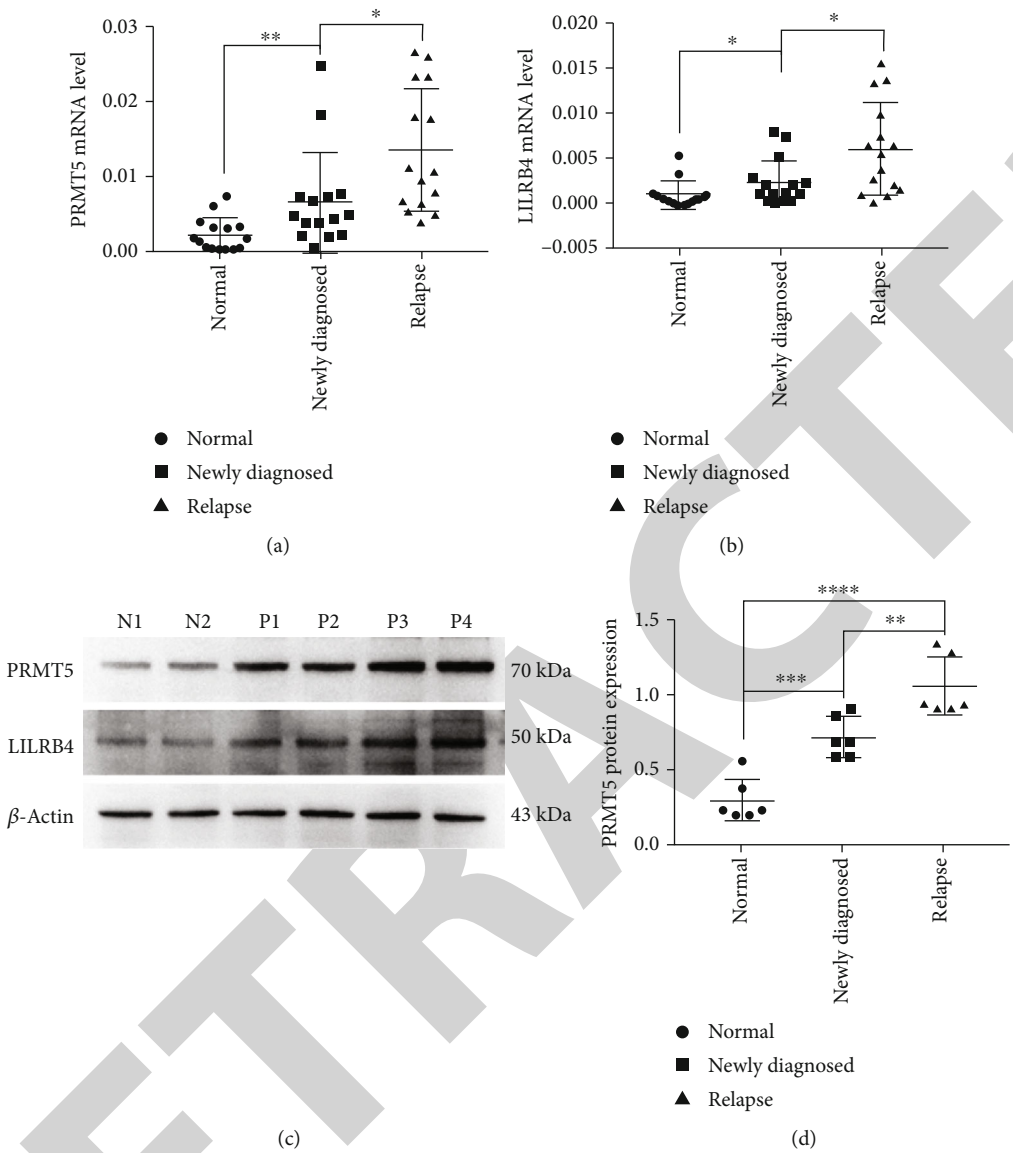

Figure 1: Continued.

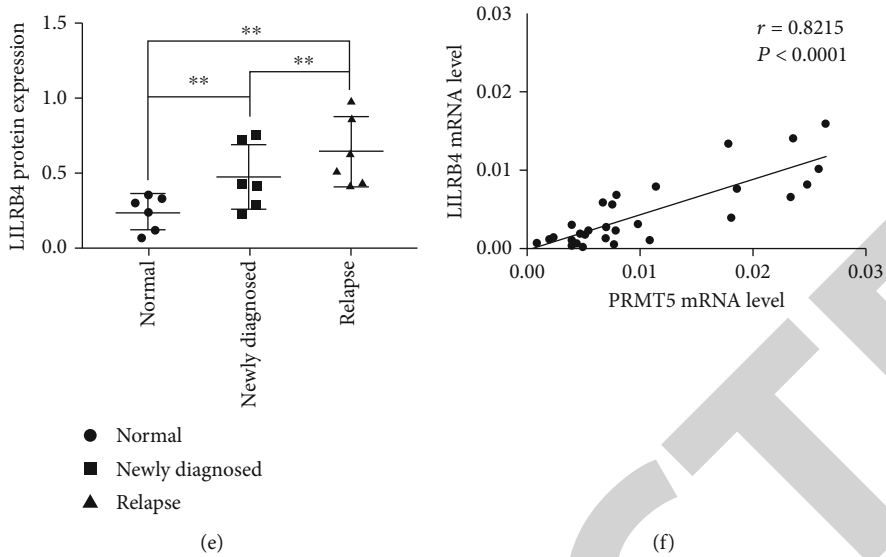

Figure 1: Real-time qPCR and Western blot analyses of the levels of PRMT5 and LILRB4 in 30 patients with AML-M5. The mRNA levels of (a) PRMT5 and (b) LILRB4 were detected by real-time qPCR in normal subjects, newly diagnosed patients, and recurrent ones. (c) Western blot analysis was performed to detect the protein abundances of PRMT5 and LILRB4 (normal persons, $n = 2$; newly diagnosed cases, $n = 2$; and recurrent cases, $n = 2$). β-Actin was used as the internal control. Western blot and subsequent grayscale analysis revealed that the expression of (d) PRMT5 and (e) LILRB4 was higher in the relapse group than that in the newly diagnosed group. (f) The analysis of correlation coefficient indicated that the expression of PRMT5 was positively correlated with that of LILRB4 ($r = 0.8215$, $P \leq 0.0001$). Each value was presented as $\log_{10}{}^{X}$. All the experiments were repeated in triplicates. The data are expressed by mean ± standard deviation ($^{*}P \leq 0.05$; $^{**}P \leq 0.01$). The 2-Δ CT method was used for quantitative presentation of relative mRNA levels. The error bar represents ±SD ($^{*}P \leq 0.05$; $^{**}P \leq 0.01$; $^{***}P \leq 0.001$; $^{****}P \leq 0.0001$).

followed by incubation for 48 h. Western blot was used to detect the downregulation efficiency of siRNA.

2.7. Transwell Migration and Invasion Assay. siRNA was used to downregulate the expression of PRMT5 in MV-4-11 and THP-1 cells, followed by assessment of the migration and invasion ability of the corresponding cells. In brief, leukemia cells (5×10^4 cells/ml) were added to the polycarbonate membrane (pore size 8 μm, BD Biosciences) for migration assay and polycarbonate membrane with fibronectin coating (pore size 8 μm, BD Biosciences) for invasion assay, respectively, and 600 μl RPMI1640 medium was added to the lower chamber of Transwell. After incubation at 37°C for 24 h, cells were observed under microscope (100x) by randomly selecting nine views from each well, aiming to count the number of cells penetrating into the lower cavity and to observe cell morphology.

2.8. Cell Adhesion Assay. In order to study the effect of PRMT5 on the adhesion ability of leukemic cells, Beibo Cell Adhesion Test Kit (Bestbio, China) was purchased to detect the cell adhesion ability of THP-1 and MV-4-11 cells after downregulating PRMT5 and the corresponding control cells at the same time. Briefly, 100 μl/well coating solution was added to the 96-well plate at 4°C overnight. After washing with PBS twice, 5×10^4/ml cells per well were inoculated and incubated at 37°C for 1 h. Afterwards, 10 μl staining solution of 37°C was added and incubated for additional 2-4 h, followed by detection of the absorbance of 450 nm by enzyme labeling instrument.

2.9. Statistical Analysis. All results were analyzed using the GraphPad Prism 7.0 software. Data were presented as mean ± SD and analyzed by either one-way ANOVA or Student's t-test. $P < 0.05$ was considered as statistically significant.

3. Results

3.1. The High Expression of PRMT5 in AML-M5 Patients. Blood samples from 30 patients with AML-M5 or AML-M4 and 20 normal controls were collected from the Hematopoietic Stem Cell Laboratory of the Affiliated Hospital of Guizhou Medical University from May 2018 to April 2020. The clinical characteristics of the patients are summarized in Table 1. RT-qPCR analysis revealed the expression of PRMT5 in AML patients. As a result, the mRNA expression of PRMT5 was the highest in the recurrent group, sequentially followed by the newly diagnosed group and normal control group (Figure 1(a)). Similarly, RT-qPCR was used to detect the expression of LILRB4 in AML patients, and the mRNA expression of LILRB4 was significantly higher in AML patients than that in normal subjects (Figure 1(b)). Patients were divided into primary diagnosis group and recurrence group. The mRNA expression of LILRB4 was significantly higher in recurrent patients than that in the primary diagnosis group (Figure 1(b)). In addition, the protein levels of PRMT5 and LILRB4 were detected by Western blot, which was consistent with those of RT-qPCR (Figure 1(c)). The protein levels of PRMT5 and LILRB4 were the highest in recurrent patients, followed by newly diagnosed patients

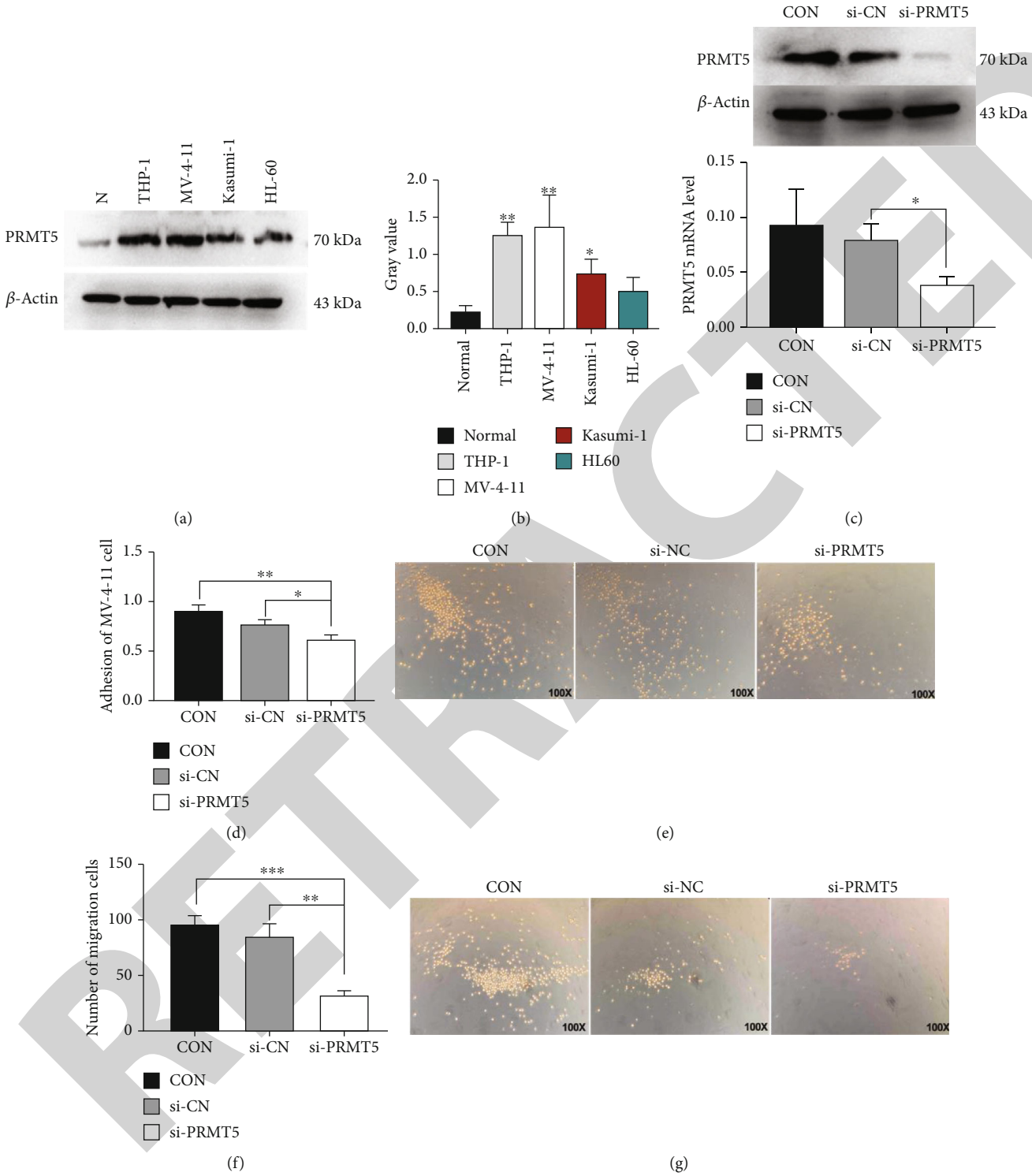

Figure 2: Continued.

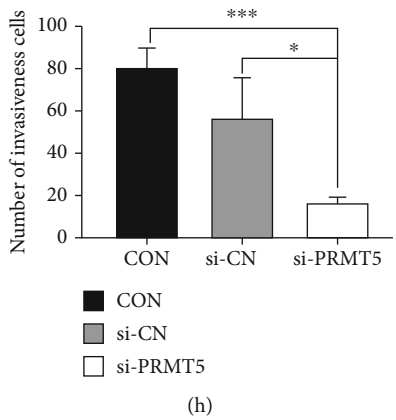

(h)

Figure 2: Detection of expression in human samples and AML cell lines. (a) Western blot was used to detect the protein level expression in PRMT5 (normal, THP-1, MV-4-11, kasum-1, and HL-60), respectively. β- Actin was used as the internal control. (b) Western blot and subsequent grayscale analysis revealed the expression of PRMT5. Downregulation of PRMT5 gene by siRNA could inhibit the migration, invasion, and adhesion of MV-4-11. (c) PRMT5 silencing by siRNA on AML. After treatment with si-PRMT5 or NC siRNA for 48 h, the expression of PRMT5 in protein (upper) and mRNA (lower) level was significantly decreased in MV-4-11 cells. (d) Adhesion assay exhibited that the adhesion capability of MV-4-11 cells in the si-PRMT5 group was significantly lower than that in the wild type group and si-CN group. (e) Transwell assay was performed to detect the migration of MV-4-11 cells in the wild type group, si-CN group, and si-PRMT5 group. (f) Quantitative analysis of the number of migrating cells in each group after 24 h indicated that the number of migrating cells in the si-PRMT5 group was significantly decreased. (g) After downregulation of PRMT5 by siRNA, the invasion of MV-4-11 cells in each group was observed. (h) Quantitative analysis revealed that the number of invasion in MV-4-11 cells was significantly decreased. Data are expressed by mean ± standard deviation ($^*P \leq 0.05$; $^{**}P \leq 0.01$; $^{***}P \leq 0.001$). The 2-Δ CT method was used for quantitative presentation of relative mRNA levels. The error bar represents ±SD. ($^*P \leq 0.05$). The images of (c, e) are under 100x magnification.

and normal control (Figures 1(d) and 1(e)). These results indicated that the expressions of PRMT5 and LILRB4 were increased in AML patients, especially in recurrent patients.

In order to determine whether PRMT5 was closely correlated with LILRB4, we investigated the correlation coefficient. $\mathrm{Log}_{10}{}^{X}$ was used to calculate the mRNA level of PRMT5 and LILRB4. According to the R value, there was a positive correlation between PRMT5 and LILRB4 (Figure 1(f)), suggesting the positive correlation between the expression of PRMT5 and LILRB4 in AML patients.

3.2. The Changes in Migration, Invasion, and Adhesion of AML Cells after Downregulating PRMT5. We detected the expression of PRMT5 in AML cell lines (THP-1, MV-4-11, kasumi-1, and HL-60) and normal human samples by Western blot. As a result, the expression of PRMT5 in cell lines was higher than in normal human samples (Figure 2(a)). Moreover, the expression of PRMT5 in THP-1 and MV-4-11 cell lines was higher than that in other cell lines. Grayscale analysis of all Western blot bands showed the significantly high expression of PRMT5 in THP-1, MV-4-11, and kasumi-1 than normal human samples. And PRMT5 expression was the highest in THP-1 and MV-4-11 (Figure 2(b)). Therefore, THP-1 and MV-4-11 were selected for subsequent experiments.

Although the increased expression of PRMT5 has been confirmed to be associated with the pathogenesis and prognosis of AML and to affect the proliferation and differentiation of AML cells, however, the effects of PRMT5 on the invasion and migration of AML cells were not well-studied. To confirm the roles of PRMT5 expression in the adhesion, invasion, and migration of AML cells, we assessed the adhesion, invasion, and migration abilities of MV-4-11 (Figure 2) and THP-1 (Figure 3) cells after downregulation of PRMT5 expression. siRNA was used to downregulate the expression of PRMT5 in AML cells, followed by assessment of the suppressed expression of PRMT5 by Western blot and RT-qPCR (Figures 2(c) and 3(b)). Afterwards, we examined the effects of PRMT5 expression on cell adhesion and found that the adhesion ability of cells was significantly decreased in the si-PRMT5 group (Figures 2(d) and 3(b)). Observation of cell morphology revealed that the morphological integrity of cells in the si-PRMT5 group was worse than that in the CON group, and the number of malformed cells in the si-PRMT5 group was significantly more than that in the CON group (Figures 2(e) and 3(c)). Transwell assay was used to detect the migration ability of the treated cells, indicating that the migration ability of the two AML cell lines in the si-PRMT5 group was significantly lower than that in the CON group (Figures 2(f) and 3(d)). We further evaluated the changes of cell invasion that were consistent with the migration assay. The number of cells infiltrating from the upper chamber to the lower chamber in the si-PRMT5 group was significantly less than that in the CON one (Figures 2(g) and 2(h) and 3(e) and 3(f)).

To further validate the results, PRMT5 inhibitors (EPZ015666) were purchased to inhibit PRMT5 expression in MV-4-11 and THP-1 cells. And Western blot was used to detect PRMT5 expression in MV-4-11 and THP-1 cells, showing that the expression of PRMT5 in the EP015666 group was significantly decreased (Figures 4(e) and 4(i)). We further examined the migration, invasion, and adhesion

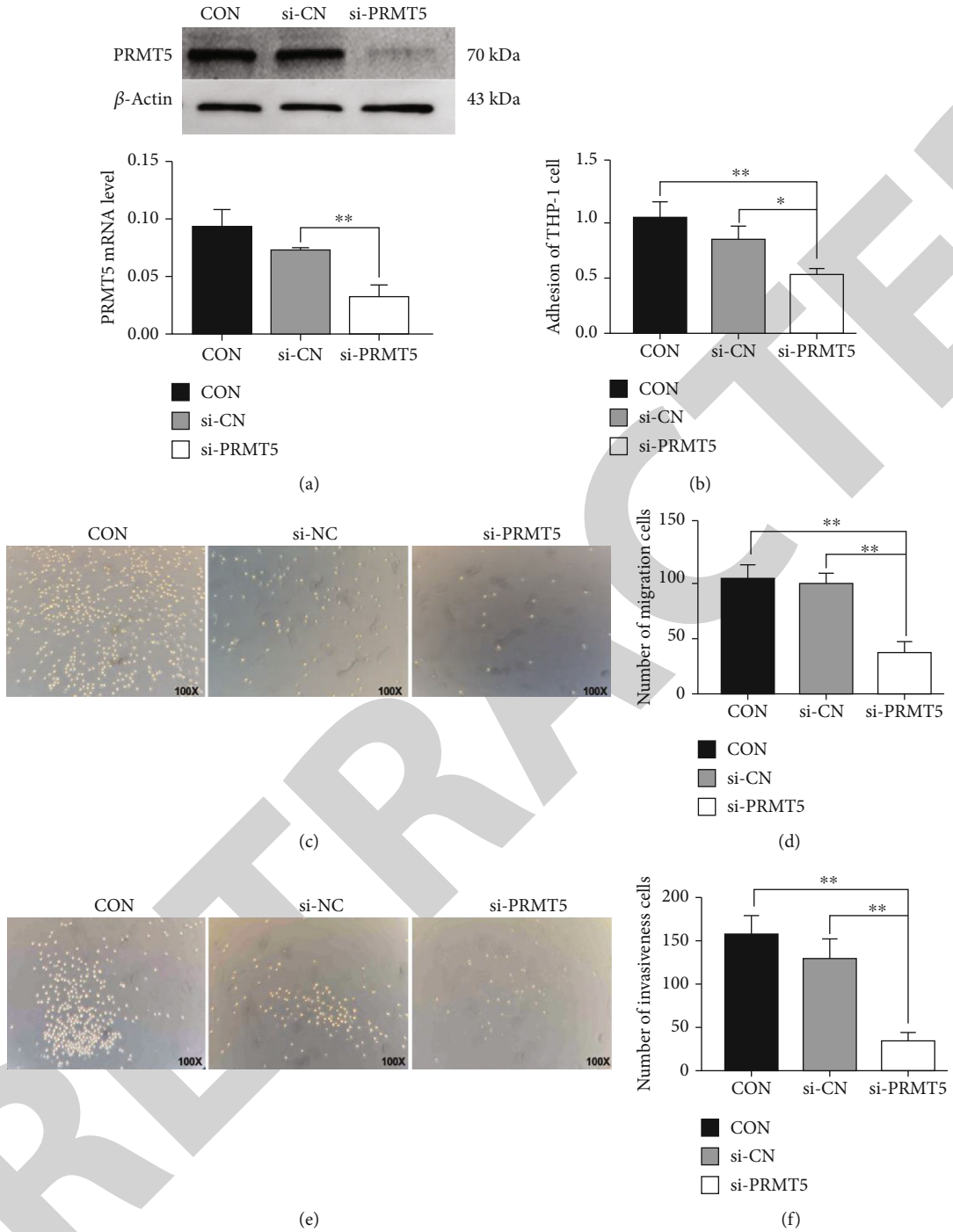

Figure 3: Downregulation of PRMT5 gene by siRNA can inhibit the migration, invasion, and adhesion of THP-1. (a) After treatment with si-PRMT5 or NC siRNA for 48 h, the expression of PRMT5 in protein (upper) and mRNA (lower) level was significantly decreased in THP-1 cells. (b) Adhesion assay revealed that the adhesion capability of THP-1 cells in the si-PRMT5 group was significantly decreased than that in the wild type group and si-CN group. (c) Transwell assay was used to detect the migration of THP-1 cells in the CON group, si-CN group, and si-PRMT5 group. (d) Quantitative analysis of the number of migrating cells in each group after 24 h indicated that the number of migrating cells in the si-PRMT5 group was significantly decreased. (e) Invasion assay was performed to detect the migration of THP-1 cells in the CON group, si-CN group, and si-PRMT5 group. (f) Quantitative analysis of the number of invasion cells in each group after 24 h indicated that the number of invasion cells in the si-PRMT5 group was significantly decreased. All the experiments were performed in triplicate. Data are expressed by mean ± standard deviation ($^{*}P \leq 0.05$; $^{**}P \leq 0.01$). 2-Δ CT was used for quantitative presentation of relative mRNA levels. The error bar represents ±SD ($^{**}P \leq 0.01$). The images of (c, e) are under 100x magnification.

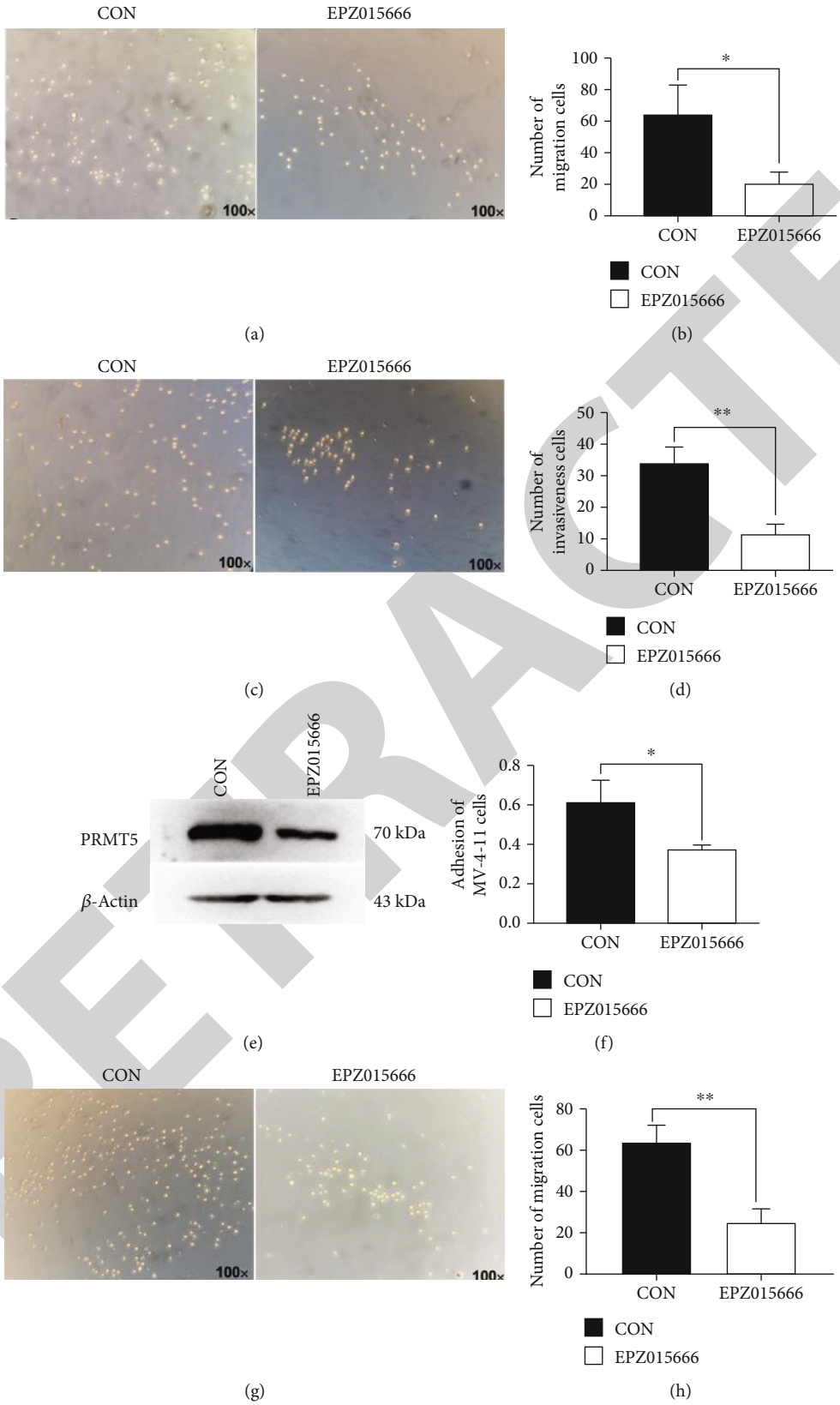

Figure 4: Continued.

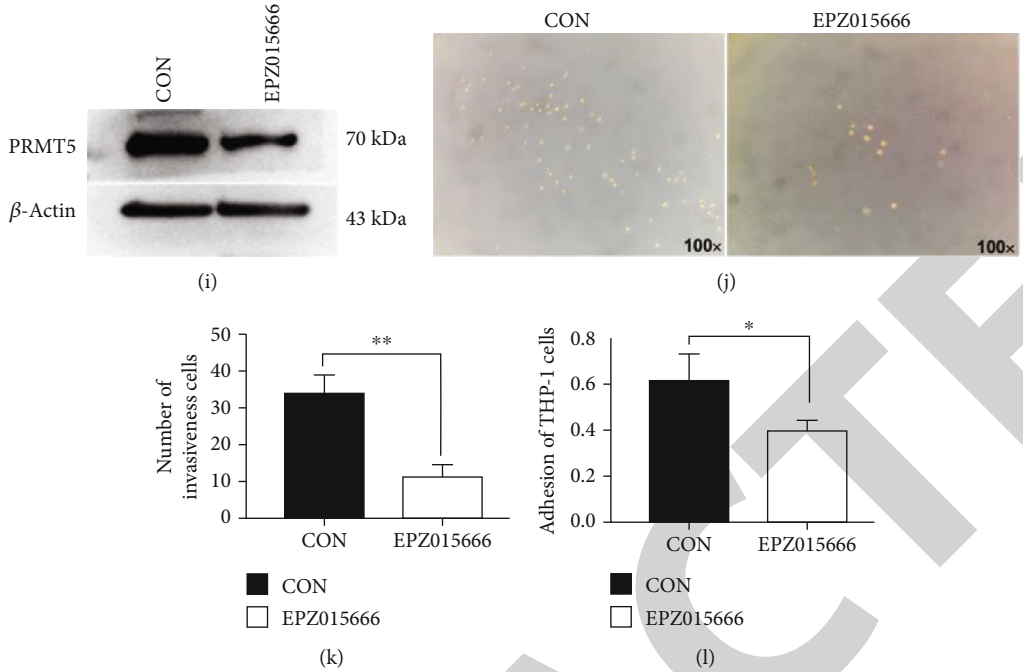

Figure 4: PRMT5 inhibitor (EPZ015666) attenuates the migration, invasion, and adhesion of AML cells. (a) After EPZ015666 treatment in MV-4-11 cells for 24 h, the numbers of cell migration in the CON group and EPZ015666 group were detected by Transwell migration study. (b) Quantification analysis of (a) indicated that the number of cells in the inhibitor group was significantly less than that in the CON group. (c) After EPZ015666 treatment in MV-4-11 cells for 24 h, the number of cell invasion in the CON group and inhibitor group was detected by Transwell invasion assay. (d) Quantification analysis of (c) indicated that the number of invasion cells in the inhibitor group was significantly less than that in the CON group. (e) After EPZ015666 treatment in MV-4-11 cells for 24 h, the protein expression of PRMT5 was changed. (f) After EPZ015666 treatment in MV-4-11 cells for 24 h, cell adhesion was detected, and the number of adherent cells in the inhibitor group was found to be significantly less than that in the CON group. After EPZ015666 treatment in THP-1 cells for 24 h, the (g, h) migration, (j, k) invasion, and (l) adhesion of THP-1 cells were detected. The above indexes in the inhibitor group were significantly lower than those in the CON group. (i) After EPZ015666 treatment in THP-1 cells for 24 h, the protein level of PRMT5 was changed. All the experiments were performed in triplicate. Data are expressed by mean ± standard deviation ($^{*}P \leq 0.05$; $^{**}P \leq 0.01$). The representative images are under 100x magnification.

abilities and morphology of THP-1 and MV-4-11 cell lines after the treatment of PRMT5 inhibitors. Based on the experimental results of MV-4-11 cells, we observed that the morphology of the cells penetrating the membrane pore after PRMT5 inhibition was worse than that of the CON group, and the cell fragments increased (Figure 4(a)). The number of cell migration in the PRMT5 inhibitor group was significantly decreased compared with that in the CON group (Figure 4(b)). Consistent with migration analysis, invasion assay revealed the similar results. (Figures 4(c) and 4(d)). Moreover, after the administration of PRMT5 in MV-4-11, the adhesion ability of AML cells was also inhibited (Figure 4(f)), which was consistent with the results after PRMT5 downregulation in MV-4-11. Similar observations were also detectable from THP-1 cells (Figures 4(g)–4(l)). Taken together, these results revealed that the expression of PRMT5 affected cell adhesion, migration, and invasion of AML cells.

3.3. PRMT5 Downregulation Decreases the Expression of LILRB4. In order to verify whether PRMT5 affected the invasiveness of AML cells by downregulating the expression of LILRB4, protein samples were extracted from AML cells after downregulating PRMT5. As a result, the expression of LILRB4 was significantly lower in the si-PRMT5 group than in the CON group of MV-4-11 cells (Figure 5(a)), and the grayscale analysis showed that the downward adjustment was statistically significant on both (Figures 5(b) and 5(c)). Similar findings were also detected on THP-1 cells (Figures 5(d)–5(f)). Thus, the expression of LILRB4 was decreased following downregulation of PRMT5 in AML cells.

3.4. PRMT5 Knockdown Affects AKT, ERK, and mTOR Pathways in AML Cells. Previous studies have shown that PRMT5 is involved in the regulation of AKT, ERK, NF-κB, and mTOR pathways [34]. Silencing of PRMT5 can lead to the inhibition of AKT and ERK pathways, which in turn inhibit mTOR pathway [35], thus affecting the apoptosis and migration of lung cancer [19]. To determine whether PRMT5 affected the expression of LILRB4 and the invasiveness of AML cells through relevant pathways, MV-4-11 cells with downregulation of PRMT5 were extracted and subjected to Western blot. Compared with the CON group and si-CN one, the phosphorylation of AKT, mTOR, and ERK pathways was inhibited in si-PRMT5 groups of both MV-4-11 (Figure 6(a)) and THP-1 cells (Figure 6(c)), while the phosphorylation of NF-κB pathway was only affected in

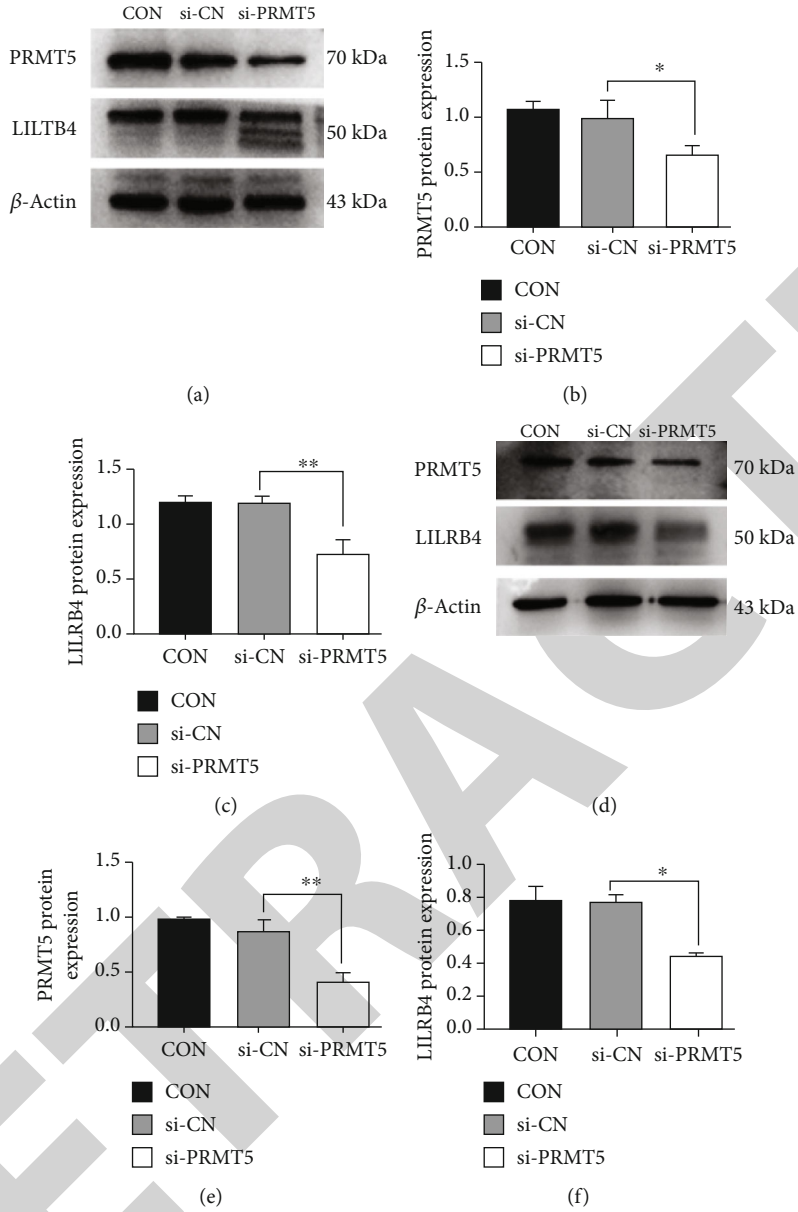

Figure 5: The effect of PRMT5 knockdown by siRNA on the protein abundance of LILRB4. (a) Western blot analysis of PRMT5 and LILRB4 protein in MV-4-11 cells of the CON group, si-CN group, and si-PRMT5 group after corresponding treatment for 48 h. β-Actin was used as the internal control. Subsequent grayscale analysis revealed the expression levels of (b) PRMT5 protein and (b) LILRB4 protein in MV-4-11 cells of the si-PRMT5 group were lower than those of other two groups. (d) Western blot analysis of PRMT5 and LILRB4 proteins in THP-1 cells of the CON group, si-CN group, and si-PRMT5 group after corresponding treatment for 48 h. β-Actin was used as the internal control. Subsequent grayscale analysis revealed that the expression levels of (e) PRMT5 protein and (f) LILRB4 protein in THP-1 cells of the si-PRMT5 group were lower than those of other two groups. All the experiments were repeated for three times. Data are expressed by mean ± standard deviation ($^{*}P \leq 0.05$; $^{**}P \leq 0.01$).

THP-1 (Figure 6(d)) but not MV-4-11 (Figure 6(b)) cells. Thus, PRMT5 knockdown by siRNA significantly decreased the phosphorylation of AKT, mTOR, and ERK pathways in AML cell lines of both MV-4-11 and THP-1 cells.

3.5. Blocking mTOR Pathway Affects the Expression of LILRB4 and Invasion, Migration, and Adhesion of AML Cells. Since AKT/mTOR and ERK/mTOR pathways were significantly affected after the downregulation of PRMT5 in AML cell lines, we speculated that PRMT5 might affect the expression of LILRB4 and the invasive capability of AML cells through AKT/mTOR and ERK/mTOR axes. Thus, we applied an inhibitor of mTOR pathway, mTOR inhibitor-3, on both MV-4-11 and THP-1 cell lines, followed by examination of both morphology and migration, invasiveness, and adhesion. As the results yielded from the experiments of MV-4-11 cells, we observed that not only the morphology (Figure 7(a)) of the cells infiltrating through the membrane barrier after inhibition of mTOR was worse than that of the CON group, with increased cell fragments,

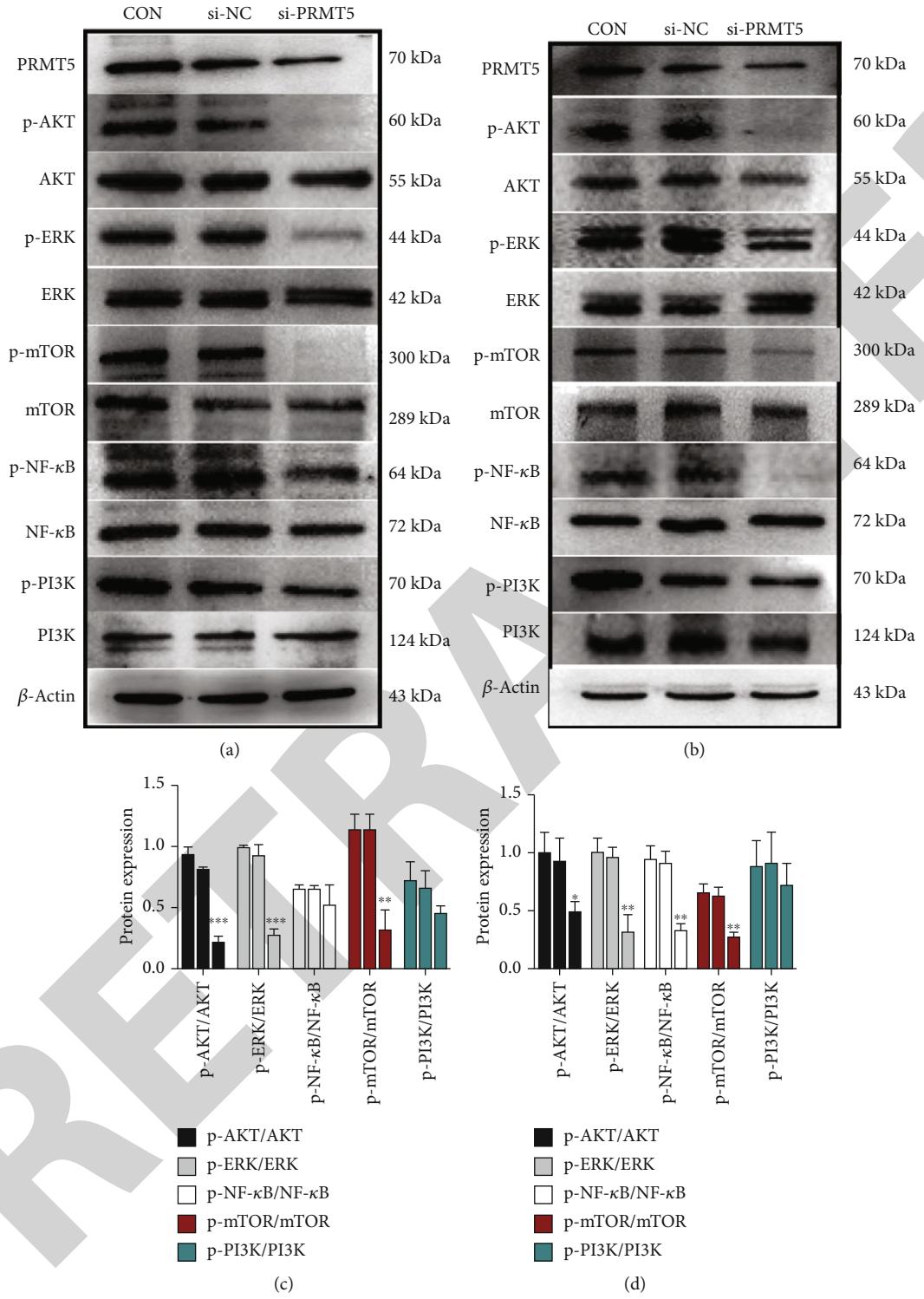

Figure 6: The effect of PRMT5 knockdown by siRNA on several signaling pathways in AML cells. (a) Western blot was used to detect the changes of p/T-AKT, p/T-ERK, p/T-mTOR, p/T-NF-κB, and p/T-PI3K in MV-4-11 cells after siRNA knockdown of PRMT5 gene. (*top*) Western blot images (β-actin as loading control); (*bottom*) image grayscale analysis of the corresponding Western blot images in triplicates. The results indicated that the expression levels of p-ERK, p-AKT, and p-mTOR were decreased in the si-PRMT5 group. (b) Western blot was used to determine the changes of p/T-AKT, p/T-ERK, p/T-mTOR, p/T-NF-κB, and p/T-PI3K in THP-1 cells after siRNA knockdown of PRMT5 gene. (*top*) Western blot images (β-actin as loading control); (*bottom*) image grayscale analysis of the corresponding Western blot images in triplicates. The results suggested that the expression levels of p-ERK, p-AKT, p-NF-κB, and p-mTOR were decreased in the si-PRMT5 group. All the experiments were repeated by three times. Data are expressed by mean ± standard deviation ($^{*}P \leq 0.05$; $^{**}P \leq 0.01$; $^{***}P \leq 0.001$).

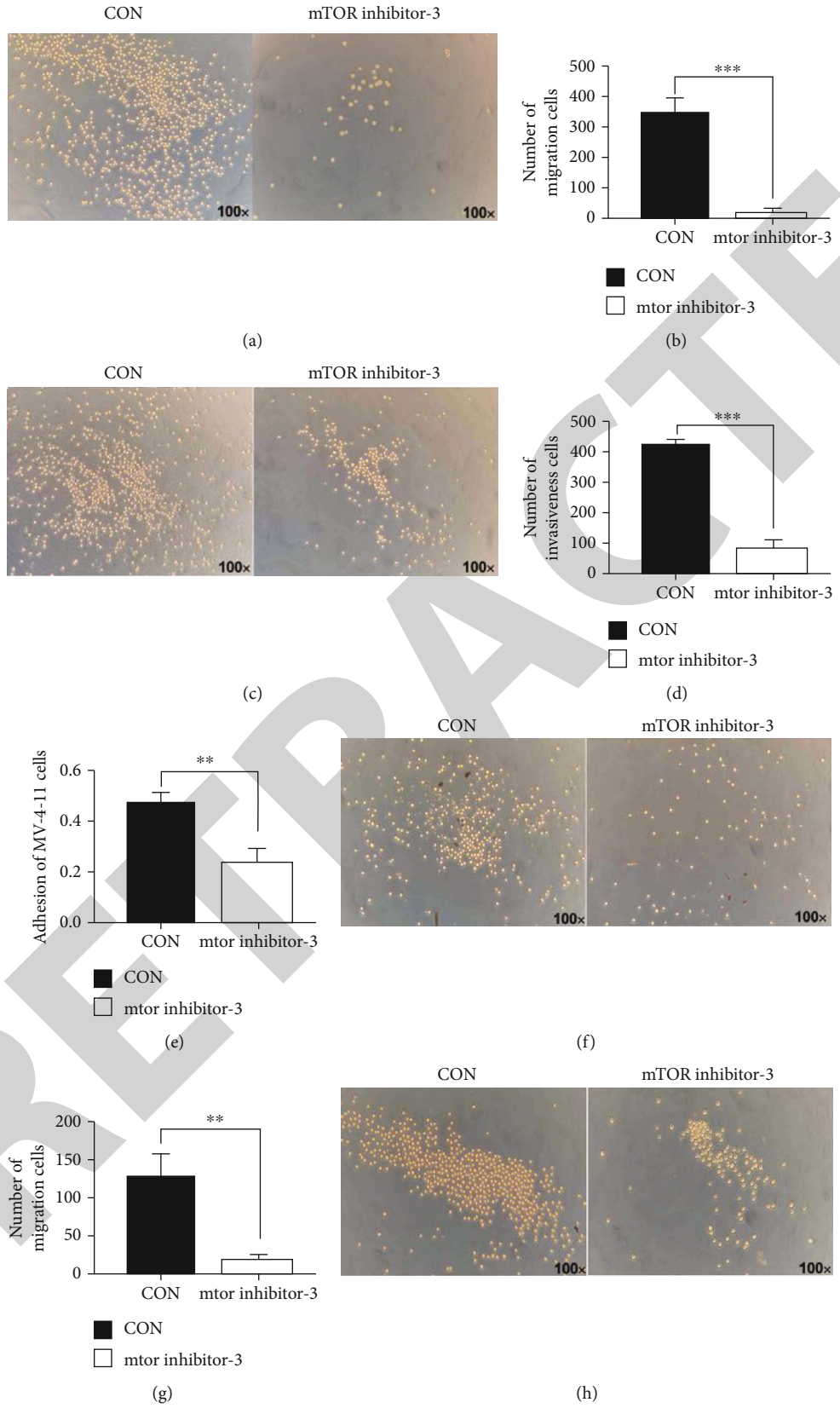

Figure 7: Continued.

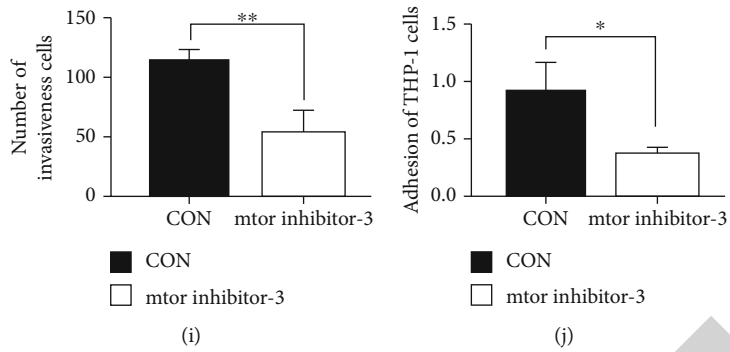

Figure 7: mTOR pathway inhibitor attenuated the migration, invasion, and adhesion of AML cells. (a) After treatment of mTOR pathway inhibitor in MV-4-11 cells for 12 h, the numbers of cell migration in the CON group and inhibitor group were detected by Transwell migration assay. (b) Quantification analysis (a) indicated that the number of cells in the inhibitor group was significantly less than that in the CON group. (c) After treatment of mTOR pathway inhibitor in MV-4-11 cells for 12 h, the numbers of cell invasion in the CON group and inhibitor group were detected by Transwell invasion assay. (d) Quantification analysis (c) indicated that the number of invasion cells in the inhibitor group was significantly less than that in the CON group. (e) After treatment of mTOR pathway inhibitor in MV-4-11 cells for 12 h, the cell adhesion was detected, and the number of adherent cells in the inhibitor group was found to be significantly less than that in the CON group. After treatment of mTOR pathway inhibitor in THP-1 for 12 h, the (f, g) migration, (h, i) invasion, and (j) adhesion of THP-1 cells were detected. The above indexes in the inhibitor group were significantly lower than those in the CON group. All the experiments were repeated by three times. Data are expressed by mean ± standard deviation ($^{*}P \leq 0.05$; $^{**}P \leq 0.01$; $^{***}P \leq 0.001$). The representative images are under 100x magnification.

but also the migration (Figure 7(b)) of cells treated by mTOR inhibitor was significantly less. Consistent with migration assay, the invasion assay yielded similar results (Figures 7(c) and 7(d)). Additionally, the inhibition of the mTOR pathway also led to the suppressed adhesion ability of AML cells (Figure 7(e)), which was consistent with outcomes after the downregulation of PRMT5. Similar observations were also obtained from THP-1 cells (Figure 7(f)–7(j)).

To further validate the results, we used PRMT5 inhibitors (EPZ015666) to inhibit PRMT5 expression in both MV-4-11 and THP-1 cells. Western blot was used to detect the changes of mTOR pathway and LILRB4 at protein level in MV-4-11 (Figure 8(a)), which revealed that the phosphorylation of mTOR pathway was inhibited (Figure 8(d), $P < 0.05$) and the expression of LILRB4 was inhibited (Figure 8(e), $P < 0.05$). Meanwhile, we observed the same changes in THP-1 cell lines (Figures 8(b)–8(h)).

In order to explore the relationship between the above changes and LILRB4, we detected the proteins of PRMT5 and LILRB4 in AML cells after blocking mTOR pathway. Therefore, after blocking mTOR pathway, the protein abundance of LILRB4 in the mTOR inhibitor-3 group was significantly lower than that in the CON group of both MV-4-11 (Figure 9(a)) and THP-1 (Figure 9(b)) cells, which were statistically significant indicated by image gray analysis (Figures 9(c) and 9(d)). These results suggested that the expression of LILRB4 was regulated by the mTOR pathway.

4. Discussion

Some studies have shown that PRMT5 is necessary for the survival of AML cells and is highly expressed in many types of leukemia, especially in M5 leukemia [20, 37]. However, the pathogenesis of AML is complex, and little is known about the specific role of PRMT5 in AML. Inhibition of PRMT5 expression has been reported to functionally exert antitumor effects and can be used as a promising therapeutic target. It can induce alternative splicing changes of a variety of essential genes through the mysterious splicing regulatory factor SRSF1 [18, 21, 38].

PRMT5 exists in the nucleus and cytoplasm. A great deal of evidence shows that PRMT5 activates or suppresses the transcription via the methylation of arginine on histone and promotes cancer by inhibiting the expression of tumor suppressor gene [1, 9, 16, 17, 20]. PRMT5 is highly expressed in malignant hematological diseases such as leukemia and lymphoma and participates in the expression and regulation of many genes [17]. It is an important regulator of cell proliferation and differentiation, which has been attracting more and more attention. It is also involved in the regulation of proliferation and survival pathway, epigenetic regulation of anticancer target genes, and organelle biogenesis [20, 35–37]. Previous studies have shown that PRMT5 is overexpressed in many malignant tumors such as acute lymphoblastic leukemia and is closely related to tumor growth [16, 17]. Several studies have shown whether PRMT5 is essential for the survival of AML cells and its expression pattern in many types of leukemia, especially in M5 leukemia [20, 37]. In this study, the effects of PRMT5 on the invasion and migration in AML cells were investigated. Firstly, the clinical samples from 30 AML-M5 patients were examined, showing that the expression of PRMT5 was high in AML-M5 patients, and the expression of PRMT was significantly higher in recurrent patients than that in other patients, indicating that the overexpression of PRMT5 was associated with the recurrence of AML (Figure 1). AML-M5 is more prone to present EMI and recurrence than other types of leukemia. According to this phenomenon, PRMT5 expression is associated with specific types of leukemia and is correlated with the invasive ability of tumor. Moreover, we

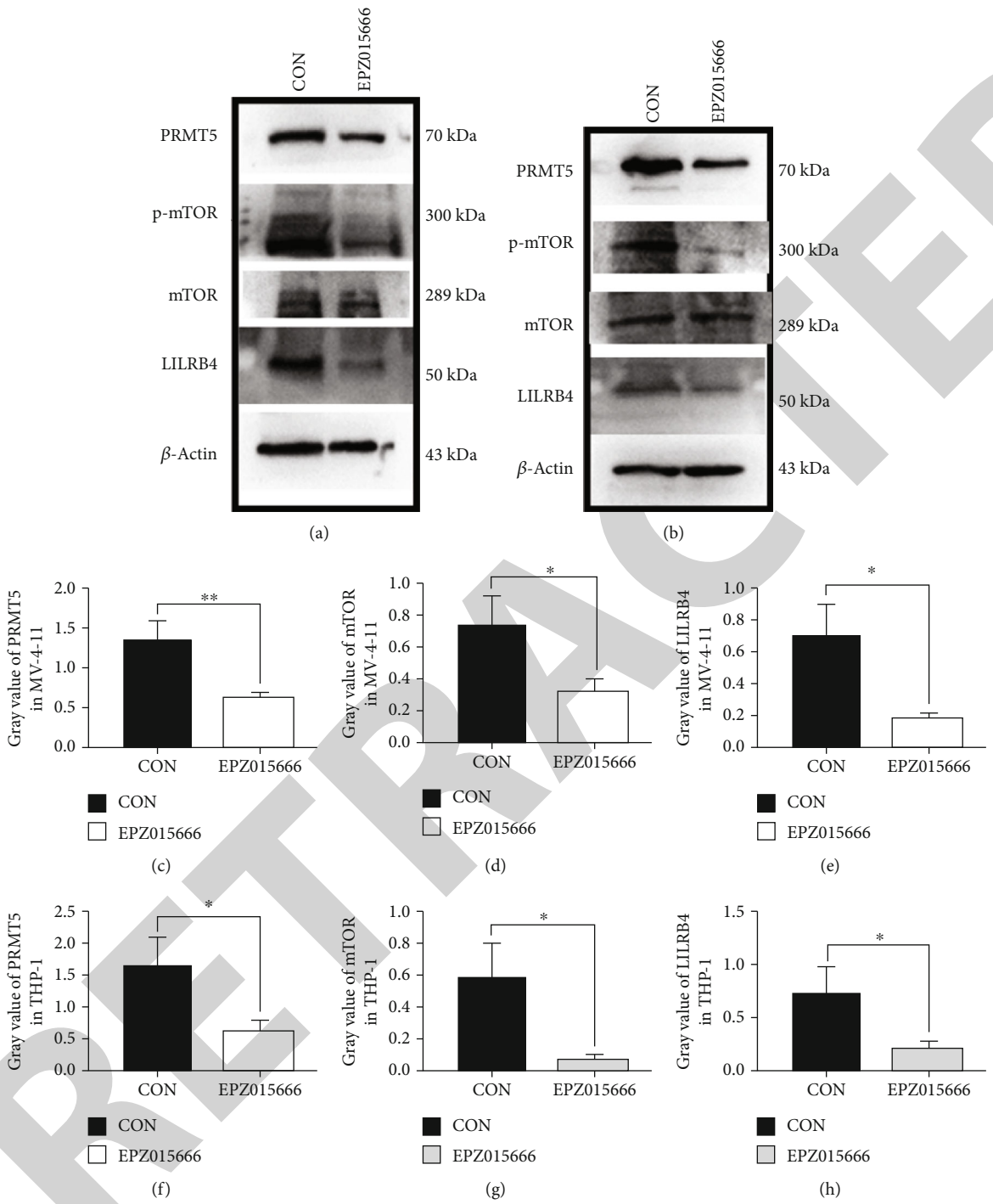

Figure 8: The effect of inhibition of PRMT5 (EPZ015666) on the expression of related genes in AML cells. (a) After treatment of MV-4-11 and THP-1 cells with PRMT5 inhibitor (EPZ015666) for 24 h, the expression of PRMT5, p/T-mTOR, and LILRB4 in the CON group and EPZ015666 group was detected by Western blot. (c) J image grayscale analysis (a) showed that PRMT5 expression was downregulated in the EPZ015666 group. (d) J image grayscale analysis (a) showed that p-mTOR expression was downregulated in the EPZ015666 group. (e) J image grayscale analysis (a) showed that LILRB4 expression was downregulated in the EPZ015666 group. β-Actin was used as the internal control. The same experiments and similar results were reproduced on THP-1 cells, as shown in (b) and (f–h). Data are expressed by mean ± standard deviation ($^{*}P \leq 0.05$; $^{**}P \leq 0.01$).

found that PRMT5 was highly expressed in AML cell lines, and the expression of PRMT5 in MV-4-11 and THP-1 was higher than kasumi-1 and HL-60 (Figures 2(a) and 2(b)). The effects of PRMT5 on the invasion and migration of AML were investigated in MV-4-11 and THP-1. siRNA and EPZ015666 inhibitor were used to inhibit PRMT5 expression. The capability of migration, invasion, and adhesion of THP-1 and MV-4-11 was significantly decreased

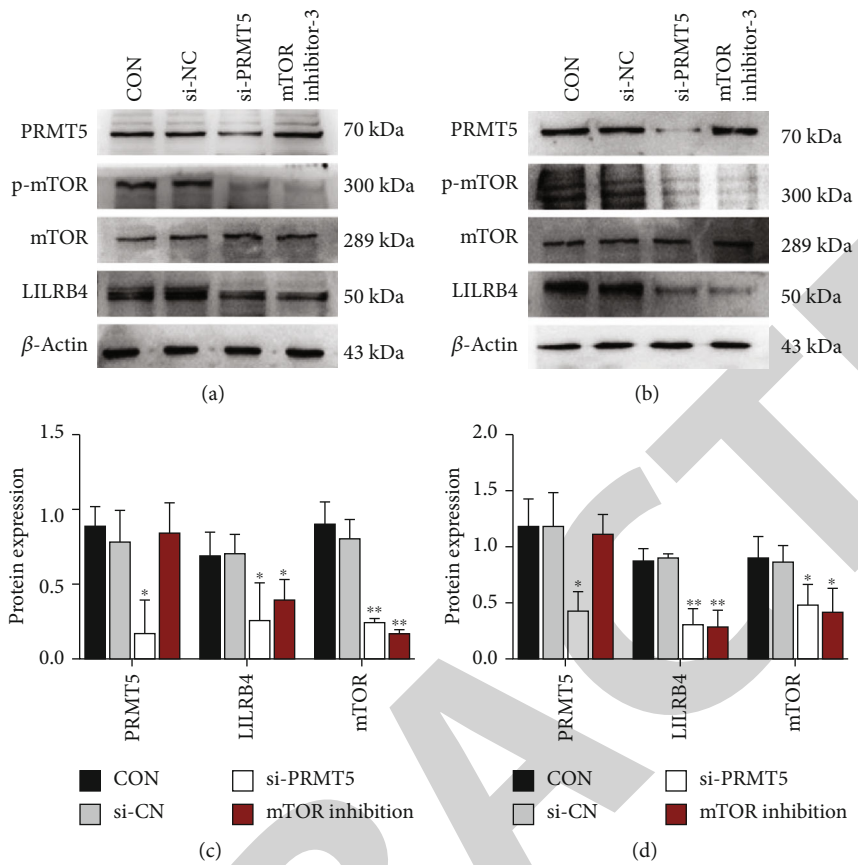

Figure 9: The effect of inhibition of mTOR pathway on the expression of related genes in AML cells. (a) After treatment of MV-4-11 and THP-1 cells with mTOR pathway inhibitor for 12 h, the expression levels of PRMT5, p/T-mTOR, and LILRB4 in the CON group, si-CN group, si-PRMT5, and mTOR inhibitor-3 group were detected by Western blot. (b) J image grayscale analysis (a) revealed that PRMT5 had no obvious downward trend, but the expression of p-mTOR and LILRB4 was significantly decreased, and the expression of PRMT5, p-mTOR, and LILRB4 was significantly decreased in the si-PRMT5 group. β-Actin was used as the loading control. The same experiments and similar results were reproduced on THP-1 cells, as shown in (c, d). Data are expressed by mean ± standard deviation ($^{*}P \leq 0.05$; $^{**}P \leq 0.01$).

(Figures 2–4). These results have shown that PRMT5 plays important roles in invasion and migration in AML-M5.

Recent studies have shown that LILRB4 is vitally involved in the pathogenesis and development of AML, and the overexpression of LILRB4 in AML-M5 is closely associated with the invasive ability of AML-M5 [26]. We further examined the expression of LILRB4 in 30 patients and found that the expression of LILRB4 in patients was higher than that in normal subjects. The expression of LILRB4 was the highest in recurrent patients (Figure 1(b)) and positively correlated with PRMT5 (Figure 1(f)), suggesting that LILRB4 may be involved in the pathogenesis of AML. There may be a certain relationship between PRMT5 and LILRB4 in regulating the invasion and migration of AML. This result is consistent with the characteristics of AML in previous studies [29], and our results further confirm that the overexpression of PRMT5 is closely associated with the expression of LILRB4 in highly invasive AML. In addition, our results provide evidence that the expression of LILRB4 is significantly decreased after downregulation of PRMT5. Meanwhile, the capability of invasion, migration, and adhesion in AML cells is also significantly decreased, similar to that following downregulation of LILRB4 expression [29]. Thus, PRMT5 may affect the invasion and migration of AML by regulating the expression of LILRB4.

In addition, the mechanism underlying the effects of PRMT5 on downstream gene expression and phenomena was also discussed. To be specific, in lung cancer, inhibition of PRMT5 expression can alleviate the trigger of enolase-1, thus reducing the invasion of lung adenocarcinoma [38]. Previous studies have also shown that PRMT5 can regulate PI3K, AKT, ERK, mTOR, and NF-κB signaling pathway [16, 17, 20, 34]. PRMT5 affects the expression of multiple essential genes by regulating splicing [21]. In this study, we selected several approaches and found that the change of mTOR pathway was the most significant. Strobl et al. have found that the inhibition of PRMT5 is consistent with the induction of p53 expression and the decrease of AKT/mTOR signal transduction in lung cancer [19]. Wei et al. have found that PRMT5 affects the apoptosis and invasion of lung cancer cells by regulating the expression of AKT/mTOR or ERK/mTOR [34]. These results suggest that PRMT5 plays a biological role in AML through the mTOR pathway. In this study, downregulation of PRMT5 was used to inhibit the

expression of LILRB4, which further decreased the invasive ability of THP-1 and MV-4-11 cells. We speculated that PRMT5 might affect the expression of LILRB4 by activating AKT/mTOR and ERK/mTOR axes. Therefore, mTOR inhibitors were used to suppress the phosphorylated expression of mTOR pathway, followed by detection of downstream phenomena and LILRB4 expression. These results showed that the expression of LILRB4 was significantly decreased, and the migration, invasion, and adhesion abilities of THP-1 and MV-4-11 were significantly decreased. The above findings indicate that the expression of LILRB4 is inhibited under suppressed mTOR phosphorylation. PRMT5 is the upstream gene of LILRB4 and regulates the expression of LILRB4 through mTOR pathway, thus affecting the invasive ability of AML.

5. Conclusions

PRMT5 is highly expressed in AML, which is a marker of poor prognosis for AML. PRMT5 plays an important role in the invasive capability of AML cells. Inhibition of PRMT5 can alleviate the invasion and migration of AML cells and improve the prognosis of AML, which is associated with the change of LILRB4 induced by PRMT5. The effects of PRMT5 on LILRB4 may be associated with its regulation on mTOR. The overexpression of PRMT5 is critically involved in the invasion and migration of AML, which could act as a new therapeutic target for AML.

Data Availability

The datasets used or analyzed in the current research can be obtained from the appropriate authors according to reasonable requirements.

Conflicts of Interest

The authors declare that they have no conflicts of interest.

Authors' Contributions

LZ wrote the manuscript. LZ and BC conceived and designed the study. LZ, BC, JX, and DM were responsible for the collection and analysis of the experimental data. XL and LW interpreted the data and drafted the manuscript. XZ and JW revised the manuscript critically for important intellectual content. All the authors read and approved the final manuscript.

Acknowledgments

This study was supported by the National Natural Science Foundation of China (No. 81960032) and Science and Technology Fund Project of Guizhou Province (No. 2018-25). And we are grateful for the clinical specimens provided by the Hematopoietic Stem Cell Laboratory of Guizhou Medical University.

References

[1] N. J. Short, M. E. Rytting, and J. E. Cortes, "Acute myeloid leukaemia," *The Lancet*, vol. 392, no. 10147, pp. 593–606, 2018.

[2] L. I. Shlush, A. Mitchell, L. Heisler et al., "Tracing the origins of relapse in acute myeloid leukaemia to stem cells," *Nature*, vol. 547, no. 7661, pp. 104–108, 2017.

[3] J. Rossignol, L. Polivka, L. Maouche-Chretien, L. Frenzel, P. Dubreuil, and O. Hermine, "Recent advances in the understanding and therapeutic management of mastocytosis," *F1000Research*, vol. 8, 2019.

[4] The Cancer Genome Atlas Research Network, "Genomic and epigenomic landscapes of adult de novo acute myeloid leukemia," *New England Journal of Medicine*, vol. 368, no. 22, pp. 2059–2074, 2013.

[5] S. Kayser and M. J. Levis, "Advances in targeted therapy for acute myeloid leukaemia," *British Journal of Haematology*, vol. 180, no. 4, pp. 484–500, 2018.

[6] A. K. Burnett, "Treatment of acute myeloid leukemia: are we making progress?," *Hematology*, vol. 2012, pp. 1–6, 2012.

[7] H. Kantarjian, "Acute myeloid leukemia–major progress over four decades and glimpses into the future," *American Journal of Hematology*, vol. 91, no. 1, pp. 131–145, 2016.

[8] P. Bose and S. Grant, "Rational combinations of targeted agents in AML," *Journal of Clinical Medicine*, vol. 4, no. 4, pp. 634–664, 2015.

[9] M. T. Bedford and S. G. Clarke, "Protein arginine methylation in mammals: who, what, and why," *Molecular Cell*, vol. 33, no. 1, pp. 1–13, 2009.

[10] P. J. Hamard, G. E. Santiago, F. Liu et al., "PRMT5 Regulates DNA Repair by Controlling the Alternative Splicing of Histone- Modifying Enzymes," *Cell Reports*, vol. 24, no. 10, pp. 2643–2657, 2018.

[11] D. Q. Tan, Y. Li, C. Yang et al., "PRMT5 modulates splicing for genome integrity and preserves proteostasis of hematopoietic stem cells," *Cell Reports*, vol. 26, no. 9, pp. 2316–2328.e6, 2019.

[12] L. C. Litzler, A. Zahn, A. P. Meli et al., "PRMT5 is essential for B cell development and germinal center dynamics," *Nature Communications*, vol. 10, no. 1, p. 22, 2019.

[13] J. Liu, Y. Liu, J. Shao et al., "Zeb1 is important for proper cleavage plane orientation of dividing progenitors and neuronal migration in the mouse neocortex," *Cell Death & Differentiation*, vol. 26, no. 11, pp. 2479–2492, 2019.

[14] Y. Amano, D. Matsubara, T. Yoshimoto et al., "Expression of protein arginine methyltransferase-5 in oral squamous cell carcinoma and its significance in epithelial-to-mesenchymal transition," *Pathology International*, vol. 68, no. 6, pp. 359–366, 2018.

[15] C. Y. Yang, L. L. Chiu, C. C. Chang, H. C. Chuang, and T. H. Tan, "Induction of DUSP14 ubiquitination by PRMT5-mediated arginine methylation," *The FASEB Journal*, vol. 32, no. 12, pp. 6760–6770, 2018.

[16] R. S. Blanc and S. Richard, "Arginine methylation: the coming of age," *Molecular Cell*, vol. 65, no. 1, pp. 8–24, 2017.

[17] A. Richters, "Targeting protein arginine methyltransferase 5 in disease," *Future Medicinal Chemistry*, vol. 9, no. 17, pp. 2081–2098, 2017.

[18] S. Kaushik, F. Liu, K. J. Veazey et al., "Genetic deletion or small-molecule inhibition of the arginine methyltransferase PRMT5 exhibit anti-tumoral activity in mouse models of

Hindawi
BioMed Research International
Volume 2021, Article ID 7865856, 17 pages
https://doi.org/10.1155/2021/7865856

Research Article

A Wavelet-Based Learning Model Enhances Molecular Prognosis in Pancreatic Adenocarcinoma

Binhua Tang, Yu Chen, Yuqi Wang, and Jiafei Nie

Epigenetics & Function Group, Hohai University, Jiangsu 213022, China

Correspondence should be addressed to Binhua Tang; bh.tang@outlook.com

Received 16 June 2021; Accepted 21 September 2021; Published 16 October 2021

Academic Editor: Suyan Tian

Genome-wide omics technology boosts deep interrogation into the clinical prognosis and inherent mechanism of pancreatic oncology. Classic LASSO methods coequally treat all candidates, ignoring individual characteristics, thus frequently deteriorating performance with comparatively more predictors. Here, we propose a wavelet-based deep learning method in variable selection and prognosis formulation for PAAD with small samples and multisource information. With the genomic, epigenomic, and clinical cohort information from The Cancer Genome Atlas, the constructed five-molecule model is validated via Kaplan-Meier survival estimate, rendering significant prognosis capability on high- and low-risk subcohorts (p value < 0.0001), together with three predictors manifesting the individual prognosis significance (p value: 0.0012~0.024). Moreover, the performance of the prognosis model has been benchmarked against the traditional LASSO and wavelet-based methods in the 3- and 5-year prediction AUC items, respectively. Specifically, the proposed model with discrete stationary wavelet base (bior1.5) overwhelmingly outperformed traditional LASSO and wavelet-based methods (AUC: 0.787 vs. 0.782 and 0.721 for the 3-year case; AUC: 0.937 vs. 0.802 and 0.859 for the 5-year case). Thus, the proposed model provides a more accurate perspective, but with less predictor burden for clinical prognosis in the pancreatic carcinoma study.

1. Introduction

Pancreatic adenocarcinoma (PAAD) cancer is one of the leading causes of global cancer-related mortality, but until now, the diagnosis and prognosis are still hysteretic with its death toll approaching the diagnosed cases [1]. Pancreatic ductal adenocarcinoma (PDAC) is the most common subtype of pancreatic cancer, named for its histological similarity to ductal cells [2, 3]. Quite a few developed countries have 3 to 4 times higher pancreatic cancer incidence than developing nations, with the highest rates in Europe, North America, Australia, and New Zealand. Notably, in many EU countries, pancreatic cancer is overtaking breast cancer as the third leading cause of cancer death [4].

In previous diagnosis and prognosis studies, Park et al. inferred prognostic markers from patient-specific gene relevance networks and identified diverse prognostic gene pairs [5]. Wang and Wei proposed a multivariate mixed model (IMIX) framework to screen genes and CNV related to the prognosis of pancreatic cancer, and the key genes identified were positively correlated with CNV status [6]. Nikolova et al. proposed a Bayesian multitasking method to infer the key genes for PAAD occurrence [7]. HiFreSP, a high-frequency subpath mining method, was proposed to identify cancer risk factors and the molecular pathways related to prognosis [8].

From the perspective of digital signal processing, S. Wang and X. Wang introduced a two-dimensional wavelet into protein structure prediction for denoising [9]. Lin et al. used stationary wavelet transform for sequence similarity analysis, where wavelet transform was used to convert complex numbers obtained from cluster mapping into feature vectors [10].

Recently, combined with a convolutional neural network (CNN), a stacked ensemble model was introduced to extract

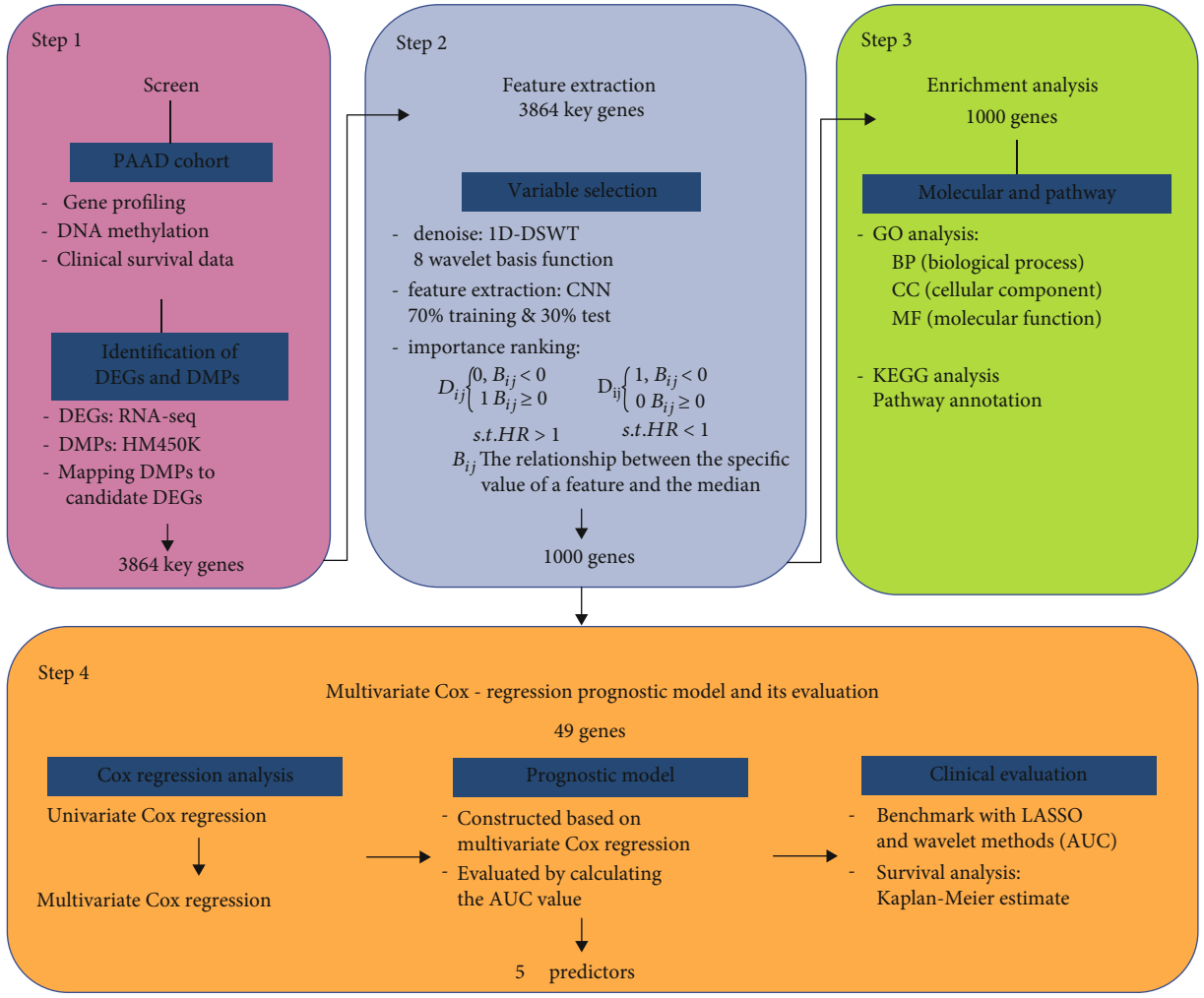

Figure 1: The pipeline to identify key genes and construct a prognostic risk model. The initial three parts mainly cover the procedures to retrieve, identify, and analyze key genes. The last part is the construction of the prognostic risk model.

features and achieve satisfactory prognosis performance [11]. Chen et al. proposed a deep-learning capsule network, CapsNetMMD, which can transform gene identification into a supervised classification problem, outperforming classic machine learning methods [12]. DeepType is also a deep learning-based algorithm for cancer subtype classification, which effectively combines supervised learning and unsupervised clustering [13]. Hao et al. proposed a sparse deep neural network, PASNet, for prognostic analysis and identification of complex biological processes related to prognostic pathways [14].

Both CNN for feature extraction and discrete wavelet transform in signal processing were adopted to tumor subtype classification in medical imaging [15]. Meintjes et al. utilized CNN and continuous wavelet transform in the classification of heart sounds [16]. In the segment study of brain tumor, wavelet transform can enhance the CNN structure, thus leading to effectively improve the image processing capability [17].

Although massive contributions were completed in cancer diagnosis and treatment, to significantly reduce its morbidity and mortality, it is still required to thoroughly identify feasible biomarkers for the occurrence and development in combination with multisource data and to comprehensively reveal its tumorigenesis mechanisms.

Therefore, this work attempted to identify the combinatorial predictors for PAAD prognosis through the integration of multisource genomic, epigenomic, and clinical information. We proposed a novel deep learning-based method with wavelet feature selection to construct the PAAD prognostic model. With the mRNA profiling (RNA-seq), DNA methylation, and corresponding clinical information retrieved from The Cancer Genome Atlas (TCGA), the constructed model was validated by the predictive ROC (receiver operating characteristics) test on the 3-year and 5-year survival rates, respectively. Together, our proposed model was compared with classic LASSO and previous wavelet-based approaches quantitatively, rendering enhanced performance with less predictor consideration.

In the rest of the paper, Section 2 presents a detailed method proposal and multisource datasets under study; Section 3 discusses the validation and comparison results for the method; Section 4 draws the conclusion and highlights the future direction.

2. Materials and Methods

Figure 1 depicts the analytic pipeline to identify candidate prognostic predictors based on multisource genomic and epigenomic profiling and clinical information for PAAD. The initial step is to retrieve multisource mRNA profiling (RNA-seq) and DNA methylation (Infinium HumanMethylation450K) data from TCGA and determine differentially expressed genes (DEGs) with the cutoff criteria ($|\log FC| \geq 1.5$ and the adjusted p value < 0.05) and determine differential methylation probes (DMPs) with the cutoff criteria ($|\text{deltaBeta}| > 0.2$ and the adjusted p value < 0.05). The key gene candidates are filtered through integrating the DEGs and DMPs; specifically, the key genes are the DEGs that interact with differential methylation probes. Secondly, a new DSWT method based on deep learning is used for feature extraction from key genes. And functional enrichment analysis was performed on the screened key genes to identify functional clues. Enrichment analysis includes Gene Ontology (GO) and Kyoto Encyclopedia of Genes and Genomics (KEGG) analysis. After performing Cox regression analysis on the genes obtained after feature selection of 56 kinds of wavelet basis functions, a prognostic model of five genes was finally formulated.

Compared with the traditional LASSO method and the latest method SWT-CNN, the predictive ability of the proposed deep learning method is significantly higher than that of LASSO [18] and SWT-CNN [19].

2.1. Gene Expression Data and DNA Methylation Data Information. The gene expression profiling, DNA methylation, and clinical information in this study were retrieved from TCGA, including 178 tumor and 4 normal samples. Table 1 lists the data statistics adopted in this study. We detected the DEGs between tumor and normal tissue samples using edgeR [20], with the $|\log FC| \geq 1.5$ and adjusted p value < 0.05 and identified the DMPs with the $|\text{deltaBeta}| > 0.2$ and adjusted p value < 0.05 as the cutoff criteria using ChAMP [21].

2.2. Deep Learning-Based DSWT Method for Feature Selection

2.2.1. One-Dimensional Stationary Wavelet Transform for Noise Removal. Wavelet transform has been widely used in signal processing and computer vision [22, 23]. Regarded as an extension of short-time Fourier transform (STFT), it can effectively solve the limitation that the shape and size of the STFT window do not change with frequency. In many signals, the low-frequency part is particularly important. Based on the Mallet algorithm, discrete wavelet transform (DWT) can effectively extract the low-frequency part of the signal, also known as noise removal [24].

With a mother wavelet $\psi((t-b)/a)$, the continuous wavelet transform of a function $x(t)$ can be formulated as.

$$CWT_x(a,b) = \frac{1}{\sqrt{a}} \int_{-\infty}^{\infty} x(t)\psi\left(\frac{t-b}{a}\right) dt, \quad (1)$$

where a denotes the scale coefficient and b the translation distance [25]. Frequently, the two parameters can be discretized by the 2-base power series as.

$$a = 2^j, b = k2^j, \quad \text{for} \forall j, k \in \mathbb{Z}. \quad (2)$$

The mother wavelet $\psi(t)$ can be further reformulated as

$$\psi_{j,k}(t) = \frac{1}{\sqrt{2^j}} \psi\left(\frac{t}{\sqrt{2^j}} - k\right). \quad (3)$$

Thus, the corresponding discrete wavelet transform is derived as

$$DWT_x(j,k) = \frac{1}{\sqrt{2^j}} \int_{-\infty}^{\infty} x(t)\psi_{jk}\left(\frac{t}{\sqrt{2^j}} - k\right) dt, \quad (4)$$

where j denotes the scale coefficient and k is the translation distance, respectively.

In this study, we adopted the one-dimensional discrete stationary wavelet transform (DSWT) due to its translational invariance. Compared with DWT, the length of each channel coefficient after decomposition is equal to the original signal. The DSWT algorithm contains two steps: (a) the input signal is divided into two coefficient sets, high and low; (b) the low-frequency coefficient set is decomposed by the method in (a). The details are depicted in Figure 2.

We use the wavelet to denoise the gene expression profiles. Here, we mainly choose the basis function of DSWT based on three parameters: (a) decomposition layers, (b) the family of wavelets, and (c) the corresponding basis function in a family of wavelets.

The number of decomposition layers has a great influence on noise removal. Too few layers may lead to a poor denoising effect, but too many layers may also lead to signal distortion. Here, we select the optimal number of decomposition layers according to the degree of distortion of the signal when setting different decomposition layers.

Here, we mainly consider 8 wavelet families and corresponding 56 basis functions, which are daubechies (basis function: db$i$, $i = 2, 3, 4, 5, 6, 7, 8$), symlets (basis function: sym i, $i = 2, 3, 4, 5, 6, 7, 8$), coiflets (basis function: coif$i$, $i = 2, 3, 4, 5$), biorSplines (basis function: bior$i$, $i = 1.1, 1.3, 1.5, 2.2, 2.4, 2.6, 2.8, 3.1, 3.3, 3.5, 3.7, 3.9, 4.4, 5.5, 6.8$), reverseBior (basis function: rbio$i$, $i = 1.1, 1.3, 1.5, 2.2, 2.4, 2.6, 2.8, 3.1, 3.3, 3.5, 3.7, 3.9, 4.4, 5.5, 6.8$), haar, dmeyer, and Fejer-Korovkin (basis function: fk$i$, $i = 4, 6, 8, 14, 18, 22$), respectively (Table 2).

For its outstanding capabilities in processing matrix-wise information, the CNN method develops rapidly and is applied in quite a few topics [26, 27]. Here, we utilized it in feature extraction. The DSWT results serve as the network

input; specifically, 70% of the input samples were selected as the training set and 30% as the test set.

2.2.2. Step Function for Determining Gene Scores. A score metric is assigned to each gene to evaluate its importance in prognosis. There are two procedures to acquire the gene score: (a) the gene weight matrix $C_{n\times m}$ obtained by CNN and (b) sparse matrix $D_{q\times m}$. Matrix C is calculated according to the output matrix A of the maximum pooling layer of CNN. A is a three-dimensional matrix with dimension $m \times n \times p$ (m is the sample size of the input of CNN, n is the number of features, and p is the number of channels). After averaging the matrix A, according to the number of channels P, we get the matrix $C_{n\times m}$. We assume the expression matrix of DEGs is $B_{q\times m}$. Here, we obtain the matrix D by the formula similar to a step function [28].

$$D_{ij} = \begin{cases} 0, & B_{ij} < 0 \\ 1 & B_{ij} \geq 0 \end{cases}, \text{s.t.} \quad HR > 1, \tag{5}$$

$$D_{ij} = \begin{cases} 1, & B_{ij} < 0 \\ 0 & B_{ij} \geq 0 \end{cases}, \text{s.t.} \quad HR < 1, \tag{6}$$

where HR is obtained by univariate Cox analysis of DEGs. The relationship between B_{ij} and 0 is corresponding to the gene expression level and its median. And the matrix $E_{q\times n}$ can be denoted as.

$$E_{q\times n} = D_{q\times m} C^T_{n\times m}. \tag{7}$$

Then, individual gene score (GS) is estimated as.

$$GS_i = \frac{1}{n} \sum_{i=1}^{n} \sum_{j=1}^{n} E_{ij}. \tag{8}$$

2.2.3. Functional Enrichment Analyses. Gene Ontology (GO) analysis is utilized to describe three types of gene products, biological process (BP), molecular function (MF), and cellular component (CC). Then, we further systematically interrogated KEGG pathways to link genomic profiling status to higher-order functional information.

2.3. Cox Regression Analysis. The Cox Proportional Hazards model, essentially a statistical regression model, is adopted to investigate the association between the survival time of patients and potential predictive factors [29].

2.3.1. Univariate Cox Regression Analysis. The genes obtained by feature selection were analyzed by a univariate Cox regression model, and the relationship between the gene expression level and its corresponding patient survival time was analyzed. The results of univariate Cox regression analysis included regression coefficient (β), risk ratio (95% confidence interval), z, Wald test results, and p value [29].

2.3.2. Multivariate Cox Regression Analysis. Cox risk regression analysis was performed to assess the mutual effect of several predictive factors on survival outcomes. Specifically, initial screening was carried out on the genes obtained by univariate Cox regression; then, multivariate Cox regression analysis was performed on the screened genes. After both univariate and multivariate analyses, a candidate gene with its p value less than 0.05 can be considered an independent predictor.

Table 1: Statistics of gene expression profiling, DNA methylation, and clinical cohort information of PAAD under study.

PAAD clinical cohort	Statistics
Tumor	178
Normal	4
Histological type	
PDAC	146
Pancreas-colloid carcinoma	4
Other	28
Survival status (tumor)	
Living	86
Deceased	93
Follow-up (months)	0.13-132.97
Age (years)	
Range	35-88
Median	61.3
Gender (tumor)	
Male	98
Female	80
#. (Epi)genomics data	
mRNA profiling (DEGs)	17240
DNA methylation (DMPs)	10648

2.4. Construction of Multivariate Cox Regression Prognostic Model. The prognostic risk score (PRS) for a multivariate Cox regression model was calculated based on a linear combination of regression coefficients and the corresponding gene expression level, respectively.

$$\text{PRS} = \sum_{i=1}^{N} \text{Exp}_i * \beta_i. \tag{9}$$

The median threshold of total risk scores divides the samples into the high-risk and low-risk groups.

To analyze the relationship between PAAD patients' risk score and overall survival and their risk score, p value < 0.05 was the significance test level, and the risk score had a significant impact on the overall survival of PAAD patients. The prognosis was predicted by the Kaplan-Meier curve and the Cox regression model, and the sensitivity was tested by the subject's working curve.

Furthermore, in evaluating model performance, the true positive rate (TPR, or sensitivity), a measure of the proportion of positive cases in the data that are correctly classified, is defined as

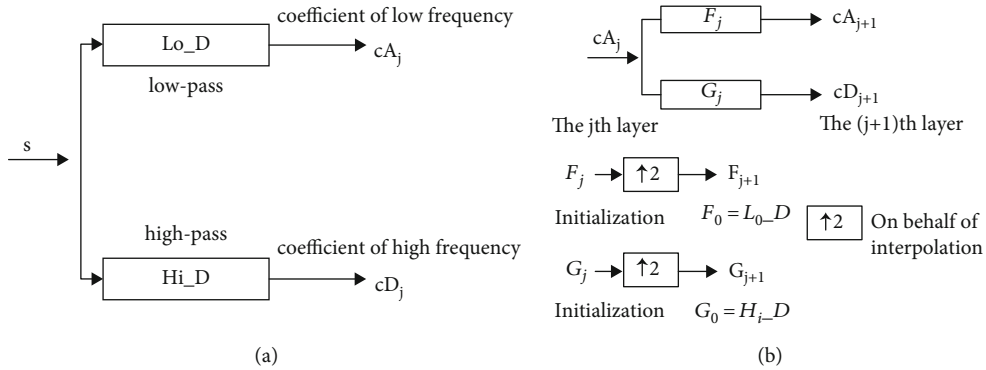

Figure 2: DSWT algorithm. (a) The input signal is divided into two coefficient sets, high and low; (b) the low-frequency coefficient set is decomposed by the method in (a). Lo_D: low pass filter; Hi_D: high pass filter.

Table 2: A total of eight typical wavelet family functions adopted in the study.

Wavelets	Description
daubechies	$\psi(t) = \sum_k g_k \phi(2t-k)$, $\phi(t)$: scale function, g_k : weight
symlets	An improvement over db and approximate symmetric wavelet function
coiflets	Compared with db, $\psi(t)$ and $\phi(t)$ have better symmetry
biorSplines	The input signal $f(t)$, $\begin{cases} \text{Decompos} : C_{j,k}(t) = \int f(t)\tilde{\psi}_{j,k}(t)dt \\ \text{Reconstruct} : f(t) = \sum_{j,k} \tilde{C}_{j,k}\psi_{j,k}(t) \\ \text{s.t.} \quad \text{the dual wavelet } \psi_{j,k}(t) \text{ and } \tilde{\psi}_{j,k}(t) \end{cases}$
reverseBior	Biorthogonal spline wavelets for which symmetry and exact reconstruction are possible
haar	$\psi(t) = \begin{cases} 1, (0 \le t < 1/2), \\ -1, (1/2 \le t \le 1), \\ 0, \text{otherwise} \end{cases}, \phi(t) = \begin{cases} 1, (0 \le t \le 1), \\ 0, \text{othewise} \end{cases}$
dmeyer	Discrete Meyer wavelet, FIR-based approximation of Meyer wavelet
Fejer-Korovkin	It has an optimal progressive resolution.

$$\text{TPR} = \frac{\text{TP}}{\text{TP} + \text{FN}}, \tag{10}$$

where TP denotes true positive and FN for false negative. And the false positive rate (FPR or fall-out), the proportion of negative cases incorrectly classified as positive cases in the data, is introduced as

$$\text{FPR} = \frac{\text{FP}}{\text{FP} + \text{TN}}, \tag{11}$$

where FP denotes false positive and TN for true negative. A ROC (receiver operating characteristic) curve, parameterized with the above measures, is utilized to evaluate the performance of a classification model at all classification thresholds. An AUC (area under the ROC curve) is introduced to measure the classification efficiency.

Table 3: Performance comparison among the eight typical wavelet-based and classic LASSO and SWT-CNN methods.

Method	Basis	AUC at 3 years	AUC at 5 years	Predictors
haar	haar	0.618	0.756	5
dmeyer	dmeyer	0.823	0.869	7
symlets	sym3	0.806	0.904	5
coiflets	coif4	0.696	0.788	5
daubechies	db7	0.804	0.867	5
biorSplines	bior1.5	0.787	0.937	5
reverseBior	rbior2.8	0.852	0.897	10
Fejer-Korovkin	fk14	0.672	0.861	5
SWT-CNN	sym4	0.721	0.859	8
LASSO		0.782	0.802	11

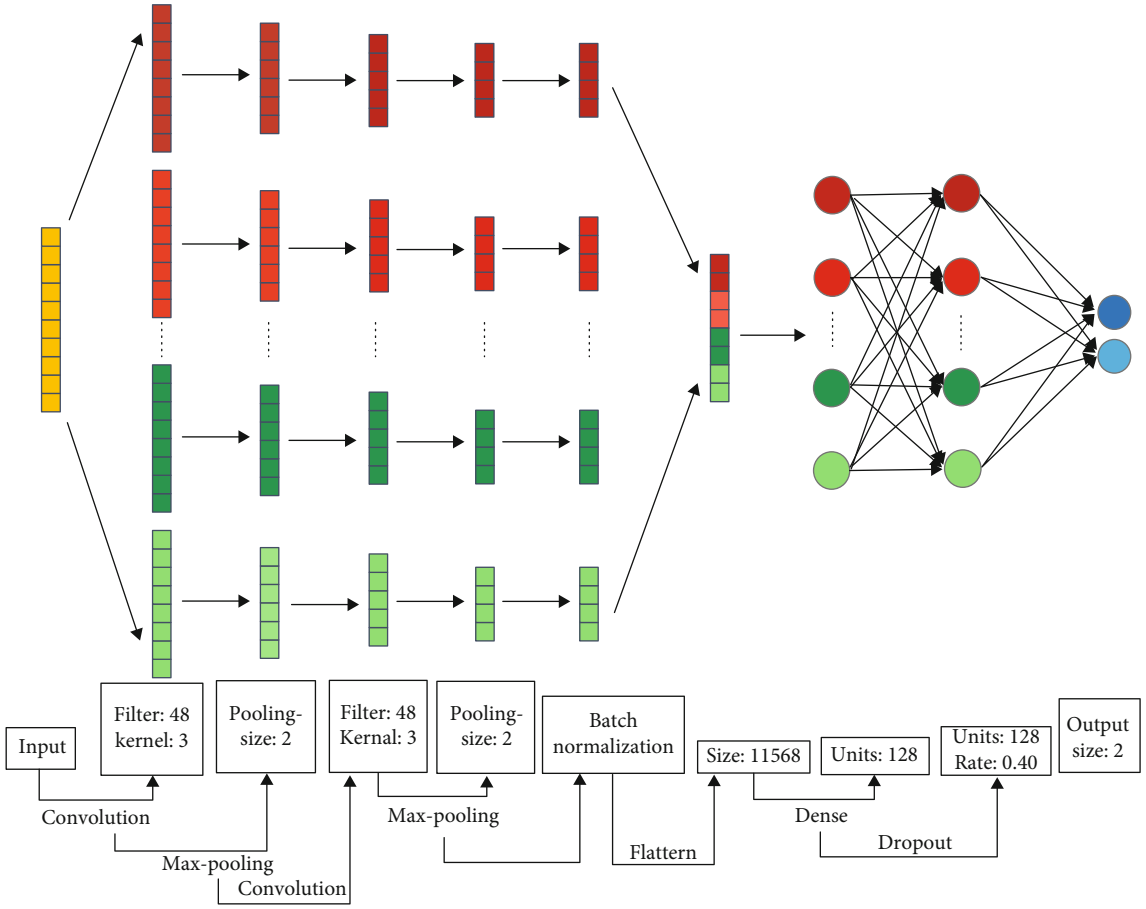

Figure 3: The CNN model structure for feature extraction. The proposed deep model consists of 9 layers, namely, convolutional layer, max-pooling layer, convolutional layer, max-pooling layer, batch normalization layer, flatten layer, hidden layer, dropout layer, and output layer, with the size and link noted above.

3. Results

We retrieved mRNA profiling data (RNA-seq) and filtered the candidate genes satisfying the cutoff criteria, $|\log FC| \geq 1.5$, and adjusted p value < 0.05, as the DEGs; in the DNA methylation dataset (Infinium HumanMethylation450K), we filtered the methylation positions satisfying the cutoff criteria, adjusted p value < 0.05, and $|\text{deltaBeta}| > 0.2$ as DMPs, then identified the key genes related to DMPs using ChAMP [21]. Then, we merged the DEGs and the genes related to DMPs as the key genes. After the screening analysis, totally 3864 gene candidates were obtained.

3.1. DSWT-Based Noise Removal Analysis. In this study, through experiment validation, it is most reasonable to set the number of decomposition layers of DSWT at 2. A total of 56 wavelet basis functions are selected to remove the noise. The optimal basis function was obtained after the prognostic analysis. The evaluation criteria of the optimal wavelet basis function include two parts: (a) the prognostic model constructed has the best prognosis performance; (b) the least number of predictors is involved in the corresponding prognostic model. The major performance comparisons are provided in Table 3, and the detailed comparison analyses on the proposed method, classic LASSO, and wavelet-based methods with diverse predictors are listed in additional file 1.

3.2. CNN-Based Feature Extraction. Since the gene positions in the expression matrix are not correlated, a one-dimensional CNN is adopted in this study to construct a 9-layer deep neural network, as depicted in Figure 3.

To achieve robust experimental results, the feature extraction process was repeated 100 times. Then, the model with the optimal predicted results of the test dataset was reserved for the subsequent analysis. The step function defined in Section 2.2.2 was utilized to score 3864 key genes, and the functional analysis was based on the top 1000 genes. Then, Cox analyses were performed based on the top 200 genes. According to the performance comparison among the constructed prognosis models, bior1.5 is adopted as the optimal wavelet basis in our proposed model.

3.3. Functional Enrichment Analysis. The key genes identified from the feature selection were further performed with GO and KEGG analyses, respectively. Figure 4 depicts the

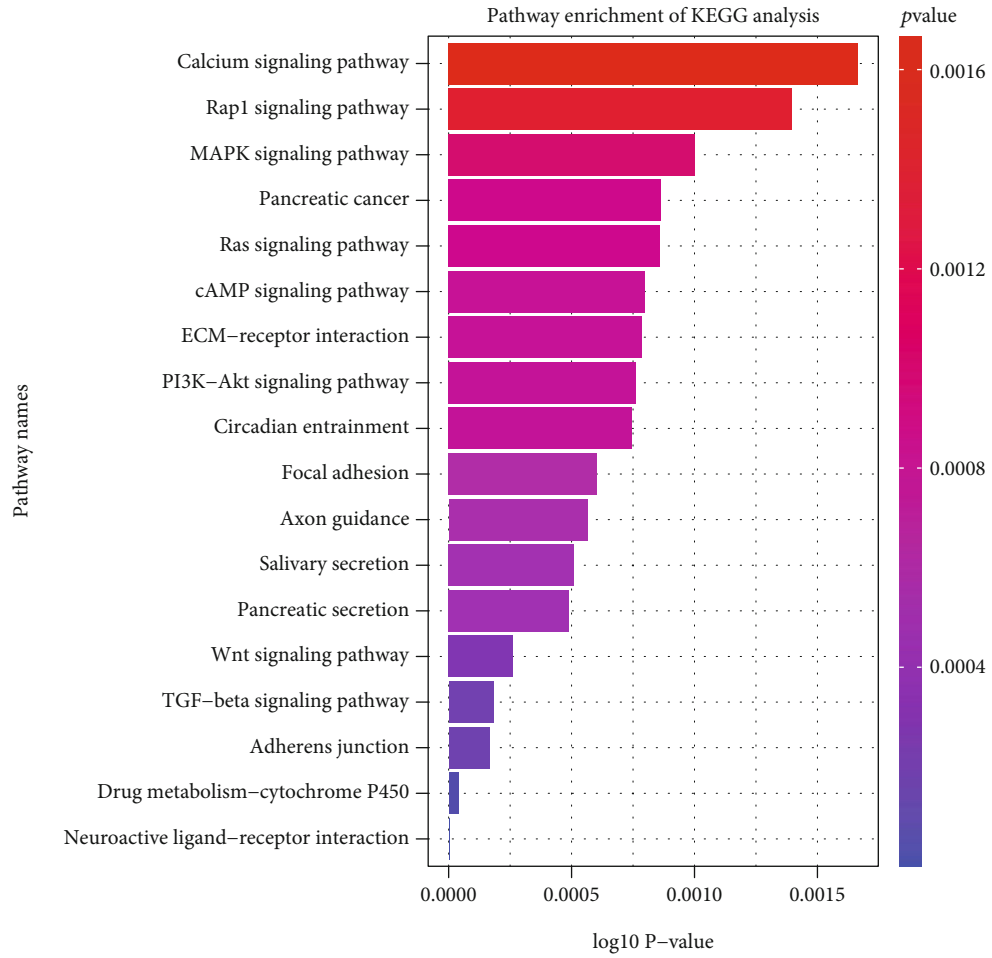

(a)

Figure 4: Continued.

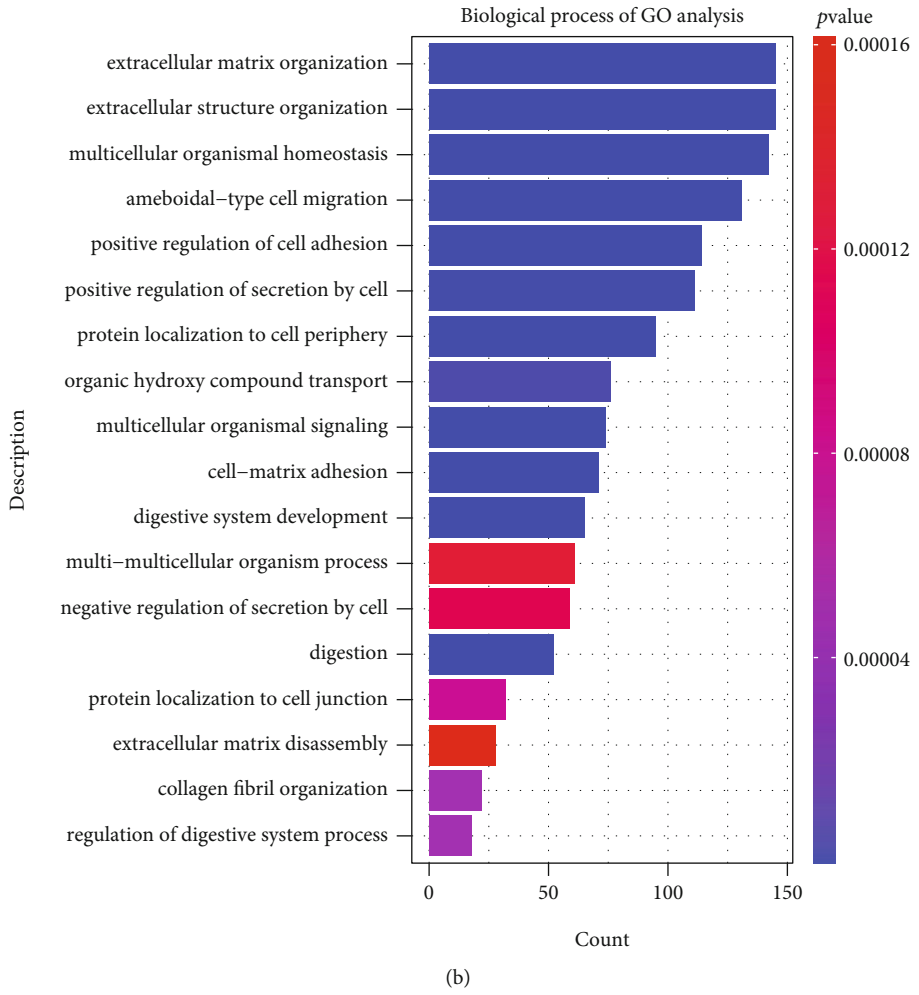

(b)

Figure 4: Continued.

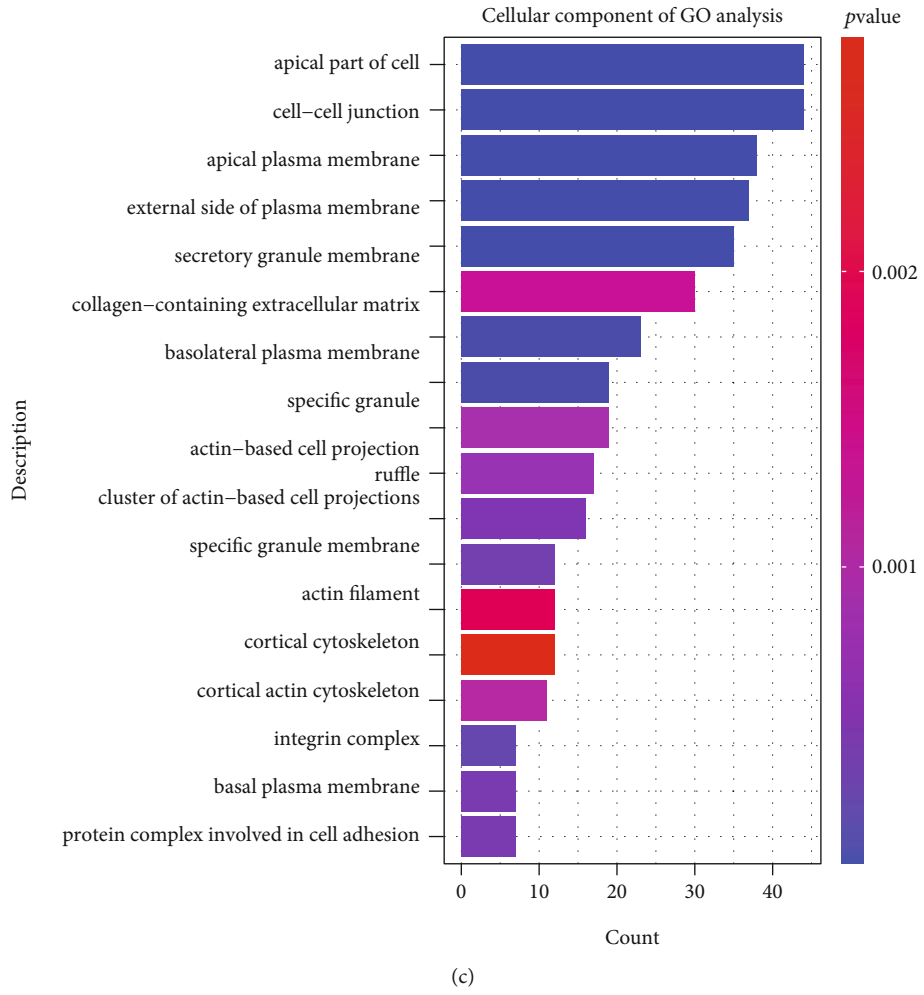

(c)

Figure 4: Continued.

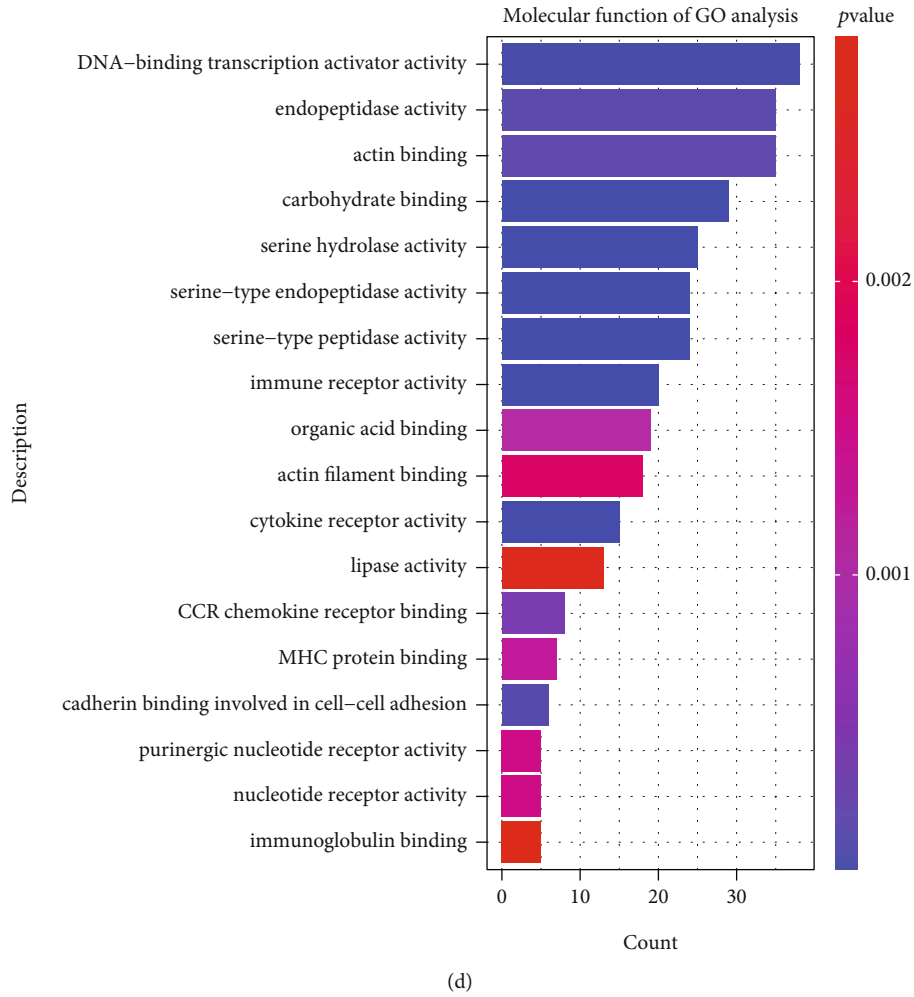

Figure 4: Illustration of KEGG and GO analysis results for the key genes in PAAD. (a) the KEGG pathways of the key genes; (b) the biological process (BP); (c) the cellular component (CC); (d) the molecular function (MF).

GO function and KEGG pathway enrichment results for the key genes.

The significantly enriched KEGG pathways of the DEGs are illustrated in Figure 4(a). These pathways mainly include MAPK signaling pathway, pancreatic cancer, pancreatic secretion, and ECM-receptor interaction. The full results of KEGG pathway analyses are shown in additional file 2. In Figures 4(b)–4(d), the results indicate that the key genes were mainly enriched in these BP terms as extracellular structure organization, extracellular matrix organization, digestion, and cell adhesion; and CC terms cover secretory granule membrane, cell-cell junction, and actin filament; MF terms include serine-type peptidase activity, endopeptidase activity, and actin binding. All the results of GO analysis about the BP, CC, and MF terms are shown in additional files 3 to 5, respectively.

3.4. Cox Regression Analysis and Construction of the Prognostic Model. First, univariate Cox regression analysis was carried out on key genes to filter satisfactory candidate predictors, wherein the stepwise regression was conducted on the results of the univariate Cox regression analysis. Afterwards, the prognostic models are further constructed with multivariate Cox analysis based on the initially filtered candidates.

The prognostic ability of the established model was evaluated by calculating the AUC value of the ROC curve to select the optimized prognostic model. The detailed decomposition results are depicted in Table 3. According to Table 3, the optimal prognosis model was acquired when the biorSplines wavelet family was selected and the smoothness was 1.5.

Comparatively, the prognostic model with the biorSplines basis bior1.5 can achieve the AUC value 0.937 with 5 predictors in the 5-year survival case; while in the 3-year survival case, the reverseBior wavelet rbio2.8 can achieve the AUC value of 0.852 on 10 predictors. However, the classic LASSO method requires at least 11 predictors to achieve the AUC, 0.782 for the 3-year case, and 0.802 for the 5-year case; the previous SWT-CNN requires at least 8 genes to achieve the AUC 0.721 for the 3-years and 0.859 for the 5-year case.

Table 4: The univariate and multivariate Cox regression analysis results.

	Univariate Cox		Multivariate Cox	
Candidates	HR (95% CI)	p value	HR (95% CI)	p value
ABHD8	0.5712 (0.4411-0.7397)	0.00001		
MCF2L	0.58195 (0.456-0.7426)	0.00003	0.6378 (0.454-0.897)	0.0097
FAM184B	0.6376 (0.5084-0.7997)	0.00010	0.7063 (0.517-0.965)	0.0287
GPRC5A	1.27261 (1.1239-1.441)	0.00010	1.0309 (0.804-1.323)	0.8108
KRT19	1.4003 (1.1809-1.6606)	0.00010	1.3305 (1.005-1.761)	0.0460
PADI1	1.1260 (1.0585-1.1978)	0.00020		
TNS4	1.1852 (1.0839-1.2961)	0.00020		
SEMA3C	1.29315 (1.1238-1.488)	0.00030		
MUCL3	1.0985 (1.0426-1.1572)	0.00040		
RNF223	1.24345 (1.102-1.4031)	0.00040		
PCAT2	1.2261 (1.0947-1.3733)	0.00040		
C6orf132	1.3850 (1.1484-1.6703)	0.00070		
C5orf49	0.8046 (0.7097-0.9123)	0.00070		
GABBR1	0.73285 (0.6096-0.881)	0.00090		
ARID3A	0.6824 (0.5442-0.8558)	0.00090		
FOSL1	1.2481 (1.0938-1.4242)	0.00100		
CHGA	0.9029 (0.8494-0.9598)	0.00100		
KRT8	1.4131 (1.1458-1.7428)	0.00120		
PLS1	1.30127 (1.1046-1.533)	0.00160		
CNIH2	0.8180 (0.7215-0.9274)	0.00170		
RYK	1.6625 (1.2059-2.2921)	0.00190		
CTSE	1.1388 (1.0482-1.2372)	0.00210		
GBP4	1.2933 (1.0965-1.5255)	0.00230	1.3814 (1.139-1.676)	0.0010
GALNT5	1.1870 (1.0626-1.3259)	0.00240	0.9135 (0.743-1.123)	0.0391
MAPT	0.83235 (0.739-0.9375)	0.00250		
TRIM59	1.4513 (1.1282-1.8671)	0.00370		
PLAC8	1.2037 (1.0616-1.3649)	0.00380		
TECPR1	0.6379 (0.4698-0.8663)	0.00400		
GRIN2C	0.7433 (0.6068-0.9105)	0.00420		
RASAL1	1.25077 (1.073-1.4579)	0.00420		
CALHM31	1.1261 (1.0353-1.2249)	0.00560		
FGF12	0.8187 (0.7081-0.9467)	0.00690		
TCEA2	0.7593 (0.6204-0.9293)	0.00760		
KRT5	1.0792 (1.0202-1.1416)	0.00790		
TINAG1	1.1122 (1.0281-1.2031)	0.00800		
KCNK3	0.8803 (0.8010-0.9674)	0.00810		
CAPN5	1.2323 (1.0548-1.4396)	0.00850		
SLCO4A1	1.1957 (1.0465-1.3663)	0.00860		
KCNK12	0.8240 (0.7122-0.9532)	0.00920		
FSTL4	0.8815 (0.8015-0.9694)	0.00930		
GPR78	1.2335 (1.0527-1.4452)	0.00940		
FOXA2	0.8482 (0.7381-0.9746)	0.02020	1.0812 (0.891-1.313)	0.4300
DUOX2	1.0933 (1.0138-1.1791)	0.02060		
HDAC4	0.7096 (0.5308-0.9487)	0.02060		
MPPED2	0.8509 (0.7413-0.9768)	0.02180		
SDK1	0.8594 (0.7549-0.9784)	0.02200		
STAC	1.1520 (1.0199-1.3012)	0.02280		
VRK2	1.3697 (1.0399-1.8043)	0.02520		
ITGBL1	1.1277 (1.0126-1.2557)	0.02860		

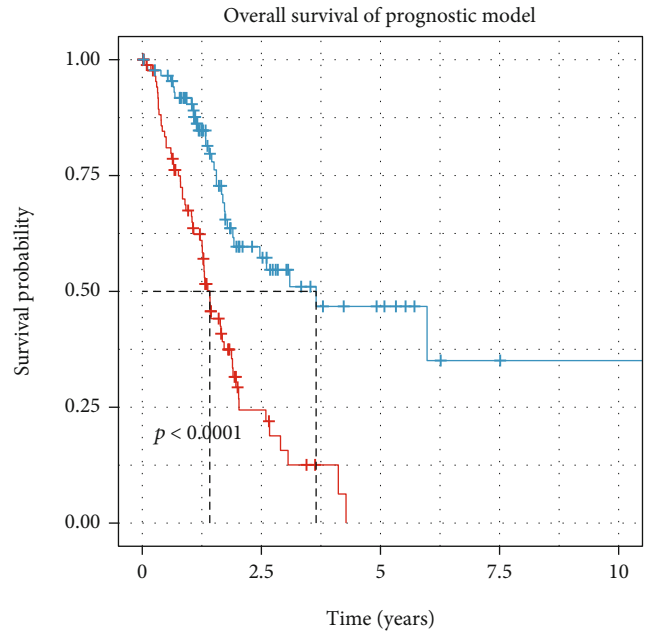

(a)

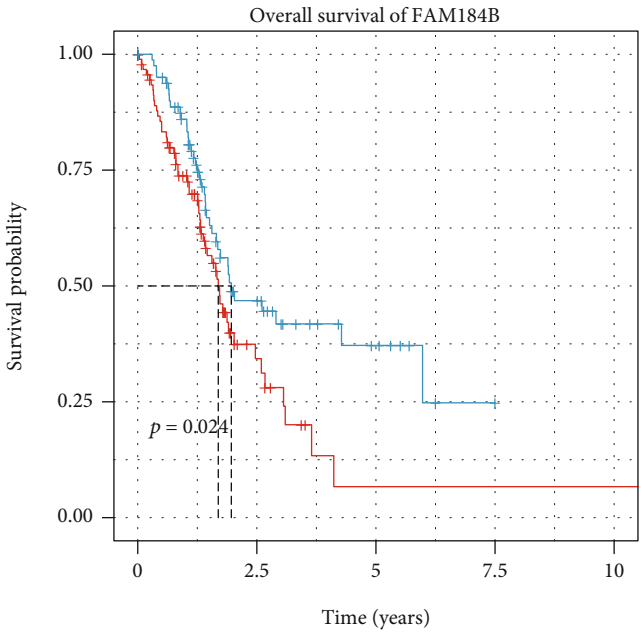

(b)

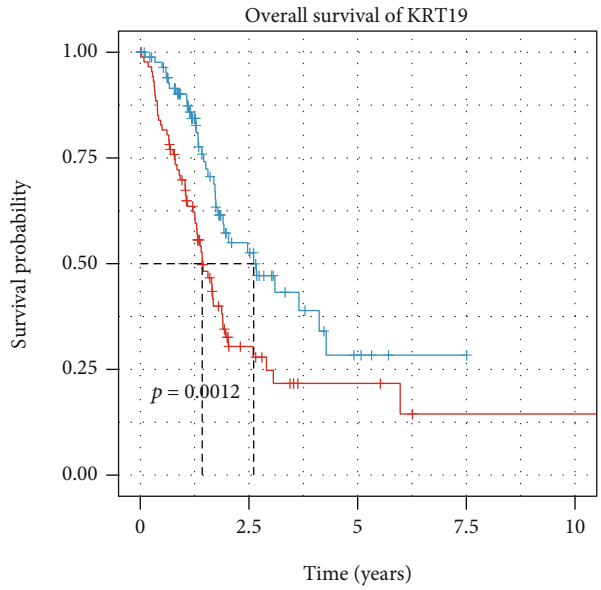

(c)

Figure 5: Continued.

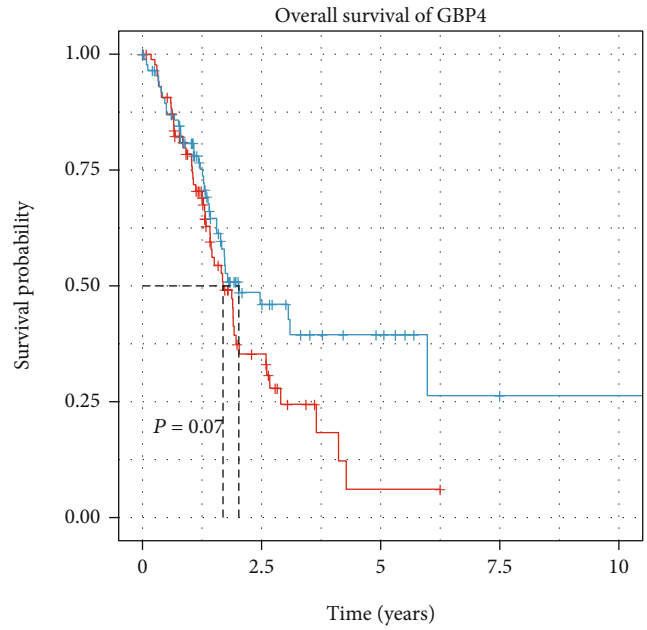

(d)

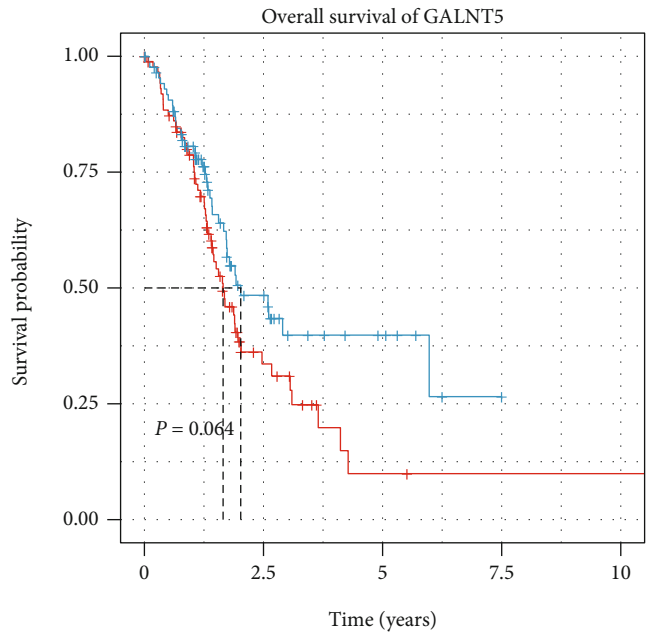

(e)

Figure 5: Continued.

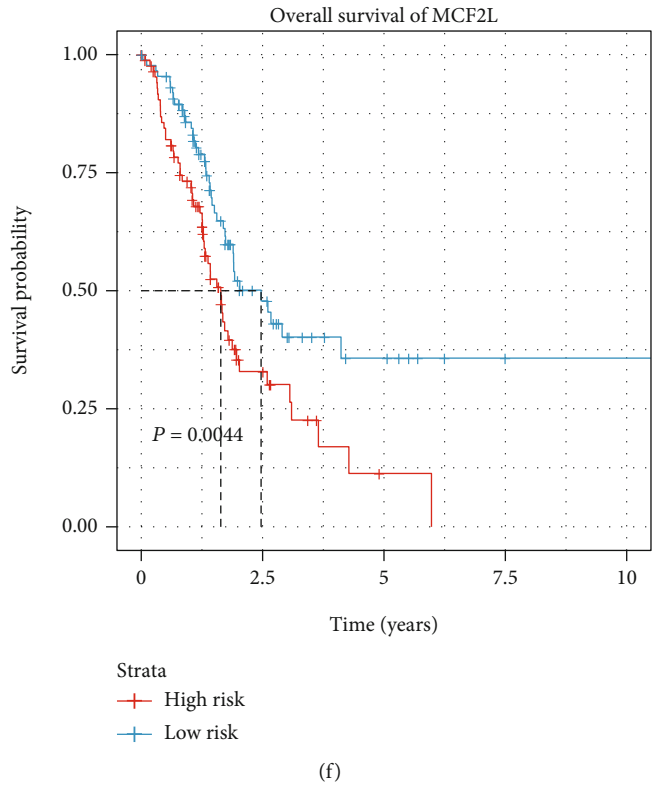

Figure 5: Kaplan-Meier survival analysis of the 5-molecule signature and individual predictors. (a) Kaplan-Meier survival curve analysis for overall survival of PAAD patients using the 5-molecule signature. Survival in the low-risk group was much longer than in the high-risk group; (b) overall survival distribution of FAM184B; (c) overall survival distribution of KRT19; (d) overall survival distribution of GBP4; (e) overall survival distribution of GALNT5; (f) overall survival distribution of MCF2L.

The results of our proposed method outperformed the other two methods overall; thus, the biorSplines basis was adopted as the variable selection in constructing the prognosis model. Then, univariate and multivariate Cox regression analyses were further performed on the predictor candidates, detailed in Table 4.

Table 4 depicts the univariate and multivariate Cox regression analysis to filter the prognosis risk candidates, wherein five molecules, namely, MCF2L, FAM184B, KRT19, GBP4, and GALNT5, were determined as the predictors. Thus, after the above quantitative comparison, the final optimal prognosis model is denoted with the five molecular risk predictors.

$$\begin{aligned} \mathrm{PRS} = {} & (-0.342 * \mathrm{Exp}_{\mathrm{FAM184B}}) + (0.300 * \mathrm{Exp}_{\mathrm{KRT19}}) \\ & + (0.318 * \mathrm{Exp}_{\mathrm{GBP4}}) + (-0.070 * \mathrm{Exp}_{\mathrm{GALNT5}}) \\ & + (-0.412 * \mathrm{Exp}_{\mathrm{MCF2L}}). \end{aligned} \quad (12)$$

3.5. Kaplan-Meier Survival Analysis. Each patient's risk score was calculated using the prediction function based on the constructed prognosis model in Equation (12). The cohorts were divided into two groups, the high-risk group and the low-risk group, respectively.

The survival rates were calculated from the high-low risk groups, and the corresponding Kaplan-Meier survival diagram is illustrated in Figure 5(a); and for the comparison of prognosis potentials of individual molecules, the other five molecular predictors are provided in Figures 5(b)–5(f). Noticeably, the three predictors involved in the 5-molecule prognosis model are statistically significant, namely, FAM184B, KRT19, and MCF2L (log-rank test p value < 0.05). Noticeably, although the five protein-coding genes have not been reported in PAAD, they have interfered with other disease or pathway dysfunction, for example, interferon-gamma signaling and cytokine signaling in immune system, GPCR pathway, and p75 NTR receptor-mediated signaling.

3.6. Comparison with Other Typical Methods. The prognostic power of the established model was evaluated by the AUC value of the ROC curve with the SWT-CNN and classic LASSO methods (Figure 6), where the AUC measure for the 3- and 5-year terms was compared, respectively. The AUC at 3 years of our proposed model is 0.787, and the AUC at 5 years is 0.937, while for the classic LASSO method, the AUC at 3 years and 5 years are 0.782 and 0.802, respectively. For the SWT-CNN method, the AUC at 3 years and 5 years are 0.721 and 0.859, respectively. The results indicate that the prognostic model proposed had a better sensitivity in predicting the survival risk of PAAD patients.

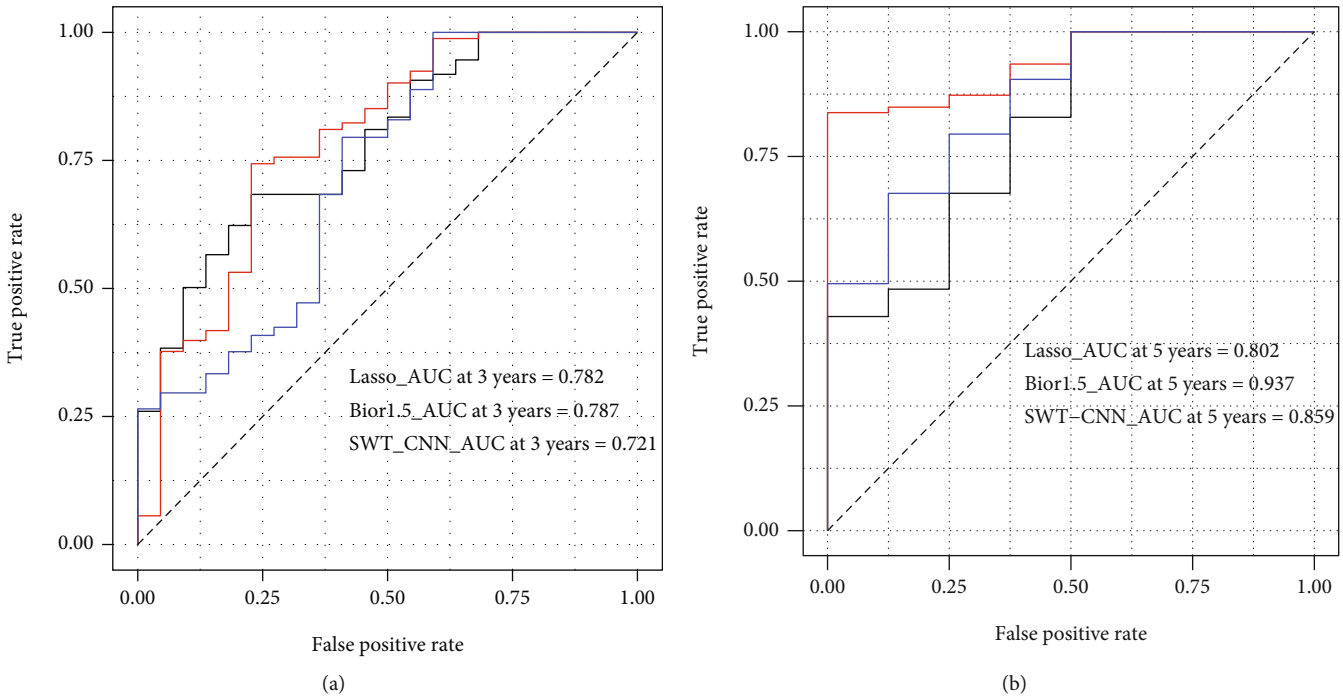

Figure 6: Performance comparison with the SWT-CNN and traditional LASSO methods. (a) AUC at 3 years: bior1.5_AUC at 3 years = 0.787, lasso_AUC at 3 years = 0.782, and SWT-CNN at 3 years = 0.721; (b) AUC at 5 years: bior1.5_AUC at 5 years = 0.937, lasso_AUC at 5 years = 0.802, and SWT-CNN at 5 years = 0.859.

4. Conclusions and Discussion

Pancreatic cancer is a high-incidence tumor type with poor clinical prognosis. There is an urgent need to develop effective methods for the prognosis prediction of pancreatic cancer. Thus, we proposed a novel CNN-based model to enhance prognosis performance in PAAD through combining wavelet transform features. In the work, we integrated mRNA expression and DNA methylation, together with cohort clinical information into PAAD prognosis formulation, from an ensemble perspective of multiple omics data.

Firstly, with the noise reduction functionality of wavelet transform in signal processing, a 1D-DSWT was utilized to denoise the identified key genes, specifically differentially expressed genes overlapping with differentially methylated loci. The number of decomposition layers, wavelet family, and basis function types are considered in the wavelet function selection for denoising, and the low-frequency part of the signal value is reserved for the subsequent analyses.

Then, a 9-layer CNN structure is trained for feature extraction after the above noise reduction process. The weights of candidate genes are obtained from feature extraction, specifically the output matrix of the CNN pooling layer, for subsequent analysis. A scoring measure is proposed for weighting important molecular predictors involved in pancreatic cancer prognosis. The score consists of three parts, the HR value obtained by univariate Cox regression analysis of the key genes, the sparse matrix constructed by the step function of HR value, and the weights derived from the CNN structure.

Through enrichment analysis of the screened genes, it indicates that these identified genes are involved in many biological activities closely related to pancreatic cancer, which manifests the biological significance of the candidates to the prognosis of pancreatic cancer.

The initial candidate genes in the scoring process were adopted for univariate Cox analysis to compress the candidate space; then after multivariate Cox regression, five molecule predictors were screened out to construct the prognosis model. To verify the survival predictive capability, the constructed model and individual predictors have been examined with survival analysis via Kaplan-Meier estimate, respectively. The constructed model has significant statistical predictive ability on high- and low-risk cases (p value: 0.00007). For the other three individual factors, it also manifested the underlying survival prognosis significance (p value: 0.0012~0.024).

Moreover, to validate the prediction performance and measure the diagnostic accuracy of quantitative tests, the proposed prognosis model was compared with the traditional LASSO and wavelet-based methods in the 3- and 5-year prediction AUC scores, respectively. In three prediction cases, our proposed model with discrete stationary wavelet base (bior1.5) got the optimal results, especially in the 5-year case. We applied the proposed method to the other tumor type, stomach adenocarcinoma (STAD). The results were superior to some previous methods, proving that our proposed method has a certain degree of robustness. The data and specific results are shown in additional file 6.

In the future study, the proposed method will be applied to diverse cancer types and multiple clinical and biological profiling data to further test its robustness and flexibility in tumor prognosis. Furthermore, combined with the characteristics of pancreatic cancer data distribution, specific processing measures for high-dimensional unbalanced data are another focus in the subsequent analysis. The processing of class imbalanced data can be further combined with feature selection to improve the model accuracy and reduce the complexity of the model.

Data Availability

The datasets used in this study are publicly available in The Cancer Genome Atlas resource portal (Materials and Methods). Additional files 1 to 6 are available at https://github.com/gladex/WavePrognosis.

Conflicts of Interest

The authors declare that they have no conflicts of interest.

Authors' Contributions

BHT and YC conceived the study, performed the analyses, and wrote the manuscript; YQW and JFN suggested on the analyses; and all approved the final manuscript.

Acknowledgments

This work was supported by the Fundamental Research Funds for the Central Universities (2019B22414), Changzhou Municipal Key S&T Program (CE20195023), and the Natural Science Foundation of Jiangsu, China (BE2016655 and BK20161196). This work made use of the resources supported by the NSFC-Guangdong Mutual Funds for Super Computing Program (2nd Phase).

Supplementary Materials

Additional file 1: the performance comparison of the proposed method. Additional file 2: the detailed results of KEGG pathway analyses. Additional file 3: the detailed results of GO analysis on the BP term. Additional file 4: the detailed results of GO analysis on the CC term. Additional file 5: the detailed results of GO analysis on the MF term. Additional file 6: the validation of the proposed method on the STAD dataset. *(Supplementary Materials)*

References

[1] F. Bray, J. Ferlay, I. Soerjomataram, R. L. Siegel, L. A. Torre, and A. Jemal, "Global cancer statistics 2018: GLOBOCAN estimates of incidence and mortality worldwide for 36 cancers in 185 countries," *CA: a Cancer Journal for Clinicians*, vol. 68, no. 6, pp. 394–424, 2018.

[2] R. L. Siegel, K. D. Miller, and A. Jemal, "Cancer statistics, 2019," *CA: a Cancer Journal for Clinicians*, vol. 69, no. 1, pp. 7–34, 2019.

[3] A. L. Warshaw and C. Fernandez-del Castillo, "Pancreatic carcinoma," *New England Journal of Medicine*, vol. 326, no. 7, pp. 455–465, 1992.

[4] J. Ferlay, C. Partensky, and F. Bray, "More deaths from pancreatic cancer than breast cancer in the EU by 2017," *Acta Oncologica*, vol. 55, no. 9-10, pp. 1158–1160, 2016.

[5] B. Park, W. Lee, and K. Han, "A new approach to deriving prognostic gene pairs from cancer patient-specific gene correlation networks," *IEEE/ACM Transactions on Computational Biology and Bioinformatics*, p. 1, 2020.

[6] Z. Wang and P. Wei, "IMIX: a multivariate mixture model approach to association analysis through multi-omics data integration," *Bioinformatics*, vol. 36, no. 22-23, pp. 5439–5447, 2021.

[7] O. Nikolova, R. Moser, C. Kemp, M. Gönen, and A. A. Margolin, "Modeling gene-wise dependencies improves the identification of drug response biomarkers in cancer studies," *Bioinformatics*, vol. 33, no. 9, pp. 1362–1369, 2017.

[8] M. Li, J. Zhao, X. Li et al., "HiFreSP: a novel high-frequency sub-pathway mining approach to identify robust prognostic gene signatures," *Briefings in Bioinformatics*, vol. 21, no. 4, pp. 1411–1424, 2020.

[9] S. Wang and X. Wang, "Prediction of protein structural classes by different feature expressions based on 2-D wavelet denoising and fusion," *BMC Bioinformatics*, vol. 20, Supplement 25, p. 701, 2019.

[10] J. Lin, J. Wei, D. Adjeroh, B. H. Jiang, and Y. Jiang, "SSAW: a new sequence similarity analysis method based on the stationary discrete wavelet transform," *BMC Bioinformatics*, vol. 19, no. 1, p. 165, 2018.

[11] N. Arya and S. Saha, "Multi-modal classification for human breast cancer prognosis prediction: proposal of deep-learning based stacked ensemble model," *IEEE/ACM Transactions on Computational Biology and Bioinformatics*, p. 1, 2020.

[12] C. Peng, Y. Zheng, and D. S. Huang, "Capsule network based modeling of multi-omics data for discovery of breast cancer-related genes," *IEEE/ACM Transactions on Computational Biology and Bioinformatics*, vol. 17, no. 5, pp. 1605–1612, 2020.

[13] R. Chen, L. Yang, S. Goodison, and Y. Sun, "Deep-learning approach to identifying cancer subtypes using high-dimensional genomic data," *Bioinformatics*, vol. 36, no. 5, pp. 1476–1483, 2019.

[14] J. Hao, Y. Kim, T. K. Kim, and M. Kang, "PASNet: pathway-associated sparse deep neural network for prognosis prediction from high-throughput data," *BMC Bioinformatics*, vol. 19, no. 1, p. 510, 2018.

[15] A. Kutlu, "A novel method for classifying liver and brain tumors using convolutional neural networks, discrete wavelet transform and long short-term memory networks," *Sensors*, vol. 19, no. 9, p. 1992, 2019.

[16] A. Meintjes, A. Lowe, and M. Legget, "Fundamental heart sound classification using the continuous wavelet transform and convolutional neural networks," in *2018 40th Annual International Conference of the IEEE Engineering in Medicine and Biology Society (EMBC)*, pp. 409–412, Honolulu, HI, USA, 2018.

[17] B. A. Savareh, H. Emami, M. Hajiabadi, S. M. Azimi, and M. Ghafoori, "Wavelet-enhanced convolutional neural network: a new idea in a deep learning paradigm," *Biomedical Engineering / Biomedizinische Technik*, vol. 64, no. 2, pp. 195–205, 2019.

[18] N. Simon, J. Friedman, T. Hastie, and R. Tibshirani, "A sparse-group Lasso," *Journal of Computational and Graphical Statistics*, vol. 22, no. 2, pp. 231–245, 2013.

[19] Y. Zhao, Y. Zhou, Y. Liu et al., "Uncovering the prognostic gene signatures for the improvement of risk stratification in cancers by using deep learning algorithm coupled with wavelet transform," *BMC Bioinformatics*, vol. 21, no. 1, p. 195, 2020.

[20] D. J. McCarthy, Y. Chen, and G. K. Smyth, "Differential expression analysis of multifactor RNA-Seq experiments with respect to biological variation," *Nucleic Acids Research*, vol. 40, no. 10, pp. 4288–4297, 2012.

[21] Y. Tian, T. J. Morris, A. P. Webster et al., "ChAMP: updated methylation analysis pipeline for Illumina BeadChips," *Bioinformatics*, vol. 33, no. 24, pp. 3982–3984, 2017.

[22] R. A. Movahed, G. P. Jahromi, S. Shahyad, and G. H. Meftahi, "A major depressive disorder classification framework based on EEG signals using statistical, spectral, wavelet, functional connectivity, and nonlinear analysis," *Journal of Neuroscience Methods*, vol. 358, p. 109209, 2021.

[23] C. Wang, Z. Yan, W. Pedrycz, M. Zhou, and Z. Li, "A weighted fidelity and regularization-based method for mixed or unknown noise removal from images on graphs," *IEEE Transactions on Image Processing*, vol. 29, pp. 5229–5243, 2020.

[24] S. G. Mallat, "A theory for multiresolution signal decomposition: the wavelet representation," *IEEE Transactions on Pattern Analysis and Machine Intelligence*, vol. 11, no. 7, pp. 674–693, 1989.

[25] D. Chen, S. Wan, and F. S. Bao, "Epileptic focus localization using discrete wavelet transform based on interictal intracranial EEG," *IEEE Transactions on Neural Systems and Rehabilitation Engineering*, vol. 25, no. 5, pp. 413–425, 2017.

[26] J. Gu, Z. Wang, J. Kuen et al., "Recent advances in convolutional neural networks," *Pattern Recognition*, vol. 77, pp. 354–377, 2018.

[27] B. Tang, Z. Pan, K. Yin, and A. Khateeb, "Recent advances of deep learning in bioinformatics and computational biology," *Frontiers in Genetics*, vol. 10, no. 214, 2019.

[28] C. Müssel, F. Schmid, T. J. Blätte, M. Hopfensitz, L. Lausser, and H. A. Kestler, "BiTrinA—multiscale binarization and trinarization with quality analysis," *Bioinformatics*, vol. 32, no. 3, pp. 465–468, 2016.

[29] D. R. Cox, "Regression models and Life-Tables," *Journal of the Royal Statistical Society: Series B (Methodological)*, vol. 34, no. 2, pp. 187–202, 1972.

Hindawi
BioMed Research International
Volume 2024, Article ID 9867817, 1 page
https://doi.org/10.1155/2024/9867817

Retraction

Retracted: Effects of High-Flux Dialysis Combined with Hemoperfusion on Serum GRP78 and miR-495-3p in Renal Failure Patients

BioMed Research International

Received 12 March 2024; Accepted 12 March 2024; Published 20 March 2024

This article has been retracted by Hindawi following an investigation undertaken by the publisher [1]. This investigation has uncovered evidence of one or more of the following indicators of systematic manipulation of the publication process:

(1) Discrepancies in scope

(2) Discrepancies in the description of the research reported

(3) Discrepancies between the availability of data and the research described

(4) Inappropriate citations

(5) Incoherent, meaningless and/or irrelevant content included in the article

(6) Manipulated or compromised peer review

The presence of these indicators undermines our confidence in the integrity of the article's content and we cannot, therefore, vouch for its reliability. Please note that this notice is intended solely to alert readers that the content of this article is unreliable. We have not investigated whether authors were aware of or involved in the systematic manipulation of the publication process.

Wiley and Hindawi regrets that the usual quality checks did not identify these issues before publication and have since put additional measures in place to safeguard research integrity.

We wish to credit our own Research Integrity and Research Publishing teams and anonymous and named external researchers and research integrity experts for contributing to this investigation.

The corresponding author, as the representative of all authors, has been given the opportunity to register their agreement or disagreement to this retraction. We have kept a record of any response received.

References

[1] W. Fan, X. Li, X. Xu, and H. Chu, "Effects of High-Flux Dialysis Combined with Hemoperfusion on Serum GRP78 and miR-495-3p in Renal Failure Patients," *BioMed Research International*, vol. 2021, Article ID 9591177, 6 pages, 2021.

Hindawi
BioMed Research International
Volume 2021, Article ID 9591177, 6 pages
https://doi.org/10.1155/2021/9591177

Research Article

Effects of High-Flux Dialysis Combined with Hemoperfusion on Serum GRP78 and miR-495-3p in Renal Failure Patients

Wei Fan, Xudong Li, Xiangjun Xu, and Hong Chu

Department of Nephrology, Affiliated Yixing People's Hospital of Jiangsu University, Wuxi, 214200 Jiangsu Povince, China

Correspondence should be addressed to Hong Chu; chaogong796757@163.com

Received 13 June 2021; Revised 20 September 2021; Accepted 21 September 2021; Published 11 October 2021

Academic Editor: Jun Yang

Objective. This study was designed to probe into the changes and clinical significance of GRP78 and miR-495-3p in renal failure (RF) patients during high-flux dialysis (HFD) combined with hemoperfusion (HP). *Methods*. Sixty-five RF patients and 74 health check-ups who were admitted in our hospital from March 2015 to February 2017 were prospectively selected, and the related characteristics were retrospectively collected for analysis. GRP78 and miR-495-3p were detected in RF patients at admission (before treatment), 12 weeks after treatment (during treatment), 24 weeks after treatment (after treatment), and the control group at admission, and the relationship between the two and the occurrence, efficacy, and recurrence of RF was analyzed. *Results*. Before treatment, the GRP78 mRNA level in RF patients was higher than that in health check-ups, while the miR-495-3p level was lower ($P < 0.05$). GRP78 mRNA in RF patients was lower than that before treatment and was the lowest after treatment. On the contrary, miR-495-3p was higher than that before treatment and was the highest after treatment ($P < 0.05$). The two had a significant effect on predicting RF before treatment, efficacy of patients, and their recurrence after treatment (all $P < 0.001$). *Conclusion*. GRP78 decreased during the treatment of high-flux hemodialysis (HF-HD) combined with systemic HP in RF patients, while miR-495-3p increased. Both of them have a good reference value for RF occurrence, treatment results, and recurrence.

1. Introduction

Renal failure (RF) is a pathological state in which all kinds of chronic kidney diseases develop to the later stage and cause partial or total loss of renal function, and it is also very common clinically [1]. The morbidity of RF is high among middle-aged and elderly people, and the main reason may be related to body function decrease of patients [2]. According to statistics, the number of RF patients in the world is as high as 13.4%, and it is increasing year by year [3, 4]. Early stage of RF is characterized by oliguria, anemia, etc., which is easily ignored by patients [5]. It is not difficult to cure early RF, and most patients can achieve a more rational state by controlling the etiology and diet [6]. But, once the disease develops to the middle and late stage, it may only be treated by kidney transplantation [7]. Thus, we always attach great importance to RF in clinical practice and constantly explored new and effective diagnosis and treatment methods [1, 8].

At the moment, RF patients usually need to be treated with blood purification, and the harmful and toxic substances in blood are removed by diffusion and ultrafiltration, so as to reduce their mortality and improve their quality of life [9, 10]. Although hemodialysis can fundamentally solve the blood toxicity of RF patients, it is gradually found that some macromolecules such as β-2 microglobulin in the blood cannot be purified, which makes the treatment ineffective and even the disease recurs [11]. In view of this situation, high-flux dialysis (HFD), which can solve the problem of macromolecules, has been developed slowly clinically [12] and has achieved remarkable therapeutic results in diseases such as RF [13]. Glucose-regulated protein is a kind of stress protein, and its synthesis quantity is obviously increased under low glucose and hypoxia, which can assist protein folding, transportation, and assembly [14]. Among them, glucose-regulated protein 78 (GRP78) is one of the most representative family members, which has been proved to be relevant to renal cancer progression [15]. However, the

role of miR-495-3p in kidney diseases has been unanimously recognized [16], but its changes in the process of HFD combined with hemoperfusion (HP) are still vague.

Therefore, by analyzing the influence of HFD combined with HP on GRP78 and miR-495-3p in RF patients, this study provides a reliable theoretical basis for future clinical evaluation of state of an illness.

2. Experiment Preparation

2.1. Research Objects. RF patients and health check-ups who were admitted in our hospital from March 2015 to February 2017 were selected for prospective analysis, and the characteristics were retrospectively collected. The subjects were selected based on the inclusion and exclusion criteria (18-65 years old; being diagnosed with chronic RF; the time of blood purification treatment was more than 6 months; using arteriovenous fistula (AVF) or semipermanent dialysis catheter as vascular access; no major organ complications occurred within 3 months. Patients with tumors or severe cardiovascular and cerebrovascular diseases, other organ dysfunction, low treatment compliance, or those transferred from one hospital to another, or during pregnancy, and pregnant women were excluded). Finally, 65 RF patients and 74 health check-ups were confirmed. This experiment has been approved by the Ethics Committee of our hospital, and the investigation was conducted with the knowledge and consent of all subjects.

3. Methods

3.1. Treatment Methods. RF patients were treated with high-flux hemodialysis (HF-HD) combined with HP after admission. They were treated with Braun Dialog$^+$ hemodialysis machine, Fresenius F60 polysulfone dialyzer (ultrafiltration coefficient: 46 ml/(h∗mmHg), screening coefficient of β2-microglobulin: 0.8), Jafron HA130 HP device, and bicarbonate dialysate. The blood flow was set to 250-280 mL/min and the dialysate flow to 600-800 mL/min. Two hours after HP, hemodialysis was performed for 2 h. In the first week of admission, both HP and hemodialysis were treated 3 times, and in the second week, only hemodialysis and one combined treatment were performed. They were treated for 12 weeks, followed by routine hemodialysis for 12 weeks.

3.2. Acquisition of Blood Samples. Altogether, 4 mL fasting venous blood was collected from RF patients at admission (before treatment), 12 weeks after treatment (during treatment), 24 weeks after treatment (after treatment), and the control group at admission, which were placed at room temperature for 30 min and centrifuged for 10 min (1505 × g, 4°C) to obtain the upper serum to be measured.

3.3. qRT-PCR Detection. Total RNA of serum was extracted by Trizol reagent, and then RNA was reverse transcribed into cDNA according to the instructions of reverse transcription kit for PCR detection. The primer sequence was designed by GENEWIZ, Inc. (Table 1). The reaction system was configured according to the kit instructions, and the reaction conditions were 95°C for 5 min, 95°C for 30 s, 60°C for 30 s and 72°C for 30 s, 40 cycles in total. The expression of target genes was calculated by $2^{-\Delta\Delta Ct}$.

3.4. Outcome Measures. The miR-495-3p and GRP78 expression levels and the β2-MG, IL-6, and TNF-α concentrations during treatment were detected. Clinical efficacy was divided into markedly effective: their clinical signs score decreased by more than 60% before and after treatment, while the urea nitrogen (UN) and serum creatinine (Scr) values decreased by more than 30%; effective: their clinical sign score decreased by more than 30% before and after treatment, while UN and Scr values decreased by more than 15%; ineffective: their clinical sign scores decreased by less than 30% before and after treatment, while UN and Scr values decreased by less than 5%; and recurrence: patients were followed up for 3 years in the form of hospital reexamination, and their recurrence rate was recorded. The relationship between miR-495-3p and GRP78 and RF occurrence, efficacy, prognosis, and recurrence was assessed.

3.5. Statistical Methods. In this experiment, GraphPad 8 (v8.4.3) was used for statistical analysis, and all the tests were repeated three times, and the results were averaged. The counting data were recorded in the form of (rate), and the comparison between groups was analyzed by Chi-square test. The measurement data were recorded in the form of (mean ± standard deviation), the comparison between groups was analyzed by independent-samples T test and that at multiple time points was assessed by repeated measures analysis of variance and Bonferroni back testing, and prediction value was tested by ROC curve analysis. The difference was statistically remarkable when $P < 0.05$.

4. Results

4.1. Comparison of Clinical Data between RF Patients and Health Check-Ups. Age, BMI, serum phosphorus, gender, smoking, drinking, exercise habits, living environment, and nationality between RF patients and health check-ups were compared, and there was no difference ($P > 0.05$) (Table 2).

4.2. Expression of GRP78 and miR-495-3p before Treatment. Before treatment, the GRP78 mRNA level in RF patients was higher than that in health check-ups (Figure 1(a)), while the miR-495-3p level was lower (Figure 1(b)) ($P < 0.05$).

4.3. Predictive Value of GRP78 and miR-495-3p for RF before Treatment. ROC curve analysis manifested that when GRP78 mRNA > 2.395 before treatment, the sensitivity and specificity of predicting RF were 58.46% and 97.30% ($P < 0.001$). When miR − 495 − 3p < 6.960 before treatment, the sensitivity and specificity were 92.31% and 60.81% ($P < 0.001$) (Figure 2).

4.4. Changes of GRP78 and miR-495-3p during Treatment. GRP78 mRNA in RF patients decreased before treatment and reached the lowest level after treatment (Figure 3(a)), while miR-495-3p increased during treatment and reached the highest level after treatment (Figure 3(b)) ($P < 0.05$).

Table 1: Primer sequence (5′-3′).

Name	Direction	Sequence
miR-495-3p	Forward	ACACTCCAGCTGGGAAACAAACATGGTGCA
	Reverse	TGGTGTCG TGGAGTCG
GRP78	Forward	CATCACGCCGTCCTATGTCG
	Reverse	CGTCAAAGACCGTGTTCTCG
Internal reference U6	Forward	CTCGCTTCGGC AGCACA
	Reverse	AACGCTTCACGAATT TGCGT

Table 2: Comparison of clinical data.

		RF patients ($n = 65$)	Health check-ups ($n = 74$)	t value or χ^2 value/P value
Age (years)		52.8 ± 7.4	50.9 ± 8.5	1.396/0.165
BMI (kg/cm^2)		22.42 ± 4.64	21.84 ± 5.06	0.701/0.485
Phosphorus (mmol/L)		2.32 ± 0.51	1.15 ± 0.09	19.400/<0.001
Urea nitrogen (mmol/L)		26.61 ± 8.06	4.54 ± 1.14	23.300/<0.001
Gender	Male	58 (89.23)	61 (82.43)	1.298/0.255
	Female	7 (10.77)	13 (17.57)	
Smoking	Yes	48 (73.85)	51 (68.92)	0.410/0.522
	No	17 (26.15)	23 (31.08)	
Drinking	Yes	38 (58.46)	47 (63.51)	0.372/0.542
	No	27 (41.54)	27 (36.49)	
Exercise habits	Yes	8 (12.31)	12 (16.22)	0.429/0.512
	No	57 (87.69)	62 (83.78)	
Living environment	Towns	48 (73.85)	59 (79.73)	0.676/0.411
	Countryside	17 (26.15)	15 (20.27)	
Nationality	Han	64 (98.46)	71 (95.95)	0.784/0.367
	Ethnic minorities	1 (1.54)	3 (4.05)	

4.5. Predictive Value of GRP78 and miR-495-3p on Efficacy of Patients during Treatment. Among the 65 patients, 53 cases were markedly effective, 10 were effective, 2 were ineffective, and the total excellent rate of treatment was 81.54% (53/64). ROC analysis of GRP78 mRNA and miR-495-3p levels in patients during treatment showed that when GRP78 mRNA < 2.175 during treatment, the sensitivity and specificity of predicting the efficacy of patients were 73.58% and 91.67%. When miR − 495 − 3p < 6.225, the sensitivity and specificity were 75.47% and 83.33% ($P < 0.001$) (Figure 4).

4.6. Predictive Value of GRP78 and miR-495-3p on Prognosis and Recurrence of Patients after Treatment. Fifty-nine patients were successfully followed up during the 3-year follow-up with a follow-up success rate of 90.77% (59/65). Among them, 8 patients relapsed renal disease, and the disease recurrence rate was 13.56% (8/51). ROC analysis of GRP78 mRNA and miR-495-3p levels after treatment manifested that when GRP78 > 1.950 after treatment, the sensitivity and specificity of predicting the recurrence of disease were 75.00% and 92.16% ($P < 0.001$). When miR − 495 − 3 p < 7.085 after treatment, the sensitivity and specificity were 87.50% and 68.63% ($P < 0.001$) (Figure 5).

5. Discussion

At present, the morbidity of RF is increasing all over the world, and it puts an increasingly serious threat to patients [17, 18]. The treatment of RF patients is the top priority in clinical research, and the effect of HF-HD combined with systemic HP on RF has been preliminarily determined [19, 20]. In order to further apply this treatment scheme clinically, this study evaluated the changes of GRP78 and miR-495-3p during HF-HD combined with systemic HP, which can provide more accurate reference for future clinical practice.

First of all, by detecting the GRP78 mRNA and miR-495-3p expression levels in the serum of RF patients before treatment and health check-ups, we found that GRP78 was highly expressed in RF, while miR-495-3p was low, which was consistent with the previous studies on GRP78 and miR-495-3p [21–23] and could support our experimental results. The most studied protein in GRP78 glycoregulatory protein family is mainly stably expressed in endoplasmic reticulum, which is involved in inhibiting aggregation of endoplasmic reticulum nascent peptides, regulating abnormal folding proteins, and maintaining calcium homeostasis in cells and endoplasmic reticulum [24, 25]. Previous studies on GRP78 are mainly related to tumors. Scholars believe that

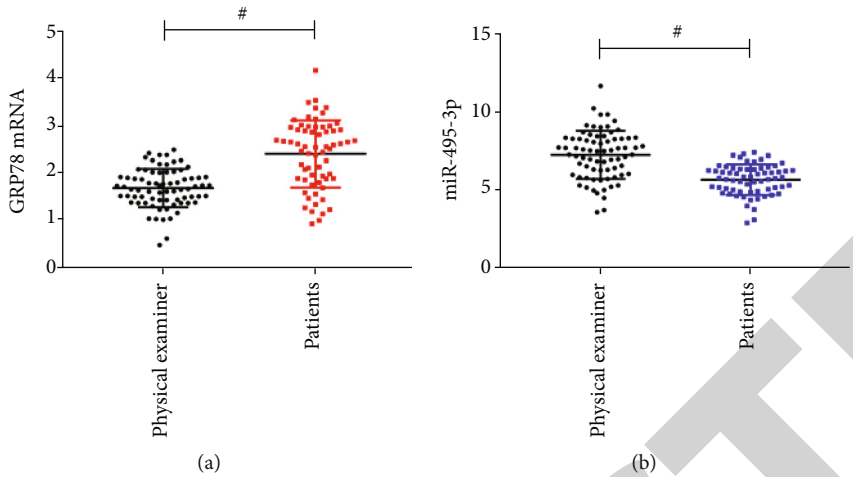

Figure 1: Expression of GRP78 and miR-495-3p before treatment. (a) GRP78 mRNA level in RF patients and health check-ups before treatment. (b) miR-495-3p level of RF patients and health check-ups before treatment. ($^{\#}P < 0.05$).

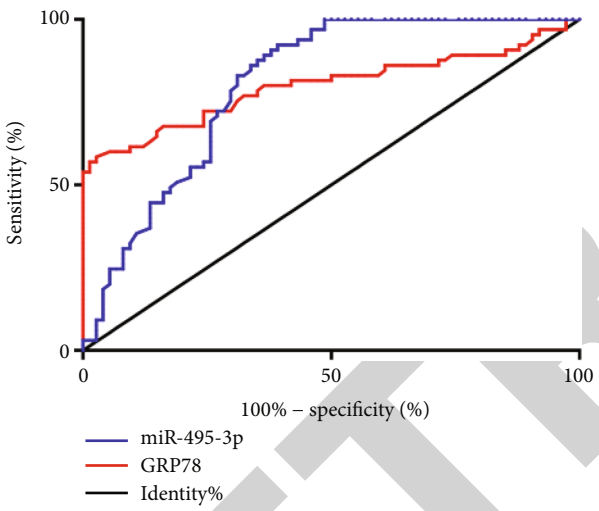

Figure 2: ROC curve of GRP78 and miR-495-3p predicting RF before treatment GRP78-AUC: 0.7983, 95% CI: 0.7183 to 0.8784 and miR-495-3p-AUC: 0.8045, 95% CI: 0.7315 to 0.8774.

tumor-related microRNA can combine with the 3′ noncoding region of GRP78 mRNA to form RNA-induced silencing complex, which eventually leads to the increase of GRP78 mRNA expression [26, 27]. The increase of GRP78 mRNA in RF patients may also be consistent with this mechanism. We speculate that it may be caused by blood flow toxicity and necrosis caused by RF, which also causes some microRNA changes, resulting in GRP78 increase. Thereinto, we found that miR-495-3p was confirmed to be relevant to sepsis in previous studies [28], and Chen et al. [29] mentioned that there might be a certain potential relationship with GRP78. In this experiment, the decrease of miR-495-3p also confirmed this view. miR-495-3p decrease in RF patients not only confirms that miR-495-3p may be involved in RF development and progression but also suggests that GRP78 increase may be caused by it. However, the specific mechanism has not been confirmed, which requires further experimental analysis. Then, through ROC curve analysis, we discovered that the expression levels of GRP78 mRNA and miR-495-3p before treatment had a good effect on predicting RF occurrence. And GRP78 has obvious specificity, and miR-495-3p has extremely high sensitivity, which can be relatively complemented in diagnosing RF and achieving the best diagnosis effect. The current clinical diagnosis of RF can only be determined through blood routine, urine routine, renal function, blood biochemistry, X-ray, radiography, isotope, renal biopsy, and other examinations [30], which not only has great negative impact on early diagnosis but also has extremely low economic effect, and it is difficult to carry out a wide range of clinical screening, which cannot achieve the best diagnosis effect. Therefore, if we can find an effective and specific serum marker of RF, it will be of great help to future clinical diagnosis and treatment. GRP78 and miR-495-3p results in this study confirmed that they might become serum markers of RF in the future.

Afterward, we detected the condition of GRP78 and miR-495-3p after 12 and 24 weeks of treatment and found that the former gradually decreased while the latter increased during the treatment, which indicated that the two could change with the treatment progress in the process of HF-HD combined with systemic HP. This suggests that by monitoring the GRP78 and miR-495-3p expression in RF patients in the future, we can have a preliminary understanding of disease progression. Vig et al. [31] and Cui et al. [32] found that GRP78 and miR-495-3p could be regarded as the outcome measures of pancreatic cancer and gastric cancer, which showed that the two had great potential in future clinical medical evaluation. In order to further analyze the significance of GRP78 and miR-495-3p in HF-HD combined with systemic HP therapy, we analyzed the significant predictive value of their levels on clinical efficacy after 12 weeks of treatment by ROC curve and found that both had extremely significant effects. This further confirms our above viewpoint. In the future, clinicians can objectively judge the efficacy of patients by detecting GRP78 and miR-495-3p and intervene in the treatment as soon as possible to achieve the best therapeutic purpose.

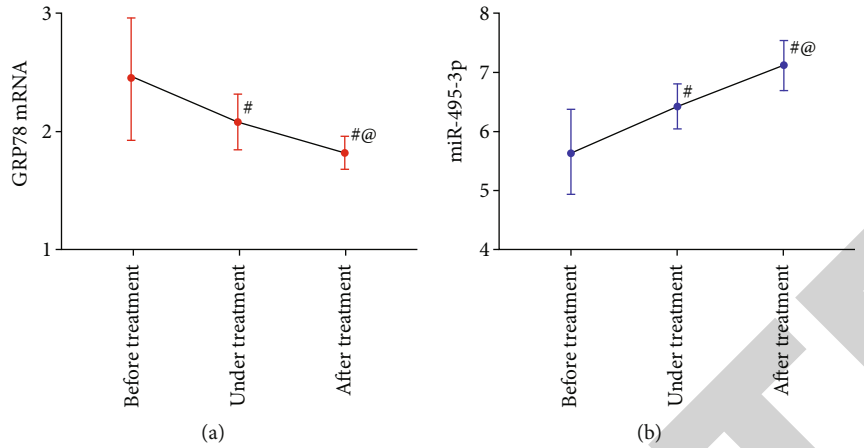

Figure 3: Changes of GRP78 and miR-495-3p during treatment. (a) Changes of GRP78 mRNA level during treatment; (b) changes of miR-495-3p level during treatment; # means compared with before treatment ($P < 0.05$); @ means compared with during treatment ($P < 0.05$).

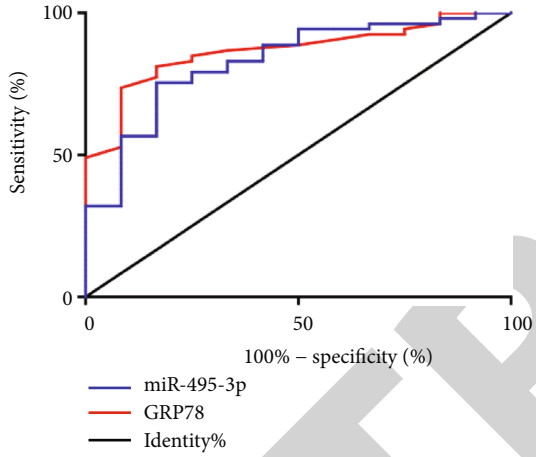

Figure 4: GRP78 and miR-495-3p are marked ROC curves in predicting the efficacy of RF patients. GRP78-AUC: 0.8656, 95% CI: 0.7691 to 0.962. miR-495-3p-AUC: 0.8286, 95% CI: 0.7033 to 0.9539.

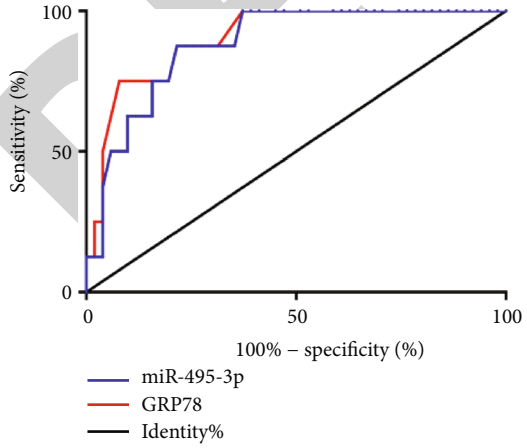

Figure 5: ROC curve of GRP78 and miR-495-3p in predicting prognosis and disease recurrence in RF patients after treatment. GRP78-AUC: 0.9044, 95% CI: 0.811 to 0.9978. miR-495-3p-AUC: 0.8811, 95% CI: 0.7815 to 0.9807.

Finally, through the follow-up of prognosis, we found that the probability of recurrence of renal disease in patients with a prognosis of 3 years was 13.56%, which also revealed that the efficacy of HF-HD combined with systemic HP was remarkable and could effectively control the prognosis and living conditions of patients. The GRP78 and miR-495-3p levels at 24 weeks after treatment can effectively predict the recurrence of the disease. First, it shows that they are relevant to RF and even renal function. Second, it proves that the two can be used as an excellent prognostic indicator of RF, which helps to evaluate the prognosis and rehabilitation of patients clinically.

There are still some shortcomings that need to be improved. For example, the related mechanism of GRP78 and miR-495-3p participating in RF needs more experimental confirmation, and ROC analysis results need more pathological data to confirm the best cut-off value. However, due to the short experimental period, we cannot evaluate the long-term prognosis of patients. We will make a more perfect experimental analysis as soon as possible in view of the above shortcomings.

To sum up, GRP78 decreases while miR-495-3p increases in RF patients undergoing HF-HD combined with systemic HP. Both of them have a good reference value for RF occurrence, treatment results, and prognosis recurrence.

Data Availability

The data used during the present study are available from the corresponding author upon reasonable request.

Conflicts of Interest

The authors declare that they have no conflicts of interest.

References

[1] C. Tuegel and N. Bansal, "Heart failure in patients with kidney disease," *Heart*, vol. 103, no. 23, pp. 1848–1853, 2017.

Hindawi
BioMed Research International
Volume 2021, Article ID 1989917, 8 pages
https://doi.org/10.1155/2021/1989917

Research Article

Bioinformatics Analysis of ZBTB16 as a Prognostic Marker for Ewing's Sarcoma

Ke Ding,[1] **Wenli Qiu**,[2] **Dianbo Yu**,[1] **Huade Ma**,[1] **Kangqi Xie**,[1] **Fuqiang Luo**,[1] **Shanlang Li**,[1] **Zaiyong Li**,[1] **and Jihua Wei**[1]

[1]*Department of Sports Medicine, Affiliated Hospital of Youjiang Medical University for Nationalities, Baise, Guangxi, China*
[2]*Department of Lab Medicine, Affiliated Hospital of Youjiang Medical University for Nationalities, Baise, Guangxi, China*

Correspondence should be addressed to Jihua Wei; jihua.wei@ymcn.edu.cn

Ke Ding and Wenli Qiu contributed equally to this work.

Received 16 August 2021; Revised 3 September 2021; Accepted 4 September 2021; Published 6 October 2021

Academic Editor: Jianxin Shi

Objective. The purpose of this study is to identify novel biomarkers for the prognosis of Ewing's sarcoma based on bioinformatics analysis. *Methods*. The GSE63157 and GSE17679 datasets contain patient and healthy control microarray data that were downloaded from the Gene Expression Omnibus (GEO) database and analyzed through R language software to obtain differentially expressed genes (DEGs). Firstly, Gene Ontology (GO) and Kyoto Encyclopedia of Genes and Genomes (KEGG) functional enrichment, protein-protein interaction (PPI) networks, and Cytoscape Molecular Complex Detection (MCODE) plug-in were then used to compute the highest scores of the module. After survival analysis, the hub genes were lastly obtained from the two module genes. *Results*. A total of 1181 DEGs were identified from the two GSEs. Through MCODE and survival analysis, we obtain 53 DEGs from the module and 29 overall survival- (OS-) related genes. ZBTB16 was the only downregulated gene after Venn diagrams. Survival analysis indicates that there was a significant correlation between the high expression of ZBTB16 and the OS of Ewing's sarcoma (ES), and the low expression group had an unfavorable OS when compared to the high expression group. *Conclusions*. High expression of ZBTB16 may serve as a predictor biomarker of poor prognosis in ES patients.

1. Introduction

Ewing's sarcoma (ES) is the second most common sarcoma of bone and soft tissue, usually occurring in children and adolescents [1]. The typical genetic feature is EWSR1 gene translocation, which leads to EWS-FLI1 gene fusion in t(11;22) [2], accounting for 85% of the ES family [3, 4], and is dominated by small round cells [5]. The early data report of the National Cancer Institute showed that the incidence of ES differed by gender, age, and race. Males accounted for 60.3%, mostly under 24 years old, and the incidence of whites was nine times that of African-Americans [6].

At present, optimal treatment of ES emphasizes multimodal therapy [7–9]. Chemotherapy is an efficient treatment for ES, and it significantly improves the 5-year overall survival (OS) rate [10, 11]. However, due to the lack of early efficient diagnosis, the high recurrence rate and distant metastasis of patients with ES lead to a poor prognosis [12], and the prognosis of patients with ES is not optimistic. Patients with ES showed poor survival in age ≥ 18 years, tumor size > 10 cm, receiving radiotherapy alone, and receiving no treatment [13]. Therefore, there is still an urgent need for new diagnoses and treatment strategies to improve long-term survival.

With the development of tumor genomics research such as high-throughput sequencing, it is of great significance to find potential prognostic treatment pathways and targets for ES. In this study, our purpose is to investigate the biomarkers related to the prognosis of ES. We processed and

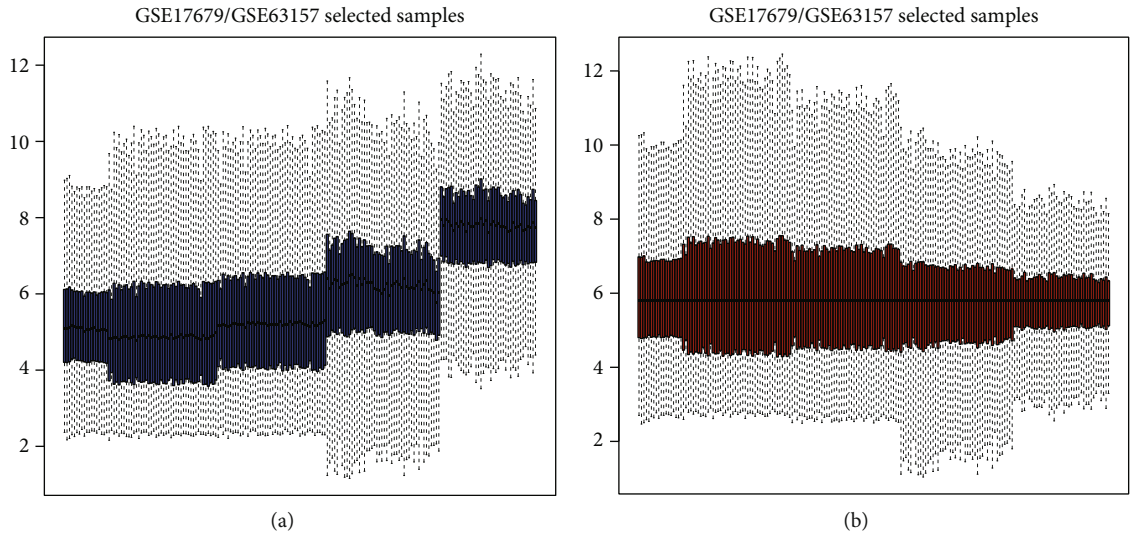

Figure 1: Normalization of ES patients' samples: (a) before normalization of total DEGs; (b) following normalization of total DEGs.

analyzed microarray data from GSE63157 and GSE17679 datasets from the Gene Expression Omnibus (GEO) database. Gene Ontology (GO) and Kyoto Encyclopedia of Genes and Genomes (KEGG) functional and pathway enrichment analysis, protein-protein interaction (PPI) network construction of pivot genes, and identification of key genes that are significantly related to OS in ES are aimed at providing therapeutic strategies for the prognosis of ES.

2. Materials and Method

2.1. Data Source and Data Processing. Based on the GEO database (https://www.ncbi.nlm.nih.gov/geo/), we obtain two microarray datasets of ES: GSE63157 and GSE17679. GSE63157 was submitted by Volchenboum SL and Andrade J et al. and GSE17679 by Savola S and Klami A et al. GSE63157 included 85 ES patient samples; GSE17679 consisted of 88 ES patient samples and 18 matched human normal skeletal muscle samples (10 ES cell line samples were deleted). The R GEOquery package (version 2.60.0) does the download annotation. GSE63157 was sampled based on the GPL5715 Affymetrix Human Exon 1.0 ST Array. GSE17679 was sampled based on the GPL570 Affymetrix Human Genome U133 Plus 2.0 Array.

2.2. Identification of DEGs. All the samples' data of GSE63157 and GSE17679 were normalized and visualized by the R "Limma" package (version 3.48.1) and also the annotation. The screening conditions for the DEGs were an absolute value of log 2FC > 2 and adj. P value < 0.05.

2.3. GO and KEGG Enrichment Analysis. The R "Clusterprofile" package (version 4.0.0) was used for GO and KEGG enrichment analysis and visualization. GO analysis was used to annotate the biological process (BP), cytological component (CC), and molecular function (MF) of DEGs, and KEGG enrichment analysis was used to understand

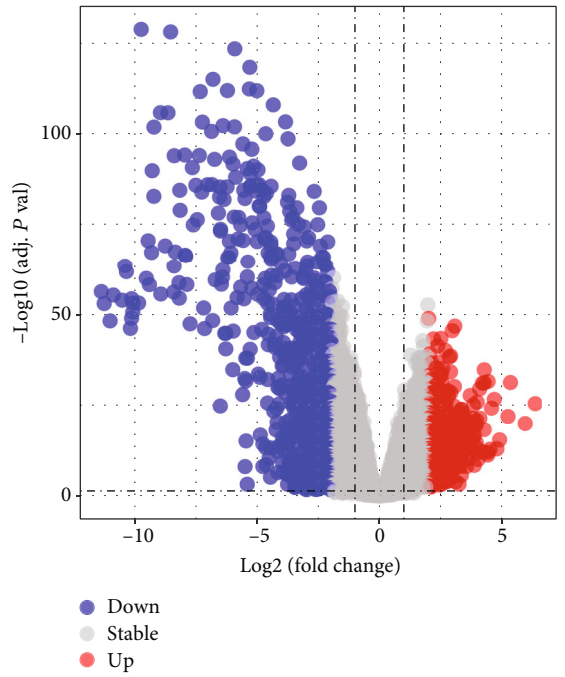

Figure 2: Screening of DEGs: (a) the volcano plot showed DEGs between ES groups and normal control groups. Grey represents the not significant change in expression. Red represents upregulation. Blue represents downregulation.

the related signaling pathways; $P < 0.05$ was statistically significant.

2.4. PPI Network Construction and Module Analysis. The online tool STRING (http://string-db.org) (version 11.0) was used to construct the PPI network of DEGs. The threshold for statistically significant interaction is a confidence score > 0.9. Cytoscape (version 3.6.1) is software providing

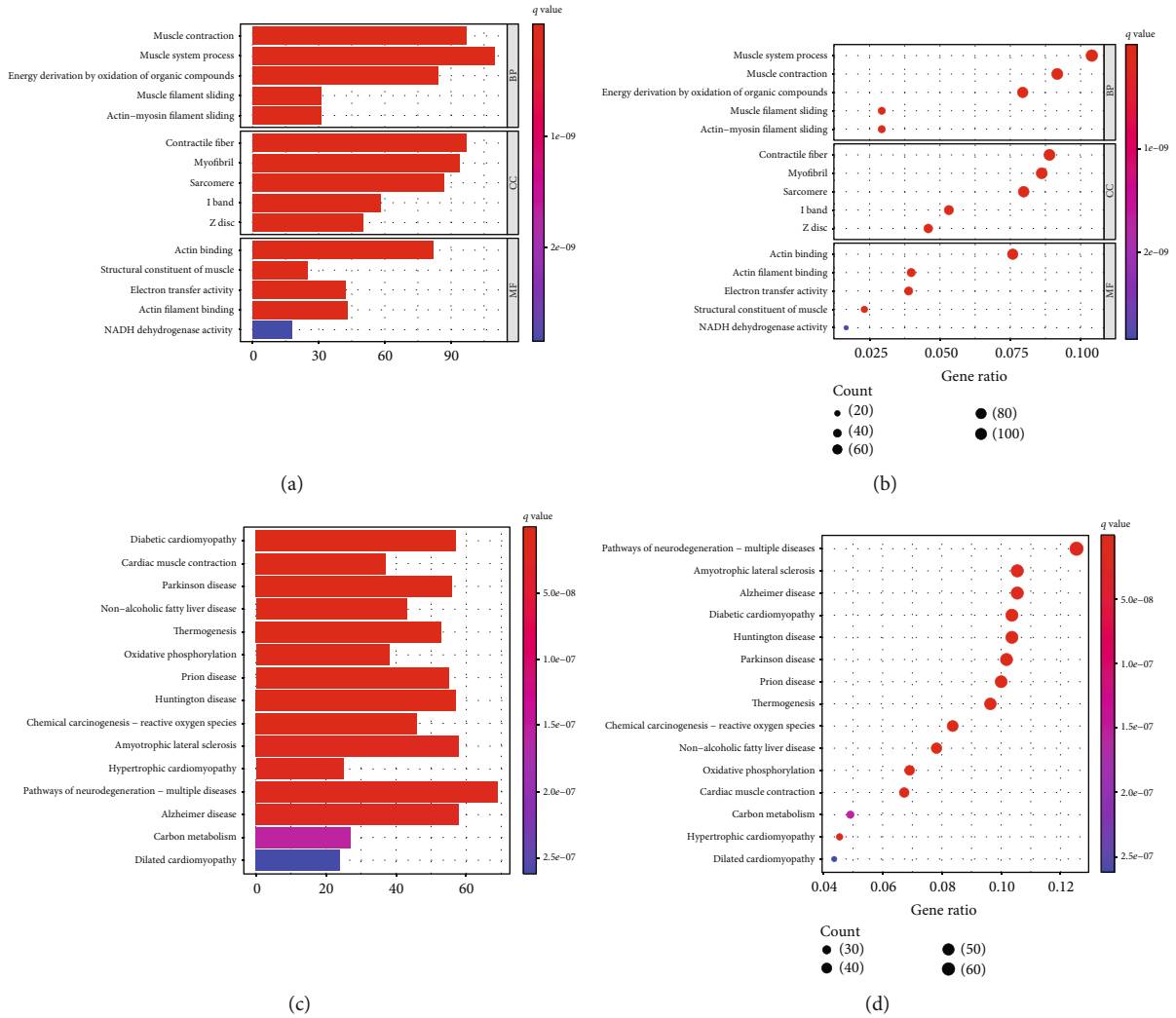

Figure 3: GO and KEGG pathway analysis of the DEGs. The color depth of nodes refers to the q-value. The size of nodes refers to the number of genes. (a) Barplot of top 5 significantly enriched biological processes, cell component, and molecular function in DEGs. (b) Bubble plot of top 5 significantly enriched biological processes, cell component, and molecular function in DEGs. (c) Barplot of top 15 significantly enriched molecular functions in DEGs. (d) Bubble plot of top 15 significantly enriched KEGG pathways in DEGs.

an open platform for the visualization of biological processes, molecular interaction networks, and integration of these networks. Molecular Complex Detection (MCODE) (version 1.5.1), a plug-in of Cytoscape, is applied to discover densely connected regions and identify the significant modules through clustering a given network. MCODE scores > 10, k-score = 2, max depth = 100, node score cut-off = 0.2, and degree cut-off = 2 were set as the criteria for the selection of significant modules.

2.5. Survival Analysis of Hub Gene. The survival data of 173 ES patients samples were integrated with the expression data of DEGs. Univariate and multivariate Cox regression analyses were performed through using the R "Survival" package to identify the DEGs associated with the OS time and clinical characteristics of ES, and the hub genes that could independently guide the prognosis were found by taking the overlap with module genes. The ES patients' samples were divided into the high expression groups and the low expression groups. The difference between the hub genes and ES was further verified by the Kaplan-Meier survival curve. A Venn diagram was used for visualization, and $P < 0.01$ was statistically significant.

3. Results

3.1. Normalization of Total DEGs. Gene expression data of GSE63157 and GSE17679 were standardized and displayed in a boxplot. The black line in (Figure 1(b)) is basically at the same level, indicating a high consistency of data.

3.2. Identification of DEGs. A total of 1181 DEGs were identified from GSE63157 and GSE17679 datasets, of which 364 were upregulated genes and 817 were downregulated genes

Table 1: GO and KEGG pathway enrichment analysis of DEGs in ES.

Term	Description	adj. *P* Val	Gene count
Biological processes			
BP	Muscle system process	$2.28E-37$	110
BP	Muscle contraction	$2.28E-37$	97
BP	Energy derivation by oxidation of organic compounds	$9.88E-36$	84
BP	Actin-mediated cell contraction	$3.57E-27$	49
BP	Muscle filament sliding	$4.52E-29$	31
Cell component			
CC	Contractile fiber	$2.45E-57$	97
CC	Myofibril	$9.39E-56$	94
CC	Sarcomere	$1.49E-52$	87
CC	I band	$5.76E-35$	58
CC	Z disc	$1.02E-28$	50
Molecular function			
MF	Actin binding	$4.51E-18$	82
MF	Structural constituent of muscle	$6.14E-18$	25
MF	Electron transfer activity	$6.67E-17$	42
MF	Actin filament binding	$8.16E-11$	43
MF	NADH dehydrogenase activity	$3.12E-09$	18
KEGG pathway			
hsa05415	Diabetic cardiomyopathy	$6.34E-19$	57
hsa04260	Cardiac muscle contraction	$6.34E-19$	37
hsa05012	Parkinson disease	$3.19E-14$	56
hsa04932	Nonalcoholic fatty liver disease	$3.19E-14$	43
hsa04714	Thermogenesis	$7.89E-14$	53
hsa00190	Oxidative phosphorylation	$5.35E-13$	38
hsa05020	Prion disease	$4.75E-12$	55
hsa05016	Huntington disease	$4.67E-11$	57
hsa05208	Chemical carcinogenesis-reactive oxygen species	$1.81E-10$	46
hsa05014	Amyotrophic lateral sclerosis	$1.84E-08$	58
hsa05410	Hypertrophic cardiomyopathy	$1.90E-08$	25
hsa05022	Pathways of neurodegeneration-multiple diseases	$2.02E-08$	69
hsa05010	Alzheimer disease	$2.18E-08$	58
hsa01200	Carbon metabolism	$1.78E-07$	27
hsa05414	Dilated cardiomyopathy	$3.06E-07$	24

DEGs = differentially expressed genes; GO = Gene Ontology; KEGG = Kyoto Encyclopedia of Genes and Genomes; BP = biological processes; CC = cell component; MF = molecular function.

(Figure 2(a)). Volcano plot of the DEGs, respectively, suggests that the expression of identified DEGs can correctly distinguish the case and normal samples.

3.3. GO and KEGG Enrichment Analysis. The R package "Clusterprofile" was used for functional enrichment analysis to assess the biological classification of DEGs (Figure 3). GO analysis showed (Figures 3(a) and 3(b)) that among biological processes, DEGs were significantly involved in the muscle system process (110 genes), muscle contraction (97 genes), energy derivation by oxidation of organic compounds (84 genes), actin-mediated cell contraction (49 genes), and muscle filament sliding (31 genes). In the cell component, DEGs were significantly involved in contractile fiber (97 genes), myofibril (94 genes), sarcomere (87 genes), I band (58 genes), and Z disc (50 genes). In molecular function, DEGs are significantly involved in binding-related projects. The molecular function includes actin binding (82 genes), structural constituent of muscle (25 genes), electron transfer activity (42 genes), actin filament binding (43 genes), and NADH

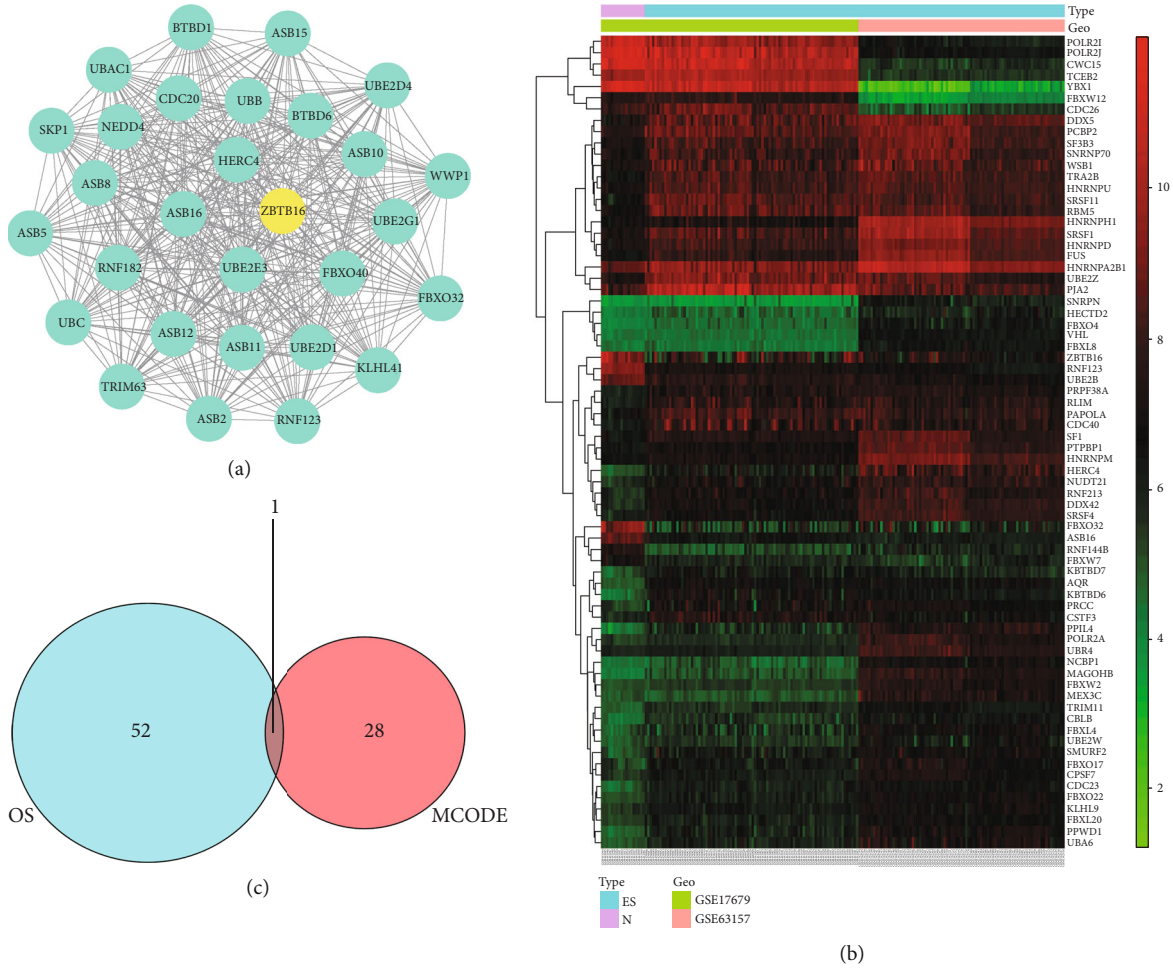

FIGURE 4: Screening of hub gene. (a) The most significant module was obtained from the PPI network with 29 nodes and 406 edges. The hub gene ZBTB16 was signature in yellow. (b) Heatmap of the top 72 differentially expressed genes in patients with ES compared with those in a normal cohort. Red represents upregulation. Green represents downregulation. (c) Venn diagram of the hub genes. The overlapping one gene is the hub gene.

dehydrogenase activity (18 genes). In addition, KEGG analysis showed (Figures 3(c) and 3(d)) that DEGs were mainly involved in diabetic cardiomyopathy (57 genes), cardiac muscle contraction (37 genes), and pathways of neurodegeneration-multiple diseases (69 genes) (Table 1).

3.4. PPI Network Construction and Module Analysis. With a total of 645 nodes and 3300 edges, the PPI network information of the DEGs from STRING was imported into Cytoscape, and the module of DEGs was constructed. We just take the module with the highest MCODE score. This module contains 29 nodes and 406 edges (Figure 4(a)).

3.5. Hub Gene Screening and Identification. Survival analysis showed that there was a total of 72 DEGs related to OS time of patients with ES (Figure 4(b)), among which 53 genes were related to clinical characteristics. The hub gene was obtained after the intersection with 29 genes in the module with the highest MCODE score (Figure 4(c)).

3.6. Survival Analysis of Hub Gene. A total of 173 ES patients have follow-up information for survival analysis. All the ES patients were divided into the high expression group ($n = 87$) and the low expression group ($n = 86$), according to the median expression levels of ZBTB16. The expression of ZBTB16 was downregulated in the ES patients group, and the OS time of patients with low expression was poorer than the high expression group. Univariate and multivariate Cox regression analyses showed that ZBTB16 may be a prognostic factor for ES. The difference is statistically significant ($P < 0.01$) (Figure 5).

4. Discussion

Ewing's sarcoma (ES) is the second most common malignant bone tumor in children and adolescents [2]. At present, vincristine, doxorubicin, cyclophosphamide, ifosfamide, and etoposide are the standard chemotherapy regimens. However, the prognosis of patients is not optimistic [14, 15] and has little effect on patients with metastasis or recurrence

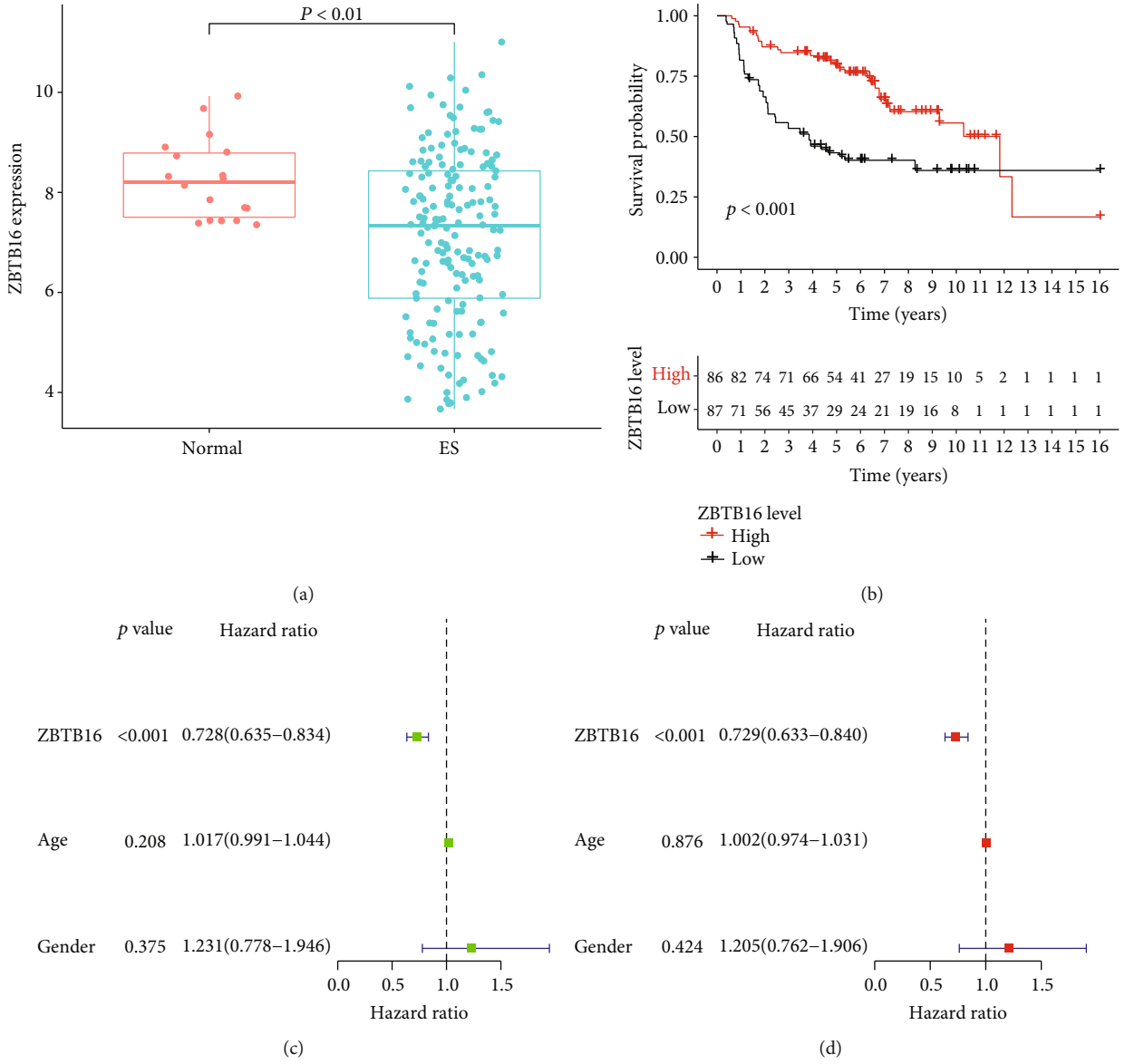

Figure 5: Survival curves of the hub gene (Kaplan-Meier plotter). (a) ZBTB16 expression in normal and ES patient tissues. Scatter plot indicating a higher expression of normal tissues when compared to ES patients ($P < 0.01$). (b) Kaplan-Meier survival curves for ZBTB16 in the high and low expression groups ($P < 0.001$). (c) Univariate Cox regression analysis for ZBTB16 ($P < 0.001$). (d) Multivariate Cox regression analysis for ZBTB16 ($P < 0.001$).

[16]. Microarray technology provides a new direction for the treatment of patients with ES. Therefore, it is necessary to explore appropriate and effective measures to guide the prognosis of treatment.

The purpose of our microarray-based analysis is to identify novel biomarkers related to the prognosis of patients with ES. Based on GSE63157 and GSE17679 datasets, 1181 DEGs were screened and identified from the ES patient group and normal control group, including 364 upregulated genes and 817 downregulated genes. Then, the functional enrichment analysis was carried out, and the interaction between DEGs was discussed. GO and KEGG pathway enrichment analysis shows that DEGs are mainly involved in the muscle system process, muscle contract, structural constituent of muscle, electron transfer activity, diabetic cardiomyopathy, and cardiac muscle contraction. These biological functions are consistent with our knowledge of ES. Based on the MCODE plug-in computing the highest score module and survival analysis filtering, we chose the overlapping one gene as the hub gene according to the two modules.

Zinc-finger and BTB domain-containing 16 (ZBTB16), also known as promyelocytic leukemia zinc finger protein (PLZF), was first found in t(11;17) chromosome translocation, and fusion with retinoic acid receptor α (RARa) was identified [17]. ZBTB16 is an important mediator that regulates the expression of neuropeptides [18], ion channels [19], or various receptors [20], to influence the response to incoming signals and/or downstream neuron signals.

ZBTB16 is expressed in various tissues and plays a variety of biological functions through the regulation of tissue-specific target genes, which is related to adipogenesis [21], myocardial remodeling [22], osteoblast differentiation [23], and obesity [24]. The enhanced expression of ZBTB16 can increase the number of mitochondria and the ability of respiration and uncoupling. Besides, ZBTB16 is associated with various tumors. ZBTB16 is a classic androgen receptor (AR) regulatory gene, which has antiproliferative activity in prostate cancer cells [25] and plays a role in inhibiting cancer by inhibiting the MAPK pathway [26]. Secondly, ZBTB16 may become a prognostic marker for breast cancer and hepatocellular carcinoma [27, 28].

Up to now, there is no literature report on the relationship between ZBTB16 and the prognosis of Ewing's sarcoma. Previous studies have found that ZBTB16 can be used to distinguish leiomyosarcomas from leiomyomas [29]. In addition, pathological studies have reported that ZBTB16 has high sensitivity and specificity in various tissue types of Primitive Neurological Tumor (PNET) [30]. This study verified the correlation between ZBTB16 and ES, and we need to further explore the relationship between ZBTB16 and the prognosis of ES. In our study, the expression of the ZBTB16 was downregulated in the ES group when compared to the control group. Survival analysis indicates that the high expression of the ZBTB16 was significantly higher than that in the low expression group, which further clarified that ZBTB16 was related to the prognosis of ES.

In a word, we confirmed that ZBTB16 provides valuable information for the prognosis of ES and may become a novel biomarker for the prognosis of ES patients. However, there are some limitations to this study. Due to the limited raw data, we did not consider the associations between ZBTB16 expression and clinicopathological factors (e.g., stage and grade) of patients with ES. Further research is needed to make up for the shortcomings of this article.

5. Conclusion

We identified ZBTB16 from the GEO database through bioinformatics analysis. Moreover, higher ZBTB16 expression patients can have a longer OS time. It may be the potential prognostic biomarker of ES. In addition, biological functions and mechanisms need to be studied further in ES.

Data Availability

The data used to support the findings of this study are available from the corresponding author upon request.

Conflicts of Interest

The authors declare that they have no conflicts of interest.

Authors' Contributions

Ding Ke and Qiu Wenli contributed equally to this work.

Acknowledgments

The study was supported by the (1) Guangxi Natural Science Foundation (Contract No. 2020GXNSFAA259068) and (2) First Batch of High-level Talent Scientific Research Projects of the Affiliated Hospital of Youjiang Medical University for Nationalities in 2019 (Contract No. R20196321).

References

[1] Y. Park, M. Chang, K.-M. Kim, and D.-H. An, "Analysis of prognostic factors in extraosseous Ewing sarcoma family of tumors: review of St. Jude Children's Research Hospital experience," *Annals of Surgical Oncology*, vol. 19, no. 12, pp. 3816–3822, 2012.

[2] H. E. Grier, "THE EWING FAMILY OF TUMORS: Ewing's Sarcoma and Primitive Neuroectodermal Tumors," *Pediatric Clinics of North America*, vol. 44, no. 4, pp. 991–1004, 1997.

[3] M.-C. Le Deley, O. Delattre, K.-L. Schaefer et al., "Impact of EWS-ETS fusion type on disease progression in Ewing's sarcoma/peripheral primitive neuroectodermal tumor: prospective results from the cooperative Euro-E.W.I.N.G. 99 trial," *Journal of Clinical Oncology*, vol. 28, no. 12, pp. 1982–1988, 2010.

[4] O. Delattre, J. Zucman, B. Plougastel et al., "Gene fusion with an _ETS_ DNA-binding domain caused by chromosome translocation in human tumours," *Nature*, vol. 359, no. 6391, pp. 162–165, 1992.

[5] M. Sbaraglia, A. Righi, M. Gambarotti, and A. P. Dei Tos, "Ewing sarcoma and Ewing-like tumors," *Virchows Archiv*, vol. 476, no. 1, pp. 109–119, 2020.

[6] M. U. Jawad, M. C. Cheung, E. S. Min, M. M. Schneiderbauer, L. G. Koniaris, and S. P. Scully, "Ewing sarcoma demonstrates racial disparities in incidence-related and sex-related differences in outcome: an analysis of 1631 cases from the SEER database, 1973-2005," *Cancer*, vol. 115, no. 15, pp. 3526–3536, 2009.

[7] R. W. Rödl, C. Hoffmann, G. Gosheger, B. Leidinger, H. Jürgens, and W. Winkelmann, "Ewing's sarcoma of the pelvis: combined surgery and radiotherapy treatment," *Journal of Surgical Oncology*, vol. 83, no. 3, pp. 154–160, 2003.

[8] J. Alvarez-SanNicolas, I. Gracia-Alegria, L. Trullols-Tarrago, A. Peiro-Ibañez, and C. Lamas-Gomez, "Prognostic factors and survival in Ewing's sarcoma treated by limb salvage surgery," *Clinical & Translational Oncology*, vol. 21, no. 10, pp. 1374–1382, 2019.

[9] K. Jamshidi, M. R. Shirazi, A. Bagherifard, and A. Mirzaei, "Curettage, phenolization, and cementation in paediatric Ewing's sarcoma with a complete radiological response to neoadjuvant chemotherapy," *International Orthopaedics*, vol. 43, no. 2, pp. 467–473, 2019.

[10] J. L. Pretz, C. M. Barysauskas, S. George et al., "Localized adult Ewing sarcoma: favorable outcomes with alternating vincristine, doxorubicin, cyclophosphamide, and ifosfamide, etoposide (VDC/IE)-based multimodality therapy," *The Oncologist*, vol. 22, no. 10, pp. 1265–1270, 2017.

[11] J. E. Oesterheld, D. R. Reed, B. A. Setty et al., "Phase II trial of gemcitabine and nab-paclitaxel in patients with recurrent Ewing sarcoma: a report from the National Pediatric Cancer Foundation," *Pediatric Blood & Cancer*, vol. 67, no. 7, 2020.

[12] A. Mendoza-Naranjo, A. El-Naggar, D. H. Wai et al., "ERBB4 confers metastatic capacity in Ewing sarcoma," *EMBO Molecular Medicine*, vol. 5, no. 7, pp. 1087–1102, 2013.

[13] Z. H. Wan, Z. H. Huang, and L. B. Chen, "Survival outcome among patients with Ewing's sarcoma of bones and joints: a population-based cohort study," *São Paulo Medical Journal*, vol. 136, no. 2, pp. 116–122, 2018.

[14] M. Chin, R. Yokoyama, M. Sumi et al., "Multimodal treatment including standard chemotherapy with vincristine, doxorubicin, cyclophosphamide, ifosfamide, and etoposide for the Ewing sarcoma family of tumors in Japan: results of the Japan Ewing Sarcoma Study 04," *Pediatric Blood & Cancer*, vol. 67, no. 5, article e28194, 2020.

[15] H. E. Grier, M. D. Krailo, N. J. Tarbell et al., "Addition of ifosfamide and etoposide to standard chemotherapy for Ewing's sarcoma and primitive neuroectodermal tumor of bone," *The New England Journal of Medicine*, vol. 348, no. 8, pp. 694–701, 2003.

[16] J. I. Albergo, C. L. L. Gaston, M. C. Parry et al., "Risk analysis factors for local recurrence in Ewing's sarcoma: when should adjuvant radiotherapy be administered?," *Bone Joint J*, vol. 100-B, no. 2, pp. 247–255, 2018.

[17] Z. Chen, N. J. Brand, A. Chen et al., "Fusion between a novel Krüppel-like zinc finger gene and the retinoic acid receptor-alpha locus due to a variant t(11;17) translocation associated with acute promyelocytic leukaemia," *The EMBO Journal*, vol. 12, no. 3, pp. 1161–1167, 1993.

[18] H. Cheng, S. J. Pablico, J. Lee, J. S. Chang, and S. Yu, "Zinc finger transcription factor Zbtb16 coordinates the response to energy deficit in the mouse hypothalamus," *Frontiers in Neuroscience*, vol. 14, 2020.

[19] A. Náray-Fejes-Tóth, C. Boyd, and G. Fejes-Tóth, "Regulation of epithelial sodium transport by promyelocytic leukemia zinc finger protein," *American Journal of Physiology. Renal Physiology*, vol. 295, no. 1, pp. F18–F26, 2008.

[20] T. Zhang, K. Dong, W. Liang et al., "G-protein-coupled receptors regulate autophagy by ZBTB16-mediated ubiquitination and proteasomal degradation of Atg14L," *eLife*, vol. 4, article e06734, 2015.

[21] M. A. Ambele, C. Dessels, C. Durandt, and M. S. Pepper, "Genome-wide analysis of gene expression during adipogenesis in human adipose- derived stromal cells reveals novel patterns of gene expression during adipocyte differentiation," *Stem Cell Research*, vol. 16, no. 3, pp. 725–734, 2016.

[22] E. Farrell, A. E. Armstrong, A. C. Grimes, F. J. Naya, W. J. de Lange, and J. C. Ralphe, "Transcriptome analysis of cardiac hypertrophic growth in MYBPC3-null mice suggests early responders in hypertrophic remodeling," *Frontiers in Physiology*, vol. 9, p. 1442, 2018.

[23] F. Marofi, G. Vahedi, S. Solali et al., "Gene expression of TWIST1 and ZBTB16 is regulated by methylation modifications during the osteoblastic differentiation of mesenchymal stem cells," *Journal of Cellular Physiology*, vol. 234, no. 5, pp. 6230–6243, 2019.

[24] C. L. Plaisier, B. J. Bennett, A. He et al., "Zbtb16 has a role in brown adipocyte bioenergetics," *Nutrition & Diabetes*, vol. 2, no. 9, article e46, 2012.

[25] F. Jiang and Z. Wang, "Identification and characterization of PLZF as a prostatic androgen-responsive gene," *Prostate*, vol. 59, no. 4, pp. 426–435, 2004.

[26] C.-L. Hsieh, G. Botta, S. Gao et al., "PLZF, a tumor suppressor genetically lost in metastatic castration-resistant prostate cancer, is a mediator of resistance to androgen deprivation therapy," *Cancer Research*, vol. 75, no. 10, pp. 1944–1948, 2015.

[27] J. He, M. Wu, L. Xiong et al., "BTB/POZ zinc finger protein ZBTB16 inhibits breast cancer proliferation and metastasis through upregulating ZBTB28 and antagonizing BCL6/ZBTB27," *Clinical Epigenetics*, vol. 12, no. 1, p. 82, 2020.

[28] A. Hui, H. Lau, C. Cao, J. Zhou, P. Lai, and S. Tsui, "Downregulation of PLZF in human hepatocellular carcinoma and its clinical significance," *Oncology Reports*, vol. 33, no. 1, pp. 397–402, 2015.

[29] M. Momeni, T. Kalir, S. Farag et al., "Immunohistochemical detection of promyelocytic leukemia zinc finger and histone 1.5 in uterine leiomyosarcoma and leiomyoma," *Reproductive Sciences*, vol. 21, no. 9, pp. 1171–1176, 2014.

[30] G. Q. Xiao, A. E. Sherrod, and K. M. Hurth, "ZBTB16: A new biomarker for primitive neuroectodermal tumor element / Ewing sarcoma," *Pathology, Research and Practice*, vol. 215, no. 10, p. 152536, 2019.

Hindawi
BioMed Research International
Volume 2021, Article ID 9458328, 11 pages
https://doi.org/10.1155/2021/9458328

Research Article

Gene Expression Characteristics of Liver Tissue Reveal the Underlying Pathogenesis of Hepatocellular Carcinoma

Congfang Guo,[1] Xiang Guo,[2] Yudong Rong,[1] Yirui Guo,[1] and Li Zhang[1]

[1]*Physical Examination Center, Tianjin First Central Hospital, Tianjin 300192, China*
[2]*College of Veterinary Medicine, Shanxi Agricultural University, Jinzhong 030801, China*

Correspondence should be addressed to Li Zhang; luzhangba26@163.com

Received 5 July 2021; Revised 6 September 2021; Accepted 7 September 2021; Published 4 October 2021

Academic Editor: Jianxin Shi

Background. Hepatocellular carcinoma (HCC) is high-mortality primary liver cancer and the most common malignant tumor in the world. This study is based on a hepatocellular carcinoma-related dysfunction module designed to explore the dysregulation of genes in liver cancer tissue. *Methods*. By downloading the relevant data on the GEO database, we performed a differential analysis of healthy liver tissue and liver cancer tissues as well as healthy liver tissue and hepatocellular carcinoma tissue and then obtained two sets of differential genes and combined them. We performed a cointerpretation analysis of these differential genes and constructed related functional disorder modules. A hypergeometric test was performed to calculate the potential regulatory effects of multiple factors on the module, and a series of ncRNA and TF regulators were identified. We obtained a total of 4479 differentially expressed genes in hepatocellular carcinoma, and these genes were clustered into ten hepatocellular carcinoma-related functional interpretation disorder modules. *Results*. Enrichment analysis revealed that these modular genes are mainly involved in signal transduction including cell cycle, TGF-beta signal transduction, and p53 signal transduction. Depending on the predictive analysis of multidimensional regulators, 323 ncRNAs and 52 TF-mediated hepatocellular carcinoma-related dysregulation modules were found to regulate disease progression. *Conclusions*. Based on a series of investigations, it was found that miR-30b-5p may participate in the peroxisome signal transduction by downregulating ABCD3-mediated module 1, thereby promoting the development and progression of hepatocellular carcinoma. Our research results not only provide a theoretical basis for biologists to study hepatocellular carcinoma further but also offer new methods and new ideas for the personalized care and treatment of hepatocellular carcinoma.

1. Introduction

Hepatocellular carcinoma (HCC) is a deadly human malignancy and one of the most common causes of cancer-related deaths worldwide. Hepatocellular carcinoma is a late stage disease associated with major vascular invasion, with a poor prognosis and low survival rate [1–3]. There are four main growth modes: trabecular type, solid type, pseudo/acinar type, and large and small beam type [4]. Hepatocellular carcinoma (HCC) is not only a heterogeneous malignancy but also a potentially fatal complication of chronic liver disease with limited treatment. Liver transplantation is the preferred treatment [5, 6]. The most common sites of extrahepatic metastases include the lung, regional lymph nodes, adrenal glands, and bone [7]. The limited treatment options for patients with advanced HCC have become a significant problem [8]. Most biologists have been involved in the pathological study of hepatocellular carcinoma. For example, Xu et al. observed that the genetic variation of the hepatitis B virus X gene (HBx) is associated with progression of hepatocellular carcinoma (HCC) and identified a novel HBx genotype that may result in the loss of proliferation-promoting function [9]. Epithelial-mesenchymal transition (EMT) is also associated with progression of hepatocellular carcinoma, which occurs during HCC progression [10]. According to previous reports, we found that regulatory T cells (Tregs) are an essential component of immune cell infiltration in the tumor microenvironment, which is closely related to the progression and metastasis of hepatocellular carcinoma [11]. Long noncoding RNAs (IncRNAs) have

essential functions in the pathogenesis of hepatocellular carcinoma, including tumor growth, proliferation, metastasis, invasion, and recurrence [12]. The occurrence and development of diseases are often related to the interpretation of genes. The interpretation of SNHG16 was significantly increased in HCC tissues and cell lines, and its overexpression was inseparable from the invasive clinicopathological features and poor prognosis of HCC patients [13]. Zhong et al. [14] found that upregulated interpretation of miR-21-5p may be a functional regulator of metabolism or apoptosis in HCC and is also a novel tumor marker for the early diagnosis of HCC. Besides, studies have shown that CircPTGR1 is a circRNA with three isoforms. CircPTGR1 is upregulated in serum exosomes of HCC patients and is associated with clinical stage and prognosis [15]. In a report by the scholar (Wang J), we found that pescadillo ribosomal biosynthesis factor 1 (PES1) is generally upregulated in HCC tissues and cells, may promote proliferation and tumorigenicity, and represents a novel prognostic marker for HCC overall survival [16]. Signal transductions also have essential regulatory functions in disease progression. Cancer stem cells (CSCs) have been identified as a small fraction of cancer cells with high self-renewal, differentiation, and tumorigenic capacity [17]. CD44v is the major isoform expressed on CSCs of various tumors and has been extensively studied. The data suggest that CD44s may be involved in the maintenance of CSC in HCC cell lines via the NOTCH3 signal transduction [18].

According to a study by a scholar (Guerrero M), we found that the mTOR pathway is overexpressed in patients with multinodular HCC and is associated with an increased tumor recurrence rate after LT (liver transplantation) [19]. According to the above-mentioned partial pathogenesis of hepatocellular carcinoma, scientists and medical personnel from all over the world are actively exploring corresponding treatments and personalized care. In the treatment of hepatocellular carcinoma, scientists such as Xu et al. pointed out that FHIT and p16 as tumor suppressor genes can effectively inhibit the proliferation of HCC, which can be used as a new indicator for clinical detection, providing an original method for clinical diagnosis [20]. The circular RNA (circRNA) hsa_circ_0079299 is considered to be overexpressed in hepatocellular carcinoma, inhibiting tumor growth in vitro and in vivo and delaying cell cycle progression. Its tumor-suppressive effect in HCC provides a new understanding of circRNA in cancer [21]. The latest advances in nanotechnology are milestones in the study of treatments for hepatocellular carcinoma. According to the study of Chi et al., the integration of imaging and treatment of arsenite-containing magnetic mesoporous silica nanoparticles has great promise for the treatment of hepatocellular carcinoma [22]. Recent studies have found that rosiglitazone metformin adduct (RZM) increases the antiproliferative effect of metformin (Met) in HCC by upregulating p21 interpretation in an AMPK-dependent manner. The results indicate that RZM may be an adjuvant for the effective treatment of HCC [23]. Besides, raloxifene inhibits the growth of hepatocellular carcinoma in vitro and in vivo, suggesting another potential strategy for HCC prevention and treatment [24]. Previous clinical studies have shown that low serum cholesterol can predict adverse outcomes in HCC patients. Cholesterol inhibits the progression of HCC by inhibiting SCAP-mediated new fatty acid synthesis [25]. In the personalized care of hepatocellular carcinoma, we should consider the burden and extent of HCC. We also discuss the patient's performance status, potential liver function, extrahepatic disease and comorbidity, and the stage of HCC at diagnosis and provide multiple treatment options and determine the best treatment option [26]. Barcelona's advanced clinical liver cancer (BCLC C) is a type of hepatocellular carcinoma staging, and the best-recommended treatment is to use sorafenib alone [27].

Percutaneous ablation and hepatectomy are recommended first-line treatment options depending on the extent of liver resection and liver function. Laparoscopic surgery (resection or ablation) is an excellent surgical procedure when the tumor is located on the surface of the liver and close to the extrahepatic organ [28]. For HCC sample studies, CYP3A4 immune response was observed in peripheral hepatocytes, and CYP3A7 immunostaining was found in normal hepatocytes. CYP3A4 metabolizes sorafenib but not by CYP3A7. Overexpression of CYP3A4 may lead to increased drug degradation, which in turn leads to clinical ineffectiveness [29]. These results suggest that positive CYP3A4 in HCC liver samples may indicate a rare response to sorafenib, suggesting the need for individualized treatment of HCC [30]. Based on the gene interpretation characteristics and functional pathways of liver tissue, we propose a comprehensive approach. Based on coexpression analysis and enrichment analysis of functional pathways, we focused on a series of core ncRNA and transcription factor regulators and revealed the underlying pathogenesis of hepatocellular carcinoma to guide personalized care and treatment.

2. Materials and Methods

2.1. Data Resource. Data interpretation profiles for hepatocellular carcinoma were obtained from GSE67764 in the NCBI Gene interpretation Omnibus database [31]. In the dataset, a gene assay to screen the expression of total RNA in liver tissues, including 3 normal liver tissues, 3 HCC paracancer specimens, and 3 HCC samples with HBV-induced hepatitis. The normal liver samples were obtained from normal hepatic tissue in three hepatic hemangioma surgical operative patients, and three matched pairs of HCC and its paracancer tissues were, respectively, obtained from three HCC surgical operative patients without any chemotherapy and radiotherapy. The dataset contains normal and disease samples from different tissues of hepatocellular carcinoma [32]. There are 3,600 related genes in cancer tissues and 1224 associated genes in adjacent tissues. To understand the genetic characteristics of liver tissue, we integrated the genes of these two different tissues to obtain a final set of differential genes.

2.2. Coexpression Analysis Identifies Relevant Functional Modules. To explore the synergistic interpretation of the dysregulated genes, we constructed a gene interpretation profile matrix for cointerpretation network analysis

(WGCNA) of these genes [33]. WGCNA is a system biology method used to describe patterns of gene association between different samples. It can be used not only to identify synergistic changes in gene sets with high intrinsic but also to communicate the link between gene interpretation behavior and sample phenotype. We used the correlation coefficient weighting value; that is, the gene correlation coefficient is taken to the Nth power, and the correlation coefficient (Pearson's coefficient) between any two genes is calculated. Since the nodes in the network are subject to scale-free systems, their characteristics are consistent with the interpretation relationship between genes, so the algorithm is more biologically significant than other algorithms. Correlation coefficients between genes construct a hierarchical clustering tree, and different branches of the clustering tree represent different gene modules; that is, different colors represent different modules.

2.3. Functional and Pathway Enrichment Analysis to Identify Dysfunction Modules. The exploration of the functions of genes and the exploration of participating signal transductions are often effective means of studying the molecular mechanisms of disease. The function and pathway involved in the module gene can characterize the dysfunction mechanism of the module during the disease process. For each functional module gene of hepatocellular carcinoma, using the Cluster profile package [34], we performed Go function (p value cutoff = 0.05, qvalueCutoff = 0.05) and KEGG Pathway (p value cutoff = 0.05, qvalueCutoff = 0.05) enrichment analysis. We screened the functions and pathways reported to be associated with the progression of hepatocellular carcinoma and mapped the bubbles.

2.4. Identification of Transcription Factors and ncRNA Regulation of Modules. Data on transcriptional and post-transcriptional target regulation relationships are included in the TRRUST v2.0 database and the RAID v2.0 database [35, 36]. TRRUST v2 is now the most comprehensive database based on manual curation for both human and mouse TF–target interactions. RAID v2.0 is aimed at providing a comprehensive and reliably assessed collection of RNA-associated interactions across organisms. Among them, we downloaded and used all human transcription factor target data in the TRRUST v2 database, involving 52 transcription factors and 52 TF-Module interaction pairs. In RAID 2.0, we set the interaction score > 0.5 and screened 323 ncRNA-Module interaction pairs on humans, involving 356 ncRNAs. These regulators often mediate disease development. To explore the driving forces of cointerpretation modules for hepatocellular carcinoma-associated genes, we performed a pivotal analysis based on these interaction data. Pivot analysis refers to the search for a driver with at least two pairs of modules in the target pair, and we calculate the significance of the interaction between the driver and the module based on the hypergeometric test. The ncRNA-he1TF with p value < 0.01 is the pivot of the significant regulatory module. We performed a statistical analysis of the pivot, and the pivotal function of the dysfunction module was identified as the core pivot. The ncRNA and TF-based target data were predicted as background sets, and the crucial regulator of the regulatory dysfunction module was obtained.

3. Results

3.1. Determining the Time Series Expression of Hepatocellular Carcinoma. Gene interpretation disorders have essential functions in the disease process. To explore the genetic dysregulation of hepatocellular carcinoma, we screened differentially the interpretation profile of hepatocellular carcinoma. We obtained two sets of differences and combined the two groups of differential genes, with a total of 4479 (Table S1). Also, these differentially expressed genes may have a direct/long association with hepatocellular carcinoma, and they may have essential regulatory functions in the development of the disease.

3.2. Identify Functional Hepatocellular Carcinoma Staging-Related Modules. We constructed interpretation profiles in patient samples for 4479 differentially expressed genes in hepatocellular carcinoma. Based on the WGCNA network for cointerpretation analysis of differentially expressed genes, ten cointerpretation modules were obtained, and these module genes showed significant clustering in the samples (Figures 1(a) and 1(b)). According to the association phenotypic analysis, we found that the first module was positively correlated with the potential pathogenesis triggered by hepatocellular carcinoma (Figures 1(c) and 1(d)). Through the introduction of differential genes into the module gene, we obtained a hub gene with strong regulation of hepatocellular carcinoma in each module and considered that these genes have essential regulatory functions in the pathogenesis of hepatocellular carcinoma. Functional modules may be involved in different functions and pathways and represent different regulatory mechanisms that mediate the development and progression of hepatocellular carcinoma.

3.3. Functional and Pathway Enrichment Analysis to Identify Dysfunction Modules. Studying the functions and pathways involved in genes is an essential means of identifying their pathogenesis. To analyze the possible dysfunction of modular gene imbalance, we performed separate enrichment analysis of functions and pathways for each module. The results showed that most of the functional modules were enriched in hepatocellular carcinoma-related functions and pathways. We performed GO function and KEGG pathway enrichment analysis on the obtained ten functional modules and received a total of 36,231 functions and 1247 KEGG pathway enrichment results. It includes 5569 molecular functions (MF), 3281 cell components (CC), and 27,381 biological processes (BP) involved in the gene (Table S2, Figures 2(a) and 2(b)). Signal transductions include cell cycle, fatty acid metabolism, TGF-beta signal transduction, and p53 signal transduction. It may be identified as a core signal transduction involved in its potential disorder mechanism. We found that these signal transductions may be closely related to the genetic profile of liver tissue in the pathogenesis of hepatocellular carcinoma.

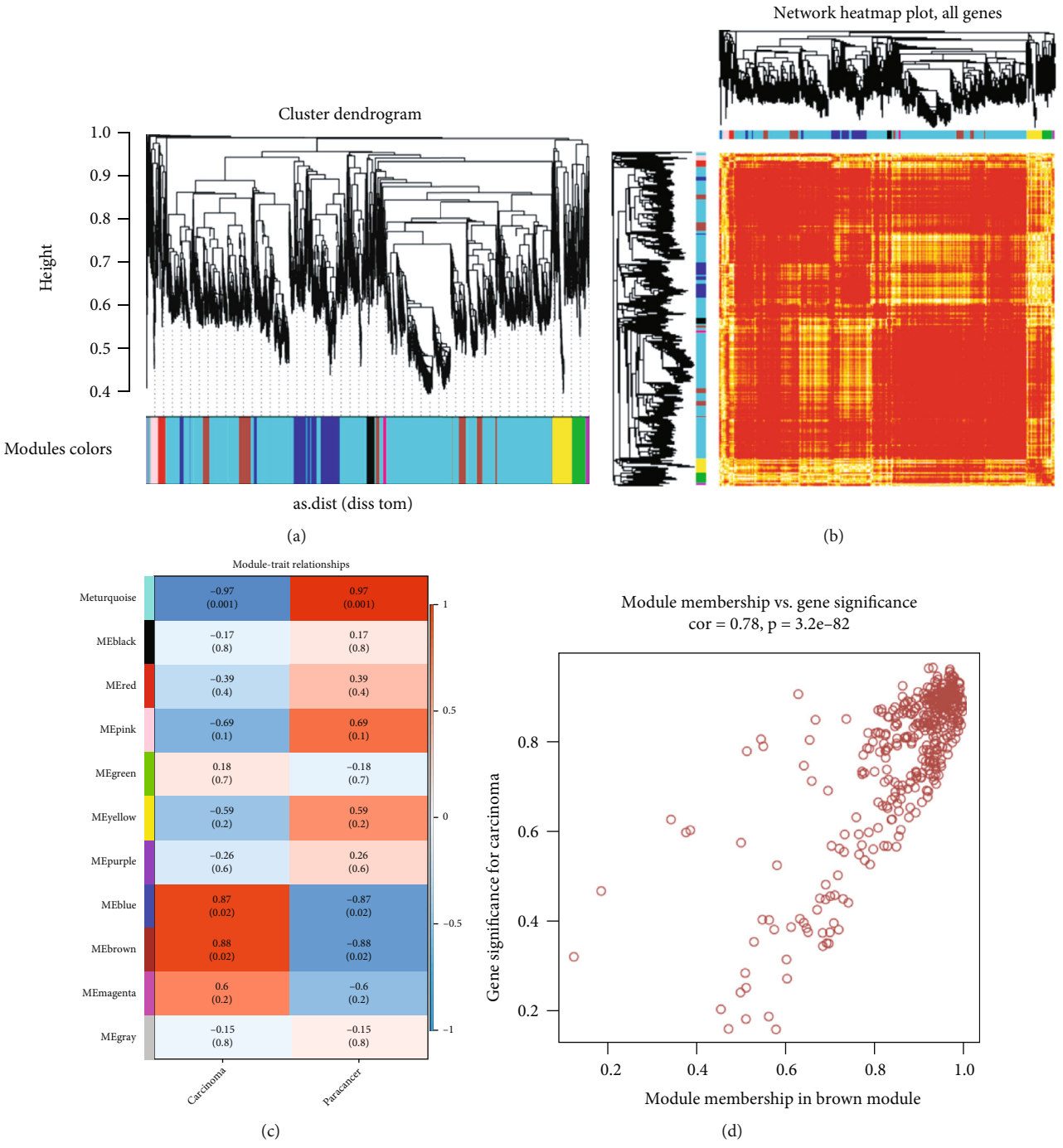

Figure 1: (a) Cointerpretation analysis clustered hepatocellular carcinoma-related differential genes into ten modules. The ten colors represent ten modules. (b) Cluster gene interpretation heat map of the module gene in the sample. (c, d) Each row represents a module, and each column represents a phenotype. The corresponding correlation coefficient maps the color of each cell. Values range from -1 to 1; the color changes from blue to white. The transition to red is a significant positive and negative correlation of the module. The darker the color, the more prominent it is in the module.

3.4. Identification of Critical Regulators Driving the Development in Hepatocellular Carcinoma. Hepatocellular carcinoma is a complex disease with multiple factors and multiple cascades, and a variety of factors naturally regulates the functional disorder module of hepatocellular carcinoma. ncRNA is considered to be an essential regulator. Scientific prediction of ncRNAs that regulate dysfunction module genes facilitates our in-depth exploration of the transcriptional regulatory mechanisms of hepatocellular carcinoma. We based on cpRNA-based pivot analysis to explore the ncRNA regulators that cause dysfunction of the module. The predicted results (Table S3, Figure 3(a)) show that 323 ncRNAs have significant regulatory effects on the module, involving 356 ncRNA-Module target pairs. These ncRNAs affect the development of hepatocellular

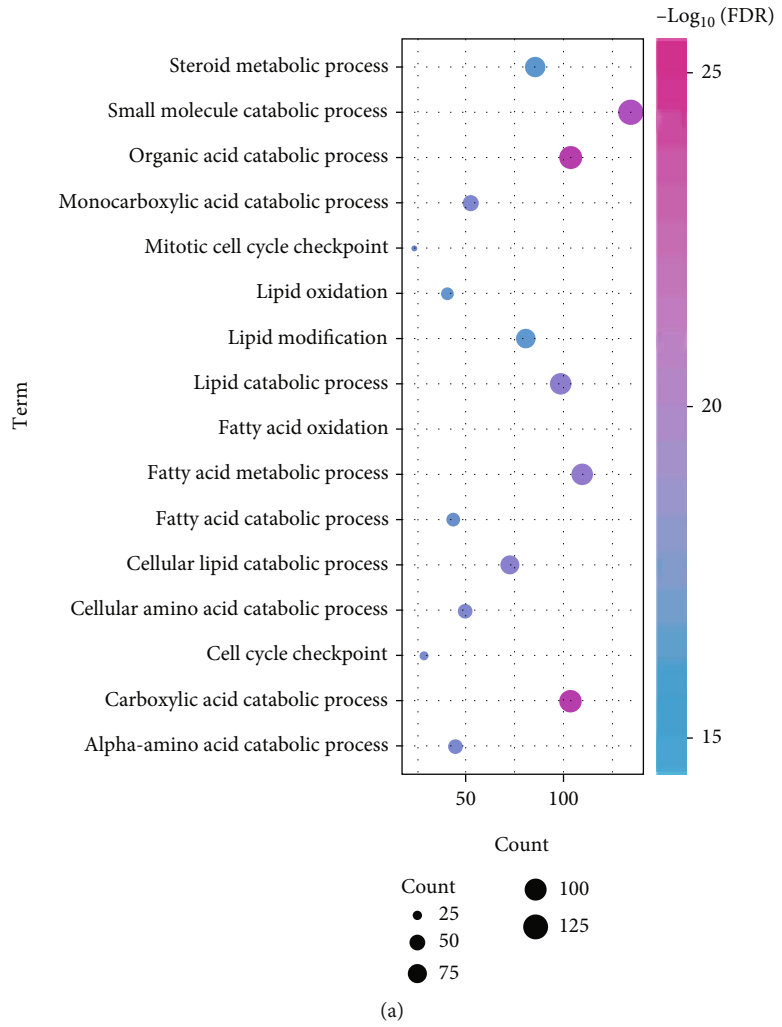

(a)

Figure 2: Continued.

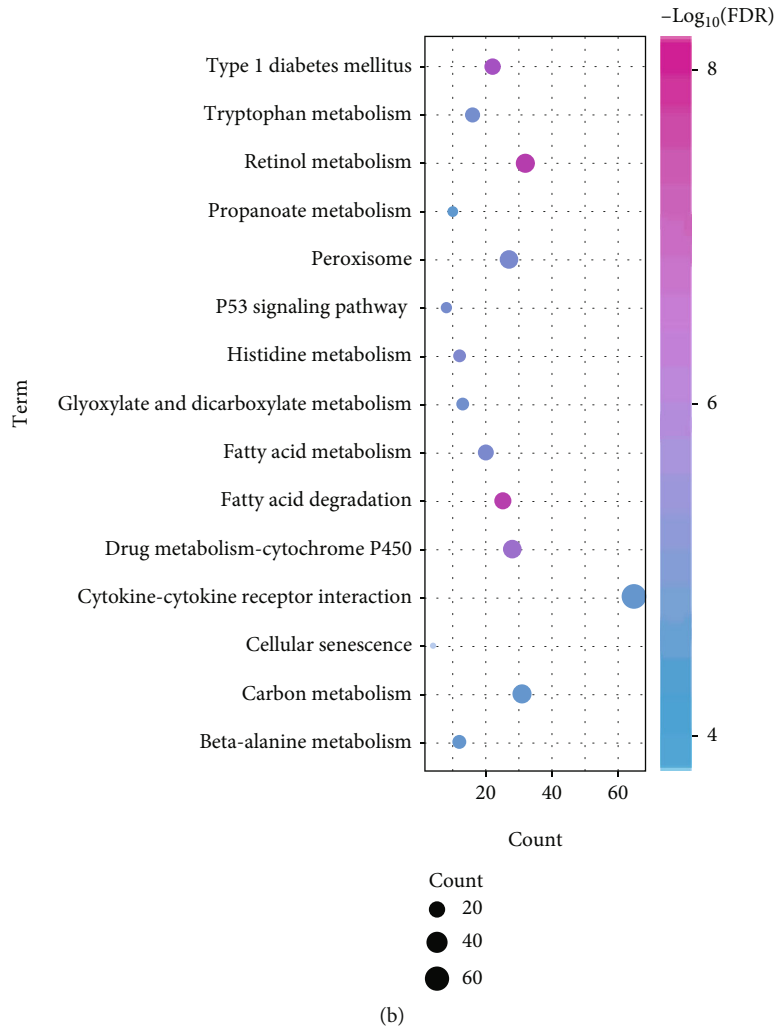

Figure 2: Modules involved in the function and pathway of the gene to identify hepatocellular carcinoma dysfunction modules. (a) Module gene GO function enrichment analysis. The deeper the color, the stronger the enrichment. The larger the circle, the more significant the proportion of the gene in the module that accounts for the GO function. (b) Module gene KEGG pathway enrichment analysis. The deeper the color, the stronger the enrichment. The larger the circle, the more significant the proportion of the gene in the KEGG pathway entry.

carcinoma to varying degrees. Besides, statistical analysis of the results revealed that miR-30b-5p and TUG1 have significant regulatory relationships with the three functional disorder modules and have essential functions in the dysfunction of the module. ncRNA (FENDRR, let-7b-5p, and let-7c-5p) exhibits a significant regulatory effect on dysfunction modules and also has critical functions in the progression of hepatocellular carcinoma. The occurrence and development of hepatocellular carcinoma are also inextricably linked to the dysregulation of transcription factors, which is also reflected in the regulation of transcription factors to dysfunction modules. Therefore, we perform a pivot analysis of the module based on the regulatory relationship of the transcription factor to the gene. The results showed that (Table S4, Figure 3(b)) a total of 52 transcription factors have significant transcriptional regulation on hepatocellular carcinoma dysfunction modules, involving 52 TF-Module regulatory pairs. For transcription factor regulatory pairs, we performed statistical analysis. We found that STAT6 mediates two modules, while TFs such as JUN, AES, and AR mediate a module that affects the development and progression of hepatocellular carcinoma. We also found that miR-30b-5p, an essential gene affecting hepatocellular carcinoma, may contribute to the development and progression of hepatocellular carcinoma by targeting ABCD3-mediated module 1 involvement in the peroxisome signal transduction (Figure 3(c)).

4. Discussion

Hepatocellular carcinoma (HCC) is one of the most common cancers in the world. This malignant tumor is associated with poor prognosis and high mortality, especially in the Chinese population [37, 38]. Liquid biopsy is noninvasive and allows repeated analyses to monitor tumor recurrence, metastasis, or treatment responses in real time. With the advanced development of new molecular techniques,

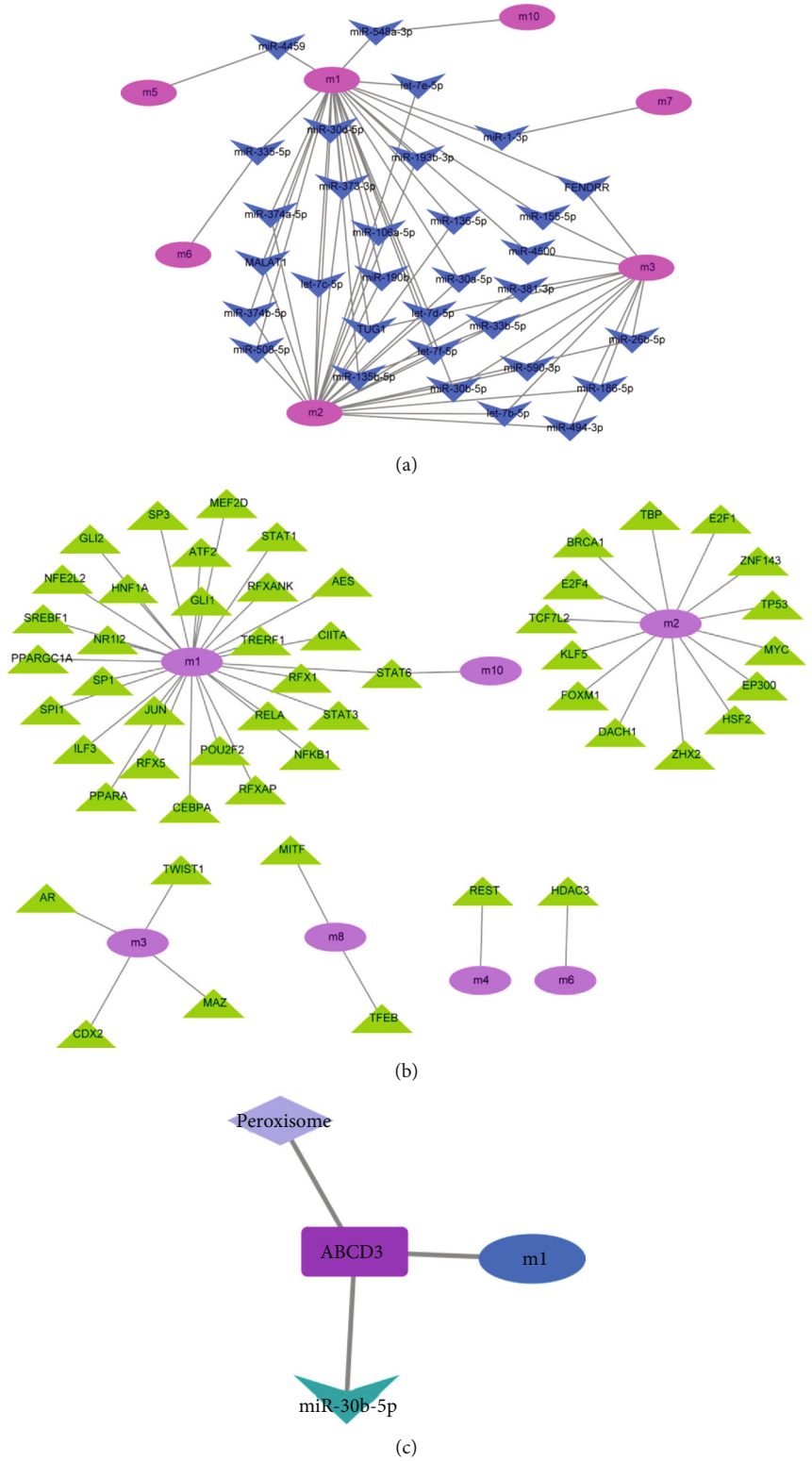

Figure 3: (a) Modulation of noncoding RNA to dysfunction modules. The color from pink to blue represents the connectivity of the nodes from large to small, that is, the more complicated the relationship with the regulation. (b) Regulatory effects of transcription factors on dysfunction modules. The color from purple to green represents the connectivity of the nodes from large to small and the more complicated the relationship with regulation. (c) Essential genes of hepatocellular carcinoma may participate in related signal transductions through target gene-mediated modules to promote the occurrence and development of diseases.

HCC circulating tumor cells (CTCs) and circulating tumor DNA (ctDNA) detection have achieved interesting and encouraging results. Based on the gene interpretation characteristics of liver tissue, we reveal that the pathogenesis of hepatocellular carcinoma guides personalized care and treatment and proposes a comprehensive method. Four thousand four hundred seventy-nine potential pathogenic genes (including MYH2, FGF21, and CYP26A1) for hepatocellular carcinoma were integrated, and cointerpretation analysis was performed with a correlated phenotype. We identified ten functional modules with synergistic interpretation and obtained the corresponding hub genes (CDCA5, TPTE2) for each module. Comprehensive studies have shown significant changes in eight protein spots in patients with hepatocellular carcinoma. Four proteins were successfully identified, including MYH2 protein, mitochondrial ATP synthase, sulfated glycoprotein-2 (SGP-2), and glial fibrillary acidic protein (GFAP). These results indicate that MYH2 protein, mitochondrial ATP synthase, SGP-2, and GFAP may be potential molecular biomarkers of hepatocellular carcinoma [39]. Also, fibroblast growth factor 21 (FGF21) has essential functions in liver metabolism and is also a potential marker for nonalcoholic fatty liver disease (NAFL). High fat, the high sucrose-induced fat-induced elevation of FGF21, may have essential functions in inhibiting hepatic pathology from NAFL to HCC [40]. During the development of HCC, decreased levels of FGF21 protein are associated with cancerous hyperproliferation and abnormal p53 and TGF-β/Smad signaling [41]. Data analysis of Lepri SR revealed that HepG2/C3A cells were exposed to genistein (5 and 50 μM).

After 12 hours, CYP1A1 and CYP1B1 were upregulated, and CYP2D6 and CYP26A1 and CYP26B1 mRNA levels were downregulated [42]. Studies have found that increased CDCA5 interpretation is not only associated with increased HCC tumor diameter and microvascular invasion but may also be associated with hepatocellular carcinoma [43]. Further studies have shown that depletion of CDCA5 can reduce the levels of ERK1/2 and AKT phosphorylation *in vitro* and *in vivo* [44]. In conclusion, CDCA 5 may be a biomarker and therapeutic target for liver cancer prognosis [45]. Based on the SNP analysis of Clifford RJ, we identified two variants while recognizing that their allele frequencies differ essentially between HCC and cirrhosis (LC). One of them is located in the PTEN homolog TPTE2 [46]. Given functional enrichment results, we found that the signal transduction that modules tend to participate includes cell cycle, fatty acid metabolism, TGF-beta signal transduction, and p53 signal transduction. According to related studies, saffron inhibits the growth of QGY-7703 cells and stops the cell cycle in the G0/G1 phase and induces cell apoptosis [47]. A-Raf and fatty acid 2-hydroxylase (FA2H) are expressed in the early stage of liver cancer, both during progression and in tumor stage. The results indicate that elevated interpretation of A-Raf and FA2H in hepatocellular carcinoma is associated with lipid metabolism disorders and cancer progression [48]. Bi et al. believe that miR-181a-5p is a negative regulator of Egr1 and can inhibit tumor proliferation in HCC by targeting the Egr1/TGF-β1/Smad pathway, which may be a potential therapeutic approach for HCC [49]. The ubiquitin-binding enzyme E2S (UBE2S) has important functions in the development of human cancer. Pan et al. demonstrated in vitro experiments that UBE2S overexpression promotes proliferation and migration of HCC cells. UBE2S knockdown inhibits HCC cell proliferation and migration by regulating the p53 signal transduction [50]. These functions and pathways involved in the modular gene produce a far-reaching network effect that comprehensively regulates the pathogenesis of hepatocellular carcinoma. We explored a range of drivers for these dysfunction modules involving ncRNA (miR-30b-5p, TUG1, FENDRR, let-7b-5p, and let-7c-5p) and transcription factors (STAT6, JUN, AES, and AR). In terms of the driving force of ncRNA, miR-30b-5p and TUG1 both regulate the three functional disorder modules. Based on clinical data, miR-30b-5p was found to be associated with a variety of clinicopathological features (survival time, tumor size, pathological stage, differentiation, and intrahepatic metastasis). It also has an inhibitory effect on cell proliferation and cell cycle of HCC cell lines [51]. Long-chain noncoding RNAs (lncRNAs) have been reported to have key regulatory functions in the development of various cancers. General studies have shown that long noncoding RNA TUG1 is essentially upregulated in HCC tissues and cell lines; knocking out TUG1 may inhibit cell proliferation, cell migration, cell invasion, and epithelial-mesenchymal transition (EMT) [52]. Also, TUG1 was confirmed to be a molecular sponge of miR-144. It was found that TUG1 interacts with miR-144 to promote proliferation and migration of HCC cells by activating the JAK2/STAT3 pathway *in vitro* [53]. The above results indicate that TUG 1 can be used as a new diagnostic biomarker and therapeutic target for HCC [54]. In the regulation of transcription factors, STAT6 essentially regulates two functional disorder modules, while TF such as AR and ATF2 has a driving effect on one module, which affects the occurrence and development of hepatocellular carcinoma. Signal transduction and transcriptional activator-6 (STAT6) is highly expressed in various human cancers. Consistent evidence suggests that STAT6 predicts poor prognosis in patients with hepatocellular carcinoma (HCC) [55]. Xiao et al. [56] found that AR/miR-520f-3p/SOX9 signaling altered HCC cells by increasing cancer stem cell (CSC) population. Luo et al. believe that the mechanism of sorafenib combined with silencing activation of transcription factor 2 (ATF2) may be related to the activation of the TNF-α/JNK3 signal transduction [57]. LEN (a linear tyrosine kinase inhibitor) may be an important therapeutic method. The efficacy of locally advanced patients who underwent selective internal radiotherapy (SIRT) was similar to that of patients treated with sorafenib [58]. For patients with HCC who are not suitable for surgery and other local area treatments, we may consider central liver stereotactic whole body radiation therapy (SBRT). This treatment regimen produces a good therapeutic response to centrally located hepatocellular carcinoma (CL-HCC) with acceptable HBT (hepatobiliary toxicity) and LC (local control) [59].

There are some limitations in our manuscript. Firstly, although the key module and key genes were identified, no in vitro experiments were performed to validate the conclusions. Secondly, given the characteristics of the dataset we

used, we could not explore the key genes by different stages. All the above would be performed in the future.

5. Conclusions

According to data mining and modularized research methods, we conducted a series of comprehensive and systematic analyses to reveal the underlying pathogenesis of hepatocellular carcinoma. According to the genetic characteristics of liver tissue, we explored the functional disorder module of hepatocellular carcinoma and revealed its pathogenesis and guided personalized care and treatment. It not only provides a new way for biologists and medical scientists to study hepatocellular carcinoma but also provides a valuable reference for its subsequent diagnostic treatment.

Data Availability

The datasets used and/or analyzed during the current study are available from the corresponding author on reasonable request.

Ethical Approval

The study was approved by the Ethics Committee of Tianjin First Central Hospital, China.

Consent

Consent is not applicable.

Conflicts of Interest

The authors declare that they have no competing interests.

Authors' Contributions

CG wrote the manuscript and collected the data. XG and YR designed the study and performed the experiment. YG and LZ were responsible for the analysis and discussion of the data. All authors read and approved the final manuscript.

Supplementary Materials

Supplementary 1. Table S1.4479 Hepatocellular carcinoma differential genes.

Supplementary 2. Table S2.36231 Functional enrichment results.

Supplementary 3. Table S3.356 ncRNA-Module target pairs.

Supplementary 4. Table S4.52 TF-Module control pairs.

References

[1] X. Zhang, L. Jin, Z. Tian et al., "Nitric oxide inhibits autophagy and promotes apoptosis in hepatocellular carcinoma," *Cancer Science*, vol. 110, no. 3, pp. 1054–1063, 2019.

[2] H. H. Lai, C. W. Li, C. C. Hong et al., "TARBP2-mediated destabilization of Nanog overcomes sorafenib resistance in hepatocellular carcinoma," *Molecular Oncology*, vol. 13, no. 4, pp. 928–945, 2019.

[3] Q. Lin, X. Huang, C. Zhong, T. Luo, X. Zeng, and S. Chen, "Improved survival with radiotherapy in hepatocellular carcinoma with major vascular invasion: a propensity-matched analysis of Surveillance, Epidemiology, and End Results database," *Cancer Medicine*, vol. 8, no. 2, pp. 515–526, 2019.

[4] M. S. Torbenson, "Morphologic subtypes of hepatocellular carcinoma," *Gastroenterology Clinics of North America*, vol. 46, no. 2, pp. 365–391, 2017.

[5] Y. Ma, C. Zhang, B. Zhang, H. Yu, and Q. Yu, "circRNA of AR-suppressed PABPC1 91 bp enhances the cytotoxicity of natural killer cells against hepatocellular carcinoma via upregulating UL16 binding protein 1," *Oncology Letters*, vol. 17, pp. 388–397, 2019.

[6] R. Samuel, M. Bilal, R. Nawgiri, S. Merwat, S. Parupudi, and P. Guturu, "Recurrence of hepatocellular carcinoma at the porta-hepatis following liver transplantation diagnosed on EUS-FNA," *Clinical Journal of Gastroenterology*, vol. 12, no. 4, pp. 336–340, 2019.

[7] Y. Shen, L. Nie, Y. Yao, L. Yuan, Z. Liu, and Y. Lv, "Seminal vesicle metastasis after liver transplantation for hepatocellular carcinoma," *Medicine*, vol. 98, no. 3, article e13770, 2019.

[8] W. D. Thompson and E. B. Smith, "Atherosclerosis and the coagulation system," *The Journal of Pathology*, vol. 159, no. 2, pp. 97–106, 1989.

[9] Q. G. Xu, S. X. Yuan, Q. F. Tao et al., "A novel HBx genotype serves as a preoperative predictor and fails to activate the JAK1/STATs pathway in hepatocellular carcinoma," *Journal of Hepatology*, vol. 70, no. 5, pp. 904–917, 2019.

[10] X. Yang, X. Du, L. Sun et al., "SULT2B1b promotes epithelial-mesenchymal transition through activation of the β-catenin/MMP7 pathway in hepatocytes," *Biochemical and Biophysical Research Communications*, vol. 510, no. 4, pp. 495–500, 2019.

[11] C. Shi, Y. Chen, Y. Chen, Y. Yang, W. Bing, and J. Qi, "$CD4^+$ $CD25^+$ regulatory T cells promote hepatocellular carcinoma invasion via TGF-β1-induced epithelial–mesenchymal transition," *Oncotargets and Therapy*, vol. 12, pp. 279–289, 2019.

[12] J. F. Huang, H. Y. Jiang, H. Cai et al., "Genome-wide screening identifies oncofetal lncRNA Ptn-dt promoting the proliferation of hepatocellular carcinoma cells by regulating the Ptn receptor," *Oncogene*, vol. 38, no. 18, pp. 3428–3445, 2019.

[13] J. Ye, R. Zhang, X. Du, W. Chai, and Q. Zhou, "Long noncoding RNA SNHG16 induces sorafenib resistance in hepatocellular carcinoma cells through sponging miR-140-5p," *Oncotargets and Therapy*, vol. Volume 12, pp. 415–422, 2019.

[14] X. Z. Zhong, Y. Deng, G. Chen, and H. Yang, "Investigation of the clinical significance and molecular mechanism of miR-21-5p in hepatocellular carcinoma: a systematic review based on 24 studies and bioinformatics investigation," *Oncology Letters*, vol. 17, pp. 230–246, 2019.

[15] G. Wang, W. Liu, Y. Zou et al., "Three isoforms of exosomal circPTGR1 promote hepatocellular carcinoma metastasis via the miR449a-MET pathway," *eBioMedicine*, vol. 40, pp. 432–445, 2019.

[16] J. Wang, J. Sun, N. Zhang et al., "PES1 enhances proliferation and tumorigenesis in hepatocellular carcinoma via the PI3K/AKT pathway," *Life Sciences*, vol. 219, pp. 182–189, 2019.

[17] N. Wang, S. Wang, M. Y. Li et al., "Cancer stem cells in hepatocellular carcinoma: an overview and promising therapeutic strategies," *Therapeutic Advances in Medical Oncology*, vol. 10, 2018.

[18] R. Asai, H. Tsuchiya, M. Amisaki et al., "CD44 standard isoform is involved in maintenance of cancer stem cells of a hepatocellular carcinoma cell line," *Cancer Medicine*, vol. 8, no. 2, pp. 773–782, 2019.

[19] M. Guerrero, G. Ferrín, M. Rodríguez-Perálvarez et al., "mTOR expression in liver transplant candidates with hepatocellular carcinoma: impact on histological features and tumour recurrence," *International Journal of Molecular Sciences*, vol. 20, no. 2, p. 336, 2019.

[20] W. Xu, X. Qi, X. Wang, and J. Sun, "Effect of interventional embolotherapy on FHIT and p16 expression in hepatocellular carcinoma patients," *Oncology Letters*, vol. 17, pp. 871–876, 2019.

[21] H. Zheng, T. Chen, C. Li et al., "A circular RNA hsa *circ* 0079929 inhibits tumor growth in hepatocellular carcinoma," *Cancer Management and Research*, vol. 11, pp. 443–454, 2019.

[22] X. Chi, R. Zhang, T. Zhao et al., "Targeted arsenite-loaded magnetic multifunctional nanoparticles for treatment of hepatocellular carcinoma," *Nanotechnology*, vol. 30, no. 17, article 175101, 2019.

[23] Y. Liu, X. Hu, X. Shan, K. Chen, and H. Tang, "Rosiglitazone metformin adduct inhibits hepatocellular carcinoma proliferation via activation of AMPK/p21 pathway," *Cancer Cell International*, vol. 19, no. 1, p. 13, 2019.

[24] H. Ma, D. Yan, Y. Wang et al., "Bazedoxifene exhibits growth suppressive activity by targeting interleukin-6/glycoprotein 130/signal transducer and activator of transcription 3 signaling in hepatocellular carcinoma," *Cancer Science*, vol. 110, no. 3, pp. 950–961, 2019.

[25] Z. Zhao, L. Zhong, K. He et al., "Cholesterol attenuated the progression of DEN-induced hepatocellular carcinoma via inhibiting SCAP mediated fatty acid de novo synthesis," *Biochemical and Biophysical Research Communications*, vol. 509, no. 4, pp. 855–861, 2019.

[26] T. Couri and A. Pillai, "Goals and targets for personalized therapy for HCC," *Hepatology International*, vol. 13, no. 2, pp. 125–137, 2019.

[27] E. G. Giannini, L. Bucci, F. Garuti et al., "Patients with advanced hepatocellular carcinoma need a personalized management: a lesson from clinical practice," *Hepatology*, vol. 67, no. 5, pp. 1784–1796, 2018.

[28] A. Vitale, M. Peck-Radosavljevic, E. G. Giannini et al., "Personalized treatment of patients with very early hepatocellular carcinoma," *Journal of Hepatology*, vol. 66, no. 2, pp. 412–423, 2017.

[29] R. L. Hesketh, A. X. Zhu, and R. Oklu, "Hepatocellular Carcinoma," *American Journal of Clinical Oncology*, vol. 38, no. 4, pp. 431–436, 2015.

[30] D. Fanni, M. Manchia, F. Lai, C. Gerosa, R. Ambu, and G. Faa, "Immunohistochemical markers of CYP3A4 and CYP3A7: a new tool towards personalized pharmacotherapy of hepatocellular carcinoma," *European Journal of Histochemistry*, vol. 60, no. 2, p. 2614, 2016.

[31] T. Barrett, S. E. Wilhite, P. Ledoux et al., "NCBI GEO: archive for functional genomics data sets–update," *Nucleic Acids Research*, vol. 41, no. D1, pp. D991–D995, 2012.

[32] Y. Yang, Y. Guo, S. Tan et al., "β-Arrestin1 enhances hepatocellular carcinogenesis through inflammation- mediated Akt signalling," *Nature Communications*, vol. 6, no. 1, p. 7369, 2015.

[33] P. Langfelder and S. Horvath, "WGCNA: an R package for weighted correlation network analysis," *BMC Bioinformatics*, vol. 9, no. 1, p. 559, 2008.

[34] G. Yu, L. G. Wang, Y. Han, and Q. Y. He, "clusterProfiler: an R package for comparing biological themes among gene clusters," *OMICS*, vol. 16, no. 5, pp. 284–287, 2012.

[35] H. Han, J. W. Cho, S. Lee et al., "TRRUST v2: an expanded reference database of human and mouse transcriptional regulatory interactions," *Nucleic Acids Research*, vol. 46, no. D1, pp. D380–D386, 2018.

[36] Y. Yi, Y. Zhao, C. Li et al., "RAID v2.0: an updated resource of RNA-associated interactions across organisms," *Nucleic Acids Research*, vol. 45, no. D1, pp. D115–D118, 2017.

[37] R. Zhang, Z. Zhang, Z. Liu et al., "Adoptive cell transfer therapy for hepatocellular carcinoma," *Frontiers in Medicine*, vol. 13, no. 1, pp. 3–11, 2019.

[38] X. Gong and S. Qin, "Study progression of anti-angiogenetic therapy and its combination with other agents for the treatment of advanced hepatocellular carcinoma," *HepatoBiliary Surgery and Nutrition*, vol. 7, no. 6, pp. 466–474, 2018.

[39] W. Wu, J. Li, Y. Liu, C. Zhang, X. Meng, and Z. Zhou, "Comparative proteomic studies of serum from patients with hepatocellular carcinoma," *Journal of Investigative Surgery*, vol. 25, no. 1, pp. 37–42, 2012.

[40] G. Singhal, G. Kumar, S. Chan et al., "Deficiency of fibroblast growth factor 21 (FGF21) promotes hepatocellular carcinoma (HCC) in mice on a long term obesogenic diet," *Molecular Metabolism*, vol. 13, pp. 56–66, 2018.

[41] Q. Zhang, Y. Li, T. Liang et al., "Loss of FGF21 in diabetic mouse during hepatocellular carcinogenetic transformation," *American Journal of Cancer Research*, vol. 5, pp. 1762–1774, 2015.

[42] S. R. Lepri, D. Sartori, S. C. Semprebon, A. Baranoski, G. C. Coatti, and M. S. Mantovani, "Genistein affects expression of cytochrome P450 (CYP450) genes in hepatocellular carcinoma (HEPG2/C3A) cell line," *Drug Metabolism Letters*, vol. 12, no. 2, pp. 138–144, 2018.

[43] Y. Tian, J. Wu, C. Chagas et al., "CDCA5 overexpression is an indicator of poor prognosis in patients with hepatocellular carcinoma (HCC)," *BMC Cancer*, vol. 18, no. 1, p. 1187, 2018.

[44] J. Wang, C. Xia, M. Pu et al., "Silencing of CDCA5 inhibits cancer progression and serves as a prognostic biomarker for hepatocellular carcinoma," *Oncology Reports*, vol. 40, pp. 1875–1884, 2018.

[45] Z. Shen, X. Yu, Y. Zheng et al., "CDCA5 regulates proliferation in hepatocellular carcinoma and has potential as a negative prognostic marker," *Oncotargets and Therapy*, vol. 11, pp. 891–901, 2018.

[46] R. J. Clifford, J. Zhang, D. M. Meerzaman et al., "Genetic variations at loci involved in the immune response are risk factors for hepatocellular carcinoma," *Hepatology*, vol. 52, no. 6, pp. 2034–2043, 2010.

[47] T. Liu, L. Tian, X. Fu, L. Wei, J. Li, and T. Wang, "Saffron inhibits the proliferation of hepatocellular carcinoma via inducing cell apoptosis," *Panminerva Medica*, vol. 62, no. 1, 2020.

[48] M. Ranjpour, S. Wajid, and S. K. Jain, "Elevated expression of A-Raf and FA2H in hepatocellular carcinoma is associated with lipid metabolism dysregulation and cancer progression," *Anti-Cancer Agents in Medicinal Chemistry*, vol. 19, no. 2, pp. 236–247, 2019.

[49] J. G. Bi, J. F. Zheng, Q. Li et al., "MicroRNA-181a-5p suppresses cell proliferation by targeting Egr1 and inhibiting Egr1/TGF-β/Smad pathway in hepatocellular carcinoma," *The International Journal of Biochemistry & Cell Biology*, vol. 106, pp. 107–116, 2019.

[50] Y. H. Pan, M. Yang, L. P. Liu, D. C. Wu, M. Y. Li, and S. G. Su, "UBE2S enhances the ubiquitination of p53 and exerts oncogenic activities in hepatocellular carcinoma," *Biochemical and Biophysical Research Communications*, vol. 503, no. 2, pp. 895–902, 2018.

[51] X. Qin, J. Chen, L. Wu, and Z. Liu, "MiR-30b-5p acts as a tumor suppressor, repressing cell proliferation and cell cycle in human hepatocellular carcinoma," *Biomedicine & Pharmacotherapy*, vol. 89, pp. 742–750, 2017.

[52] C. He, Z. Liu, L. Jin et al., "lncRNA TUG1-mediated Mir-142-3p downregulation contributes to metastasis and the epithelial-to-mesenchymal transition of hepatocellular carcinoma by targeting ZEB1," *Cellular Physiology and Biochemistry*, vol. 48, no. 5, pp. 1928–1941, 2018.

[53] A. Michalski and B. Rozental-Ratajczyk, "Coexistence of lung cancer with other malignant neoplasms," *Pneumonologia Polska*, vol. 53, pp. 137–142, 1985.

[54] A. S. Machikhin, V. E. Pozhar, A. V. Viskovatykh, and L. I. Burmak, "Acousto-optical tunable filter for combined wideband, spectral, and optical coherence microscopy," *Applied Optics*, vol. 54, no. 25, pp. 7508–7513, 2015.

[55] T. Qing, Z. Yamin, W. Guijie, J. Yan, and S. Zhongyang, "STAT6 silencing induces hepatocellular carcinoma-derived cell apoptosis and growth inhibition by decreasing the RANKL expression," *Biomedicine & Pharmacotherapy*, vol. 92, pp. 1–6, 2017.

[56] Y. Xiao, Y. Sun, G. Liu et al., "Androgen receptor (AR)/miR-520f-3p/SOX9 signaling is involved in altering hepatocellular carcinoma (HCC) cell sensitivity to the Sorafenib therapy under hypoxia via increasing cancer stem cells phenotype," *Cancer Letters*, vol. 444, pp. 175–187, 2019.

[57] L. Luo, L. Cai, L. Luo, Z. Tang, and X. Meng, "Silencing activating transcription factor 2 promotes the anticancer activity of sorafenib in hepatocellular carcinoma cells," *Molecular Medicine Reports*, vol. 17, pp. 8053–8060, 2018.

[58] H. Wang, H. Wang, Z. Yu, and H. Liu, "Alternative treatment strategies to sorafenib in patients with advanced hepatocellular carcinoma: a meta-analysis of randomized phase III trials," *Oncotargets and Therapy*, vol. Volume 11, pp. 5195–5201, 2018.

[59] S. Lazarev, C. Hardy-Abeloos, O. Factor, K. Rosenzweig, and M. Buckstein, "Stereotactic body radiation therapy for centrally located hepatocellular carcinoma: outcomes and toxicities," *Journal of Cancer Research and Clinical Oncology*, vol. 144, no. 10, pp. 2077–2083, 2018.

Hindawi
BioMed Research International
Volume 2024, Article ID 9858395, 1 page
https://doi.org/10.1155/2024/9858395

Retraction

Retracted: The Functionalities and Clinical Significance of Tumor-Infiltrating Immune Cells in Esophageal Squamous Cell Carcinoma

BioMed Research International

Received 12 March 2024; Accepted 12 March 2024; Published 20 March 2024

This article has been retracted by Hindawi following an investigation undertaken by the publisher [1]. This investigation has uncovered evidence of one or more of the following indicators of systematic manipulation of the publication process:

(1) Discrepancies in scope

(2) Discrepancies in the description of the research reported

(3) Discrepancies between the availability of data and the research described

(4) Inappropriate citations

(5) Incoherent, meaningless and/or irrelevant content included in the article

(6) Manipulated or compromised peer review

The presence of these indicators undermines our confidence in the integrity of the article's content and we cannot, therefore, vouch for its reliability. Please note that this notice is intended solely to alert readers that the content of this article is unreliable. We have not investigated whether authors were aware of or involved in the systematic manipulation of the publication process.

Wiley and Hindawi regrets that the usual quality checks did not identify these issues before publication and have since put additional measures in place to safeguard research integrity.

We wish to credit our own Research Integrity and Research Publishing teams and anonymous and named external researchers and research integrity experts for contributing to this investigation.

The corresponding author, as the representative of all authors, has been given the opportunity to register their agreement or disagreement to this retraction. We have kept a record of any response received.

References

[1] J. Zhang, H. Wang, H. Wu, and G. Qiang, "The Functionalities and Clinical Significance of Tumor-Infiltrating Immune Cells in Esophageal Squamous Cell Carcinoma," *BioMed Research International*, vol. 2021, Article ID 8635381, 9 pages, 2021.

Hindawi
BioMed Research International
Volume 2021, Article ID 8635381, 9 pages
https://doi.org/10.1155/2021/8635381

Research Article

The Functionalities and Clinical Significance of Tumor-Infiltrating Immune Cells in Esophageal Squamous Cell Carcinoma

Jishuai Zhang,[1] Haifeng Wang,[2] Haitao Wu,[3] and Guangliang Qiang[4]

[1]*Department of Thoracic Surgery, Feicheng Hospital Affiliated to Shandong First Medical University, Shandong Province, China*
[2]*Department of Thoracic Surgery, No.1 People's Hospital of Ningyang County, Shandong Province, China*
[3]*Oncology Department, No.1 People's Hospital of Ningyang County, Shandong Province, China*
[4]*Department of Thoracic Surgery, China-Japan Friendship Hospital, Chaoyang District, Beijing, China*

Correspondence should be addressed to Guangliang Qiang; qianghecheng3500@163.com

Received 23 June 2021; Revised 11 August 2021; Accepted 16 August 2021; Published 27 September 2021

Academic Editor: Jun Yang

Tumor-infiltrating immune cells have been implicated in the tumorigenesis and progression of esophageal squamous cell carcinoma (ESCC). However, the functionalities and clinical significance of immune cells remain largely unveiled. In this study, the gene expression data from the Cancer Genome Atlas (TCGA) and Gene Expression Omnibus (GEO) were extracted. The relative infiltrating levels were estimated by single-sample gene set enrichment analysis. Some cytotoxic immune cells were attenuated, and resting cytotoxic immune cells were accumulated in ESCC. Remarkably, we also observed that infiltrating levels of macrophage M2 and resting natural killer (NK) cells were increased in nonresponders of CRT, and T cells that had anticancer activities such as activated memory CD4 and T helper 2 (Th2) cells were significantly reduced in ESCC tissues of the nonresponders. Moreover, the high infiltrations of the resting natural killer (NK) and dendritic cell (DC) were observed to result in a shorter overall survival in ESCC. Consistently, high expression of immune checkpoint genes, CTLA4 and HAVCR2, was associated with poor prognosis. Furthermore, STAT5B, a key transcription factor, as well as its target genes, involved in the regulation of T cells, was significantly downregulated in ESCC, especially subgroup I, indicating that downregulation of STAT5B might be associated with reduced T cell-mediated anticancer activity. In conclusion, the present study significantly improved our understanding of the regulatory roles of immune cells in ESCC.

1. Introduction

Esophageal squamous cell carcinoma (ESCC) is a major type of tumors occurring in the esophagus, accounting for more than 70% of total esophageal cancer cases worldwide [1]. The 5-year survival rate of esophageal cancer is less than 25%, which makes it one of the leading causes of cancer-related deaths [2]. Risk factors for ESCC include alcohol consumption, tobacco smoking, and other unhealthy lifestyles [3], and though the incidence of ESCC has been declining in Western countries, it still remains an important public health concern in East Asia and Africa [1].

For cancers that are closely associated with chronic inflammation, such as colorectal carcinoma, hepatocellular carcinoma, and ESCC, inflammatory mediators released by immune cells are often responsible for abnormal cell proliferation, genomic instability, oncogene activation, and angiogenesis [4]. Also, responses to therapy are affected by inflammation and immunity [5]. Since immunotherapy has emerged as a promising treatment for patients with advanced-stage ESCC, many recent studies are placing emphasis on the composition and function of immune cells in tumor microenvironment, and the relationship between immune cell infiltrating and ESCC survival has attracted much attention. In a previous research, immunohistochemistry was applied to measure the infiltration of T cells and the expression of immune checkpoint proteins in ESCC patients, including PD-1, TIGIT, PD-L1, and PD-L2, and

the abundance of these checkpoint proteins was found to be associated with patients' prognoses [6]. Another study has hinted that intraepithelial CD4+ lymphocyte infiltration could contribute to favorable prognosis in ESCC [7]. Moreover, the abundance of CD103 + CD8+ tumor-infiltrating lymphocytes (TILs), which was a subpopulation of CD8+ TILs, was found to be associated with better overall survival of ESCC patients [8]. Infiltration of macrophages, such as CD68+ and CD204+, in ESCC was also evaluated, and a higher CD8+/CD204+ ratio could serve as a positive prognostic indicator for ESCC patients [9].

Considering the diversity of distinct tumor-infiltrating immune cells, the landscape of immune cell infiltrating in ESCC still remains largely unveiled. Here, we estimated the relative infiltrating levels of the immune cells in ESCC and characterized their functionalities and clinical significance.

2. Materials and Methods

2.1. Data Collection. The gene expression data from the Cancer Genome Atlas (TCGA) project [10] were collected from UCSC Xena database [11]. We only retained 81 esophageal squamous cell carcinoma (ESCC) and 11 adjacent normal tissues with detailed clinical information. The expression values were normalized to log2 (FPKM (Fragment Per Kilobase Per Million Reads) +1) [12]. The gene expression data of responders and nonresponders of preoperative chemoradiotherapy (CRT) were collected from Gene Expression Omnibus (GEO) with accession GSE45670 and normalized by MAS5 (MicroArray Suite 5.0) by previous study [13].

2.2. Estimation of Infiltrating Levels. A total of 570 genes representing 26 types of immune cells, fibroblast, and endothelial cells were collected from previous study. The relative infiltrating levels were estimated by single-sample gene set enrichment analysis (ssGSEA), which were implemented in R *gsva* package [14]. Single-sample GSEA (ssGSEA), an extension of Gene Set Enrichment Analysis (GSEA), calculates separate enrichment scores for each pairing of a sample and gene set. Each ssGSEA enrichment score represents the degree to which the genes in a particular gene set are coordinately up- or downregulated within a sample.

2.3. Overrepresentation Enrichment Analysis. Prior to the overrepresentation enrichment analysis, we identified the differentially expressed genes in each subgroup by pairwise Wilcoxon rank-sum test and fold change methods (FDR < 0.05 and fold change > 2) [15]. The overrepresentation enrichment analysis was implemented in R *clusterProfiler* package [16, 17].

2.4. Hierarchical Clustering Analysis. The gastric cancer samples were clustered based on the infiltrating levels of the 28 cells. The Ward method and Euclidean distance were used in this analysis. The default options were selected for the other parameters.

2.5. Survival Analysis. The univariable Cox proportional hazard regression analysis was used to identify infiltrating cells associated with overall survival. The survival analysis was implemented in R *survival* and visualized by R survminer package.

3. Results

3.1. The Differential Infiltrating Cells between Esophageal Squamous Cell Carcinoma and Adjacent Normal Tissues. In this study, we collected gene expression data of 81 esophageal squamous cell carcinoma (ESCC) and 11 adjacent normal tissues from the Cancer Genomics Atlas (TCGA). The relative infiltrating levels of 28 cells in ESCC and adjacent normal tissues were estimated by the single-sample enrichment analysis (ssGSEA). Among these cells, 11 were differentially infiltrated into ESCC tissues, of which, endothelial cells and resting CD4 memory cells were found to be decreased in ESCC (Figure 1(a)). Particularly, macrophage M1, regulatory T cells (Tregs), and T helper 1 cells (Th1) were significantly infiltrated into ESCC tissues, and their corresponding marker genes were observed highly expressed in ESCC (Figure 1(b)). These results indicated that the immune cells were highly coinfiltrated into the ESCC tissues, and the ESCC tissues exhibited an inflammatory phenotype.

3.2. The Association between Tumor-Infiltrating Immune Cells and Response of Preoperative Chemoradiotherapy (CRT). As the immune cells were associated with the response of drug treatment, we collected the gene expression data of responders and nonresponders of preoperative CRT. The differential analysis revealed that infiltrating levels of macrophage M2 and resting natural killer (NK) cells were increased in nonresponder ESCC tissues (Figures 2(a) and 2(b), Wilcoxon rank-sum test, $P < 0.05$), suggesting that macrophage M2 and resting NK cells might be associated with the resistance of CRT. In contrast, the T cells that had anticancer activities such as activated memory CD4 and T helper 2 (Th2) cells were significantly reduced in ESCC tissues of the nonresponders, suggesting that these cells mediated anticancer activity might promote the sensitivity of CRT in ESCC. These results revealed that the tumor-infiltrating levels of immune cells were closely associated with the response of CRT in ESCC.

3.3. Immune Subtypes of ESCC Samples. As the ESCC samples exhibited variable infiltrating levels of immune cells due to intertumor heterogeneity, we classified the ESCC samples into three subgroups based on the infiltrating levels of immune cells by hierarchical clustering analysis. As shown in Figure 3(a), the subgroups II and III had significantly higher immune cell infiltrating levels than subgroup I. The survival analysis revealed that subgroup I had a better prognosis than the other two subgroups (Figure 3(b)), suggesting that the high infiltration of immune cells might be associated with poor prognosis. Particularly, high infiltrations of the resting natural killer (NK) and dendritic cell (DC) were observed to result in a shorter overall survival in ESCC (Figures 3(c) and 3(d)). These results indicated that the immune profiles were significantly different and associated with overall survival in ESCC samples.

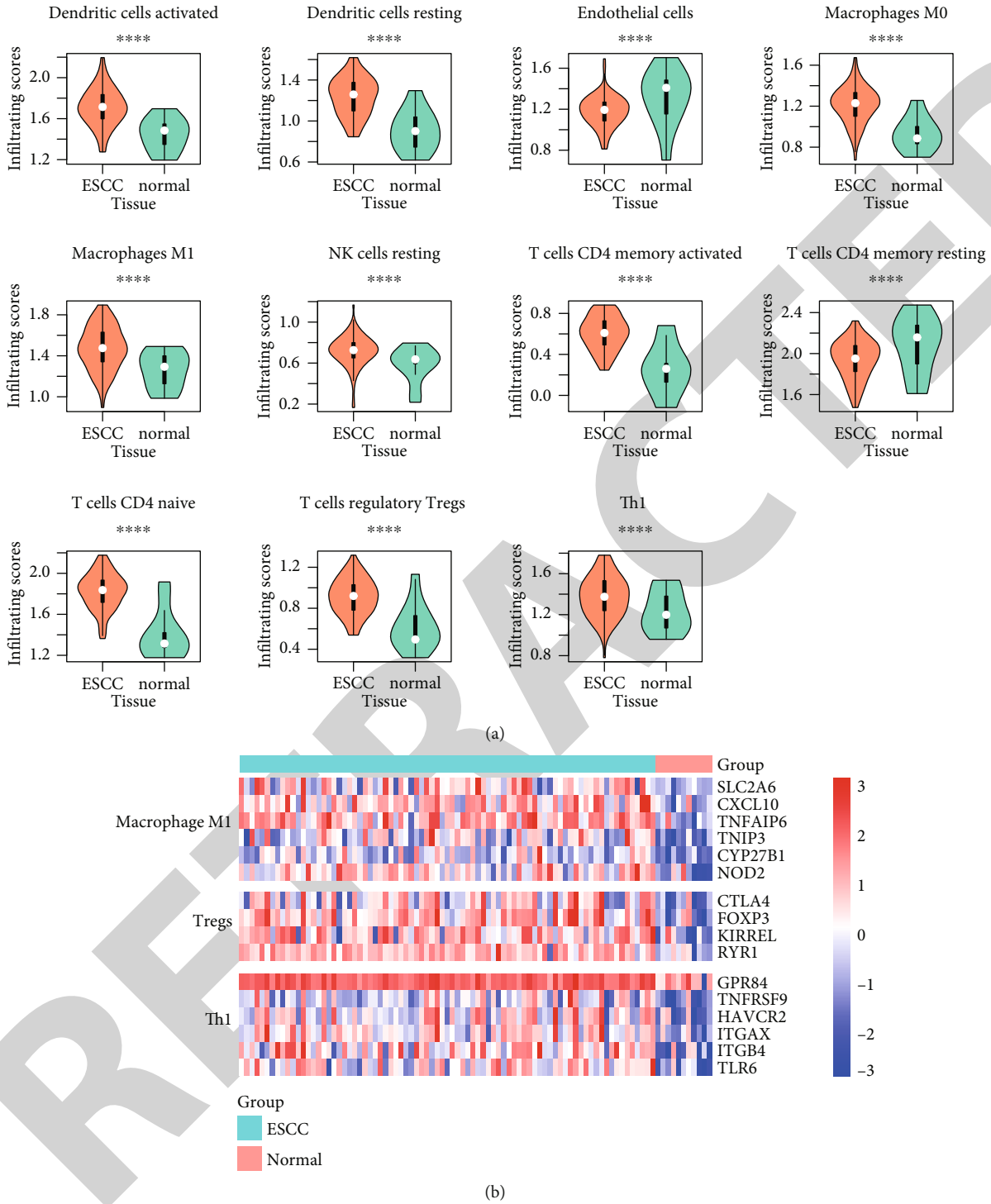

Figure 1: The differentially infiltrating levels of immune cells between ESCC and adjacent normal tissues. (a) The differentially infiltrating immune cells and their infiltrating levels in ESCC and normal tissues. (b) The expression patterns of marker genes in macrophage M1, Tregs, and Th1. The expression levels were scaled at -3 to 3. $^{****}P < 0.0001$.

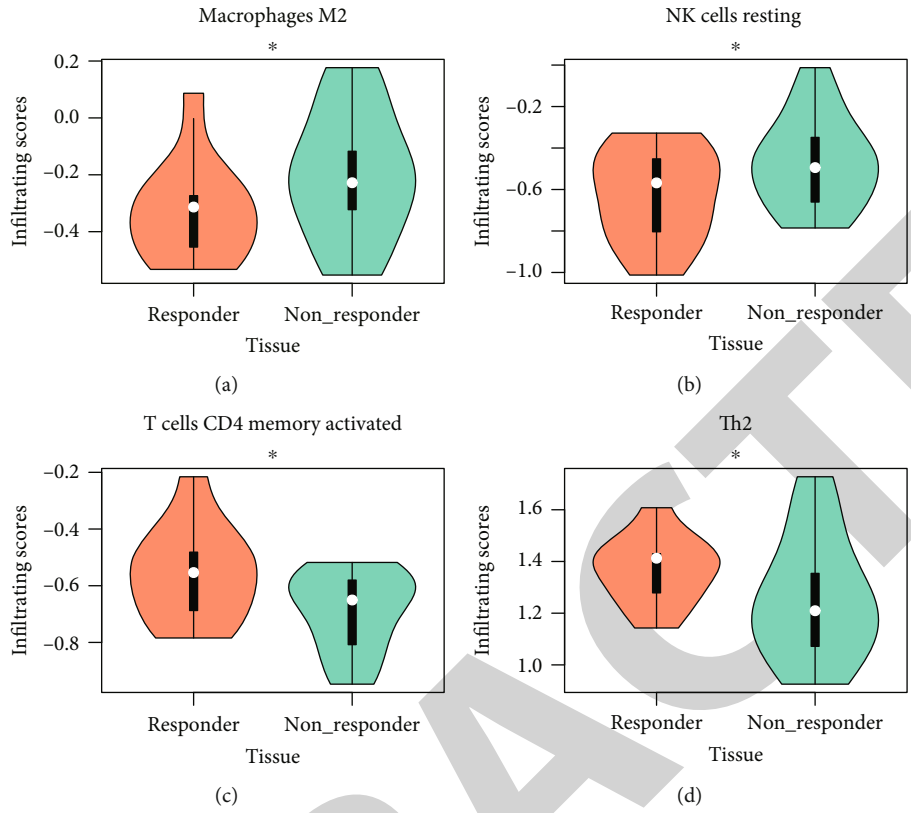

Figure 2: The immune cells associated with the response of chemoradiotherapy. The infiltrating levels of macrophage M2, resting NK cells, activated memory CD4 cells, and Th2 are displayed in (a–d). $^{*}P < 0.05$.

3.4. The Immune Checkpoints in ESCC. As the inflammatory phenotypes were observed in ESCC, we attempted to examine whether the immune checkpoints were associated with the immune evasion in ESCC. Based on the three immune subgroups in ESCC, we found that CTLA4 and HAVCR2 (TIM-3) were significantly upregulated in subgroups II and III (Figures 4(a) and 4(b)). CTLA4 and TIM-3 were well-known regulators of inhibiting the anticancer activity of immune cells. These results indicated that the immune checkpoint inhibitors might be applied to the treatment of ESCC samples with higher infiltration of immune cells.

3.5. The Downregulated Genes and Pathways in ESCC. As the upregulated signatures were characterized by the inflammatory phenotypes in ESCC, we then investigated the downregulated genes and pathways. We found that the synthesis and metabolic activity-related pathways were significantly attenuated in ESCC (Figure 5(a)). Furthermore, we also found the STAT5B, a key transcription factor involved in the regulation of T cells, was significantly downregulated in ESCC, especially subgroup I (Figure 5(b)). Consistently, the lower expressions were observed in target genes of STAT5B such as ENPP2, TAL1, CD247, SLAMF1, IRF4, BATF, and IRF8. These results indicated that downregulation of STAT5B might be associated with reduced T cell-mediated anticancer activity.

4. Discussion

Tumor-infiltrating immune cells play a role in the regulation of tumor progression and are often found in esophageal squamous cell carcinoma (ESCC). However, the landscape of immune cell infiltrating in ESCC still remains largely unveiled. In this study, we estimated the infiltrating levels of immune cells in 81 ESCC and 11 adjacent normal tissues. Macrophage M1, regulatory T cells (Tregs), and T helper 1 cells (Th1) were significantly infiltrated into ESCC tissues, and their corresponding marker genes were observed highly expressed in ESCC (Figure 1(b)). Particularly, Tregs and Th1 were dysregulated and contributed to the initiation and propagation in ESCC [18]. The high infiltration of these cells showed that the functionalities of these immune cells might be impaired in ESCC. As the immune cells were associated with the response of drug treatment [19], we observed that infiltrating levels of macrophage M2 and resting natural killer (NK) cells were increased in nonresponders of CRT, and T cells that had anticancer activities such as activated memory CD4 and T helper 2 (Th2) cells were significantly reduced in ESCC tissues of the nonresponders. In accordance with these results, M2 has been found to result in poor response of chemotherapy [20], and increased infiltration of activated memory CD4 in ESCC patients with chemoradiotherapy was a favorable indicator of ESCC prognosis [21].

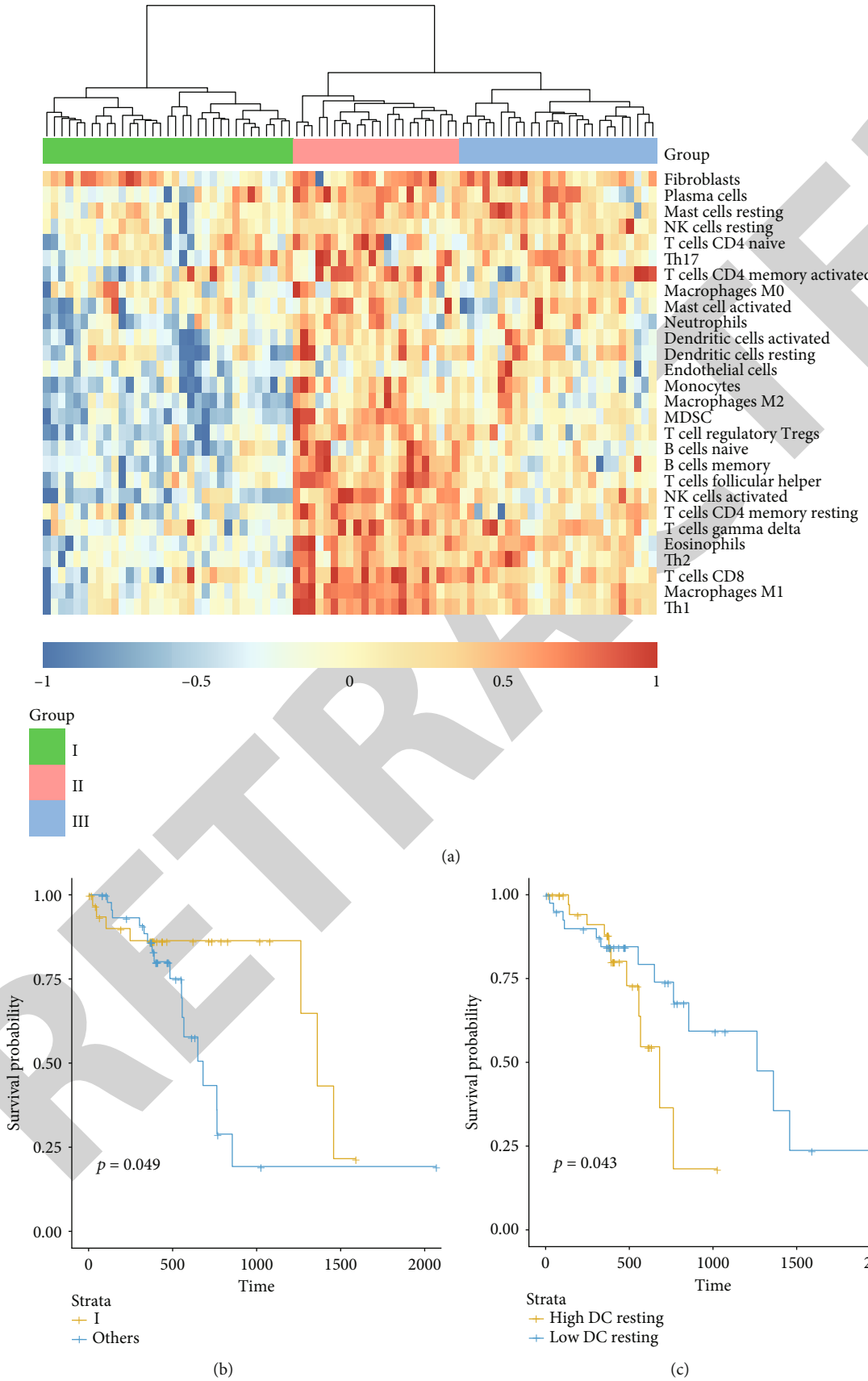

Figure 3: Continued.

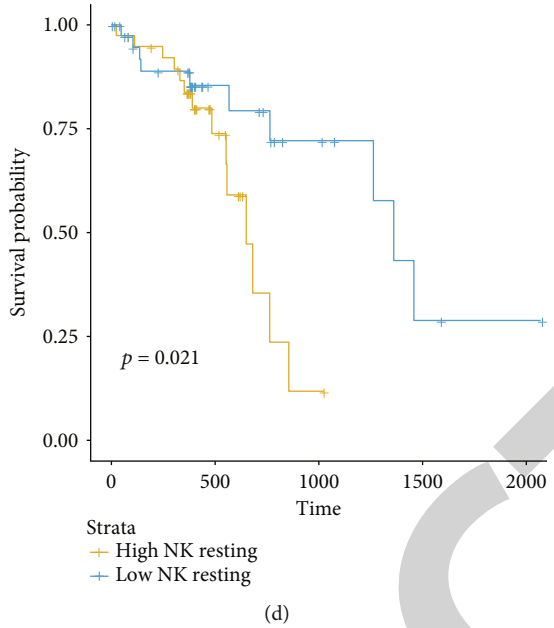

Figure 3: The immune subtypes and clinical significance in ESCC. (a) The hierarchical clustering of the ESCC samples by the infiltrating levels of immune cell. (b) The prognostic difference between subtypes I and others. (c, d) The prognostic significance of resting DC and NK cells, respectively.

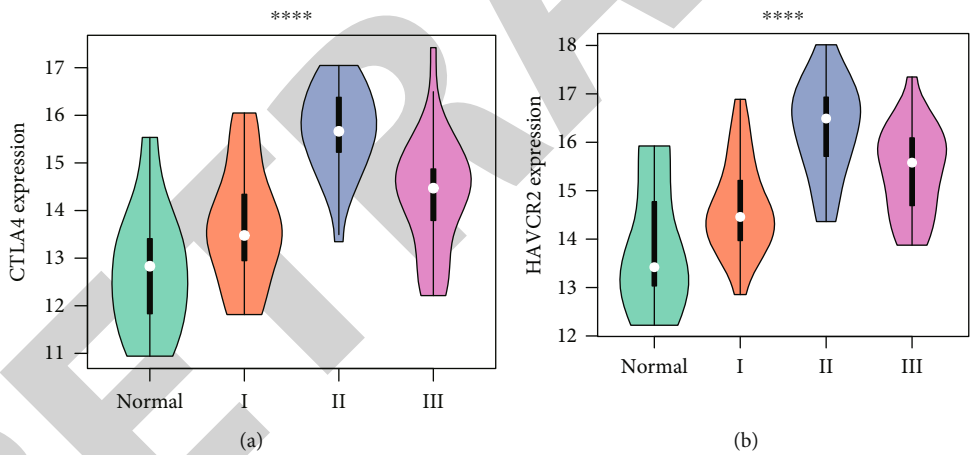

Figure 4: The expression patterns of immune checkpoint genes in the immune subtypes. The upregulations of two immune checkpoint genes, CTLA4 and HAVCR2 (TIM-3), in subtypes II and III are displayed in (a, b), respectively. $^{****}P < 0.0001$.

As the ESCC samples exhibited variable infiltrating levels of immune cells due to intertumor heterogeneity, we found that the ESCC samples could be classified into three subgroups based on the infiltrating levels of immune cells. The worse prognosis in patients with high infiltration of immune cells was also observed by previous study [22]. Particularly, high infiltrations of the resting natural killer (NK) and dendritic cell (DC) were observed to result in a shorter overall survival in ESCC (Figures 3(c) and 3(d)). The attenuated cytotoxicity in NK and DC might be the cause of poor prognosis. Notably, CTLA4 and HAVCR2 (TIM-3) were significantly upregulated in subgroups II and III (Figures 4(a) and 4(b)). High expression of CTLA4 and HAVCR2 was associated with poor prognosis [23, 24], and the two proteins might be the potential immunotherapeutic targets in ESCC [25].

As the upregulated signatures were characterized by the inflammatory phenotypes in ESCC, we found that the synthesis and metabolic activity-related pathways were significantly attenuated in ESCC, suggesting that the normal function of esophagus might be impaired [26, 27]. Furthermore, we also found the STAT5B, a key transcription factor involved in the regulation of T cells, was significantly downregulated in ESCC, especially subgroup I (Figure 5(b)). Consistently, the lower expressions were observed in target genes of STAT5B such as ENPP2, TAL1, CD247, SLAMF1, IRF4,

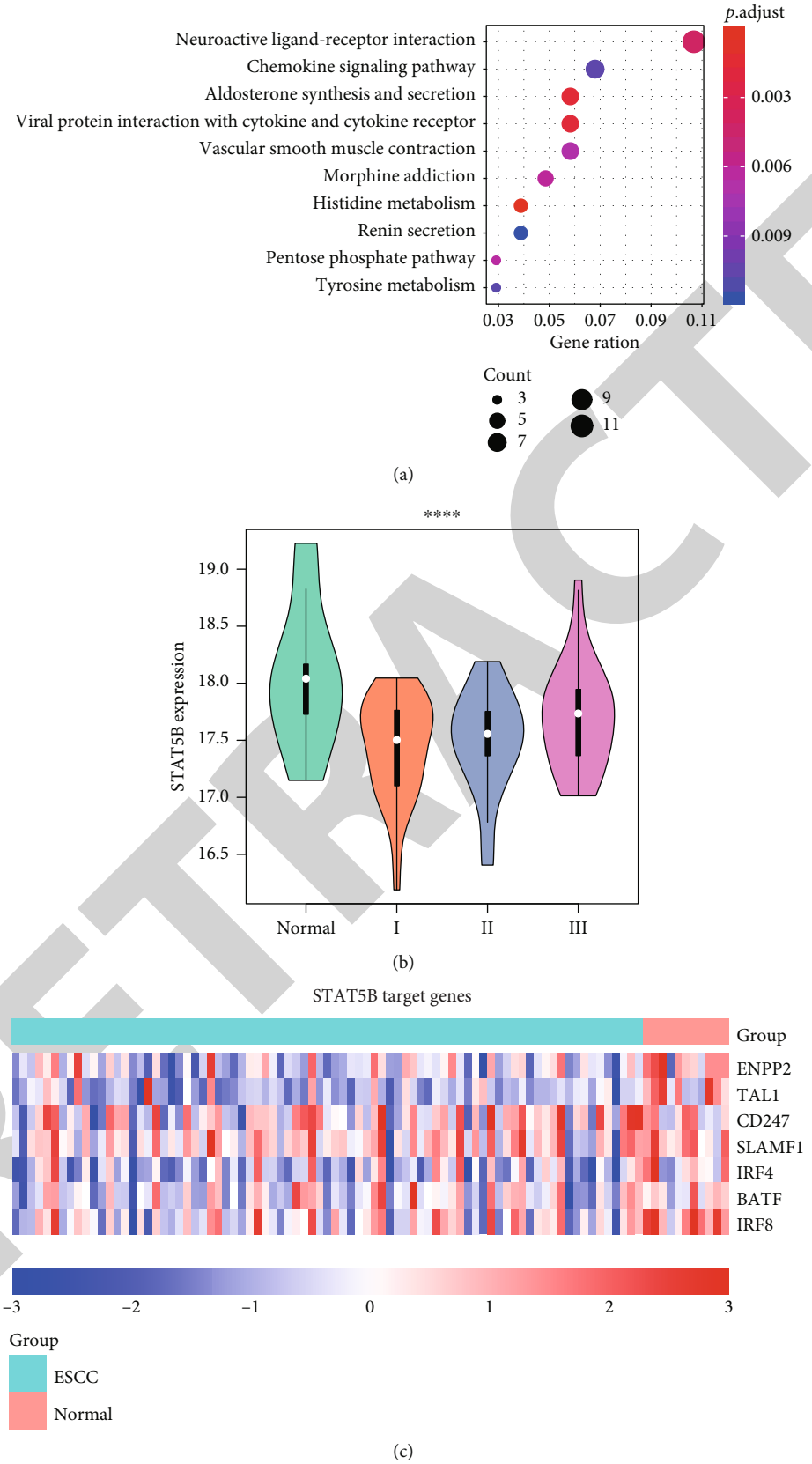

Figure 5: The aberrantly inactivated pathways in ESCC. (a) The pathways enriched by downregulated genes in ESCC. The node size represents the number of genes included in the pathway, and the node color represents the statistical significance. (b) The STAT5B expression pattern in normal tissues and immune subtypes. (c) The downregulated target genes of STAT5B. $^{****}P < 0.0001$.

BATF, and IRF8, indicating that downregulation of STAT5B might be associated with reduced T cell-mediated anticancer activity.

There are some limitations in our study. First, it lacks the validation by our own data. Second, in vitro and in vivo experiments are still needed to validate.

In summary, the present study systematically characterized the immune cells infiltrated in the ESCC tissues and identified some key immune cells associated with CRT, and key regulators implicated in ESCC.

Data Availability

All the data can be downloaded from the Cancer Genome Atlas (TCGA) and Gene Expression Omnibus (GEO) with accession GSE45670.

Conflicts of Interest

The authors declare that they have no conflicts of interest.

Acknowledgments

This research was supported by the Fundamental Research Funds for the Central Universities (Grant No. 3332020078).

References

[1] Y. Sasaki, M. Tamura, R. Koyama, T. Nakagaki, Y. Adachi, and T. Tokino, "Genomic characterization of esophageal squamous cell carcinoma: insights from next-generation sequencing," *World Journal of Gastroenterology*, vol. 22, no. 7, pp. 2284–2293, 2016.

[2] E. O. Then, M. Lopez, S. Saleem et al., "Esophageal cancer: an updated surveillance epidemiology and end results database analysis," *World journal of oncology*, vol. 11, no. 2, pp. 55–64, 2020.

[3] L. S. Engel, W. H. Chow, T. L. Vaughan et al., "Population attributable risks of esophageal and gastric cancers," *Journal of the National Cancer Institute*, vol. 95, no. 18, pp. 1404–1413, 2003.

[4] E. Shacter and S. A. Weitzman, "Chronic inflammation and cancer," *Oncology (Williston Park)*, vol. 16, no. 2, pp. 217–226, 2002.

[5] S. I. Grivennikov, F. R. Greten, and M. Karin, "Immunity, inflammation, and cancer," *Cell*, vol. 140, no. 6, pp. 883–899, 2010.

[6] J. J. Zhao, Z. Q. Zhou, P. Wang et al., "Orchestration of immune checkpoints in tumor immune contexture and their prognostic significance in esophageal squamous cell carcinoma," *Cancer Management and Research*, vol. Volume 10, pp. 6457–6468, 2018.

[7] K. Chen, Z. Zhu, N. Zhang et al., "Tumor-infiltrating CD4+ lymphocytes predict a favorable survival in patients with operable esophageal squamous cell carcinoma," *Medical science monitor: international medical journal of experimental and clinical research*, vol. 23, pp. 4619–4632, 2017.

[8] L. Han, Q. L. Gao, X. M. Zhou et al., "Characterization of CD103(+) CD8(+) tissue-resident T cells in esophageal squamous cell carcinoma: may be tumor reactive and resurrected by anti-PD-1 blockade," *Cancer Immunology, Immunotherapy*, vol. 69, no. 8, pp. 1493–1504, 2020.

[9] K. Hatogai, S. Kitano, S. Fujii et al., "Comprehensive immunohistochemical analysis of tumor microenvironment immune status in esophageal squamous cell carcinoma," *Oncotarget*, vol. 7, no. 30, pp. 47252–47264, 2016.

[10] J. Kim, R. Bowlby, A. J. Mungall et al., "Integrated genomic characterization of oesophageal carcinoma," *Nature*, vol. 541, no. 7636, pp. 169–175, 2017.

[11] M. Goldman, B. Craft, M. Hastie et al., "Visualizing and interpreting cancer genomics data via the Xena platform," *Nature Biotechnology*, vol. 38, no. 6, pp. 675–678, 2020.

[12] X. Shi, T. Huang, J. Wang et al., "Next-generation sequencing identifies novel genes with rare variants in total anomalous pulmonary venous connection," *eBioMedicine*, vol. 38, pp. 217–227, 2018.

[13] J. Wen, H. Yang, M. Z. Liu et al., "Gene expression analysis of pretreatment biopsies predicts the pathological response of esophageal squamous cell carcinomas to neo-chemoradiotherapy," *Annals of oncology: official journal of the European Society for Medical Oncology*, vol. 25, no. 9, pp. 1769–1774, 2014.

[14] S. Hanzelmann, R. Castelo, and J. Guinney, "GSVA: gene set variation analysis for microarray and RNA-seq data," *BMC Bioinformatics*, vol. 14, no. 1, 2013.

[15] C. Gu, Z. Huang, X. Chen et al., "TEAD4 promotes tumor development in patients with lung adenocarcinoma via ERK signaling pathway," *Biochimica et Biophysica Acta - Molecular Basis of Disease*, vol. 1866, no. 12, p. 165921, 2020.

[16] G. Yu, L. G. Wang, Y. Han, and Q. Y. He, "clusterProfiler: an R package for comparing biological themes among gene clusters," *Omics: a journal of integrative biology*, vol. 16, no. 5, pp. 284–287, 2012.

[17] C. Gu, X. Shi, Z. Huang et al., "A comprehensive study of construction and analysis of competitive endogenous RNA networks in lung adenocarcinoma," *Biochim Biophys Acta Proteins Proteom*, vol. 1868, no. 8, p. 140444, 2020.

[18] H. Samiei, B. Sadighi-Moghaddam, S. Mohammadi et al., "Dysregulation of helper T lymphocytes in esophageal squamous cell carcinoma (ESCC) patients is highly associated with aberrant production of miR-21," *Immunologic Research*, vol. 67, no. 2-3, pp. 212–222, 2019.

[19] L. Bracci, G. Schiavoni, A. Sistigu, and F. Belardelli, "Immune-based mechanisms of cytotoxic chemotherapy: implications for the design of novel and rationale-based combined treatments against cancer," *Cell Death and Differentiation*, vol. 21, no. 1, pp. 15–25, 2014.

[20] K. Sugimura, H. Miyata, K. Tanaka et al., "High infiltration of tumor-associated macrophages is associated with a poor response to chemotherapy and poor prognosis of patients undergoing neoadjuvant chemotherapy for esophageal cancer," *Journal of Surgical Oncology*, vol. 111, no. 6, pp. 752–759, 2015.

[21] X. Chen, W. Zhang, D. Qian et al., "Chemoradiotherapy-induced CD4(+) and CD8(+) T-cell alterations to predict patient outcomes in esophageal squamous cell carcinoma," *Frontiers in Oncology*, vol. 9, p. 73, 2019.

[22] Y. Li, Z. Lu, Y. Che et al., "Immune signature profiling identified predictive and prognostic factors for esophageal squamous cell carcinoma," *Oncoimmunology*, vol. 6, no. 11, p. e1356147, 2017.

[23] B. Shan, H. Man, J. Liu et al., "TIM-3 promotes the metastasis of esophageal squamous cell carcinoma by targeting epithelial-mesenchymal transition via the Akt/GSK-3β/Snail signaling

Hindawi
BioMed Research International
Volume 2024, Article ID 9769323, 1 page
https://doi.org/10.1155/2024/9769323

Retraction

Retracted: Curcumin Improves Pulmonary Hypertension Rats by Regulating Mitochondrial Function

BioMed Research International

Received 12 March 2024; Accepted 12 March 2024; Published 20 March 2024

This article has been retracted by Hindawi following an investigation undertaken by the publisher [1]. This investigation has uncovered evidence of one or more of the following indicators of systematic manipulation of the publication process:

(1) Discrepancies in scope

(2) Discrepancies in the description of the research reported

(3) Discrepancies between the availability of data and the research described

(4) Inappropriate citations

(5) Incoherent, meaningless and/or irrelevant content included in the article

(6) Manipulated or compromised peer review

The presence of these indicators undermines our confidence in the integrity of the article's content and we cannot, therefore, vouch for its reliability. Please note that this notice is intended solely to alert readers that the content of this article is unreliable. We have not investigated whether authors were aware of or involved in the systematic manipulation of the publication process.

Wiley and Hindawi regrets that the usual quality checks did not identify these issues before publication and have since put additional measures in place to safeguard research integrity.

We wish to credit our own Research Integrity and Research Publishing teams and anonymous and named external researchers and research integrity experts for contributing to this investigation.

The corresponding author, as the representative of all authors, has been given the opportunity to register their agreement or disagreement to this retraction. We have kept a record of any response received.

References

[1] J. Chen, W. Jiang, F. Zhu, Q. Wang, H. Yang, and J. Wu, "Curcumin Improves Pulmonary Hypertension Rats by Regulating Mitochondrial Function," *BioMed Research International*, vol. 2021, Article ID 1078019, 10 pages, 2021.

Hindawi
BioMed Research International
Volume 2021, Article ID 1078019, 10 pages
https://doi.org/10.1155/2021/1078019

Research Article

Curcumin Improves Pulmonary Hypertension Rats by Regulating Mitochondrial Function

Jing Chen,[1] Wen Jiang,[2] Fei Zhu,[1] Qiong Wang,[1] Haiyan Yang,[3] and Jinhua Wu[2]

[1]*Department of Pharmaceutics, Zhoushan Women and Children Hospital, 316000, Zhoushan, Zhejiang Province, China*
[2]*Department of Teaching & Research, Zhoushan Women and Children Hospital, 316000, Zhoushan, Zhejiang Province, China*
[3]*Department of Internal Medicine, Zhoushan Women and Children Hospital, 316000, Zhoushan, Zhejiang Province, China*

Correspondence should be addressed to Jinhua Wu; wujinhua7611@163.com

Received 13 June 2021; Revised 19 July 2021; Accepted 11 August 2021; Published 30 August 2021

Academic Editor: Chang Gu

Objective. To investigate the role of curcumin in regulating pathogenesis of pulmonary arterial smooth muscle cells (PASMCs) derived from pulmonary arterial hypertension (PAH) model. *Methods*. Male Sprague Dawley rats were injected with monocrotaline (MCT) to establish the PAH experimental model. The rats were divided into control group, MCT group, and curcumin group. At the end of the study, hemodynamic data were measured to determine pulmonary hypertension. Proliferation ability of PASMCs, a remodeling indicator of pulmonary artery and right ventricle, was detected. In addition, the morphology and function of mitochondria, antiglycolysis and antiproliferation pathways, and genes were also analyzed. *Results*. Curcumin may function by reversing MCT-mediated pulmonary vascular remodeling in rats. Curcumin effectively improved pulmonary vascular remodeling, promoted PASMC apoptosis, and protected mitochondrial function. In addition, curcumin treatment suppressed the PI3K/AKT pathway in PASMCs and regulated the expression of antiproliferative genes. *Conclusion*. Curcumin can improve energy metabolism and reverse the process of PAHS. However, there were side effects of curcumin in MCT-induced rats, suggesting that the dosage should be treated with caution and its toxicological mechanism should be further studied and evaluated.

1. Introduction

Pulmonary arterial hypertension (PAH) is determined by alterations of pulmonary vascular function and structure caused by a variety of factors, leading to a progressive increase in pulmonary vascular resistance. Subsequently, it leads to a clinicopathological syndrome characterized by right ventricular remodeling and right heart failure [1]. The prevalence rate of PAH of all kinds has exceeded 30~50 per 1 million people, making it one of the most important diseases endangering human beings [2]. Despite the improvement of modern drugs and treatment methods, the prognosis of PAH patients is still poor, and the annual mortality rate of 2.5% for females and 0.9% for males has been maintained in the past ten years [3]. Current studies have shown that the degree of increased pulmonary artery pressure is only moderately correlated with clinical prognosis. The functional state of the right ventricle is an independent predictor of clinical symptoms and survival prognosis [4, 5]. Clinical studies have confirmed that different patients show significantly different right ventricular adaptive response and clinical prognosis in response to the same pulmonary vascular resistance [6]. Therefore, it is of great clinical significance to maintain effective right ventricular structure and function. At present, the clinical understanding of right ventricular remodeling mechanism and drug therapy is mainly derived from the left ventricle. Surprisingly, classic drugs that inhibit left ventricular remodeling and left heart failure cannot effectively improve or reverse the right ventricular function and improve the survival rate in PAH patients [7]. It suggests that there are still other mechanisms for right ventricular remodeling and occurrence and development of heart failure. Unfortunately, there is still a lack of an effective and recognized right ventricular specific treatment strategy in clinical practice [8], which is mainly due to the long-term neglect of the importance of

right ventricular in PAH course development and the incomplete clarification of the exact mechanism of PAH right ventricular remodeling. An in-depth study of the cellular and molecular mechanisms of PAH right ventricular remodeling has important scientific significance and clinical value for the prevention and treatment of right heart failure and the reversal of functions [9].

Mitochondria are the "power factories" of cells, providing 80% of the energy needed for cell life and play an important role in cell metabolism and physiological processes. It is worth noting that basically all PAH pathological processes seem to be unrelated, and molecules with abnormal expression can be explained by abnormal mitochondrial function. Only cell proliferation and apoptosis are balanced to maintain normal biologic states, while the mitochondria of PAH patients exhibited an antiapoptotic and overproliferative effect in pulmonary artery smooth muscle cell (PASMC), leading to pulmonary vascular remodeling. At the same time, PASMC of PAH patients is also enhanced in the condition of constant oxygen, and mitochondrial function is inhibited, which are strikingly similar to tumor cells [10]. In addition, when PAH occurs, there are molecular markers of tumor cells on the blood vessels, which have been proved to play an important role in the pathological process of PAH [11]. More and more studies have found that various pathological manifestations of PAHS can be explained by the metabolic theory originally used for tumors, and mitochondrial abnormalities are the core of this theory [12]. PASMC also has the characteristic of enhanced glycolysis reaction of tumor cells. Pyruvate dehydrogenase kinase (PDK) plays an important role in PAH generation. PDK prevents pyruvate from entering mitochondria to participate in the Krebs cycle, and insufficient electron production in mitochondrial electron transport chain results in reduced mROS production [13]. At the same time, enhanced glycolysis also promoted pyruvate synthesis of amino acids needed for excessive cell proliferation in the cytoplasm. This mechanism was beneficial to overproliferated cells and promoted pulmonary vascular remodeling.

Curcumin is a kind of fat-soluble phenolic pigment extracted from the traditional Chinese medicine curcuma, which is widely used as food additive. A large number of studies have shown that curcumin has anti-inflammatory, antioxidant, antiviral, scavenging oxygen free radicals, antifibrosis, anticoagulation, lipid regulation, and other pharmacological effects. Curcumin has been paid more and more attention by medical workers at home and abroad because of its low toxicity and good safety [14–16]. Curcumin can significantly reduce aortic injury and neovascularization thickness. Curcumin reduces the expression of CD36 circulating inflammatory factors (IL-1, TNF-α, and CRP), intracellular adhesion molecules, vascular cell adhesion molecules, P-selectivity, monocyte chemoattractant protein 1, and mRNA induced by high-fat diet. The study found that low-density lipoprotein gene knockout mice significantly improved early atherosclerosis lesions and lipid exudation in the aortic arch after 18 weeks of long-term curcumin feeding. Curcumin reduces plasma lipid levels, including apolipoprotein B and cholesterol ester transfer protein, and increases the expression of high-density lipoprotein and liver apolipoprotein A1 [17]. Chen et al. investigated the potential effect of curcumin on hypertrophy of cardiomyocytes and the possible mechanism, and the results showed that curcumin inhibited hyperglycemic and insulin-induced cardiac hypertrophy through the PPAR/AKT/NO signaling pathway [18]. In addition, curcumin has other pharmacological effects, such as antifibrosis, neuroprotective effect, promoting wound healing, and reversing multidrug resistance (MDR) of cancer cells. Wang et al. showed that intraperitoneal injection of curcumin could significantly reduce bleomycin-induced pulmonary inflammation and fibrosis response [19]. The mechanism was that curcumin could effectively reduce normal lung tissue and primary pulmonary fibrosis and fibrosis promoting factors and reduce collagen deposition by inhibiting transforming growth factor B. However, the regulation mechanism of curcumin on pulmonary hypertension is still unclear.

It has not been reported whether curcumin inhibits HPA through improving mitochondrial metabolism in hypoxia-induced pulmonary hypertension (HPH) disease model. In this study, through the establishment of HPA rat model and hypoxia PASMC model, the effect mechanism of curcumin on HPA through the regulation of mitochondrial pathway was explored. The purpose of this study was to investigate the role of curcumin in regulating PASMC proliferation and apoptosis, so as to reverse PAH by improving mitochondrial metabolism. This may contribute to the clinical application of curcumin as a new therapeutic agent.

2. Methods

2.1. Grouping and Treatment of Experimental Animals. Eighteen male SD rats were randomly divided into three groups: normal control group, MCT group, and curcumin group ($30\,mg{\cdot}kg^{-1}$) administrated by gavage. MCT was given with $50\,mg{\cdot}kg^{-1}$ by subcutaneous injection in one time to prepare the rat pulmonary hypertension model. The animals were given the same dose of saline once a day for 18 consecutive days in the normal group and the model group, and their weight was recorded daily.

The end point was 25 days. The animals were anesthetized with isoflurane and fixed, and the relevant physiological and biochemical indexes such as hemodynamics, organ index, pulmonary inflammatory factors, and immunohistochemistry were measured. For separating and building of rat endothelial cell line, the SD rats were disinfected and anesthetized, and their lung small arteries were isolated from the lung tissues and then treated with 1 mL 0.2% collagenase digestion. I treat lung small artery after digestion of floc centrifugal fragments, to the upper collagenase after joining medium placed at 37°C and 5% CO_2 cultivation in the box. PASMCs of primary generation were obtained after 3 days, and cells were collected for experiment after cell passage to 4~6 generations. Cell starvation for 12 h synchronizes the cell cycle, followed by intervention.

2.2. Cell Activity Was Detected by CCK-8. PASMCs were prepared into single-cell suspension and inoculated into 96-well plates, incubated in a constant temperature incubator for

24 h. The grouping method was the same as before. Each group had 6 holes, and blank groups without cells were set around them, and the corresponding incubator was placed for culture. At the end of the intervention, the medium and CCK-8 reagent are added to each well, and the medium is placed in the incubator in a short time to avoid light, and the absorbance of each hole is set at 450 nm after 1~2 h.

2.3. Pulmonary Artery Pressure and Right Cardiac Hypertrophy Measurement. SD rats were anesthetized with isoflurane, and the right external jugular vein was separated after fixation, and the pressure tube was intubated into the pulmonary artery. The mean pulmonary artery pressure (mPAP) of every rat was measured by the physiological recorder [6]. Rats were bleeding to death, and full heart is removed, a complete separation of the right ventricle (right ventricle, RV) and left ventricle and the interventricular septum (left ventricle plus septum, LV + *S*). After being drained and weighed, the right cardiac hypertrophy index (RVHI) = [RV/(LV + *S*)] was recorded and calculated to reflect the condition of right cardiac hypertrophy.

2.4. Detection of Pulmonary Vascular Remodeling Index. The upper lobe of the right lung of rats was fixed in 4% paraformaldehyde for 24 h, and the lung tissues were embedded in paraffin for HE staining. The prepared HE staining sections were observed under a common light microscope, and the small pulmonary arteries in 6 different visual fields were randomly selected to be photographed. The Image-pro Plus 6.0 Image analysis software was used to analyze the wall area to total area (WA/TA) of small and medium-sized pulmonary arteries to reflect the degree of pulmonary vascular structural remodeling.

2.5. Histological Morphology of Pulmonary Artery Was Determined by HE Staining. The left lung tissue of the rats was fixed on the foam board, and the lung tissue was cut with a scalpel 0.5 cm away from the tip of the lung, and the tissue was fixed in neutral formaldehyde for 24 h. After the tissue was removed, the rats were dehydrated with ethanol, embedded in paraffin, and sliced, and then, HE staining was performed. The pulmonary vascular morphology of each group was observed under an optical microscope. In addition, pulmonary artery with a diameter of about 100 μm was used for quantitative analysis of its morphology using the image analysis software. The ratio of the transection area of the vessel wall to the transection area of the vessel was used as an indicator to measure the remodeling of hypoxic pulmonary vessels.

2.6. Immunohistochemical Method Was Used to Detect Ki67 and Apoptosis-Related Proteins Bax and Caspase-3. The left lung tissue of the rats was fixed on the foam board with a pin, and the lung tissue was cut 0.5 cm from the tip of the lung with a scalpel. The pulmonary artery with a diameter of 100 m was isolated and exhaled. The pulmonary artery was fixed with 4% paraformaldehyde and embedded in paraffin, and sections with a thickness of 5 m were prepared for immunohistochemical staining. The slices were dewaxed, followed by the addition of primary antibody at 4°C overnight, followed by the addition of secondary antibody, and dehydrated to seal the slices. The number of positive cells of Ki67, Bax, and caspase-3 in 5 different fields was observed under an optical microscope and then analyzed statistically.

2.7. Detection of ATP Content. The tissue was made into 10% homogenate and centrifuged at 2000 × g for 10 min. The supernatant was centrifuged at 1000 × g for 15 min, and the protein was quantified by the Lowry method. The isolated mitochondria were made into suspension with cold homogenate medium, and the contents of ATP were determined.

2.8. Preparation of Electron Microscope Samples. The mice in each group were fixed by heart perfusion with 4% glutaraldehyde. The mice were quickly taken out and cut into 1 mm^3 small pieces and fixed in 4% glutaraldehyde electron microscope solution. According to the preparation procedure of electron microscope samples, the mice were rinsed, dehydrated, soaked, and embedded in epoxy resin. After ultrathin sections, the slices were fished to the copper net and then dried for lead and uranium double staining. The alterations of cell morphology and ultrastructure were observed under transmission electron microscope.

2.9. Serum LDH Level Detection. 1 ml mouse blood was obtained by eyeball blood sampling method, centrifuged at 3000 × g for 15 min, and the supernatant was stored in -80°C refrigerator. Serum LDH levels were analyzed by enzyme-linked immunosorbent assay (Roche company). The specific operation was carried out in strict accordance with the instructions of the kit. The OD value of 450 nm was recorded for drawing the standard curve and calculating the level of the sample to be measured.

2.10. Western Blot Was Used to Detect Protein Expression. Total protein of lung tissue samples and PASMCs was extracted from each group, and the total protein concentration was determined. 40 g cell protein samples and 60 g tissue protein samples were subjected to gel electrophoresis, transferred to PVDF membrane, sealed with skim milk, and incubated at 4°C overnight for primary antibody including p-AKT (abcam,1/1000) and p-PI3K (abcam, 1/1000). Incubate the secondary antibody after washing the next day, and run the imager for exposure after rinsing. Quantity One was used to determine the gray value of each strip, and GAPDH was taken as the internal reference. The ratio of the gray value of proteins in each group to the corresponding GAPDH was the relative expression quantity of the histone, and the expression difference of proteins in each group was compared.

2.11. Real-Time PCR (RT-PCR). Total cellular RNA was extracted using TRIzol and preserved in a -80°C refrigerator. The extracted RNA was subjected to reverse transcription using a cDNA first-strand synthesis kit (TaKaRa, PrimeScript RT Master Mix, RR036A). The reverse transcription synthesis was performed at 37°C for 15 min and 85°C for 5 s and finally preserved at 4°C. PCR amplification of the target genes and the internal reference GAPDH was carried out using SYBR Premix Ex Taq II, RR820A (Takara, Dalian, China). Primer sequences of PKM2 were as follows: forward:

5′-CTCTCACAGTTGAATGTCCTTG-3′ and reverse: 5′-CTCCTTGTCAGCAGAATGAAG-3′. Primer sequences of MCT1 were as follows: forward: 5′-AGAAGGCTGGGGCTCATTTG-3′ and reverse: 5′-AGGGGCCATCCACAGTCTTC-3′. Primer sequences of PTEN were as follows: forward: 5′-CTCTCACAGTTGAATGTCCTTG-3′ and reverse: 5′-ATCCGGTCAGCAGAATGAAG-3′. Primer sequences of SRC were as follows: forward: 5′-GGTCAATCGGCTCATTTG-3′ and reverse: 5′-GTGTCCATCCACAGTCTTC-3′. RT-PCR was conducted at 95°C for 30 s, 95°C for 5 s, and 60°C for 30 s, for a total of 40 cycles. Expression level of target gene was calculated by the 2–ΔΔCt method.

2.12. Statistical Analysis. The difference of indicators between 3 groups was analyzed by *t*-test and $P < 0.05$ indicated that the difference was statistically significant. The SPSS21.0 statistical software was used for analysis. Multigroup comparisons were performed by one-way ANOVA, and pairwise comparisons were performed by the LSD-t method.

3. Results

3.1. Curcumin Improves Vascular Remodeling. Right ventricular systolic pressure (RVSP) and mean pulmonary arterial pressure (mPAP) were significantly raised in MCT-induced rats but decreased after curcumin administration (Figures 1(a) and 1(b)). Furthermore, MCT-mediated pulmonary arterioles were observably remodeled. However, after curcumin delivery, this influence was significantly reduced by increasing the mean median thickness, lumen/total ratio, and pulmonary WT% ($P < 0.05$) as shown in Figures 1(c)–1(f). These results illustrate that curcumin may function by reversing MCT-mediated pulmonary vascular remodeling in rats.

3.2. Curcumin Can Improve Ventricular Function. Compared with the control group, RVHI in MCT group was observably higher but decreased after curcumin delivery (Figure 2(a)). In addition, after curcumin delivery, RV fibrosis was also uniformly reversed. In the MCT group, RV fibrosis was boosted compared with the control group, while curcumin group was reversed (Figure 2(b)). Of note, RV thickness and interventricular septum diameter (IVSD) boosted in the MCT group but decreased in the curcumin group ($P < 0.05$), as shown in Figures 2(c) and 2(d). Tricuspid annular plane systolic excursion (TAPSE), an indicator of RV systolic function, also improved after curcumin delivery. Compared with the control group, TAPSE decreased in the MCT group and boosted in the curcumin group (Figure 2(e)). Therefore, our results suggested that curcumin normalizes right ventricular function by reducing pulmonary artery pressure.

3.3. Curcumin Promotes Apoptosis of PASMC. To evaluate the influence of curcumin on PASMC proliferation, lung tissue sections were stained. The percentage of Ki67 positive cells around pulmonary artery in the MCT group was significantly boosted. However, this influence was reversed after curcumin administration ($P < 0.05$; Figure 3(a)). To further confirm the involved influence, PASMCs were isolated from all three groups for culture. The OD value of the MCT group was higher than that of the control group, while that of the curcumin group was lower than that of the MCT group ($P < 0.05$; Figure 3(b)), suggesting curcumin inhibited the proliferation of PASMC in PAH rat models.

In addition, lung tissue sections were stained to detect apoptotic markers Bax and caspase-3. Compared with the control group, the percentage of Bax and caspase-3 positive cells in the MCT group diminished, while that in the curcumin group triggered (both $P < 0.05$) as shown in Figures 3(c) and 3(d). Therefore, curcumin can markedly promote the apoptosis of PASMC in MCT-mediated PAH models.

3.4. Curcumin Improves Function of Mitochondrial. Morphological analysis showed that compared with the control group, MCT administration markedly reduced the number of normal mitochondria and triggered the number of mitochondrial fragments. After curcumin administration, the influence was weakened (Figures 4(a) and 4(b)). To assess mitochondrial function, ATP content in lung tissue was measured. The results showed that the ATP level in the MCT group was lower than that in the control group. However, the curcumin group triggered compared with the MCT group (Figure 4(c)). Serum LDH concentration was measured to further reflect the metabolic state. LDH in the MCT group was boosted compared with that in the control group, while that in the curcumin group was decreased (Figure 4(d)) and showed that curcumin markedly protected mitochondrial functions in MCT-induced PAH rat models.

3.5. Curcumin Inhibits the PI3K/AKT Pathway in PASMCs. Next, we investigated whether curcumin mediates the proliferation and apoptosis of PASMC by hindering the PI3K/AKT pathway. Compared with the control group, the expression of p-PI3K and p-AKT was augmented in the MCT group ($P < 0.05$). Compared with the MCT group, the expression of p-PI3K and p-AKT in the curcumin group was decreased (all $P < 0.05$; Figure 5(a)). These findings illustrate the curcumin PASMC proliferation inhibition by PI3K/AKT pathway.

3.6. Curcumin Mediated the Expression of Antiproliferative Genes in PASMCs. Compared with the control group, the relative expressions of PKM2, MCT1, and SRC in the MCT group were augmented, respectively, while PTEN was diminished (all $P < 0.05$). After curcumin administration, the protein levels of PKM2, MCT1, and SRC were suppressed while PTEN were diminished, respectively, compared with the MCT group ($P < 0.05$; Figures 5(b)–5(f)). These results indicated that curcumin could significantly induce the expression of antiglycolysis and antiproliferation genes in PASMCs.

4. Discussion

Changing the imbalance of proliferation/apoptosis of smooth muscle and endothelial cells has long been a key strategy to prevent vascular remodeling. There is evidence that promoting smooth muscle cell apoptosis under hypoxic exposure, such as artificially induced expression of smooth muscle cell tumor suppressor gene P27, can effectively improve vascular remodeling [20]. However, after administration of a

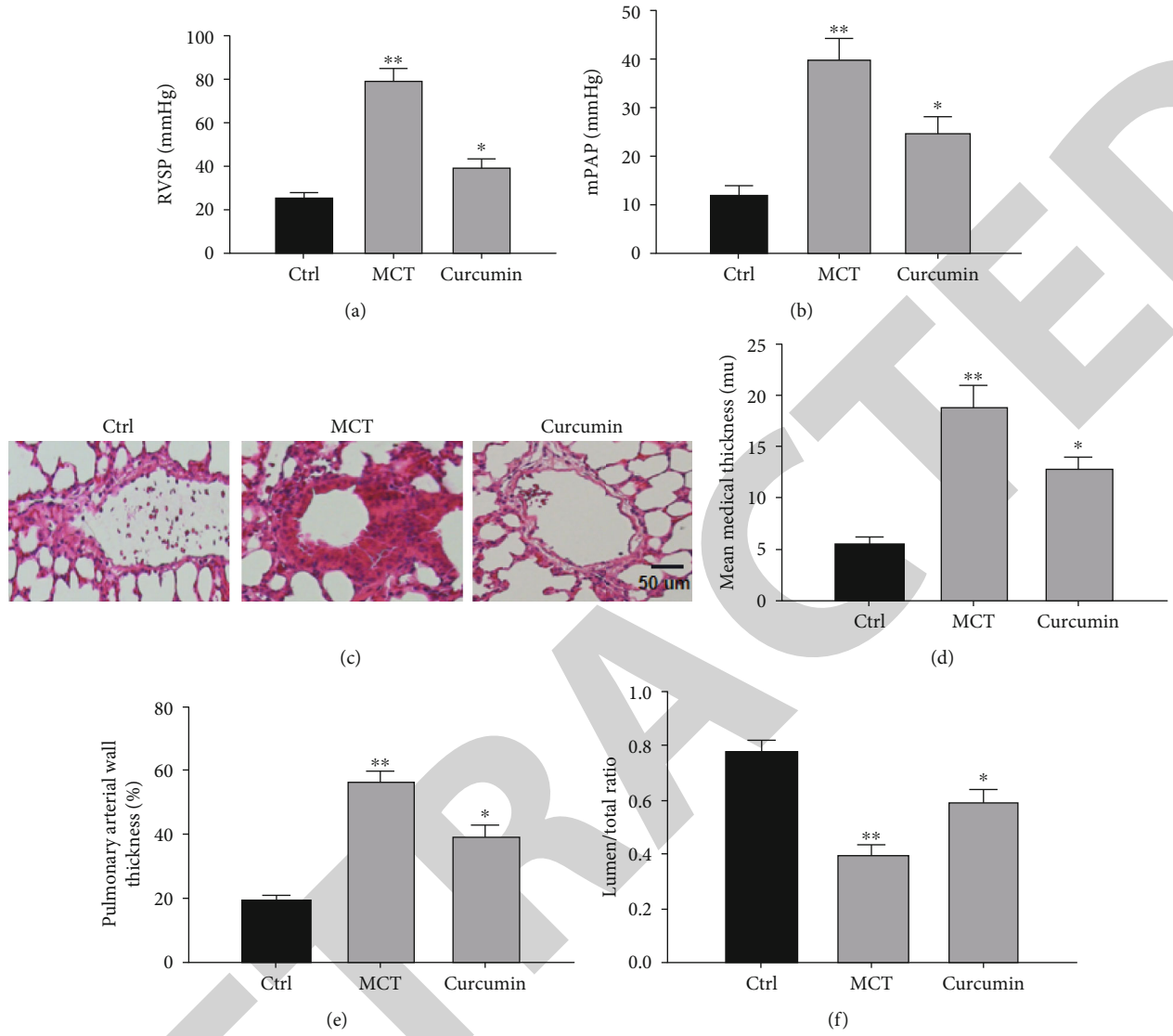

Figure 1: Curcumin improves vascular remodeling. (a) Data results of RVSP (mmHg). (b) Data results of mPAP. (c) Images of HE-stained sections from indicated groups. (d) Data results of artery media thickness. (e) Statistical analysis of pulmonary arterial wall thickness. (f) Data results of lumen of total ratio. $^{*}P < 0.05$ and $^{**}P < 0.01$. Magnification: 400x.

broad-spectrum inhibitor of caspase-3 in rats, hypoxia-induced apoptosis of endothelial cells was reduced and hypoxia-induced pulmonary vascular remodeling was significantly inhibited. Apoptosis of smooth muscle cells is involved in the reversal process of vascular remodeling. In the process of reoxygenation, the production of reactive oxygen species in cells increases and mediates cell apoptosis. After the removal of reactive oxygen species, its apoptosis can be significantly inhibited [20, 21]. Other pathways including activation of P53, inhibition of STAT3 pathway, inhibition of mitochondrial division, activation of autophagy, and inhibition of NLRP3 inflammasome activation can all inhibit hypoxia-induced smooth muscle cell proliferation and endothelial cell injury and improve vascular remodeling [22].

Herein, we demonstrate that curcumin significantly reduces pulmonary vascular remodeling in the rat model of pulmonary hypertension. Another recent study showed that curcumin treatment significantly restored mitochondrial structure, thereby inhibiting PAHs. Notably, we demonstrate that curcumin can improve mitochondrial metabolism, inhibit PASMC proliferation, promote apoptosis, and ultimately reduce pulmonary vascular remodeling and RV dysfunction. In addition, we found that curcumin plays a protective role in PAH by inhibiting the PI3K/AKT pathway. In terms of molecular mechanism, curcumin treatment attenuates the expression of antiglycolysis and antiproliferation genes mediated by MCT treatment.

In recent years, mitochondria have attracted much attention as a research hotspot. Mitochondria not only serve as an energy factory, but also as a transfer station for the collection and transmission of various intracellular signals, which are widely involved in cell autophagy, inflammatory response, proliferation/apoptosis, and other cellular biological processes. Under hypoxic exposure, the mitochondrial structure

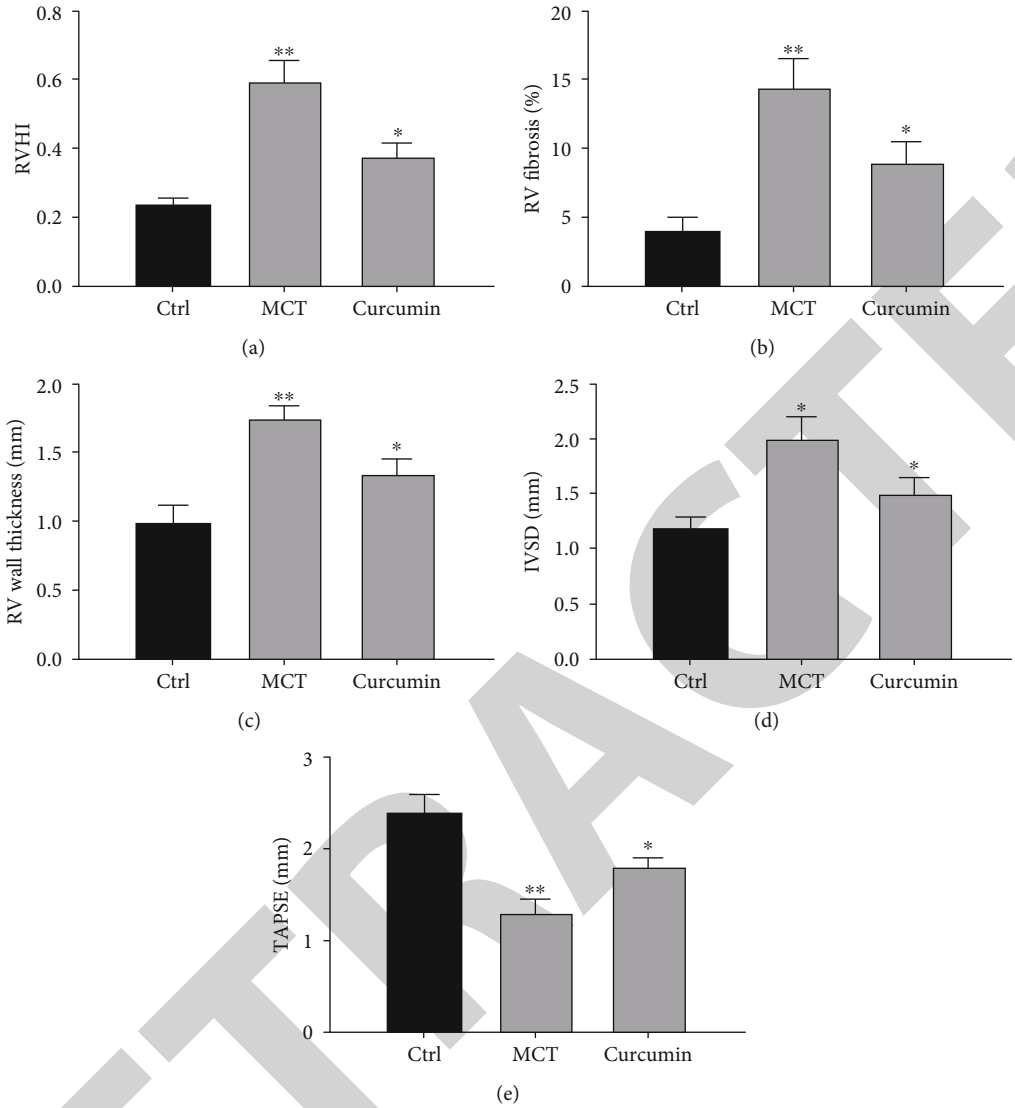

Figure 2: Curcumin can improve ventricular function. (a) RVHI was the ratio of RV weight to LV + S weight, RV was stained with picrosirius red and analyzed. (b) Data results of RV fibrosis. (c) Data results of RV wall thickness. (d) Statistical analysis of IVSD. (e) Data results of apical four chamber notch. $^{*}P < 0.05$ and $^{**}P < 0.01$.

and function of endothelial cells and smooth muscle cells were abnormally changed. Smooth muscle cells in vascular remodeling exhibit malignant proliferation similar to cancer cells. Even in the presence of sufficient oxygen, mitochondrial aerobic oxidation is inhibited and glycolytic metabolism is enhanced. Mitochondrial membrane potential and mitochondrial oxygen free radical were also changed. A series of abnormalities in mitochondria can activate downstream-related pathways, thereby activating the transcription of proliferation-related genes and promoting cell proliferation [23, 24]. Reduced concentration of mitochondrial calcium can inhibit the activity of Ca2+-dependent enzymes in mitochondria, including pyruvate dehydrogenase (PDH), isocitrate dehydrogenase, α-ketoglutarate dehydrogenase, and ATP synthase, which inhibit glucose oxidation and promote glycolysis. The reduction of the intermediate α-ketoglutarate (α-KG) and mitochondrial oxygen free radicals relieved the inhibition of HIF prolyl hydroxylase and inhibited the activity of P53, thereby activating HIF-1α at the transcription and protein levels. At the same time, HIF-1α inhibits mitochondrial biosynsis and promotes the expression of glycosylated enzymes such as pyruvate dehydrogenase kinase (PDK), which phosphorylates PDH, thus forming a positive feedback regulation of amplification and further promoting smooth muscle cell proliferation. In another key cell of vascular remodeling, hypoxia can cause mitochondrial crista fracture and swelling in endothelial cells and also activate mitochondrial autophagy, damaging mitochondrial biosynthetic [25–27], which leads to endothelial cell damage, activation of the NF-κB pathway-mediated inflammatory molecule expression, inhibition of NO production, and promotion of contractibility factor secretion.

As for PHA-related research fields, it has been reported that caspase-1 can regulate inflammatory factors and participate in the occurrence and development of PHA [28]. IL-1

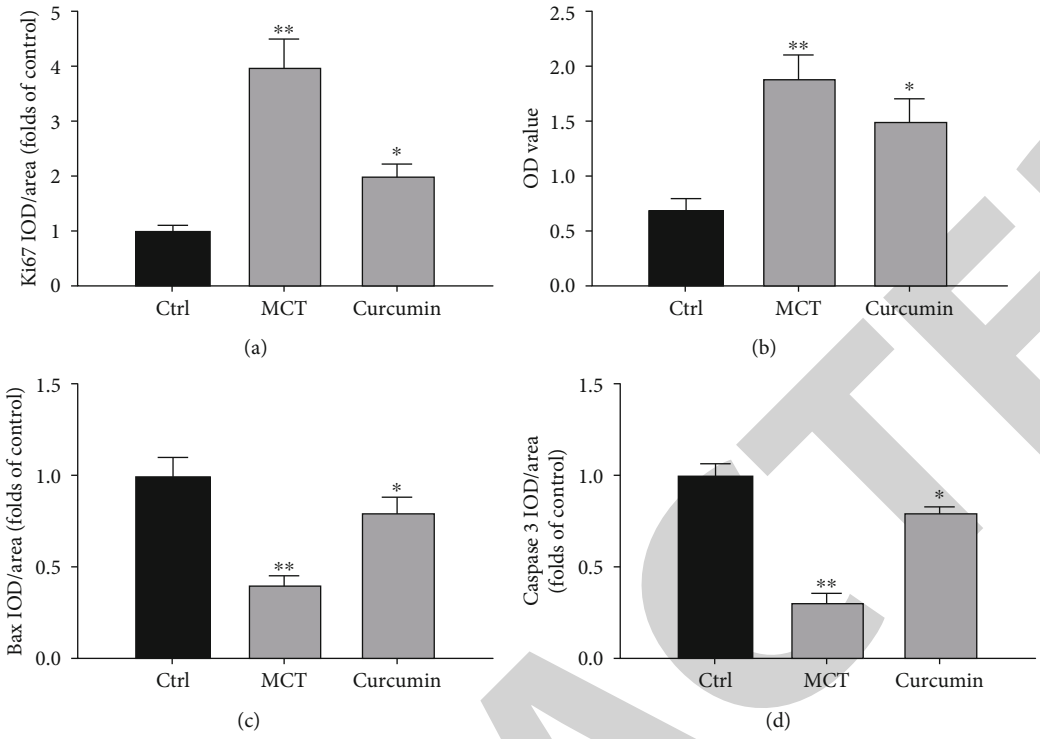

Figure 3: Curcumin promotes apoptosis of PASMC. (a) Quantitative analysis of Ki67 positive rate of immunohistochemical staining. (b) The OD value of PASMCs was quantitatively analyzed. (c) Quantitative analysis of the positive rate of Bax. (d) Quantitative analysis of caspase-3 positive rate. $^{*}P < 0.05$ and $^{**}P < 0.01$.

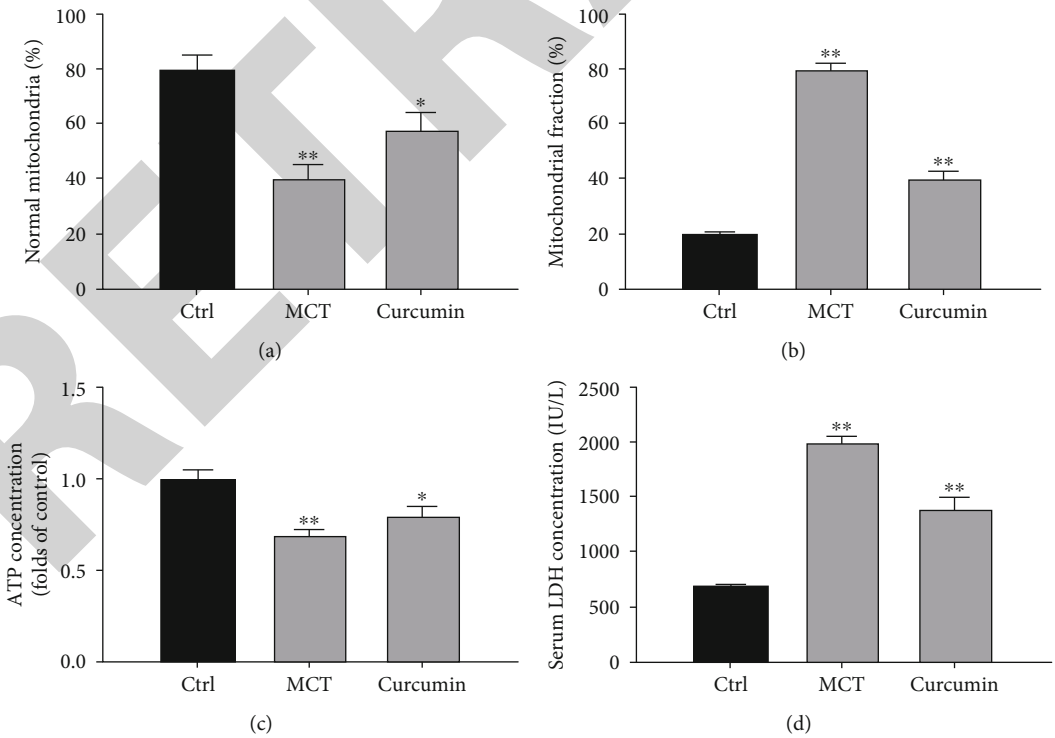

Figure 4: Curcumin improves function of mitochondrial. (a) Statistical analysis of normal mitochondrial percent of RV. (b) Statistical analysis of mitochondrial fragment percent of RV. (c) Effect of curcumin on mitochondrial function in vivo study. Statistical analysis of relative ATP levels in lung tissue. (d) Effect of curcumin on serum LDH concentration. $^{*}P < 0.05$ and $^{**}P < 0.01$.

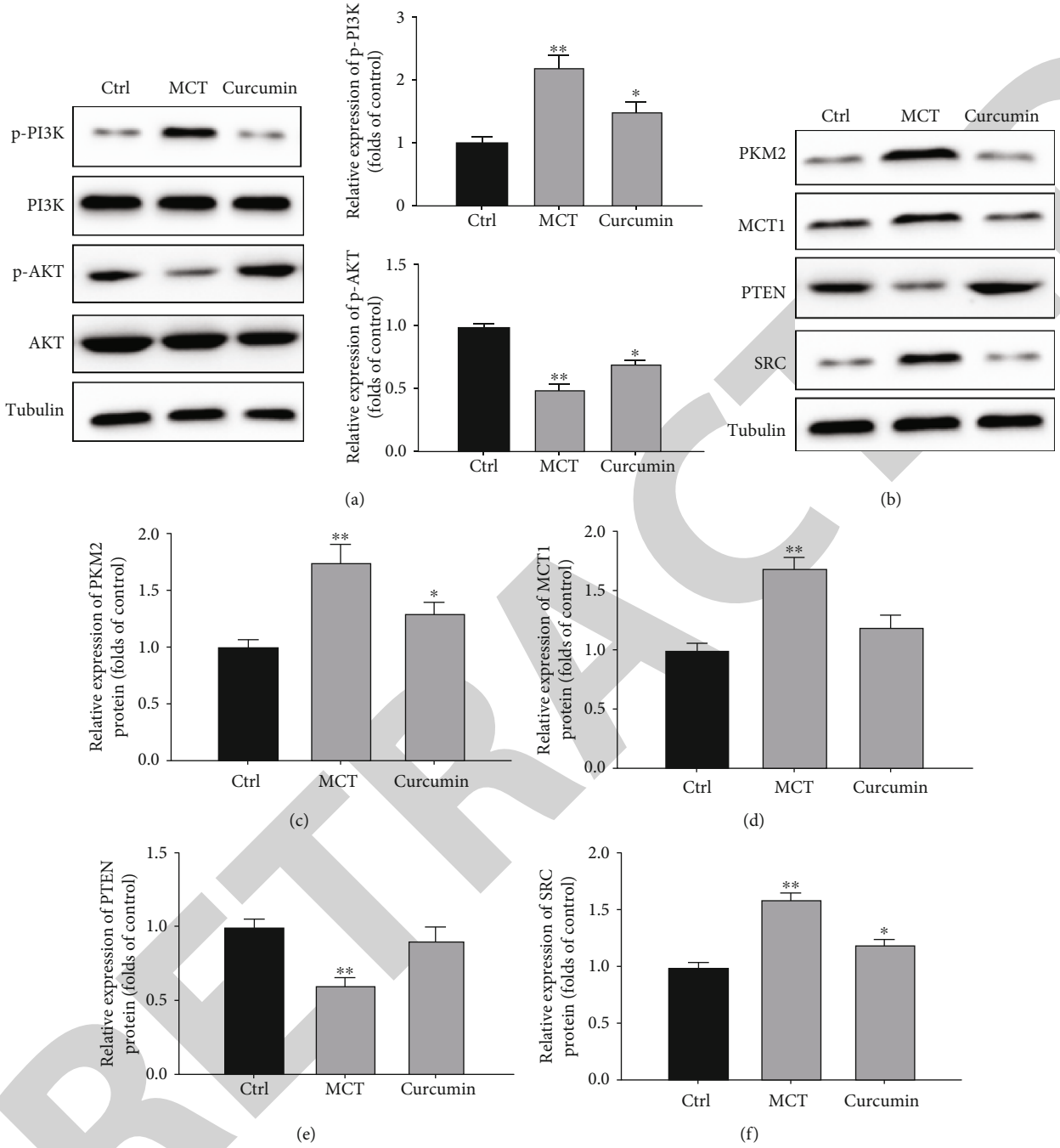

Figure 5: Curcumin mediated the expression of antiproliferative genes in PASMCs. (a) Relative expression of p-PI3K and p-AKT. (b) Relative expression of PKM2, MCT1, PTEN, and SRC. (c) Quantitative analysis of relative expression of PKM2. (d) Quantitative analysis of relative expression of MCT1. (e) Quantitative analysis of relative expression of PTEN. (f) Quantitative analysis of relative expression of SRC. $^{*}P < 0.05$ and $^{**}P < 0.01$.

can mediate the recruitment of macrophages around pulmonary vessels in mice, promote the abnormal proliferation of PASMCs, and cause pulmonary vascular remodeling, which is closely related to the disease progression of PHA [29, 30]. Curcumin could inhibit the secretion of IL-1 by inhibiting NLRP3 inflammasome, thus playing an anti-inflammatory role. Since inflammation is one of the important pathological mechanisms of hypoxia injury, curcumin may inhibit the activation of caspase-1 by inhibiting NLRP3 inflammasome, thereby reducing the maturation and release of IL-1, reducing the proliferation of inflammation-induced PASMCs, improving the remodeling of blood vessels, and ultimately reducing pulmonary artery pressure in PHA rats.

5. Conclusion

Pulmonary hypertension is a serious disease characterized by pulmonary vascular structure and remodeling, right heart

failure, and eventual death. Mitochondrial metabolic changes have recently been recognized as a new feature of PAH. Therefore, correcting mitochondrial metabolism can inhibit the excessive proliferation of PASMCs and promote its apoptosis, which is the core mechanism of PAH. Our results show that curcumin can reduce pulmonary artery pressure and remodeling, so it may be a new drug for PAH. Overall, our data suggest that curcumin is effective in reducing pulmonary artery pressure and reversing pulmonary artery remodeling but should be used with caution.

Data Availability

The data used during the present study are available from the corresponding author upon reasonable request.

Conflicts of Interest

The authors declare that they have no conflicts of interest.

References

[1] M. Humbert, N. W. Morrell, S. L. Archer et al., "Cellular and molecular pathobiology of pulmonary arterial hypertension," *Journal of the American College of Cardiology*, vol. 43, no. 12, pp. S13–S24, 2004.

[2] R. Rafikov, J. James, N. McClain, S. P. Tofovic, and O. Rafikova, "Role of gender in regulation of redox homeostasis in pulmonary arterial hypertension," *Antioxidants*, vol. 8, no. 5, p. 135, 2019.

[3] A. E. Lammers, "Predicting prognosis of children with pulmonary arterial hypertension: the importance of multimodal expert assessment," *Heart*, vol. 100, no. 17, pp. 1305–1307, 2014.

[4] J. J. Ryan and S. L. Archer, "The right ventricle in pulmonary arterial hypertension: disorders of metabolism, angiogenesis and adrenergic signaling in right ventricular failure," *Circulation Research*, vol. 115, no. 1, pp. 176–188, 2014.

[5] M. G. George, L. J. Schieb, C. Ayala, A. Talwalkar, and S. Levant, "Pulmonary hypertension surveillance: United States, 2001 to 2010," *Chest*, vol. 146, no. 2, pp. 476–495, 2014.

[6] V. Gurtu and E. D. Michelakis, "Emerging therapies and future directions in pulmonary arterial hypertension," *Canadian Journal of Cardiology*, vol. 31, no. 4, pp. 489–501, 2015.

[7] G. Ruocco, A. Gavazzi, S. Gonnelli, and A. Palazzuoli, "Pulmonary arterial hypertension and heart failure with preserved ejection fraction: are they so discordant?," *Cardiovascular Diagnosis and Therapy*, vol. 10, no. 3, pp. 534–545, 2020.

[8] K. Yada, L. A. Roberts, N. Oginome, and K. Suzuki, "ffect of Acacia Polyphenol Supplementation on Exercise-Induced Oxidative Stress in Mice Liver and Skeletal Muscle," *Antioxidants*, vol. 9, no. 1, 2019.

[9] T. Stącel, R. Antończyk, M. Latos et al., "Extracorporeal Membrane Oxygenation as a Postoperative Left Ventricle Conditioning Tool After Lung Transplantation in Patients With Primary Pulmonary Artery Hypertension: First Polish Experience," *Transplantation Proceedings*, vol. 52, no. 7, pp. 2113–2117, 2020.

[10] B. Ahn, R. Ranjit, P. Premkumar et al., "Mitochondrial oxidative stress impairs contractile function but paradoxically increases muscle mass via fibre branching," *Journal of Cachexia Sarcopenia and Muscle*, vol. 10, no. 2, pp. 411–428, 2019.

[11] J. James, M. Valuparampil Varghese, M. Vasilyev et al., "Complex III inhibition-induced pulmonary hypertension affects the mitochondrial proteomic landscape," *International Journal of Molecular Sciences*, vol. 21, no. 16, p. 5683, 2020.

[12] L. Mei, Y. M. Zheng, T. Song et al., "Rieske iron-sulfur protein induces FKBP12.6/RyR2 complex remodeling and subsequent pulmonary hypertension through NF-κB/cyclin D1 pathway," *Nature Communications*, vol. 11, no. 1, p. 3527, 2020.

[13] Y. Guo, X. Liu, Y. Zhang, H. Qiu, F. Ouyang, and Y. He, "3-Bromopyruvate ameliorates pulmonary arterial hypertension by improving mitochondrial metabolism," *Life Sciences*, vol. 256, article 118009, 2020.

[14] M. Sarighieh, V. Montazeri, A. Shadboorestan, M. H. Ghahremani, and S. N. Ostad, "The inhibitory effect of curcumin on hypoxia inducer factors (Hifs) as a regulatory factor in the growth of tumor cells in breast cancer stem-like cells," *Drug Research*, vol. 70, no. 11, pp. 512–518, 2020.

[15] B. Ren, Y. F. Zhang, S. S. Liu et al., "Curcumin alleviates oxidative stress and inhibits apoptosis in diabetic cardiomyopathy via Sirt1-Foxo1 and PI3K-Akt signalling pathways," *Journal of Cellular and Molecular Medicine*, vol. 24, no. 21, pp. 12355–12367, 2020.

[16] A. Girme, G. Saste, A. K. Balasubramaniam, S. Pawar, C. Ghule, and L. Hingorani, "Assessment of *Curcuma longa* extract for adulteration with synthetic curcumin by analytical investigations," *Journal of Pharmaceutical and Biomedical Analysis*, vol. 191, article 113603, 2020.

[17] M. Tian, X. Zhang, L. Wang, and Y. Li, "Curcumin induces ABCA1 expression and apolipoprotein A-I-mediated cholesterol transmembrane in the chronic cerebral hypoperfusion aging rats," *The American Journal of Chinese Medicine*, vol. 41, no. 5, pp. 1027–1042, 2013.

[18] R. Chen, X. Peng, W. du et al., "Curcumin attenuates cardiomyocyte hypertrophy induced by high glucose and insulin *via* the PPAR γ/Akt/NO signaling pathway," *Diabetes Research and Clinical Practice*, vol. 108, no. 2, pp. 235–242, 2015.

[19] Z. Wang, Z. Chen, B. Li et al., "Curcumin attenuates renal interstitial fibrosis of obstructive nephropathy by suppressing epithelial-mesenchymal transition through inhibition of the TLR4/NF-κB and PI3K/AKT signalling pathways," *Pharmaceutical Biology*, vol. 58, no. 1, pp. 828–837, 2020.

[20] R. Yamanaka, A. Hoshino, K. Fukai et al., "TIGAR reduces smooth muscle cell autophagy to prevent pulmonary hypertension," *American Journal of Physiology-Heart and Circulatory Physiology*, vol. 319, no. 5, pp. H1087–H1096, 2020.

[21] H. He, Y. Luo, Y. Qiao et al., "Curcumin attenuates doxorubicin-induced cardiotoxicity via suppressing oxidative stress and preventing mitochondrial dysfunction mediated by 14-3-3γ," *Food & Function*, vol. 9, no. 8, pp. 4404–4418, 2018.

[22] X. Shi, T. Huang, J. Wang et al., "Next-generation sequencing identifies novel genes with rare variants in total anomalous pulmonary venous connection," *eBioMedicine*, vol. 38, pp. 217–227, 2018.

[23] C. Salaud, A. Alvarez-Arenas, F. Geraldo et al., "Mitochondria transfer from tumor-activated stromal cells (TASC) to primary *Glioblastoma* cells," *Biochemical and Biophysical Research Communications*, vol. 533, no. 1, pp. 139–147, 2020.

[24] T. Chen, G. Wu, H. Hu, and C. Wu, "Enhanced fatty acid oxidation mediated by CPT1C promotes gastric cancer

Hindawi
BioMed Research International
Volume 2024, Article ID 9807363, 1 page
https://doi.org/10.1155/2024/9807363

Retraction

Retracted: Protective Effect of Luteolin on D-Galactosamine (D-Gal)/Lipopolysaccharide (LPS) Induced Hepatic Injury by in Mice

BioMed Research International

Received 12 March 2024; Accepted 12 March 2024; Published 20 March 2024

This article has been retracted by Hindawi following an investigation undertaken by the publisher [1]. This investigation has uncovered evidence of one or more of the following indicators of systematic manipulation of the publication process:

(1) Discrepancies in scope

(2) Discrepancies in the description of the research reported

(3) Discrepancies between the availability of data and the research described

(4) Inappropriate citations

(5) Incoherent, meaningless and/or irrelevant content included in the article

(6) Manipulated or compromised peer review

The presence of these indicators undermines our confidence in the integrity of the article's content and we cannot, therefore, vouch for its reliability. Please note that this notice is intended solely to alert readers that the content of this article is unreliable. We have not investigated whether authors were aware of or involved in the systematic manipulation of the publication process.

Wiley and Hindawi regrets that the usual quality checks did not identify these issues before publication and have since put additional measures in place to safeguard research integrity.

We wish to credit our own Research Integrity and Research Publishing teams and anonymous and named external researchers and research integrity experts for contributing to this investigation.

The corresponding author, as the representative of all authors, has been given the opportunity to register their agreement or disagreement to this retraction. We have kept a record of any response received.

References

[1] Y. Pu, Z. Yang, and X. Mo, "Protective Effect of Luteolin on D-Galactosamine (D-Gal)/Lipopolysaccharide (LPS) Induced Hepatic Injury by in Mice," *BioMed Research International*, vol. 2021, Article ID 2252705, 8 pages, 2021.

Hindawi
BioMed Research International
Volume 2021, Article ID 2252705, 8 pages
https://doi.org/10.1155/2021/2252705

Research Article

Protective Effect of Luteolin on D-Galactosamine (D-Gal)/Lipopolysaccharide (LPS) Induced Hepatic Injury by in Mice

Yiwei Pu, Zhaocong Yang, and Xuming Mo

Department of Cardiothoracic Surgery, Children's Hospital of Nanjing Medical University, Nanjing, China

Correspondence should be addressed to Zhaocong Yang; yangzhaocong34@126.com
and Xuming Mo; mohsuming15@njmu.edu.cn

Received 9 June 2021; Accepted 19 July 2021; Published 29 July 2021

Academic Editor: Jun Yang

To observe the effects of luteolin on galactosamine (D-Gal)/lipopolysaccharide (LPS) induced liver injury in mice. Male C57BL/6 mice were randomly divided into 4 groups: normal control group, D-GaI/LPS group, D-GaI/LPS + luteolin (Lu, 20 mg/kg), and D-GaI/LPS + luteolin (Lu, 40 mg/kg). Mice in the normal control group and D-GaI/LPS group were given distilled water while other groups were given drugs in 7 days by gavage. 4 hours after the continuous administration, Gal (700 mg/kg) and LPS (10 mg/kg) were injected intraperitoneally. Mice in the normal control group were given the same volume of vegetable oil solution. 24 h after the establishment of the mice model, blood and liver samples were collected. Hematoxylin (HE) staining was used to observe the changes of hepatic histopathology. Alanine aminotransferase (ALT) and glutamic oxalacetic transaminase (AST) in serum, interleukin-6 (IL-6), interleukin-1β (IL-1β), and tumor necrosis factor (TNF-α) were measured by related kits. Western blotting was used to demonstrate the expression levels of related inflammation proteins. Lu significantly reduced levels of proinflammatory cytokines including interleukin-6 (IL-6), interleukin-1β (IL-1β), and tumor necrosis factor-α (TNF-α) in serum and liver. Lu restored the pathological changes after galactosamine (D-Gal)/lipopolysaccharide (LPS) treatment. In addition, Lu regulated proteins levels of the NLRP3/NF-κB pathway in liver. Lu exhibited therapeutical effects on D-GaI/LPS induced liver injury in mice which might be related to the regulation of the NLRP3/NF-κB pathway.

1. Introduction

Acute hepatic failure (AFT) is a serious clinical syndrome, which is the result of a large number of hepatocyte deaths [1]. The prognosis of acute liver failure is very poor, and there is no effective treatment unless liver transplantation. Drug-induced liver injury (DILI) is a major cause of AFT which is one of the leading causes for liver transplantation [2]. The liver injury caused by simultaneous injection of d-galactosamine (d-gal) and lipopolysaccharide (LPS) has been widely used to study the pathogenesis of AFT [3–5]. Although it is well known that hepatocyte is the main target cell of AFT, hepatocyte (such as macrophages and neutrophils) has an inflammatory reaction. The mechanism of liver injury induced by d-gal/LPS is not completely clear [6]. Therefore, it is urgent to study the mechanism of AFT and the drug treatment.

D-galactosamine is a classic model for the preparation of acute liver injury. The main pathogenic component of bacterial lipopolysaccharide gram-negative bacteria can cause systemic inflammatory response syndrome, which can lead to acute liver injury and multiple organ failure. D-galactosamine (D-gal) can increase the sensitivity of mice to lipopolysaccharide and aggravate the lethal effect of lipopolysaccharide. Therefore, D-galactosamine (D-gal) and lipopolysaccharide (LPS) were used to replicate the liver injury model of mice in this experiment.

NLRP3 inflammasome (Nucleotide-binding and oligomerization domain-like receptors3 inflammasome), a newly discovered pattern recognition receptor (PRRs), is an important membership of host immune defense system, including NLRP3 molecules, ligand molecules ASC (apoptosis-associated spec-like protein), and procaspase-1, which is composed of three molecules whose binding state regulates the activity

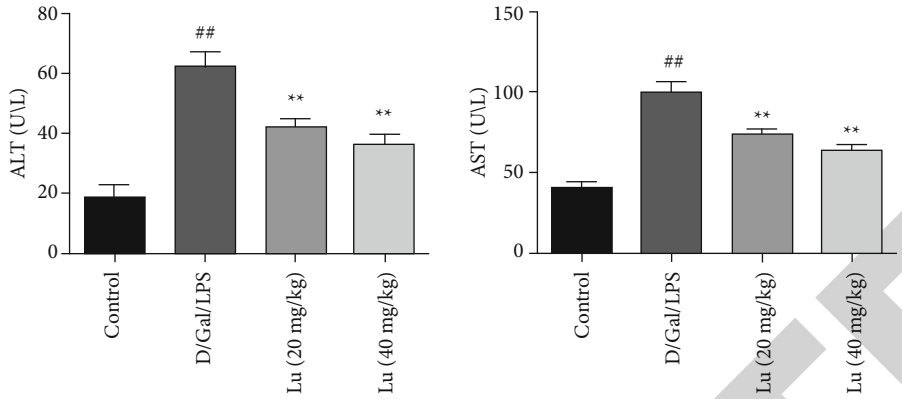

Figure 1: Effects of Lu on ALT and AST in liver injury mice induced by D-GaI/LPS. The values are presented as the mean ± standard deviation. $^{*}P < 0.05$ compared to the D-GaI/LPS group; $^{**}P < 0.01$ compared to the D-GaI/LPS group; $^{\#}P < 0.01$ compared to the control group, $^{\#\#}P < 0.01$ compared to the control group.

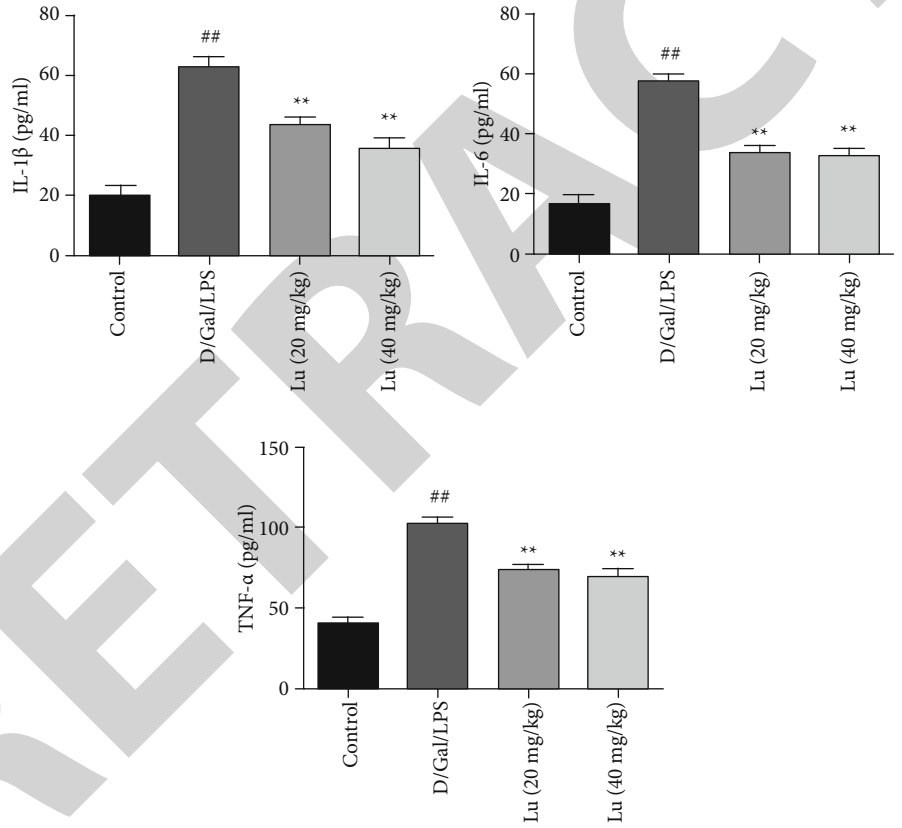

Figure 2: Effects of Lu on cytokines in serum of D-GaI/LPS-induced liver injury mice. The values are presented as the mean ± standard deviation. $^{*}P < 0.05$ compared to the D-GaI/LPS group; $^{**}P < 0.01$ compared to the D-GaI/LPS group; $^{\#}P < 0.01$ compared to the control group, $^{\#\#}P < 0.01$ compared to the control group.

of NLRP3 inflammasome corpuscles [7]. In the liver, NLRP3 inflammasome corpuscles were mainly expressed in hepatocyte. NLRP3 inflammasome consists of NLRP3, ASC, and caspase-1. Caspase-1 is crucial to the conversion of IL-1β immature type to active type. The response of NLRP3 to stimulus requires NF-κB signaling.

Luteolin (3′, 4′, 5,7–tetrahydroxyflavone, Lu), a common flavonoid found in various plants, is reported to have various pharmacological correlations, including free radical scavenging anticancer and anti-inflammatory activities [8, 9]. However, there are still few studies on whether Lu is beneficial for acute liver failure. Luteolin has also been shown to exhibit a therapeutic effect on liver injury induced by tetrachloromethane (CCl4) [10], ethanol [11], or acetaminophen [12] in mice. Therefore, our research is aimed at evaluating the effects of Lu on acute liver failure and exploring its possible mechanism.

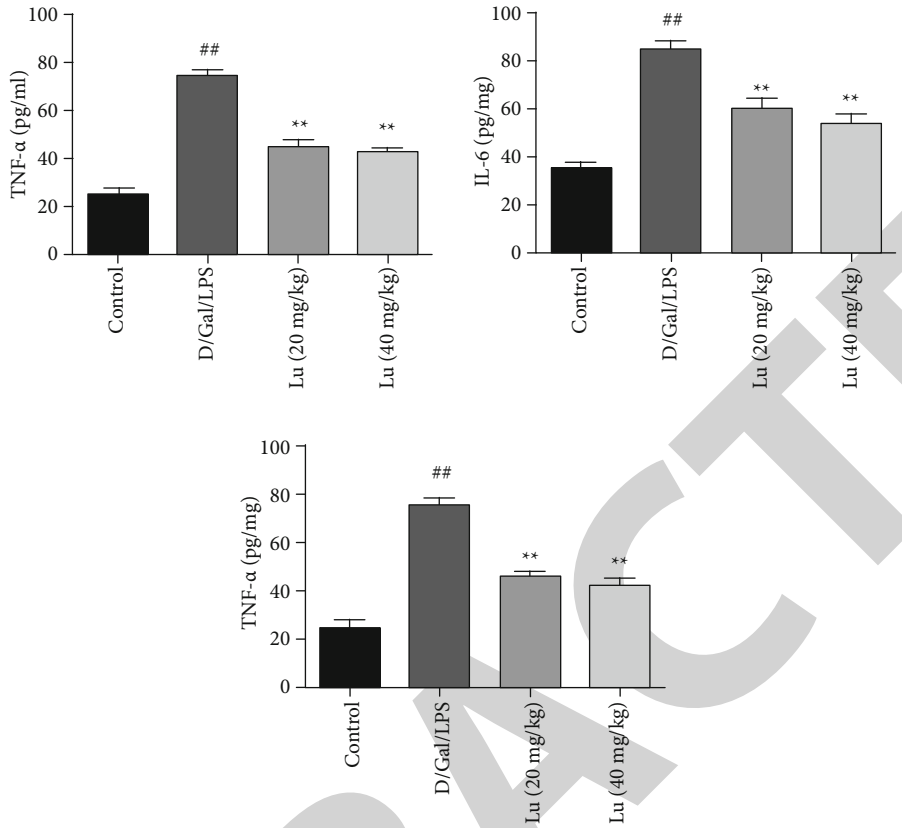

Figure 3: Effects of Lu on cytokines in liver of D-GaI/LPS-induced liver injury. The values are presented as the mean ± standard deviation. $^{*}P < 0.05$ compared to the D-GaI/LPS group; $^{**}P < 0.01$ compared to the D-GaI/LPS group; $^{\#}P < 0.01$ compared to the control group, $^{\#\#}P < 0.01$ compared to the control group.

2. Materials and Methods Reagents and Kits

Lu was obtained from Sigma-Aldrich (Saint Louis, MO, USA). Gal and LPS were obtained from Sigma Aldrich (St. Louis, USA). Interleukin- (IL-) 6, IL-1β, and tumor necrosis factor- (TNF-) α enzyme-linked immunosorbent assay (ELISA) kits were obtained from Elabscience (Wuhan, China). Primary antibodies were purchased from Cell Signaling Technology. The commercial kits of alanine aminotransferase (ALT) and glutamic oxalacetic transaminase (AST) were purchased from Jiancheng Bioengineering Institute (Nanjing, China).

2.1. Animals. 60 male C57BL/6 mice (20-22 g) were purchased from the experimental animal center of Nantong University, Certificate No. SCXK (Su) 2012-0001. Animal welfare and experimental procedures strictly abide by the ethical guidelines of the National Institutes of Health and were approved by the Institutional Animal Research Committee of Nanjing Medical University.

2.2. Experimental Procedure. 60 male C57BL/6 mice were randomly divided into 4 groups, 15 in each group: control group, D-GaI/LPS group, D-GaI/LPS + Lu (20 mg/kg), and D-GaI/LPS + Lu (20 mg/kg) (40 mg/kg). Lu (20, 40 mg/kg) was given continuously by gastric perfusion for 7 days, while the control group and the D-GaI/LPS group were given the same amount of distilled water. Four hours after the last administration, D-GaI (700 mg/kg) and LPS (10 mg/kg) were injected intraperitoneally to mice, while the control group was injected intraperitoneally with equal volume of solvent. After 24 h, the animals were sacrificed to collect the blood and liver tissue.

2.3. HE Staining of Liver Tissue. C57BL/6 mice liver tissue was fixed in 4% neutral formalin solution. The liver tissue was then embedded in paraffin and cut into 4 mm thick slices. Finally, hematoxylin-eosin staining (HE staining) was performed to observe the histopathological changes of the liver under optical microscope.

2.4. Biochemical Assays in Serum. The levels of ALT and AST were determined by commercial kits according to the manufacturer's instructions.

2.5. Determination of Cytokines in Serum and Liver. The contents of IL-1β, IL-6, and TNF-α in serum and liver of mice of each group were detected according to ELISA kit instructions.

2.6. Determination of NLRP3/NF-κB-Related Protein in Liver. The total protein in liver tissue of mice in each group was extracted with RIPA lysate, centrifuged at 12,000 rpm for 15 minutes, and supernatant was collected. The BCA kit was used to quantify the proteins of each group. The protein samples of each group were subjected to SDS-polyacrylamide gel electrophoresis and then transferred to PVDF membrane.

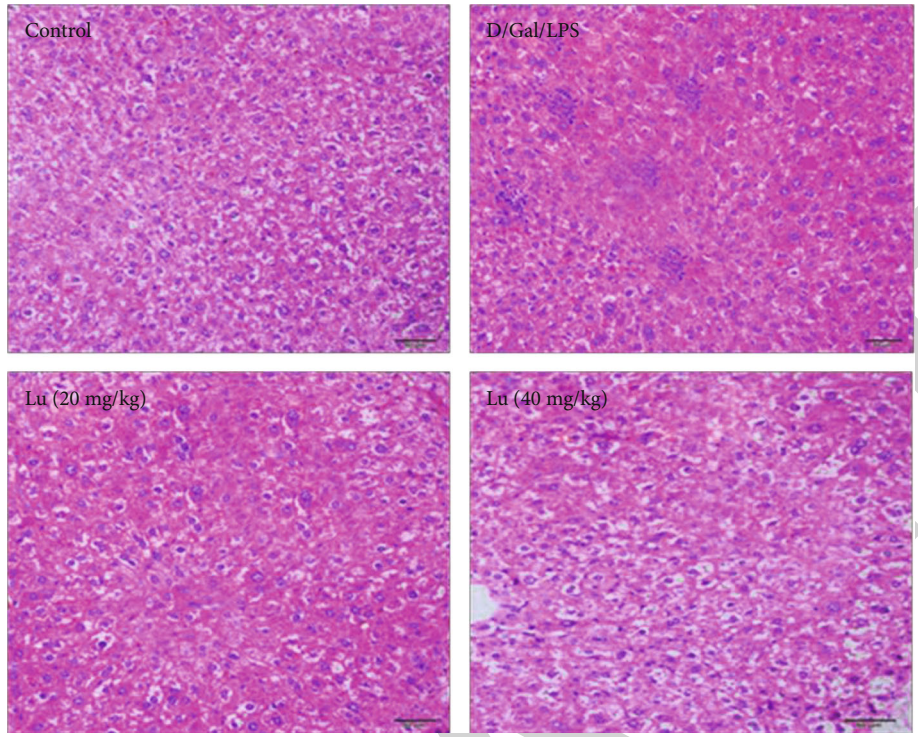

Figure 4: Effect of Lu on liver tissue pathological changes in D-GaI/LPS-induced liver injury mice (×200). The values are presented as the mean ± standard deviation. $^{*}P < 0.05$ compared to the D-GaI/LPS group; $^{**}P < 0.01$ compared to the D-GaI/LPS group; $^{\#}P < 0.01$ compared to the control group, $^{\#\#}P < 0.01$ compared to the control group.

Then, the PVDF membrane was placed in 5 % skimmed milk and sealed for 2 h. After 2 hours of sealing, PVDF membrane was placed in the corresponding primary antibody and incubated overnight at 4°C. The next day was washed 4 times with TBST for 8 min each time. Then, the PVDF membrane was placed in the second antibody solution and incubated for 2 h at room temperature in a shaking table. PVDF membrane was removed and washed 4 times with TBST for 8 min each time. The gel imaging system was used to expose and scan the bands to analyze the gray value of each band.

2.7. Immunohistochemistry. The expressions of NLRP3 and p-NF-κBP65, in the liver of mice, were detected by immunohistochemical method. In short, liver tissue was fixed with 4 % paraformaldehyde (PFA), embedded in paraffin, and sliced. Paraffin sections were dewaxed in xylene and absolute ethanol, microwave in sodium citrate buffer, and washed with PBS. Endogenous peroxidase activity was blocked by 3 % hydrogen peroxide for 20 min. Each sample was blocked with 5% goat serum for 20 minutes and then treated with primary antibodies NLRP 3 (1 : 200) and p-NF-κBp65 (1 : 200), overnight at 4°C. The next day, after washing with PBS for 3 times, each sample was treated with goat anti-rabbit IgG secondary antibody for 20 min, then the horseradish enzyme-labeled streptavidin working solution was incubated for 20 min, and washed with PBS for 3 times. Then stained with 3-3′ diaminobenzidine (DAB) and then stained with hematoxylin. After dehydration and drying, the slices were fixed with neutral glue and observed under a microscope.

2.8. Statistical Analysis. All the experimental data were expressed as mean standard deviation, and one-way ANOVA was performed with statistical software. $P < 0.05$ showed that the difference was statistically significant.

3. Results

3.1. Effects of Lu on ALT and AST in Liver Injury Mice Induced by D-GaI/LPS. As is shown in Figure 1, compared with the control group, the contents of ALT and AST in the model group were significantly increased after injection of D-GaI/LPS. Compared with the model group, Lu (20, 40 mg/kg) could significantly reduce ALT and AST contents.

3.2. Effects of Lu on Cytokines in Serum of D-GaI/LPS-Induced Liver Injury Mice. As is shown in Figure 2, compared with the control group, the levels of IL-1β, IL-6, and TNF-α in the serum of mice in the model group were significantly increased. Compared with the model group, the contents of IL-1β, IL-6, and TNF-α in Lu (20, 40 mg/kg) groups were significantly lower than those in the model group.

3.3. Effects of Lu on Cytokines in Liver of D-GaI/LPS-Induced Liver Injury Mice. As is shown in Figure 3, compared with the control group, the levels of IL-1β, IL-6, and TNF-α in the liver of mice in the model group were significantly increased. Compared with the model group, the contents of IL-1β, IL-6, and TNF-α in Lu (20, 40 mg/kg) groups were significantly lower than those in the model group.

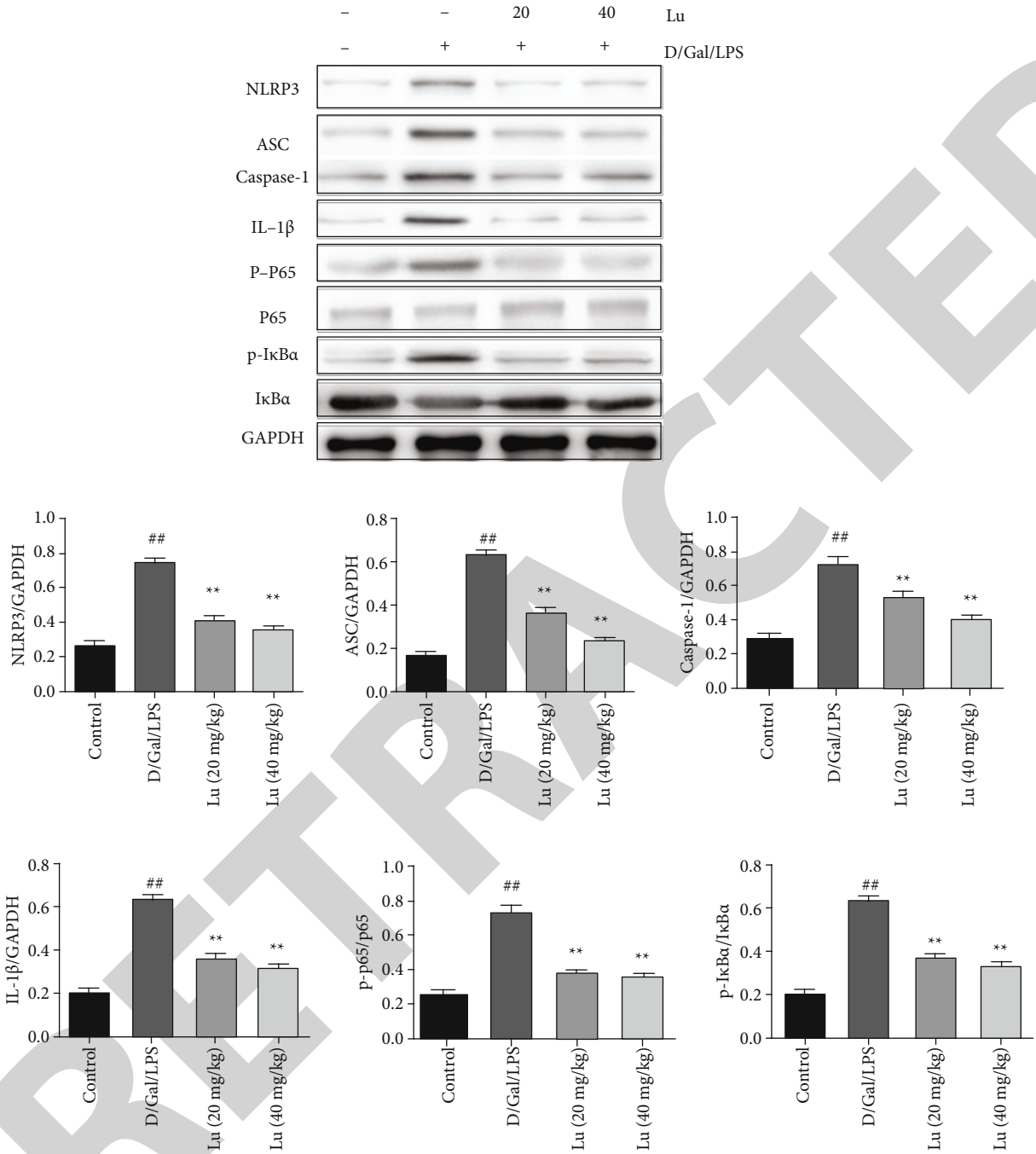

Figure 5: Effect of Lu on the expression of NLRP3/NF-κB pathway protein in liver of D-GaI/LPS-induced liver injury mice. The values are presented as the mean ± standard deviation. $^{*}P < 0.01$ compared to the D-GaI/LPS group; $^{**}P < 0.01$ compared to the D-GaI/LPS group; $^{\#}P < 0.01$ compared to the control group, $^{\#\#}P < 0.01$ compared to the control group.

3.4. Effect of Lu on Liver Tissue Pathological Changes in D-GaI/LPS-Induced Liver Injury Mice. As shown in Figure 4, the liver tissue structure of the mice in the control group is normal and the cell morphology is normal. In the model group, the liver tissue structure was abnormal, liver cells were denatured, and inflammatory cells infiltrated. Compared with the model group, the liver structure and hepatocyte morphology in Lu (20, 40 mg/kg) groups were basically normal, and inflammatory cell infiltration was reduced.

3.5. Effect of Lu on the Expression of NLRP3/NF-κB Pathway Protein in Liver of D-GaI/LPS-Induced Liver Injury Mice. As shown in Figure 5, compared with the group, the expression of NLRP3, ASC, Caspapse-1, IL-1β, p-IκBα, and p-NF-κBp65 protein in the model group were significantly increased. Compared with the model group, the expression of NLRP3, ASC, Caspapse-1, IL-1β, p-IκBα, and p-NF-κBp65 protein in liver tissue of mice in Lu (20, 40 mg/kg) groups was significantly decreased.

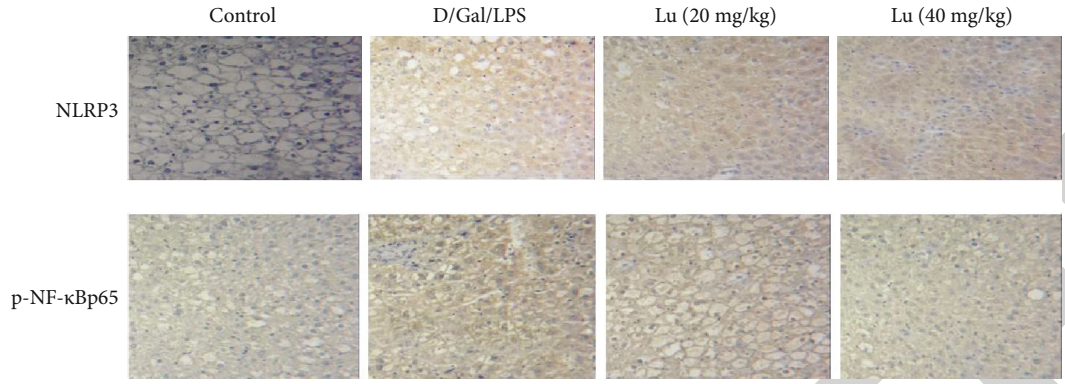

Figure 6: Effect of Lu on the expression of NLRP3 and p-NF-κBp65 in liver of D-GaI/LPS-induced liver injury mice by immunohistochemistry. The values are presented as the mean ± standard deviation. $^{*}P < 0.05$ compared to the D-GaI/LPS group; $^{**}P < 0.01$ compared to the D-GaI/LPS group; $^{\#}P < 0.01$ compared to the control group, $^{\#\#}P < 0.01$ compared to the control group.

3.6. Effect of Lu on the Expression of NLRP3 and p-NF-κBp65 in Liver of D-GaI/LPS-Induced Liver Injury Mice by Immunohistochemistry. As shown in Figure 6, compared with the control group, the expression of NLRP3 and p-NF-κBp65 in the model group was significantly increased. Compared with the model group, the expression of NLRP3 and p-NF-κBp65 in liver tissue of mice in Lu (20, 40 mg/kg) groups was significantly decreased.

4. Discussion

The liver injury model induced by D-GaI/LPS was used in this study. It was found that Lu could significantly reduce ALT and AST activities and reduce the content of proinflammatory cytokines such as IL-1β, IL-6, and TNF-α in serum and liver induced by D-GaI/LPS. The results of western blot suggest that Lu may have protective effects on liver injury via inhibiting NLRP3/NF-κB pathway.

Alanine aminotransferase (ALT) and aspartate aminotransferase (AST) are both present in liver. When the hepatocyte membrane is damaged or the cell is necrotic, the enzymes entering the supernatant increase. ALT and AST activities in the supernatant can sensitively reflect the degree of hepatocyte injury [13]. In the early stage of acute liver injury, ALT change is the most sensitive, and it is the main item to diagnose hepatocyte parenchymal damage. ALT level is often parallel to the severity of the disease. However, when liver injury occurs, AST increases to a higher level than ALT. At that time, AST is the main indicator of the degree of liver injury. ALT mainly exists in hepatocyte plasma, while AST exists in hepatocyte plasma and is distributed in mitochondria. AST and ALT are commonly used indicators of liver fibrosis. Previous studies have shown that the administration of D-GaI/LPS distinctly increased the activities of ALT and AST. However, pretreatment with flavonoid strikingly reduced AST and ALT activities [14]. Our study showed the change of serum enzyme of ALT and AST levels was consistent with the above results.

Inflammatory reaction is one of the important causes of liver injury. Inhibition of inflammatory reaction can improve the symptoms of liver injury [15]. Therefore, anti-inflammatory protection of liver cells is crucial in the treatment of liver injury. After the occurrence of liver parenchymal injury, hepatocyte is activated to release more inflammatory mediators IL-1β, IL-6, and TNF-α, which could influence HSC and Kuffer cells. It forms positive feedback regulation, resulting in more cytokines and aggregation, thus, promoting the development of liver injury [16]. The contents of IL-1β, IL-6, and TNF-α in liver injury serum were significantly higher than those in the normal control group and gradually increased with the aggravation of liver injury. IL-1β, IL-6, and TNF-α participate in the whole process of the occurrence and development of acute liver injury [17]. In this study, the expression of IL-1β, IL-6, and TNF-α in serum and liver was significantly increased under the stimulation of D-GaI/LPS. Lu could inhibit the production and release of inflammatory factors in serum and liver of mice with liver injury induced by D-GaI/LPS. Park et al. found that luteolin administration significantly ameliorated the increased TNF-α production and COX-2 expression in GalN/LPS-induced hepatitic ICR mice [18]. Attiq et al. reported Lu abrogates the LPS-induced inflammatory responses in human plasma, especially decreased the expression of IL-1β and IL-6 [19].

TNF-α secretion is regulated by The TLR4/NF-κB signaling pathway in liver [20, 21]. NF-κB belongs to Rel protein family, in which the heterodimer composed of p65 and p50 is a trimer formed by combining NF-κB with IκBα in resting state and exists in cytoplasm in inactive form. NF-κB was reported regulating the inflammation in CCl4 exposure-induced hepatitis to ameliorate liver injury [22, 23]. When stimulated by external signals, it activates a series of protein kinases, such as NLRP3 inflammasome, thus, mediating inflammatory reactions [24]. LPS could cause the expression and activation of NLRP3, while luteolin treatment could inhibit the expression and activation of NLRP3 [25]. There was no report that luteolin is effective in LPS-induced liver failure through NLRP3/NF-κB inflammatory pathway. NLRP3 inflammasome is a protein complex composed of receptor protein, apoptosis-associated specific-like protein (CARD), ASC, and effector molecule pro-caspase-1. It forms a cysteine proteolytic enzyme (Caspase) self-shearing that can lead to inflammatory aspartic acid specificity. The latter causes host inflammatory response by activating proinflammatory factors IL-1β and IL-18. The existing literature has

proved the inflammatory regulatory effect of the NLRP3/NF-κB pathway in the course of liver injury [26]. This study proves that Lu can significantly reduce the increased production of NLRP3, ASC, Caspapse-1, IL-1β, p-IκBα, and p-NF-κBp65 caused by D-GaI/LPS.

5. Conclusion

To sum up, our experiment shows that Lu can improve the liver injury induced by D-GaI/LPS in mice, and the effect may be through NLRP3/NF-κB signal pathway, and the specific mechanism needs further study.

Data Availability

The raw data could be accessed by contact the corresponding author if necessary.

Conflicts of Interest

No potential conflicts of interest were disclosed.

Acknowledgments

We would like to acknowledge the funding from the China Postdoctoral Science Foundation (2019M651904), a Key Project supported by the Medical Science and Technology Development Foundation, Nanjing Municipality Health Bureau (ZKX19039), the National Natural Science Foundation of China (81970265, 82000303), and the Natural Science Foundation of Jiangsu Province (BK20180144).

References

[1] J. H. Hoofnagle, R. L. Carithers Jr., C. Shapiro, and N. Ascher, "Fulminant hepatic failure: summary of a workshop," *Hepatology*, vol. 21, no. 1, pp. 240–252, 1995.

[2] J. C. Fernandez-Checa, P. Bagnaninchi, H. Ye et al., "Advanced preclinical models for evaluation of drug induced liver injury - consensus statement by the european drug-induced liver injury network [pro- euro-dili-net]," *Journal of Hepatology*, 2021.

[3] T. Nakama, S. Hirono, A. Moriuchi et al., "Etoposide prevents apoptosis in mouse liver with D-galactosamine/lipopolysaccharide-induced fulminant hepatic failure resulting in reduction of lethality," *Hepatology*, vol. 33, no. 6, pp. 1441–1450, 2001.

[4] A. Kuhla, C. Eipel, N. Siebert, K. Abshagen, M. D. Menger, and B. Vollmar, "Hepatocellular apoptosis is mediated by TNFα-dependent Fas/FasLigand cytotoxicity in a murine model of acute liver failure," *Apoptosis*, vol. 13, no. 12, pp. 1427–1438, 2008.

[5] C. Eipel, E. Kidess, K. Abshagen et al., "Antileukoproteinase protects against hepatic inflammation, but not apoptosis in the response of D-galactosamine-sensitized mice to lipopolysaccharide," *British Journal of Pharmacology*, vol. 151, no. 3, pp. 406–413, 2007.

[6] A. O. Shakil, D. Kramer, G. V. Mazariegos, J. J. Fung, and J. Rakela, "Acute liver failure: clinical features, outcome analysis, and applicability of prognostic criteria," *Liver Transplantation*, vol. 6, no. 2, pp. 163–169, 2000.

[7] W. M. Lee, "Acute liver failure," *The New England Journal of Medicine*, vol. 329, no. 25, pp. 1862–1872, 1993.

[8] A. Mignon, N. Rouquet, M. Fabre et al., "LPS challenge in D-galactosamine-sensitized mice accounts for caspase-dependent fulminant hepatitis, not for septic shock," *American Journal of Respiratory and Critical Care Medicine*, vol. 159, no. 4, pp. 1308–1315, 1999.

[9] M. Imran, A. Rauf, T. Abu-Izneid et al., "Luteolin, a flavonoid, as an anticancer agent: a review," *Biomedicine & Pharmacotherapy*, vol. 112, p. 108612, 2019.

[10] R. Domitrović, H. Jakovac, C. Milin, and B. Radošević-Stašić, "Dose- and time-dependent effects of luteolin on carbon tetrachloride-induced hepatotoxicity in mice," *Experimental and Toxicologic Pathology*, vol. 61, no. 6, pp. 581–589, 2009.

[11] G. Liu, Y. Zhang, C. Liu et al., "Luteolin alleviates alcoholic liver disease induced by chronic and binge ethanol feeding in mice," *The Journal of Nutrition*, vol. 144, no. 7, pp. 1009–1015, 2014.

[12] M. Tai, J. Zhang, S. Song et al., "Protective effects of luteolin against acetaminophen-induced acute liver failure in mouse," *International Immunopharmacology*, vol. 27, no. 1, pp. 164–170, 2015.

[13] R. J. Kaufman, "Stress signaling from the lumen of the endoplasmic reticulum: coordination of gene transcriptional and translational controls," *Genes & Development*, vol. 13, no. 10, pp. 1211–1233, 1999.

[14] Y. He, Z. Xia, D. Yu et al., "Hepatoprotective effects and structure-activity relationship of five flavonoids against lipopolysaccharide/d-galactosamine induced acute liver failure in mice," *International Immunopharmacology*, vol. 68, pp. 171–178, 2019.

[15] D. Ron and P. Walter, "Signal integration in the endoplasmic reticulum unfolded protein response," *Nature Reviews. Molecular Cell Biology*, vol. 8, no. 7, pp. 519–529, 2007.

[16] C. Xu, B. Bailly-Maitre, and J. C. Reed, "Endoplasmic reticulum stress: cell life and death decisions," *The Journal of Clinical Investigation*, vol. 115, no. 10, pp. 2656–2664, 2005.

[17] R. V. Rao, H. M. Ellerby, and D. E. Bredesen, "Coupling endoplasmic reticulum stress to the cell death program," *Cell Death and Differentiation*, vol. 11, no. 4, pp. 372–380, 2004.

[18] C. M. Park and Y. S. Song, "Luteolin and luteolin-7-O-glucoside protect against acute liver injury through regulation of inflammatory mediators and antioxidative enzymes in GalN/LPS-induced hepatitic ICR mice," *Nutrition Research and Practice*, vol. 13, no. 6, pp. 473–479, 2019.

[19] A. Attiq, J. Jalil, K. Husain, H. F. Mohamad, and A. Ahmad, "Luteolin and apigenin derived glycosides from *Alphonsea elliptica* abrogate LPS-induced inflammatory responses in human plasma," *Journal of Ethnopharmacology*, vol. 275, p. 114120, 2021.

[20] S. Zhao, J. Jiang, Y. Jing et al., "The concentration of tumor necrosis factor-α determines its protective or damaging effect on liver injury by regulating Yap activity," *Cell Death & Disease*, vol. 11, no. 1, p. 70, 2020.

[21] H. Wang, X. Wei, X. Wei et al., "4-hydroxybenzo[d]oxazol-2(3H)-one ameliorates LPS/D-GalN-induced acute liver injury by inhibiting TLR4/NF-κB and MAPK signaling pathways in mice," *International Immunopharmacology*, vol. 83, p. 106445, 2020.

[22] M. Seif, M. Deabes, A. el-Askary et al., "Ephedra sinica mitigates hepatic oxidative stress and inflammation via